Influence of Polyolefin Contamination on the Thermal Characteristics of Bottle Grade Recycled Polyethylene Terephthalate

By

Bachir ITIM

Thesis submitted in partial fulfilment of the requirements
of London Metropolitan University for the Degree of

DOCTOR OF PHILOSOPHY

September 2015

ACKNOWLEDGEMENTS

I would like to thank Dr Mathew Philip and Dr Dominic Spillane for the support and advices they gave me during the course of my research studies and to whom I am extremely grateful.

❖

Sincere thanks to all my lecturers and staff at London Metropolitan University, especially Professor Shah Hashemi and Dr Ahmed Farid.

❖

With regards to this research studies, I am thankful to the management team, in particular Nick Cliffe at Closed Loop Recycling Limited for supplying the *recycled bottle grade PET flakes.*

❖

Thanks to my family and friends, especially to my mother who taught me the importance of hard work and education. Also, I thank my brother Mekki for his continuous encouragement, and congratulation to my daughter, Warda, for her continuous academic achievement.

❖

Finally, to my soul mate Dr Inara and the close ones Edgars and Maria with love and gratitude for all their help and encouragement, without which this thesis would never have been written. Whose love, patience and support have helped me through the difficult and demanding years of my research studies at London Metropolitan University and to whom I dedicate this entire thesis.

❖

ABSTRACT

During the *mechanical recycling*, especially during the *sorting* and *separation process* of *bottle grade PET*, cross contamination with *polyolefin* is inevitable. Very small number of *polyolefin bottles, caps* and *closures* pass through the separation process and get recycled with *PET bottles* and affect the final characteristics of the recyclate. The effect of this cross contamination and the *influence* of *polyolefin contamination* on the *overall characteristics* of *bottle grade recycled PET*, especially the *thermal characteristics* with emphasis on *crystallinity*, were thoroughly investigated. The investigation showed that the inclusion of *polyolefin contamination* influenced the overall characteristics of the *bottle grade rPET matrix* and indicated *incompatibility* of *polyolefin contaminants* and *rPET-bg*. This influence had an impact on the *viscosity, elasticity* and *strength* of the *rPET-bg matrix*. Furthermore, the *crystallinity* of the *rPET-bg matrix* showed the impact of *polyolefin contamination* as a result of variation of *cooling rates* and that *cross-linking* and *chain branching* predominated over *chain scissions* as a result of *repetitive extrusions*. The crystallisation process of the *non contaminated rPET-bg* and *rPET-bg contaminated with polyolefin* depended on many influencing factors, such as *impurities, cross-linking, chain branching, chain scissions, cooling rates* and *repetitive extrusion cycles*. Also, the crystallisation mechanism fully depended on the *nucleation* and *growth rates* and that *competition* between *nucleation* and *molecular mobility* was influenced by the variation of *cooling rates* and *repetitive extrusion cycles.* As a result, the *thermal characteristics* were greatly influenced by the inclusion of *polyolefin contamination*, especially *crystallinity*, as shown and validated by the *Avrami* and *Ozawa models* and that the findings are a step forward and an original insight on the *influence* of *polyolefin contamination* at industrial scale.

Keywords: *Bottle grade rPET, polyolefin contamination, crystallinity, chains scission, cross-linking, chain branching.*

TABLE OF CONTENTS

Stage 1

Stage 2

LIST OF TABLES

LIST OF FIGURES

LIST OF SYMBOLS & ABBREVIATIONS

Abbreviation for Plastics **Meaning**

PET .....Poly(ethylene terephthalate)
PEN .....Poly(ethylene naphthalate)
PBT .....Poly(butylene terephthalate)
PTT .....Poly(trimethylene terephthalate)
rPET ..... recycled Poly(ethylene terephthalate)
HDPE .....High Density Polyethylene
PP .....Polypropylene

Abbreviation for Analyses and Testing

DSC .....Differential Scanning Calorimetry
FTIR .....Fourier Transform Infra-Red spectrometry
MFR/I ..... Melt Flow Rate/Index

Abbreviation of Chemical Compounds

-COO- ..... Ester Chemical Functional group
C-O ..... Carbon Oxygen Single Bond
C=O ..... Carbonyl Functional group
C-H ..... Carbon Hydrogen bond
C=C .....Carbon Carbon Double Bond
C-O-C ..... Ether group
n .....Number of repeated units in a polymer chain
O .....Oxygen
C ..... Carbon
H ..... Hydrogen
BHET ..... bis(hydroxyethyl terephthalate)
DMT ..... Dimethyl Terephthalate
DEG ..... Diethylene glycol
EG ..... Ethylene Glycol
TPA ..... Terephthalic Acid

Abbreviation of Chemical Compounds **Meaning**

PMDA ..... Pyromellitic dianhydride
SEBS ..... Styrene/ethylene-butylene/styrene
E-EA ..... Ethylene-ethyl acrylate
MA or MAH ..... Maleic anhydride
GMA ..... Glycidyl methacrylate
DAP ..... Diallyl phthalate

Abbreviation of Processes

MPPC .....Melt Phase Polycondensation
SSP .....Solid State Polycondensation
Extr.....Extruded or Extrusion
Inj. Moulded.....Injection Moulded
ISBM.....Injection Stretch Blow Moulding

Other abbreviations **Units**

T_g ..... [^oC].....Transition Glass Temperature
T_c .....[^oC].....Crystallisation Temperature
$T_{m.}$.....[^oC].....Melting Temperature
$T_{d.}$.....[^oC]..... Degradation Temperature
ΔH_m .....[J.g^{-1}].....Heat of Fusion, Enthalpy of Melting
ΔH_c .....[J.g^{-1}].....Heat of Crystallisation, Enthalpy of Crystallisation
E.....[GPa]..... Modulus (Elastic Modulus)
σ_{UTS}.....[MPa]..... Tensile Stress at Yield
σ_f.....[MPa]..... Tensile Stress at Failure or Break
e.....Strain
$\%\ elong$.....[%].....% Elongation
IS .....[J.m^{-2}].....Impact Strength
$I.V$ or $[\eta]$ ..... [dL/g].....Intrinsic viscosity
% .....Percentage

Units	Meaning
^{o}C	Degree Celcius
$J.g^{-1}$	Joule Per Gram
rpm	Revolution per Minute
s^{-1}	Per Second
N	Newton
mm	Millimetre
mins	Minutes
dL/g	Decilitre per gram
g.	Gram
kg.	Kilogram
g.10mins	Gram Per 10minutes
Bar	Pressure
MPa	Mega-Pascal
GPa	Giga-Pascal
$J.m^{-2}$	Joule Per Square Meter

Other

ICI	Imperial Chemical Industries
ASTM	American Society for Testing and Materials
ISO	International Organisation for Standardisation
u	Mean Value
S_E	Standard Error
σ	Standard Deviation
n	Number of tested samples or specimens
CI	Confidence Interval
URRC	United Resource Recovery Corporation
NA	Not Applicable
min	Minimum
max	Maximum
(1)	Equation Number
[?]	Reference Number

Chapter 1

Introduction

1.1 Introduction

Plastic waste is one of the major issues in the UK. A balanced production and consumption of plastics is of paramount importance in overcoming current and future environmental problems resulting from incineration or land-filling and their impact on soil and air qualities [1]. The worldwide production of plastics rose to 299 million tonnes in 2013, from which 20% were produced by European countries, where polyethylene terephthalate, PET, represented 6.9% [2]. *Reduce, reuse* and *recycle* became the main targets and pressure for sustainable use and recycling is continuously exerted by the *European Union Legislations.* The *EU Waste Framework Directive 2008* [3] requires all member states to recycle at least 50% of waste by 2015. *The Climate Change Bill 2008* [4] requires the UK to reduce CO_2 emissions by at least 26% by 2020 compared to 1990 levels. *The Climate and Energy Package* [5] set by the *EU* leaders in March 2007 aiming at reducing the *EU* greenhouse gas emissions by *20%* compared to 1990 levels, increasing the share of *EU* energy consumption produced from renewable resources to *20%* and improving the *EU* energy efficiency by *20%*.

PET is well established engineering polyester synthesised by polycondensation of bis(hydroxyethyl terephthalate), BHET, either by *transesterification* of *dimethyl terephthalate* and *ethylene glycol* [6] or by *direct esterification* of *terephthalic acid* and *ethylene glycol* [7] and then polymerised by *step-growth polycondensation* [8], during which, the weight average molecular weight of the PET produced in the first stage of polycondensation is increased from 15000$g.mol^{-1}$ to reach 27000$g.mol^{-1}$or higher by solid state polycondensation, SSP [9, 10]. The SSP is usually performed at lower temperatures to overcome the polymer's thermal degradation. The polymer molecular weight is increased for processing and material characteristics purposes, such as overcoming processability complications for certain engineering applications which require high

molecular weight polymers. The high molecular weight of PET is a determinant factor in extrusion and injection mouldings for the production of fibres, filaments, films and especially bottles. The most used process for PET bottles is injection stretch blow moulding, ISBM. The vast use of PET bottles manufacturing increased post-consumer waste dramatically and recycling capacities are in continuous increase to overcome the cost of using virgin PET, *Zhang* and *Wen* [11]. Advances in recycling techniques allowed the recycling of post-consumer PET waste *mechanically* into new recycled PET for re-use, *Shen et al.* [12] or *chemically converted* by reversing the process of polymerisation (depolymerisation) and breaking the polymer chains into basic chemical compounds. Depolymerisation of PET by *chemolysis* is performed either by *hydrolysis*, *Liu et al.* [13], *methanolysis, Kurokawa et al.* [14], *glycolysis, Ghaemy et al.* [15] and other processes. Chemical compounds *chemically converted* from PET are re-used to produce virgin PET due to their high pure state. Whereas *mechanically* recycled PET is usually contaminated by polymeric materials, mainly polyolefin or other foreign materials, which affect the fundamental inherited properties of the recycled PET.

Bottle grade recycled PET referred to in future as rPET-bg can be used as an alternative to virgin bottle grade PET and reduces environmental issues related to landfilling and incineration. rPET-bg is considered to lose its inherited properties through recycling and reprocessing cycles, as reported by *Lopez et al.* [16]. During mechanical recycling, rPET-bg gets cross-contaminated with other polymeric materials, especially polyolefin. This cross contamination is a major issue in rPET-bg recycling industry because of its influence on the thermal and mechanical characteristics of the final produce. Furthermore, during reprocessing of the contaminated rPET-bg, the transparency of the final product is altered as a result of contamination. The present research work focuses on the influence of polyolefin contamination, HDPE and PP contamination on the characteristics of rPET-bg; research works were done in this field by *Navarro et al.* [17], *Friedrich et al.* [18] and other reasearchers, respectively on the mechanical and processing characteristics of rPET and PET. Additionally, processing behaviour and crystallisation kinetics of engineering grades have been extensively studied, *Kim et al.* [19], *Jabarin* [20], *Tant* and *Culberson* [21] and other researchers. However, studies on rPET-bg contaminated with polyolefin have been rare. The effect of this type of contamination on the crystallisation of rPET-bg is particularly important because HDPE and PP bottles, caps and closures are easily mixed

with rPET-bg during recycling. Their presence in small amounts in rPET-bg can significantly affect crystallinity during multiple extrusions. Some researchers have studied the degradation of rPET during processing and concluded
that chain scission can occur and that formation of grafted copolymers and crystallisation can be facilitated, as reported by *Paci* and *La Mantia* [22], *Torres et al.* [23] and *Pospíšil et al.* [24] and others concluded that during repetitive extrusion, chain scission predominated and no chain branching or cross-linking were observed which decreased capabilities and crystallinity, as reported by *Camacho* and *Karlsson* [25] and *Badía et al.* [26], in contrast, others concluded that cross-linking and chain branching occur during extrusion, as reported by *Assadi et al.* [27] and *Nait-Aliet al.* [28].

1.2 Polymer Structure

A Polymer is a long chain of molecules of very high molecular weight, measured in the tens to hundreds of thousands grams/mole [10]. Technological advances have also allowed the manufacture of ultra high molecular weight polymers of millions grams/mole [29]. Because of its high molecular weight, a polymer is sometimes referred to as a *macromolecule*. The *monomer*, the polymer basic unit, is unique to each polymer and forms its fundamental characteristics. Polymers exhibit very different physical properties compared to their monomers, dependent on the *length* of the *polymer chains*.
The presence of small amounts of very long or very short chains can have great effects on properties of polymers. Polymers vary in chemical structure of monomer unit, 3D structure, length of chains and distribution and molecular weights. There are natural and synthetic polymers. Natural polymers, such as cellulose, proteins rubber occur in nature and can be extracted. Rubber is a natural polymer which needs to be vulcanised before applications. Synthetic polymers, such as polyolefin and polyesters, are synthesised from petroleum oil. Many polymers *crystallise* and the size, shape and organisation of crystallites depend on the way crystallisation is achieved. Other polymers are *amorphous* due to entanglement and irregular distribution of chains [30].

1.2.1 Average Molecular Weights and their Distribution

Polymers always contain chains with a range of lengths. The average length of the polymer chain determines an *average molecular weight*, which is the average of all the chain lengths in a sample. A polymer is not usually characterised by a single *average molecular weight*. Several molecular weight averages, such as number-average, $\boldsymbol{M_N}$, weight-average, $\boldsymbol{M_W}$, viscosity-average, $\boldsymbol{M_V}$, and z-average, $\boldsymbol{M_Z}$, are frequently used and are dependent on the particular method of measurement, as reported by *Jabarin* and *Balduff* [31] and *Moore* [32].

Colligative properties of solutions, such as *boiling point elevation, freezing point depression* and *osmotic pressure* are sensitive to the *number* of molecules present and not influenced by the *size* of any particle in the mixture. The calculated ratio of *total weight* and *number* of polymer molecules for *colligative properties* is the *number-average molecular weight*, $\boldsymbol{M_N}$, and is measured by ***osmometry*** and is given by the following equation:

$$M_N = \frac{\sum_i N_i M_i}{\sum_i N_i} \tag{1.1}$$

Where: $\boldsymbol{N_i}$ is the number of molecules of molecular weight $\boldsymbol{M_i}$.

Light transmitted through a very dilute polymer solution is sensitive to changes in number of *large molecules*. The *scattering intensity* at any given angle is a function of the second power of the *molecular weight*. Because of this s*quare* function, *large molecules* contribute much more to the *molecular weight* than *small molecules*. So, the *weighted* average obtained is the *weight-average molecular weight*, $\boldsymbol{M_W}$, and is measured by ***light scattering***. This measure is better correlated with polymer properties, such as *melt viscosity*, *tensile properties* and *light scattering* and is given by the following equation:

$$M_W = \frac{\sum_i N_i M_i^2}{\sum_i N_i M_i} \tag{1.2}$$

A dilute solution of a polymer flowing through a capillary encounters *frictional resistance* resulting from the presence of *different sized molecules*. By measuring the rate of flow, we are measuring the *molecular volumes* of the polymer molecules in the solution. *Large molecules* increase more the *interactions* and *viscosity* than *small* molecules. The relevant *average* obtained is the *viscosity-average molecular weight*, $\boldsymbol{M_V}$ [33], and is measured by ***dilute solution viscosities*** and can be correlated with polymer *melt viscosity* when we consider extrusion and moulding properties and is given by the following equation:

$$M_V = \left(\frac{\sum N_i M_i^{1+a}}{\sum N_i M_i} \right)^{\frac{1}{a}} \tag{1.3}$$

Where: ***a*** is Mark-Houwink viscometric exponent, as reported by *Galeski et al.* [34]

In a polymer diluted solution subjected to a centrifugal field at low speed, at thermodynamic equilibrium, the *molecules* become distributed according to their molecular sizes. In the centrifuge, the *extremely large molecules* are more important and settle most in the induced gravitational field and the *average* obtained is the *z-average molecular weight*, $\boldsymbol{M_Z}$. This is measured by ***centrifugation*** and may be correlated with polymer tensile properties, such as *flexural stiffness* and *toughness* and is given by the following equation:

$$M_Z = \frac{\sum_i N_i M_i^3}{\sum_i N_i M_i^2} \tag{1.4}$$

As the molecular weight determined is biased to particular molecular properties, two different measures of molecular weights together provide a useful means for assessing the range of molecular weights in a polymer. This leads to the term, ***Polydispersity*** (***d***) which is defined as the measure of *width of the molecular weight distribution* for a polymer and is the *ratio* of $\boldsymbol{M_W}$ to $\boldsymbol{M_N}$. If all the molecules in a polymer sample are of similar size, then all of the molecular weight averages are identical. The closer the polydispersity approaches a value of ***one***, the narrower is the molecular weight distribution. In a distribution, $\boldsymbol{M_P}$ is the ***peak maxima***, as reported by *Granath* and *Kyist* [35] and *Milana et al.* [36].

$$d = \frac{M_W}{M_N} > 1 \qquad (1.5)$$

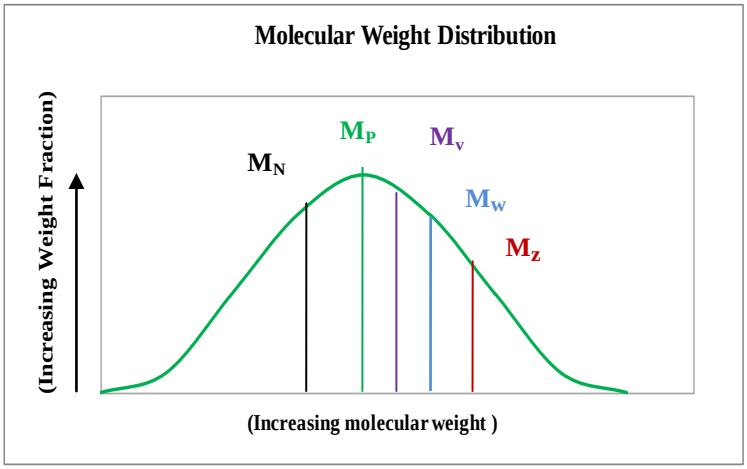

Figure 1.1 Molecular Weights Distribution

The processability and properties of a polymer can be predicted by the shape of the *distribution* and the value of either $\boldsymbol{M_W}$ or $\boldsymbol{M_N}$. If the *breadth* of the distribution *narrows*, properties such as *strength*, *toughness* and *viscosity* often tend to *increase* and the *processing* of the polymer becomes more complicated and difficult.

Each *average-molecular weight* is determined by a single specific method as seen previously but only *Gel permeation chromatography*, *GPC*, is used for measuring *average-molecular weights* and their *distribution* [31].

1.2.2 Amorphous and Semi-crystalline Polymers

The molecular arrangement of chains is an important factor in determining properties of polymers. In the solid state, polymers exhibit two types of morphology; *amorphous* and *semi-crystalline*, as *fully crystalline* polymers are very rare. Polymer morphology is also influenced by the size and shape of the sub-groups of the monomers. If the monomers are large and irregular, it is difficult for their polymer chains to arrange themselves in ordered structures and so more *amorphous structures* are formed. However, smaller monomers and monomers that have very regular structures will form more *crystalline regions*. Amorphous polymers have long chains with large molecular weights and arranged and oriented randomly. These chains can twist and curve around one-another. Long linear chains have a characteristic entanglement and exhibit a stress relaxation by reptation or retraction under thermal conditions. Frequently, amorphous polymers have been visualised as a mass of wet spaghetti in order to indicate the randomness in an amorphous polymer, where the different chains are in contact with each other and can slide past each other but are not necessarily in parallel with each other, resulting in certain separation between the chains and greater occupied volume than in crystalline structure, where the chains are parallel, as reported by *Robertson* [37]. Amorphous polymers have glass-like, transparent appearances. The amorphous or glass-like structures don't show range orders and the chains are highly tangled.

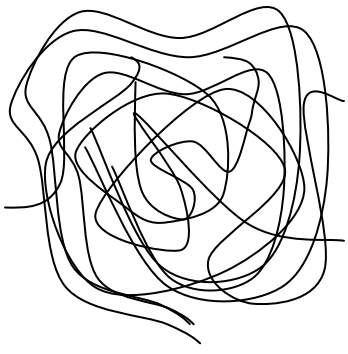

Figure 1.2 Amorphous Polymer Structure

An amorphous region is formed when the chains have little orientation throughout the bulk polymer as the chain segments remain too far apart for significant secondary bonding between them. The *glass transition temperature*, T_g, is the point at which the randomly distributed polymer chains are transformed from a rubbery solid into a glassy solid.

The morphology of most polymers is *semi-crystalline*. *Semi-crystalline* polymers exhibit mixtures of small *crystalline* and *amorphous regions* and melt over a range of temperature instead of at a single melting point. Crystalline regions require greater force to deform them than amorphous regions. This combination of *crystalline* and *amorphous structures* forms polymers with better *strength*, *stiffness* and *toughness*, as reported by *Badia et al.* [38].

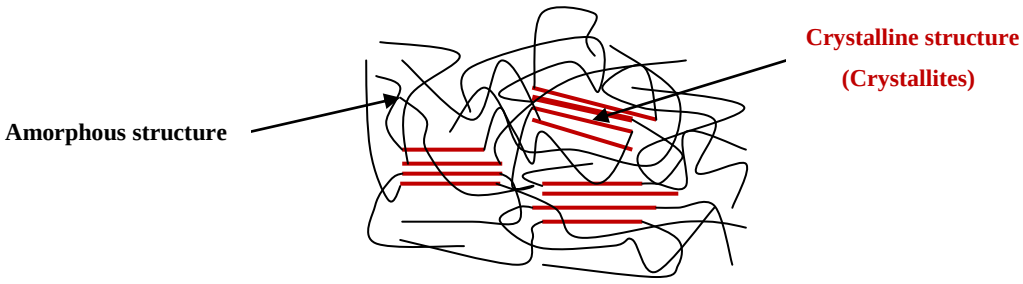

Figure 1.3 Semi-crystalline Polymer Structure

The *degree of polymerisation* is an important factor in determining the *crystallinity* of a polymer. High degree of polymerisation yields long chains with high molecular weights, high degree of entanglement and low degree of mobility which contribute to the increased formation of *amorphous regions* in a polymer. These long chains have greater strength because they become tangled between layers and add to the *strength* and *stiffness* of the polymer. Whereas, low degree of polymerisation is a factor in creating small chains with low molecular weights capable of fast organising, packing, folding and forming *crystalline regions*. But the crystalline structure of small chains of low molecular weights is generally weak because only weak *Van der Waals forces* hold them together, which can

allow slipping of crystalline layers and causing breakage or failure of the polymer structure. The degree of crystallinity is quantified based on the density and factors such as bulk side groups, chain complexity, branching and randomness of copolymers make it harder to crystallise. Another important factor is the *rate of cooling* or quenching of the polymer melt. The *crystallisation process* is sensitive to this rate and influences the formation of *amorphous* structures in linear polymers.

The *crystalline regions* show high degrees of ordered molecular *chains* which have the ability of folding on each other to form microscopic *lamellae*. These folded *lamellae* grow out radially into *three dimensional spherical crystallites* or *spherulites* [39]. *Spherulites* literally little spheres, with diameters in the range of 0.5-100 μm [30] are characteristics of polymer morphology. The microstructure of *spherulites* is therefore a polycrystalline form of equivalent radiating and branching units which tend to form a spherical geometry. During crystallisation, the growth of *spherulites* is *time* dependent at given *temperature*.

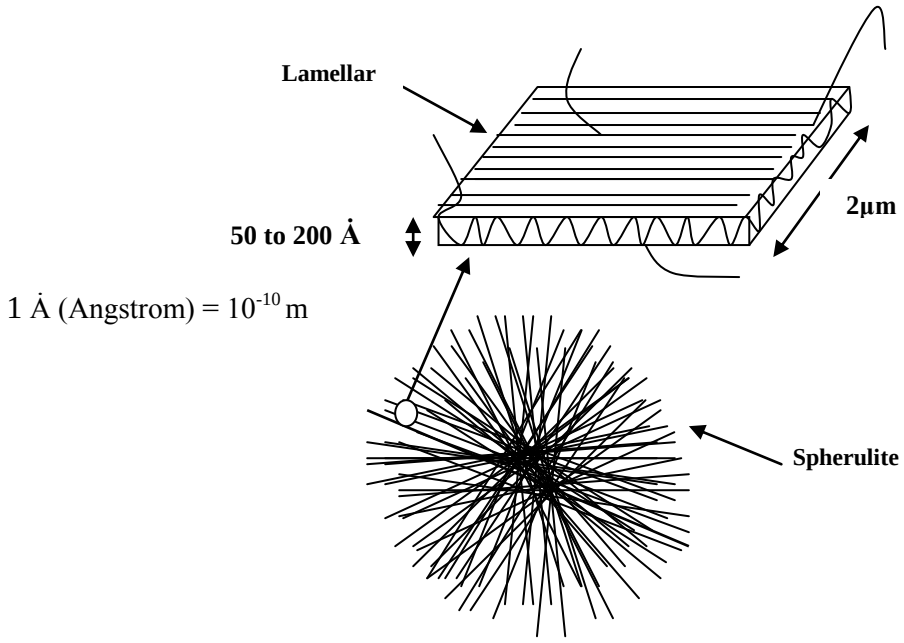

Figure 1.4 Lamellar and Spherulite

1.2.3 Crystallisation Process

The process of forming crystals from the melt or solution is known as crystallisation. This process is achieved in two stages, *nucleation* and *growth*. *Nucleation* is initiated by the formation of primary *stable nuclei* [40]. For the primary nuclei to form, the free energy barrier associated with the polymer chains disentangling and straightening must be crossed; the larger the fold period, the greater the barrier and the slower the rate of nucleation. In most cases, nucleation starts on the surfaces of impurities or on added nucleating agents. These *nuclei* contribute to the formation of *spherulites* and grow *linearly* with *time*. Then, the *growth* of spherulites from *heterogeneous nuclei* continues until reaching the maximum crystallisation temperature, $\boldsymbol{T_c}$, were they filled all the *area* under the *exotherm*. Radial growth rates *increase* and nucleation densities *decrease* with crystallisation temperature. Heterogeneous nuclei are likely to form into smaller particles with decreasing temperature. Also, with decreasing temperature, these small particles become more active and increase the density of nuclei. This stage of transformation of heterogeneous nuclei into spherulites, is called *primary crystallisation* and usually proceeds at high rate, and continues until most of the spherulite areas collide together. Many researchers [41, 42] have attributed the deviation of the primary crystallisation process to a *secondary nucleation* and *secondary* crystallisation. This secondary crystallisation takes place and proceeds at lower rate up to the end of the process, where the crystallites' *growth* changes from *spherulitic* to *fibrillar* and developing within the boundaries of the spherulites according to *Hillier's two-stage crystallisation* [43] and transforming the remaining amorphous domains between the formed s*pherulites*. *Verhoyen et al.* [44] consider that the secondary crystallisation occurs well after the primary has stopped and the two follow their own *Avrami* kinetic equation.

1.2.4 Evaluation of Crystallisation for Isothermal Process

The estimation of isothermal crystallisation parameters is normally performed using the data obtained from the crystallisation exotherms with a basic assumption that the amount of crystallinity obtained is linearly proportional to the heat released during crystallisation. By integrating the heat evolved during crystallisation, a relationship [45, 46] between relative crystallinity and time can be obtained as described below:

$$X_t = \frac{\int_0^t \frac{dH_c}{dt} dt}{\Delta H_c} \qquad (1.6)$$

Where: X_t is the relative crystallinity, t is the elapsed time and dH_c is the released heat during crystallisation time interval dt. ΔH_c is the total enthalpy of crystallisation and is given by the following relationship [47].

$$\Delta H_c = \int_0^{\infty} \frac{dH_c}{dt} dt \qquad (1.7)$$

For *isothermal crystallisation*, the *primary crystallisation* is described by the *Johnson-Mehl-Avrami-Kolmogorov equation*, or *JMAK equation*, which was popularized by *Melvin Avrami* in series of papers [48, 49, 50] and very often called *Avrami equation*.

This equation describes the *time* dependent *relative crystallinity*, X_t,.

$$1 - X_t = \exp(-Z_t t^n) \qquad (1.8)$$

Where: X_t is the relative crystallinity at time t, n is *Avrami exponent* and Z_t is a rate constant and both are *temperature* dependent and diagnostic of the crystallisation mechanism.

The plot of relative crystallinty, $\boldsymbol{X_t}$ Vs ***time*** shows that transformations follow a characteristic *"S" shape* or *sigmoidal profile* as shown below:

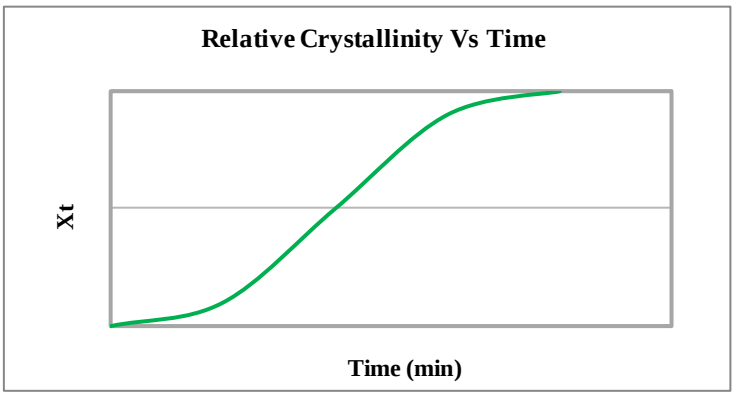

Figure 1.5 *Avrami's* Relative Crystallinity as function of time

The linearised logarithmic form of equation **(1.8)** is written as follow:

$$\ln\left[-\ln(1-X_t)\right] = n\ln t + \ln Z_t \qquad (1.9)$$

Plotting $\ln[-\ln(1-X_t)]$ Vs ln*t* generates two linear sections relative to *primary* and *secondary* crystallisations, where $\boldsymbol{n}$ and $\boldsymbol{Z_t}$ are obtained from the ***slope*** and ***intercept*** of the *primary* linear section respectively.

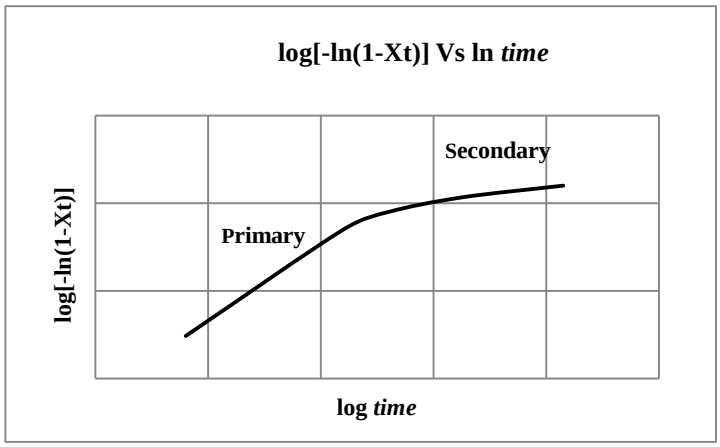

Figure 1.6 *Avrami* Plot of $\log[-\ln(1-X_t)]$ Vs log*t*

1.2.5 Evaluation of Crystallisation for Non-isothermal Process

For *non-isothermal crystallisation*, the Avrami equation **(1.8)** can still describe the primary phase of crystallisation and the linearised form is written as follow:

$$\log\left[-\ln(1-X_t)\right] = n\log t + \log Z_t \qquad (1.10)$$

A Plot of $[-\ln(1-X_t)]$ Vs log*t* can provide the values of ***n*** and $\boldsymbol{Z_C}$.

For *non-isothermal process* and because of the influence of *cooling rates*, the ***intercept log*** $\boldsymbol{Z_t}$ was *corrected* into ***log*** $\boldsymbol{Z_C}$ [45].

$$\log Z_C = \frac{\log Z_t}{a} \qquad (1.11)$$

Where: ***a*** is the cooling rate.

An alternative approach to describe the *non-isothermal crystallisation*, is the *Ozawa equation* [51], describing the development of relative crystallinity as function of temperature, $\boldsymbol{X_T}$,

$$1 - X_T = \exp\left[-\frac{K_T}{a^m}\right] \qquad (1.12)$$

Where: $\boldsymbol{X_T}$ is the relative crystallinity at temperature ***T***, $\boldsymbol{K_T}$ is a cooling function dependent on the global rate of crystallisation and ***m*** is *Ozawa exponent* and both of them diagnostic of the crystallisation mechanism and ***a*** is the cooling rate.

A relationship [11] between relative crystallinity and temperature can be obtained as described below:

$$X_T = \frac{\int_0^T \frac{dH_c}{dT} dT}{\int_0^\infty \frac{dH_c}{dT} dT} \tag{1.13}$$

Where: $\boldsymbol{X_T}$ is the relative crystallinity, $\boldsymbol{T}$ is the temperature and $\boldsymbol{dH_c}$ is the released heat at temperture interval $\boldsymbol{dT}$.

The plot of relative crystallinty, $\boldsymbol{X_T}$ Vs ***temperature*** shows the following curve characteristics with a negative exponent ***(-m)***:

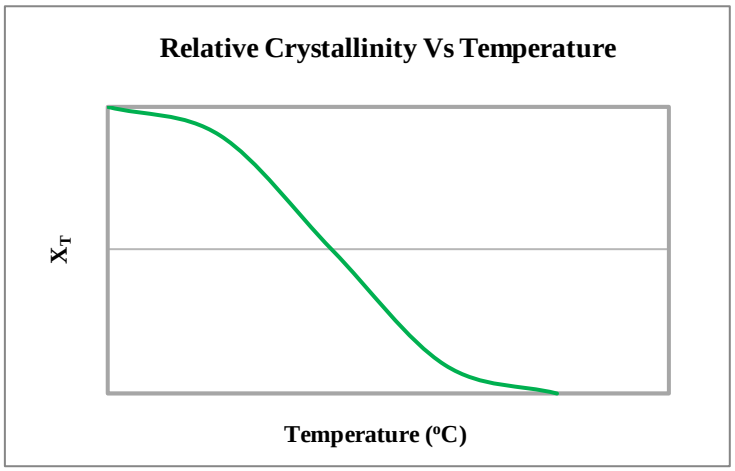

Figure 1.7 *Ozawa's* Relative Crystallinity as function of Temperature for Non-Isothermal Crystallisation

The linearised form of equation **(1.12)** is written as follow:

$$\log\left[-\ln(1-X_T)\right] = \log K_T - m\log a \qquad (1.14)$$

A plot of log [-ln(1-X_T)] Vs log*a* at a given ***temperature*** generates a ***straight line***, where ***-m*** is the ***slope*** of the linear equation and $\boldsymbol{K_T}$ is calculated from the value of the ***intercept log*** $\boldsymbol{K_T}$.

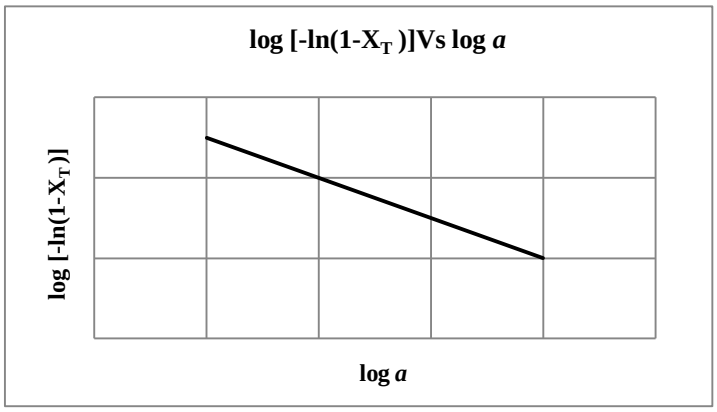

Figure 1.8 *Ozawa's* Plot of log[-ln(1-X_T)] Vs log*a*
for Non-Isothermal Crystallisation

The *Avrami* and *Ozawa exponents*, respectively ***n*** and ***m***, take different values depending on the growth mechanism as tabulated below.

(n, m)	Mechanism	Shape
2	Rod-Shaped Growth from Sporadic Nuclei	1 Dimension
2	Disc- Shaped Growth from Instantaneous Nuclei	2 D
3	Disc-Shaped Growth from Sporadic Nuclei	2 D
3	Spherulitic Growth from Instantaneous	3 D
4	Spherulitic Growth from Sporadic Nuclei	3 D

Table 1.1 Growth Characteristics [52]

1.3 Aims and Objectives

This research work investigates the influence of small amounts of *polyolefin contamination, HDPE* or *PP*, on the overall characteristics and processability of *rPET-bg*. In particular, the work will focus on the *thermal characteristics*, with emphasis on *crystallinity* and *crystallisation process*, and the aims and objectives are summarised below.

Firstly, rPET-bg flakes will be studied and their physical and flow properties will be assessed by DSC, FTIR and MFR analyses. Then, the flakes will be converted into pellets by extrusion. Extruded samples will be analysed similarly to investigate changes to physical and flow after extrusion. Then, injection moulded specimens will be produced to investigate the variation of previously discussed properties and to determine their mechanical capability. The interrelationship between the properties will then be studied.

Secondly, batches of *rPET-bg* "contaminated" with *HDPE* and *rPET-bg* with *PP* at various % weight-weight will be studied. *Extruded pellets* and *injection moulded specimens* which will be analysed as previously done with the *non contaminated rPET-bg*. Correlations and comparisons between the non *contaminated rPET-bg* and contaminated batches of *rPET-bg* will then be made and depending on the outcomes, a *suitable contaminated batch* will be investigated further to determine the influence of *polyolefin contamination* on the *rPET-bg main matrix* for that *batch*.

Thirdly, as the *cooling rate* is an important processing parameter which influence the thermal characteristics in the field of bottle manufacturing and the *repetitive extrusions* is a method of choice in compounding *recycled polymers*, therefore extruded samples of *non contaminated rPET-bg* and a *suitable contaminated rPET-bg batch* will be thermally analysed by DSC at various *cooling rates*. In addition, both materials will be *extruded repetitively* for *5 cycles* (*repetitive* or *multiple extrusions*) and their thermal characteristics will be quantified at each step to determine the influence of *contaminant* on the *rPET-bg main matrix* during the crystallisation process. Finally, the crystallisation process will be analysed using the *Avrami* and *Ozawa equations* to validate the findings.

Chapter 2

Literature Review

2.1 Poly(ethylene terephthalate)

In 1941 PET was discovered in Britain by *John Rex Whinfield* and *James Tennant Dickson*. This discovery was the result of advancing the work and research on the study of polyesters previously covered by *Wallace Hume Carothers*. The polymer that became polyester resulted from the *direct esterification* of *terephthalic acid* and *ethylene glycol* by *Whinfield* and *Dickson*, as reported in the literature [53].

2.1.1 Synthesis of PET Monomer

The PET monomer bis(hydroxyethyl terephthalate), BHET, is synthesised either by transesterification or direct esterification [6, 7], as described below, to give PET polymer of basic unit formula $C_{10}H_8O4$ and the following structure,

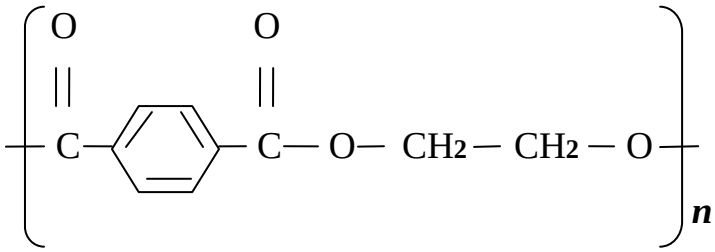

Figure 2.1 PET Structure

Where: ***n*** is the number of repeat units in the polymer chain.

The transesterification consists of reacting dimethyl terephthalate, DMT, and ethylene glycol, EG, to produce the PET monomer, BHET, as reported by *Lin* and *Baliga* [54]. Consequently, other oligomers and methanol are produced too, which indicates the role of end groups in this reaction, as reported by *Collins et al.* [55].

The transesterification requires the use of an acid catalyst, such as acetates of calcium, manganese, cobalt, cadmium, lead and zinc, to accelerate the reaction, as reported by *Ravindranath* and *Mashelkar* [56] and the reaction takes the pattern described in *Figure 2.2* below.

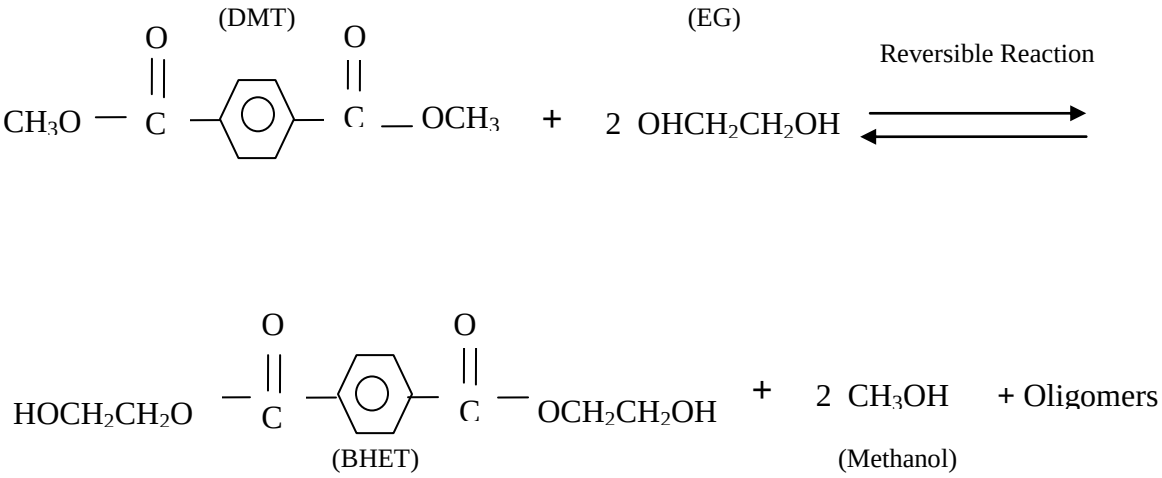

Figure 2.2 Synthesis Reaction of BHET by Transesterification

The industrial process as illustrated in *Figure 2.3* below, consists of dissolving the solid DMT in a *Tank*, then mixing it with EG in the presence of a suitable catalyst in a *Mixer*. The reaction takes place within a temperature range of *140-200^{o}C* at a pressure of *1atm* in a *Reactor*. The ideal temperature is *180 ^{0}C*. Because the reaction is reversible, the removal of unwanted chemicals, such as methanol and other non reacted monomers is performed by separation in a *Separation Column* in order to achieve complete conversion and production of the BHET. The un-reacted EG is re-injected again into the reactor. Catalysts are used to accelerate the residence time required for complete conversion.

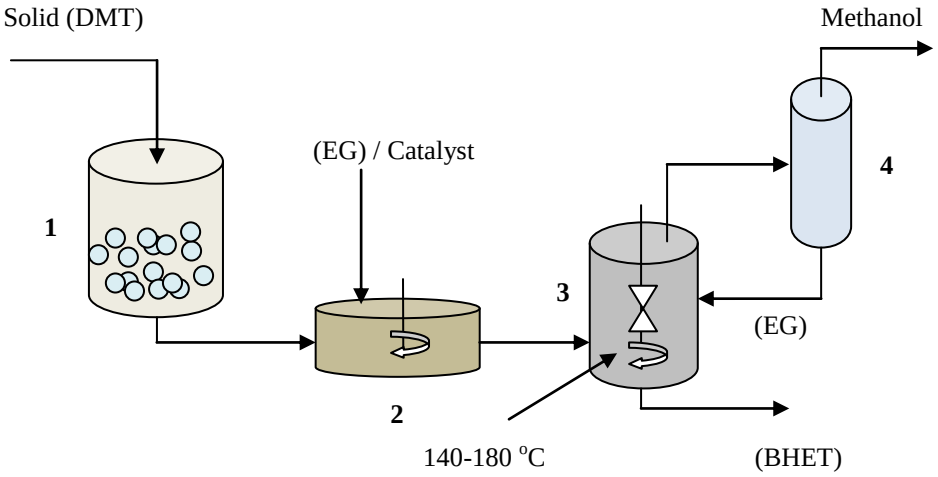

Figure 2.3 Schematic Industrial Synthesis of BHET by Transesterification

The direct esterification consists of reacting terephthalic acid, TPA, and ethylene glycol, EG, to produce the BHET. Consequently, other oligomers and water are produced too.

The direct esterification is self-catalysed by the carboxylic acid groups and does not require catalysts and takes the pattern described in *Figure 2.4* below.

.

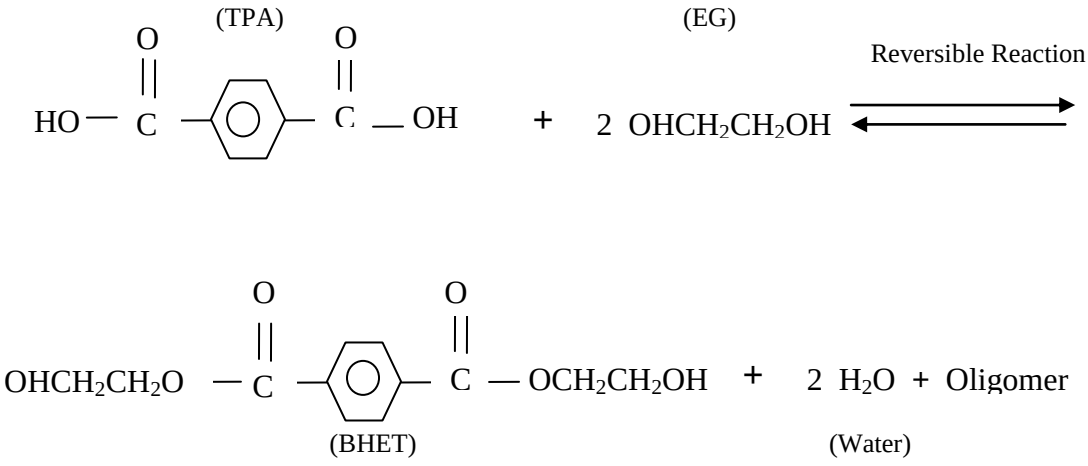

Figure 2.4 Synthesis Reaction of BHET by Direct Esterification

Referring to *Figure 2.5* below, the industrial process consists of mixing the TPA with EG in a *Mixer*, then the mixture is transferred to series of stirred *Tank Reactors*, where they react together within a temperature range of *220-260^{o}C*. The temperature range is higher than that of transesterification because of the poor solubility of TPA at atmospheric pressure. Because the reaction is reversible, it's necessary to remove the produced acetaldehyde and water by separation in a *Fractionator*, from where the un-reacted chemicals are re-injected again into the stirred *Tank Reactors*. The conversion and production of the BHET is then achieved.

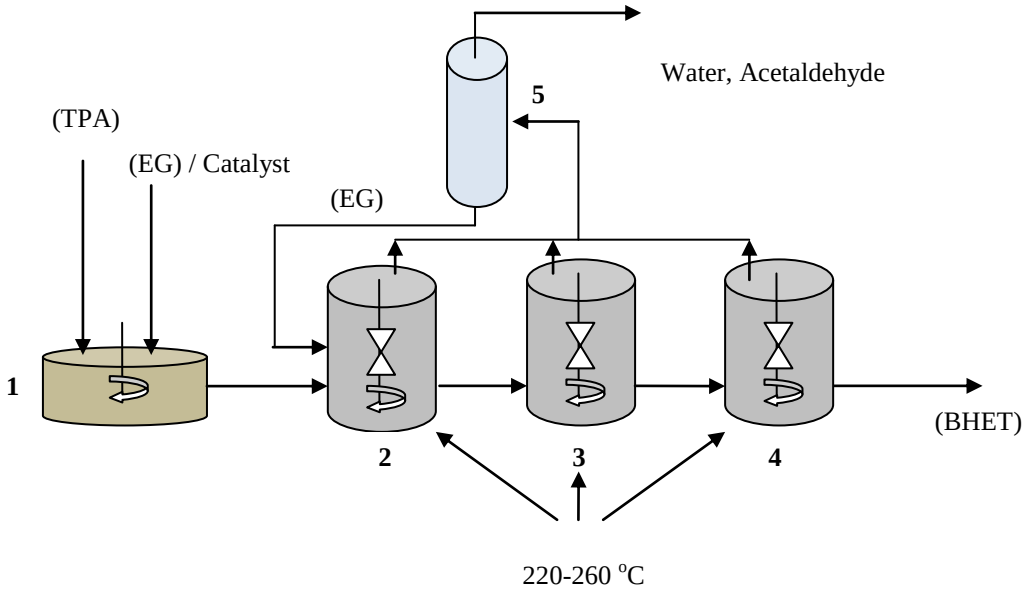

Figure 2.5 Schematic Industrial Synthesis of BHET by Direct Esterification

Note: The diagrams in *Figures 2.3* and *2.5* are the work of the student to schematically summarise the information reported by *Lin* and *Baliga* [54], *Collins et al.* [55] and *Ravindranath* and *Mashelkar* [56] about these processes.

By comparing the above syntheses, the following table lists the different products achieved.

Reaction Steps	Product 1	Product 2	By-Product	Prepolymer	Catalysts
Transesterification	DMT	EG	Methanol	BHET + Oligomers	Required
Direct Esterification	TPA	EG	Water	BHET + Oligomers	Not Required

Table 2.1 Transesterification and Direct Esterification Reactions Comparison

2.1.2 Synthesis of PET

The synthesis of PET is performed by step-growth polycondensation in two ways depending on the polymer grade required, as reported by *Sorenson* and *Cambell* [57].

- During the melt phase polycondensation, MPPC, the BHET and other oligomers are produced, either by transesterification or direct esterification, as described previously in (***Section 2.1.1***), then, BHET is polymerised under further catalytically accelerated transesterification reaction using antimony trioxide, as reported by *Youk et al.* [58]. As the catalysts used during transesterification help the creation of diethylene glycol, DEG, therefore prior to polycondensation, phosphorous acid or its esters are added in the purpose to inactivate the glycols by-product. Furthermore, to prevent any thermal degradation of the polymer, which results in discoloration (yellowing), it is recommended to add metaphosphoric acid and its alkali metal salts when using the catalyst titanium tetrabutylate. The polycondensation reaction is performed under a controlled range of temperature of 270 – 285^{o}C because the thermal properties of PET are sensitively affected by polycondensation catalysts and temperature which promote hydrolytic cleavage of chains due to the formation of autocatalytic carboxylic groups as reported by *Zimmermann et al.* [59]. The weight average molecular weight of the PET produced under the above discussed synthesis processes range between *15000-25000g.mol^{-1}*.

Because the processing techniques, such as injection or extrusion require high molecular weight polymers, as reported in the literature [60], these lower molecular weight polymers are difficult to process for certain engineering applications and therefore further increase in molecular weight is necessary to produce processable PET for engineering applications.

- Solid State Polycondensation, SSP, is required to overcome the problem of lower molecular weight PET. The weight average molecular weight is increased by SSP to reach 27000g.mol^{-1}or as high as 38000g.mol^{-1}, primarily because of some side ester interchange reactions involved, as reported in the literature [61, 62]. *Coover et al.* [63] indicated that an organo-titanium compound has to be used as a catalyst in a solid-phase polymerization process for preparing linear super-polyesters. The SSP process is performed at lower temperatures to overcome the problem of thermal degradation and deterioration of properties as result of the presence of catalysts at high temperatures.

2.1.3 Degradation of PET

Degradation is the change in the molecular structure of a polymer accompanied by the creation of other products that affect the overall integrity of the polymer. A decrease in molecular weight is usually a common sign of degradation. PET like other polyesters can undergo various processes of degradations, such as thermal (under the influence of heat alone), oxidative (under oxygen and heat), photo-oxidative (under oxygen and light), hydrolytic (in the presence of moisture) and chemical degradation (in the presence of various solvolytic agents, such as water, alcohol, acid, alkali or amine) referred to in *Section 2.1.6.* In the case of thermal degradation, there is a splitting cleavage of the C-O bonds of the polymer backbone and creation of new bonds resulting in new products. As a result of the use of metal catalysts during polycondensation, the ester bonds become less stable and subjected to splitting. The changes create side reactions, which lead to changes in the properties of the produced PET. Also, during production, there is transformation by intermolecular dehydration of EG to DEG. This dehydration is acid catalysed and leads to further creation of ester bondage through the splitting of the water formed. Hence the number of carboxylic end groups increases and the reactions propagate further.

Once condensed in the PET during the polycondensation, the DEG is not completely removed and certain percentage remains in the final product. The remaining small percentage of DEG in the PET decreases the melt temperature, the light and thermo-oxidative stabilities and lowers the mechanical properties as reported by *Binsack* [8]. Other most important side reaction is the thermal degradation, during which, ester end groups transesterify and generate acetaldehyde. Acetaldehyde is an unwanted by-product in the production and manufacture of *PET*. It is also produced during the degradation of *EG* and during the thermo-oxidative degradation, as reported in the literature [64]. In the case of thermo-oxidative degradation, the high processing temperature of PET melt initiates the degradation process, where further chemical reactions due to the fact that the ethylene glycol or EG units tends towards forming hydrogen peroxide and this lead to the formation of free radicals, such as O, CH, OOH radicals. The excess of formed radicals can result in cross-linking and deformation in the molecular structure of PET, as reported in the literature [65]. Formation of cyclic low molecular weight oligomers and acetaldehyde were detected in PET matrix, when processed at various temperatures, as reported by *Samperi et al.* [66]. In studying the thermo-mechanical and thermo-oxidative degradation of bottle grade PET, *Romao et al.* [67] showed that low molar mass compounds, mainly cyclic and linear di-acid oligomers, increased proportionally with time and chain scissions affected the stability of these oligomers and DEG helped the formation of hydroxyl radicals in the polymeric matrix**.** In the case of hydrolytic degradation, the water present in the PET pellets before processing, as a result of poor drying, is the main factor of this kind of degradation, where decrease of viscosity and molecular weight results from the splitting of the ester bonds and the rate of propagation is faster than during thermo-oxidative and photo-oxidative degradations, as reported by *Cooney et al* [68]. In the case of photo-oxidative degradation, the lengthy sunlight exposition of the PET is the main factor in affecting the structure, influencing and speeding up the process by splitting molecular bonds, as reported by *Wypych* [69] and *Arnold* [70].

2.1.4 PET Grades and their Applications

The main PET grades are in the form of fibres, films and bottle grades, where each grade category has various sub-grades of specific characteristics and applications. The trade name of fibre grade firstly used in England was Terylene, which was manufactured by Imperial Chemical Industries, ICI. DuPont manufactured its fibre grade under the name of Dacron and was the first to start the manufacturing of the fibre grade. Mylar is the film grade in use, which is manufactured by DuPont Tejjin films. Terylene was used by ICI as a film grade too. The manufacturing of the film grades started around the same time as the fibre grade. *Bottle grades* have molecular weights around $27000 g.mol^{-1}$ and an intrinsic viscosity of *0.90 dL/g* [10] and their manufacturing started later than the fibre and film grades.

PET grades are characterised by their high strength, high resistance to stretching and abrasion and their resilience. Their dielectric properties are exceptional. Also, have excellent chemical resistance to acids and weather but can lose some strength under sunlight. They have good water-proof properties, excellent clarity and good recyclability. PET grades are extensively used in the manufacture of clothes because of their light weight, tear resistance and fast drying. Also, used in making acid resistant ropes, safety belts and packaging, especially in bottles manufacturing. PET grades are differentiated and characterised by their intrinsic viscosities, I.V or [η].

Intrinsic viscosities of PET grades are ranged between 0.40 to 1.00 dL/g depending on their applications, as reported by *Gupta* and *Bashir* [71].

PET Grade	Intrinsic Viscosities (I.V),[η]- (dL/g)	Applications
Fibre	0.40 - 0.70 / 0.72 - 0.98	Textile / Technical
Film	0.60 - 0.70 / 0.70 - 1.00	Biaxially oriented / Sheet for thermoforming
Bottle	0.70 - 0.78 / 0.78 – 0.85	Water Bottles / Carbonated soft drink

Table 2.2 Intrinsic Viscosities and Applications of PET Grades

2.1.5 PET Bottles Manufacturing Process

PET is processed by various techniques and the most popular are extrusion and injection mouldings. Extrusion is mainly to produce fibres, filaments, films, bottles and other products. The blending of *PET* with other olefins is performed by extrusion. In contrast, bottles are mostly manufactured by injection blow moulding and the most used process for PET bottles is injection stretch blow moulding, ISBM.

PET Bottles are manufactured in two ways; single or two stages process. The single stage consists of producing performs, tube like shaped model as illustrated in *Figure 2.6* below, by injection moulding and immediately after, the produced preforms are stretched and air blown into bottles in the same manufacturing unit. The two stage bottle production consists of producing preforms and then shaping them at a later stage, i.e. preforms can be sold or stored for a time waiting to be shaped. At later stage, the cold preforms are heated and softened at a temperature just above the glass transition temperature, T_g, then stretched and air blown into bottles. Finally, the bottles are ejected from the mould, quality inspected then packed and stored.

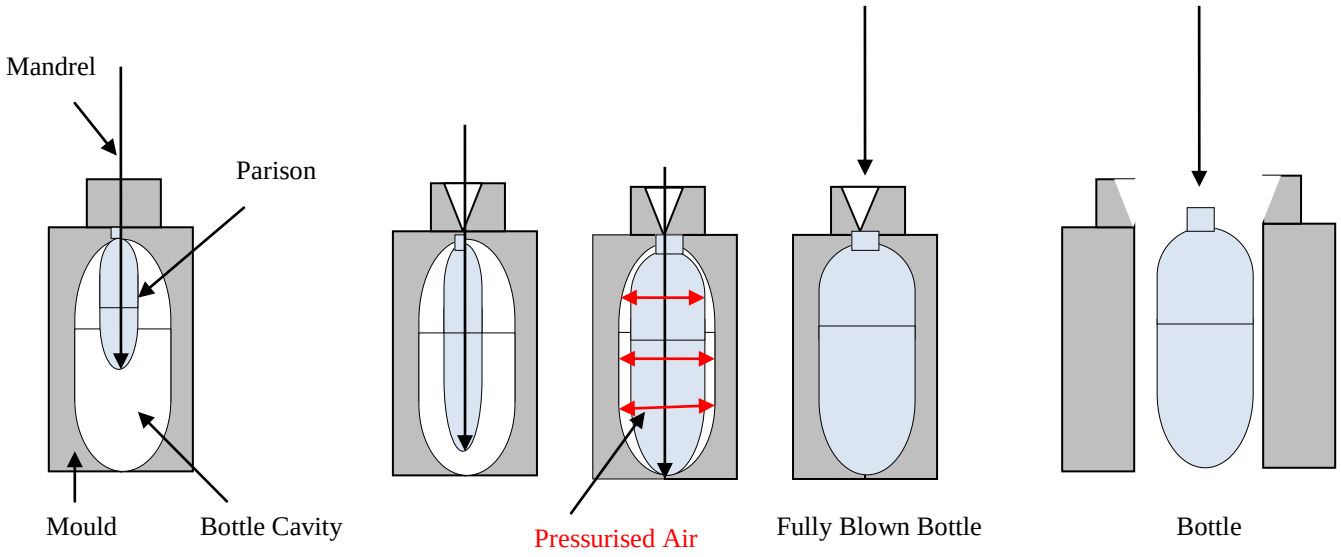

Figure 2.6 Simplified Inj. Stretch Blow Moulding, *ISBM*, of PET Bottles

Note: The diagram in *Figure 2.6* is the work of the student.

2.1.6 Recycling of PET

The recycling of PET is of paramount importance in tackling environmental problems, especially land-filling and soil contaminations due to the slow decomposition rate of PET. The growing demand of packaging materials, for the production of bottles and other products, increased the recycling capacities to overcome the cost of using virgin PET. Post consumer PET is recycled in two ways, either recycled mechanically and treated chemically or decontaminated and transformed into flakes for re-use or completely chemically converted into chemical raw materials, i.e. reversing the process of polymerisation or depolymerisation by chemolysis.

- Mechanical and **chemical treatment recycling** [72] consists of sorting stage, where mixed bales of PET and HDPE bottles are placed in conveyors, opened and the dispersed bottles pass through a perforated rotating drum where impurities and bottle caps are removed. Everything metal is removed by a powerful electromagnet and additionally aluminium contaminants are removed by an eddy current separator. Paper, films and other objects are separated from the bottle by air jet. Once impurities are removed, then the bottles are sorted by type and colour. Sorting machines using optical recognition systems are used to separate the bottles by material types but contamination still remains. The sorted bottles are finally investigated manually to remove any persisting contaminants. Then, granulating and washing stage, where the bottles pass through granulators and chopped into small sized flakes and transported to the next step through pressurised tubes. Then, the flakes are washed by hot water at 80^{o}C and weak solution of caustic soda to clean them from any persistent impurities, such as labels, glue or ink.
Finally, decontamination of PET bottles, in the purpose to return to recycled PET-bg its food-grade characteristics, where the PET fakes are super cleaned by removing any persistent contaminants on the surface-layers. Then, the flakes are dried by hot air and to complete the reaction process, the flakes pass through a rotating furnace and remain for 4 hours and then cooled in a water tank, rinsed and finally dried.

- **Chemical conversion recycling** known as chemolysis is a reversing process or a degradation process (depolymerisation), i.e. the PET is decomposed chemically into basic raw materials. This process proved to have advantages on the mechanical recycling. This process is able to recover the PET to its fundamental basic components and to recover a valuable material that is economically challenging to recycle. When PET is mechanically recycled, small amounts of contamination can find their way into the final recycled material and therefore compromise its performance. But with chemical recycling, post consumer PET is totally converted, meaning that contamination is removed. The resulting raw chemicals, such as DMT, TPA, EG, BHET and other materials can be recovered and re-used to produce virgin PET free from impurities. Despite its advantageous results the chemical recycling of PET is highly expensive, as reported in the literature [73]. Many chemical processes are employed in chemical recycling of PET, such as methanolysis, hydrolysis, glycolysis and other processes, as reported by *Paszun* and *Spychaj* [74].

- The **methanolysis process** involves depolymerisation of post-consumer PET with methanol in the presence of transesterification catalysts and yields dimethyl terephthalate, DMT, and ethylene glycol, EG. Methanolysis is performed at temperature range and pressure respectively of 160-300^{o}C and up to 7MPa, as reported by *Milgrom* [75].
The resulting yield of DMT from methanolysis of recycled PET usually does not exceed 90% , as reported by *Marathe et al.* [76]. Among the important features of methanolysis as a process for the chemical recycling of PET compared to glycolysis are the allowance to use low quality PET feed because of the easier purification of the obtained DMT and tolerance of high level of contamination, as reported in the literature [77]. *Cornell* [78] reported that problems associated with catalyst poisoning due to the presence of water can occur and that the cost of the recovery of DMT is usually high.

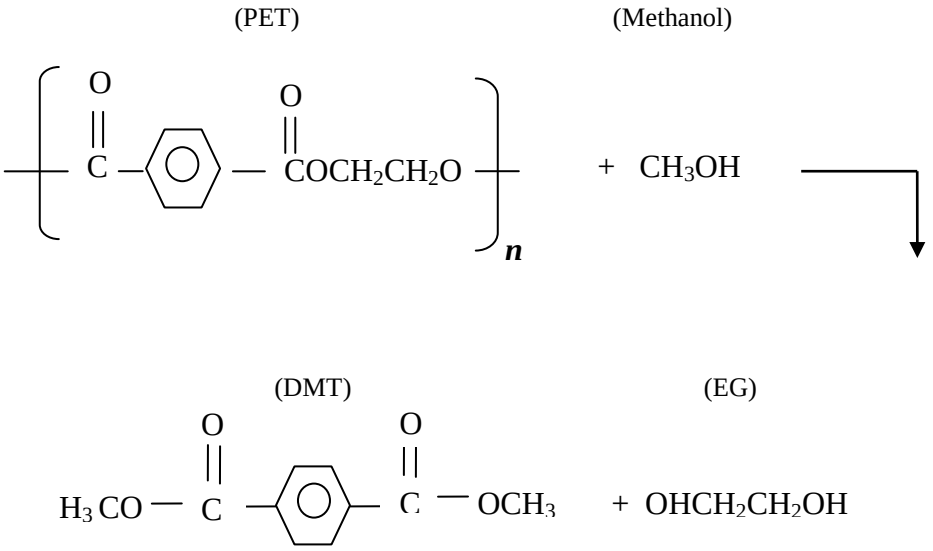

Figure 2.7 Simplified Methanolysis Reaction of PET

- The **glycolysis process** is performed by heating the post-consumer PET with a glycol (ethylene glycol, diethylene glycol or other) in the presence of catalysts (amines, alkoxydes or other) and yields short chain oligomers and even low molecular weight *hydroxyl-terminated* products. Glycolysis is performed under normal pressure at temperature range of 180-250^{o}C and usually proceeds for 3-8 hours and carried out with ethylene glycol, EG, as reported in the literature [79, 80]. The result of deep polymer glycolysis by EG is primarily BHET. Also, the glycolysis reaction has been found to be catalysed by acetates of Zn, Mn, Co, Pb and others. For these catalysts, *Baliga* and *Wong* [81] have reported that the initial rate of depolymerisation at 190^{o}C followed this pattern: Zn > Pb > Mn > Co. In the same study, these authors have also investigated glycolysis reactions of clear and green recycled PET flakes and reported that the colour pigment did not affect the extent of depolymerisation. *Chen et al.* [82] reported that the depolymerisation reaction is accelerated at higher pressure and the reaction is achieved in less than 3 hours. Similar results are reported by *Campanelli et al.* [83], in their study on kinetics of glycolysis of molten state blow moulded PET at temperatures range 245-265^{o}C. *Guclu et al.* [84] reported that PET dissolves readily in EG above 170^{o}C in zinc acetate-catalysed gycolysis of PET waste.

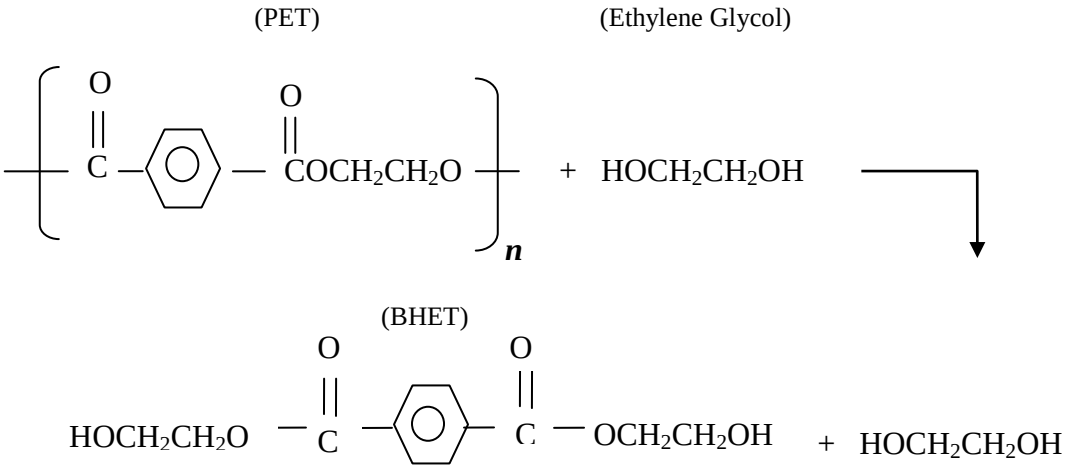

Figure 2.8 Simplified Glycolysis Reaction of PET

- The **hydrolysis process** of PET waste can be performed in three ways, acid- catalysed, alkaline-catalysed or neutral hydrolysis. The hydrolysis uses aqueous systems at elevated temperature and pressure to yield terephthalic acid, TA, and ethylene glycol, EG.

The **acid hydrolysis** of PET can be performed at 150^{o}C using concentrated sulphuric acid as reported by *Yoshioka et al.* [85] or other concentrated mineral acids, such as phosphoric acic as reported by *Kamatani et al.* [86]. Additional *research work* [87] reported a process in which PET bottles are consumed in nitric acid at temperatures in the range of 70-100^{o}C and at atmospheric pressure, where the final products were TA and EG and where the latter was partially oxidised to oxalic acid; a product which is more expensive than TA or EG.

The **alkaline hydrolysis** of PET is usually performed using an aqueous solution of sodium hydroxide or potassium hydroxide as reported by *Kao et al.* [88] and that the hydrolysis to be performed above the melting temperature of PET as reported by *Campanelli et al.* [89]. *Yoshioka et al.* [90] described an alkaline hydrolysis for the conversion of PET into TA and oxalic acid in a concentrated sodium hydroxide solution and determined that the optimal conditions were 250^{o}C, reaction time of 5 hours and oxygen pressure of 5MPa. In their kinetic study alkaline hydrolysis, *Kao et al.* [91] found

that potassium hydroxide is reactively more suited than sodium hydroxide. Also, potassium hydroxide hydrolysis yielded higher molar ratio at 160°C for 30 min under autogenic pressure and showed total polymer disintegration as reported by *Wan et al.* [92].

The **neutral hydrolysis** of PET is performed in the absence of acidic or alkaline catalysts by using water at neutral pH and temperature range of 200-300°C and at pressure range of 1-4MPa as reported by *Campanelli et al.* [89, 93]. *Campanelli et al.* [89] and *Kao et al.* [88] confirmed that the rate of hydrolysis of PET is faster in the molten state than in the solid state, especially at temperature above 245°C. Also, *Campanelli et al.* described that the catalytic effect of Zn catalyst at temperatures of 250-265°C and sodium salts is attributed to electrolytic destabilised PET/water interface. It is worth noting that neutral hydrolysis is environmentally friendly but impurities in the PET are passed in the obtained feedstock of TA meaning that extra and sophisticated purification is required.

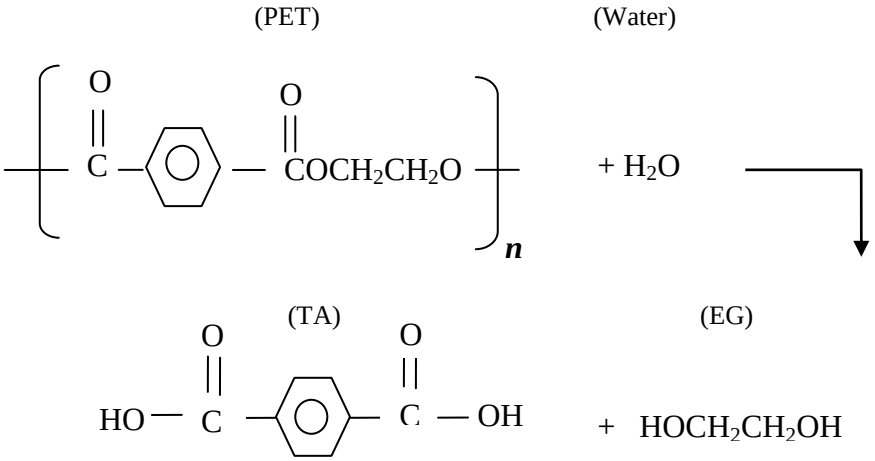

Figure 2.9 Simplified Hydrolysis Reaction of PET

In light of the above mechanical and chemical recycling processes of post-consumer PET, it became apparent that the final recycled PET properties undergo various physical changes. The quantity and quality of the available post-consumer PET are the major considerations in the choice of mechanical versus chemical recycling. Mechanical recycling of post-consumer bottle grade PET and its conversion by the melt reprocessing routes requires high molecular weight PET, hence, mechanical recycling is more suitable for bottle grade PET despite the level of contamination resulting from cross-contamination with other polymeric material, such as HDPE, PP or others, which can affect the processability and the properties of the obtained recyclate. *Noritake et al.* [94] used different techniques and showed that decomposition of PET and reduction of its physical and chemical properties can happen when subjected to high-pressure steam treatment, however new polymerisation can occur due to presence of free radicals and chemical groups present after treatment. The result showed that PET can be easily converted into new product. *Lopez et al.* [95] and *Hamad et al.* [96] respectively reported that after mechanical recycling, the material properties undergo significant decline in terms of molecular weight and tensile properties. Mechanical recycling involves the use of large amounts of water and PET is very sensitive to hydrolytic degradation and known to undergo thermal and hygrothermal degradation, which complicate its reprocessing and results in reduction of both molecular weight and applications of the recyclate. Therefore, drying the mechanically recycled flakes to a very low moisture level prior to reprocessing is of paramount importance. In contrast, the chemical recycling methods are more suitable for recycling diverse feedstock without consideration of molecular weights or level of contamination. The important advantages of the chemical recycling methods related to post-consumer PET is the removal of any physical or chemical impurities to the polymer by purification of the obtained chemicals. But it is worth noting that to achieve high rate of depolymerisation and high yield and quality of targeted products, it is important to characterise the available feedstock for the level and type of contamination and chemical composition prior to selecting the most appropriate recycling method.

2.2 PET recycling and PET Blends

This section investigates the existing research work in the area of PET recycling and PET blends with polyolefin, focusing on the melt processing and degradation, compatibility in PET blends and effect of multiple extrusions and crystallisation.

As a semi-crystalline material, the physical and mechanical properties of PET, depend on its microstructure and therefore is determined by the rate of crystallisation and the degree of crystallinity. In order to control the rate of crystallisation and the degree of crystallinity for improving and obtaining desired morphology and properties, various studies on crystallisation kinetics were performed to determine the changes in properties [97, 98, 99].

In a polymer blend, chemical reactions between the polymers or interchange reactions are very important in understanding the fundamental interactions in polymer compatibility. These interchange reactions can take place between functional groups belonging to molecules with different chemical compositions at elevated melt temperatures and in the presence of catalysts, especially in PET blends.

In their studies on recycled PET, *Awaja* and *Pavel* [100, 101] showed that pyromellitic dianhydride (PMDA*)* added at a specific % composition to rPET did facilitate the improvement in mechanical properties and the quality of the blend was superior to virgin PET. Blends of extruded recycled PET and virgin PET in the presence of chain extender, at various loadings, were injection moulded to produce bottles and showed that with 20% recycled content, PET gave optimum burst pressure and top load resistance. Additionally, with 29% rPET minimum liquid permeation and carbonation loss were obtained. These findings showed the importance of PMDA as a compatibiliser and chain extender in a blend of rPET and PET. Since both polymers are compatible and the interchange interaction is high likely to happen, this is expected that improvement is the main outcome of this work. *Oromiehie et al* [102] reported that, results of compounding PET and a mixture of virgin and recycled PET, with and without polypropylene functionalised with maleic anhydride, showed decreased intrinsic viscosity and molecular weight with increased loading of recycled PET in the blend. The decrease was attributed to the thermal exposure and shear degradation of recycled PET. This finding showed that improvement of blend properties is proportional to rPET loading and vice versa, and showing the high degree of degradation of the rPET.

Incarnato et al. [103] used PMDA as a chain extender for rPET-bg and found that with an amount between 0.50 and 0.75% the chain extending reaction produces an increase of M_w and branching phenomena that modify the rPET and make it suitable for film blowing and blow moulding processes. *Daver et al.* [104] reported that recycled PET modified with low molecular weight modifier, PMDA, by reactive extrusion exhibited higher complex viscosity and higher storage modulus compared to unmodified recycled PET. Also, this increase in complex viscosity was proportional to the increase in percentage of PMDA in recycled PET and contributed to increase in molecular weight and the formation of branching at concentration above 0.25 weight % PMDA. These findings showed the important role of PMDA in restoring the rPET chains and creating extra branching resulting in improved rPET, also giving an insight about the state of degradation of the rPET without chain extender and the effects of PMDA as compatibiliser, in improving the properties of rPET when blended with PET.

The current research work involves the presence of polyolefins, HDPE or PP in the recycled PET matrix. Being a polar polymer, PET is known to be immiscible with HDPE or PP which are non polar polymers. Blending recycled PET and HDPE or PP wastes and creating new materials are the main driving forces for the development of PET/HDPE or PET/ PP blends. Appropriate compatibilisers are necessary to overcome the problem of immiscibility in PET/HDPE or PET/PP, especially when the dispersed phase concentration exceeds 5 to 10% weight as reported by *Utracki* [105]. These compatibilisers enhance the degree of miscibility and molecular interfacial adhesion between the blended polymers and to improve impact strength and other mechanical properties. The main compatibilisers can be styrene block co-polymers, such as styrene/ethylene-butylene/styrene (SEBS), or a triblock co-polymer and ethylene co-polymer, such as ethylene-ethyl acrylate (E-EA) co-polymer. For reactive compatibilisation, either type of the above compatibilisers has to contain reactive functionality, such as maleic anhydride (MA) or epoxy-glycidyl methacrylate (GMA).

Research was done on blends of rPET and polyolefins for ecological and commercial reasons. It is well known that the mechanical properties of the recycled materials would decrease due to the decomposition and degradation of polymer chains. Some investigations have been done concerning the control of degradation in polymers during recycling by creating blends and or introducing additives. Several studies have been reported in the literatures on the usage of a third polymer component for compatibilised

PET and polyolefin blends in order to improve the mechanical properties, thermal stability, and toughness of the blends. The improvements of toughness for such blends have been reported with the compounding of ethylene-glycidyl methacrylate copolymer in rPET [106, 107]. *Yao* and *Beatty* [108] showed that PET and HDPE are incompatible in blending because of their immiscibility which is a result of their different molecular structures, polarities and crystallisation behaviours. The poor interactions between the molecular structures of these polymers make it difficult to achieve good dispersion during the mixing and lead to poor adhesion. *Carte* and *Moet* [109] reported that poor mechanical properties were the result of uncompatibilised PET/HDPE blends and reported an increase in break elongation of 600% in compatibilised PET/HDPE blend with 17% maleic anhydride grafted SEBS by reactive extrusion. Also, *Kim et al.* [110] reported improved morphological and mechanical properties and 10% of compatibiliser was enough to increase the notched impact strength in compatibilised PET/HDPE blends. During the melt blending by extrusion of PET-bg and HDPE in the presence of EPDM and SEBS as physical compatibiliser, *Traugott et al.* [111] reported that modulus and yield strength were reduced but elongation and impact strength improved significantly and further decrease was shown with increasing HDPE content. This showed that despite that the compatibiliser did bond physically the two phases of PET and HDPE, it could not form molecular bridges across the interface of their incompatible molecular phases. *Kalfoglou et al.* [112] compared various compatibilisers at various loadings blends of rPET-bg and HDPE by reactive extrusion and found that the effectiveness of compatibilisers containing epoxy (GMA) were better than compatibilisers containing anhydride (MA) because GMA is more reactive with hydroxyl and carboxyl end groups of PET. *Kim et al.* [113] used HDPE grafted with a blocked isocyanate for reactively compatibilising PET and HDPE and noticed improved compatibility in the blend, shown by the smaller size of the dispersed phase and the resulting superior mechanical properties. *Pracella et al.* [114] reported that melt mixing by extrusion of blends of post-consumer PET and polyolefin, HDPE and PP in the presence of compatibilisers, showed improvement of morphology, crystallisation behavior, thermal stability, rheological, and dynamic-mechanical properties of the blends. In their study of injection moulded recycled PET and PP blends, at different loadings in the presence of a compatibiliser, *Friedrich et al.* [115] reported that mechanical properties, such as flexural modulus and strength of the

samples were 50% better than those of the clean PP. On the other hand, fillers such as talc or $CaCO_3$ were used in order to improve the thermal resistance and flame retardancy of rPET / rPP blends [116, 117]. *Inoya et al.* [118, 119] has reported on hydrogenated block-copolymer of SEBS for improving the compatibility of rPET with PP blends. *Heino et al.* [120] reported that reactions between the GMA-functionalised SEBS and PET lead to improved mixing between PET and PP phases and lead to smaller dispersed phase domains and stabilised morphology compared to MA-functionalised one. Also, this improved interfacial adhesion was reflected by the shift in $\boldsymbol{T_g}$ of the PET towards that of PP. *Zhu et al.* [121] reported that the introduction of bi-functional co-agent, diallyl phthalate (DAP), during the blending of rPET with PP by reactive extrusion, with and without PP-g-MAH/DAP (PP grafted with both MAH and DAP), significantly enhanced the grafting degree of MA, decreased the chain scission of PP, increased the crystallisation temperature of grafted PP due to the nucleation of grafted groups, chemical reactions took place between PP-g-MAH/DAP and rPET and enhanced the interface adhesion in PP/rPET blend.

Paci and *La Mantia* [22] reported that during repetitive processing of PET, the main cause of degradation is the presence of small amounts of water, leading to hydrolytic chain scission and other polymeric contaminants and concluded that both chain scission and chain extension occur during processing. By repetitively extruding PE and PP, *Camacho* and *Karlsson* [25] reported that PP showed better thermal stability than PE and in both cases chain scission predominated and no chains branching or crosslinking were observed during the repetitive extrusions. As the current research work involves polymeric contaminants, such as HDPE and PP, these results are of paramount importance when investigating the outcome of such contaminants in relation to what was reported. It is worth noting that mixing thoroughly the polymer melts by twin screw extrusion enhances the blending in the barrel and yields well compounded polymers and that optimised processing conditions, screw speed and % torque, are important factors during the blending process. *Pospíšil et al.* [24] reported that during processing, as a result of thermo-mechanical degradation, reactions between macromolecules and relevant macro-radicals can occur, resulting in formation of grafted copolymers in some blends. This finding is mostly achievable in a blend of compatible polymers, so will it be considered in cases of rPET/HDPE or rPET/PP? *Giraldi et al.* [122, 123] focussed on the

influence of screw speed and torque in the improvement of the thermo-mechanical properties of injection moulded recycled PET with glass fibre and showed that optimised screw speed and torque significantly increased the mechanical performance and the positive effect on the interfacial adhesion matrix-fibre. Also, their study on compounding recycled PET showed the importance of screw speed on melt compounding and adhesion of the blend. Furthermore, the use of repetitive extrusion in investigating the potential of blended materials and the effects of thermo-mechanical influence on the final properties is of paramount importance. *Badía et al* [26], by using simulation processing techniques, showed that recycled PET subjected to repetitive extrusion showed signs of thermo-mechanical degradation resulted in chain scission reaction which decreased its capabilities and crystallinity, in the other hand, the irreversible structural changes studied by *Assadi et al* [27] during the extrusion of *PET* using different testing techniques, such as the steric exclusion chromatography and rheometry, showed that crosslinking occurs after repetitive extrusion operation. Also, *Nait-Ali et al.* [28] , in their study of the kinetics of PET post mechanical recycling extrusion, reported that two types of oxidative macromolecular changes take place successively; Chain scissions and chain branching, respectively in the well oxygenated zones of the extruder barrel (feed and die) and in poorly oxygenated zones (middle of the barrel). Additionally, *Pawlak et al.* [124] found that all PET regrinds contained additional mixture of other polymers ranging between 0.1–5 weight % and that the presence of more than 50 ppm PVC makes PET worthless for film forming due to reduced strength as a result of catalysed hydrolysis initiated by PVC. *Giannotta et al* [125] reported evidence of the effect of impurities, resulting from recycling, on the degradation of compounded virgin and recycled PET by extrusion resulting in lower melt viscosity and molecular weight and the presence of high concentration of carboxylic end groups. This finding is very important, because chain scission and chain branching are likely to be promoted simultaneously by the presence of high concentration of free radicals in the polymer melt. In their comparative study of thermal and mechanical properties of homogeneous and heterogeneous recycled PET bottles and virgin PET, *Torres et al.* [23] reported that the presence of contaminants, such as soil, and residual moisture, facilitated the crystallisation of recycled PET compared to virgin *PET* and initiated chains' cleavage during processing. This finding is in line with the role of short chains in the formation of crystallites. In their DSC study of injection

moulded recycled PET and recycled PET blended with engineering PET, *Fann et al.* [126] reported that the degree of crystallinity of recycled PET specimen was higher compared to engineering PET and when blended, the degree of crystallinity of the blend follow the pattern of the recycled PET, even in 20% of rPET in the blend. Again, this finding showed that the presence of short chains helped the increase in crystallinity. *Hao et al.* [127] studied the effect of inclusion of silicon nitrile nanoparticles (Si_3N_4) into PET matrix as a heterogeneous nucleating agent, and the non-isothermal crystallisation behaviour of recycled PET-silicon nitride nanocomposites investigation by differential scanning calorimetry showed accelerated nucleation and slow growth rate of PET, especially with Si_3N_4 content more than 1 wt%. This showed the effectiveness of silicon nitrile in increasing interaction between the PET chains and the Si_3N_4 nanoparticles and that growth rate can be hindered by the addition of silicon nitrile above certain amounts. *Tao* and *Mai* [128] reported that the non-isothermal crystallisation and melting behaviour, and the crystallisation morphology of extruded blends of recycled PET / PP compatibilised with various amounts (2–10 weight %) of PP-g-MA or PP-g-GMA showed chemical reactions of rPET with PP-g-MA and PP-g-GMA. These reactions resulted in increased crystallisation temperatures of rPET and PP due to the heterogeneous nucleation effect on each other. The melting peak temperature of rPET in PP/rPET blends compatibilised by PP-g-MA was lower than that of compatibilised by PP-g-GMA, indicating that PP-g-MA had stronger reactivity with rPET. And the crystallisation was influenced by the melting behaviour of rPET in the blends.

2.3 Scope of the Work

In light of the above information on PET, it became clear that inherited catalysts from the polycondensation stage can affect the thermal stability of PET properties, even at later stages of processing and melt recycling. And under high temperature, they can promote hydrolytic cleavage of chains due to the formation of autocatalytic carboxylic groups which degrade and deteriorate the properties. PET can undergo various processes of degradations, such as thermal, oxidative, photo-oxidative, hydrolytic and chemical degradation during its life cycle. Additionally, during the mechanical recycling processes of post-consumer PET, the properties of the final recyclate undergo further physical changes. Mechanical recycling is more suitable for post-consumer bottle grade PET, *rPET-bg*. Its conversion by the melt reprocessing routes requires high molecular weight PET and so, during the mechanical recycling, especially during the sorting and separation process, cross contamination with other plastic materials can occur easily. Bottles of HDPE, bottle caps of PP and mostly the PP caps' closures of PET bottles can pass through the separation process and get recycled with PET bottles. This cross contamination influences the properties of the final rPET-bg, and the final properties of the recyclate deteriorate with respect to virgin PET. Various research works were performed in order to improve the quality of the obtained recyclate, especially in tackling the problem of incompatibility between PET and other polymeric contaminants, such as polyolefin and others, through blending; these works showed that improvement of immisciblity, phase dispersion, morphological, mechanical and physical properties of recycled PET blended with either PET or HDPE or PP are fully dependent on physical and reactive compatibilisers and on the degree of their effectiveness in terms of interaction and reactivity. Also, the post mechanical recycling impurities, such as soil, polymeric and other contaminants, showed clear influence on the properties and crystallisation behaviour of the recycled PET. To overcome problems related to deterioration of properties, most of existing works dealt with cases, such as compatibilisation of PET and other polymeric material, suitability of various compatibilsers, effectiveness of compatibilisers on the improvement of properties of blends and their crystallisation. However, work dealing with cases, such as studying the effects of polyolefin contaminants on recycled PET-bg without further addition of additives, was rare. It is assumed that properties of most recycled material deteriorate as a result of recycling, especially post melt recycling, as for the case of rPET-bg.

In my belief, this assumption and the probability that this deterioration happen is arguable. Existing works showed that unless compatibilisers are used, properties cannot be improved and so, what if this outcome is not applicable for all cases? As seen through the literature review cited, even virgin PET still contains inherited chemicals, such as catalysts and other by-products. Furthermore, the partial degradation of PET during its life cycle and during recycling can be prone to unexpected changes in properties, and that combination of inherited and other chemicals during processing can trigger unexpected changes. From this assumption, the idea of investigating the influence of the presence of small amounts of HDPE or PP on the properties of the rPET-bg matrix without any addition of additives, germinated.

Additionally, the effects of thermo-mechanical degradation during the compounding or blending process by extrusion, the role of extrusion variables, injection moulding cooling rates and repetitive extrusions on the properties of contaminated and non contaminated rPET-bg matrix in general and thermal characteristics in particular, will reveal any hidden facts related to recycled PET-bg. Finally, the current research work, by investigating the above assumption, will contribute further to existing knowledge and will fill gaps related to the influence of small amounts of polyolefin contamination on the thermal characteristics and the crystallisation kinetics of rPET-bg without any supportive additives. In this research work, bottle grade recycled PET will be purposely contaminated with small amounts of HDPE or PP and the effects and influence of such contamination on the characteristics and processability, without using additives, will be investigated. This investigation will relate thermal characteristics to processability and further understanding of the influence of these polyolefin contaminants will be revealed. It is hoped that this will help industrial recycling and processing facilities reach targets in terms of decreasing polymeric wastes and improving efficiency and productivity when dealing with contaminated rPET.

Chapter 3

Experimental

3.1 Materials

3.1.1 Bottle Grade Recycled PET, *rPET-bg*

The recycled PET used in this work was bottle grade in the form of *flakes* of different sizes and colours as shown in *Figure 3.1*, supplied by *Closed Loop Recycling limited* [72] without any additional information or processing guidelines.

Figure 3.1 Mixed bottle grade rPET Flakes

3.1.2 High Density Polyethylene, *HDPE*

The HDPE grade used was HMA 025 [129], manufactured by ExxonMobil Chemical and characterised by its excellent dimensional stability, impact strength, high stiffness and with the following properties.

Properties	Nominal Values	Test Methods
Melting Temperature	134°C	ASTM D3418
Peak Crystallisation (DSC)	116°C	ASTM 3418
MFR/I (190°C /2.16 kg)	8g /10min	ASTM D1238
Density	0.964g/cm^3	ExxonMobil
Tensile Strength	26MPa	ISO 527-2/1A/50
Tensile Elongation @ Break	100%	ISO 527-2/1A/50

Table 3.1 Some Properties of HDPE grade HMA 025

3.1.3 Polypropylene, *PP*

The *PP* grade used was 7011L1 [130], manufactured by ExxonMobil Chemical and characterised by its high melt viscosity and impact strength at low temperature and with the following properties.

Properties	Nominal Values	Test Methods
Melting Temperature (DSC)	161°C	ISO 3146
Peak Crystallisation (DSC)	112°C	ISO 3146
MFR/I (230°C /2.16 kg)	1g /10min	ISO 1133
Density	0.9g/cm^3	ExxonMobil
Tensile Strength	26MPa	ISO 527-2/50

Table 3.2 Some Properties of PP grade 7011L1

As a guideline, the following are some properties of virgin PET:

Properties	Nominal Values
Melting Temperature Range (*Tm*)	250 - 260 ^{o}C
Glass Transition Temperature (*Tg*)	70 - 80 ^{o}C
MFR/I (230^{o}C /2.16 kg)	35.08g /10min
Density (ρ)	1.30 – 1.40g/cm ^{3}
Amorphous, semi-crystalline	30 – 40%
Tensile Elasticity (*E*)	2.10 – 3.10GPa
Tensile Strength (*s*)	55 – 80MPa

Table 3.3 Some Properties of PET [131]

Note: For additional information, material data sheets are available in ***Appendix 2***.

3.2 Methods and Processes

3.2.1 Differential Scanning Calorimetry, *DSC*

In thermal analysis, *differential thermal analysis*, DTA, and *differential scanning calorimetry*, DSC, are both used for the determination of characteristic temperatures. Additionally, DSC allows for the determination of *caloric* values such as the heat of melting and heat of crystallisation. For both DTA and DSC, the primary measuring signal during a measurement is the *temperature difference* between a *sample* and a *reference* in micro-volt, µV (thermal voltage). Additionally, for DSC, this temperature difference is converted into *heat flow* in watt, W, by means of appropriate sensitivity calibration and this possibility does not exist for a purely DTA instrument. Then, the measured data are transformed by the computer program into *thermograms* as shown below [132, 133].

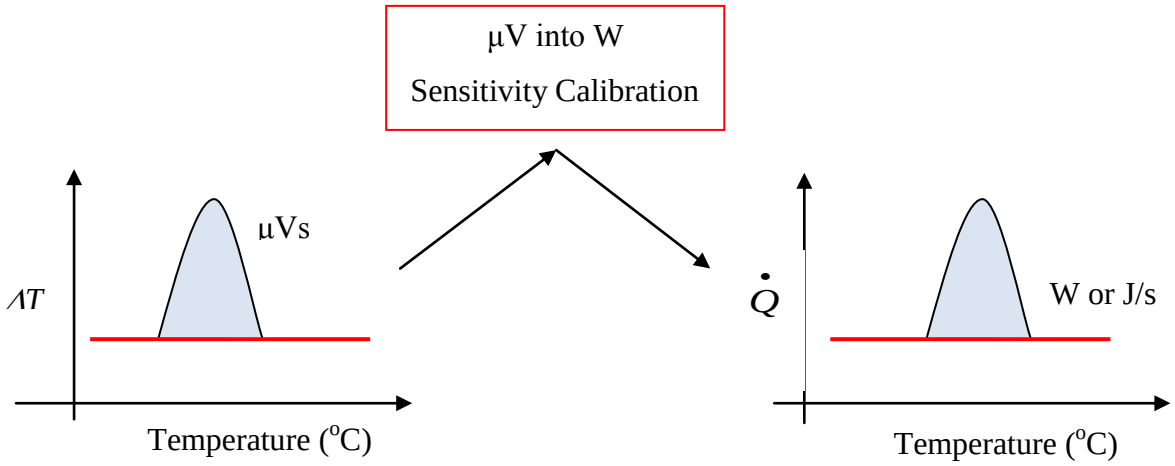

Figure 3.2 DTA Thermogram

Figure 3.3 DSC Thermogram

Where: ΔT is the *temperature difference* in micro-volt second (µVs) for DTA,

$\dot{Q}$ is the *heat flux* or *heat flow* per *unit time* in (W or J/s) for DSC.

Differential scanning calorimetry, DSC, provides information on the thermal transition phases of polymers and determines a range of characteristics, including glass transition temperature, T_g, crystallisation temperature, T_c, melting temperature, T_m, degradation temperature, T_d, enthalpies of melting and crystallisation, ΔH_m and ΔH_c, and % crystallinity, X_c, of polymers. This technique is used for determining the quantity of heat that is either absorbed or released by a sample of substance undergoing a physical or chemical change. Because of this change, the internal energy, known as enthalpy, ΔH, is altered. It is this change of enthalpy between two states which is of interest during experimentation. Melting, evaporation or glass transition, are processes which absorb more energy, such processes increase the enthalpy and called *endothermic*. In contrast, crystallisation and decomposition which release energy and consequently lower the enthalpy are called exothermic processes. This enthalpy, ΔH, is determined by the following relationship [134].

$$\Delta h = C_p.dT \qquad (3.1)$$

Where: $\boldsymbol{\Delta h}$ is the *enthalpy* in Joule (J),

$\boldsymbol{C_p}$ is the *heat capacity* in (J/^{o}C or J/K),

$\boldsymbol{dT}$ is the *temperature difference* in (^{o}C or K).

By dividing both parts in **(3.1)** by the sample *mass*, the *specific enthalpy*, $\boldsymbol{\Delta H}$ is obtained:

$$\Delta H = \frac{\Delta h}{m} = \frac{C_p.dT}{m} \rightarrow ?$$

And,

$$\Delta H = \left(\frac{C_p}{m}\right).dT = c_p.dT \rightarrow ?$$

$$\Delta H = c_p.dT \qquad (3.2)$$

Or the integration form as follow,

$$\Delta H = \int c_p . dT \qquad (3.3)$$

Where: ***ΔH*** is the *specific enthalpy* in (J/g),

c_p is the *specific heat capacity* in (J/^{o}C.g or J/K.g),

Experimentally, the *specific heat capacity*, ***c_p***, which represents the quantity of energy needed to raise the temperature of 1g of substance by 1^{o}C at constant pressure, is determined by measuring the *heat flux*, which represents the quantity of heat transferred (heat flow) per *unit time* and *mass* and it is measured as a function of *temperature* and/or *time*. As *heat flux* is determined by the control and the *heating/cooling rate* and *mass* are known during practical analysis, so the *specific heat capacity* can be determined from the direct proportional relationship with the *heat flux* from the following relationship:

$$\frac{\dot{Q}}{m} = v.c_p \qquad (3.4)$$

Where: $\dot{Q}$ is the *heat flux* or *heat flow* per *unit time* in (W or J/s),

c_p is the *specific heat capacity* in (J/^{o}C.g or J/K.g),

m is the *sample mass* in (g),

v is the *heating/cooling rate* in (^{o}C/min or K/min).

From the relationship **(3.4)**, the *heating/cooling rate* is known to be,

$$v = \frac{dT}{t} \qquad (3.5)$$

Where: ***dT*** is the *temperature difference* in (^{o}C or K) and ***t*** is *time* in (min or s).

By replacing **(3.5)** in **(3.4)**, the *specific heat capacity* in terms of *heat-flux* is as follow,

$$c_p = \frac{\frac{\dot{Q}}{m}}{\frac{dT}{t}} \rightarrow ?$$

$$c_p = \frac{\dot{Q}.t}{m.dT} \tag{3.6}$$

By replacing **(3.6)** in **(3.2)**, a relationship between *heat-flux* and *specific enthalpy* is as follow,

$$\Delta H = c_p.dT = \frac{\dot{Q}.t}{m.dT}(dT) = \frac{\dot{Q}.t}{m} \rightarrow ?$$

$$\Delta H = \frac{\dot{Q}.t}{m} \tag{3.7}$$

Where: ***ΔH*** is the *specific enthalpy* in (J/g),

$\dot{Q}$ is the *heat flux* or *heat flow* per unit time in (J/s),

t is the *time* in (min or s),

m is the *sample mass* in (g),

In DSC, the sample *pan* can either be kept open or sealed depending on the material tested. Pans or crucibles exist in a variety of shapes and sizes, depending on the type of apparatus and application, and made of high thermal conductivity materials, especially aluminum which is the most widely used. The *reference* normally consists of an *empty pan* similar to the *sample one*. The measurement of the energy flow to and from a *sample* during a temperature controlled program is performed against the *reference.* The energy required to keep both *sample* and *reference* at the same temperature is converted into *heat flow* and subsequently, by means of a computer program, the data are converted into a thermogram showing a curve of heat flow *versus* temperature/or time as shown in *Figure 3.4* below.

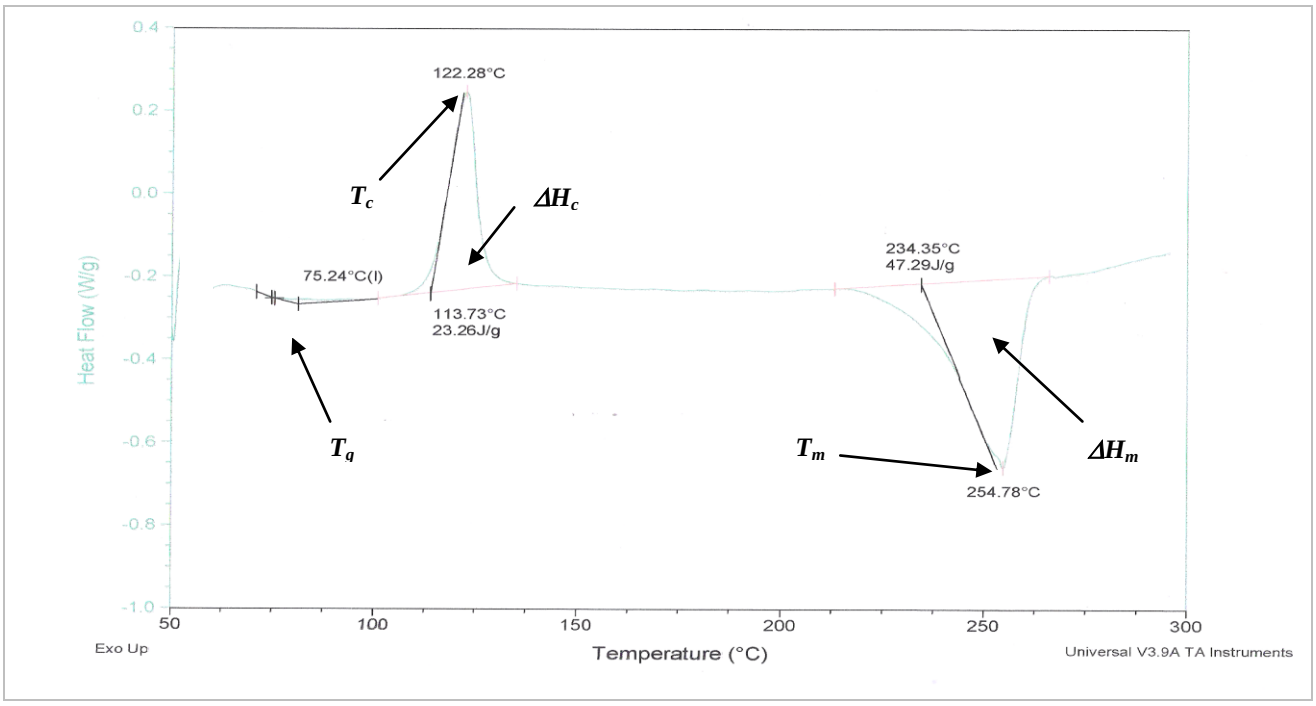

Figure 3.4 DSC Curve Showing Phase Transitions of rPET in the Heating Mode

Where: T_g is the glass transition temperature, T_c is the cold crystallisation temperature, T_m is the melting temperature, ΔH_c and ΔH_m are respectively, the enthalpies of cold crystallisation and melting.

The base line of the DSC curve is the linear part which shows that no reaction or transition is taking place and where the heat is equal to zero.

3.2.1.1 DSC Measuring Techniques

The measurement standards [135, 136] identify two methods for measuring the difference between thermal transitions in a *sample* and in a *reference* material. These two different measuring techniques are *heat-flux DSC* and *power-compensated DSC*. In *heat flux DSC*, shown in *Figure 3.5*, the *sample*, *S*, and the *reference*, *R*, pans are heated or cooled in the same furnace chamber according to a controlled temperature program.

The temperature difference between the *sample* and the *reference* is measured continuously. As long as the sample and reference respond to the temperature program, the heat flux into both of them remains constant. The advantage of *heat flux DSC* is its robustness and give a stable baseline of heating curve and permit a clear measurement of T_g. In *power compensated DSC*, shown in *Figure 3.6*, the *sample* and the *reference* crucible are heated or cooled in separated *two small furnaces* and each one is controlled independently by a primary heating program. So, if an *exothermic* or *endothermic* reaction in the *sample* leads to a temperature difference between the two small furnaces, power (energy) is added or removed from the *sample furnace* to compensate for the energy change in the *sample*. The difference in *thermal power* is the change in *heat flux* relative to the *reference thermal power*.

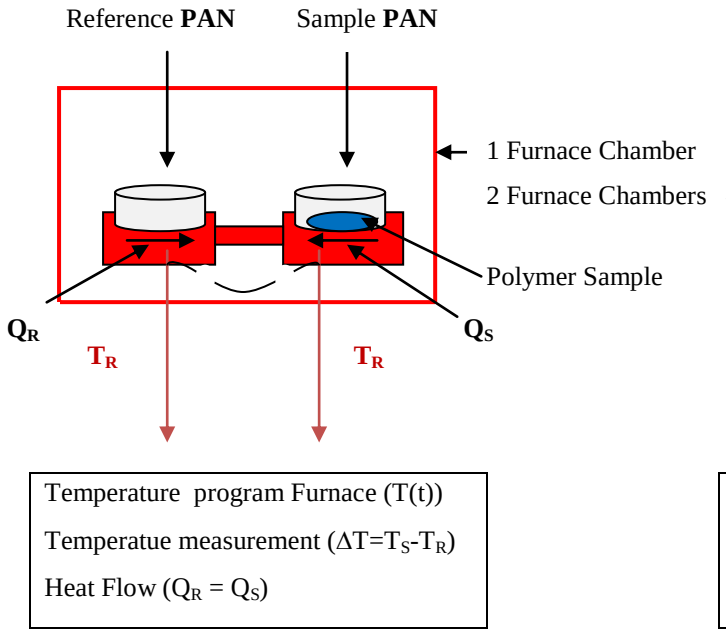

Figure 3.5 Heat Flux DSC

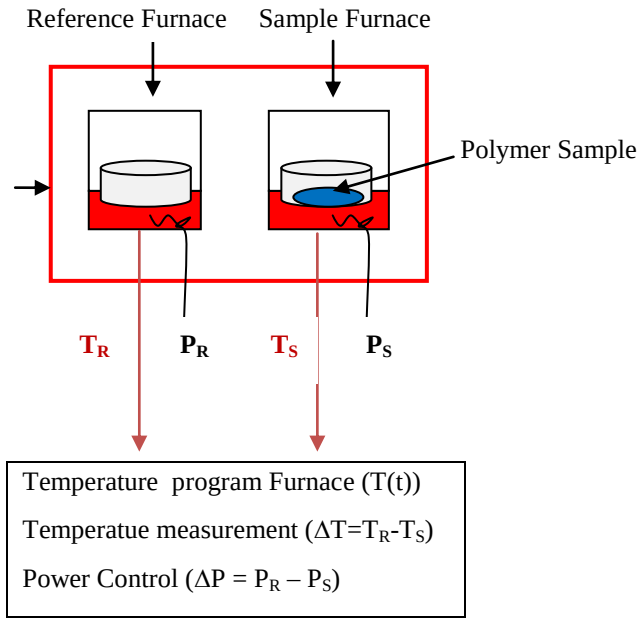

Figure 3.6 Power Compensated DSC

3.2.1.2 Procedure

The measuring technique used in this work was *heat flux DSC* performed by means of a *TA Instrument 2010* calorimeter, shown in *Figure 3.7* below, having a furnace chamber similar to the diagram shown in *Figure 3.5* and *Figure 3.8* below, interfaced to a PC computer using *TA Instrument* conversion programs, *V4.4E* and *Universal V3.9A*, to follow the variation of the rate of *heat evolution* with *time*.

Figure 3.7 *TA Instrument 2010* Calorimeter

Figure 3.8 Furnace Chamber of *TA 2010*

As indium is suitable for calibrating the medium temperature range of many polymers, so, to ensure accuracy of measurement, the *temperature* and *energy calibration*s [137] of the calorimeter were done, on every sample, from the point and enthalpy of melting of pure indium [138], respectively T_m = 156.6°C and ΔH_m = 28.5 J.g^{-1} and using standard aluminium pans. The calibration measurement was conducted dynamically at different heating rates. Then, the indium melting points obtained were plotted against heating rates and the extrapolation point at heating rate zero was compared to the literature value as reported by *Höhne* [139]. During experiment, DSC calorimeter uses a purging gas, such as helium, argon, nitrogen, which flows through the cell at a constant rate to ensure that the atmospheric conditions are as uniform as possible in all experiments. In this work, the samples were analysed in nitrogen atmosphere at controlled flow rate of 20ml/min. The heating and cooling rates were set as per experiment requirement, as described below.

In this work, *3 runs* of each sample were performed. Before each run, the operating parameters; *temperature, heating/cooling rates* and analysis condition were set in the computer program. For each run, the sample was weighed, flattened, put into a *sample pan* (also called *crucible*), encapsulated, transferred to its holder in the calorimeter furnace and submitted to the *temperature program*, where the measurement was performed against a *reference.*

- In *experiments 1* to *8*, samples of masses no more than *20mg*, as recommended by standard [135] for glass transition studies, were analysed *dynamically* in the *heating mode* at a *rate* of $10^oC/min$ up to300^oC and determined their glass transition, crystallisation and melt temperatures and enthalpies of melting.

- In *experiment 9*, samples of masses no more than *10mg*, as recommended by standard [135] for melting and crystallisation studies, were analysed in the heating mode at *10, 15, 20* and $25^oC/min$, up to 300^oC and isothermally kept for *2 minutes* at 300^oC to complete melting. Then, the samples were cooled *non-isothermally*, at *cooling rates* of *10, 15, 20* and $25^oC/min$ from 300^oC to completion of crystallisation and determined the values of the relative crystallinity as previously described by *equation* **(1.6)** in *Section 1.2.3.1* and *equation* **(1.13)** in *Section 1.2.3.2*. Also, validation for non-isothermal crystallisation process was performed as described in *Section 1.2.3.2*.

- In *experiment 10*, samples of masses no more than *10mg*, as recommended by standard [135] for melting and crystallisation studies, were analysed at a heating rate of $10^oC/min$, up to 300^oC and isothermally kept for *2 minutes* at 300^oC to complete melting. Then, the samples were cooled from 300^oC at the same rate of $10^oC/min$. And determined the relative crystallinity as previously described by *equation* **(1.6)** in *Section 1.2.3.1*. Also, validation for non-isothermal crystallisation process was performed as described in *Section 1.2.3.2*.

3.2.1.2.1 Glass Transition

The temperature range over which amorphous polymers or amorphous sections of semicrystalline thermoplastics mark a change from a glassy state to a rubbery state or vice versa, is called glass transition. As per standard [135], the glass transition temperature, T_g, is the midpoint of the glass transition temperature range and at which half of the change in specific heat capacity is attained. The mobility of polymer chains is greater above T_g than below it, where the chains are frozen. In a DSC curve, the T_g position depends on the orientation, crystallisation and other factors such as crosslinking and residual stress.

In this work, the T_g was determined as per standard and as shown in *Figure 3.9* below. Two baselines were extrapolated from the first and the last points where deviations were detected from the baselines; the points of detected deviation were respectively, $\boldsymbol{T_{ig}}$ and $\boldsymbol{T_{fg}}$. Then, a tangent of the step-like change was drawn and the $\boldsymbol{T_g}$, or $\boldsymbol{T_{mg}}$, was determined as being the temperature at mid-point of the line joining the two intersection points of the tangent and extrapolated baselines, i.e. $\boldsymbol{T_{eig}}$ and $\boldsymbol{T_{efg}}$, where it is assumed that half of the change in specific heat capacity has occurred.

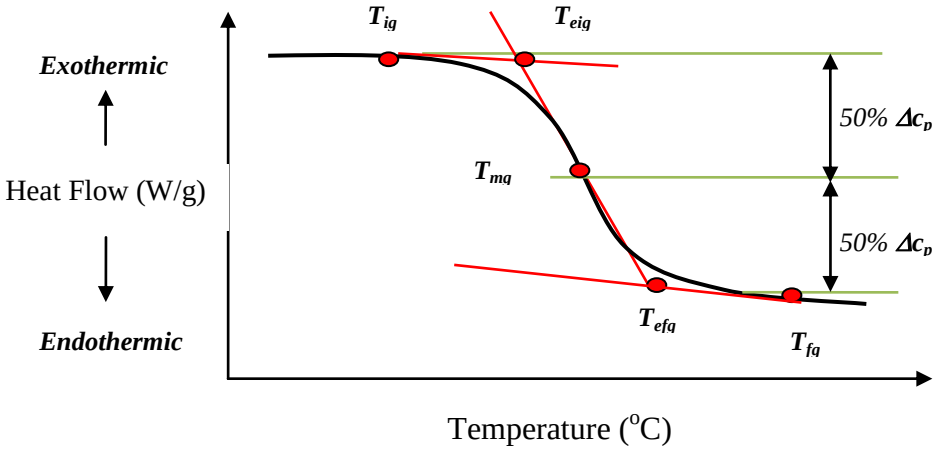

Figure 3.9 Temperatures of Glass Transition

Where:

$\boldsymbol{T_{ig}}$ – *Onset temperature* (first detectable deviation from the baseline).

$\boldsymbol{T_{eig}}$ – *Extrapolated onset temperature* (tangent-baseline intersection below $\boldsymbol{T_g}$).

$\boldsymbol{T_{mg}}$ – *Midpoint temp. or* $\boldsymbol{T_g}$ (at which 50% of the change in specific heat capacity occurs).

$\boldsymbol{T_{efg}}$ – *Extrapolated end temperature* (tangent-baseline intersection above $\boldsymbol{T_g}$).

$\boldsymbol{T_{fg}}$ – *End temperature* (last detectable deviation from the baseline).

$\boldsymbol{\Delta c_p}$ – *Endothermic change in specific heat capacity*.

3.2.1.2.2 Melting

The transformation or change of a solid from a crystalline state into an amorphous state is called melting. During the melting process, the solid does not encounter a loss of mass or chemical change of its structure. The melting process requires absorption of heat and therefore, it is an endothermic change and depends heavily on the thermal and mechanical history of the sample. In a DSC curve, the amount of heat absorbed during the melting of crystalline fractions is called the enthalpy of melting, ΔH_m, and characterised by the area under the endotherm. As per standard [135], the melting temperature, T_m, shown as T_{pm} in *Figure 3.10* below, is the temperature at which most of the crystallites melt. It is at the melting end temperature, T_{fm}, that all the crystallites are melted and it is considered the experimental melting temperature [140]. The melt profile depends on the orientation, crystallisation and heating rate.

In this work, the T_m and ΔH_m were determined as per standard and as shown in *Figure 3.10* below. A baseline was extrapolated between the first and the last points where deviations were detected from the baseline; the points of detected deviation were respectively, $\boldsymbol{T_{im}}$ and $\boldsymbol{T_{fm}}$. Then, two extrapolated linear sections of the endotherm were drawn and the $\boldsymbol{T_m}$, or $\boldsymbol{T_{pm}}$, was determined as being the temperature of peak maximum, at the intersection of the extrapolated linear sections, where it is assumed that most of the crystallites have melted.

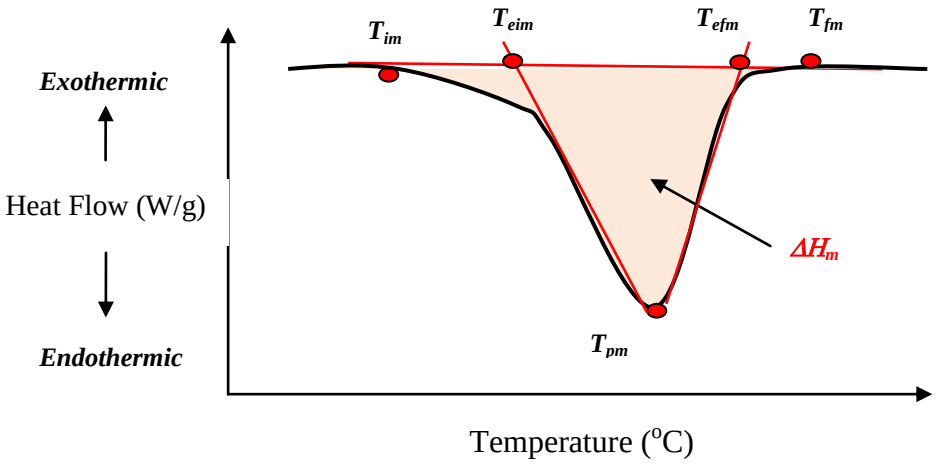

Figure 3.10 Temperatures and Enthalpy of Melting

Where:

T_{im} – *Melting onset temperature* (first detectable deviation from the baseline).

T_{eim} – *Extrapolated onset temp.* (extrap. linear falling peak edge - baseline intersection).

T_{pm} – *Melting peak temp. or* T_m (temperature of the peak maximum).

T_{efm} – *Extrapolated end temp.* (extrap. linear rising peak edge - baseline intersection).

T_{fm} – *End temperature* (last detectable deviation from the baseline).

ΔH_m – *Quantity of heat absorbed or enthalpy of melting.*

3.2.1.2.3 Crystallisation

The transformation or change of a material from the liquid amorphous state into a crystalline state is called crystallisation. During the crystallisation process, the material does not require any heat, instead it releases heat and therefore, it is an exothermic change. In a DSC curve, the amount of heat released during crystallisation is called the enthalpy of crystallisation, ΔH_c, and characterised by the area under the exotherm. As per standard [135, 141], the crystallisation temperature, T_c, shown as T_{pc}, in *Figure 3.11* below, is the temperature at which the crystallisation rate is at its maximum. Crystallisation can occur during the heating of the material, called cold crystallisation, and usually occurs if the material was rapidly cooled from the melt. Crystallisation from the melt occurs when

the temperature falls under the theoretical equilibrium melting temperature, T_m^0, this is the temperature where $T_m = T_c$ of a 100% crystalline fraction. The cooling rate, nucleation and growth are determinant factors during crystallisation.

In this work, the T_c and ΔH_c were determined as per standards and as shown in *Figures 3.11* and *3.12* below. In both heating and cooling modes, a baseline was extrapolated between the first and the last points where deviations were detected from the baseline; the points of detected deviation were respectively, $\boldsymbol{T_{ic}}$ and $\boldsymbol{T_{fc}}$. Then, two extrapolated linear sections of the exotherm were drawn and the $\boldsymbol{T_c}$, or $\boldsymbol{T_{pc}}$, was determined as being the temperature of peak maximum, at the intersection of the extrapolated linear sections, where it is assumed that the crystallisation rate is at its maximum. The area under the exotherm represents the amount of heat released during crystallisation, i.e. the enthalpy of crystallisation, ΔH_c.

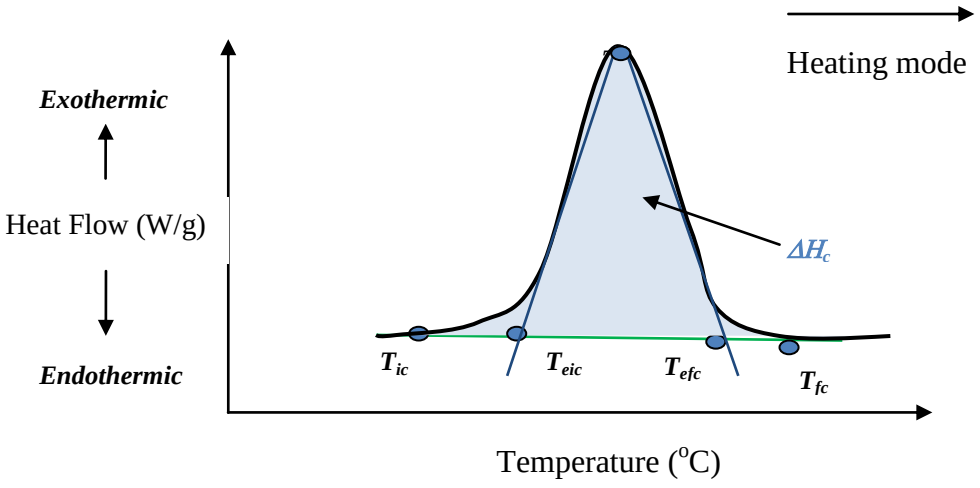

Figure 3.11 Temperatures and Enthalpy of Cold Crystallisation in Heating Mode

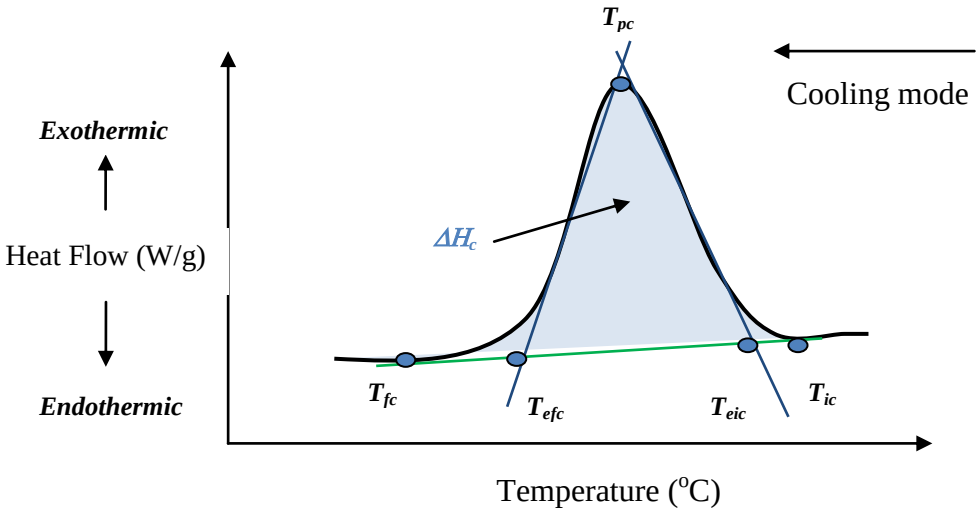

Figure 3.12 Temperatures and Enthalpy of Crystallisation in Cooling Mode

Where:

T_{ic} – *Start of crystallisation* (first detectable deviation from the baseline).

T_{eic} – *Extrapolated onset temp.* (extrap. linear rising peak edge - baseline intersection).

T_{pc} – *Crystallisation peak temp. or* T_c (temperature of the peak maximum).

T_{efc} – *Extrapolated end temp.* (extrap. linear falling peak edge -baseline intersection).

T_{fc} – *End temperature* (last detectable deviation from the baseline).

ΔH_c – *Quantity of heat released or enthalpy of crystallisation.*

3.2.1.2.4 Degree of Crystallinity, X_c

The crystallinity of a material, which is expressed in %, is the crystalline fraction of a complete crystallisation, was determined using the following relationship:

In the heating mode as reported in the literature [131],

$$X_c = \frac{\Delta H_m}{\Delta H_m^0}.100 \qquad (3.8)$$

A 100% crystalline fraction of PET is reported in the literature [140] to have an enthalpy, ΔH_m^0 of *140 J.g*$^{-1}$, within a melting temperature range of *240-260*^oC and at a heating rate of *10*^oC*/min*.

In the cooling mode, related to the heat of fusion as reported in the literature [142],

$$X_c = \frac{\Delta H_c}{\Delta H_m^0 . m} .100 \qquad (3.9)$$

Where: $\boldsymbol{X_c}$ is the *% crystallinity*,

$\boldsymbol{\Delta H_m}$ and $\boldsymbol{\Delta H_c}$ are respectively the *enthalpies* of *melting* and *crystallisation*,

ΔH_m^0 is the *enthalpy* of *melting* of a *100% crystalline fraction*,

m is the *sample mass*.

3.2.2 Fourier Transform Infrared, *FTIR*

Infrared spectroscopy is a preferred technique for materials analysis. The main infrared sub-regions are *near*, *middle* and *far* infrared. The infrared region is within a wavenumber range of *12800-10cm*$^{-1}$, where FTIR represents the mid-range, with a wavenumber range of *4000-200cm*$^{-1}$, or equivalent wavelength range of *2.5-50μm* [144].

The positions of atoms in molecules are not fixed but subjected to a number of different vibrations, each vibration occurs independently of all others around it and the atoms behave as simple harmonic oscillators. A variety of vibrations are possible, *stretching*, *bending*, *rocking* and *twisting*. The energy level of infrared light corresponds to the energy required by the molecule to vibrate. When the alignment of the electric field and the bond's dipole takes place, a shortening of the bonds happen; the absorption of the infrared light as a consequence changes the dipole of the bonds as they vibrate. Each type of bond requires a specific amount of infrared energy and therefore, the energy of infrared light absorbed indicates the type of functional group present in the sample. In spectroscopy, the *wavenumber*, $\bar{\nu}$ is defined as the number of *waves* per *centimeter*, and is also the *reciprocal* of the *wavelength*, λ, and also equals to the *frequency* divided by the *velocity of light*, *c*. The resulting spectrum obtained represents the molecular absorption or transmission, creating a molecular fingerprint of the sample, where each molecular structure produces a unique infrared spectrum. This makes infrared spectroscopy useful for several types of qualitative and quantitative analyses, which give a positive

identification of every different kind of material and determines the amount of material present through the size of the peaks in the spectrum. The resulting spectrum is a plot of either *absorbance* or *transmittance* versus infrared *wavenumber*. The *absorbance* and *transmittance* are determined by the following relationships:

For *Absorbance*,

$$A = \log\left(\frac{I_0}{I_t}\right) \tag{3.10}$$

For *Transmittance*,

$$T = \frac{I_t}{I_0} \tag{3.11}$$

Where:

A is *absorbance*, ***T*** is *transmittance*,

$\boldsymbol{I_0}$ is the *initial intensity* entering the sample,

$\boldsymbol{I_t}$ is the *intensity transmitted* after sample absorption.

Because of its accuracy, Fourier Transform Infrared, FTIR, became the preferred method of infrared spectroscopy and with the aid of modern conversion algorithms software, *FTIR* became an excellent tool for quantitative analysis. As in any analysis technique, the original infrared spectroscopy instruments were of the *dispersive* type, which separate the individual frequencies of energy emitted from the *infrared source* by using a *visible prism* that separates visible light into its colours or *frequencies*. Prism was later upgraded to *grating*, which is a more modern *dispersive* element that separates better the frequencies of *infrared* energy. The *detector* measures the amount of *intensity* which passes through the *sample* and compares it with the intensity passing through the *reference*, the reference can be *air*. *FTIR* uses an infrared prism which works exactly the same as a *visible* prism but *FTIR* is preferred over *dispersive* method because of its precision, fast scanning, high sensitivity, mechanically simple and no need for external calibration. And it was specifically developed to overcome the limitations of the *dispersive* instruments and their slow and individual scanning process. So, the method for measuring all of the infrared frequencies *simultaneously* and faster by the use of a very simple optical device called *interferometer*, which produces a unique type of signal which has all of the infrared frequencies *encoded* into it and allow a very fast measurement of signals in matter of a

second, this *interferometer* allowed the *FTIR* spectrometers to became preferred over the *dispersive* instruments [145, 146].

3.2.2.1 FTIR Measuring Technique

The measurement standard [143] identifies the practices for quantitative analysis. Infrared energy is emitted from a *source* of a spectrometer, where an *infrared beam* of controlled amount of energy, is emitted through an *interferometer*, a *sample* and a finally a *detector* as shown in *figure 3.13*. Once in the *interferometer*, the infrared beam is divided into two optical beams by a *beamsplitter*. The two beams reflect off of the mirror and are recombined when they meet back at the *beamsplitter*. The use of the *interferometer* results in very fast measurements and the resulting signal is called an *interferogram* which has a unique property, i.e. all frequencies are being measured *simultaneously* as the *interferogram* is measured. To allow the measured *interferogram* signal to be interpreted, it must be converted into a *frequency spectrum* with the desired spectral information for analysis, and to do this, a *decoding* is performed by computer software using a mathematical technique called *Fourier transformation*.

During analysis, and for scaling purposes for the absorption intensity, a *background spectrum* of the reference, which is *air*, is measured before analysis, as shown in *Figure 3.14* below. A *background* measurement is done without any *sample* in the beam and used by the *detector* and compared to the *sample spectrum* to determine the *% transmittance*. This methodical step, results in a *spectrum*, as shown in *Figure 3.15* below, without presence of instrumental characteristics and therefore, all spectral information exhibited are strictly due to the sample. One *background spectrum* can be used for many *sample measurements* because it is characteristic of the *instrument* itself.

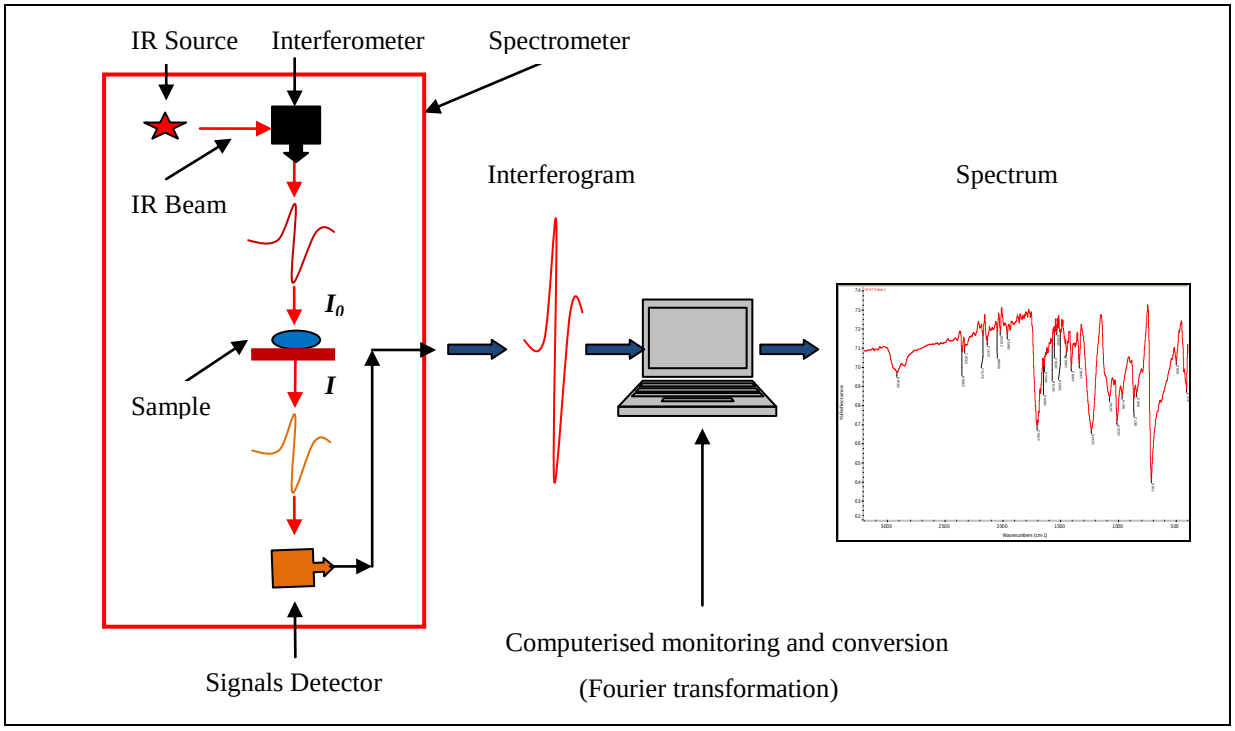

Figure 3.13 Schematic Representation of the FTIR Analysis

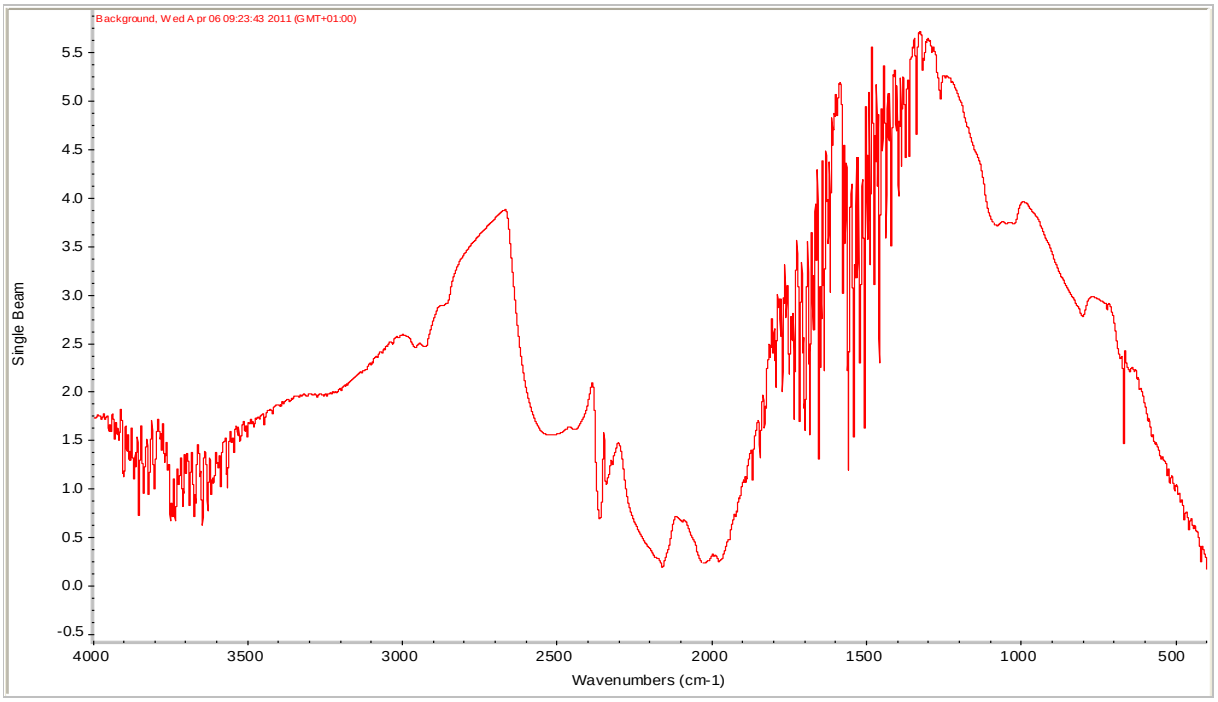

Figure 3.14 Background Single Beam of *Nicolet 380* Spectrometer

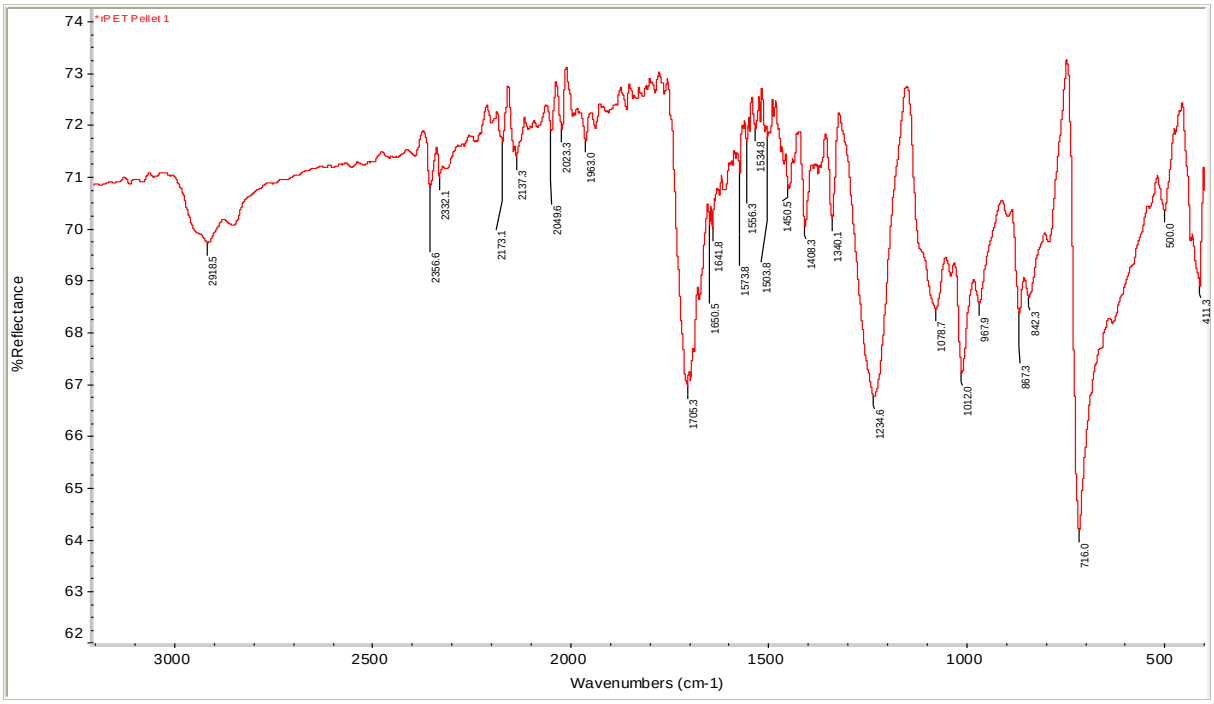

Figure 3.15 FTIR Spectrum of a rPET-bg Sample

3.2.2.2 Procedure

The measuring technique used in this work was FTIR performed by means of a *Nicolet 380* spectrometer; having a high-energy source with pinned source position for easy replacement, a *rapid scanning* electromagnetic drive *interferometer* with an XT-KBr *beamsplitter* of a range *11000-375 cm*$^{-1}$ and pinned-in-place *detectors* for easy-exchange, and using *air* as *reference*, as shown in *Figures 3.13* and *3.16*, interfaced to a PC computer using *OMNIC* conversion programs to follow the scanning progress.

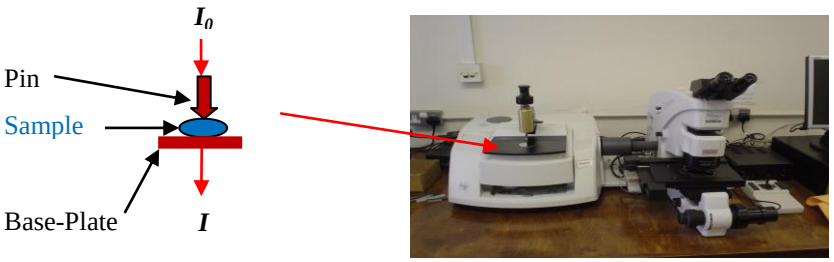

Figure 3.16 *Nicolet 380* Spectrometer

In this work, FTIR analysis was performed in *experiments 1* to *8*, where *3 scans* of each sample were taken. After cleaning thoroughly the testing *plate* and the *pin*, and to eliminate any instrumental influence on the samples' scanning as per standard [143], a *background single beam*, as in *Figure 3.14* above, was taken for each population of samples of rPET, rPET/HDPE and rPET/PP. Then, *3 thin discs* (film) of each sample were tested within a *rapid scanning* frequency range of *4000-400cm*$^{-1}$ and the curve option was set to *% reflectance* versus *wavenumber*. Each *sample* was carefully placed between the *pin* and the *plate* in the *testing area* of the spectrometer and *scanned*. Once the *data* and the *spectrum* were collected, the used sample was removed and scanning continued with *samples 2* and *3*. Once all the data and spectra were collected, the machine was cleaned and switched off. The spectra's curves were analysed, smoothed and the peaks were extracted and compared to the available literature and determined the various molecular groups.

3.2.3 Melt Flow Rate, *MFR*

In flow analysis, the melt flow rate, MFR, is a testing used to determine the ease of flow and represents a qualitative control index of thermoplastics, which is critically influenced by the physical properties and molecular structure of the polymer and the conditions of measurement. MFR is also known as melt flow index, MFI or simply melt index. The standard designation is melt mass-flow rate or MFR expressed in *g/10min* representing the equivalent *mass* in (g) of a polymer flowing through the barrel of a capillary rheometer for a time of *10 minutes*. An alternative quantity is the melt volume flow rate, MVR, expressed in *cm*^{3}*/10min*. The MVR is converted to MFR measurement by multiplying the result by the melt *density* value for the thermoplastic material. For accuracy of measurement, each sample is usually tested *3 times* and the average is used in determining the MFR as follow:

MFR determination,

$$MFR = \left(\frac{m_{average}(g)}{t_{average}(s)} \right) . \left(\frac{600(s)}{10(\text{min})} \right) \qquad (3.12)$$

MFR determination from *MVR*,

$$MFR = MVR.\rho \qquad (3.13)$$

Where: ***MFR*** is the *melt flow rate* expressed in (g/10min),

MVR is the *melt volume rate* expressed in (cm^3/10min),

$\boldsymbol{m_{average}}$ is the *average mass* in (g) and $\boldsymbol{t_{average}}$ is the *average time* in (s),

$\boldsymbol{\rho}$ is the *density* of the tested thermoplastic in (g/cm^3).

3.2.3.1 MFR Measuring Technique

The measurement standards [147, 148] identify the practices for the determination of the melt mass-flow rate, MFR, and the melt volume rate of thermoplastics by using an extrusion plastometer. The thermoplastic is heated to its molten state for a specific time and then extruded through a die with a specified length and orifice diameter under prescribed conditions of temperature, load, and piston position in the barrel as shown in *Figure 3.17*. The standards described many measuring procedures, the main two used procedures are *procedure A*; based on the measurement of the mass of extruded material through the die over a given period of time, and used to determine the melt flow rate, MFR, whereas, *procedure B* is an automatically timed measurement, used to determine both melt flow rate, MFR, and melt volume rate, MVR, of thermoplastic materials.

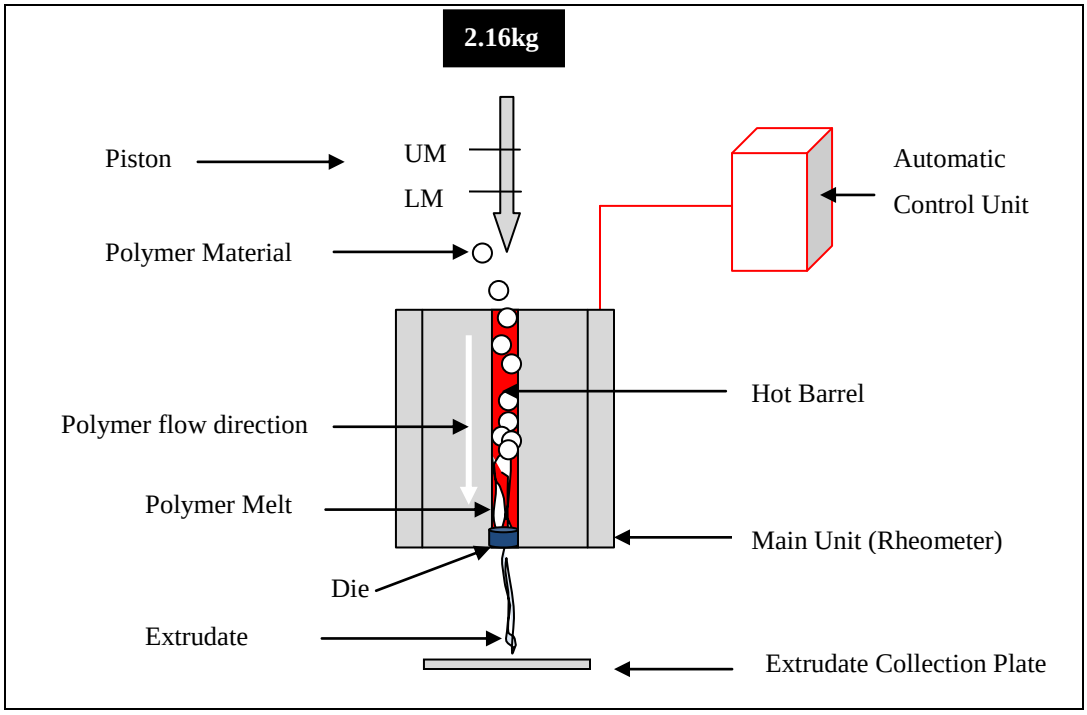

Figure 3.17 Schematic Representation of the MFR Testing

3.2.3.2 Procedure

The MFR testing was performed using procedure *A* by means of a *Davenport* capillary rheometer; having an automatic control unit, a *piston* of *9.48mm* diameter, a die of *1mm* diameter and *8.4mm* length and various test *loads*, used to simulate the processing pressure, ranged from *1.2* to *21.6 kg* to permit measuring polymer materials of various viscosities, as shown in *Figure 3.18*. A load of *2.16kg* was used to compare the results with *reference materials* measured under similar load. A measuring *funnel* of *20cm*^{3} was used to feed the material into the barrel.

Figure 3.18 *Davenport* Rheometer

In this work, MFR testing was performed in *experiments 1* to *8*, where *3 samples* of each population of samples of rPET, rPET/HDPE and rPET/PP were measured. After cleaning thoroughly the *barrel* and the *testing area,* the *melt temperature* was set to $260^{o}C$. Once the *melt temperature* was reached, an amount of $20cm^{3}$ of material was fed into the barrel and given *5 minutes* to reach molten state. Then, the piston was introduced in the barrel and the *2.16kg* load was applied on the *piston* and the collection of *extrudates* started when the *lower marking, LM,* on the piston, shown in *Figure 3.17*, was level with the inlet of the barrel and finished once the *upper marking, UM,* on the piston was reached. The pressure applied by the load allowed the polymer melt to extrudate through the *die*. The extrudates were collected at *3 periods* of *time*; *5, 10* and *15* seconds and weighted. Then, the melt flow rate, MFR, of the materials was determined by application of the MFR *equation* **(3.12)** shown previously and compared to the available literature.

3.2.4 Tensile Testing

The tensile testing provides information on the material's mechanical properties which can be used to provide data for research, development and engineering design as well as quality control and specification. This testing helps understand the material's mechanical potential and its process history through the measured tensile modulus, $\boldsymbol{E}$, stresses at yield, $\boldsymbol{\sigma_y}$, stress at break or failure, $\boldsymbol{\sigma_f}$, and the maximum elongation at yield, $\boldsymbol{\%\, e}$, of the tested materials. These measured properties define the material's mechanical applications through the understanding of factors, such as stiffness, strength and toughness. The main typical specifications in tensile testing are the *dimensions* of the tested *specimen, dumbbell*, the cross-head speed, the gage length and the testing *temperature* and computer *program* to perform data conversion. The measurement performed takes in consideration the continuous variation of the material *extension* under continuous *tensile force* and the resulting data is converted into a *load* versus *elongation* curve as shown in *Figure 3.19* below.

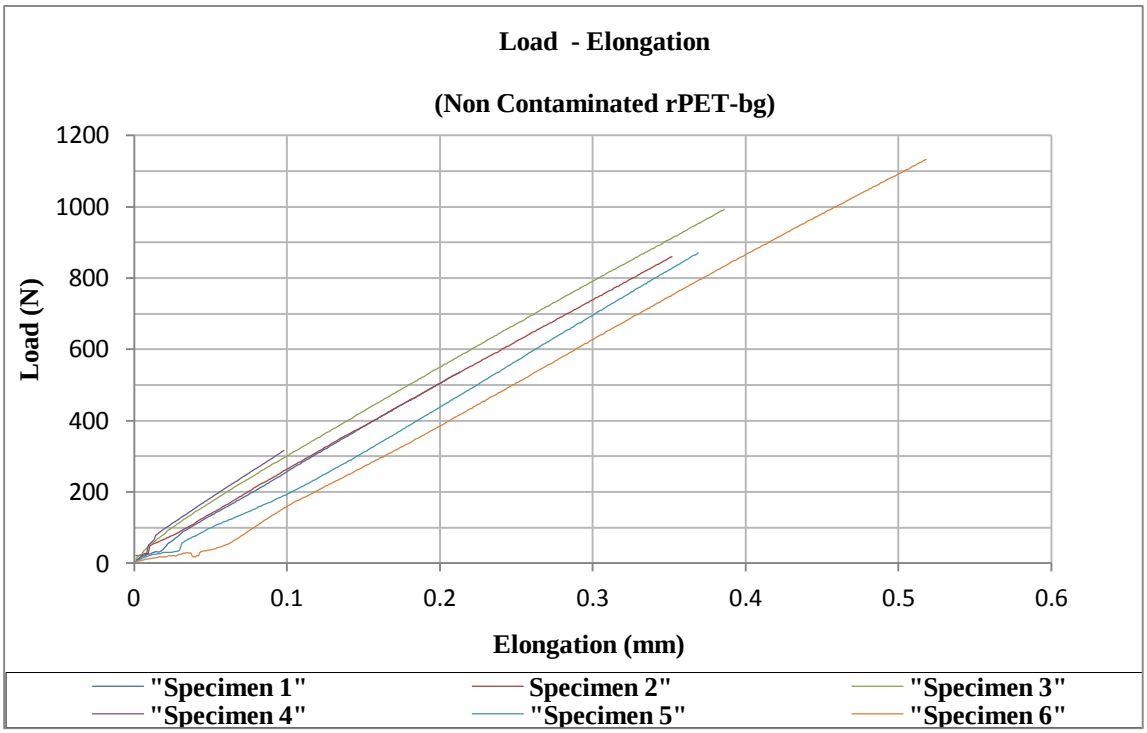

Figure 3.19 Curves of Dumbbells of non contaminated rPET-bg (1 to 6)

3.2.4.1 Tensile Measuring Technique

The measurement standards [149, 150] identify the general practices for the determination of the tensile properties. As per standards, this method is used to investigate the tensile properties of test specimens and for determining the tensile strength, tensile modulus and the various aspects of the tensile stress/strain relationship under a cross-head *speed* range of *5-50mm/min*, a *gauge length* range of *50-75mm*. This method is suitable for moulded, extruded and casted thermoplastics. A measured specimen, *dumbbell*, is placed between the *grips* of the tensile machine to maintain the specimen during the extensional test as shown in *Figure 3.20* below, sensors are placed in contact with the specimen at the mid-point to detect the variation of signals and transmits them to the *monitoring program*, and a *control unit* for setting the required data and dimensions of the specimen. The movable part of the tensile machine subjects the specimen to a controlled and balanced extensional *force* until the *specimen* fails or break. The length of extension is set by evaluating a maximum practical elongation individual to each material. The detected signals of the variation of elongation under the applied load of extension are monitored and converted

by the computer program into graphs representing curves of *stress* versus *elongation*, and the data supplied is also used to evaluate the various aspects of tensile stress/strain relationship.

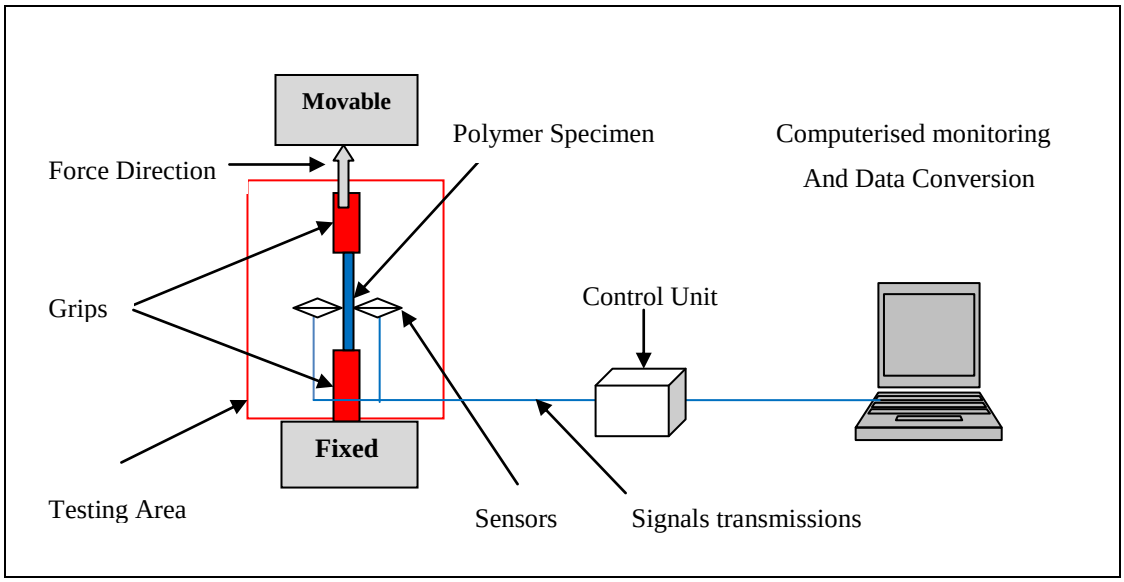

Figure 3.20 Schematic Representation of the Tensile Testing

3.2.4.2 Procedure

The tensile load-extension testing was performed by means of a *Tinius Olsen* tensile machine as shown in *Figure 3.21*; having a control unit, an *extensional force* of *10kN*, an *extensional length* up to *1500mm*. The applied loads were calibrated by standard weight. The testing machine was interfaced to a PC computer recording the response of samples to the extensional applied load using *Star* computer *program* for events monitoring and conversion of data.

Figure 3.21 *Tinius Olsen* Tensile Testing Machine

In this work, tensile testing was performed in *experiments 1* to *8*, where *6 dumbbells* of each population of samples of rPET, rPET/HDPE and rPET/PP were measured. After cleaning thoroughly the *testing area*, the test data were set into the control unit with an *extensional force* of *10kN*, an *extensional length* of *1500mm*, a cross-head *speed* of *5mm/min* and a *gauge* of *50mm* and pre-loaded to zero. Each tested *dumbbell* had a gauge length of *50mm*, a width of *10mm* and a thickness of *4mm*. These dimensions were input in the control unit for each *dumbbell test*. Each *dumbbell* was placed carefully between the grips as shown in *Figure 3.22*. The tests were conducted at room temperature between *23* and *25°C*. Each *dumbbell* was tested until failure, i.e. until breakage and end of testing. The monitored and converted data were extracted from the computer and plotted as *load-elongation curves* as shown in *Figure 3.19* and later converted to *stress*/*strain* curves as shown in *Figure 3.23* and determined the *stress* at *yield*, *stress* at *failure or break*, *strain* at *yield* and the secant *modulus* and finally all the results obtained were compared to the available literature and interpreted.

Figure 3.22 A *Dumbbell* under Test

The *stress- strain* curves were plotted after converting the *loads* and *elongations* into *stresses* and *strains* in the purpose to extract the individual *tensile characteristics* of each material from the curve of *stress* versus *strain*, as shown in *Figure 3.23* below.

The *load* was converted into *stress* using the following relationship.

$$\sigma = \frac{P}{A} \tag{3.14}$$

Where: $\boldsymbol{\sigma}$ is the *tensile stress* in ($N.m^{-2}$ or MPa),

$\boldsymbol{P}$ is the *load* applied in (N),

$\boldsymbol{A}$ is the *cross-sectional area* in (m^2) subjected to tensile testing.

The *elongation* was converted into *strain* using the following relationship.

$$e = \frac{\Delta L}{L} \tag{3.15}$$

Where: $\boldsymbol{e}$ is the *strain* (*Dimensionless*),

$\Delta \boldsymbol{L}$ is the *elongation* during the testing in (*mm*),

$\boldsymbol{L}$ is the *initial tested length or (gauge length)* in (*mm*).

From the stress-strain curves, the secant *modulus*, elastic modulus, ***E***, is extracted by from the value of the *slope* of the *stress-strain* curve at the starting *linear portion*; by dividing the amount of *stress* of any point within the linear portion (between two points $\boldsymbol{\sigma_{y1}}$ and $\boldsymbol{\sigma_{y2}}$) and the amount of equivalent *strain* of the same point within the linear portion (between two point $\mathbf{e_{x1}}$ and $\mathbf{e_{x2}}$).

$$E = \frac{\sigma_y}{e_x} \tag{3.16}$$

Where: $\boldsymbol{E}$ is the *modulus* in (GPa), which is the *slope* of the *stress-strain* curve $\boldsymbol{(\sigma - e)}$.

$\boldsymbol{\sigma_y}$ is the amount of stress of any point within the starting linear portion $\boldsymbol{(\sigma_{y2} - \sigma_{y1})}$

$\boldsymbol{e_x}$ is the amount of equivalent strain of the same point within the starting linear portion $\boldsymbol{(e_{x2} - e_{x1})}$.

Note: The first points of stress, σ_{y1}, and strain, e_{x1}, are zeroed, i.e they are taken as the starting points of the linear portion. So, the subtraction $\sigma_{y2} - \sigma_{y1}$ and $e_{x2} - e_{x1}$ give the value at point 2, which is the one used in the calculation.

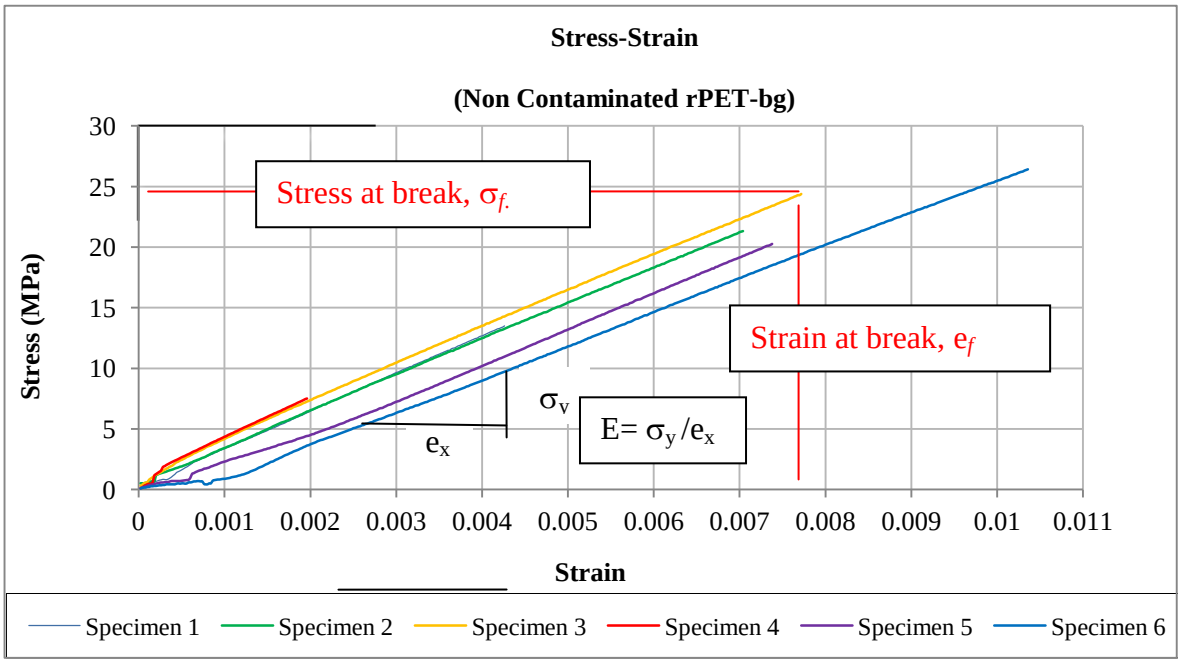

Figure 3.23 Stress-Strain Curves of rPET-bg Dumbbells (1 to 6)

3.2.5 Impact Testing

The Charpy impact testing provides information on the material's mechanical efficiency under conditions favourable to brittle fracture. This test measures the impact energy resulting from the work done by the pendulum's striker at the point of impact with the specimen. When impact happens, the test specimen starts to absorb energy and undergoes plastic deformation. The test specimen continues to absorb energy until saturation where it fractures or breaks. This testing helps understand and evaluate the material's toughness; the impact energy decreases when the yield strength is increased. At failure or fracture, the energy absorbed by a tough material is much greater than that's absorbed by brittle one. The main typical specifications in Charpy impact testing are the test specimen dimensions, the testing temperature and the weight of the pendulum's striker.

3.2.5.1 Impact Measuring Technique

The measurement standard [151] identifies the practices for the determination of the charpy unnotched impact properties under defined conditions. The impact energy absorbed in breaking an unnotched specimen at its *mid-point area*, referred to the original *cross-sectional area* of the specimen, is expressed in *kilo-joule/m*^{2}. As per standards, this method is used to investigate the *brittleness* and *toughness* of a material. The test *specimen* (impact bar), supported at its ends as a horizontal *beam*, is impacted by a single blow of a *striker* (rod of pendulum) at the *mid-point* of the beam, as shown in *Figure 3.24*. The *specimen* while absorbing the *energy* released by the *striker*, it undergoes elastic transformation to its maximum capacity until it fails either by yielding or fracturing depending on the material's properties. The *energy* absorbed by the *specimen* is calculated and displayed in the control unit's screen. As per standard, the *specimen* dimension, *type 1*, should have a length $L = 80 \pm 2mm$, a width $B = 10 \pm 0.2mm$ and a thickness $t = 4 \pm 0.2mm$ and a set consisting of *10 specimens* should be tested at temperature of 23^oC. This method is suitable for moulded, extruded, casted thermoplastics with or without fillers.

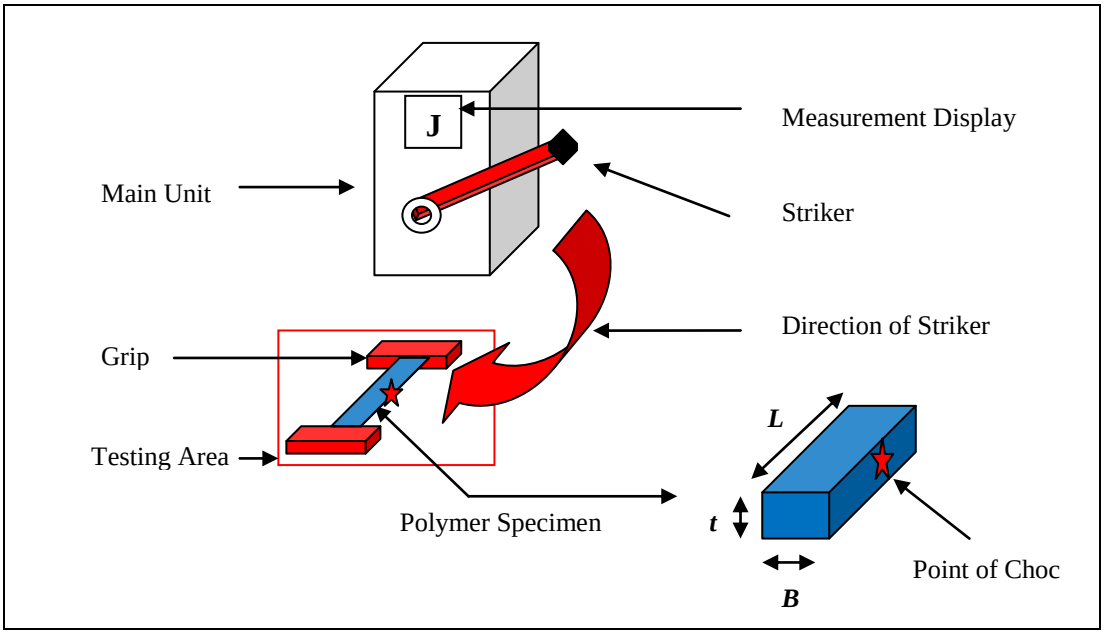

Figure 3.24 Schematic Representation of the Charpy Impact Testing

3.2.5.2 Procedure

The impact testing was performed by means of a *Ceast 6545* impact tester as shown in *figure 3.25*; fitted with a device for calculating and displaying the *energy absorbed* by the tested *specimen* and a *striker, model 6545,* of a potential energy of *50J* striking at a *speed* of *3.46m/s*. The *Ceast 6545* is not equipped with *impact strength* calculation device.

Figure 3.25 *Ceast 6545* Charpy Impact Testing Machine

In this work, impact testing was performed in *experiments 1* to *8*, where *10 specimens (Impact bars)* of each population of samples of rPET, rPET/HDPE and rPET/PP were measured. After cleaning thoroughly the *testing area*, the *striker* (pendulum) was tested to check its performance and adjusted as to hit the *specimen* at the *mid-point area* and put to a ready for use position. Then, each of the *10 specimens* was fixed between the *2 grips*. Each tested *specimen* had a *cross-sectional area* within a tolerance as per standard, described previously. Each *specimen* was placed carefully between the grips as shown in *Figure 3.24*. The tests were conducted at room temperature around $23^{o}C$. Each *specimen* was tested under a *single striker blow*. For each *specimen*, the *test* started by releasing the *striker* and hitting the specimen with a *single blow*, the *energy* absorbed by the specimen was recorded and the tested *specimen* was removed. At the end, the machine was thoroughly cleaned and switched off. The Charpy *impact strengths* were calculated using *equation* (**3.17**) below. The results obtained were compared to the available literature and interpreted.

The *impact strength* was calculated using the following relationship.

$$IS = \frac{E_a}{A} \tag{3.17}$$

Where: ***IS*** is the *Impact Strength* expressed in (kJ/m^2),

E_a is the *energy absorbed to break the specimen* (Impact bar) in (*kJ*),

A is the *cross-sectional area* of the specimen, of *width* ***B*** and *thickness* ***t***, in (m^2),

3.2.6 Extrusion Process

3.2.6.1 Description of the Process

Extrusion is a processing technique for moulding materials into fibres, profiles, pipes, sheets and other commodity or engineering products. Extrusion moulding is a process capable of manufacturing various materials, such as plastics, ceramics, metals and composites. This process allows consistent, efficient and continuous production. Polymer materials need to be of high molecular weights to be extruded efficiently. The extrusion machine or *extruder* is the principal equipment of this process. It consists of a *hopper*, a *barrel* with a *screw* and ending with a *die*. Different machines have different configuration but the principle of processing is similar. Extrusion is the process of choice in compounding and blending of materials by using twin screws design and other sophisticated filtration and removal of volatiles (Gases) during the process. Compounding extruders are more developed and complex than those used for general extrusion purposes. The measurement standard [152] identifies the practices of extrusion of materials. The extrusion principle consists of *feeding* the material into the barrel at the *feed zone* and melting and plasticising it in the *compression zone* by means of fixed *heating elements* around the barrel and by the additional heat generated by the shear of rotating screws. Then, the *rotating screws* continuously force the *molten material* towards the *metering zone*, where it is fully compressed and pass through the orifice of a *die*.

It is the *die* which dictates the shaping of the final produce, as shown in *Figure 3.26*. The properties of the final produce are fully dependent on the processing parameters, such as *temperature*, *pressure*, *shear*, *torque*, *filtration* and *screws speed*. Balanced and optimised processing conditions are of paramount importance in achieving good results. In addition, the material processing properties, such as the *flow* characteristics, degree of *degradation* and reaction to *cooling*, are determinant factors in assessing the final produce efficiency and its capability in withstanding the purposes of applications. Once extruded, the final produce is cooled, measured and cut to the desired specifications, quality controlled, sorted and packed.

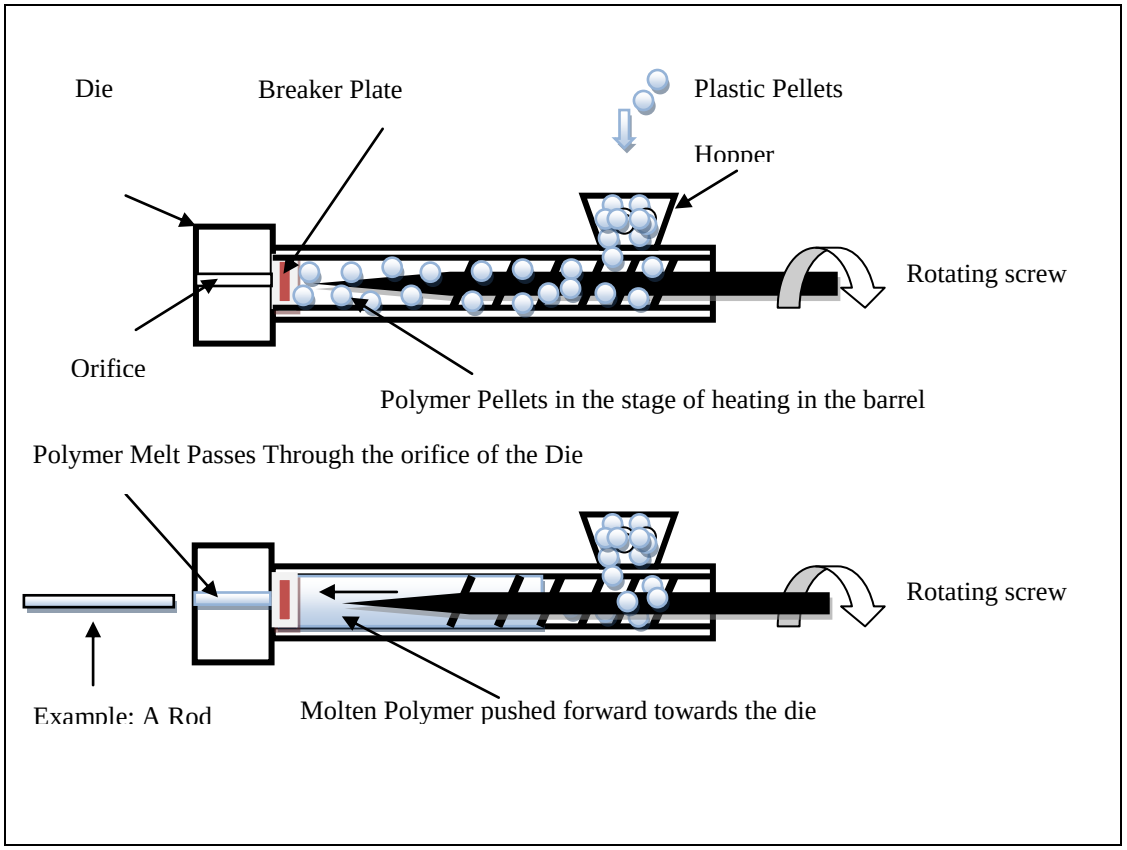

Figure 3.26 Schematic Representation of the Extrusion Moulding Process Steps

3.2.6.2 Procedure

The extrusion moulding was performed by means of a Twin screw *Leistritz* extrusion machine as shown in *Figure 3.27*; having a haul-off *Accrapak system-model 750/1* and a *Brook Crompton series 2000* shredder, as shown in *Figure 3.28*.

Figure 3.27 *Leistritz* Extrusion Machine

Figure 3.28 Extrusion Haul-off

Prior to experimentation, test processing was performed to familiarise fully with the operating system of the *Leistritz* machine and test pellets of rPET-bg flakes were produced. The heating zones of the *Leistritz* were optimised around the PET processing temperature range of *250-260^{o}C* as in *Table 3.3*, *Section 3.1.3*. The uniformly distributed heat over the *barrel zones* with temperatures ranging from *250^{o}C* at *feed* to a *die* temperature of *270^{o}C*, allowed the extrusion of well dimensioned pellets, as shown in *Figure 3.29*. These optimised processing conditions, listed in *table 3.4* below, were set to extrude all the required pellets of non contaminated rPET-bg and contaminated rPET-bg with HDPE or PP. The highest temperature of *270^{o}C* was far less than *280^{o}C*, at which degradation of PET in presence of contaminants can occur, as reported by *Awaja* and *Pavel* [153].

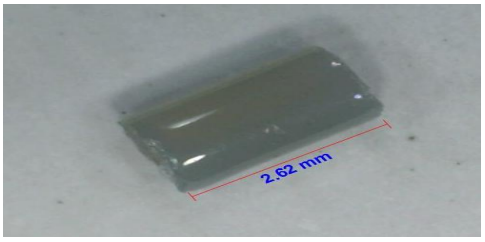

Figure 3.29 rPET-bg Extruded Pellet

Barrel rear (Feed Zone 01)		Barrel middle (Compression Zone 02)			Barrel front (Metering Zone 03)		Die (Zone 04)	Screw Speed
250°C	250°C	260°C	260°C	270°C	270°C	270°C	270°C	120 rpm

Table 3.4 Temperature Settings of the Leistritz Extruder

In this work, rPET-bg flakes were extruded into pellets in *experiment 1*. The flakes were collected from the bulk material randomly, cleared from any impurities and weighted to the required amount of *2.2kg*; the reason of choosing this amount is explained in *Section 3.2.7.2* below. Once the operating temperatures of the extruder were reached, the twin screw started slowly and the flakes were fed into the barrel in very small amounts. Once the extrudate started to flow through the die, it was pulled along the length of the water bath, then, shred into pellets and collected at the end of the haul-off section. Continuous observation of the flakes' behaviour during processing, appearance of the extrudates, screw speed and % torques were performed and data recorded.

Similarly, in *experiments 3* to *5*, respectively amounts of rPET-bg flakes were contaminated by thorough mixing with amounts of *5%*, *10%* and *15%* HDPE, as listed in *Table 3.5*, were *extruded* into contaminated *pellets*, as previously mentioned with the non contaminated rPET-bg and performed under the same extrusion processing conditions, as in *Table 3.4* above. And similar methodology applied in *experiments 6* to *8*, where respectively amounts of rPET-bg flakes were contaminated with amounts of *5%*, *10%* and *15%* PP.

The amount of *2.2 kg* represented *100%* weight of rPET-bg contaminated with HDPE or PP. The individual amounts of materials were determined depending on the percentages of contamination, *5%*, *10%* or *15%*, and mixed thoroughly before being extruded into *pellets*.

Example: *95%* rPET-bg / *5%* HDPE

$$2.2\ kg \quad \rightarrow \quad 100\%\ (95\%\ \text{rPET-bg} + 5\%\ \text{HDPE})$$
$$x \quad \leftarrow 95\%\ \text{rPET-bg}$$

$$x = \frac{2.2kg.95\%}{100\%} = 2.09kg$$

Where: ***x*** is the mass of rPET-bg corresponding to *95%* of the total mass, and the mass of *5%* HDPE is simply the difference between the masses, as tabulated below:

recycled PET-bg	*95%*	*90%*	*85%*
recycled PET-bg mass (kg)	2.09	1.98	1.87
HDPE or PP	*5%*	*10%*	*15%*
HDPE or PP mass (kg)	0.11	0.22	0.33
Total mass (kg)	**2.2**	**2.2**	**2.2**

Table 3.5 Percentages and masses of Materials

In *experiments 9*, an amount of *2.09kg* of rPET-bg flakes was contaminated by thorough mixing with an amount of *0.11kg* of PP, equivalent to *5%* PP, as listed in *Table 3.5*. This amount was *extruded once* under the same processing conditions listed in *Table 3.4* above. And in *experiments 10*, the same amount of *2.09kg* of rPET-bg flakes was mixed thoroughly with *0.11kg* of PP and *repetitively extruded* for *5 cycles* under the same processing conditions listed in *Table 3.4* above. Continuous observation of the flakes' behaviour during processing, appearance of the extrudates, screw speed and % torques were performed and data recorded.

Finally, after each extrusion operation, the extruder was purged, cleaned and switched off. The *extruded pellets* of non contaminated rPET-bg and the rPET-bg contaminated with HDPE or PP at various percentages were respectively taken to the next stages.

- Analysis of the pellets by DSC, FTIR and MFR.
- Injection moulding the extruded pellets into *dumbbells* and *impact bars*.

3.2.7 Injection Moulding Process

3.2.7.1 Description of the Process

Injection moulding is the process of choice for mass production of various commodity and engineering materials, such as plastics, ceramics, metals and composites. Packaging accessories, electrical housings, toys, bottles, caps and closures are among the products manufactured by injection moulding. Bottles are mostly manufactured by injection blow moulding and the most used process for PET bottles is injection stretch blow moulding, ISBM, which is a complicated and widely used in bottle manufacturing, as previously described in *Section 2.1.5*, this process allows efficient and continuous large amounts of products in short time. As for extrusion, polymer materials need to be of high molecular weights and require higher MFR to be injection moulded efficiently. The injection machine consists of three main sections, *injection unit*, *mould assembly* and *clamping unit*. Different machines have different configuration but the principle of processing is similar. Injection moulding machines are efficiently precise and ranging between small to very large machines up to 7000 tons of *clamping capacity*. The standard [154] identifies the practices of injection moulding of test specimens of thermoplastics materials. As for extrusion, the injection moulding principle consists of *feeding* the material from the hopper into the barrel at the *feed zone* and melting and plasticising it in the *compression zone* by means of fixed *heating elements* around the barrel of the *injection unit*. The material is fed into the *barrel* by means of a *reciprocating screw*. Unlike the extrusion screw, the injection moulding *reciprocating screw* is designed to rotate *forward* to push and *inject* the molten material and moves *backward* while rotating and *feeding* with the material from the *hopper*, as shown in *Figure 3.30*. The *barrel* is the main heating

chamber of the machine. Once heated to the required *processing conditions*, the material is then pushed forward by the *reciprocating screw* towards the *nozzle* and *injected* under high pressure into the *mould cavity* through the runner system, where the injected molten material very quickly takes the shape of the cavity of the mould. Once the mould cavity is filled, *packing pressure*, as shown in *Figure 3.33* below, is applied to pack the material to counterbalance any shrinkage due to the *cooling process*. Then, the material solidifies for a set of *cooling time* under a *clamping pressure* applied on the *mould parts* to maintain them closed and to allow the well cooling and solidification of the product before *ejection*. After solidification of the material, the *mould* opens automatically and the product is *ejected* by the *ejection system*. The final product is a replica of the mould cavity, as shown in *Figures 3.34* and *3.35* below.

The properties of the final product are fully dependent on the processing parameters, such as *melt temperature, injection time, packing- pressure, melt orientation, cooling time* and *cooling rates*. Also, balanced and optimised processing conditions are determinant in processing products with controlled *crystallisation* during *cooling*, products which can fit the purposes of their applications. Finally, the product is inspected to detect any anomalies or deficiency, sorted and packed.

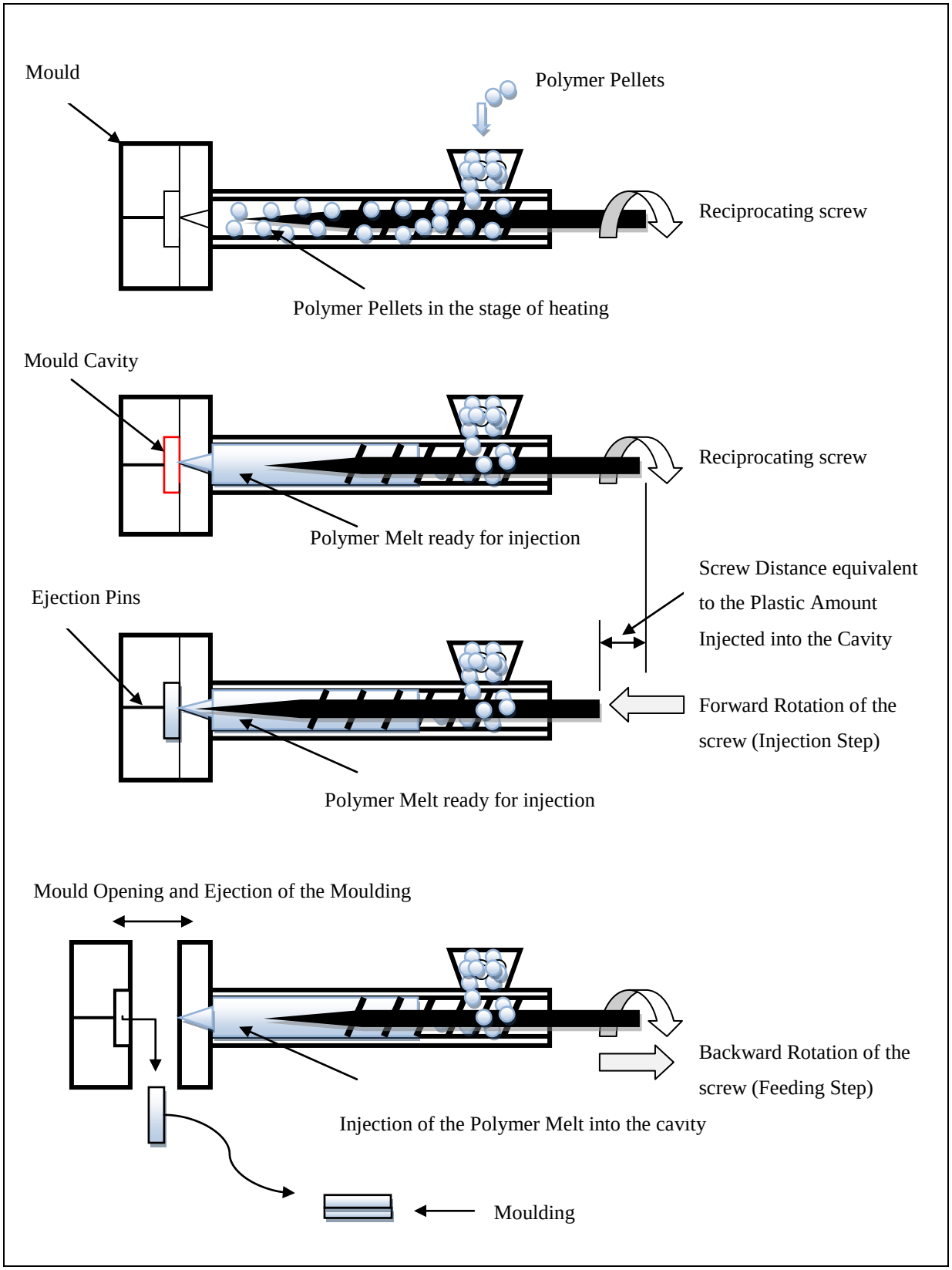

Figure 3.30 Schematic Representation of the Injection Moulding Process Steps

3.2.7.2 Procedure

The extrusion moulding was performed by means of a *Klöckner Ferromatik*, model *F60*, injection moulding machine, as shown in *Figure 3.30*; having *clamping force* around *600 kN*, a *desiccant dryer model-Dri Air AHM1* and a pair of removable mould parts to produce dumbbells and impact bars, as shown in *Figure 3.31*.

Figure 3.31 *Klockner Ferromatik* Machine

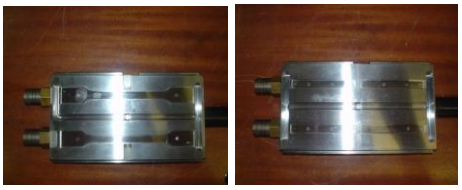

Figure 3.32 Mould Parts

Prior to experimentation, all the processed materials were dried in advance for *5 hours* under a temperature of *120^{o}C*. In the beginning, *test processing* was performed to familiarise with the operating system of the *Klockner Ferromatic* injection moulding machine. The processing conditions of the *Klockner Ferromatic* were optimised around the PET processing temperature range of *250-260^{o}C*. Unlike extrusion, for injection moulding, to allow excellent flow of material it was necessary to increase the temperature of the *nozzle zone* to *190 ^{o}C*, this did not affect the material due to the very short *time of residence*. The optimised processing conditions with temperatures ranging from *260^{o}C* at *feed* to a *nozzle* temperature of *290^{o}C*, allowed the processing of fully dimensioned *test mouldings*. These optimised processing conditions, as listed in *Table 3.6* below, were set to produce all the required *dumbbells* and *impact bars* of non contaminated rPET-bg and contaminated rPET-bg with HDPE or PP.

Material	Melt Temperatures (°C)				Injection Pressure (Bars)	Packing Pressure (Bars)	Mould Temp. (°C)	Injection Time (s)	Packing Pressure (%)
	Rear Zone	Middle Zone	Front Zone	Nozzle Zone					
rPET-bg	260	260	270	290	180	75	60	1.35	45%

Table 3.6 Temperature Settings of the Klockner Ferromatik

During the optimisation of the processing conditions, the *shot volume*, i.e. moulding weight, was optimised simultaneously. The high injection pressure generated mouldings filled to *76%* of the full *shot volume*, equivalent to a *screw-back distance* of length **A**. The remaining *volume* was optimised by applying a *packing pressure*, which increased the *screw-back distance* of length **A** with an additional displacement of length **B** equals to *20%* of **A**. Then, an additional *cushioning*, where the *screw-back distance* of length (**A+B**) was gradually increased with a displacement of length **C** equals to *10%*, as shown in *figure 3.32*. The back-screw distance (**A+B+C**) was slightly optimised and balanced until well dimensioned mouldings of *dumbbells* and *impact bars*, as shown in *figures 3.33* to *3.35*, were obtained free of any flashing.

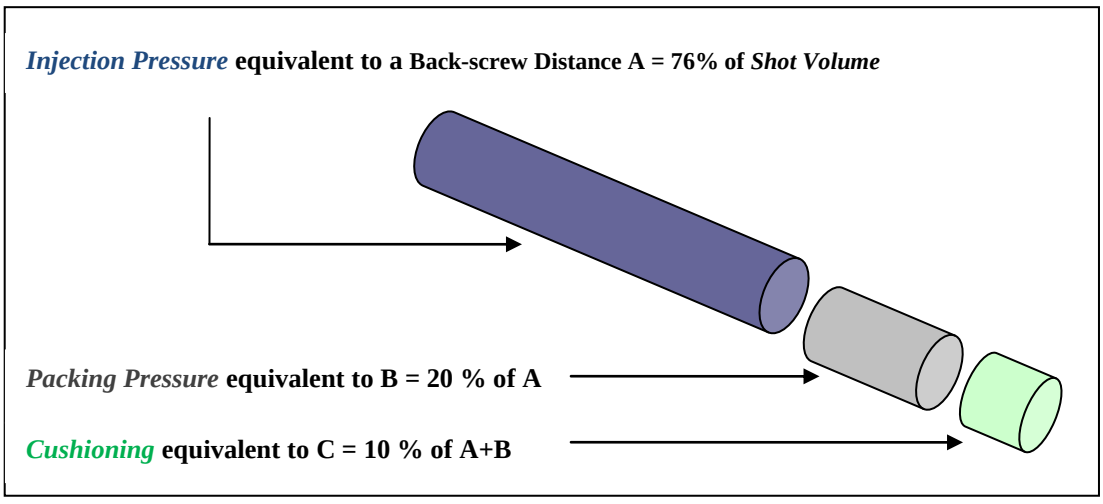

Figure 3.33 Shot Volume and Screw-back Displacement Relationship

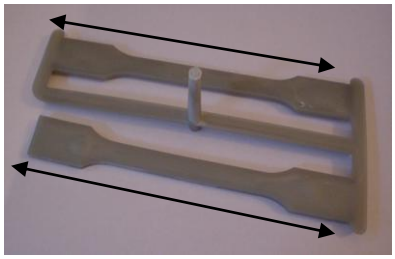

Figure 3.34 Moulding of 2 Dumbbells

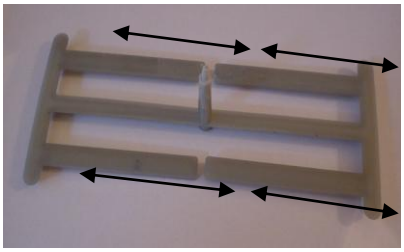

Figure 3.35 Moulding of 4 Impact Bars

Then, test mouldings of *optimised shot volume* were produced, weighted and a maximum *average weight* of *40g* per moulding was taken as reference. An amount of *2.2kg* was assumed enough to produce at least *55* mouldings; it was assumed that approximately 50% of the mouldings will be rejected during processing and approximately 50% of the remaining *specimens* may fail during the mechanical testing. Also, this amount of *2.2kg* is equivalent to *333 bottles* of *500ml* and a weight of *6.6 g* each, which was considered the lightest bottle made by *KRONES* [155].

In this work, *extruded pellets* of non contaminated rPET-bg were injection moulded into *dumbbells* and *impact bars* in *experiment 1*. The 10 best of the produced mouldings were analysed visually, checked for any anomalies and the selection was narrowed to 5 of the 10 mouldings, which were weighted and their *dimensions of interest* measured and recorded, as shown in *Figure 3.36* below.

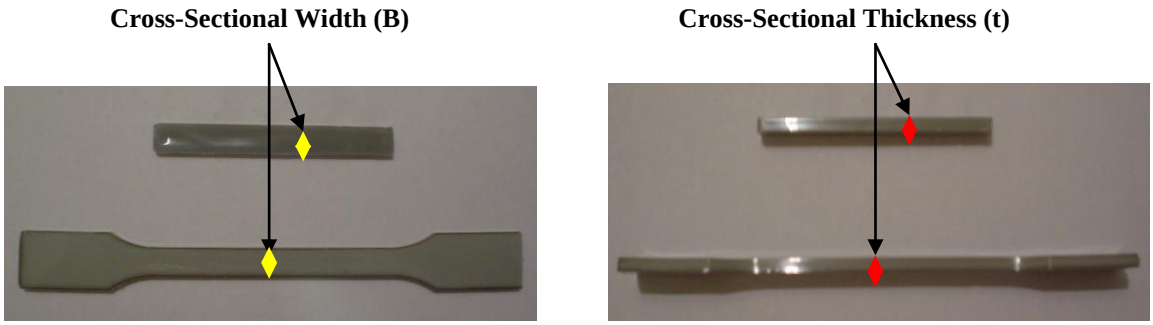

Figure 3.36 Dimensions of Interest of Specimens

Similarly, in *experiments 3* to *5*, respectively *extruded pellets* of rPET-bg contaminated with *5%*, *10%* and *15%* HDPE were injection moulded into *dumbbells* and *impact bars*, and selection was done as previously cited with the non contaminated rPET-bg mouldings. And similar methodology applied in *experiments 6* to *8,* where respectively *extruded pellets* of rPET-bg contaminated with *5%*, *10%* and *15%* PP were injection moulded into *dumbbells* and *impact bars.*

Finally, after each processing operation, the injection machine was purged, switched off, the operating area cleaned thoroughly and the *dumbbells and impact bars* of non contaminated rPET-bg and the rPET-bg contaminated with HDPE or PP at various percentages were respectively taken to the next stage.

- Analysis of *samples* from the *mouldings* by DSC, FTIR and MFR.
- Testing the *dumbbells* and *impact bars* for their tensile and impact properties.

3.3 Chronology of Experimental Work

The experimental work was performed in *10 experiments*; *8 experiments* were performed in *stage 1* and *2* experiments in *stage 2*.

Stage 1

Experiment 1: *Non Contaminated rPET-bg*

This experiment dealt with the identification and the investigation of the *thermal*, *spectroscopic* and *flow* properties of the non contaminated rPET-bg flakes and their *extrusion* into *pellets* and investigation of the variation of properties thereafter.

The sequential events of the experiment were as follow:

- Analysis of the non contaminated rPET-bg flakes for their thermal properties by DSC, as described in *Section 3.2.1.2*.
- Analysis of the non contaminated rPET-bg flakes for their spectroscopic properties by FTIR, as described in *Section 3.2.2.2*.
- Analysis of the non contaminated rPET-bg flakes for their flow properties by MFR, as described in *Section 3.2.3.2*.
- *Extrusion* of the non contaminated rPET-bg flakes into non contaminated *pellets*, as described in *Section 3.2.6.2*.
- Analysis of non contaminated *extruded samples* by DSC, FTIR and MFR.

Experiment 2: *Non Contaminated rPET-bg*

This experiment dealt with the *injection moulding* of non contaminated rPET-bg *extruded pellets* into *dumbbells* and *impact bars* and investigation of the variation of properties thereafter.

The sequential events of the experiment were as follow:

- *Injection moulding* of the *extruded pellets* into tensile *dumbbells* and *impact bars*, as described in *Section 3.2.7.2*.
- Analysis of *injection moulded samples* by DSC.
- Analysis of *injection moulded samples* by FTIR.
- Analysis of *injection moulded samples* by MFR.
- *Tensile* testing of the *dumbbells*, as described in *Section 3.2.4.2*.
- *Impact* testing of the *bars*, as described in *Section 3.2.5.2*.

The following *Flow Chart 1* shows the methodical steps of *experiments 1* and *2*:

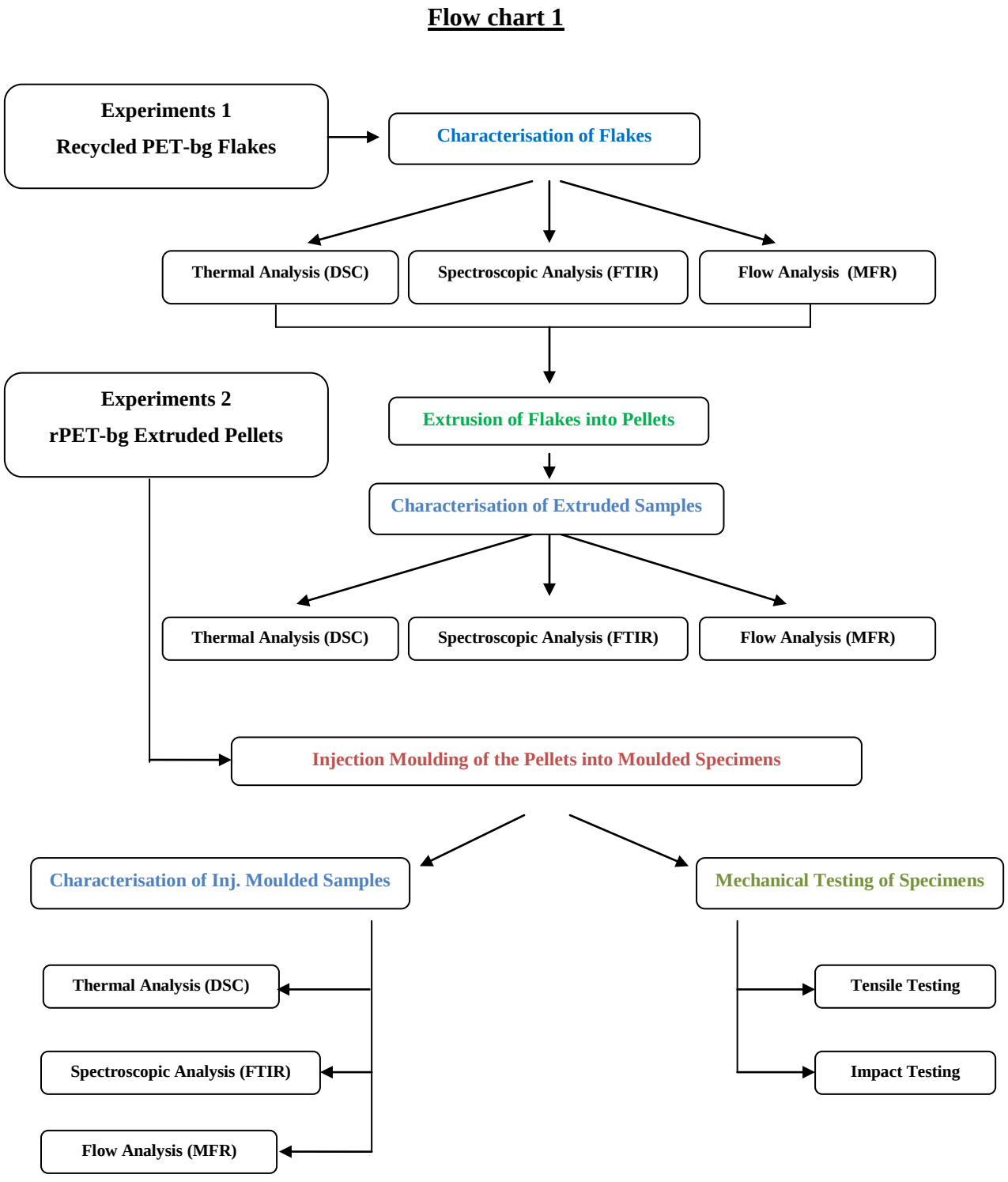

Figure 3.37 Flow Chart Showing the Steps in *Experiments 1* and *2*

Experiments 3 to 5: *rPET-bg Contaminated* with *HDPE*

These experiments dealt with the contamination of rPET-bg flakes with small amounts of HDPE at various percentages, ranging from *5%, 10%* and *15%* and the investigation of their influence on the properties of the matrix.

The sequential events of the experiment were as follow:

Experiment 3: *95% rPET-bg Contaminated* with *5% HDPE*

- *Extrusion* of the rPET-bg flakes contaminated with *5%* HDPE into *pellets.*
  .
- Analysis of *extruded samples* by DSC, FTIR and MFR.
- *Injection moulding* of the *extruded pellets* into tensile *dumbbells* and *impact bars.*
- Analysis of *injection moulded samples* by DSC, FTIR and MFR.
- *Tensile* testing of the *dumbbells* and *impact* testing of the *bars.*

Experiment 4: *90% rPET-bg Contaminated* with *10% HDPE*

- The sequential events in this experiment were similar to those performed in *experiment 3*.

Experiment 5: *85% rPET-bg Contaminated* with *15% HDPE*

- The sequential events in this experiment were similar to those performed in *experiment 3* and *4*.

Experiments 6 to 8: *rPET-bg Contaminated* with *PP*

These experiments dealt with the contamination of rPET-bg flakes with small amounts of PP at various percentages, ranging from *5%, 10%* and *15%* and the investigation of their influence on the properties of the matrix.

The sequential events of the experiment were as follow:

Experiment 6: *95% rPET-bg Contaminated* with *5% PP*

- *Extrusion* of the rPET-bg flakes contaminated with *5%* HDPE into *pellets.*
  .
- Analysis of *extruded samples* by DSC, FTIR and MFR.
- *Injection moulding* of the *extruded pellets* into tensile *dumbbells* and *impact bars.*
- Analysis of *injection moulded samples* by DSC, FTIR and MFR.
- *Tensile* testing of the *dumbbells* and *impact* testing of the *bars.*

Experiment 7: *90% rPET-bg Contaminated* with *10% PP*

- The sequential events in this experiment were similar to those performed in *experiment 6.*

Experiment 8: *85% rPET-bg Contaminated* with *15% PP*

- The sequential events in this experiment were similar to those performed in *experiment 6* and *7.*

The following *Flow Chart 2* shows the methodical steps followed in *experiments 3 to 8*.

Flow chart 2

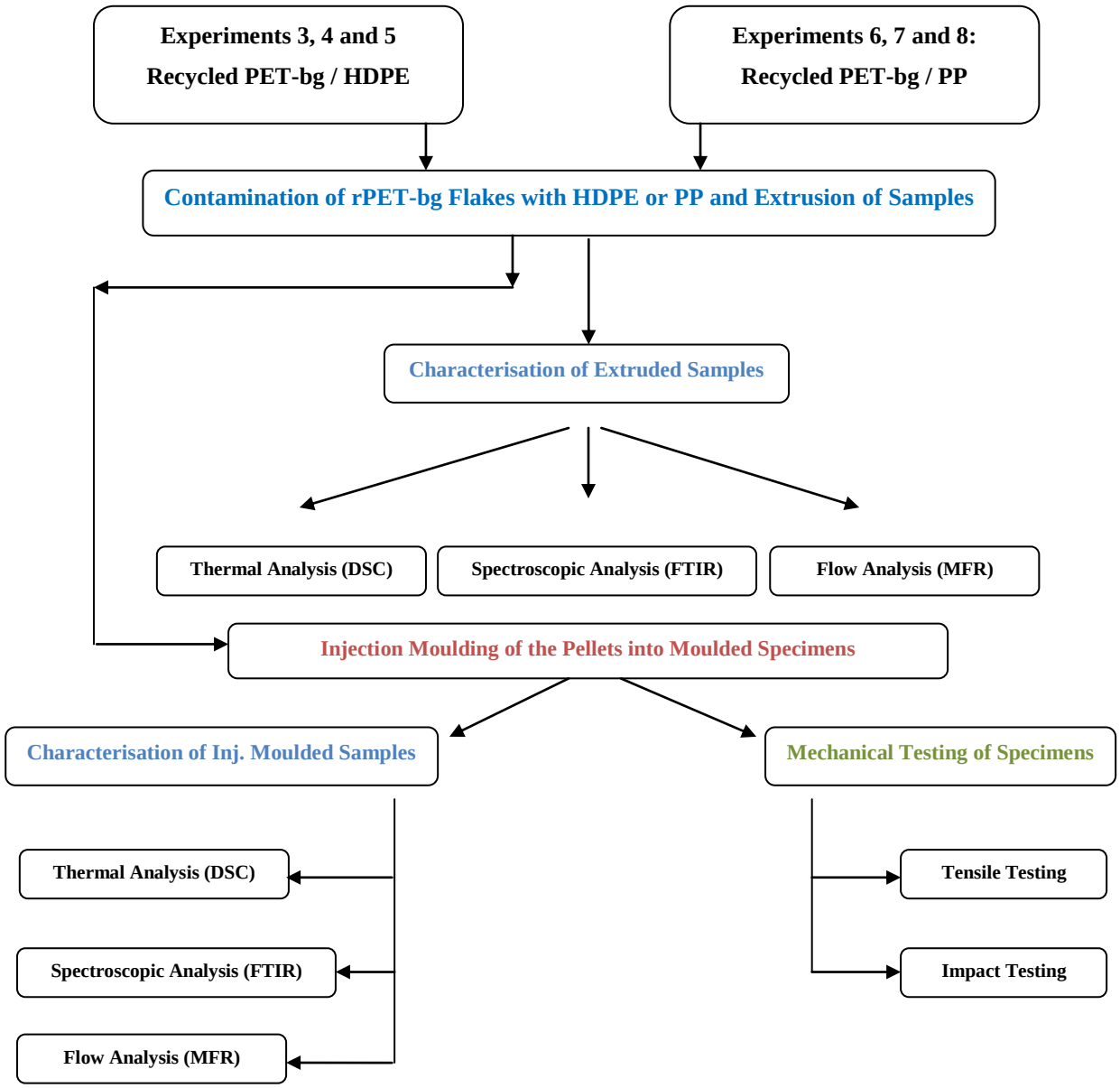

Figure 3.38 Flow Chart Showing the Steps in *Experiments 3 to 8*

Stage 2

Experiment 9: *rPET-bg Contaminated* with *5% PP*

This experiment dealt with the investigation of the effects of *cooling rates* on the *thermal characteristics* of non contaminated rPET-bg and rPET-bg contaminated with 5% PP, with emphasis on *crystallinity*, for *non-isothermal-crystallisation* process, as described in *Section 3.2.1.2*. The results were analysed by *Avrami* and *Ozawa equations* for *non-isothermal crystallisation process*, as described respectively in *Section 1.2.3.2*.

The sequential events of the experiment were as follow:

- *Extrusion* of the rPET-bg flakes contaminated with *5%* PP into *pellets*, as described in *Section 3.2.6.2.*
  .
- Analysis of *extruded samples* by DSC at a heating / cooling rate of $10^{o}C/min$, as described in *Section 3.2.1.2*.
- Analysis of *extruded samples* by DSC at a heating / cooling rate of $15^{o}C/min$.
- Analysis of *extruded samples* by DSC at a heating / cooling rate of $20^{o}C/min$.
- Analysis of *extruded samples* by DSC at a heating / cooling rate of $25^{o}C/min$.
- Analysis of obtained data by *Avrami equation* for non-isothermal crystallisation.
- Analysis of obtained data by *Ozawa equation* for non-isothermal crystallisation.

Experiment 10: *rPET-bg Contaminated* with *5% PP*

This experiment dealt with the investigation of the effects of *repetitive extrusion* on the *thermal characteristics* of non contaminated rPET-bg and rPET-bg contaminated with *5% PP*, with emphasis on *crystallinity*, for *non-isothermal* process, as described in *Section 3.2.1.2*. The results were analysed by *Avrami equation* for *non-isothermal process*, as described in *Section 1.2.3.2*.

The sequential events of the experiment were as follow:

- *1st extrusion cycle* of rPET-bg flakes contaminated with *5%* PP into *pellets*, as described in *Section 3.2.6.2* and analysis of *extruded samples* by DSC at heating/cooling rate of *10°C/min*, as described in *Section 3.2.1.2*.

- *2nd extrusion cycle* of rPET-bg flakes contaminated with *5%* PP into *pellets* and analysis of *extruded samples* by DSC, as in *1st extrusion cycle*.

- *3rd extrusion cycle* of rPET-bg flakes contaminated with *5%* PP into *pellets* and analysis of *extruded samples* by DSC, as in *1st extrusion cycle*.

- *4th extrusion cycle* of rPET-bg flakes contaminated with *5%* PP into *pellets* and analysis of *extruded samples* by DSC, as in *1st extrusion cycle*.

- *5th extrusion cycle* of rPET-bg flakes contaminated with *5%* PP into *pellets* and analysis of *extruded samples* by DSC, as in *1st extrusion cycle*.

- Analysis of obtained data by *Avrami equation* for non-isothermal crystallisation.

The following *Flow Chart 3* shows the methodical steps of *experiment 9*:

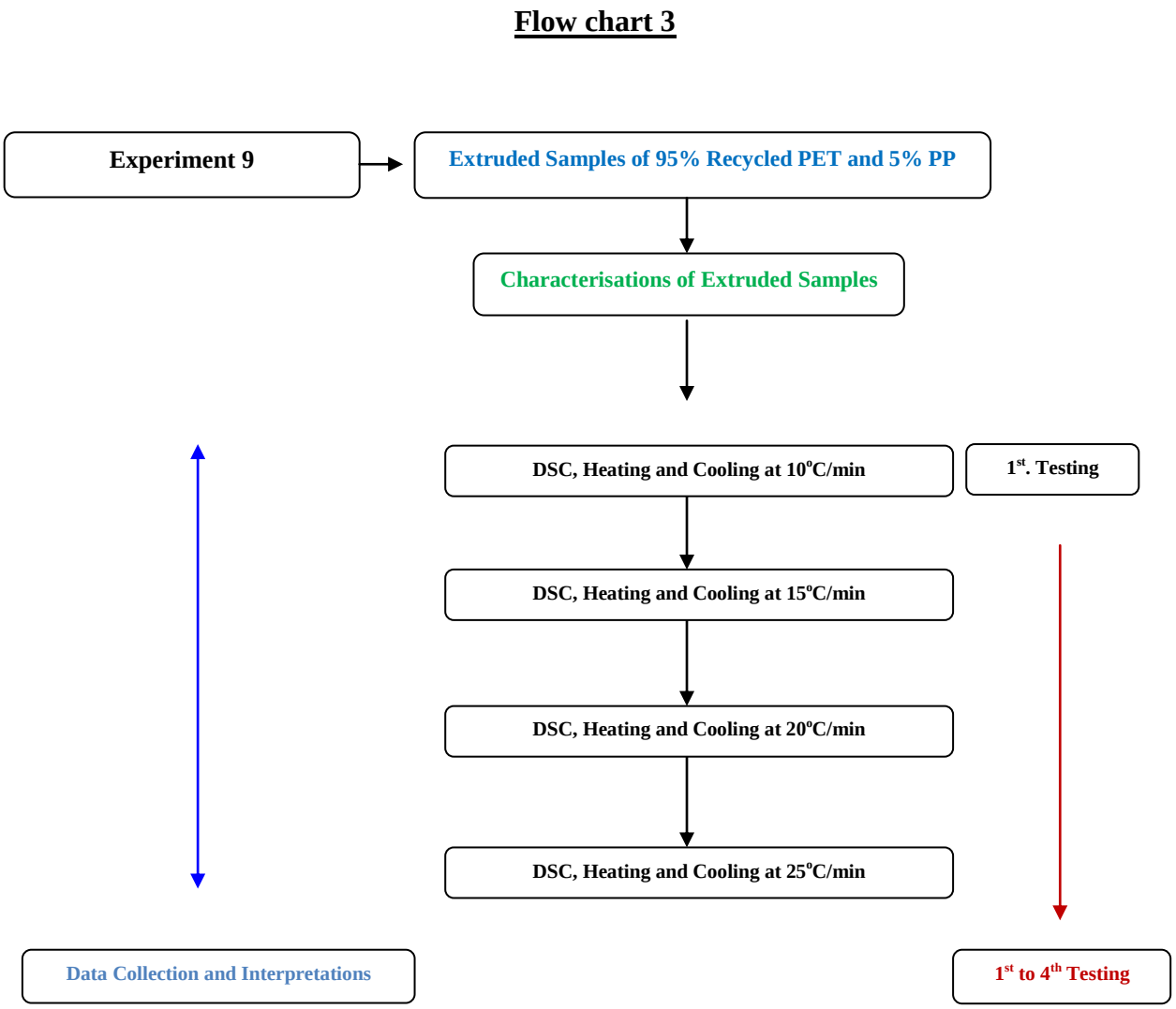

Figure 3.39 Flow Chart Showing the Steps in *Experiment 9*

The following *Flow Chart 4* shows the methodical steps of *experiment 10*:

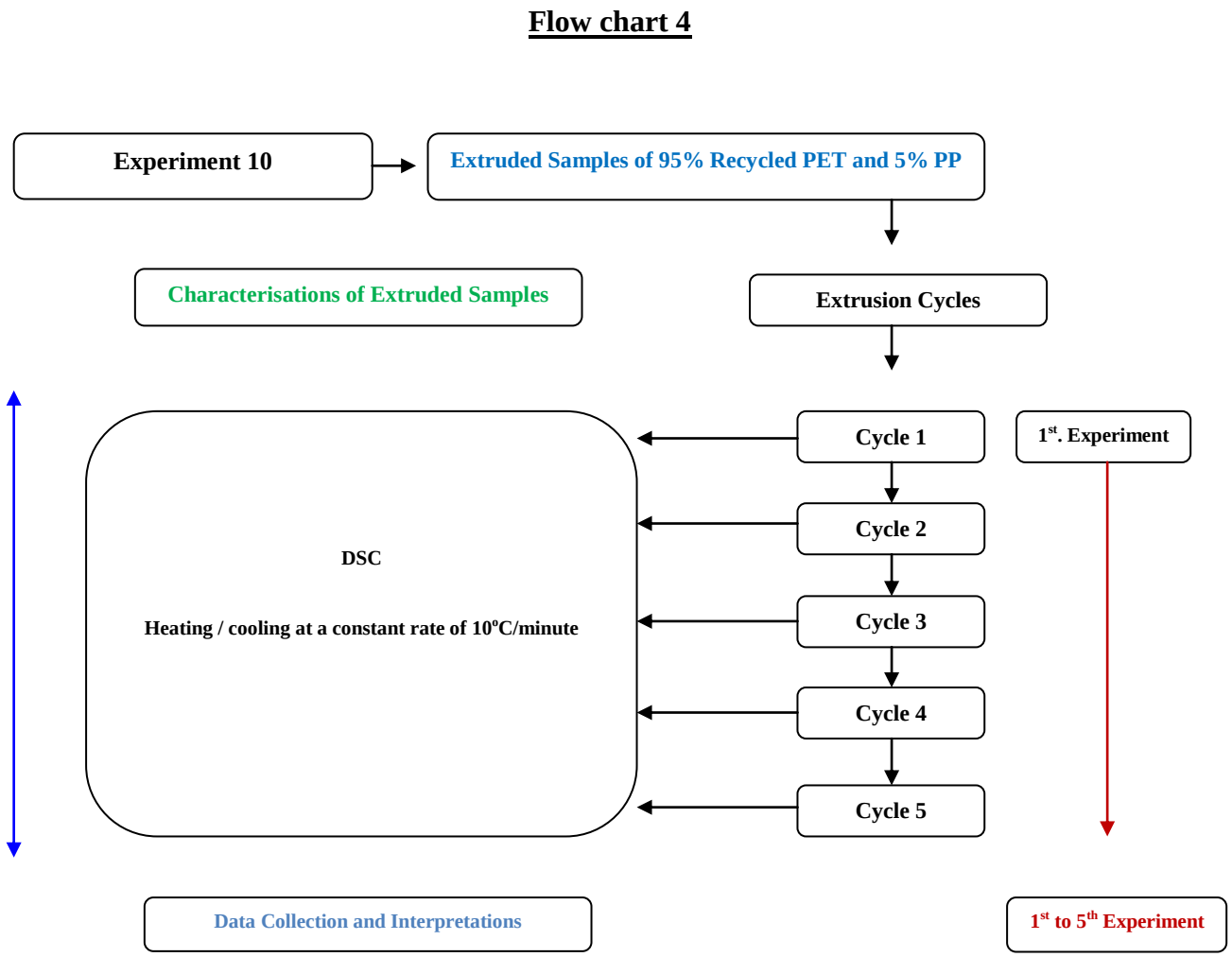

Figure 3.40 Flow Chart Showing the Steps in *Experiment 10*

The following *Flow Chart 5* shows the methodical steps of analyses:

Flow chart 5

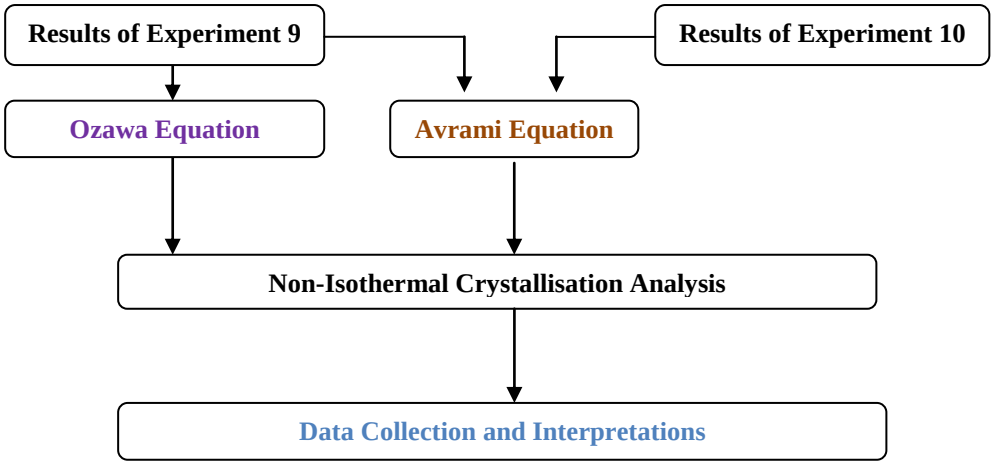

Figure 3.41 Flow Chart Showing the *Validation Analyses* in *Experiments 9* and *10*

Due to the volume of data obtained during the performance of experiments, it was decided to present the results and their discussions under individual chapters in the purpose to avoid confusion and facilitate the understanding of the contents.

In each chapter, the results were presented first and discussed individually. Then, comparative discussions were performed to shed the light on the various changes. Additionally, more data are still recorded in appendices and available for further consultation.

The *results* (*observations*) obtained in each experiment, for each analysis or test, were evaluated statistically. The statistical tool used to evaluate and determine the *acceptance* or *rejection* of *observations* (*results*) is *Dixon's Q Test*; this simplified test proved efficient in determining *outliers* within the samples' *observations*. Finally, the *samples' means* were estimated with *error margins* and at *95% confidence interval* as described in ***Appendix 9***.

The data obtained in both ***stages*** were statistically analysed for their validity, accurately, investigated, compared with other research works, interpreted and correlated.

Note: - Results and discussions of ***Stage 1*** are reported in ***Chapters 4, 5*** and ***6.***
Additional information of ***Stage 1*** is available in ***Appendices 4, 5*** and ***6***.

- Results and discussions of ***Stage 2*** are reported in ***Chapters 7*** and ***8.***
Additional information of ***Stage 2*** is available in ***Appendices 7*** and ***8***.

Stage 1

Chapter 4

Non Contaminated rPET-bg

4.1 Results and Discussions

This section discusses the various experimental results of non contaminated rPET-bg obtained in *experiments 1* and *2*, in the purpose to identify and investigate the various properties and the potential of the supplied rPET-bg flakes before and after processing.

As previously mentioned in *Section 3.1.1*, the recycled PET-bg flakes were supplied without any technical information which is typical for recycled materials sourced from wastes even where the product range is restricted as in the case of rPET-bg. Samples of *non contaminated flakes*, *extruded pellets* and injection moulded *dumbbells* and *impact bars* were analysed for their thermal, spectroscopic, flow and mechanical properties, as described in *Section 3.2*.

4.1.1 DSC results of *Flakes*

In *experiment 1*, the DSC analysis yielded the data below.

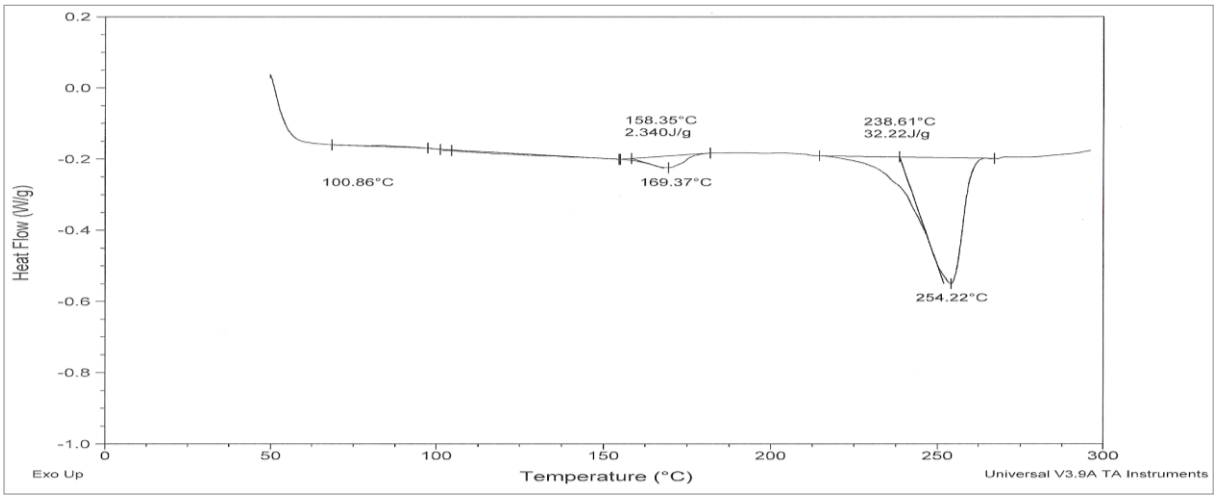

Figure 4.1 DSC Thermogram of non contaminated rPET-bg Flake 1

Material	**Samples of non contaminated rPET-bg Flakes**							
	T_g (°C)	T_m (°C)	ΔH_m (J/g)	T_c (°C)	ΔH_c (J/g)	ΔH_m^0 (J/g)	X_c (%)	T_d (°C)
Run 1	100.86	254.22 169.37	32.22 2.34	Nil	Nil	140	23.01	Nil
Run 2	100.92	254.51 168.96	20.09 0.99	Nil	Nil	140	14.35	Nil
Run 3	119.84*	253.56 167.05	23.98 1.17	Nil	Nil	140	17.13	Nil
Mean (μ)	**100.89**	**254.10** **168.46**	**25.43** **1.50**				**18.16**	
STDEV (σ)	0.04	0.49	6.19				4.42	
ST. Error ($S_E = \sigma/n^{0.5}$)	0.03	0.28	3.58				2.55	
CI (95%), ($\mu \pm 1.96S_E$)	$\mu \pm 0.06$	$\mu \pm 0.55$	$\mu \pm 7.01$				$\mu \pm 5.01$	

Table 4.1 DSC Data of non contaminated rPET-bg Flakes

*: This' an "outlier" displayed but not included in the calculation.
Data in blue is related to rPET-bg (secondary crystals melting peak).

Note: Additional DSC Thermograms are available in ***Appendix 4 (1)***.

From the above results, the average *glass transition temperature*, T_g, of *100.89±0.06°C* was within the *PET* glass transition broad range of *69-115°C* as reported in the literatures [156, 157]. The flakes exhibited *multiple endothermic transitions* shown in the form of *double melting peaks* of average *melting temperatures*, T_m, respectively *168.46°C* and *254.10 ±0.55°C*; this phenomenon is characteristic of *PET*. In their works, *Rodriguez et al.* [158], *Mathot* [159] and *Kampert et al.* [160] reported that this behaviour related to endothermic transitions is linked to the partial melting and re-crystallisation and re-melting of crystals, which re-organised in more effective orientation as the temperature increased. *Wang et al.* [161] went further and concluded, in their extensive investigation of the nature of secondary crystallisation of PET, that the first melting peak is that of the secondary crystals and the second melting peak is attributed to the primary crystals; where the respective enthalpies, ΔH_m, of flakes were *1.50 J.g^{-1}* and *25.43±7.01 J.g^{-1}*. The *primary* crystals *average* T_m of *254.10 ±0.55°C* is within the PET melting temperature range of *255-265°C* as reported by *Awaja* and *Pavel* [153]. Other literature [162] reported that *265°C* is for higher crystalline PET. The *degree of crystallinity*, X_c, of *18.16±5.01%* is low and typical for a bottle grade material. The absence of *exotherms* gave an insight on the molecular chains entanglement and that their re-organisation and orientation were over-ridden by a fast melting; this showed that the flakes originated from a product which was very fast cooled at processing and that chains re-organisation and crystallisation were prevented in the purpose to produce a transparent product. Furthermore, the flakes *average enthalpy* of *25.43±7.01 J.g^{-1}*compared with that of crystalline PET of *140 J.g^{-1}*, as reported in the literature [131], showed that the flakes originated from an *amorphous* material which underwent cooling stages at elevated cooling rates resulted in low crystal domains which required less heat consumption for melting. Hence, the flakes originated from an *amorphous* material intended to produce clear and transparent products, such as *bottles*.

In addition to what the thermal analysis by DSC revealed, spectroscopic analysis by FTIR was performed to gather more information about the flakes origin.

4.1.2 FTIR results of *Flakes*

In *experiment 1*, the FTIR analysis yielded the data below.

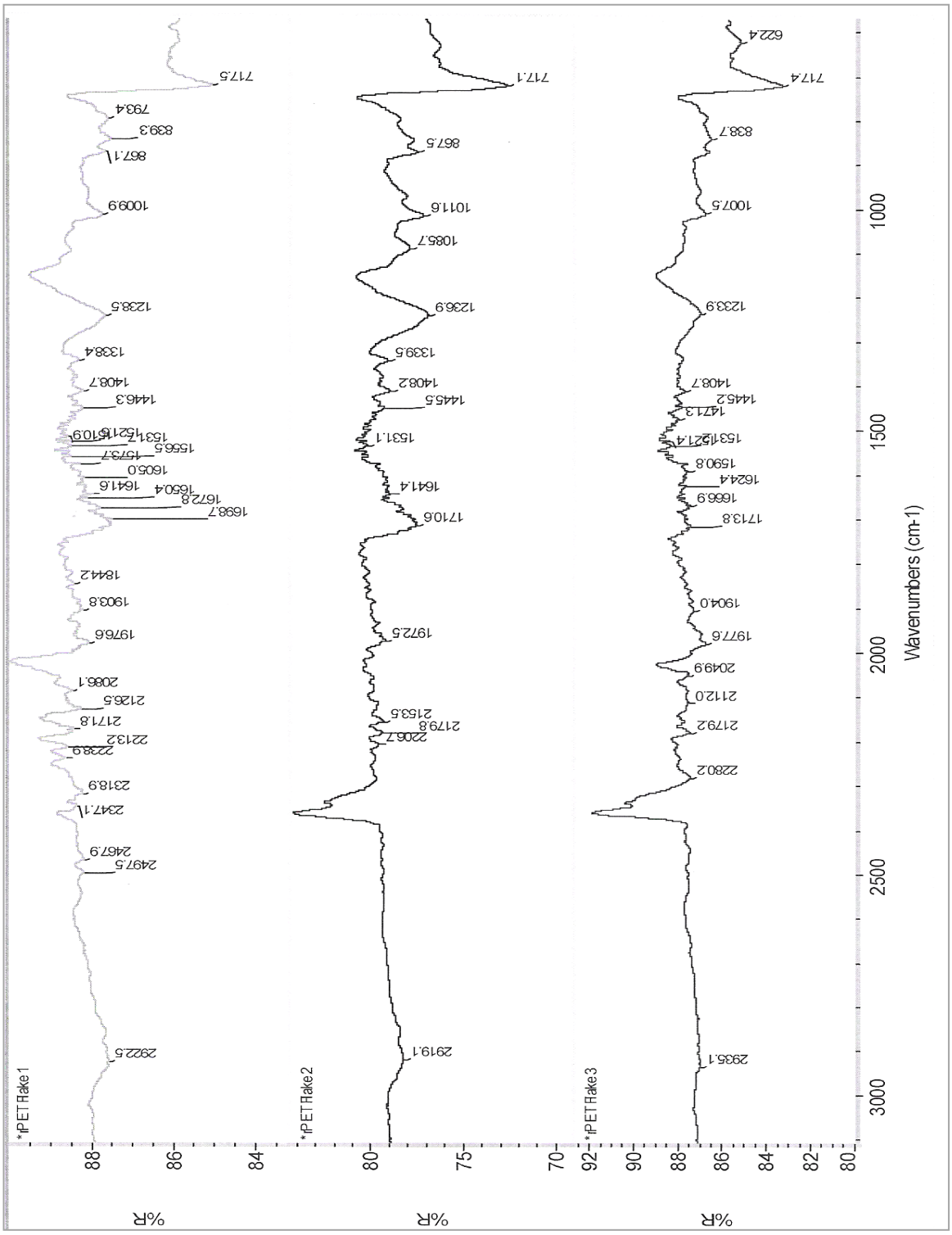

Figure 4.2 FTIR Spectra of non contaminated rPET-bg Flakes

Material	Samples of non contaminated rPET-bg Flakes

Wavenumber (cm^{-1})			Bond	Wavenumber (cm^{-1})	Compound Type
Scan 1	**Scan 2**	**Scan 3**			
2922	2919	2935	C-H	2850-2960	Alkane
1698	1710	1713	C=O	1670-1760	Ester
1521 to 1605	1531	1521 to 1590	C=C	1500-1600	Ester Ar. Ring
717 to 867	717 to 867	622 to 838	and C-H	Below 900	Ester Ar. Ring
1238	1085 to 1239	1233	C-O	1000-1260	Ester

Table 4.2 FTIR Data of non contaminated rPET-bg Flakes

The results above showed the presence of molecular *bonds* and *groups* similar to the ones of *PET* molecular structure, shown in *Figure 4.3* below.

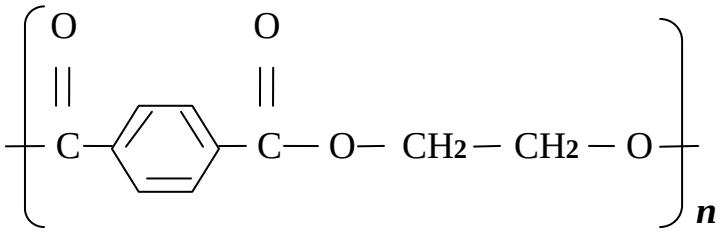

Figure 4.3 Molecular Repeat Unit of PET

The infrared spectra of the *flakes* illustrated various bonds, such as *C-H*, *C=C*, strong *C=O*, *C-O* and the broad *C-H* bonds. By correlating the results to the literature [163], the investigation confirmed that the absorptions occurring between *622* and *867cm*$^{-1}$ fall into the level expected for the *C-H bending* of an *aromatic ring group* of an *ester* (below *900cm*$^{-1}$). The absorptions occurring between *1521* and *1605 cm*$^{-1}$ fall into the range expected for *C=C stretch* of an *aromatic ring group* of an *ester* (*1500-1600cm*$^{-1}$). The strong *absorptions* occurring between *1698* and *1713cm*$^{-1}$ fall into the absorption expected for *C=O stretch* of an *ester* (*1670-1760cm*$^{-1}$). And the *absorptions* occurring between *1085* and *1239cm*$^{-1}$ fall into the range expected for *C-O stretch* of an *ester* (*1000-1260cm*$^{-1}$). And, one can see the *C=C*, *C=O* and *C-O* which fall into the 'fingerprint' region of an ester. Also, the presence of absorptions between *2919* and

2935cm^{-1}, where high frequency is explained by the low mass of the *hydrogen atom*, fall into the absorption expected for the *broad C-H stretch* of an *alkane* (*2850-2960cm^{-1}*). The mentioned *molecular groups* were identified as being identical or within the absorptions of those of *PET*.

Furthermore, the flow analysis by MFR of the flakes revealed the following result.

4.1.3 MFR results of *Flakes*

In *experiment 1*, the MFR analysis yielded the data below.

Material	**Samples of non contaminated rPET-bg Flakes**		
Extrudates	**Weight (g)**	**Time (s)**	**MFR (g/10min)**
Run 1	1.502	15	60.080
Run 2	1.046	10	62.760
Run 3	0.510	05	61.200
Mean (μ)			**61.35**
STDEV (σ)			1.35
ST. Error ($S_E = \sigma/n^{0.5}$)			0.78
CI (95%), ($\mu \pm 1.96 S_E$)			$\mu \pm 1.52$

Table 4.3 MFR of non contaminated rPET-bg Flakes

The *melt flow* results above showed the material ease in flowing with minimal resistance and the flakes' *average MFR value* of *61.35±1.52 g/10min* compared to the average MFR of virgin PET which is around *35g/10min* as mentioned in *Table 3.3, Section 3.1.3*, indicated reduced *viscosity* as a result of molecular chains-scissions as a result of processing and *recycling*. In their work, *Baker* and *Barry* [164] reported that *extrusion blow moulding* requires a melt flow rate no more than *2g/10min*, whereas other processes, such as *injection* and *blow mouldings* require *higher melt rates* in a range of *6-60g/10min*. As a comparison, the *average MFR value* of *61.35±1.52 g/10min* showed that the flakes

originated from a material used in a process requiring materials of high melt index, such as *injection moulding* or *blow moulding*, a process mainly using engineering materials of excellent ease of flow coupled with excellent stretch-ability, such as *PET*, and intended to produce complex products, such as *bottles*.

Still in *experiment 1*, after analysing and *partially* identifying the *non contaminated* rPET-bg flakes by DSC, FTIR and MFR, the *flakes* were *extruded* into *non contaminated pellets* and samples were analysed again by DSC, FTIR and MFR and the variations of properties after *extrusion* were investigated.

In terms of extrusion processing, the uniform distribution of heat and the residence time of the material allowed the machine's twin-screw to extrude at stable speed and torque. The speed fluctuated between *110* and *115 rpm* and the % torque between *50* and *60*, as shown in *Table 4.4* below. At these processing conditions, the non contaminated rPET-bg was extruding uniformly with certain dimension stability and producing acceptable *extruded pellets*, as shown in *Figure 4.2 below*.

Material	Screw Speed			% Torque		
	Min. (rpm)	Max. (rpm)	Mean (rpm)	Min. (%)	Max. (%)	Mean (%)
Non Contaminated rPET-bg	110	115	112.50 ± 2.5	50	60	55 ± 5

Table 4.4 Screw Speed and % Torque of non contaminated rPET-bg

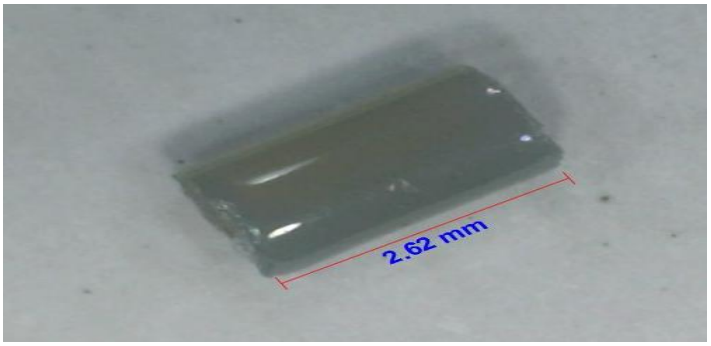

Figure 4.4 A non contaminated rPET-bg Extruded Pellet

The visual observation showed *extrudates* with no swelling or cracking, brittle, not ductile, with typical *PET* characteristics, and grey transparent, as shown in *Table 4.5* below. These are the result of well optimised processing conditions. The resulting grey transparent colour of the *extruded pellets* showed that the multi-coloured rPET-bg *flakes* were homogeneously melted and well compounded in the *extruder* barrel. The microscopic analysis of a cross-sectional area of an *extruded pellet*, magnified 400 times, showed embedded *particulates* considered as *contaminants* in the main matrix of rPET-bg, as shown in *Figure 4.3* below; the presence of these particulates confirmed that the flakes were *recycled* and encountered direct contact with soil and the filtration during the recycling process was inadequate.

Material	Swelling	Brittleness	Ductility	Colour
rPET-bg Extruded Pellets	No	High	No	Grey- Transparent

Table 4.5 Visual Characteristics of non contaminated rPET-bg Extruded Pellets

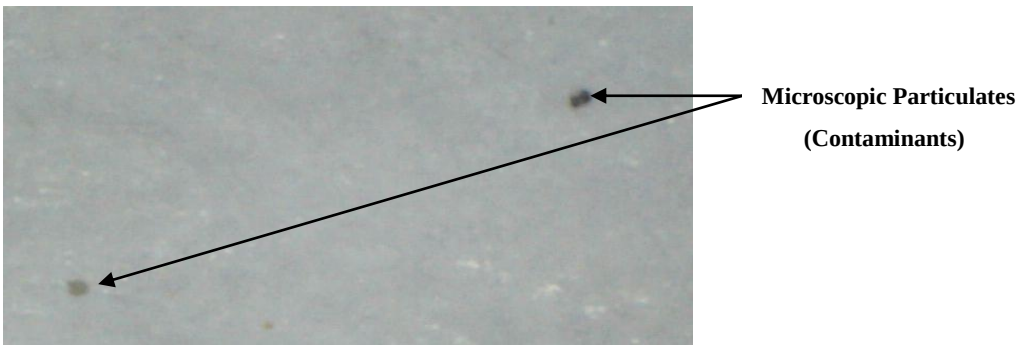

Figure 4.5 Cross-sectional Area of a non contaminated rPET-bg Extruded Pellet magnified 400 times

4.1.4 DSC results of *Extruded Samples*

In *experiment 1*, the DSC analysis yielded the data below.

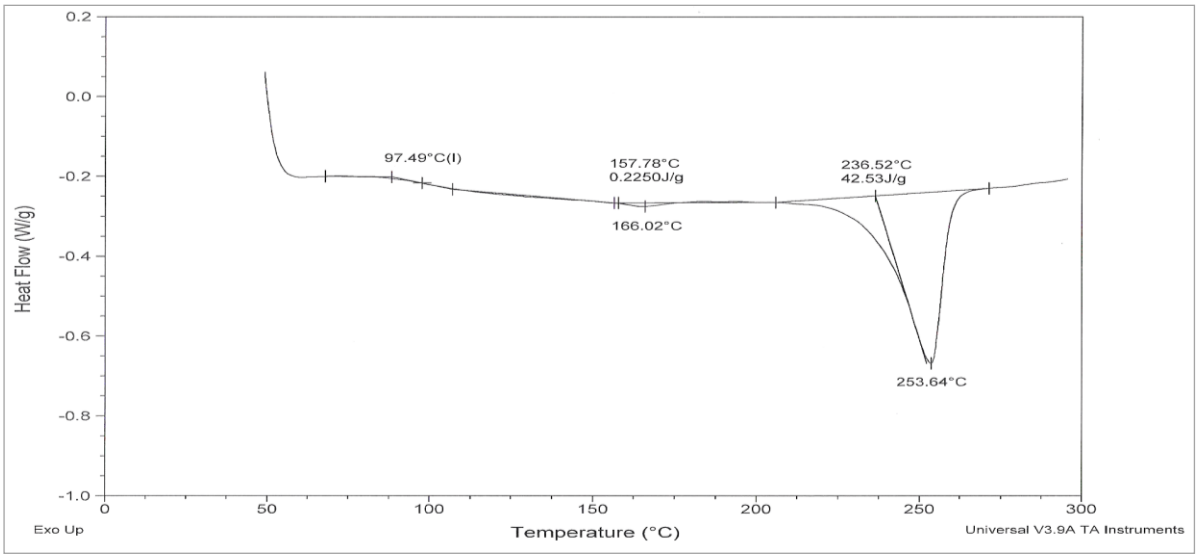

Figure 4.6 DSC Thermogram of non contaminated rPET-bg Extruded Sample 1

Material	**Extruded Samples of non contaminated rPET-bg**							
	T_g (°C)	T_m (°C)	ΔH_m (J/g)	T_c (°C)	ΔH_c (J/g)	ΔH_m^0 (J/g)	X_c (%)	T_d (°C)
Run 1	97.49	253.64 166.02	42.53 0.22	Nil	Nil	140	30.38	Nil
Run 2	104.71	255.85	26.69	Nil	Nil	140	19.06	Nil
Run 3	105.70	254.38 138.94	32.04 0.00	Nil	Nil	140	22.89	Nil
Mean (μ)	**102.63**	**254.62** **152.48**	**33.75** **0.22**				**24.11**	
STDEV (σ)	4.48	1.13	8.06				5.76	
ST. Error ($S_E = \sigma/n^{0.5}$)	2.59	0.65	4.65				3.32	
CI (95%), ($\mu \pm 1.96 S_E$)	$\mu \pm 5.07$	$\mu \pm 1.27$	$\mu \pm 9.12$				$\mu \pm 6.51$	

Table 4.6 DSC Data of non contaminated rPET-bg Extruded Samples

Data in blue is related to rPET-bg (secondary crystals melting peak).

Note: Additional DSC Thermograms are available in ***Appendix 4*** **(*3*)**.

The *extruded samples* average T_g of 102.63 ± 5.07^oC compared to the average T_g of flakes of 100.89 ± 0.06^oC, as shown in *Table 4.7* below, showed broader range of glass transition indicating sporadic domains of short polymer chains, which were further orientated in the convergent flow at the die area, allowed some degree of chains' relaxation and straightening under balanced rate of cooling. This broader range of glass transition indicated that the polymer chains of the extrudates, or *extruded pellets*, were cooled and relaxed at balanced rate.

Materials	T_g (°C)		
	Mean (μ)	**ST. Error ($S_E = \sigma/n^{0.5}$)**	**CI (95%) ($\mu \pm 1.96 S_E$)**
rPET-bg Flakes	**100.89**	0.03	$\mu \pm 0.06$
rPET-bg Extruded Samples	**102.63**	2.59	$\mu \pm 5.07$

Table 4.7 Glass Transition Temperature of non contaminated rPET-bg Flakes and Extruded Samples

The *extruded samples* average T_m of 254.62 ± 1.27^oC compared with the *flakes'* average T_m of 254.10 ± 0.55^oC, as shown in *Table 4.8* below, showed an increase in melting temperature. This is caused by the chains'-scissions; under the heat of the barrel, the polymer melt was subjected to certain degree of thermo-mechanical degradation and chains'-scission; higher number of smaller chains were created which helped in the formation of more tiny *primary crystals* during cooling. The melting of the higher number of tiny *primary crystals* created, contributed to further increase in T_m. The material underwent thermal changes and the *multiple endothermic peaks* exhibited before *extrusion* were minimised due to homogeneous melting of crystals and balanced cooling during extrusion.

Materials	T_m (°C)		
	Mean (μ)	**ST. Error ($S_E = \sigma/n^{0.5}$)**	**CI (95%) ($\mu \pm 1.96S_E$)**
rPET-bg Flakes	**254.10**	0.28	$\mu \pm 0.55$
rPET-bg Extruded Samples	**254.62**	0.65	$\mu \pm 1.27$

Table 4.8 Melting Temperature of non contaminated rPET-bg Flakes and Extruded Samples

The *extruded samples* average ΔH_m of *33.75±9.12J.g*$^{-1}$ compared with the *flakes'* average ΔH_m of *25.43±7.01 J.g*$^{-1}$, as shown in *Table 4.9* below, showed the effect of increased number of *primary crystals*, as explained previously, which required more heat to complete melting. The increased enthalpy confirmed the proportional relationship with melting temperature, which increased too.

Materials	ΔH_m (J.g^{-1})		
	Mean (μ)	**ST. Error ($S_E = \sigma/n^{0.5}$)**	**CI (95%) ($\mu \pm 1.96S_E$)**
rPET-bg Flakes	**25.43**	3.58	$\mu \pm 7.01$
rPET-bg Extruded Samples	**33.75**	4.65	$\mu \pm 9.12$

Table 4.9 Heat of Fusions of non contaminated rPET-bg Flakes and Extruded Samples

The *extruded samples* average X_c of *24.11±6.51 %* compared with the *flakes'* average X_c of *18.16±5.01 %*, as shown in *Table 4.10* below, confirmed that some degree of ordered sporadic *crystal* domains of short chains were created following extrusion, and that the balanced cooling of the extrudates allowed the polymer chains to relax, orientate and helped achieving this order of packing due to the small sizes and ease of mobility of the created short chains. These sporadic crystal domains failed to re-organise during heating, which explained the absence of cold crystallisation exotherms.

Materials	X_c (%)		
	Mean (μ)	**ST. Error ($S_E = \sigma/n^{0.5}$)**	**CI (95%) ($\mu \pm 1.96 S_E$)**
rPET-bg Flakes	**18.16**	2.55	$\mu \pm 5.01$
rPET-bg Extruded Samples	**24.11**	3.32	$\mu \pm 6.51$

Table 4.10 % Crystallinity of non contaminated rPET-bg Flakes and Extruded Samples

4.1.5 FTIR results of *Extruded Samples*

In *experiment 1*, the FTIR analysis yielded the data below.

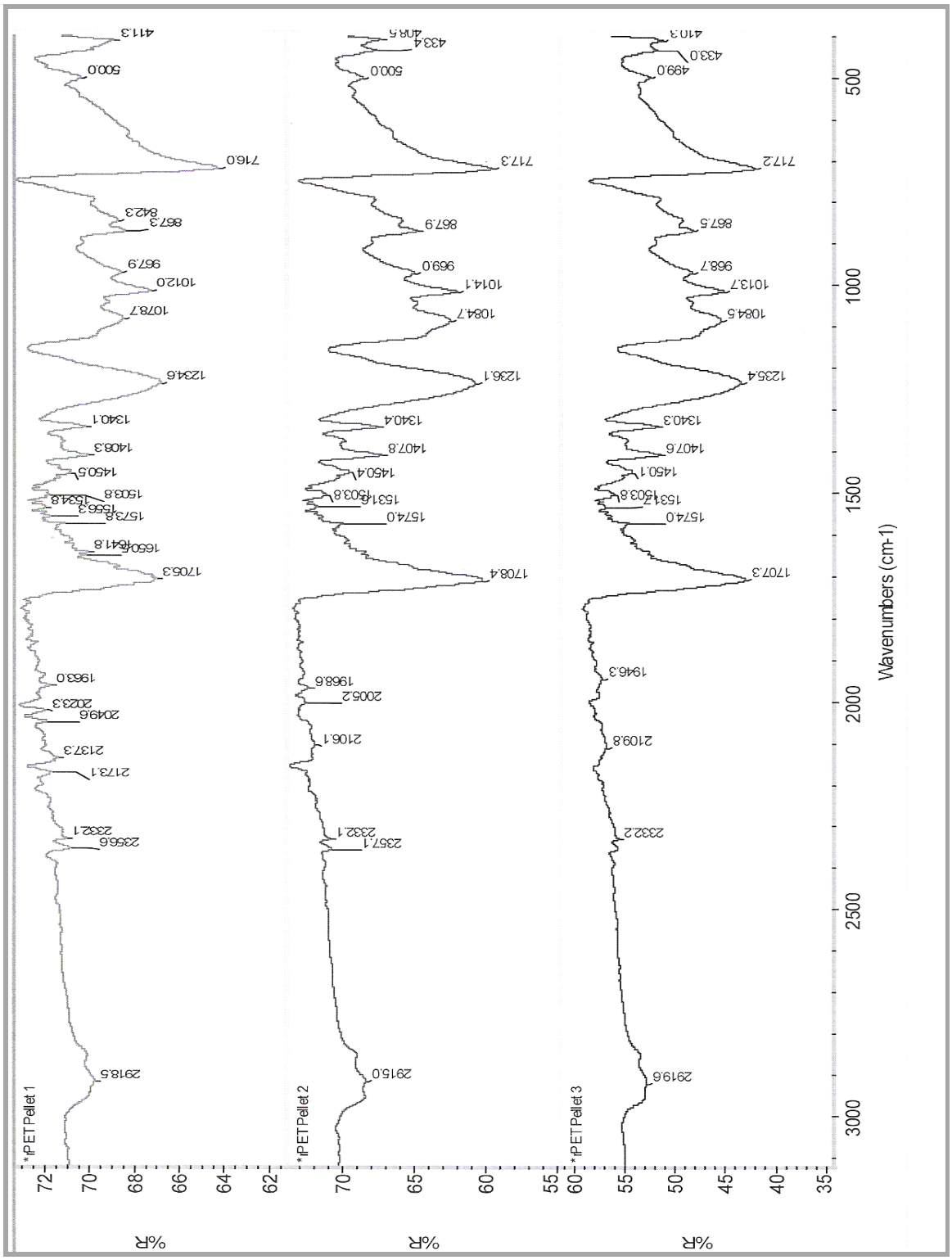

Figure 4.7 FTIR Spectra of non contaminated rPET-bg Extruded Samples

Material	Extruded Samples of non contaminated rPET-bg				
Wavenumber (cm^{-1})			Bond	Wavenumber (cm^{-1})	Compound Type
Scan 1	Scan 2	Scan 3			
2918	2915	2919	C-H	2850-2960	Alkane
1705	1708	1707	C=O	1670-1760 stretch	Ester
1503 to 1573	1503 to 1570	1503 to 1574	C=C	1500-1600	Ester Ar. Ring
411 to 867	410 to 867	410 to 867	C-H	Below 900	Ester Ar. Ring
1234	1084 to 1236	1084 to 1235	C-O	1000-1260	Ester

Table 4.11 FTIR Data of non contaminated rPET-bg Extruded Samples

The results, shown in *Table 4.12* below, showed decreased absorptions of most molecular bonds; the *aromatic ester ring C-H* absorptions at (*622-867cm^{-1}*) in the *flakes* decreased to (*410-867cm^{-1}*) in the *extruded samples*, the *aromatic ester ring C=C* absorptions at (*1521-1605 cm^{-1}*) in the *flakes* decreased to (*1503-1574 cm^{-1}*) in the *extruded samples*, the *ester C=O* absorptions at (*1698-1713cm^{-1}*) in the *flakes* decreased to (*1705-1708cm^{-1}*) in the *extruded samples*, the *ester C-O* absorptions at (*1085-1239cm^{-1}*) in the *flakes* decreased to (*1084-1236cm^{-1}*) in the *extruded samples* and the *alkane group* broad *C-H* absorption at (*2919-2935cm^{-1}*) in the *flakes* decreased to (*2915-2919cm^{-1}*) in the *extruded samples;* these fair shifting to lower values indicated generation of large bonds' strains. The peak shifting towards a lower absorptions meant the *absorption intensity decreased* as a result of the *increased density* caused by the newly created crystals which affected the freedom of bonds' vibrations; the frequency of vibration is inversely proportional to the density of vibrating molecules, i.e. the higher density due to newly created scrystalline domains, reduced the vibration frequency and the absorption, and the reduced absorptions confirmed the increase of % crystallinity shown by the DSC analysis.

Material	Non contaminated rPET-bg

Flakes	Extruded Samples	Reference		
Wavenumber (cm^{-1})	**Wavenumber (cm^{-1})**	**Bonds**	**Wavenumber (cm^{-1})**	**Compound Type**
2919 to 2935	2915 to 2919	C-H	2850-2960	Alkane
1698 to 1713	1705 to 1708	C=O	1670-1760 stretch	Ester
1521 to 1605	1503 to 1574	C=C	1500-1600	Ester Ar. Ring
622 to 867	410 to 867	C-H	Below 900	Ester Ar. Ring
1085 to 1239	1084 to 1236	C-O	1000-1260	Ester

Table 4.12 FTIR Data of non contaminated rPET-bg Flakes and Extruded Samples

4.1.6 MFR results of *Extruded Samples*

In *experiment 1*, the MFR analysis yielded the data below.

Material	Extruded Samples of non contaminated rPET-bg		
Extrudates	**Weight Averages (g)**	**Time (s)**	**MFR (g/10min)**
Run 1	**1.860**	15	74.387
Run 2	**1.253**	10	75.160
Run 3	**0.611**	05	73.360
Mean (μ)			**74.30**
STDEV (σ)			0.90
ST. Error ($S_E = \sigma/n^{0.5}$)			0.52
CI (95%), ($\mu \pm 1.96 S_E$)			$\mu \pm 1.02$

Table 4.13 MFR of non contaminated rPET-bg Extruded Samples

The average *MFR* of the *extruded samples* of *74.30±1.02 g/10min*, shown in *Table 4.14* below, compared to the *flakes'* average of *61.35±1.52 g/10min*, indicated that the *material* underwent molecular chains'-scissions resulting in *short chains* with high ability of orientation, easiness in packing and shearing at high rate which decreased the *viscosity* of the material resulting in a higher flow rate.

Materials	**MFR (g/10mins)**		
	Mean (μ)	**ST. Error ($S_E = \sigma/n^{0.5}$)**	**CI (95%) ($\mu \pm 1.96 S_E$)**
rPET-bg Flakes	**61.35**	0.78	$\mu \pm 1.52$
rPET-bg Extruded Samples	**74.30**	0.52	$\mu \pm 1.02$

Table 4.14 MFR of non contaminated rPET-bg Flakes and Extruded Samples

In *experiment 2*, the *non contaminated* rPET-bg *extruded pellets* were injection moulded into *dumbbells* and *impact bars*. Then, *injection moulded samples* were analysed again by DSC, FTIR, MFR and the *dumbbells* and *impact bars* were tested for their tensile and impact properties and investigated and the results are as below.

It was not possible to process directly the *flakes* by injection moulding because of their *sizes* which ranged between *8.20* and *10.38mm*, as shown in *Figure 4.8* (*a, b, c*) below, these sizes were larger than the recommended requirement for recycled PET processing by injection moulding as reported in many literatures [162], and *Pawlak A et al.* [165] reported that for successful *PET recycling*, as a minimum requirement, the *flakes* should be between *0.4 and 8.00mm*. So, the *flakes* were firstly *extruded* into *pellets* prior to their *injection moulding* into *dumbbells* and *impact bars*.

Figure 4.8 (a, b, c) Dimensions of non contaminated rPET-bg Flakes magnified 25 times

During injection moulding, the uniform melting, injection time, packing and cooling and the optimised processing conditions shown in *Table 4.15* below, allowed the processing of good mouldings of non contaminated rPET-bg, as shown in *Figures 4.9* and *4.10* below.

Material	Melt Temperatures (^{o}C)				Injection Pressure (Bars)	Packing Pressure (Bars)	Mould Temp. (^{o}C)	Injection Time (s)	Packing Pressure (%)
	Rear Zone	Middle Zone	Front Zone	Nozzle Zone					
rPET-bg	260	260	270	290	180	75	60	1.35	45%

Table 4.15 Injection Moulding Processing conditions of non contaminated rPET-bg

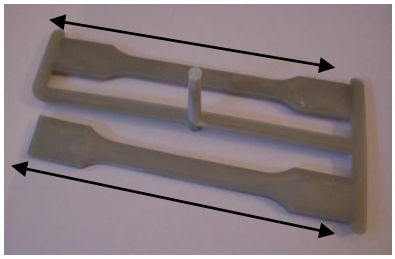

Figure 4.9 A Moulding of 2 Dumbbells

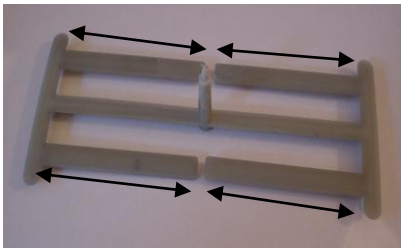

Figure 4.10 A Moulding of 4 Impact Bars

The visual observation of *dumbbells* and *impact bars* mouldings showed full packing and homogeneous dimensioning without any external anomalies. The microscopic analysis of a cross-sectional area of an *injection moulded segment*, magnified 400 times, showed insignificant embedded *contaminant* in the main matrix of rPET-bg, as shown in *Figure 4.11* below.

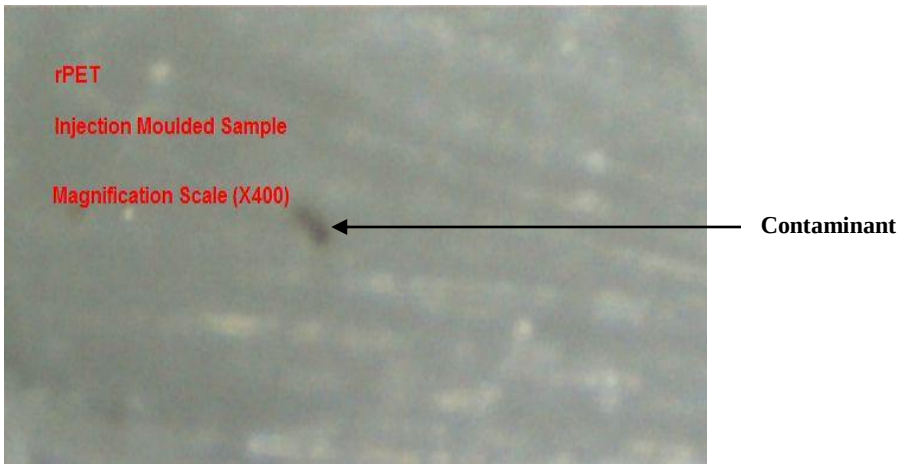

Figure 4.11 Cross-sectional Area of non contaminated rPET-bg Inj. Moulded Sample magnified 400 times

4.1.7 DSC results of *Injection Moulded Samples*

In *experiment 2*, the DSC analysis yielded the data below.

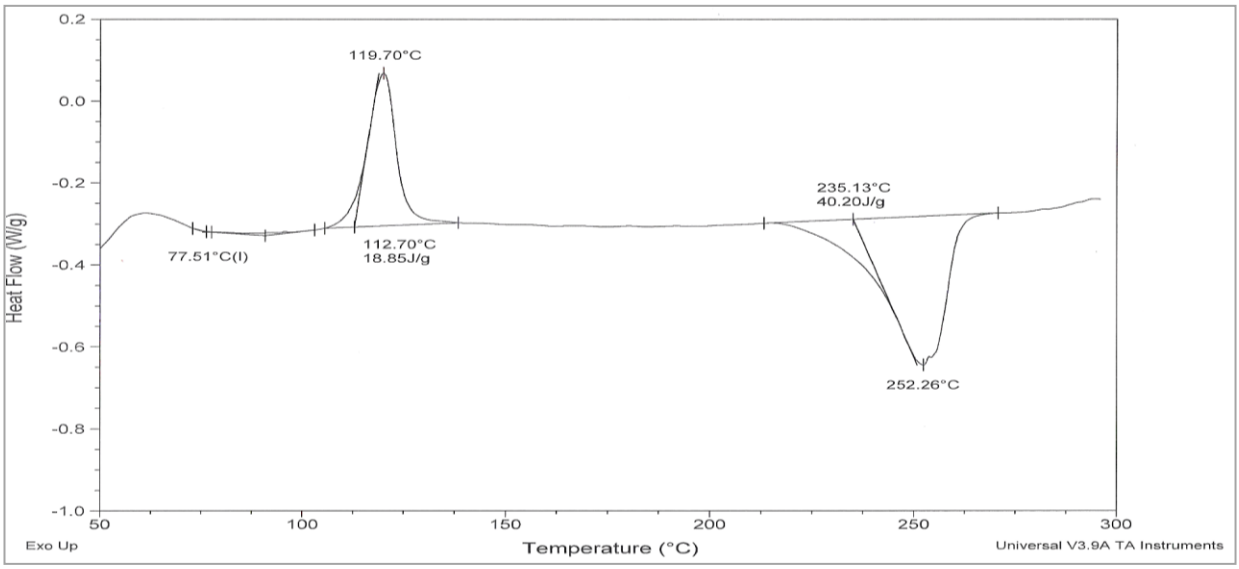

Figure 4.12 DSC Thermogram of non contaminated rPET-bg Inj. Moulded Sample 1

Material	**Injection Moulded Samples of non contaminated rPET-bg**							
	T_g (^{o}C)	T_m (^{o}C)	ΔH_m (J/g)	T_c (^{o}C)	ΔH_c (J/g)	ΔH_m^0 (J/g)	X_c (%)	T_d (^{o}C)
Run 1	77.51	252.26	40.20	119.70	18.85	140	28.71	Nil
Run 2	75.24	254.78	47.29	122.28	23.26	140	33.78	Nil
Run 3	86.05	254.54	51.16	118.70	28.26	140	36.54	Nil
Mean (μ)	**79.60**	**253.86**	**46.22**	**120.23**	**23.46**		**33.01**	
STDEV (σ)	5.70	1.39	5.56	1.85	4.71		3.97	
ST. Error ($S_E = \sigma/n^{0.5}$)	3.29	0.80	3.21	1.07	2.72		2.29	
CI (95%), ($\mu \pm 1.96 S_E$)	$\mu \pm 6.45$	$\mu \pm 1.57$	$\mu \pm 6.29$	$\mu \pm 2.09$	$\mu \pm 5.33$		$\mu \pm 4.49$	

Table 4.16 DSC Data of non contaminated rPET-bg Inj. Moulded Samples

Note: Additional DSC Thermograms are available in ***Appendix 4*** **(5)**.

Following injection moulding, the multiple endothermic phenomena were completely eradicated by further heating, this conclusion was in line with what was reported by *Lu* and *Hay* [45] related to the effect of heating rate on minimising multiple endothermic phenomena. The presence of cold crystallisation peaks indicated that the molecular chains were strained, and depending upon the cooling conditions encountered. So, upon heating during DSC heating runs, an amount of energy was released in each run, as a result of the transformation of the strained or amorphous domains into crystalline ones. These noticeable areas under the exotherms, indicated the presence of amorphous domains, which could crystallise, were retained in the samples after cooling crystallisation.

The *inj. moulded samples* average T_g of $79.60 \pm 6.45^{o}C$ compared to *extruded samples* average of $102.63 \pm 5.07^{o}C$ and the flakes' average of $100.89 \pm 0.06^{o}C$, as shown in *Table 4.17* and *Figure 4.13* below, showed narrow range of glass transition indicating the presence of new more ordered crystal domains resulting from good flow orientation, stress less bevahiour of the melt in the cavity and history of slow and balanced cooling of mouldings, where chains mobility was favoured by optimum flow behaviour of the melt under optimised conditions.

Materials	T_g (°C)		
	Mean (μ)	**ST. Error ($S_E = \sigma/n^{0.5}$)**	**CI (95%) ($\mu \pm 1.96 S_E$)**
rPET Flakes	**100.89**	0.03	$\mu \pm 0.06$
rPET Extruded Samples	**102.63**	2.59	$\mu \pm 5.07$
rPET Inj. Moulded Samples	**79.60**	3.29	$\mu \pm 6.45$

Table 4.17 Glass Transition Temperature of non contaminated rPET-bg Flakes, Extruded and Inj. Moulded Samples

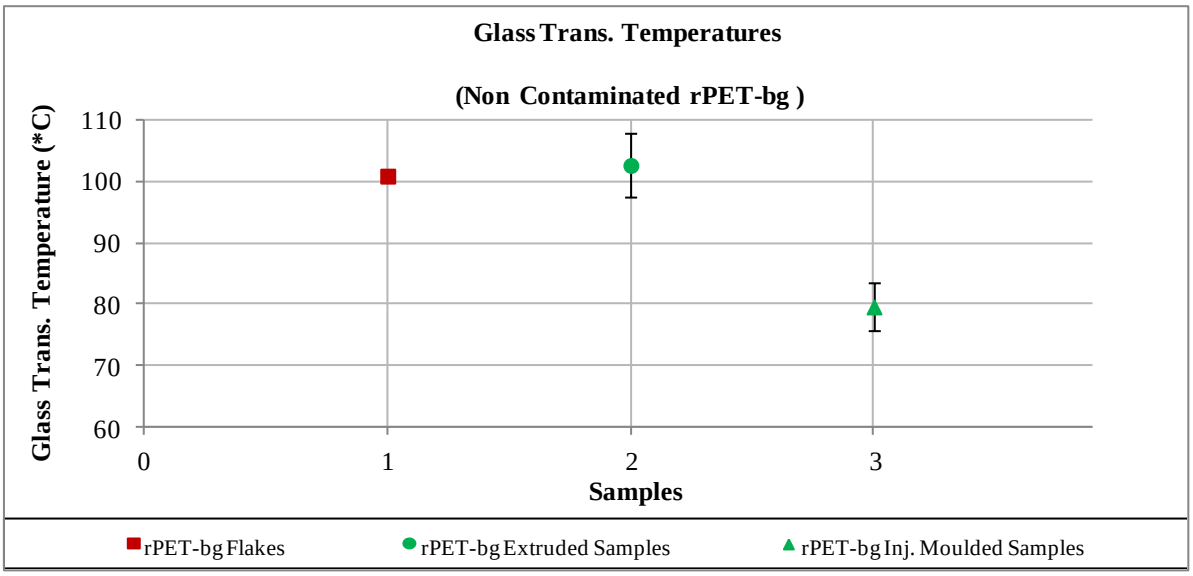

Figure 4.13 Glass Transition Temperature of non contaminated rPET-bg Flakes, Extruded and Inj. Moulded Samples

The average *inj. moulded samples* T_m of 253.86 ± 1.57^oC compared with the *extruded samples* of 254.62 ± 1.27^oC and the *flakes'* of 254.10 ± 0.55^oC, shown in *Table 4.18* and *Figure 4.14* below, showed a decrease indicating that the number of short polymer chains increased as a result of further processing and degradation, i.e. additional chains'-scissions, were sporadically dispersed within the matrix, which allowed melting of the dispersed small crystalline domains at lower temperature.

Materials	T_m (^{o}C)		
	Mean (μ)	**ST. Error** ($S_E = \sigma/n^{0.5}$)	**CI (95%)** ($\mu \pm 1.96 S_E$)
rPET Flakes	**254.10**	0.28	$\mu \pm 0.55$
rPET Extruded Samples	**254.62**	0.65	$\mu \pm 1.27$
rPET Inj. Moulded Samples	**253.86**	0.80	$\mu \pm 1.57$

Table 4.18 Melting Temperature of non contaminated rPET-bg Flakes, Extruded and Inj. Moulded Samples

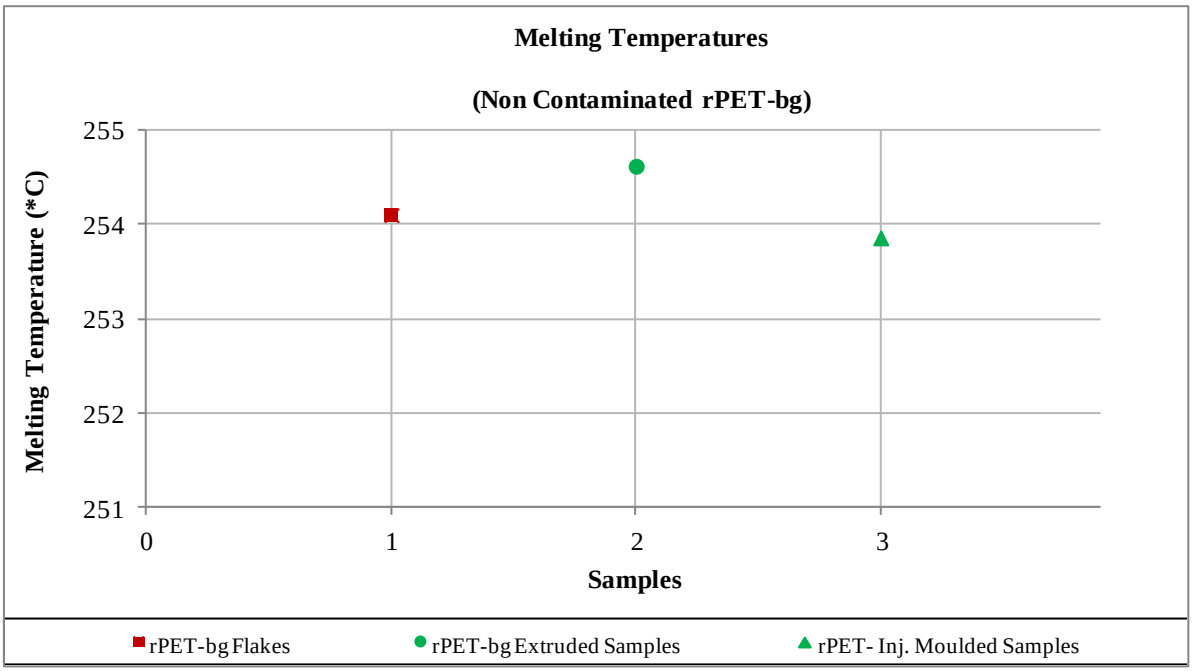

Figure 4.14 Melting Temperature of non contaminated rPET-bg Flakes, Extruded and Inj. Moulded Samples

The average injection moulded samples' *heat of fusion* or *enthalpy of melting* ΔH_m of *46.22±6.29 J.g*$^{-1}$ compared with *extruded samples'* of *33.75±9.12J.g*$^{-1}$ and the *flakes'* of *25.43±7.01 J.g*$^{-1}$, shown in *Table 4.19* and *Figure 4.15* below, showed the increased energy consumption to melt the additional numerous small crystalline domains which were created after inj. moulding; this additional crystal fractions formed following a well distribution of *material's* melt within the mould cavity and its balanced cooling rate.

Materials	ΔH_m (J.g^{-1})		
	Mean (μ)	**ST. Error ($S_E = \sigma/n^{0.5}$)**	**CI (95%) ($\mu \pm 1.96 S_E$)**
rPET Flakes	**25.43**	3.58	$\mu \pm 7.01$
rPET Extruded Samples	**33.75**	4.65	$\mu \pm 9.12$
rPET Inj. Moulded Samples	**46.22**	3.21	$\mu \pm 6.29$

Table 4.19 Heat of Fusions of non contaminated rPET-bg Flakes, Extruded and Inj. Moulded Samples

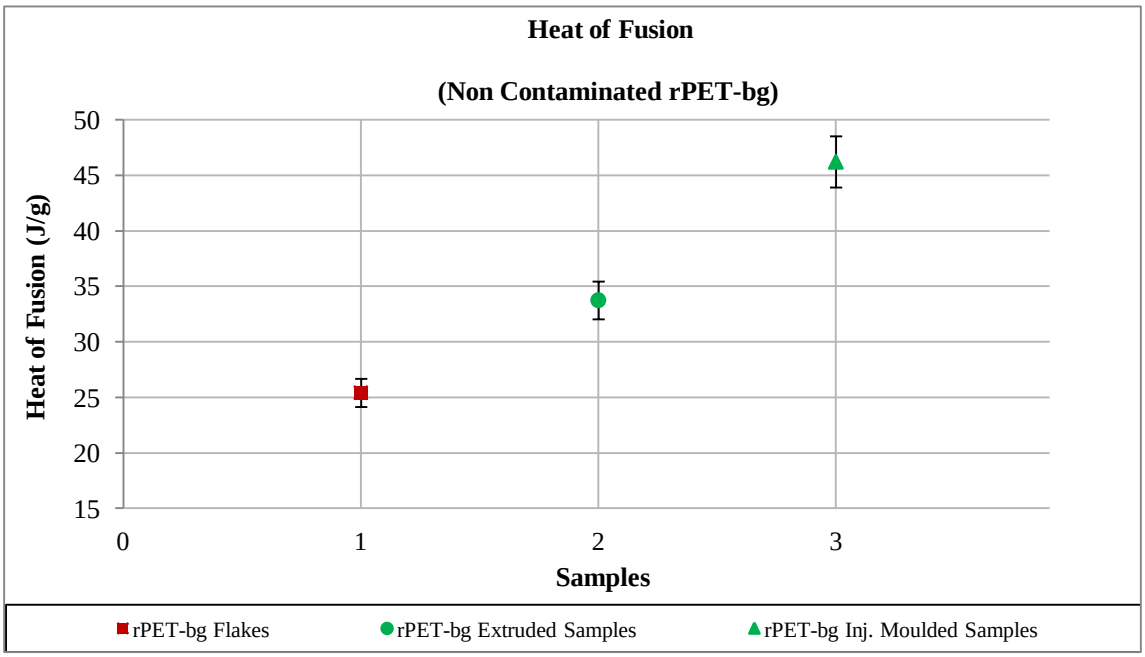

Figure 4.15 Heat of Fusions of non contaminated rPET-bg Flakes, Extruded and Inj. Moulded Samples

Cold crystallisation peaks were exhibited with a *crystallisation temperature* of *120.23±2.09 °C*, neither the *flakes* nor the *extruded samples* did exhibit cold crystallisation peaks, once again, this showed the presence of numerous ordered crystal domains created as a result of melt orientation in the cavity and history of slow and balanced cooling of material. These conditions helped increasing the degree of *crystallinity* to an average of *33.01±4.49* compared to the *extruded samples* of *24.11±6.51 %* and the flakes' of *18.16±5.01 %*, as shown in *Table 4.20* and *Figure 4.16* below. The optimised melt flow rate within the mould cavity and the balanced cooling time and rate were predominant factors in influencing the degree of crystallinity. Furthermore, the mould temperature of *60°C* contributed to the improvement of *crystallinity* through the improved flow, dispersion and orientation of polymer melt in the cavity; this allowed to establish a proportional relationship of *mould temperature* and *degree of crystallinity*, meaning that cooling rates are of paramount importance in dictating the final degree of crystallinity; this conclusion is in line with what was reported by *Crawford* [166] and *Akkapeddi et al.* [167] that for improved crystallinity of *PET*, the mould temperature can be increased as high as *140°C*.

Materials	X_c (%)		
	Mean (μ)	**ST. Error ($S_E = \sigma/n^{0.5}$)**	**CI (95%) ($\mu \pm 1.96 S_E$)**
rPET Flakes	**18.16**	2.55	$\mu \pm 5.01$
rPET Extruded Samples	**24.11**	3.32	$\mu \pm 6.51$
rPET Inj. Moulded Samples	**33.01**	2.29	$\mu \pm 4.49$

Table 4.20 % Crystallinity of non contaminated rPET-bg Flakes, Extruded and Inj. Moulded Samples

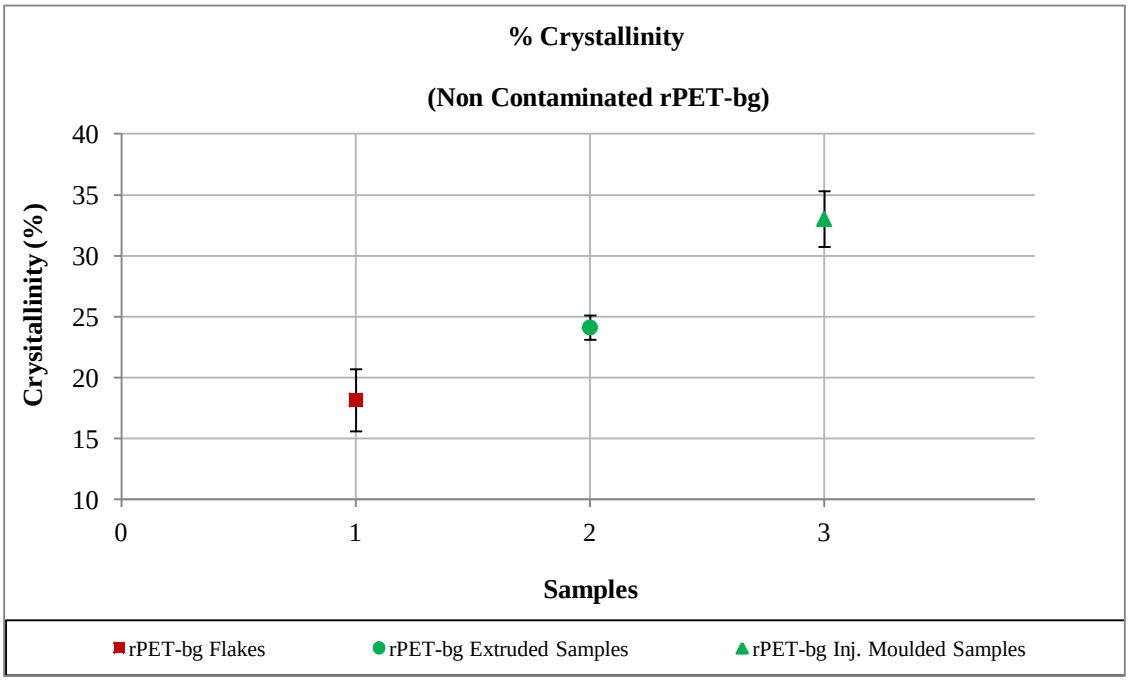

Figure 4.16 % Crystallinity of non contaminated rPET-bg Flakes, Extruded and Inj. Moulded Samples

4.1.8 FTIR results of *Injection Moulded Samples*

In *experiment 2*, the FTIR analysis yielded the data below.

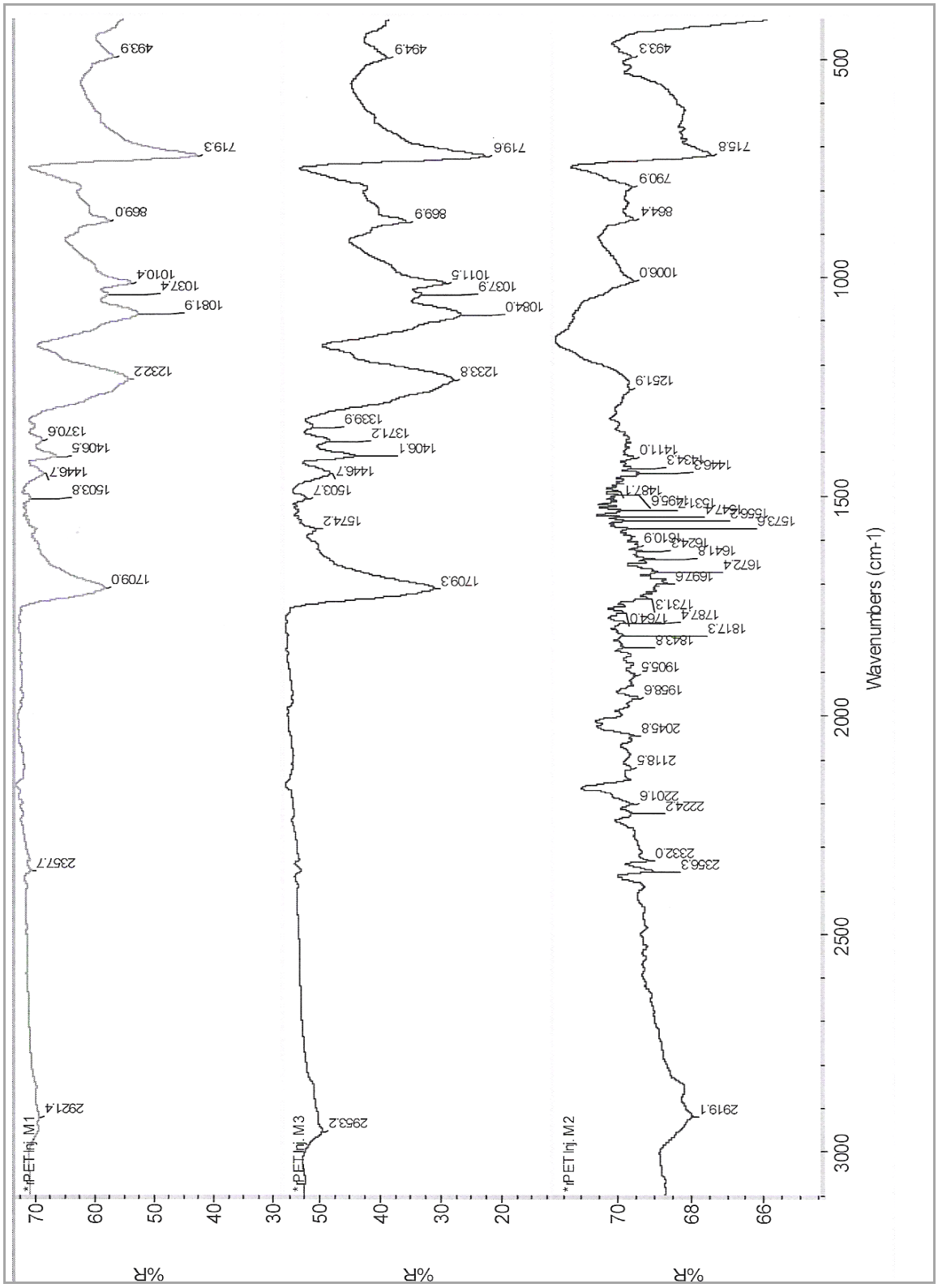

Figure 4.17 FTIR Spectra of non contaminated rPET-bg Inj. Moulded Samples

Material	Injection Moulded Samples of non contaminated rPET-bg				
Wavenumber (cm^{-1})			Bond	Wavenumber Range (cm^{-1})	Compound Type
Scan 1	Scan 2	Scan 3			
2921	2919	2953	C-H	2850-2960	Alkane
1709	1697 to 1731	1709	C=O	1670-1760	Ester
1503	1531to 1573	1503to 1574	C=C	1500-1600	Ester Ar. Ring
493 to 869	493 to 864	494 to 869	C-H	Below 900	Ester Ar. Ring
1081 to 1232	1251	1084 to 1233	C-O	1000-1260	Ester

Table 4.21 FTIR Data of rPET-bg Inj. Moulded Samples

The results, shown in *Table 4.22* below, showed that the absorptions of most molecular bonds, the *aromatic ester ring C-H,* the *aromatic ester ring C=C,* the *ester C=O*, the *ester C-O* and the *allkane* group broad *C-H*, either stabilised or slightly increased in the *inj. moulded samples* compared to *extruded samples* and *flakes*; this indicated unbalanced molecular strains as a result of heterogeneous absorptions caused by heterogeneous distribution of sporadic crystals. As a result of sporadic dispersion, the additional number of sporadic crystals allowed relaxation of overall molecular bonds' strains and allowed additional freedom of vibration of bonds, which allowed increased absorptions. The increased absorptions indicated increased crystals generated as a result of further processing confirmed the increase of % crystallinity shown by the DSC analysis.

Material	Non contaminated rPET-bg

Flakes	Extruded Samples	Inj. Moulded Samples	Reference		
Wavenumber (cm^{-1})	**Wavenumber (cm^{-1})**	**Wavenumber (cm^{-1})**	**Bonds**	**Wavenumber (cm^{-1})**	**Compound Type**
2919 to 2935	2915 to 2919	2919 to 2953	C-H	2850-2960	Alkane
1698 to 1713	1705 to 1708	1697 to 1731	C=O	1670-1760	Ester
1521 to 1605	1503 to 1574	1503 to 1574	C=C	1500-1600	Ester Ar. Ring
622 to 867	410 to 867	493 to 869	C-H	Below 900	Ester Ar. Ring
1085 to 1239	1084 to 1236	1081 to 1233	C-O	1000-1260	Ester

Table 4.22 FTIR Data of non contaminated rPET-bg Flakes, Extruded and Inj. Moulded Samples

4.1.9 MFR results of *Injection Moulded Samples*

In *experiment 2*, the MFR analysis yielded the data below.

Material	Inj. Moulded Samples of rPET

Extrudates	Weight (g)	Time (s)	MFR (g/10min)
Run 1	2.123	15	84.920
Run 2	1.532	10	91.920
Run 3	0.932	05	111.840

Mean (μ)	**96.23**
STDEV (σ)	13.97
ST. Error ($S_E = \sigma/n^{0.5}$)	8.06
CI (95%), ($\mu \pm 1.96 S_E$)	$\mu \pm 15.81$

Table 4.23 MFR of non contaminated rPET-bg Inj. Moulded Samples

The comparative *melt flow* results, shown in *Table 4.24* and *Figure 4.18* below, showed that the average *injection moulded samples' MFI* of *96.23±15.80g/10min* increased compared to the *extruded samples* and the *flakes*, indicating additional chains' scissions resulting in increased short chains of low molecular weights which lead to decreased melt *viscosity*. The increased short chains lead to higher degree of chains' orientation which explained the increase of % crystallinity previously discussed.

Materials	**MFR (g/10mins)**		
	Mean (μ)	**ST. Error ($S_E = \sigma/n^{0.5}$)**	**CI (95%) ($\mu \pm 1.96S_E$)**
rPET Flakes	**61.35**	0.78	$\mu \pm 1.52$
rPET Extruded Samples	**74.30**	0.52	$\mu \pm 1.02$
rPET Inj. Moulded Samples	**96.23**	8.06	$\mu \pm 15.80$

Table 4.24 MFR of non contaminated rPET-bg Flakes, Extruded and Inj. Moulded Samples

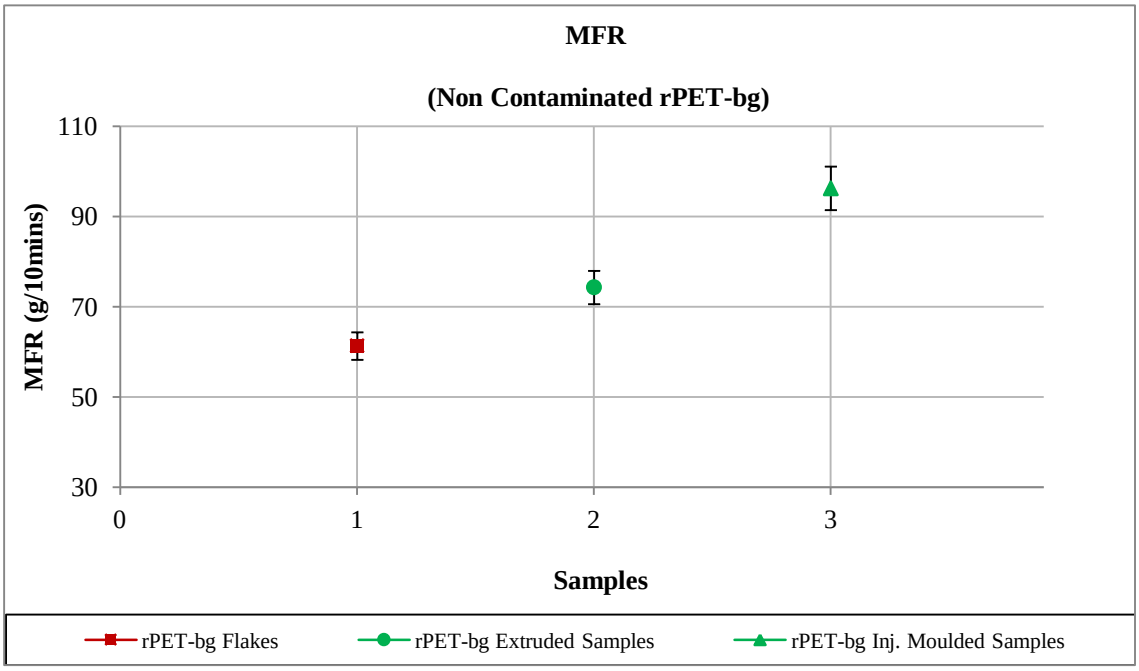

Figure 4.18 MFR of non contaminated rPET-bg Flakes, Extruded and Inj. Moulded Samples

4.1.10 Tensile Testing results of *Injection Moulded Dumbbells*

In *experiment 2*, the tensile testing yielded the data below.

.

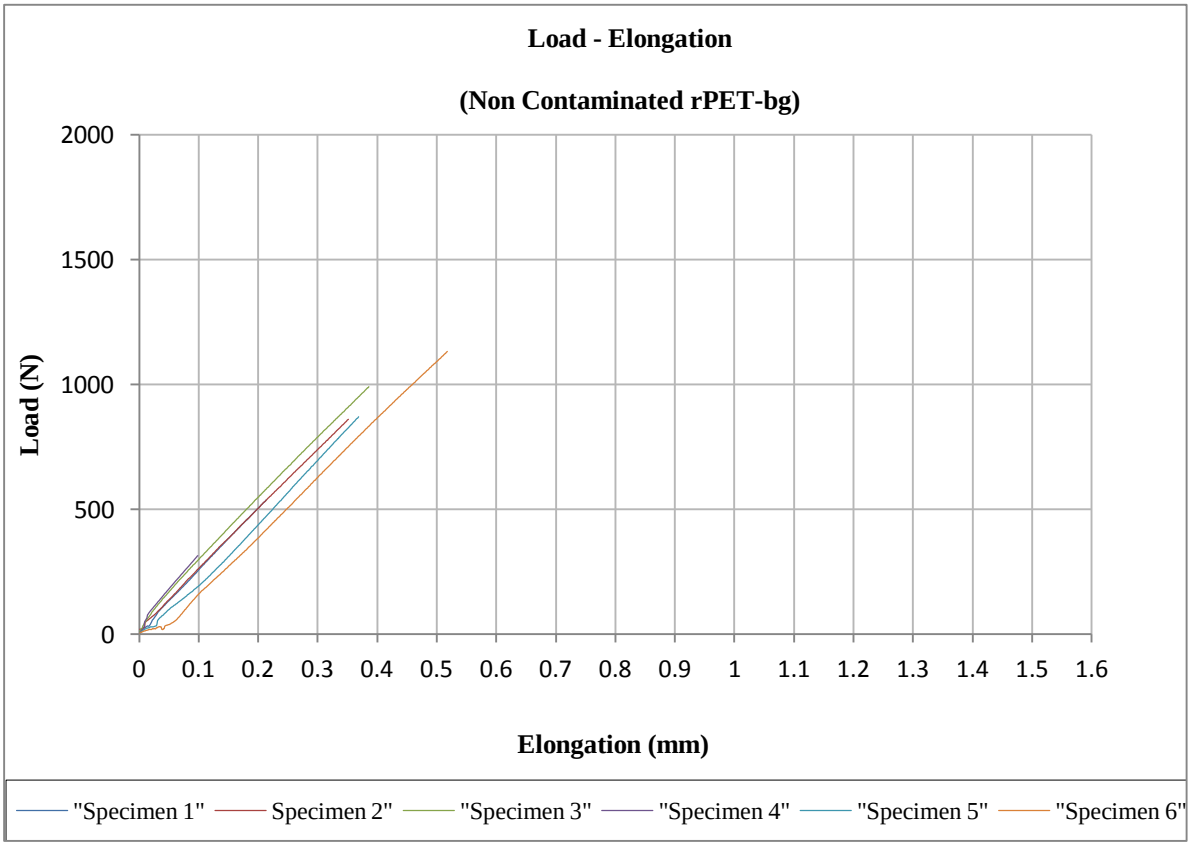

Figure 4.19 Tensile Curves of non contaminated rPET-bg Dumbbells

The *load-elongation* curves, shown in *Figure 4.19* above, were converted into *stress-strain* curves, as shown in *Figure 4.20* below, from which the tensile data were extracted, as previously described in *Section 3.2.4.2* and the results are listed in *Table 4.25* and the extracted *modulus, E*, is shown in *Table 4.26* below.

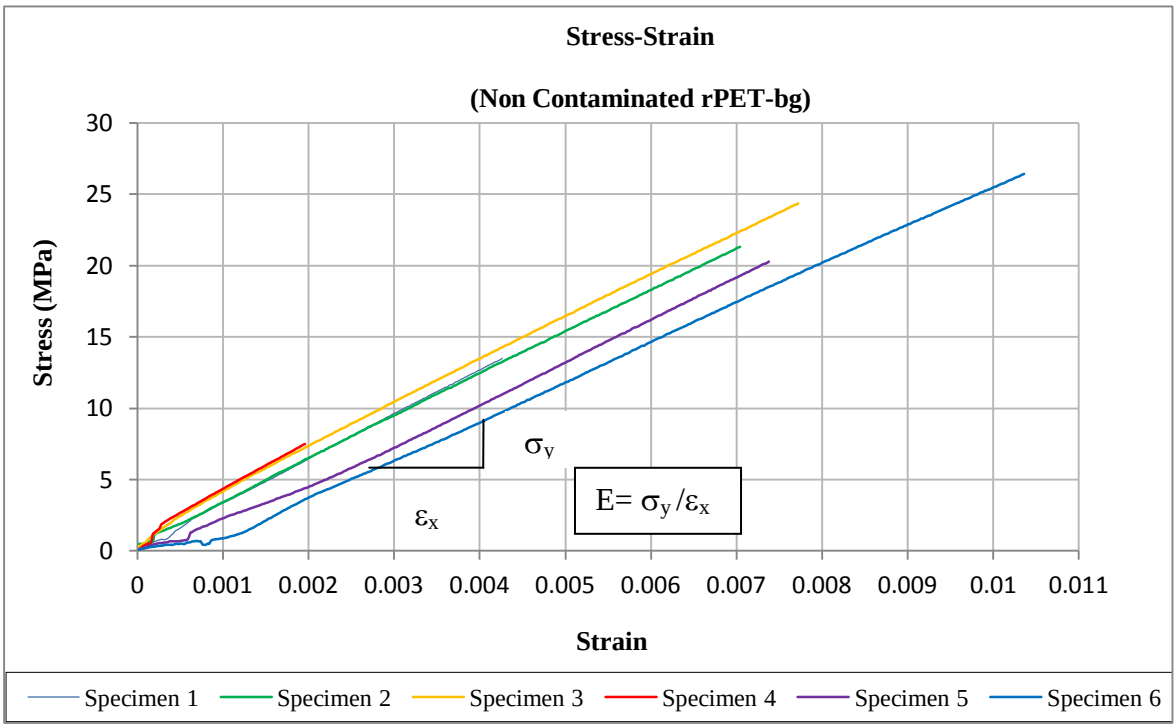

Figure 4.20 Stress-Strain Curves of non contaminated rPET-bg Dumbbells (1 to 6)

Dumbbells	Modulus, E GPa	Yield Stress, σ_y (MPa)	Stress @ Break, σ_f (MPa)	Strain @ Yield
1	3.11	13.50	13.50	0.004
2	3.05	21.31	21.31	0.007
3	3.11	24.37	24.37	0.008
4	3.33	7.50	7.50	0.002
5	2.98	20.27	20.27	0.007
6	2.77	26.42	26.42	0.010
Mean (μ)	**3.06**	**18.90**	**18.90**	**0.007**
STDEV (σ)	0.18	7.12	7.12	0.00
ST. Error ($S_E = \sigma/n^{0.5}$)	0.07	2.91	2.91	0.00
CI (95%), ($\mu \pm 1.96 S_E$)	$\mu \pm 0.15$	$\mu \pm 5.69$	$\mu \pm 5.69$	$\mu \pm 0.00$

Table 4.25 Tensile Data of non contaminated rPET-bg Dumbbells

Material	rPET-bg

	Stress , (MPa)			Strain, e_x			$E = (\sigma_y / e_x)$	
Specimen	σ_{y1}	σ_{y2}	σ_y	e_{x1}	e_{x2}	e_x	**MPa**	**GPa**
1	3.361	12.675	9.314	0.001	0.004	0.003	3104.67	3.11
2	3.419	9.511	6.092	0.001	0.003	0.002	3046.00	3.05
3	4.175	13.503	9.328	0.001	0.004	0.003	3109.33	3.11
4	2.667	5.999	3.332	0.0005	0.0015	0.001	3332.00	3.33
5	7.237	19.150	11.913	0.003	0.007	0.004	2978.25	2.98
6	6.327	14.639	8.312	0.003	0.006	0.003	2770.67	2.77

Mean (μ)	**3.06**
STDEV (σ)	0.18
ST. Error ($S_E = \sigma/n^{0.5}$)	0.07
CI (95%), ($\mu \pm 1.96 S_E$)	$\mu \pm 0.15$

Table 4.26 Tensile Modulus of non contaminated rPET-bg

The tensile results of *dumbbells*, shown in *Figure 4.19* and *Table 4.25* above, showed a *yield stress*, $\boldsymbol{\sigma_{UTS}}$, value of *18.90±5.69MPa* which is less than half the value of *PET* range of *55-75MPa,* indicating that the *flakes* originated from *recycled material* which lost its strength due to degradation in tensile properties. The strain at yield of *0.007±0.00* is still within the *PET* range of *0.005-0.015Pa* as reported in the literature [156]. The tensile *stress at break*, $\boldsymbol{\sigma_f}$, of *18.90±5.69MPa* which is less than half the value of *PET* of *50MPa*, as reported in the literature [157], indicated again that the flakes originated from a *recycled material*. Under tensile testing, all the *dumbbells* failed and broke sharply without yielding, as shown in *Figure 4.19* above and *Figure 4.21* below, indicating a characteristic of a *brittle material*, such as *PET*.

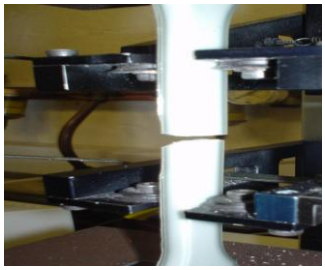

Figure 4.21 Sharp Failure of a non contaminated rPET-bg Dumbbell

The average *elastic modulus*, ***E***, of *3.06±0.15GPa* is still within the *PET* range of *2.8-3.1GPa* [166]. The above *equality* of *yield stress* and *stress at break* showed that the *material* in question was *very brittle*. The above combination of degree of *brittleness* and *elastic tensile modulus* indicated similarities with *PET* characteristics.

4.1.11 Impact Testing results of *Injection Moulded Impact Bars*

In *experiment 2*, the impact testing yielded the data below.

Material	**Non contaminated rPET-bg**
Specimen	Impact Bars

Number	**Width (B) (mm)**	**Thickness (t) (mm)**	**Energy Absorbed (J)**	**Impact Strength ($kJ.m^{-2)}$**
1	10.04	4.01	0.09	**2.24**
2	9.98	4.00	0.10	**2.51**
3	10.01	3.99	0.08	**2.00**
4	10.06	4.02	0.11	**2.72**
5	10.01	4.04	0.09	**2.23**
6	10.03	3.97	0.12	**3.01**
7	10.00	4.03	0.07	**1.74**
8	10.01	4.05	0.11	**2.71**
9	9.99	4.01	0.10	**2.50**
10	10.03	4.02	0.09	**2.23**
Mean	**10.02**	**4.01**	**0.10**	**2.39**
STDEV	0.024	0.024	0.015	0.38
ST. Error ($S_E = \sigma/n^{0.5}$)	0.008	0.007	0.005	0.12
CI (95%), ($\mu \pm 1.96 S_E$)	$\mu \pm 0.015$	$\mu \pm 0.015$	$\mu \pm 0.009$	$\mu \pm 0.23$

Table 4.27 Charpy Impact Data of non contaminated rPET-bg Impact Bars

The average *un-notched impact strength* of *2.39±0.23 $kJ.m^{-2}$* is within the equivalent *theoretical un-notched PET* value of *2.76 $kJ.m^{-2}$*, where the literature [156] reported that a *notched PET* of *3.6$kJ.m^{-2}$* is theoretically equivalent to an *un-notched PET* of *2.76$kJ.m^{-2}$* Once again, the reduced *impact strength* suggested a *recycled* material which originated from a *PET* source.

4.1.12 Overall Data Comparison

	T_g (^oC)	T_m (^oC)	ΔH_m ($J.g^{-1}$)	X_c (%)	MFI (g/10mins)
Extruded Samples *Compared to* **Flakes**	↑	↑	↑	↑	↑
Inj. Moulded Samples *Compared to* **Extruded Samples**	↓	↓	↑	↑	↑

Table 4.28 Comparison of non contaminated rPET-bg Samples

Where: ↑ means increase, ↓ means decrease.

The above comparison, shown in *Table 4.28*, showed overall increase of properties following the extrusion and injection moulding of flakes. These variations showed the effect of the processing heat in generating thermo-mechanical degradation and resulting in chains'-scission, resulting in higher number of smaller sporadic chains dispersed all over the matrix and helped the formation of more tiny sporadic crystallites under favourable conditions of cooling. Similarly, the processing allowed the increase of molecular chains'-scissions, which resulted in increased *short chains* with high ability of orientation and packing and ease of shearing at high rate which lead to increased *crystallinity*, decreased *viscosity* and increased *melt flow rate*.

4.2 Conclusion

In light of the above investigation, the determined thermal, spectroscopic and flow properties showed that the *flakes* originated from an *amorphous* material which underwent cooling stages at elevated cooling rates; a *processing technique* using engineering materials of excellent ease of flow coupled with excellent stretch-ability, such as *PET* and intended to produce clear and *transparent* products, such as *bottles.* Also, the determined tensile and impact properties showed characteristics, such as *brittleness* and *impact strength*, similar and inherited from *PET*. Furthermore, some characteristics showed *history* of *processing* and *degradation* in properties and presence of *contaminants*, such as soil particulates, which confirmed that the flakes originated from a *recycled* source of mixed batches of different colours and encountered direct contact with soil either before or at recycling stage. The obtained information allowed the identification of the *flakes* supplied by *Closed Loop Recycling limited* as *recycled bottle grade PET*, or *rPET-bg*.

Stage 1

Chapter 5

rPET-bg Contaminated with HDPE

5.1 Results and Discussions

This section discusses the various experimental results of rPET-bg contaminated with HDPE obtained in *experiments 3* to *5*. The purpose was to identify the influence of small amounts of HDPE on the properties and processability of non contaminated rPET-bg previously studied in *Chapter 4*.

Samples of rPET-bg were contaminated with *5%, 10%* and *15%* of HDPE and investigated. For comparative reasons, same methodology was performed as previously done in *Chapter 4* and as described in *Section 3.2* and *Experiments 3* to *5, Section 3.4*, i.e. contaminated samples were extruded, injection moulded and analysed by DSC, FTIR, MFR and tested for their tensile and impact properties. A step by step comparison was performed and the results of the influence of HDPE on the main matrix of rPET-bg are discussed below.

The contaminated samples showed good, uniform heat distribution which allowed apparent decrease in twin-screw speed in the increasing order of contamination % loadings, as shown in *Table 5.1* and *Figure 5.1* below, indicated homogeneous melt mixture of the two materials and the capability of HDPE in reducing the viscosity of the melt translated by the decreased screw-speed. In theory, the viscosity is inversely proportional to the shear rate, translated into material processing behaviour, this means that the screw speed is inversely proportional to the viscosity; the higher viscosity conveys lower screw speed and higher % torque. The results below showed decreased screw speed which meant increased viscosity in the ascending order of % contamination, but the % torque, which is proportional to viscosity, decreased rather than increasing; this suggested a homogeneous mixing coupled with unbalanced overall dispersion of the HDPE in the rPET-bg matrix; where very small HDPE and matrix chains were created as a result of thermo-mechanical degradation, especially at the high processing temperatures applied. Also, the inclusion of these small amounts of HDPE cannot be dispersed at equal rates within the matrix. And, the increased viscosity is attributed to the *melt flow* property of HDPE, which is *8g /10min*, as shown in *Table 3.1*, *Section 3.1.2*, compared to the non contaminated rPET-bg flakes' of *61.35g/10min* previously determined and shown in *Table 4.3*, *Section 4.1.3*, increased the viscosity of the contaminated materials quantitatively by interaction.

Extruded Samples	Screw Speed			% Torque		
	Min. (rpm)	Max. (rpm)	Mean (rpm)	Min. (%)	Max. (%)	Mean (%)
Non contaminated rPET-bg	110	115	112.50 ± 2.5	50	60	55 ± 5
95% rPET-bg / 5% HDPE	100	105	102.50 ± 2.5	40	50	45 ± 5
90% rPET-bg / 10% HDPE	95	100	97.50 ± 2.5	35	45	40 ± 5
85% rPET-bg / 15% HDPE	85	90	87.50 ± 2.5	30	40	35 ± 5

Table 5.1 Screw Speed and % Torque of extruded rPET-bg contaminated with HDPE

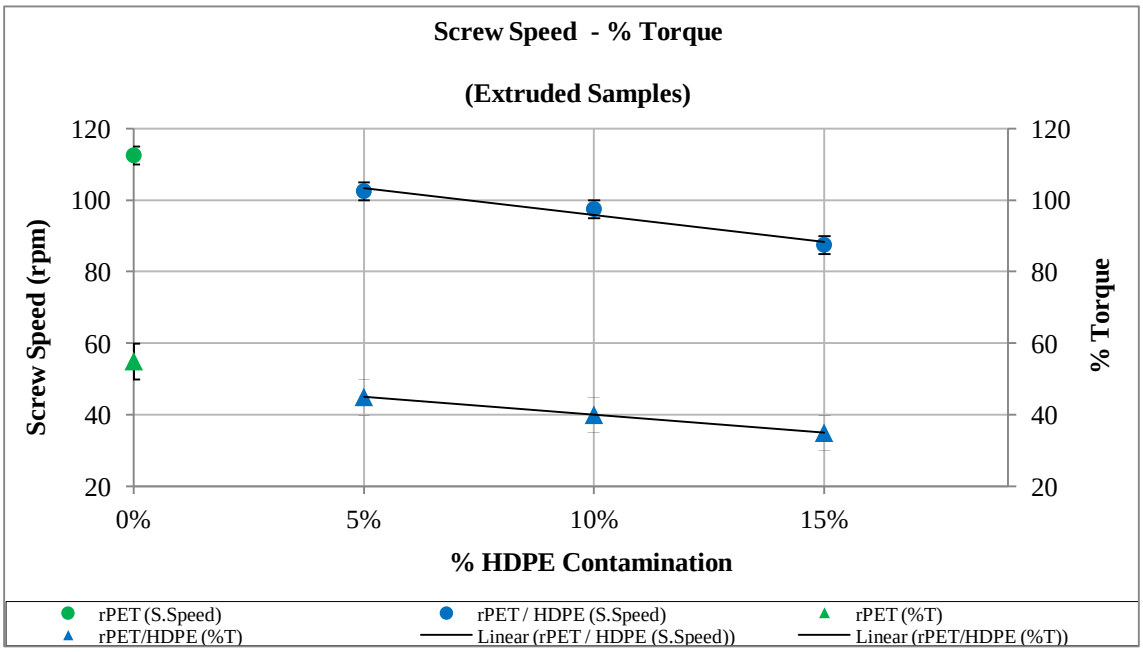

Figure 5.1 Screw Speed and % Torque of extruded rPET-bg contaminated with HDPE

The produced *extrudates*, as shown in *Table 5.2* below, showed low swelling, medium to high degree of brittleness and low degree of ductility compared to non contaminated rPET-bg. These variations showed the balanced mixing of the melt, combination and interchange in properties, resulting in increased crystalline fractions after cooling.

Extruded Samples	Swelling	Brittleness	Ductility	Colour
Non contaminated rPET-bg	No	High	No	Grey- Transparent
95% rPET-bg / 5% HDPE	Low	High	No	Grey- Transparent
90% rPET-bg / 10% HDPE	Low	Medium	Low	Grey- Transparent
85% rPET-bg / 15% HDPE	Low	Medium	Low	Grey- Transparent

Table 5.2 Extruded Pellets of rPET-bg contaminated with 5% HDPE

5.1.1 DSC results of *Extruded Samples*

In *experiments 3, 4* and *5*, the DSC analysis yielded the data below.

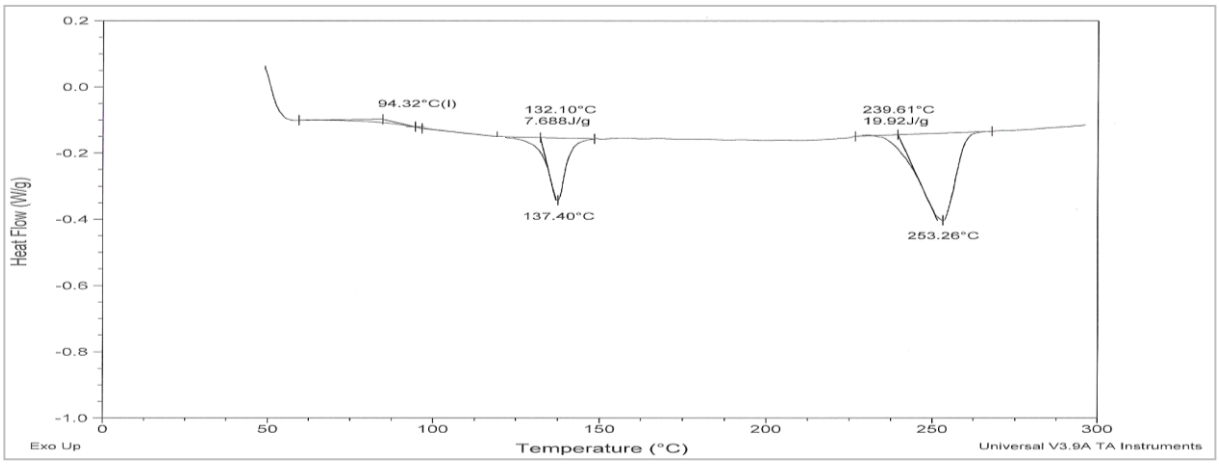

Figure 5.2 Thermogram of Extruded Sample 1 of rPET-bg contaminated with 5% HDPE

	T_g (^oC)	T_m (^oC)	ΔH_m (J/g)	T_c (^oC)	ΔH_c (J/g)	ΔH_m^0 (J/g)	X_c (%)	T_d (^oC)
Run 1	94.32	253.26	19.92	Nil	Nil	140	14.23	Nil
Run 2	76.79	252.03	30.40	123.63	14.23	140	21.71	Nil
Run 3	75.13	251.98	26.60	Nil	Nil	140	19.00	Nil
Mean (μ)	**82.08**	**252.42**	**25.64**				**18.31**	
STDEV (σ)	10.63	0.72	5.31				3.79	
ST. Error ($S_E = \sigma/n^{0.5}$)	6.14	0.42	3.06				2.19	
CI (95%), ($\mu \pm 1.96 S_E$)	$\mu \pm 12.03$	$\mu \pm 0.82$	$\mu \pm 6.00$				$\mu \pm 4.29$	

Table 5.3 DSC Data of Extruded Samples of rPET-bg Contaminated with 5% HDPE

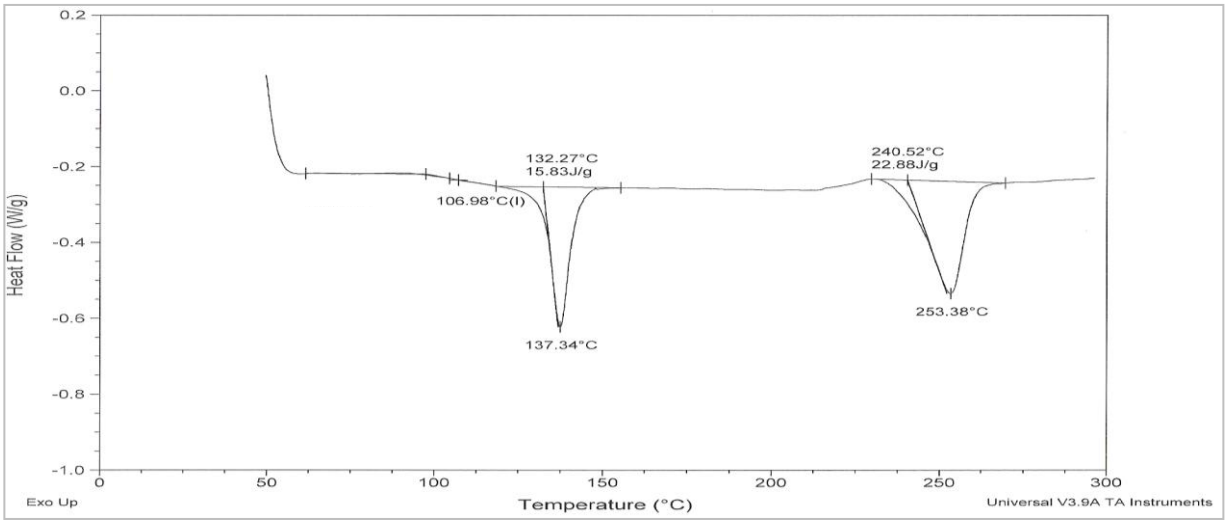

Figure 5.3 Thermogram of Extruded Sample 1 of rPET-bg contaminated with 10% HDPE

	T_g (^{o}C)	T_m (^{o}C)	ΔH_m (J/g)	T_c (^{o}C)	ΔH_c (J/g)	ΔH_m^0 (J/g)	X_c (%)	T_d (^{o}C)
Run 1	106.98	253.38	22.88	Nil	Nil	140	16.34	Nil
Run 2	108.09	254.54	25.44	Nil	Nil	140	18.17	Nil
Run 3	85.28	252.49	24.27	Nil	Nil	140	17.34	Nil
Mean (μ)	**100.12**	**253.47**	**24.20**				**17.28**	
STDEV (σ)	12.86	1.03	1.28				0.91	
ST. Error ($S_E = \sigma/n^{0.5}$)	7.42	0.59	0.74				0.53	
CI (95%), ($\mu \pm 1.96 S_E$)	$\mu \pm 14.55$	$\mu \pm 1.16$	$\mu \pm 1.45$				$\mu \pm 1.07$	

Table 5.4 DSC Data of Extruded Samples of rPET-bg Contaminated with 10% HDPE

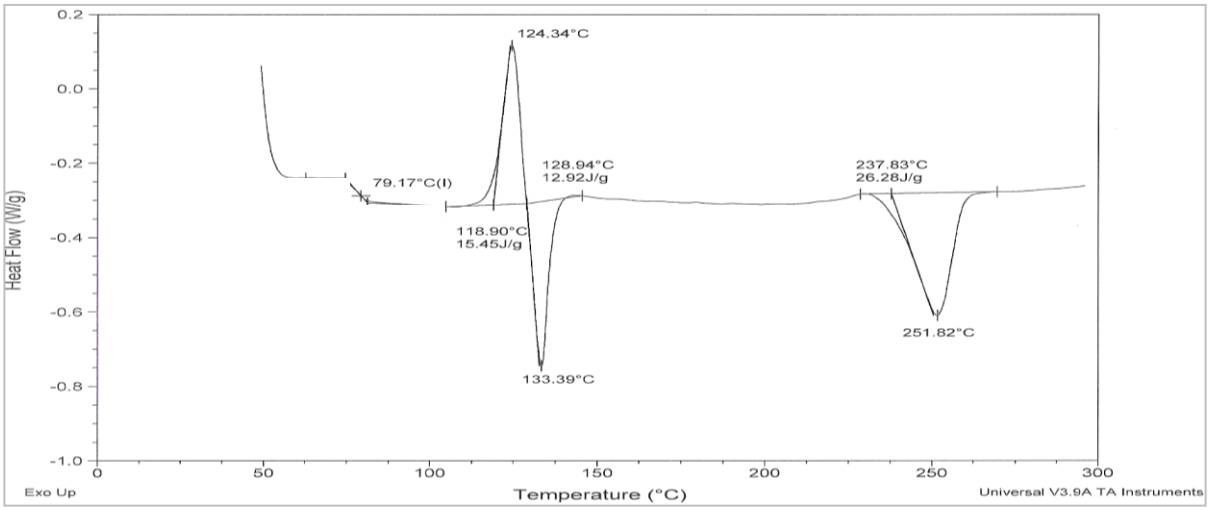

Figure 5.4 Thermogram of Extruded Sample 1 of rPET-bg contaminated with 15% HDPE

Run 1	79.17	251.82	26.28	124.34	15.45	140	18.77	Nil
Run 2	85.12	253.54	24.77	Nil	Nil	140	17.69	Nil
Run 3	74.41	252.59	22.94	Nil	Nil	140	16.39	Nil
Mean (μ)	**79.57**	**252.65**	**24.66**				**17.62**	
STDEV (σ)	5.37	0.862	1.67				1.19	
ST. Error ($S_E = \sigma/n^{0.5}$)	3.10	0.497	0.97				0.69	
CI (95%), ($\mu \pm 1.96 S_E$)	$\mu \pm 6.07$	$\mu \pm 0.975$	$\mu \pm 1.89$				$\mu \pm 1.35$	

Table 5.5 DSC Data of Extruded Samples of rPET-bg Contaminated with 15% HDPE

Note: Additional DSC Thermograms are available in ***Appendix 5*** **(***1, 2, 3***)**.

Compared to non contaminated rPET-bg, as shown in *Table 5.6* and *Figure 5.5* below, the inclusion of HDPE decreased the T_g, in all cases, indicating dispersed very small HDPE chains which filled the interstices by sliding between the matrix chains and creating certain degree of disorder which lead to narrowed range of glass transition; with the processing temperatures applied, the HDPE chains were more prone to degradation and scissions than those of the matrix, so the assumption is that more very small chains of HDPE and formation of cyclic low molecular weight oligomers can be created in PET matrix, when processed at various temperatures, as reported by *Samperi et al.* [66] and *Romao et al.* [67] . During the cooling, in extrusion process, these very small HDPE chains cooled at lower temperature and did not allow the matrix chains to reach that supercooling point easily and crystallise in time. This allowed reduced crystalline domains due to the branching phenomena exerted by the HDPE chains which filled the interstices. So, during the DSC heating mode, the very small HDPE chains started their transition earlier than those of the matrix and allowed quick transition of the overall contaminated materials, resulting in decreased T_g with increasing % HDPE loadings. Except for the 10% which showed rather higher value, this may be attributed to soil contamination which can trigger fast formation of very localised crystalline domain, which increased the time and temperature scales of glass transition.

Extruded Samples	T_g (°C)		
	Mean (μ)	**ST. Error ($S_E = \sigma/n^{0.5}$)**	**CI (95%) ($\mu \pm 1.96 S_E$)**
Non contaminated rPET-bg	**102.63**	2.59	$\mu \pm 5.07$
95% rPET-bg / 5% HDPE	**82.08**	6.14	$\mu \pm 12.03$
90% rPET-bg / 10% HDPE	**100.12**	7.42	$\mu \pm 14.55$
85% rPET-bg / 15% HDPE	**79.57**	3.10	$\mu \pm 6.07$

Table 5.6 Glass Transition Temperature of Extruded Samples of rPET-bg Contaminated with HDPE

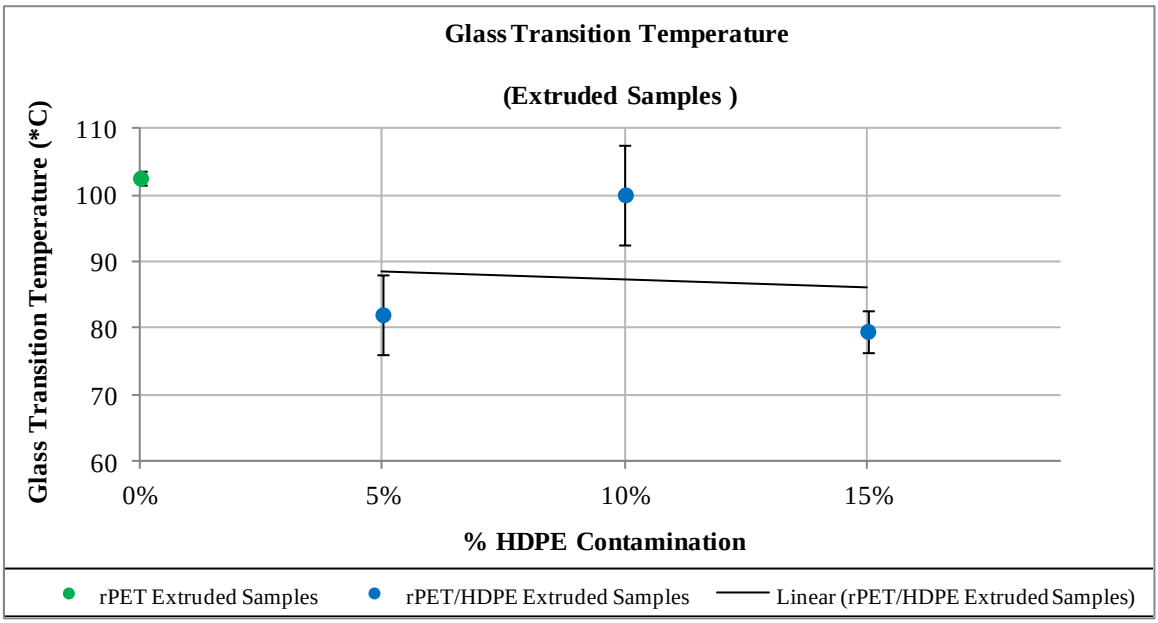

Figure 5.5 Glass Transition Temperature of Extruded Samples of rPET-bg Contaminated with HDPE

Compared to non contaminated rPET-bg, as shown in *Table 5.7* and *Figure 5.6* below, the HDPE played a role in decreasing the $\boldsymbol{T_m}$, in all cases. The increased degree of melting of the primary crystals and the shifting to lower melting temperatures explained the fast sliding of layers because of the absence of chemical secondary bonding or adhesions between the molecular chains shown by the exhibition of individual melting peaks; this indicated *incompatibility* and *immiscibility* of the polar PET and the non polar HDPE, as reported by *Kim et al.* [113], which resulted in lack of chemical secondary bonding, as reported by *Yao* and *Beatty* [108]. Secondary bonding promotes inter-molecular interaction and especially in thermoplastics, where it is improved by the presence of polar groups, such as *C-O, C-Cl, C-F, O-H* and *N-H bonds*. It is possible that the very small dispersed chains, created during extrusion, which filled the interstices, melted earlier and helped the earlier and faster melting of the matrix crystalline domains, where the degree of entropy of the very small crystalline domains was higher and the melting completed at lower temperatures. One can see, the effect of soil contamination exhibited by a still high $\boldsymbol{T_m}$ for the 10% HDPE which required higher temperature for achieving total melting of the very localised crystalline domain, assumed around a soil particulate

Extruded Samples	T_m (°C)		
	Mean (μ)	**ST. Error ($S_E = \sigma/n^{0.5}$)**	**CI (95%) ($\mu \pm 1.96 S_E$)**
Non contaminated rPET-bg	**254.62**	0.65	$\mu \pm 1.27$
95% rPET-bg / 5% HDPE	**252.42**	0.42	$\mu \pm 0.82$
90% rPET-bg / 10% HDPE	**253.47**	0.59	$\mu \pm 1.16$
85% rPET-bg / 15% HDPE	**252.65**	0.50	$\mu \pm 0.97$

Table 5.7 Melting Temperature of Extruded Samples of Extruded Samples of rPET-bg Contaminated with HDPE

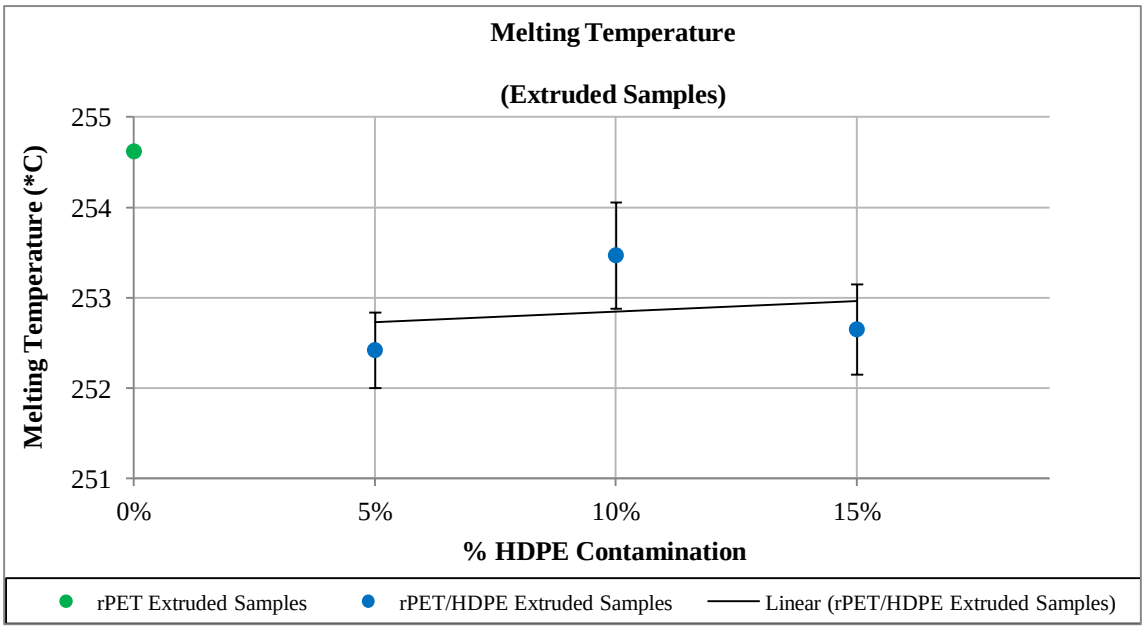

Figure 5.6 Melting Temperature of Extruded Samples of rPET-bg Contaminated with HDPE

Compared to non contaminated rPET-bg, as shown in *Table 5.8* and *Figure 5.7* below, the HDPE decreased ΔH_m is attributed to the fast melting of the HDPE crystals which improved the overall balanced rate of melting, resulting in less heat absorption, in all cases; the premature melting of the very small dispersed HDPE chains entangled within the matrix chains, allowed an overall melting equilibrium which required less heat absorption for melting.

Extruded Samples	ΔH_m (J.g^{-1})		
	Mean (μ)	**ST. Error ($S_E = \sigma/n^{0.5}$)**	**CI (95%) ($\mu \pm 1.96 S_E$)**
Non contaminated rPET-bg	**33.75**	4.65	$\mu \pm 9.12$
95% rPET-bg / 5% HDPE	**25.64**	3.06	$\mu \pm 6.00$
90% rPET-bg / 10% HDPE	**24.20**	0.74	$\mu \pm 1.45$
85% rPET-bg / 15% HDPE	**24.66**	0.97	$\mu \pm 1.89$

Table 5.8 Heat of Fusion of Extruded Samples of rPET-bg Contaminated with HDPE

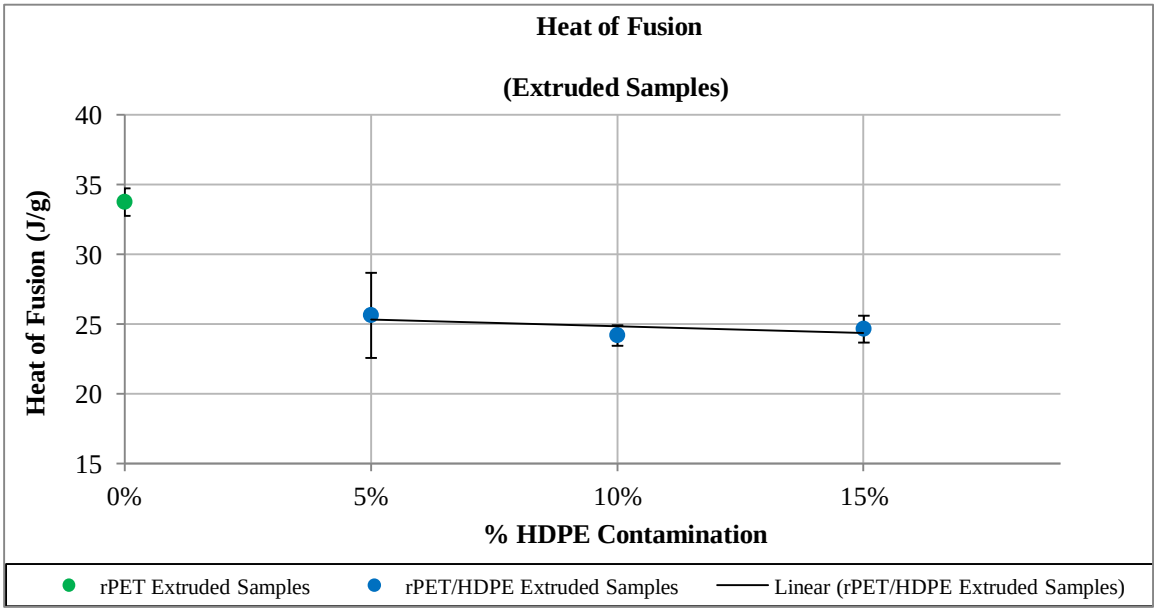

Figure 5.7 Heat of Fusion of Extruded Samples of rPET-bg Contaminated with HDPE

Compared to non contaminated rPET-bg, as shown in *Table 5.9* and *Figure 5.8* below, the absence of cold crystallisation peaks confirmed that very small chains of HDPE were created as a result of thermo-mechanical degradation and as discussed previously, these very small HDPE chains cooled at lower temperature in the interstices of the matrix chains and did not allow crystallisation to occur normally during the cooling stage of extrusion, and resulted in very dispersed crystalline domains. So, during the DSC heating, the absence of cold crystallisation peaks is attributed to the fast melting of the HDPE crystals which improved the overall transition phases, where orientation and packing of the chains were overridden by a fast melting, except in rare cases. And the reduced $\boldsymbol{X_c}$ confirmed the pattern of the crystalline domains as being numerous but dispersed as a result of HDPE inclusion.

Extruded Samples	X_c **(%)**		
	Mean (μ)	**ST. Error** ($S_E = \sigma/n^{0.5}$)	**CI (95%)** ($\mu \pm 1.96 S_E$)
Non contaminated rPET-bg	**24.11**	3.32	$\mu \pm 6.51$
95% rPET-bg / 5% HDPE	**18.31**	2.19	$\mu \pm 4.29$
90% rPET-bg / 10% HDPE	**17.28**	0.53	$\mu \pm 1.04$
85% rPET-bg / 15% HDPE	**17.62**	0.69	$\mu \pm 1.35$

Table 5.9 % Crystallinity of Extruded Samples of rPET-bg Contaminated with HDPE

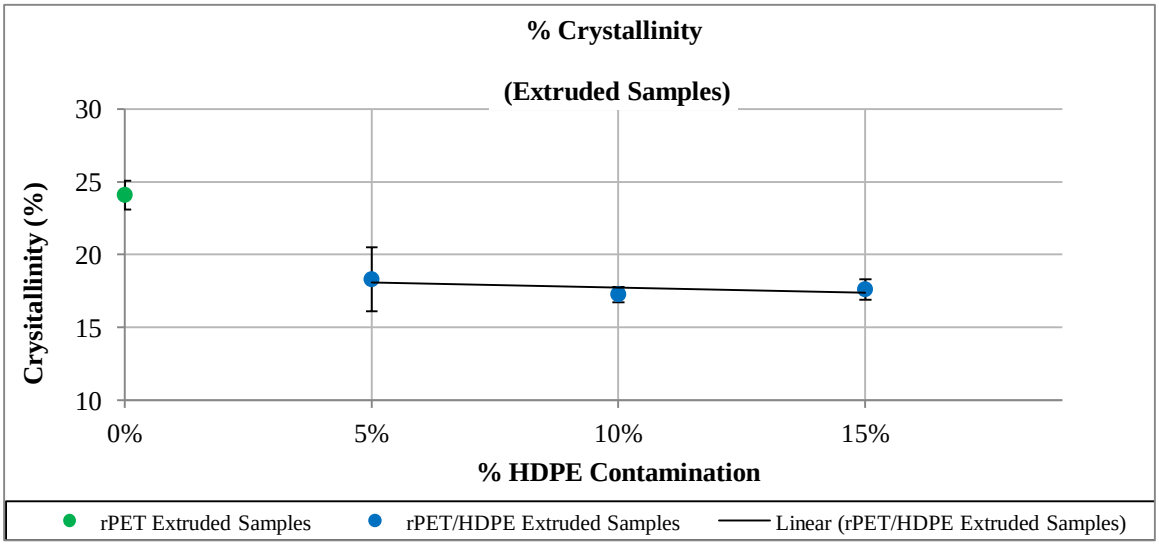

Figure 5.8 % Crystallinity of Extruded Samples of rPET-bg Contaminated with HDPE

5.1.2 FTIR results of *Extruded Samples*

In *experiments 3, 4* and *5*, the FTIR analysis yielded the data below.

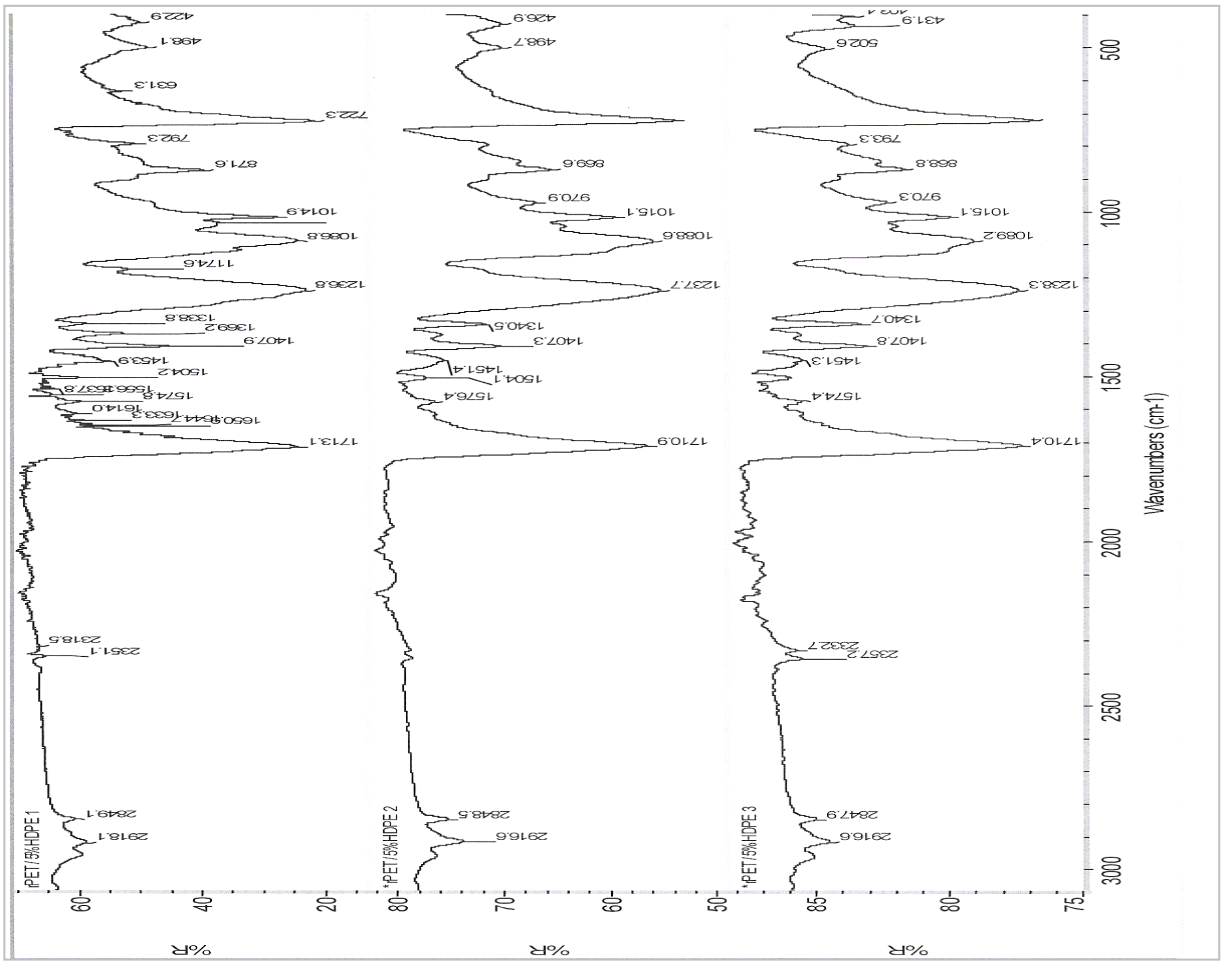

Figure 5.9 FTIR Spectra of Extruded Samples of rPET-bg contaminated with 5% HDPE

Wavenumber (cm^{-1})			Bond	Wavenumber Range (cm^{-1})	Compound Type
Scan 1	**Scan 2**	**Scan 3**			
2918	2916	2916	C-H	2850-2960	Alkane
1713	1710	1710	C=O	1670-1760	Ester
1504 to 1574	1504 to 1576	1574	C=C	1500-1600	Ester Ar. Ring
422 to 871	426 to 869	431 to 868	and C-H	Below 900	Ester Ar. Ring
1086 to 1236	1088 to 1237	1089 to 1238	C-O	1000-1260	Ester

Table 5.10 FTIR Data of Extruded Samples of rPET-bg Contaminated with 5% HDPE

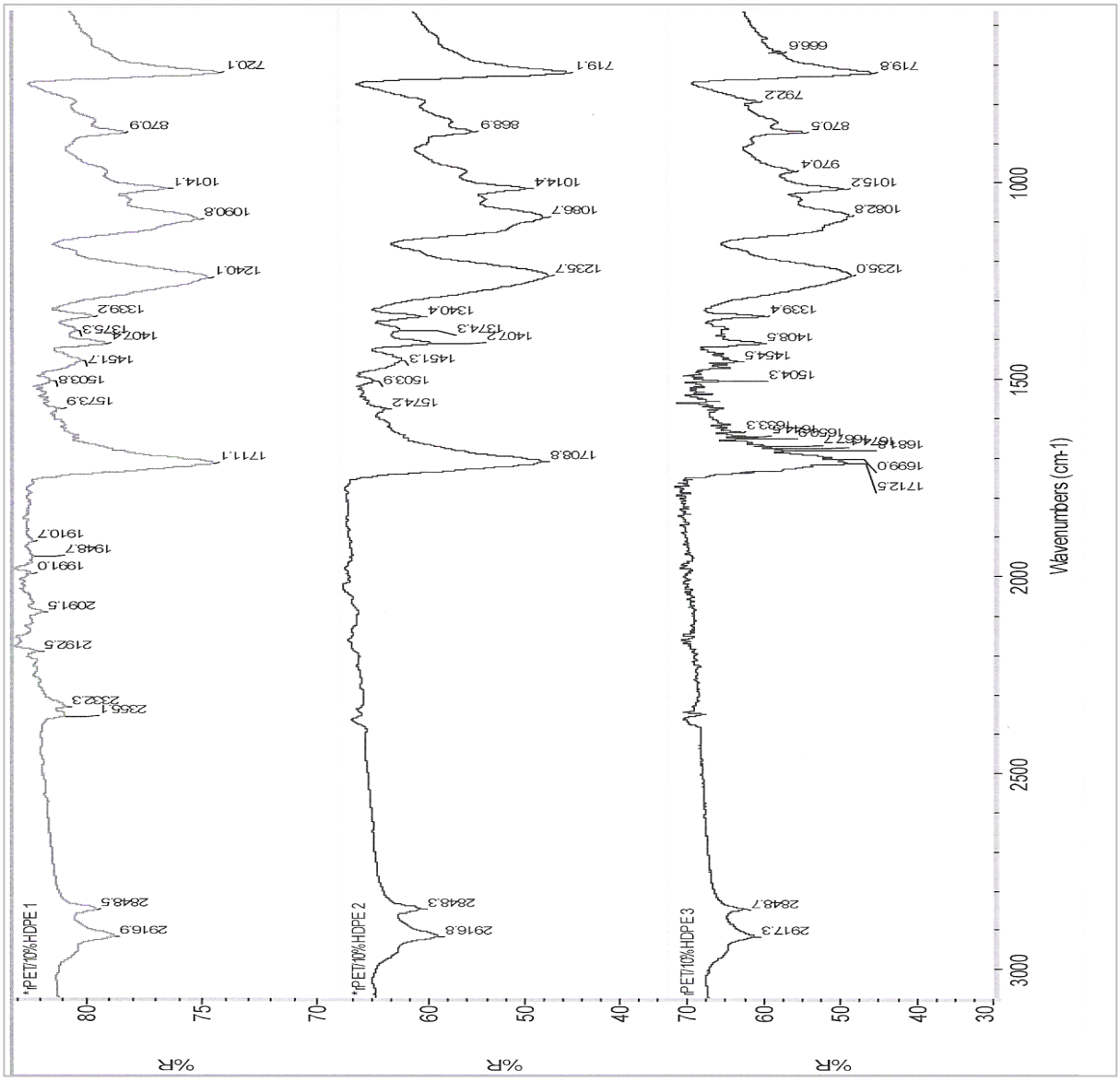

Figure 5.10 Spectra of of Extruded Samples of rPET-bg contaminated with 10% HDPE

Wavenumber (cm^{-1})			Bond	Wavenumber (cm^{-1})	Compound Type
Scan 1	**Scan 2**	**Scan 3**			
2916	2916	2917	C-H	2850-2960	Alkane
1711	1708	1699 to 1712	C=O	1670-1760	Ester
1503 to 1573	1503 to 1574	1504	C=C	1500-1600	Ester Ar. Ring
720 to 870	719 to 868	666 to 870	C-H	Below 900	Ester Ar. Ring
1090 to 1240	1086 to 1235	1082 to 1235	C-O	1000-1260	Ester

Table 5.11 FTIR Data of Extr. Samples of rPET-bg Contaminated with 10% HDPE

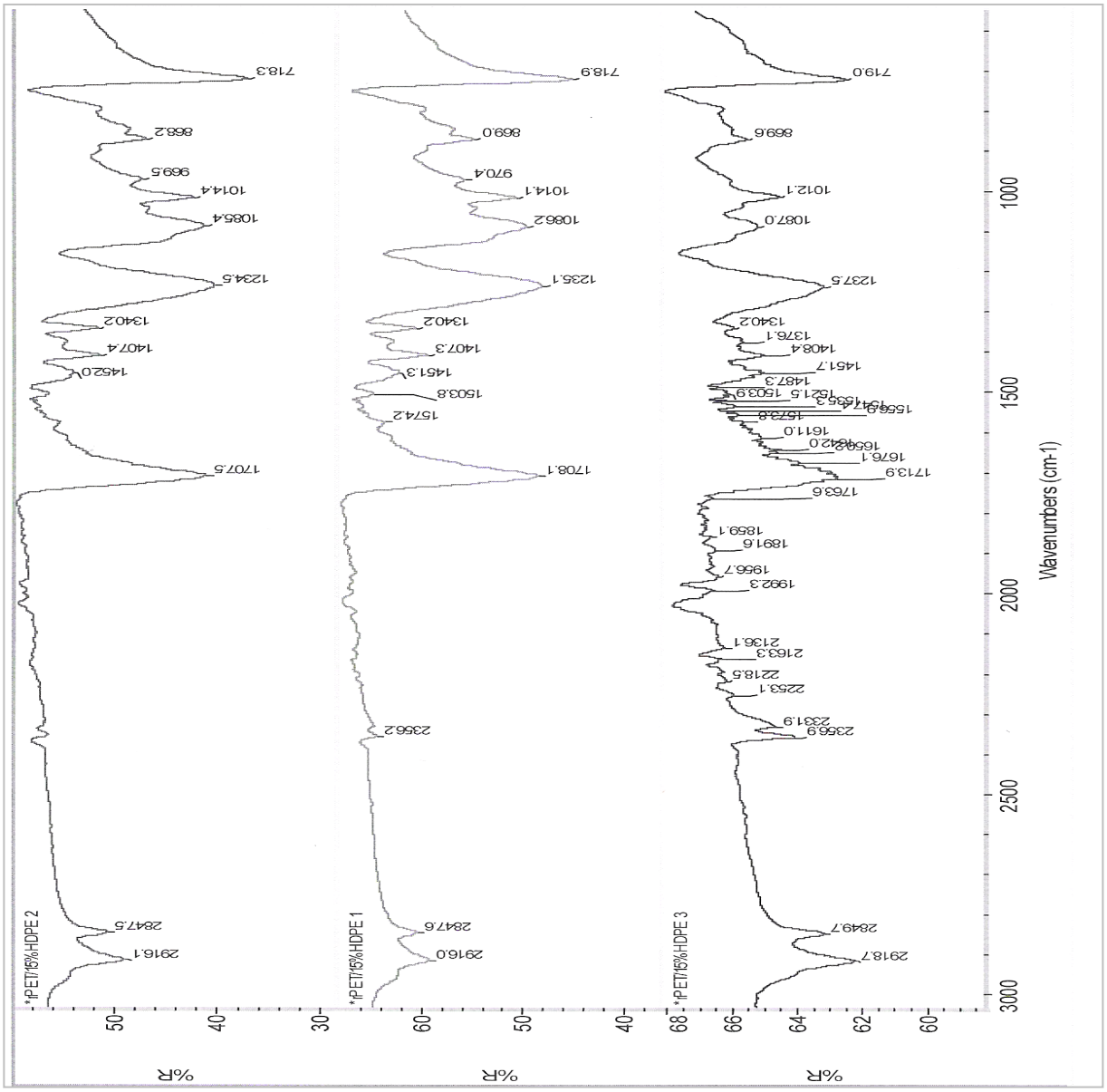

Figure 5.11 Spectra of of Extruded Samples of rPET-bg contaminated with 15% HDPE

Wavenumber (cm^{-1})			Bond	Wavenumber (cm^{-1})	Compound Type
Scan 1	**Scan 2**	**Scan 3**			
2916	2916	2918	C-H	2850-2960	Alkane
1708	1707	1713	C=O	1670-1760	Ester
1503 to 1574	?	1503 to 1573	C=C	1500-1600	Ester Ar. Ring
718 to 869	718 to 868	719 to 869	C-H	Below 900	Ester Ar. Ring
1086 to 1235	1085 to 1234	1087 to 1237	C-O	1000-1260	Ester

Table 5.12 FTIR Data of Extr. Samples of rPET-bg Contaminated with 15% HDPE

The results, shown in *Table 5.13* below, showed additional absorptions at (*2847-2849cm^{-1}*) which fall into the range expected for the *broad C-H stretch* of an *alkane* (*2850-2960cm^{-1}*) resulted from the vibration frequencies of the included *HDPE* molecular *alkane bonds*. The absorptions of most bonds, the *aromatic ester ring C-H*, the *aromatic ester ring C=C*, the *ester C=O*, the *ester C-O* and the *allkane* group broad *C-H*, showed instability in vibration levels, which indicated, as seen previously, unbalanced molecular strains as a result of heterogeneous absorptions and dispersion of sporadic crystals and as a result of various levels of absorptions due to the various interactions generated by the inclusion of HDPE. As the energy level of infrared light corresponds to the energy required to cause molecular vibrations, therefore, the *extruded samples*' molecular bonds in the batches of *rPET-bg contaminated with HDPE* compared to their counterpart of *non contaminated rPET-bg* showed slight increase and stability of vibrations; this indicated additional intermolecular hydrogen interaction as a result of the infrared light interacting with the resonant vibrational frequency of the bonds. The shown levels of absorptions and interactions between bonds indicated decreased strains as a result of further processing and confirmed the slight stability of % crystallinity shown by the DSC analysis.

Material	**Extruded Samples of rPET-bg** (1) **Compared to rPET-bg / HDPE** (5%, 10% and 15%)

Samples (1)	**5% HDPE)**	**10% HDPE**	**15% HDPE**	**Reference**		
Wavenumber (cm^{-1})				**Bonds**	**Wavenumber (cm^{-1})**	**Compound Type**
2915 to 2919	2916 to 2919 2847 to 2849	2916 to 2917 2848	2916 to 2918 2847 to 2849	C-H	2850-2960	Alkane
1705 to 1708	1710 to 1713	1699 to 1712	1707 to 1713	C=O	1670-1760 stretch	Ester
1503 to 1574	1504 to 1576	1503 to 1574	1503 to 1574	C=C	1500-1600	Ester Ar. Ring
410 to 867	422 to 871	666 to 870	718 to 869	C-H	Below 900	Ester Ar. Ring
1084 to 1236	1086 to 1238	1082 to 1240	1085 to 1237	C-O	1000-1260	Ester

Table 5.13 FTIR Data of Extruded Samples of rPET-bg contaminated with HDPE

5.1.3 MFR results of *Extruded Samples*

In *experiments 3, 4* and *5*, the MFR analysis yielded the data below.

Material	**Extruded Samples of 95% rPET-bg Contaminated with 5% HDPE**		
Extrudates	**Weight Averages (g)**	**Time (s)**	**MFR (g/10min)**
Run 1	**1.09**	15	43.52
Run 2	**0.68**	10	41.00
Run 3	**0.32**	05	38.84
Mean (μ)			**41.12**
STDEV (σ)			2.34
ST. Error ($S_E = \sigma/n^{0.5}$)			1.35
CI (95%), ($\mu \pm 1.96 S_E$)			$\mu \pm 2.65$

Table 5.14 MFR of Extruded Samples of rPET-bg Contaminated with 5% HDPE

Run 1	**1.24**	15	49.48
Run 2	**0.82**	10	49.50
Run 3	**0.40**	05	48.48
Mean (μ)			**49.15**
STDEV (σ)			0.58
ST. Error ($S_E = \sigma/n^{0.5}$)			0.34
CI (95%), ($\mu \pm 1.96 S_E$)			$\mu \pm 0.66$

Table 5.15 MFR of Extruded Samples of rPET-bg Contaminated with 10% HDPE

Run 1	**1.41**	15	56.45
Run 2	**0.95**	10	57.08
Run 3	**0.46**	05	55.08
Mean (μ)			**56.20**
STDEV (σ)			1.02
ST. Error ($S_E = \sigma/n^{0.5}$)			0.59
CI (95%), ($\mu \pm 1.96 S_E$)			$\mu \pm 1.16$

Table 5.16 MFR of Extruded Samples of rPET-bg Contaminated with 15% HDPE

Compared to non contaminated rPET-bg, as shown in *Table 5.17* and *Figure 5.12* below, one can see the effect of HDPE in decreasing the *MFR* in the contaminated rPET-bg, which is attributed to the *melt flow* property of HDPE of *8g /10min* as shown in *Table 3.1, Section 3.1.2*; if the inclusion of HDPE influenced the MFR of contaminated samples because of its low MFR, so the decrease should be higher with increasing % HDPE contamination, instead, at 5% HDPE contamination, the MFR is lower than at 15% HDPE contamination. This indicated that at 5% HDPE, the chains of HDPE were easily dispersed homogeneously within the rPET-bg matrix, between the interstices, and entangled the main chains. This sort of entanglement acted and delayed the shear rate of lamellae and increased the viscosity during the flow of the melt, i.e. decreases the MFR. Whereas, at 10 and 15% HDPE contamination, the contamination dispersion is more localised than widely dispersed, which in terms of flow, the viscosity was unbalanced and larger areas were unaffected by the contamination and therefore the average MFR followed the flow behaviour of the matrix, resulting in higher MFR average at higher % HDPE contamination. Additionally, the incompatibility of HDPE and rPET-bg was a predominant factor in promoting chains scissions during degradation and increasing shear of the contaminated lamellae. And this incompatibility, can only be overcome by the use of appropriate compatibilisers, especially when the dispersed phase concentration exceeds *5* to *10%* weight, as reported by *Utracki* [105].

Extruded Samples	**MFR (g/10mins)**		
	Mean (μ)	**ST. Error ($S_E = \sigma/n^{0.5}$)**	**CI (95%) ($\mu \pm 1.96 S_E$)**
Non contaminated rPET-bg	**74.30**	0.52	$\mu \pm 1.02$
95% rPET-bg / 5% HDPE	**41.12**	1.35	$\mu \pm 2.65$
90% rPET-bg / 10% HDPE	**49.15**	0.38	$\mu \pm 0.66$
85% rPET-bg / 15% HDPE	**56.20**	0.59	$\mu \pm 1.16$

Table 5.17 MFR of Extruded Samples of rPET-bg Contaminated with HDPE

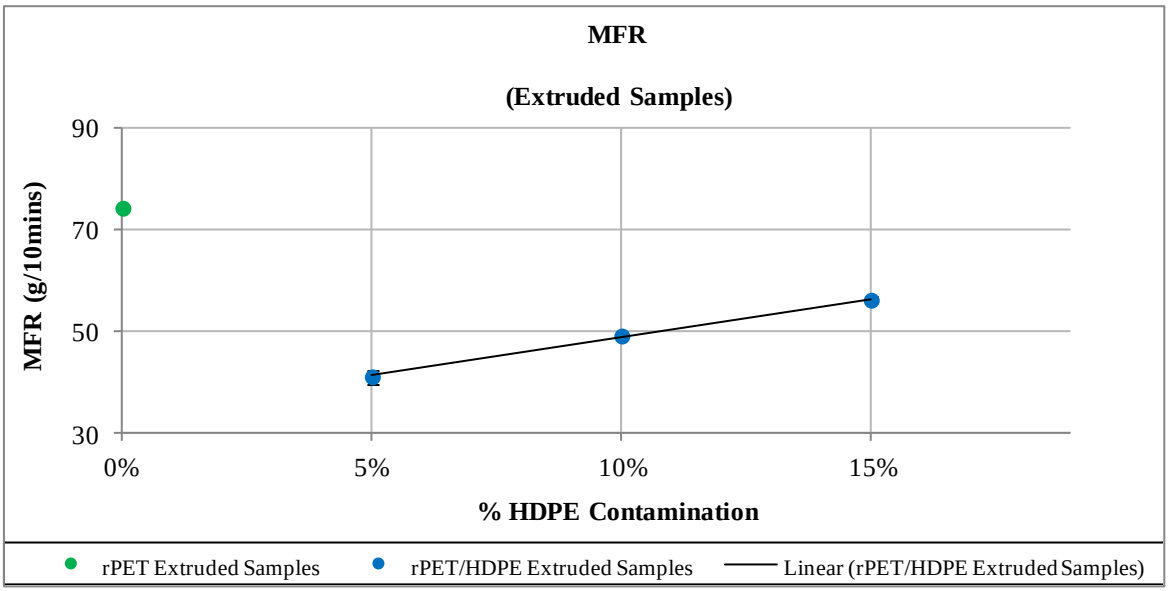

Figure 5.12 MFR of Extruded Samples of rPET-bg Contaminated with HDPE

By analysis of *Figure 5.13* below, the curves of rPET- bg contaminated with HDPE showed the inverse proportionality between MFR and % torque; the % torque of the screw during extrusion indicates the melt flow behaviour in terms of viscosity, i.e. % torque and viscosity are proportional and consequently, the MFR is inversely proportional to the viscosity. As reported in the literature [168], [169], the higher shear rate of melt lamellae yield a higher MFR and results in low viscosity, and this rule is obeyed in this case.

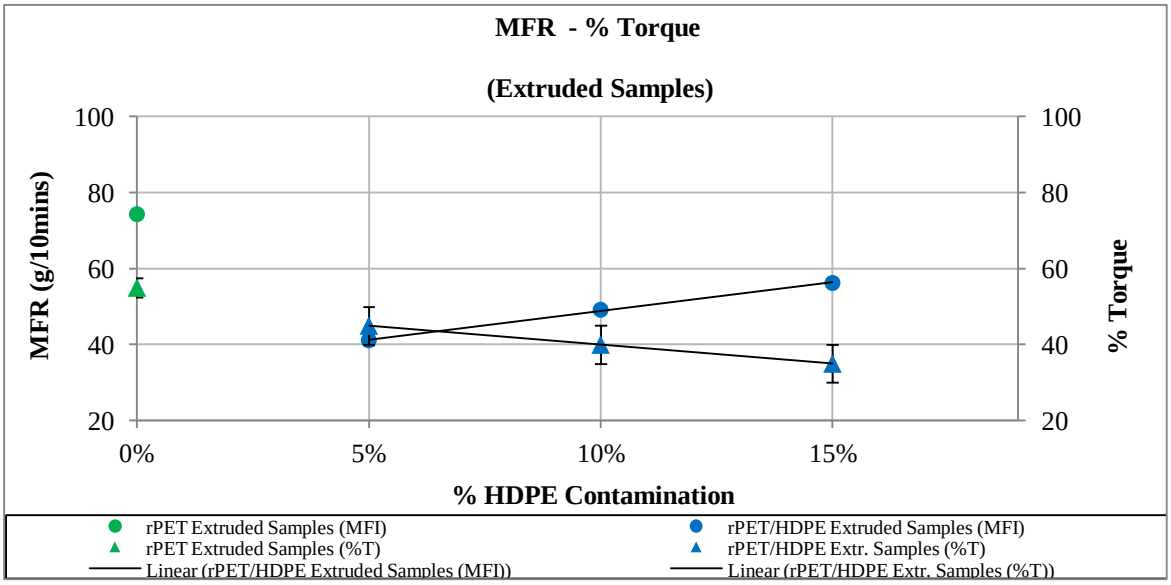

Figure 5.13 MFR Compared to % Torque of Extruded Samples of rPET-bg Contaminated with HDPE

Furthermore, by analysis of *Figure 5.14* below, the curves of rPET- bg contaminated with HDPE showed inverse proportionality between MFR and screw speed; the screw speed in extrusion is inversely proportional to viscosity, so if screw speeds decreased this means that chains-scissions were happening at high rate and increasing the concentrations of the very small HDPE and matrix chains, which lead to increased viscosity resulting in extruded samples which yielded increased MFR.

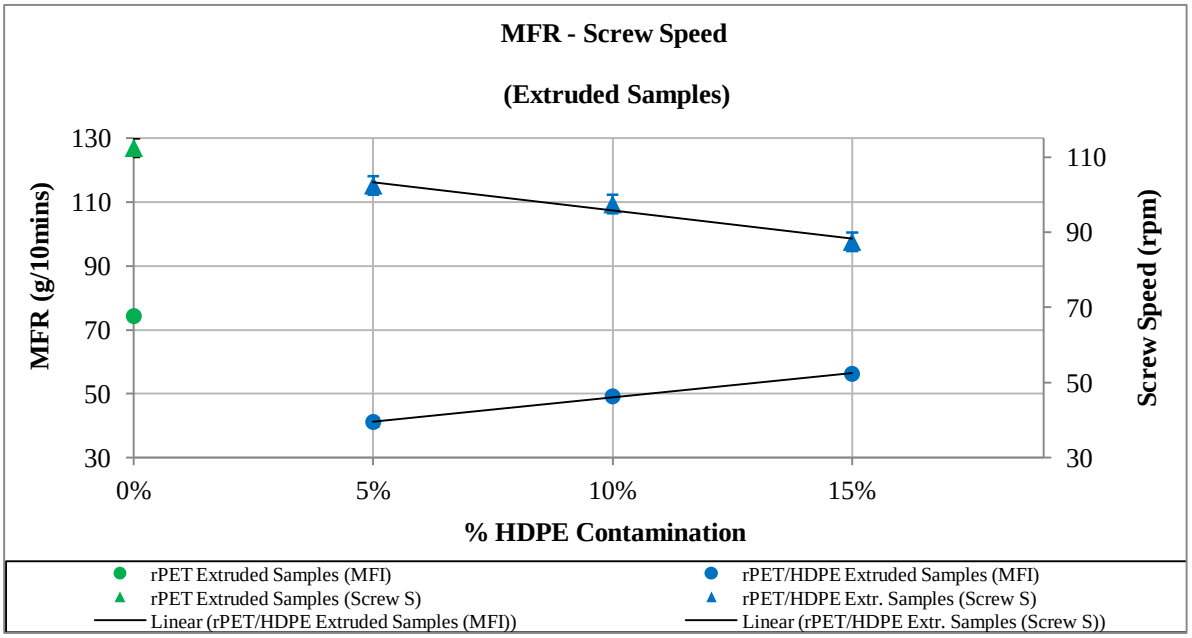

Figure 5.14 MFR Compared to Screw Speed of Extruded Samples of rPET-bg Contaminated with HDPE

In *experiments 3*, *4* and *5*, the *extruded pellets* of rPET-bg, contaminated respectively with *5%*, *10%* and *15%* HDPE, were injection moulded into *dumbbells* and *impact bars*. Again, *injection moulded samples* were analysed by DSC, FTIR, MFR and the *dumbbells* and *impact bars* were tested for their tensile and impact properties and investigated and the results are shown and discussed below.

During injection moulding, the optimised processing conditions resulted in variations of injection and packing pressures, as shown in *Table 5.18* below, the decreased injection and packing pressures with increasing % HDPE contamination, indicated ease of flow, balanced distribution, orientation and packing of the contaminated materials in the mould cavity. Compared to non contaminated rPET-bg, the contaminated materials showed homogeneous blending and melting of the extruded pellets in the barrel of the injection machine and indicated good flow properties of the contaminant, HDPE.

Injection Moulded Samples	**Injection Pressure (Bars)**	**Packing Pressure (Bars)**	**Mould Temp. (^{o}C)**	**Injection Time (s)**	**Packing Pressure (%)**
Non contaminated rPET-bg	**180**	**75**	60	1.35	45%
95% rPET-bg / 5% HDPE	**170**	**72**	60	1.35	45%
90% rPET-bg / 10% HDPE	**170**	**70**	60	1.35	45%
85% rPET-bg / 15% HDPE	**170**	**67**	60	1.35	45%

Table 5.18 Variation of Injection Moulding Condition of rPET-bg Contaminated with HDPE

5.1.4 DSC results of *Injection Moulded Samples*

In *experiments 3, 4* and *5*, the DSC analysis yielded the data below.

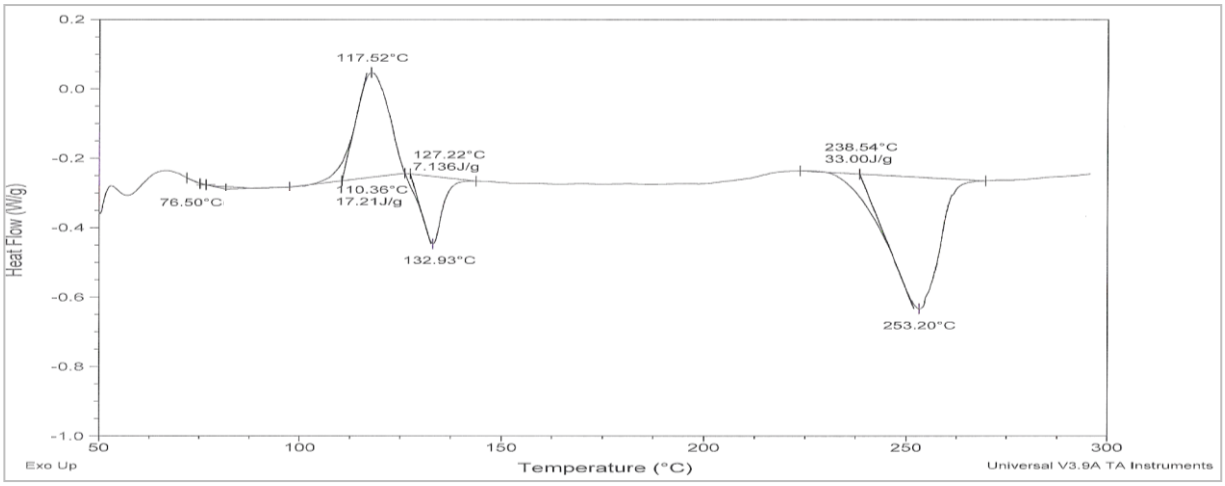

Figure 5.15 Thermogram of Inj. Moulded Sample 1 of rPET-bg contaminated with 5% HDPE

	T_g (°C)	T_m (°C)	ΔH_m (J/g)	T_c (°C)	ΔH_c (J/g)	ΔH_m^0 (J/g)	X_c (%)	T_d (°C)
Run 1	76.50	253.20	33.00	117.52	17.21	140	23.57	Nil
Run 2	74.77	254.18	37.10	117.08	21.17	140	26.50	Nil
Run 3	77.43	253.77	34.31	118.01	21.98	140	24.51	Nil
Mean (μ)	**76.23**	**253.72**	**34.80**	**117.54**	**20.12**		**24.86**	
STDEV (σ)	1.35	0.49	2.09	0.46	2.55		1.50	
ST. Error ($S_E = \sigma/n^{0.5}$)	0.78	0.28	1.21	0.27	1.47		0.86	
CI (95%), ($\mu \pm 1.96 S_E$)	$\mu \pm 1.53$	$\mu \pm 0.56$	$\mu \pm 2.37$	$\mu \pm 0.53$	$\mu \pm 2.89$		$\mu \pm 1.69$	

Table 5.19 DSC Data of Inj. Moulded Samples of rPET-bg Contaminated with 5% HDPE

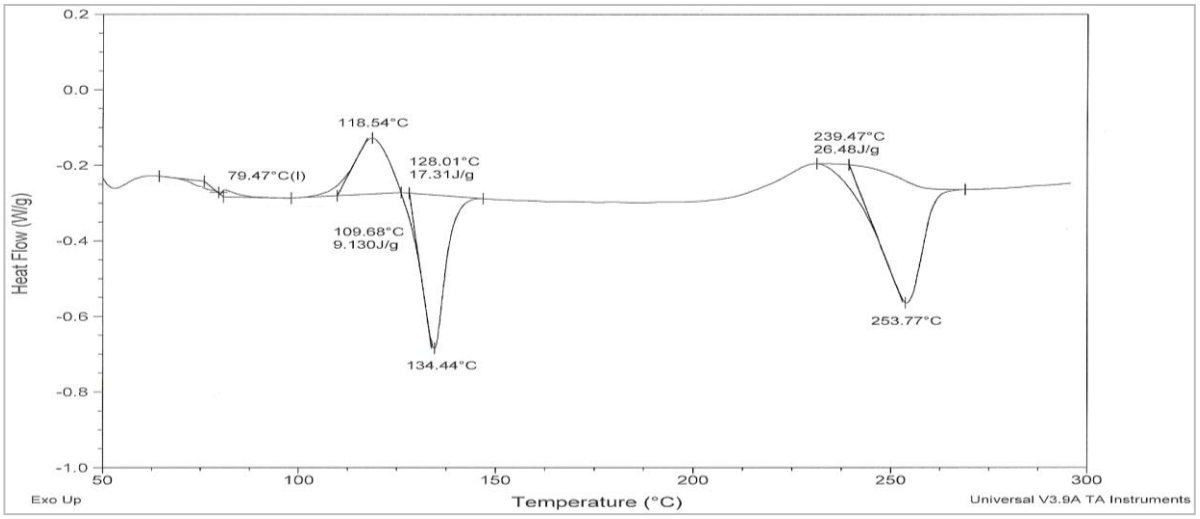

Figure 5.16 Thermogram of Inj. Moulded Sample 1 of rPET-bg contaminated with 10% HDPE

	T_g (^{o}C)	T_m (^{o}C)	ΔH_m (J/g)	T_c (^{o}C)	ΔH_c (J/g)	ΔH_m^0 (J/g)	X_c (%)	T_d (^{o}C)
Run 1	79.47	253.77	26.48	118.54	9.13	140	18.91	Nil
Run 2	75.00	251.68	26.28	118.06	15.48	140	18.77	Nil
Run 3	72.79	251.88	25.22	119.25	15.42	140	18.01	Nil
Mean (μ)	**75.75**	**252.44**	**25.99**	**118.62**	**13.34**		**18.57**	
STDEV (σ)	3.40	1.15	0.68	0.60	3.65		0.48	
ST. Error ($S_E = \sigma/n^{0.5}$)	1.96	0.67	0.39	0.346	2.11		0.28	
CI (95%), ($\mu \pm 1.96 S_E$)	$\mu \pm 3.85$	$\mu \pm 1.30$	$\mu \pm 0.77$	$\mu \pm 0.677$	$\mu \pm 4.13$		$\mu \pm 0.55$	

Table 5.20 DSC Data of Inj. Mould. Samples of rPET-bg Contaminated with 10% HDPE

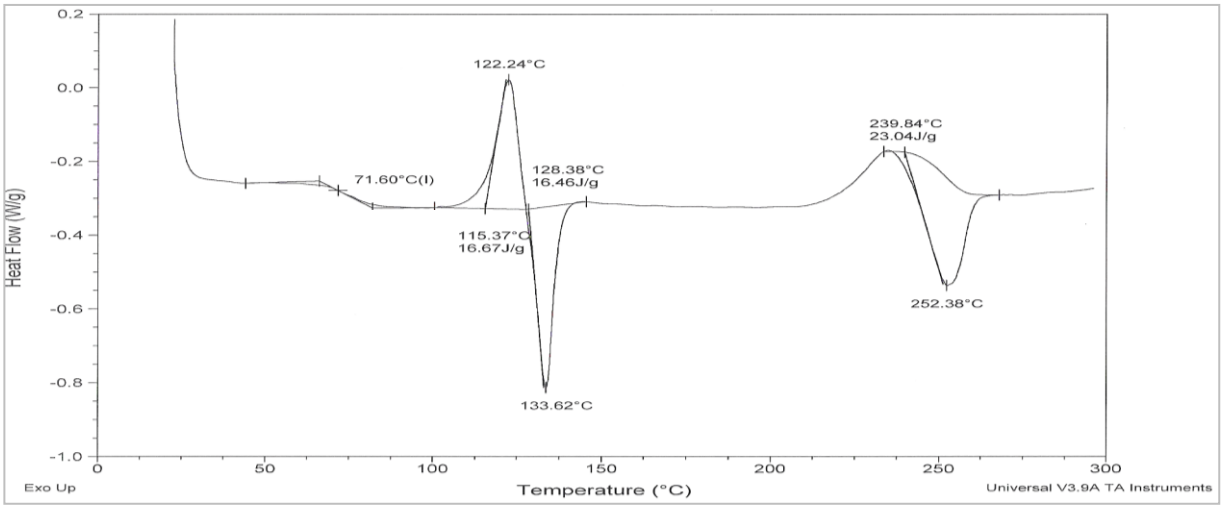

Figure 5.17 Thermogram of Inj. Moulded Sample 1 of rPET-bg contaminated with 15% HDPE

	T_g (^{o}C)	T_m (^{o}C)	ΔH_m (J/g)	T_c (^{o}C)	ΔH_c (J/g)	ΔH_m^0 (J/g)	X_c (%)	T_d (^{o}C)
Run 1	71.60	252.38	23.04	122.24	16.67	140	16.46	Nil
Run 2	73.05	251.97	26.08	122.15	14.72	140	18.63	Nil
Run 3	75.28	253.24	28.45	121.15	16.08	140	20.32	Nil
Mean (μ)	**73.31**	**252.53**	**25.86**	**121.85**	**15.82**		**18.47**	
STDEV (σ)	1.85	0.65	2.71	0.60	1.00		1.94	
ST. Error ($S_E = \sigma/n^{0.5}$)	1.07	0.37	1.57	0.35	0.58		1.12	
CI (95%), ($\mu \pm 1.96 S_E$)	$\mu \pm 2.10$	$\mu \pm 0.73$	$\mu \pm 3.07$	$\mu \pm 0.68$	$\mu \pm 1.13$		$\mu \pm 2.19$	

Table 5.21 DSC Data of Inj. Mould. Samples of rPET-bg Contaminated with 15% HDPE

Note: Additional DSC Thermograms are available in ***Appendix 5*** **(***7, 8, 9***).**

Compared to non contaminated rPET-bg, as shown in *Table 5.22* and *Figure 5.18* below, the T_g of the rPET-bg contaminated with HDPE decreased orderly with increasing % HDPE contamination in all cases, indicating presence of small amorphous domains of very small chains; these amorphous domains were restricted by the decreased packing pressure in cavity, which promoted balanced orientation, straightening and packing of the material chains during the cooling process of injection moulding and formation of ordered crystalline domains. The chains of the amorphous domains required short scales of time and temperatures to re-arrange during the DSC heating process, resulting in decreased T_g with increasing % HDPE contamination.

Inj. Moulded Samples	**T_g (°C)**		
	Mean (μ)	**ST. Error ($S_E = \sigma/n^{0.5}$)**	**CI (95%) ($\mu \pm 1.96 S_E$)**
Non contaminated rPET-bg	**79.60**	3.29	$\mu \pm 6.45$
95% rPET-bg / 5% HDPE	**76.23**	0.78	$\mu \pm 1.53$
90% rPET-bg / 10% HDPE	**75.75**	1.96	$\mu \pm 3.85$
85% rPET-bg / 15% HDPE	**73.31**	1.07	$\mu \pm 2.10$

Table 5.22 Glass Transition Temperature of Inj. Moulded Samples of rPET-bg Contaminated with HDPE

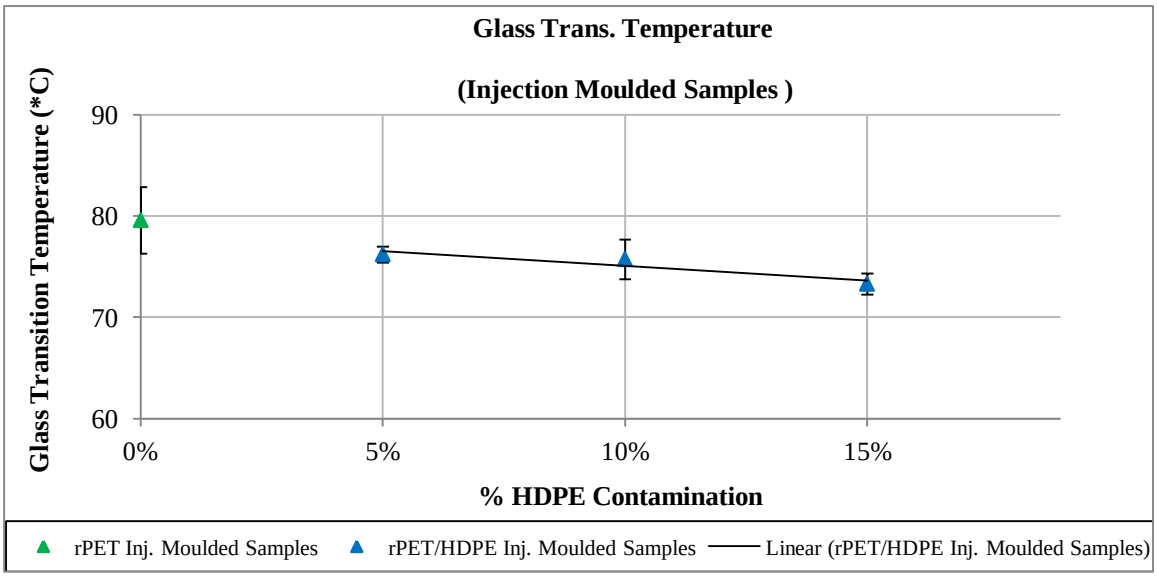

Figure 5.18 Glass Transition Temperature of Inj. Moulded Samples of rPET-bg Contaminated with HDPE

Compared to non contaminated rPET-bg, as shown in *Table 5.23* and *Figure 5.19* below, following injection moulding, and due to optimised cooling, additional crystalline domains were created as a result of well balanced flow, orientation and packing which allowed stress relaxation of the materials molecular chains and the enhancement of straightening. The T_c of the rPET-bg contaminated with HDPE are still lower than that of non contaminated rPET-bg which indicated that HDPE chains entangled the matrix chains and decreased their relaxation, and decreased the packing pressure. The increase of T_c in the contaminated materials is proportional to the increase in % HDPE contamination, which indicated that the increased very short chains, allowed additional creation of crystalline domains. During the DSC heating mode amorphous domains resulting from retained in samples were able to re-crystallise and release certain amounts of energy, as shown by cold crystallisation exotherms, which also indicated chains relaxation and straightening.

Inj. Moulded Samples	**T_c (^{o}C)**		
	Mean (μ)	**ST. Error ($S_E = \sigma/n^{0.5}$)**	**CI (95%) ($\mu \pm 1.96 S_E$)**
Non contaminated rPET-bg	**120.23**	1.07	$\mu \pm 2.09$
95% rPET-bg / 5% HDPE	**117.54**	0.27	$\mu \pm 0.53$
90% rPET-bg / 10% HDPE	**118.62**	0.35	$\mu \pm 0.68$
85% rPET-bg / 15% HDPE	**121.85**	0.35	$\mu \pm 0.68$

Table 5.23 Cold Crystallisation Temperature of Inj. Moulded Samples of rPET-bg Contaminated with HDPE

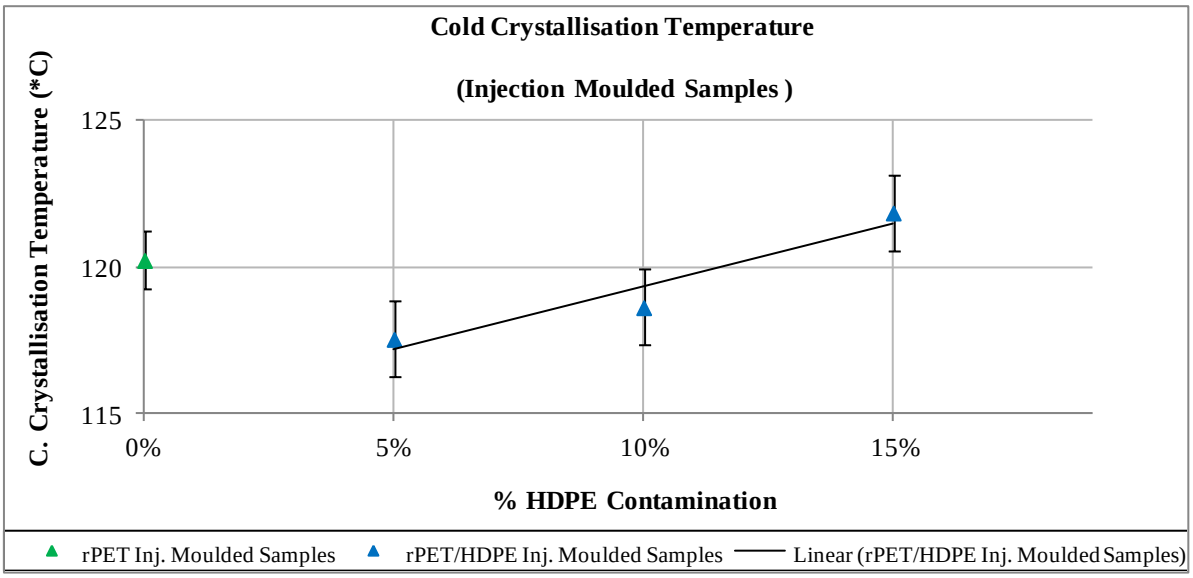

Figure 5.19 Cold Crystallisation Temperature of Inj. Moulded Samples of rPET-bg Contaminated with HDPE

Compared to non contaminated rPET-bg, as shown in *Table 5.24* and *Figure 5.20* below, the decrease of enthalpy of cold crystallisation ΔH_c indicated presence of very small crystalline domains coupled with very small and sporadically dispersed large number of very small chains which released reduced amounts of heat to straighten during the DSC heating mode and that HDPE chains by melting prematurely prevented the completion of cold crystallisation, which was overridden by overall melting.

Inj. Moulded Samples	ΔH_c (J.g^{-1})		
	Mean (μ)	**ST. Error ($S_E = \sigma/n^{0.5}$)**	**CI (95%) ($\mu \pm 1.96 S_E$)**
Non contaminated rPET-bg	**23.46**	2.72	$\mu \pm 5.33$
95% rPET-bg / 5% HDPE	**20.12**	1.47	$\mu \pm 2.89$
90% rPET-bg / 10% HDPE	**13.34**	2.11	$\mu \pm 4.13$
85% rPET-bg / 15% HDPE	**15.82**	0.58	$\mu \pm 1.13$

Table 5.24 Heat of Cold Crystallisation of Inj. Moulded Samples of rPET-bg Contaminated with HDPE

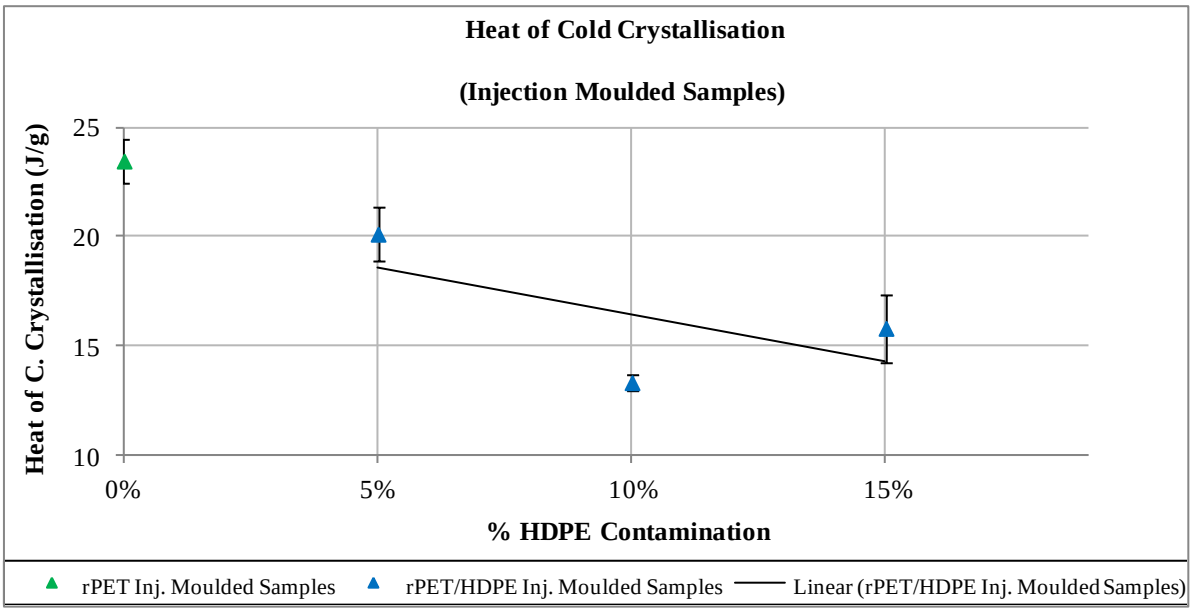

Figure 5.20 Heat of Cold Crystallisation of Inj. Moulded Samples of rPET-bg Contaminated with HDPE

Compared to non contaminated rPET-bg, as shown in *Table 5.25* and *Figure 5.21* below, following injection moulding, the T_m slightly decreased in all cases and depended on particular packing of crystalline domains in the various contaminated materials. Again, the presence of prematurely melted crystalline domains including HDPE coupled with a low degree of packing of very small chains allowed fast melting and resulted in reduced T_m. The extra processing heat of inj. moulding did not affect the miscibility factor; the *incompatibility* and *immiscibility* persisted as shown by the presence of both individual melting peaks.

Inj. Moulded Samples	**T_m (^{o}C)**		
	Mean (μ)	**ST. Error ($S_E = \sigma/n^{0.5}$)**	**CI (95%) ($\mu \pm 1.96 S_E$)**
Non contaminated rPET-bg	**253.86**	0.80	$\mu \pm 1.57$
95% rPET-bg / 5% HDPE	**253.72**	0.28	$\mu \pm 0.56$
90% rPET-bg / 10% HDPE	**252.44**	0.67	$\mu \pm 1.30$
85% rPET-bg / 15% HDPE	**252.53**	0.37	$\mu \pm 0.73$

Table 5.25 Melting Temperature of Inj. Moulded Samples of rPET-bg Contaminated with HDPE

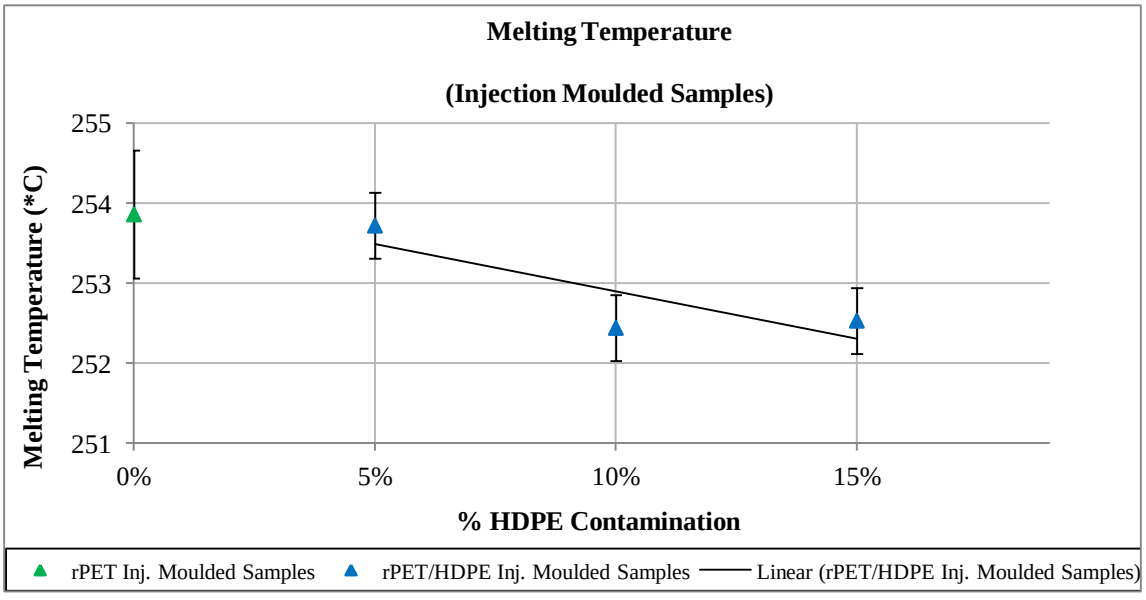

Figure 5.21 Melting Temperature of Inj. Moulded Samples of rPET-bg Contaminated with HDPE

Compared to non contaminated rPET-bg, as shown in *Table 5.26* and *Figure 5.22* below, the balanced melting of the ordered crystalline domains created certain balanced in heat absorption, resulting in a gradual decrease of the overall enthalpy of melting ΔH_m. Without doubt, the inclusion of HDPE and the created very small crystalline domains, which included HDPE chains, were predominant factors in quantitatively easing the melting process and consequently in reducing the melting enthalpy.

Inj. Moulded Samples	ΔH_m (J.g^{-1})		
	Mean (μ)	**ST. Error ($S_E = \sigma/n^{0.5}$)**	**CI (95%) ($\mu \pm 1.96 S_E$)**
Non contaminated rPET-bg	**46.22**	3.21	$\mu \pm 6.29$
95% rPET-bg / 5% HDPE	**34.80**	1.21	$\mu \pm 2.37$
90% rPET-bg / 10% HDPE	**25.99**	0.39	$\mu \pm 0.77$
85% rPET-bg / 15% HDPE	**25.86**	1.57	$\mu \pm 3.07$

Table 5.26 Heat of Fusion of Inj. Moulded Samples of rPET-bg Contaminated with HDPE

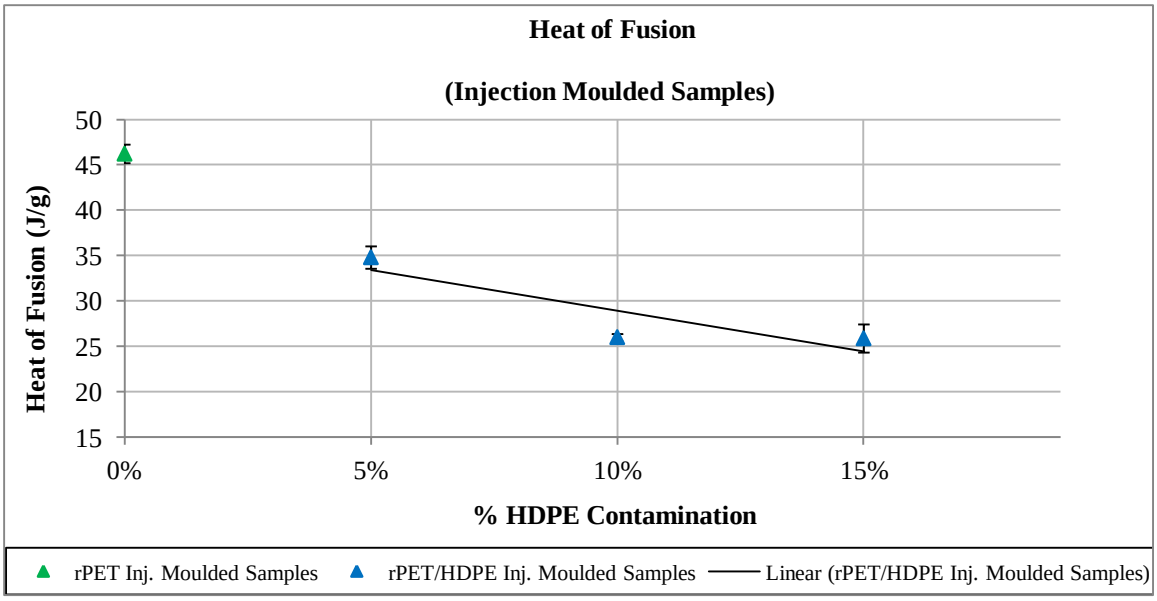

Figure 5.22 Heat of Fusion of Inj. Moulded Samples of rPET-bg Contaminated with HDPE

Compared to non contaminated rPET-bg, as shown in *Table 5.27* and *Figure 5.23* below, the % crystallinity, X_c, of the rPET-bg contaminated with HDPE decreased orderly with increasing % HDPE contamination in all cases, indicating that the very small HDPE chains filled the interstices existing between the matrix chains and created entanglement and prevented ordered packing. The degree of disorder was proportional to the % HDPE contamination; higher % HDPE contamination conveyed higher disorder of chains and resulted in lower crystallinity and vice versa. And the reduced X_c confirmed the pattern of the crystalline domains as being numerous but dispersed as a result of influence of HDPE inclusion.

Inj. Moulded Samples	**X_c (%)**		
	Mean (μ)	**ST. Error ($S_E = \sigma/n^{0.5}$)**	**CI (95%) ($\mu \pm 1.96 S_E$)**
Non contaminated rPET-bg	**33.01**	2.29	$\mu \pm 4.49$
95% rPET-bg / 5% HDPE	**24.86**	0.86	$\mu \pm 1.69$
90% rPET-bg / 10% HDPE	**18.57**	0.28	$\mu \pm 0.55$
85% rPET-bg / 15% HDPE	**18.47**	1.12	$\mu \pm 2.19$

Table 5.27 % Crystallinity of Inj. Moulded Samples of rPET-bg Contaminated with HDPE

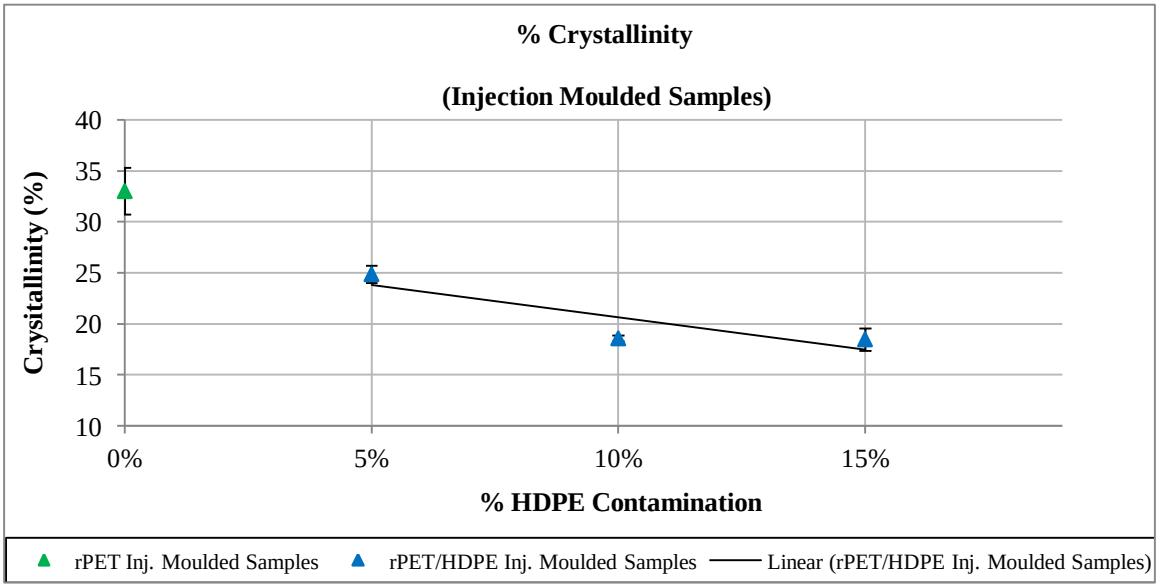

Figure 5.23 % Crystallinity of Inj. Moulded Samples of rPET-bg Contaminated with HDPE

5.1.5 FTIR results of *Injection Moulded Samples*

In *experiments 3, 4* and *5*, the FTIR analysis yielded the data below.

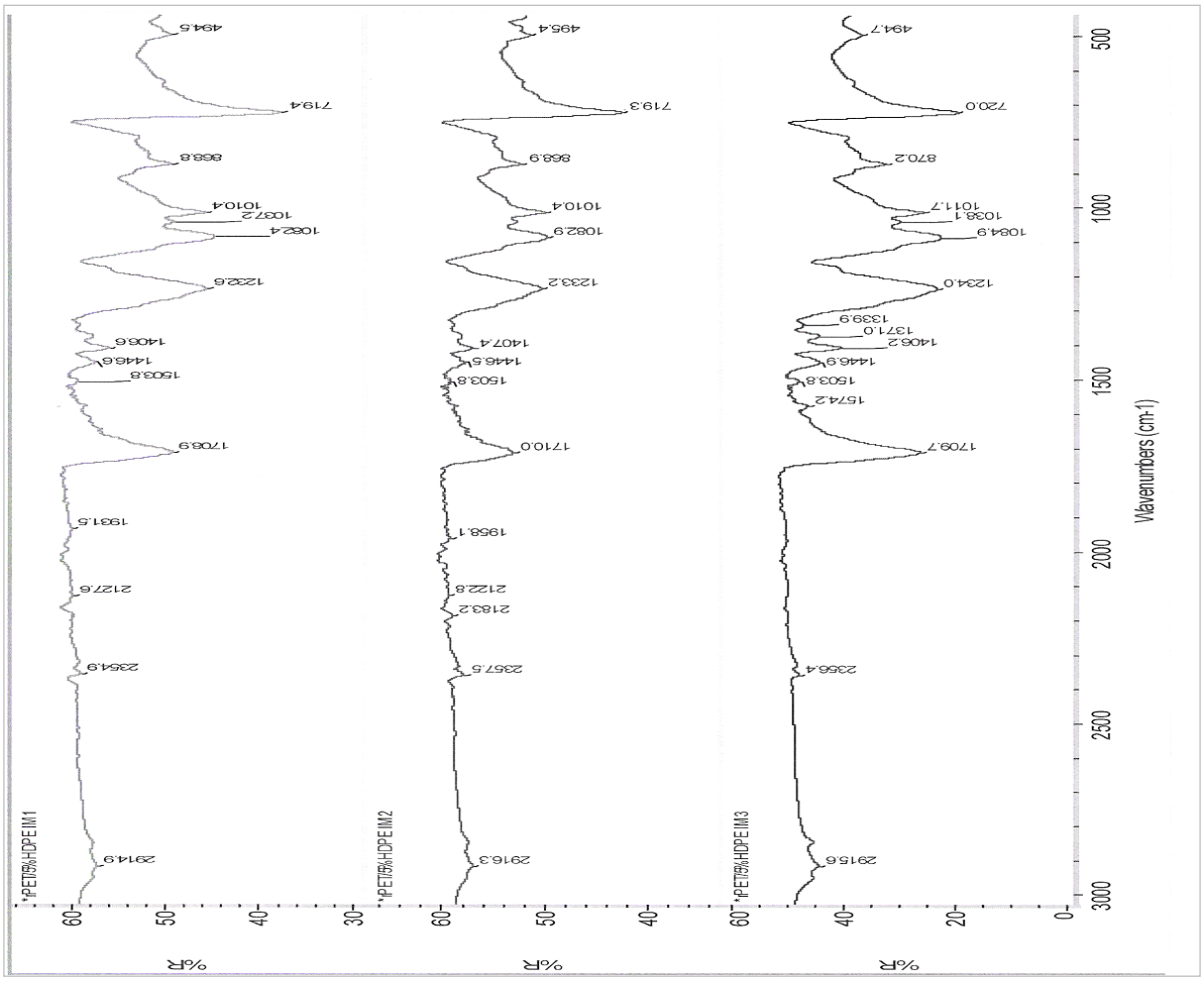

Figure 5.24 FTIR Spectra of Inj. Moulded Samples of rPET-bg contaminated with 5% HDPE

Wavenumber (cm^{-1})			Bond	Wavenumber (cm^{-1})	Compound Type
Scan 1	**Scan 2**	**Scan 3**			
2914	2916	2915	C-H	2850-2960	Alkane
1708	1710	1709	C=O	1670-1760	Ester
1503	1503	1503 to 1574	C=C	1500-1600	Ester Ar. Ring
494 to 868	494 to 868	494 to 870	C-H	Below 900	Ester Ar. Ring
1082 to 1232	1082 to 1232	1084 to 1234	C-O	1000-1260	Ester

Table 5.28 FTIR Data of Inj. M/ Samples of rPET-bg Contaminated with 5% HDPE

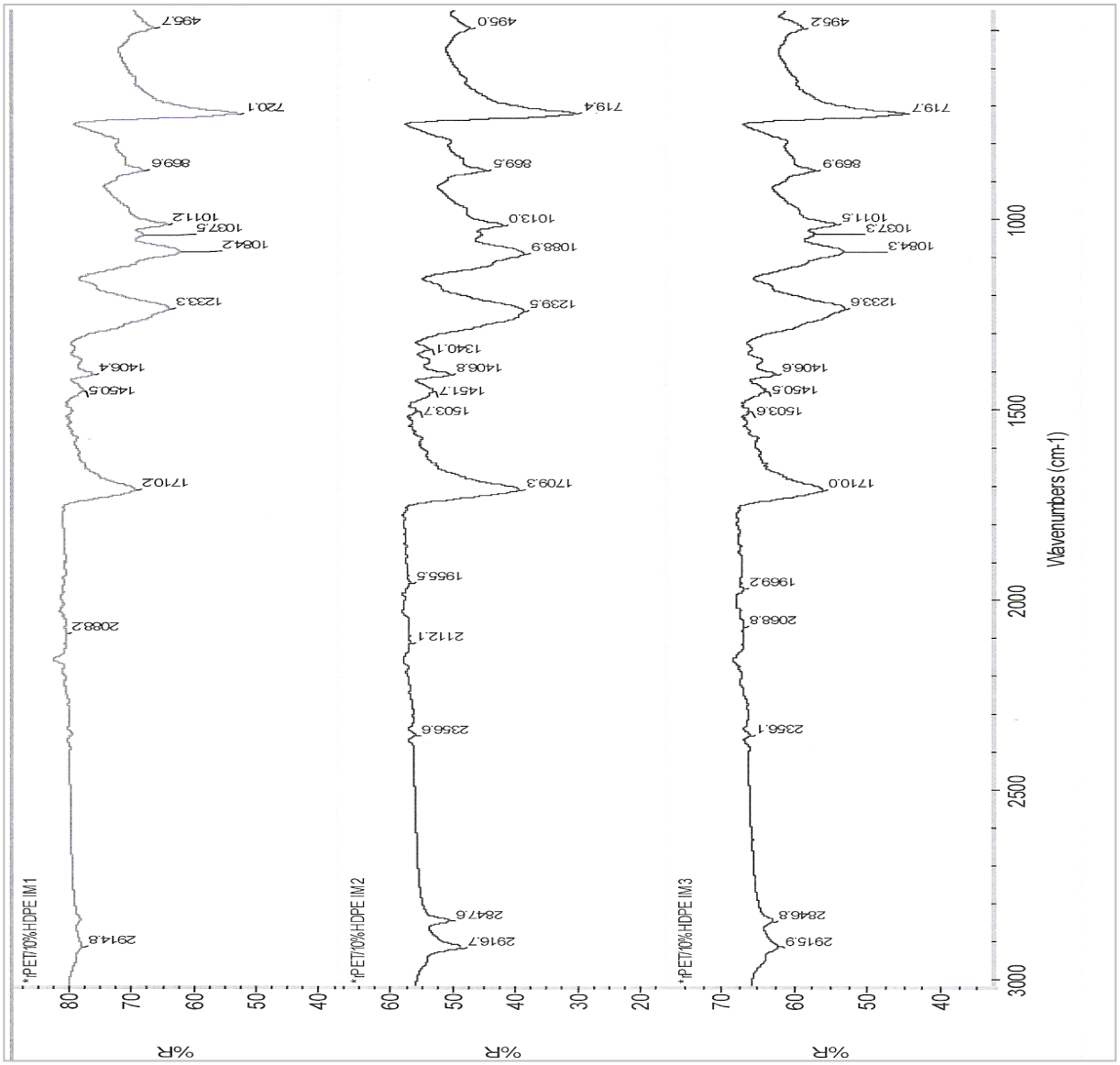

Figure 5.25 FTIR Spectra of Inj. Moulded Samples of rPET-bg contaminated with 10% HDPE

Wavenumber (cm^{-1})			Bond	Wavenumber (cm^{-1})	Compound Type
Scan 1	**Scan 2**	**Scan 3**			
2914	2916	2915	C-H	2850-2960	Alkane
1710	1709	1710	C=O	1670-1760	Ester
?	1503	1503	C=C	1500-1600	Ester Ar. Ring
495 to 869	495 to 869	495 to 869	C-H	Below 900	Ester Ar. Ring
1084 to 1233	1088 to 1239	1084 to 1233	C-O	1000-1260	Ester

Table 5.29 FTIR Data of Inj. M/ Sample of rPET-bg Contaminated with 10% HDPE

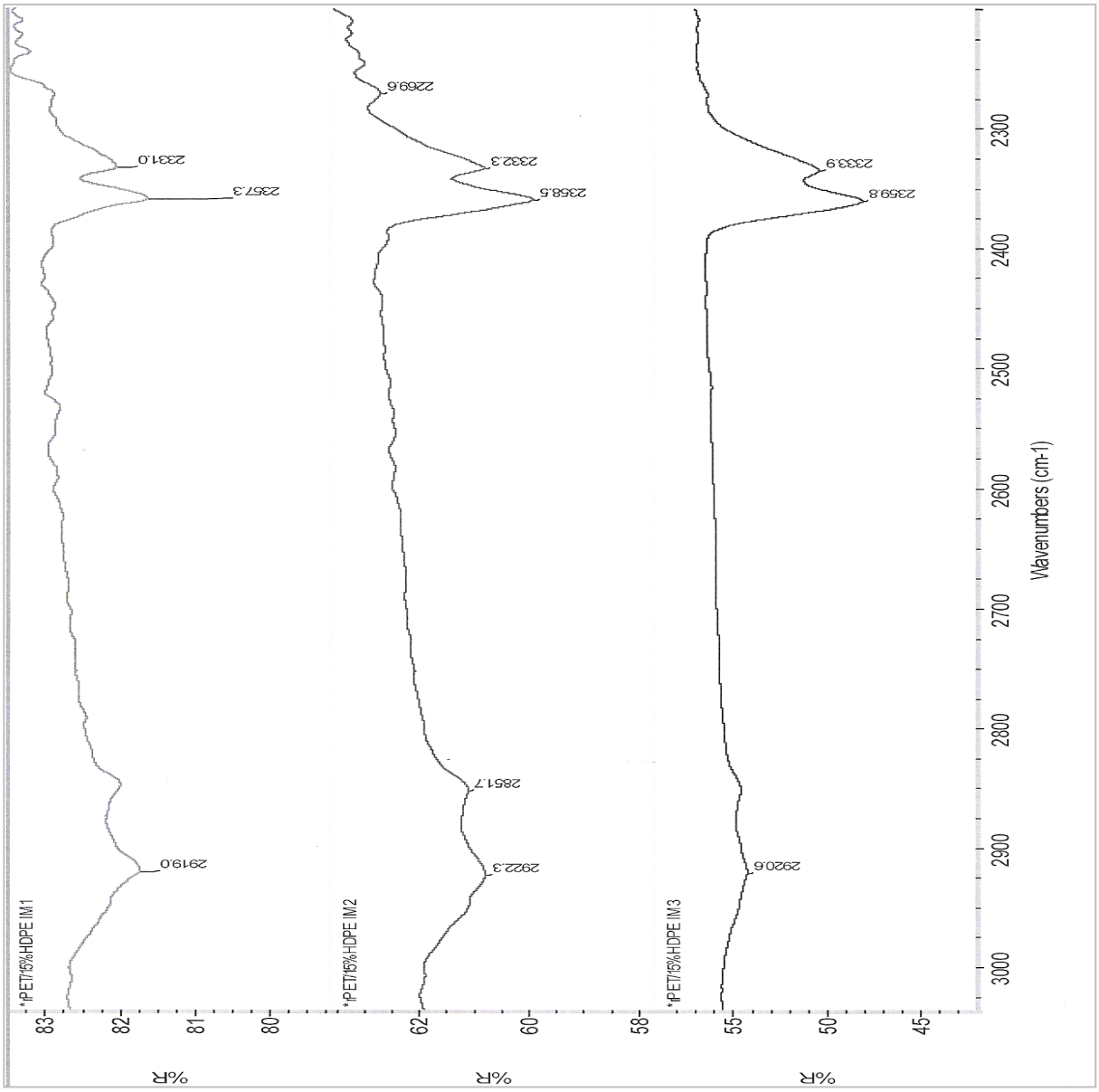

Figure 5.26 Spectra of Inj. Moulded Samples of rPET-bg contaminated with 15% HDPE

Wavenumber (cm^{-1})			Bond	Wavenumber (cm^{-1})	Compound Type
Scan 1	**Scan 2**	**Scan 3**			
2848 to 2919	2851 to 2922	2846 to 2920	C-H	2850-2960	Alkane
1707	1709	1713	C=O	1670-1760	Ester
1503	1574	1574	C=C	1500-1600	Ester Ar. Ring
718 to 866	719 to 869	718 to 869	C-H	Below 900	Ester Ar. Ring
1088 to 1233	1086 to 1237	1085 to 1235	C-O	1000-1260	Ester

Table 5.30 FTIR Dta of Inj. M/ Samples of rPET-bg Contaminated with 15% HDPE

The results, shown in *Table 5.31* below, showed slight stability in the absorption of *broad C-H stretch* of HDPE. The range of absorptions of most bonds, the *aromatic ester ring C-H*, the *aromatic ester ring C=C*, the *ester C=O*, the *ester C-O* and the *allkane* group broad *C-H*, in the *inj. moulded samples* compared to their counterpart of *non contaminated rPET-bg*, showed apparent stability and increase of vibrations due to dipole changes and mostly the strong dipole of the *ester C-O*; this indicated high level of vibrational freedom due to reduced chains' strain and reduced bonds' stiffness, as a result of dispersed and reduced crystalline domains. *Boutevin et al.* [170] and *Guerrero et al.* [171] in their studies on PET / HDPE blends reported changes in dipoles due to the inclusion of graft copolymers and compatibilisers; which indicated that the inclusion of HDPE affected the overall vibrational behaviour of the matrix molecular bonds.

Material	**Injection Moulded Samples of rPET-bg** (1) **Compared to rPET-bg / HDPE** (5%, 10% and 15%)

Samples (1)	**5% HDPE**	**10% HDPE**	**15% HDPE**	**Reference**		
Wavenumbers (cm^{-1})				**Bonds**	**Wavenumber Range (cm^{-1})**	**Compound Type**
2919 to 2953	2914 to 2916	2914 to 2916 2846 to 2847	2919 to 2922 2846 to 2851	C-H	2850-2960	Alkane
1697 to 1731	1708 to 1709	1709 to 1710	1707 to 1713	C=O	1670-1760	Ester
1503 to 1574	1503 to 1574	1503	1503 to 1574	C=C	1500-1600	Ester Ar. Ring
493 to 869	494 to 870	495 to 869	718 to 869	C-H	Below 900	Ester Ar. Ring
1081 to 1233	1082 to 1234	1084 to 1239	1085 to 1237	C-O	1000-1260	Ester

Table 5.31 FTIR Data of Injection Moulded Samples of rPET-bg contaminated with HDPE

5.1.6 MFR results of *Injection Moulded Samples*

In *experiments 3, 4* and *5*, the MFR analysis yielded the data below.

Extrudates	Weight (g)	Time (s)	MFR (g/10min)
Run 1	**1.22**	15	48.92
Run 2	**0.80**	10	47.88
Run 3	**0.43**	05	51.72
Mean (μ)			**49.51**
STDEV (σ)			1.99
ST. Error ($S_E = \sigma/n^{0.5}$)			1.15
CI (95%), ($\mu \pm 1.96 S_E$)			$\mu \pm 2.25$

Table 5.32 MFR of Inj. Moulded Samples of rPET-bg contaminated with 5% HDPE

Run 1	**1.41**	15	56.40
Run 2	**0.91**	10	54.72
Run 3	**0.50**	05	59.88
Mean (μ)			**57.00**
STDEV (σ)			2.63
ST. Error ($S_E = \sigma/n^{0.5}$)			1.52
CI (95%), ($\mu \pm 1.96 S_E$)			$\mu \pm 2.98$

Table 5.33 MFR of Inj. Moulded Samples of rPET-bg contaminated with 10% HDPE

Run 1	**1.53**	15	61.36
Run 2	**1.30**	10	78.06
Run 3	**0.56**	05	66.72
Mean (μ)			**68.71**
STDEV (σ)			8.53
ST. Error ($S_E = \sigma/n^{0.5}$)			4.92
CI (95%), ($\mu \pm 1.96 S_E$)			$\mu \pm 9.65$

Table 5.34 MFR of Inj. Moulded Samples of rPET-bg contaminated with 15% HDPE

The comparative *melt flow* results, shown in *Table 5.35* and *Figure 5.27* below, showed that the inclusion of HDPE increased the viscosity of non contaminated rPET-bg; one can see the influence of the HDPE chains, by entangling the matrix chains, especially in the interstices, allowed reduction of sliding and shear and increasing the viscosity, especially at low % HDPE contamination. The increase of MFR in the contaminated materials was proportional to the % HDPE contamination, which indicated gradual increase of shear in the HDPE lamellae; the more % HDPE included, the more shear was encountered resulting in increase of MFR within the contaminated materials, as result of the influence of molecular weights on the viscosity ratio, as reported by *Mbarek et al.* [172].

Inj. Moulded Samples	**MFR (g/10mins)**		
	Mean (μ)	**ST. Error ($S_E = \sigma/n^{0.5}$)**	**CI (95%) ($\mu \pm 1.96 S_E$)**
Non contaminated rPET-bg	**96.23**	8.06	$\mu \pm 15.80$
95% rPET-bg / 5% HDPE	**49.51**	1.15	$\mu \pm 2.25$
90% rPET-bg / 10% HDPE	**57.00**	1.52	$\mu \pm 2.98$
85% rPET-bg / 15% HDPE	**68.71**	4.92	$\mu \pm 9.65$

Table 5.35 MFR of Injection Moulded Samples of rPET-bg contaminated with HDPE

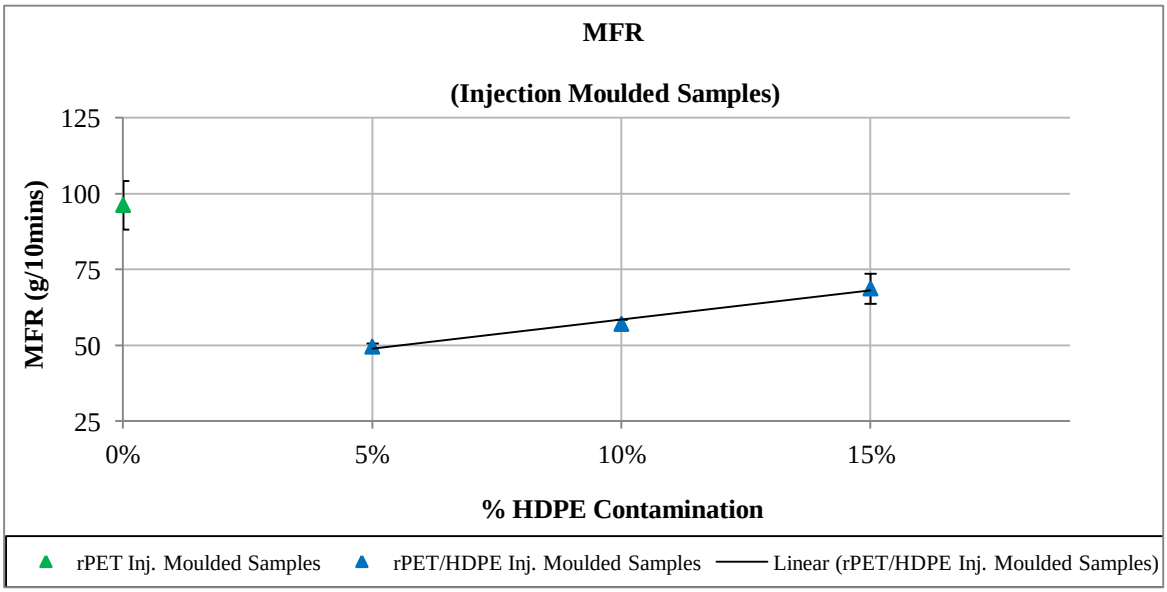

Figure 5.27 MFR of Injection Moulded Samples of rPET-bg contaminated with HDPE

5.1.7 Tensile Testing results of *Injection Moulded Dumbbells*

In *experiments 3, 4* and *5*, the tensile testing yielded the data below.

The collected data were converted into *stress-strain* curve as shown in *Figure 5.28* and from which the tensile properties were extracted and shown in *Table 5.36* below.

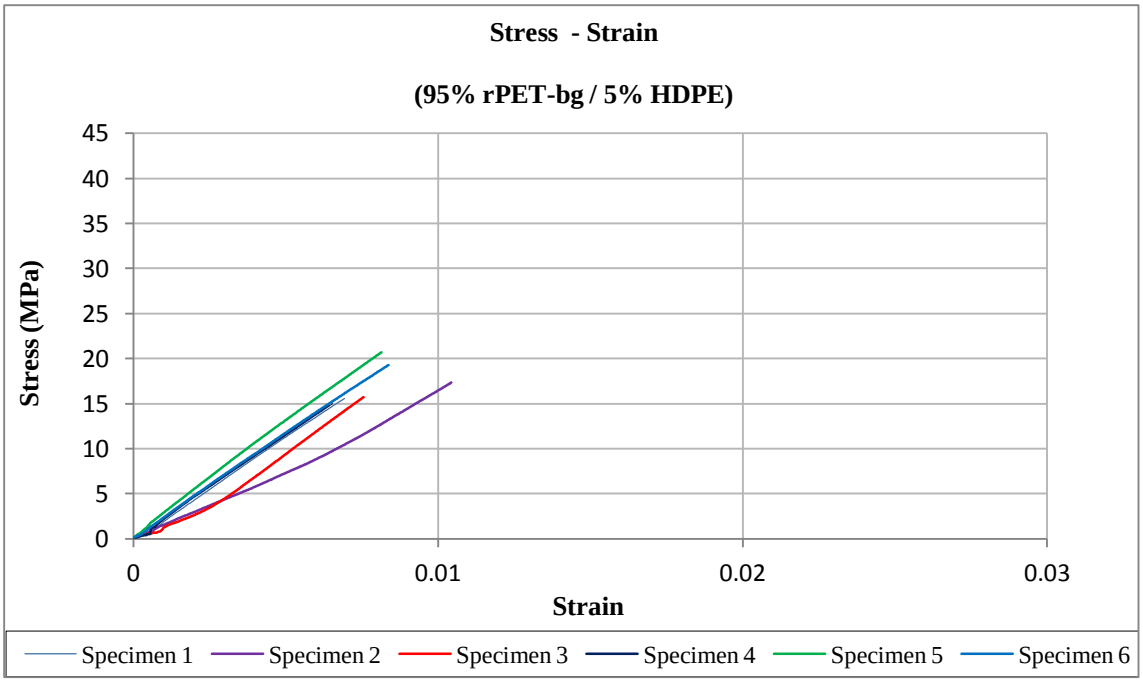

Figure 5.28 Stress-Strain Curves of Dumbbells of rPET-bg contaminated with 5% HDPE (1 to 6)

Material	95% rPET-bg contaminated with 5% HDPE			
Dumbbells	Modulus, E (GPa)	Yield Stress, σ_y (MPa)	Stress @ Break, σ_f (MPa)	Strain @ Yield, e_y
1	2.30	15.56	15.56	0.007
2	1.93	17.38	17.38	0.010
3	2.47	15.73	15.73	0.008
4	2.29	15.03	15.03	0.006
5	2.48	20.68	20.68	0.008
6	2.29	19.25	19.25	0.008
Mean (μ)	**2.29**	**17.27**	**17.27**	**0.008**
STDEV (σ)	0.20	2.27	2.27	0.00
ST. Error ($S_E = \sigma/n^{0.5}$)	0.08	0.93	0.93	0.00
CI (95%), ($\mu \pm 1.96 S_E$)	$\mu \pm 0.16$	$\mu \pm 1.82$	$\mu \pm 1.82$	$\mu \pm 0.00$

Table 5.36 Tensile Data of Dumbbells of rPET-bg contaminated with 5% HDPE

From the stress-strain curves, the *stress at yield, stress at failure* (break), *strain at yield* and the secant *modulus*, elastic modulus, were extracted as previously described in *Figure 3.23*, *Section 3.2.4.2*, i.e. by extrapolation and for the *modulus* by extracting the value of the *slope* of the *stress-strain* curve at the starting *linear portion*; by dividing the amount of *stress* of any point within the starting linear portion (between two points σ_{y1} and σ_{y2}) and the equivalent amount of *strain* of the same point of the linear portion (between two point e_{x1} and e_{x2}).

Note: The original values of first points of stress, σ_{y1}, and strain, e_{x1}, were zeroed, i.e they were taken as the starting points of the linear portion. So, the subtraction $\sigma_{y2} - \sigma_{y1}$ and $e_{x2} - e_{x1}$ gave the value at point 2, which is the one used in the calculation.
Calculation done by Excel and data displayed was rounded to the nearest decimal.

The results are shown in *Table 5.37* below. The same applied for results at 10% and 15% HDPE contamination.

Material	95% rPET-bg contaminated with 5% HDPE

	Stress , (MPa)			Strain, e_x			$E = (\sigma_y / e_x)$	
Specimen	σ_{y1}	σ_{y2}	σ_y	e_{x1}	e_{x2}	e_x	MPa	GPa
1	4.298	13.516	9.218	0.002	0.006	0.004	2304.50	2.30
2	2.992	7.341	4.349	0.002	0.005	0.003	1449.67	1.93
3	4.500	14.386	9.886	0.003	0.007	0.004	2471.50	2.47
4	4.734	13.902	9.168	0.002	0.006	0.004	2292.00	2.29
5	5.537	17.960	12.423	0.002	0.007	0.005	2484.60	2.48
6	4.845	16.274	11.429	0.002	0.007	0.005	2285.80	2.29

Mean (μ)	**2.29**
STDEV (σ)	0.20
ST. Error ($S_E = \sigma/n^{0.5}$)	0.08
CI (95%), ($\mu \pm 1.96 S_E$)	$\mu \pm 0.16$

Table 5.37 Tensile Modulus of Dumbbells of rPET-bg contaminated with 5% HDPE

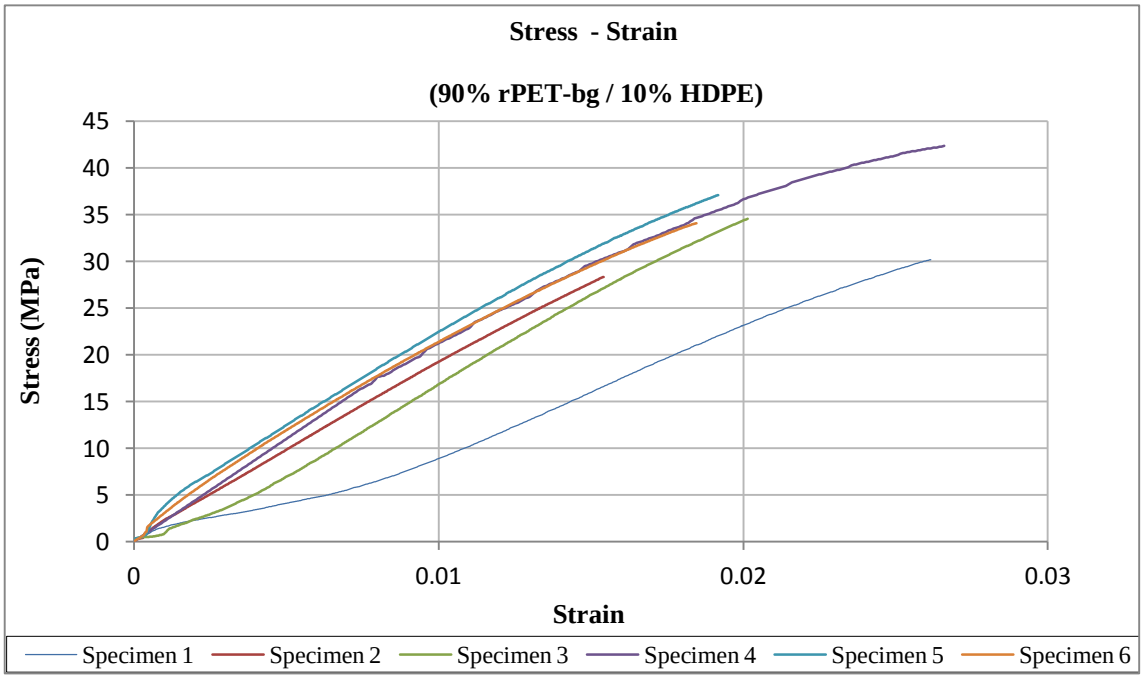

Figure 5.29 Stress-Strain Curves of Dumbbells of rPET-bg contaminated with 10% HDPE (1 to 6)

Material	90% rPET-bg contaminated with 10% HDPE			
Dumbbells	Modulus, E (GPa)	Yield Stress, σ_y (MPa)	Stress @ Break, σ_f (MPa)	Strain @ Yield, e_y
1	1.42	30.17	30.17	0.026
2	1.88	28.36	28.36	0.015
3	2.01	34.53	34.53	0.020
4	2.21	42.40	42.40	0.027
5	2.00	37.08	37.08	0.019
6	1.96	34.10	34.10	0.018
Mean (μ)	**1.91**	**34.44**	**34.44**	**0.021**
STDEV (σ)	0.26	5.01	5.01	0.00
ST. Error ($S_E = \sigma/n^{0.5}$)	0.11	2.05	2.05	0.00
CI (95%), ($\mu \pm 1.96 S_E$)	$\mu \pm 0.21$	$\mu \pm 4.01$	$\mu \pm 4.01$	$\mu \pm 0.00$

Table 5.38 Tensile Data of Dumbbells of rPET-bg contaminated with 10% HDPE

Material	90% rPET-bg contaminated with 10% HDPE

	Stress , (MPa)			Strain, e_x			$E = (\sigma_y / e_x)$	
Specimen	σ_{y1}	σ_{y2}	σ_y	e_{x1}	e_{x2}	e_x	MPa	GPa
1	8.923	23.158	14.235	0.010	0.020	0.010	1423.50	1.42
2	9.888	19.294	9.406	0.005	0.010	0.005	1881.20	1.88
3	12.765	20.797	8.032	0.008	0.012	0.004	2008.00	2.01
4	6.589	15.423	8.834	0.003	0.007	0.0040	2208.50	2.21
5	12.455	20.473	8.018	0.005	0.009	0.004	2004.50	2.00
6	9.933	17.785	7.852	0.004	0.008	0.004	1963.00	1.96

Mean (μ)	**1.91**
STDEV (σ)	0.26
ST. Error ($S_E = \sigma/n^{0.5}$)	0.11
CI (95%), ($\mu \pm 1.96 S_E$)	$\mu \pm 0.21$

Table 5.39 Tensile Modulus of Dumbbells of rPET-bg contaminated with 10% HDPE

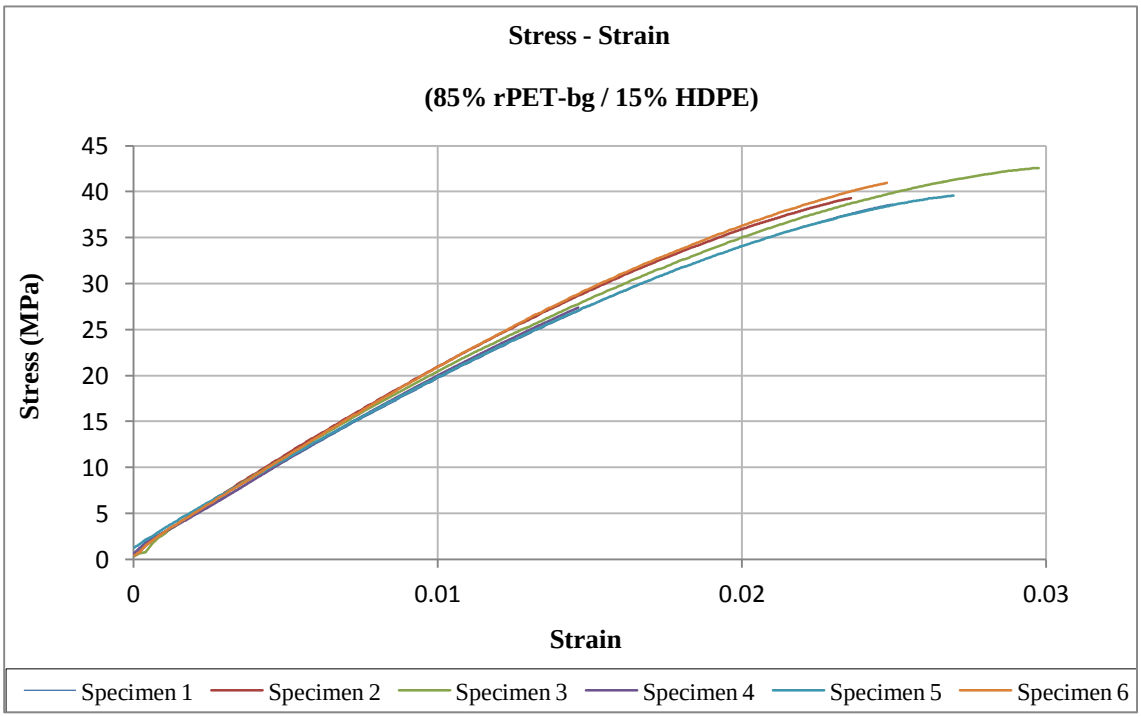

Figure 5.30 Stress-Strain Curves of Dumbbells of rPET-bg contaminated with 15% HDPE (1 to 6)

Material	**85% rPET-bg contaminated with 15% HDPE**			
Dumbbells	**Modulus, E (GPa)**	**Yield Stress, σ_y (MPa)**	**Stress @ Break, σ_f (MPa)**	**Strain @ Yield, e_y**
1	1.85	38.71	38.71	0.025
2	2.01	39.28	39.28	0.024
3	1.96	42.56	42.56	0.030
4	1.95	27.38*	27.38*	0.0150
5	1.81	39.59	39.59	0.027
6	1.98	41.00	41.00	0.025
Mean (μ)	**1.93**	**40.23**	**40.23**	**0.024**
STDEV (σ)	0.08	1.55	1.55	0.51
ST. Error ($S_E = \sigma/n^{0.5}$)	0.03	0.69	0.69	0.21
CI (95%), ($\mu \pm 1.96 S_E$)	$\mu \pm 0.06$	$\mu \pm 1.36$	$\mu \pm 1.36$	$\mu \pm 0.41$

Table 5.40 Tensile Data of Dumbbells of rPET-bg contaminated with 15% HDPE

*: This' an "outlier" displayed but not included in the calculation.

Material	85% rPET-bg contaminated with 15% HDPE

	Stress , (MPa)			Strain, e_x			$E = (\sigma_y / e_x)$	
Specimen	σ_{y1}	σ_{y2}	σ_y	e_{x1}	e_{x2}	e_x	MPa	GPa
1	10.617	16.167	5.55	0.005	0.008	0.003	1850.00	0.018
2	9.293	15.329	6.036	0.004	0.007	0.003	2012.00	0.020
3	7.109	16.891	9.782	0.003	0.008	0.005	1956.40	0.020
4	8.717	14.555	5.838	0.004	0.007	0.0030	1946.00	0.019
5	9.083	18.120	9.037	0.004	0.009	0.005	1807.40	0.018
6	11.141	19.052	7.911	0.005	0.009	0.004	1977.75	0.020

Mean (μ)	**0.019**
STDEV (σ)	0.00
ST. Error ($S_E = \sigma/n^{0.5}$)	0.00
CI (95%), ($\mu \pm 1.96 S_E$)	$\mu \pm 0.00$

Table 5.41 Tensile Modulus of Dumbbells of rPET-bg contaminated with 15% HDPE

Note: Other Graphs are available in ***Appendix 5*** **(***13, 14, 15***)**.

The tensile results of *dumbbells*, shown in *Figures 5.28*, *5.29* and *5.30* and *Tables 5.36, 5.38* and *5.40* above, showed clearly the influence of the inclusion of HDPE contamination on the overall tensile characteristics of non contaminated rPET-bg.

Under tensile testing, the *dumbbells* with 5% still failed and broke sharply but the ones with 10% and 15% showed some degree of yielding, as shown in *Figures 5.28*, *5.29* and *5.30* above and *Figure 5.31* below, the curves curvatures indicated a characteristic of *brittle* materials tending towards being ductile with increasing % HDPE contamination from 5% to 15%. It would appear that the crystalline phase is reinforcing the amorphous regions in rPET-bg and as the % crystallinity increase fracture occurred at lower strain.

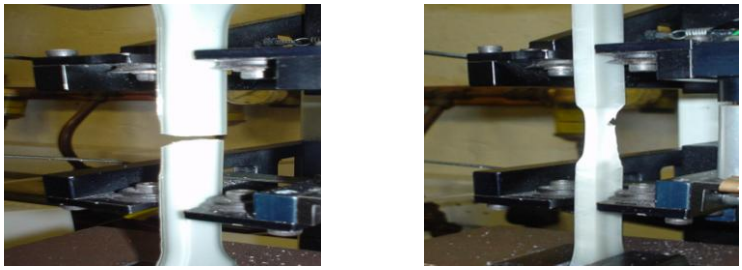

Figure 5.31 Sharp Failure of rPET-bg Dumbbell (Left) Compared to Necked Dumbbell of rPET-bg contaminated with 15% HDPE (Right)

The discussions below show the variations in terms of individual characteristics, such as modulus, stress at yield and at break and strain at yield of the materials.

Compared to non contaminated rPET-bg, as shown in *Table 5.42* and *Figure 5.32* below, the inclusion of HDPE decreased the *stiffness* of the non contaminated rPET-bg matrix; this random decrease of stiffness was attributed to the degree of *crystallinity* and secondary bonding, where an increase in secondary bonding between the molecular chains of polymers increases *stiffness* and vice versa; the decrease in elastic modulus is attributed to the materials' *incompatibility* and *immiscibility* due the difference in *polarity* between the contaminant and the host matrix. *Chen et al.* [173] and *Pracella et al.* [174] reported that tensile properties were enhanced in blends of rHDPE / rPET in the presence of compatibilisers. Similarly, *Lei et al.* [175] reported that toughness was significantly enhanced in rPET/HDPE in the presence of compatibilisers; which is not the case in this work, where no compatibilsers were used. And as previously seen, the *crystallinity* decreased in the contaminated materials orderly with increasing % HDPE, this showed proportionality between % crystallinity and stiffness. And the *elastic modulus* is a *stiffness* factor, therefore, the *stiffness* decreased with increasing % HDPE too.

Materials	Elastic Modulus, E, (GPa)		
	Mean (μ)	**ST. Error ($S_E = \sigma/n^{0.5}$)**	**CI (95%) ($\mu \pm 1.96 S_E$)**
Non contaminated rPET-bg	**3.10**	0.07	$\mu \pm 0.15$
95% rPET-bg / 5% HDPE	**2.27**	0.08	$\mu \pm 0.16$
90% rPET-bg / 10% HDPE	**1.91**	0.11	$\mu \pm 0.21$
85% rPET-bg / 15% HDPE	**1.93**	0.03	$\mu \pm 0.06$

Table 5.42 Modulus of rPET-bg contaminated with HDPE

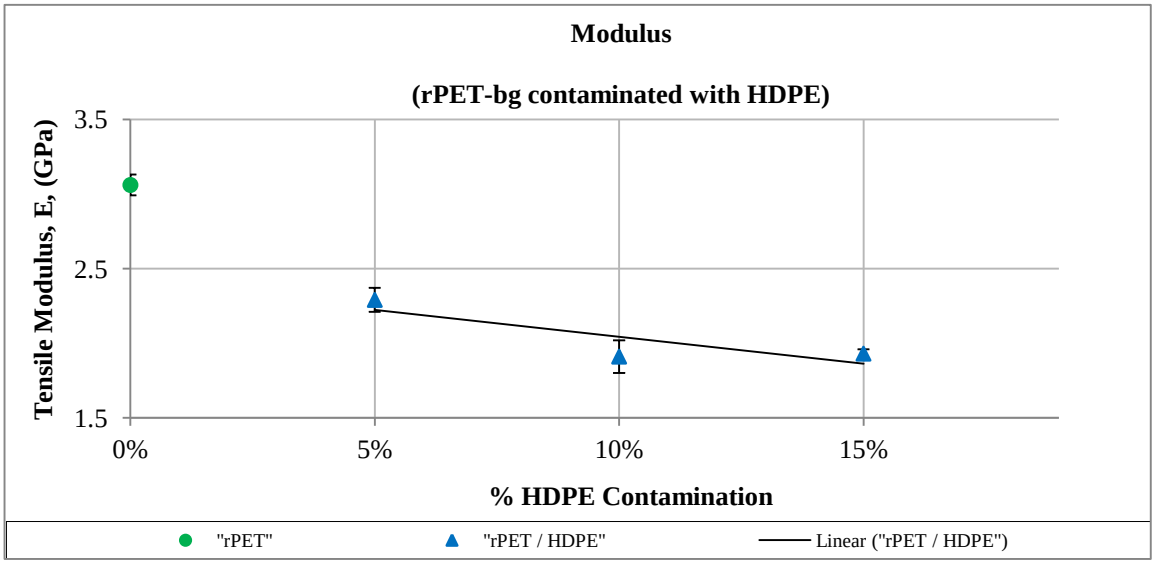

Figure 5.32 Modulus of rPET-bg contaminated with HDPE

Compared to non contaminated rPET-bg, as shown in *Table 5.43* and *Figure 5.33* below, the *stress at yield*, σ_y , increased dramatically by the inclusion of HDPE, because under tensile testing the yielding is inversely proportional to crystallinity, so the reduction in crystallinity coupled with the branching of HDPE triggered a fracture mechanism change from craze crack growth for rPET-bg, to ductile shear yielding for the contaminated materials and allowed additional strength.

Materials	**Stress at Yield, σ_y (MPa)**		
	Mean (μ)	**ST. Error ($S_E = \sigma/n^{0.5}$)**	**CI (95%) ($\mu \pm 1.96 S_E$)**
Non contaminated rPET-bg	**18.90**	2.91	$\mu \pm 5.69$
95% rPET-bg / 5% HDPE	**17.30**	0.93	$\mu \pm 1.82$
90% rPET-bg / 10% HDPE	**34.44**	2.05	$\mu \pm 4.01$
85% rPET-bg / 15% HDPE	**40.23**	0.69	$\mu \pm 1.36$

Table 5.43 Stress at Yield of rPET-bg contaminated with HDPE

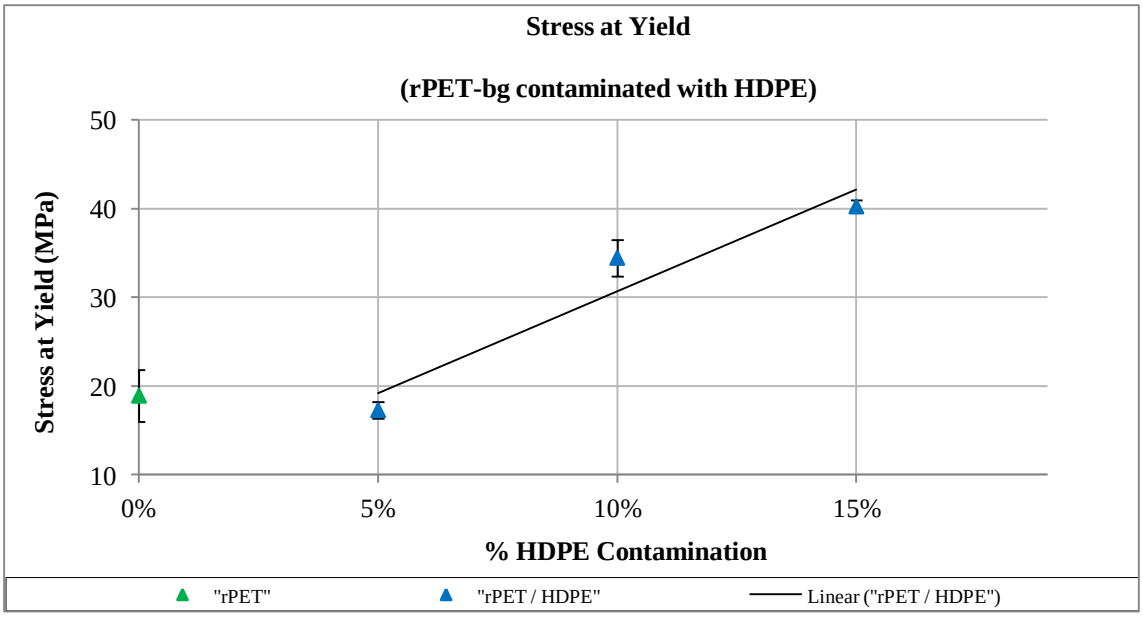

Figure 5.33 Stress at Yield of rPET-bg contaminated with HDPE

Compared to non contaminated rPET-bg, as shown in *Table 5.44* and *Figure 5.34* below, the *stress at break*, σ_f , equated the *yield stress* in the contaminated materials; this showed HDPE characteristics coupled with PET stiffness and their capabilities in withholding tensile elongations under stress. In one hand, the incompatibility and lack of strong molecular bonding and adhesion between the contaminant and matrix chains allowed limited flexibility of the molecular chains and resisted failure due to entanglement. But in the other hand, the stress at break increased in the contaminated materials, with increasing % HDPE contamination, indicating more flexibility of the HDPE chains and capability of stretching under maximum strain due to its branching.

Materials	**Stress at Break, σ_f, (MPa)**		
	Mean (μ)	**ST. Error ($S_E = \sigma/n^{0.5}$)**	**CI (95%) ($\mu \pm 1.96 S_E$)**
Non contaminated rPET-bg	**18.90**	2.91	$\mu \pm 5.69$
95% rPET-bg / 5% HDPE	**17.27**	0.93	$\mu \pm 1.82$
90% rPET-bg / 10% HDPE	**34.44**	2.05	$\mu \pm 4.01$
85% rPET-bg / 15% HDPE	**40.23**	0.69	$\mu \pm 1.36$

Table 5.44 Stress at Break of rPET-bg contaminated with HDPE

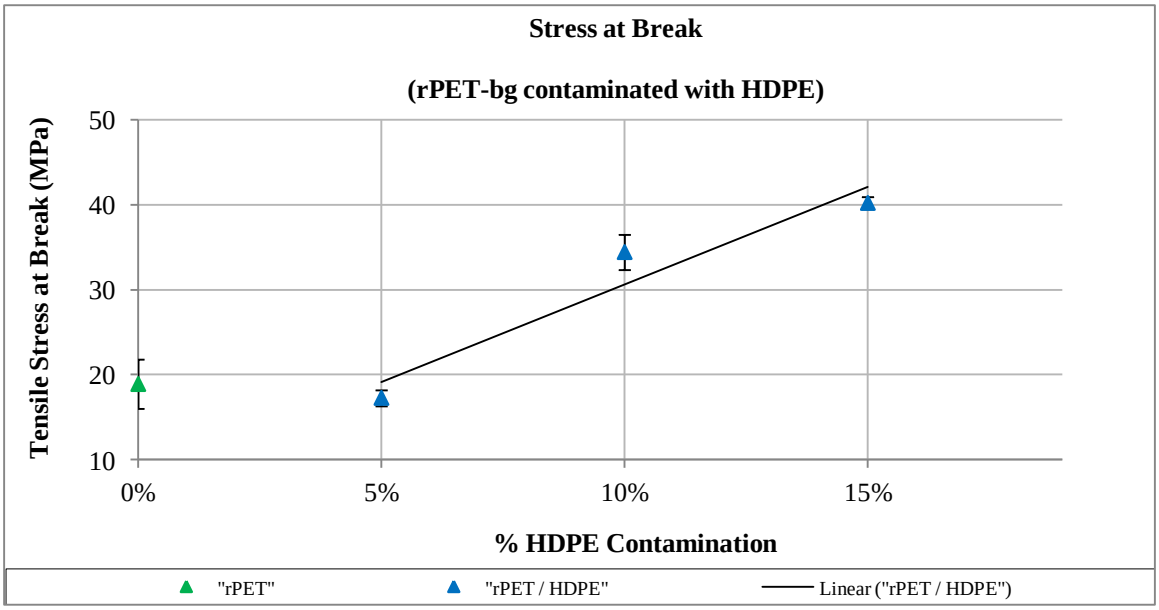

Figure 5.34 Stress at Break of rPET-bg contaminated with HDPE

Compared to non contaminated rPET-bg, as shown in *Table 5.45* and *Figure 5.35* below, the *strain at yield* showed the influence of the inclusion of HDPE and increased with increasing the % HDPE contamination; this indicated the degree of strength created by the HDPE chains in resisting yielding by maintaining the matrix chains and resisting the brittle fracture mechanism inherited from rPET-bg under tensile strain and showed the proportionality between stress at yielding and the strain encountered.

Materials	**Strain at Yield, e_y**		
	Mean (μ)	**ST. Error ($S_E = \sigma/n^{0.5}$)**	**CI (95%) ($\mu \pm 1.96 S_E$)**
Non contaminated rPET-bg	**0.007**	0.00	$\mu \pm 0.00$
95% rPET-bg / 5% HDPE	**0.008**	0.00	$\mu \pm 0.00$
90% rPET-bg / 10% HDPE	**0.021**	0.00	$\mu \pm 0.00$
85% rPET-bg / 15% HDPE	**0.024**	0.00	$\mu \pm 0.00$

Table 5.45 Strain at Yield of rPET-bg contaminated with HDPE

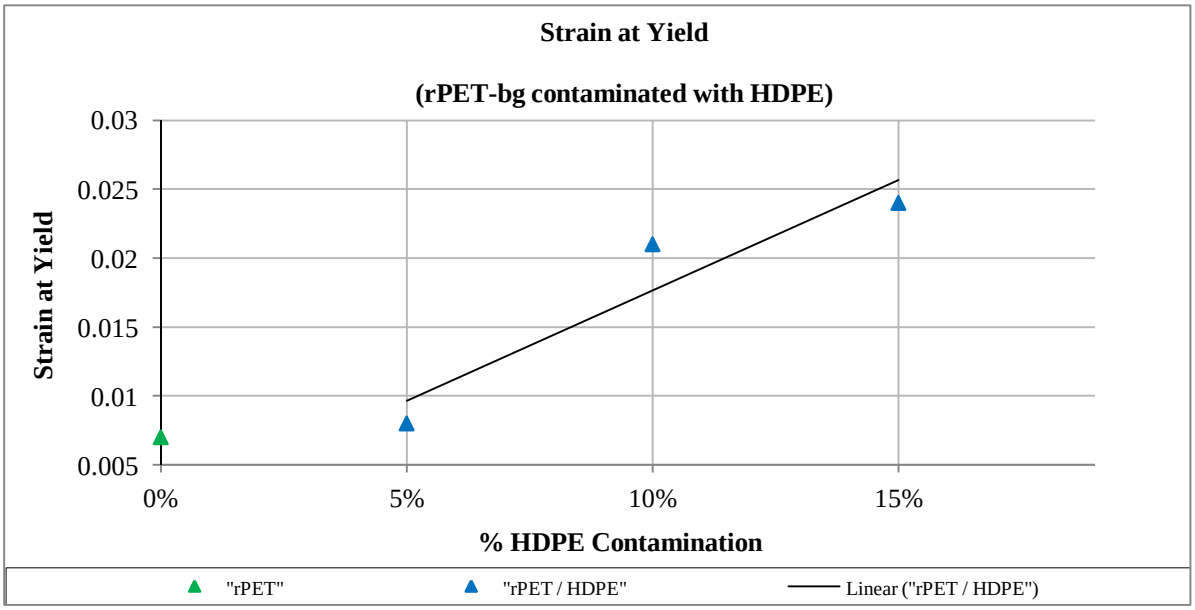

Figure 5.35 Strain at Yield of rPET-bg contaminated with HDPE

5.1.8 Impact Testing results of *Injection Moulded Impact Bars*

In *experiments 3, 4* and *5*, the impact testing yielded the data below.

Number	Width (B) (mm)	Thickness (t) (mm)	Energy Absorbed (J)	Impact Strength ($kJ.m^{-2}$)
1	10.02	4.07	0.13	**3.19**
2	10.05	4.05	0.14	**3.44**
3	10.08	4.10	0.21	**5.08**
4	10.03	4.08	0.16	**3.91**
5	10.06	4.02	0.18	**4.45**
6	9.99	4.09	0.15	**3.67**
7	10.05	4.10	0.14	**3.40**
8	10.02	4.07	0.12	**2.94**
9	10.06	4.05	0.16	**3.93**
10	10.03	4.09	0.14	**3.41**
Mean	**10.04**	**4.07**	**0.15**	**3.74**
STDEV	0.03	0.03	0.03	0.63
ST. Error ($S_E = \sigma/n^{0.5}$)	0.01	0.01	0.01	0.20
CI (95%), ($\mu \pm 1.96 S_E$)	$\mu \pm 0.02$	$\mu \pm 0.02$	$\mu \pm 0.02$	$\mu \pm 0.39$

Table 5.46 Charpy Impact Strength of rPET-bg contaminated with 5% HDPE

1	10.04	4.11	0.78	**18.90**
2	10.01	4.05	0.49	**12.09**
3	10.03	4.06	0.75	**18.42**
4	10.08	4.04	0.55	**13.51**
5	10.02	4.10	0.64	**15.58**
6	10.05	4.09	0.72	**17.52**
7	10.05	4.05	0.51	**12.53**
8	10.02	4.07	0.63	**15.45**
9	10.03	4.11	0.56	**13.58**
10	10.06	4.09	0.67	**16.28**
Mean	**10.04**	**4.08**	**0.63**	**15.39**
STDEV	0.02	0.03	0.10	2.42
ST. Error ($S_E = \sigma/n^{0.5}$)	0.01	0.01	0.03	0.77
CI (95%), ($\mu \pm 1.96 S_E$)	$\mu \pm 0.01$	$\mu \pm 0.02$	$\mu \pm 0.06$	$\mu \pm 1.50$

Table 5.47 Charpy Impact strength of rPET-bg contaminated with 10% HDPE

Number	Width (B) (mm)	Thickness (t) (mm)	Energy Absorbed (J)	Impact Strength ($kJ.m^{-2}$)
1	10.02	4.11	1.20	**29.14**
2	10.05	4.12	1.23	**29.71**
3	10.03	4.09	1.19	**29.01**
4	10.02	4.10	1.16	**28.24**
5	10.04	4.08	1.21	**29.54**
6	10.03	4.10	1.15	**27.96**
7	10.04	4.09	1.25	**30.44**
8	10.02	4.10	1.21	**29.45**
9	10.02	4.11	1.19	**28.90**
10	10.06	4.08	1.26	**30.70**
Mean	**10.03**	**4.10**	**1.21**	**29.31**
STDEV	0.01	0.01	0.03	0.86
ST. Error ($S_E = \sigma/n^{0.5}$)	0.00	0.00	0.01	0.27
CI (95%), ($\mu \pm 1.96 S_E$)	$\mu \pm 0.01$	$\mu \pm 0.01$	$\mu \pm 0.02$	$\mu \pm 0.53$

Table 5.48 Charpy Impact Strength of rPET-bg contaminated with 15% HDPE

Compared to non contaminated rPET-bg, as shown in *Table 5.49* and *Figure 5.36* below, the inclusion of HDPE showed increased *impact strength* with increasing % HDPE contamination; this dramatic increase indicated intermolecular ramifications and entanglement between the different chains which was translated in reduced *crystallinity* and decreased *modulus*. The complex entanglement and the degree of branching of HDPE structure improved the degree of strength in the contaminated materials and required high energy absorption to relax the chains rigidity and overcome any resistance to failure and completion of breakage. This property improvement is in line with what was reported by *Boutevin et al.* [170] in their study of improving the properties of PET/HDPE blends by including graft copolymers; this indicated that the inclusion of HDPE and the effect of processing generated various graft copolymers due to the generated oligomers as a result of degradation during processing, as reported by *Samperi et al.* [66], *Romao et al.* [67] and *Cooney et al* [68].

Materials	Impact Strengths (J/m^2)		
	Mean (μ)	**ST. Error ($S_E = \sigma/n^{0.5}$)**	**CI (95%) ($\mu \pm 1.96 S_E$)**
Non contaminated rPET-bg	**2.40**	0.12	$\mu \pm 0.23$
95% rPET-bg / 5% HDPE	**3.74**	0.20	$\mu \pm 0.39$
90% rPET-bg / 10% HDPE	**15.39**	0.77	$\mu \pm 1.50$
85% rPET-bg / 15% HDPE	**29.31**	0.27	$\mu \pm 0.53$

Table 5.49 Charpy Impact Strength of rPET-bg contaminated with HDPE

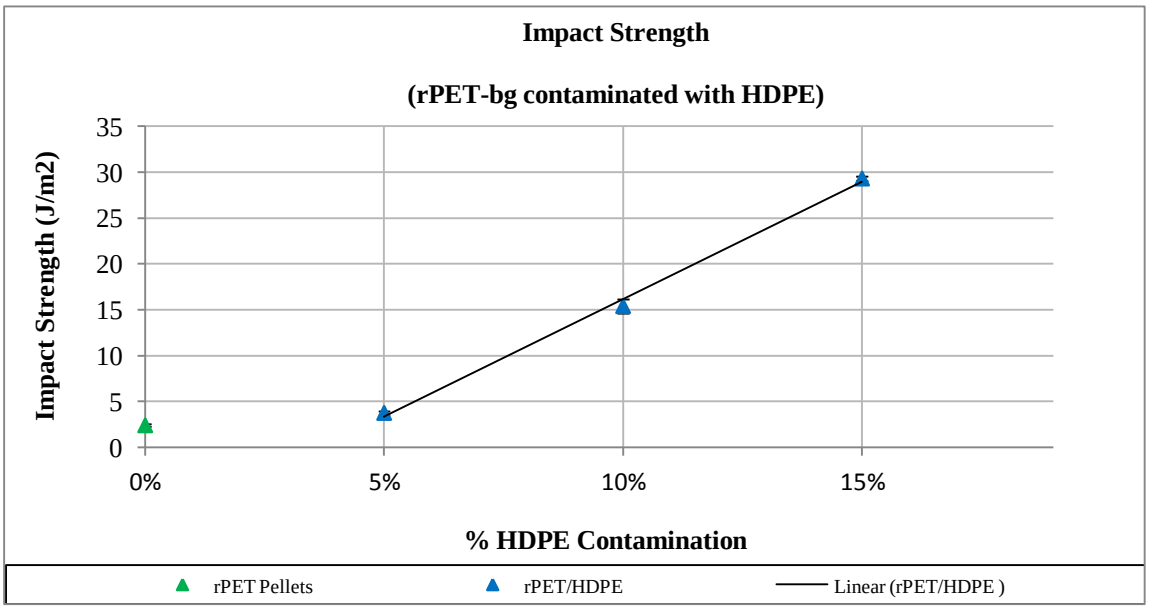

Figure 5.36 Impact Strengths of rPET-bg contaminated with HDPE

5.1.9 Overall Data Comparisons

In terms of processing, the inclusion of HDPE, as shown in *Table 5.50* below, showed decreased screw speed with increased % HDPE contamination, which indicated increased viscosity; this increase in viscosity is attributed to the *melt flow* property of HDPE, which is *8g /10min* in *Table 3.1, Section 3.1.2* compared to the non contaminated rPET-bg flakes' of *61.35g/10min* previously determined and shown in *Table 4.3, Section 4.1.3*, this large gap in MFR is the main contributor to such increase. In contrast, the % torque, which is proportional to viscosity, should increase accordingly but decreased instead; this suggested the presence of high volume of very short chains, resulting from thermo-mechanical degradation, homogeneously mixed but dispersed randomly, which allowed high shear despite the localised high viscosity generated. The same high volume of very short chains decreased the melt injection and packing pressures during injection moulding; indicating ease of flow, balanced melt distribution, orientation and packing of the contaminated materials in the mould cavity.

	***Screw Speed* (*rpm*)**	***% T***	***Injection Pressure* (*Bar*)**	***Packing Pressure* (*Bar*)**
Extruded Samples **rPET-bg / HDPE** *compared to* **rPET-bg**	↓	↓		
Inj. Moulded Samples **rPET-bg / HDPE** *compared to* **rPET-bg**			↓	↓

Table 5.50 Variation of Processing Conditions of rPET-bg contaminated with HDPE

In terms of thermal and flow properties, the inclusion of HDPE, as shown in *Table 5.51* below, decreased the T_g, indicating the presence of dispersed very small chains, created as result of thermo-mechanical degradation, which created certain degree of disorder which lead to narrowed range of glass transition. Also, the size of these chains allowed ordered arrangement into orderly crystalline domains formed as a result of balanced orientation, straightening and packing of the material chains during the cooling process of injection moulding. These ordered crystalline domains required short scales of time and temperatures to re-arrange during DSC heating. Also, the T_c decreased in most cases, except at 15%, which indicated that HDPE more chains prevented additional arrangement and straightening of chains. The increased T_c in the contaminated materials is proportional to the increase in % HDPE contamination; the result of increased very short chains and additional crystalline domains which required increase in temperature for chains relaxation and straightening during the cold crystallisation process. The inclusion of HDPE decreased the enthalpy of cold crystallisation ΔH_c, indicating that the crystalline domains were very small and dispersed and as such they did not release large amounts of heat during re-arrangement and straightening and that HDPE prevented the completion of cold crystallisation, which was overridden by overall melting. The HDPE decreased the T_m in all cases due to the absence of chemical bonding or adhesions between the molecular chains shown by the exhibition of individual melting peaks, which indicated *incompatibility* and *immiscibility* of the polar PET and the non polar HDPE, resulting in lack of chemical bonding, increased entropy and melting at lower temperatures due to the premature melting of crystalline domains containing HDPE coupled with a low degree of packing of very small chains. The decreased ΔH_m is attributed to the fast melting of the HDPE crystals which improved the overall balanced rate of melting, resulting in less heat absorption. The HDPE decreased the % X_c confirming that the pattern of the crystalline domains as being numerous but dispersed as a result of influence of HDPE inclusion. The % X_c decreased with increasing % HDPE contamination in all cases, indicating that the very small HDPE chains filled the interstices and created entanglement and prevented ordered packing; the higher % HDPE contamination conveyed random chains packing and resulted in lower crystallinity and vice versa. The inclusion of HDPE influenced and decreased the *MFR* in the contaminated rPET-bg, which is attributed to the *melt flow* property of HDPE of *8g /10min* as in (*Table 3.1, Section 3.1.2*); the inclusion of HDPE influenced the MFR of contaminated samples, which decreasing with decreasing the % HDPE

contamination; the inclusion of HDPE, increased the viscosity of non contaminated rPET-bg and consequently decreased the MFR, indicating reduction of sliding and shear of lamellae. The decrease is proportional to % HDPE contamination and its more pronounced at lower % HDPE contamination; at 5% HDPE, the chains of HDPE were easily dispersed homogeneously within the rPET-bg matrix, whereas, at 10 and 15% HDPE contamination, the dispersion is more localised than widely dispersed.

	T_g (^oC)	T_c (^oC)	ΔH_c ($J.g^{-1}$)	T_m (^oC)	ΔH_m ($J.g^{-1}$)	X_c (%)	*MFI* (*g/10min*)
Extruded Samples **rPET-bg / HDPE** *compared to* **rPET-bg**	↓	NA	NA	↓	↓	↓	↓
Inj. Moulded Samples **rPET-bg / HDPE** *compared to* **rPET-bg**	↓	↓	↓	↓	↓	↓	↓

Table 5.51 Variation of Thermal and Flow Properties
of rPET-bg contaminated with HDPE

In terms of tensile and impact properties, as shown in *Table 5.52* below, the inclusion of HDPE decreased the *stiffness* of the non contaminated rPET-bg matrix, which is attributed to the decreased *crystallinity* and *incompatibility* of the contaminant and the host matrix; the decreased secondary bonding between the molecular chains decreased the *stiffness*. As the *elastic modulus, **E***, is a *stiffness* factor, therefore, the *stiffness* decreased with increasing % HDPE. In contrast, the *yield stress,* σ_y , increased dramatically by the inclusion of HDPE, because under tensile testing the yielding is inversely proportional to crystallinity, so the decreased crystallinity triggered a fracture mechanism change from craze crack growth, for rPET-bg, to ductile shear yielding for the contaminated materials. Similarly, the *stress at break,* σ_f , increased; the stress at break increased with increasing % HDPE contamination, indicating more flexibility of the HDPE chains and capability of stretching under maximum strain.

The *strain at yield* increased with increasing the % HDPE contamination; this indicated the degree of strength created by the HDPE chains in resisting yielding by maintaining the matrix chains and resisting the brittle fracture mechanism inherited from rPET-bg under tensile strain. Lastly, the inclusion of HDPE showed increased *impact strength* with increasing % HDPE contamination, as a result of entanglement between the different chains, reduced *crystallinity* and decreased *modulus*. The branching characteristics of HDPE structure improved the degree of strength in the contaminated materials and required high energy absorption to relax the chains rigidity and overcome any resistance to failure and completion of breakage.

	E **(*GPa*)**	σ_y **(*MPa*)**	σ_f **(*MPa*)**	***e*** ***at Yield***	***I.S*** **($J.m^{-2}$)**
Inj. Moulded Samples **rPET-bg / HDPE** *compared to* **rPET-bg**	↓	↑	↑	↑	↑

Table 5.52 Variation of Tensile and Impact Properties of Inj. Moulded Samples of rPET-bg contaminated with HDPE

The injection moulded samples of contaminated rPET-bg with HDPE, as shown in *Table 5.53* below, showed variations of properties following the effect of processing heat in generating thermo-mechanical degradation and chains'-scission. The decreased $\boldsymbol{T_g}$ indicated slow and balanced cooling of well orientated melt under optimised conditions. The decreased $\boldsymbol{T_m}$ indicated sporadic very small crystalline domains which melted with ease helped by a premature melting of HDPE and the increase of $\boldsymbol{\Delta H_m}$ indicated a large number of small sporadic crystalline domains which required additional cumulative heat absorbtion to complete melting. The increase in % crystallinity confirmed the presence of large number of small crystalline domains and their capability in arranging orderly, straightening and packing. The increased MFR indicated the influence of the high shear and reduced viscosity exerted by the HDPE chains within the main matrix.

	T_g (^oC)	T_m (^oC)	ΔH_m ($J.g^{-1}$)	X_c (%)	MFI (g/10min)
Inj. Moulded Samples *compared to* **Extruded Samples** *of* **rPET-bg contaminated with HDPE**	↓	↓	↑	↑	↑

Table 5.53 Comparison of Inj. Moulded Samples to Extruded Samples of rPET-bg contaminated with HDPE

Where: ↑ means increase, ↓ means decrease.

5.2 Conclusion

In light of the above investigation, it was shown that the inclusion of small amounts of *HDPE*, as a polymeric contaminant at *5%*, *10%* and *15 %*, influenced the overall properties of the *rPET-bg* matrix. The thermal, spectroscopic, flow and mechanical analyses confirmed the presence of very small polymer chains, resulting from thermo-mechanical degradation encountered during processing operations. These very short chains allowed the formation of sporadic crystalline domains. The exhibition of individual melting peaks indicated *incompatibility* and *immiscibility* of the polar PET and the non polar HDPE, resulting in lack of chemical bonding which influenced many properties. The premature melting of HDPE primary crystals improved the overall balanced rate and the decreased *crystallinity* confirmed the influence of HDPE inclusion in creating sporadic and dispersed small crystalline domains. Additionally, the HDPE allowed an increase in shear and decrease in viscosity shown by a substantial decrease in MFR. Furthermore, the tensile and impact properties showed decrease of *stiffness* as a result of decreased *crystallinity* and indicated *incompatibility* of the contaminant, HDPE, and the rPET-bg. In contrast, the HDPE inclusion showed a fracture mechanism change from craze crack growth, for rPET-bg, to ductile shear yielding for the contaminated materials. The branching characteristics of HDPE structure increased the degree of impact strength, resulting in high energy absorption at failure.

Stage 1

Chapter 6

rPET-bg Contaminated with PP

6.1 Results and Discussions

This section discusses the various experimental results of rPET-bg contaminated with PP obtained in *experiments 6* to *8*. As previously seen with rPET-bg contaminated with HDPE in *Chapter 5*, these experiments investigated the influence of small amounts of PP on the properties and processability of non contaminated rPET-bg previously studied in *Chapter 4*.

Samples of rPET-bg were contaminated with *5%, 10%* and *15%* of PP and investigated. For comparative reasons, same methodology was performed as previously done in *Chapters 4* and *5* and as described in *Section 3.2* and *Experiments 6* to *8, Section 3.4*, i.e. contaminated samples were extruded, injection moulded and analysed by DSC, FTIR, MFR and tested for their tensile and impact properties. The results of the influence of PP on the main matrix of rPET-bg are discussed below.

Compared to non contaminated rPET-bg, and unlike with rPET-bg contaminated with HDPE, the twin-screw speed and % torque, as shown in *Table 6.1* and *Figure 6.1* below, indicated instability but overall ease of flow due to the PP dimensional stability; the instability of the parameters may be attributed to the combination of dimensional stability coupled with *melt flow* property of PP, which is *1g /10min* as shown in *Table 3.2, Section 3.1.3* compared to the non contaminated rPET-bg flakes' of *61.35g/10min* previously determined and shown in *Table 4.3, Section 4.1.3*. The general assumption is that chains-scissions due to degradation coupled with the flow dimensional stability of PP overridden the effect of its low MFR on the overall flow properties of the contaminated rPET-bg, and as a result, the included small amounts of PP dispersed and melted with ease within the matrix, translated by a

decrease in screw speed and a much lower decrease of % torque, indicating that the viscosity decreased much more with the inclusion of PP than with HDPE as previously seen.

Extruded Samples	Screw Speed			% Torque		
	Min. (rpm)	Max. (rpm)	Mean (rpm)	Min. (%)	Max. (%)	Mean (%)
Non contaminated rPET-bg	110	115	112.50 ± 2.5	50	60	55 ± 5
95% rPET-bg / 5% PP	97	103	100.00 ± 3.0	28	40	34 ± 6
90% rPET-bg / 10% PP	95	101	98.00 ± 3.0	30	41	36 ± 6
85% rPET-bg / 15% PP	96	103	99.50 ± 3.5	27	38	33 ± 6

Table 6.1 Screw Speed and % Torque of extruded rPET-bg contaminated with PP

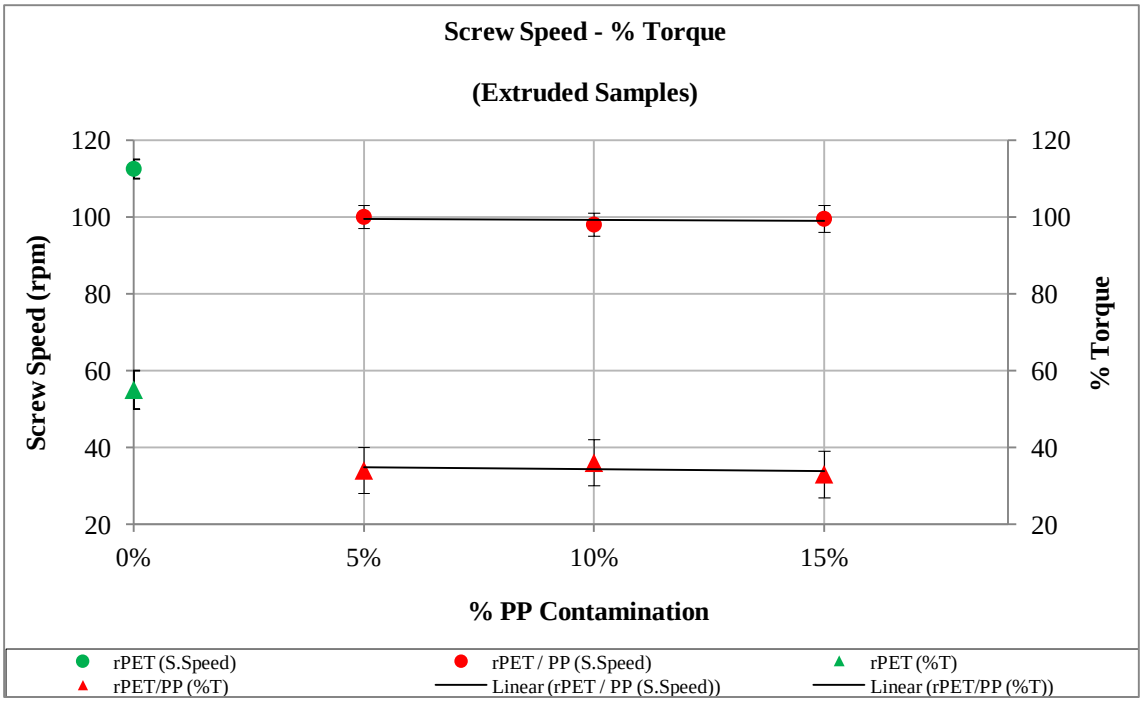

Figure 6.1 Screw Speed and % Torque of extruded rPET-bg contaminated with PP

Compared to non contaminated rPET-bg, as shown in *Table 6.2* below, brittleness decreased and apparent degree of ductility can be seen compared to non contaminated rPET-bg. These variations are the result of homogeneous mixing of the melt, combination of properties and improved crystalline fractions; this is in line with what was reported by *Pracella et al.* [114] that melt mixing by extrusion of blends of post-consumer PET and PP in the presence of compatibilisers, showed improvement in many properties. Despite the absence of compatibilisers, it appears that the inclusion of PP improved certain properties..

Extruded Samples	Swelling	Brittleness	Ductility	Colour
Non contaminated rPET-bg	No	High	No	Grey- Transparent
95% rPET-bg / 5% PP	Low	Low	Medium	Grey- Transparent
90% rPET-bg / 10% PP	Low	Low	Low	Grey- Transparent
85% rPET-bg / 15% PP	Low	Low	Low	Grey- Transparent

Table 6.2 Extruded Pellets of rPET-bg contaminated with 5% PP

6.1.1 DSC results of *Extruded Samples*

In *experiments 6, 7* and *8*, the DSC analysis yielded the data below.

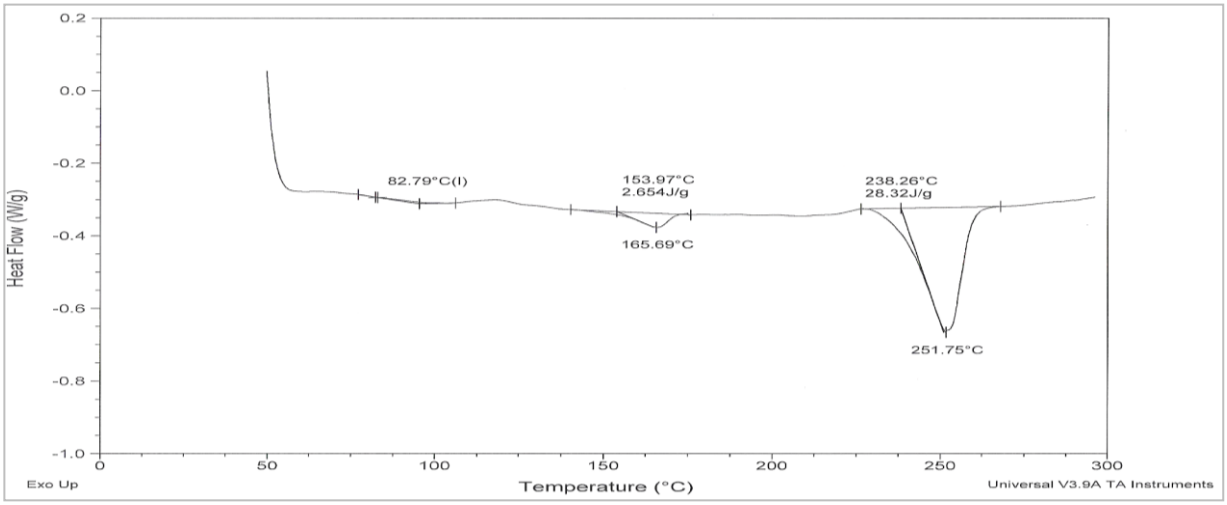

Figure 6.2 Thermogram of Extruded Sample 1 of rPET-bg contaminated with 5% PP

	T_g (^oC)	T_m (^oC)	ΔH_m (J/g)	T_c (^oC)	ΔH_c (J/g)	ΔH_m^0 (J/g)	X_c (%)	T_d (^oC)
Run 1	82.79	251.75	28.32	Nil	Nil	140	20.23	Nil
Run 2	85.92	254.08	21.84	125.62	17.17	140	15.60	Nil
Run 3	101.98	251.52	30.19	Nil	Nil	140	21.56	Nil
Mean (μ)	**90.23**	**252.45**	**26.78**				**19.13**	
STDEV (σ)	10.29	1.42	4.38				3.13	
ST. Error ($S_E = \sigma/n^{0.5}$)	5.94	0.82	2.53				1.81	
CI (95%), ($\mu \pm 1.96S_E$)	$\mu \pm 11.65$	$\mu \pm 1.60$	$\mu \pm 4.96$				$\mu \pm 3.54$	

Table 6.3 DSC Data of Extruded Samples of rPET-bg Contaminated with 5% PP

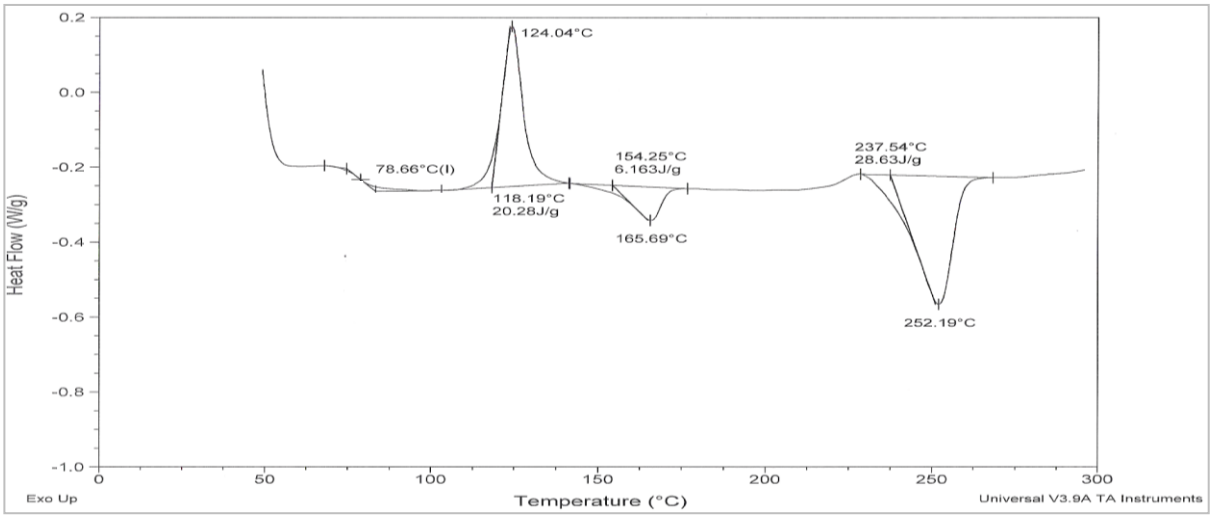

Figure 6.3 Thermogram of Extruded Sample 1 of rPET-bg contaminated with 10% PP

	T_g (^{o}C)	T_m (^{o}C)	ΔH_m (J/g)	T_c (^{o}C)	ΔH_c (J/g)	ΔH_m^0 (J/g)	X_c (%)	T_d (^{o}C)
Run 1	78.66	252.19	28.63	124.04	20.28	140	20.45	Nil
Run 2	73.58	254.24	28.17	Nil	Nil	140	20.12	Nil
Run 3	94.97	253.11	26.58	Nil	Nil	140	18.99	Nil
Mean (μ)	**82.40**	**253.18**	**27.79**				**19.85**	
STDEV (σ)	11.18	1.03	1.08				0.77	
ST. Error ($S_E = \sigma/n^{0.5}$)	6.45	0.59	0.62				0.44	
CI (95%), ($\mu \pm 1.96 S_E$)	$\mu \pm 12.65$	$\mu \pm 1.16$	$\mu \pm 1.22$				$\mu \pm 0.87$	

Table 6.4 DSC Data of Extruded Samples of rPET-bg Contaminated with 10% PP

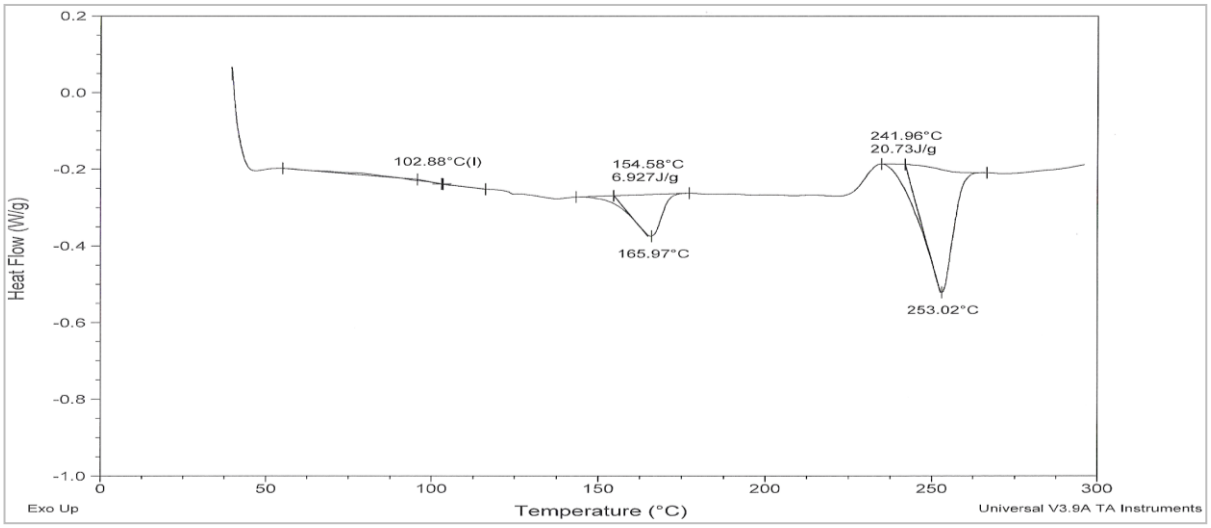

Figure 6.4 Thermogram of Extruded Sample 1 of rPET-bg contaminated with 15% PP

	T_g (^{o}C)	T_m (^{o}C)	ΔH_m (J/g)	T_c (^{o}C)	ΔH_c (J/g)	ΔH_m^0 (J/g)	X_c (%)	T_d (^{o}C)
Run 1	102.88	253.02	20.73	Nil	Nil	140	14.81	Nil
Run 2	94.39	255.30	24.12	Nil	Nil	140	17.23	Nil
Run 3	102.67	252.60	23.29	Nil	Nil	140	16.64	Nil
Mean (μ)	**99.98**	**253.64**	**22.71**				**16.22**	
STDEV (σ)	4.84	1.45	1.77				1.26	
ST. Error ($S_E = \sigma/n^{0.5}$)	2.80	0.84	1.02				0.73	
CI (95%), ($\mu \pm 1.96 S_E$)	$\mu \pm 5.48$	$\mu \pm 1.64$	$\mu \pm 2.00$				$\mu \pm 1.43$	

Table 6.5 DSC Data of Extruded Samples of rPET-bg Contaminated with 15% PP

Note: Additional DSC Thermograms are available in ***Appendix 6*** **(***1, 2, 3***)**.

Compared to non contaminated rPET-bg, as shown in *Table 6.6* and *Figure 6.5* below, the average $\boldsymbol{T_g}$ decreased in all cases, indicating well dispersion of PP chains within the rPET-bg matrix, probably creating some degree of chains entanglement, resulting in a narrowed glass transition. As a result of thermo-mechanical degradation, chains scissions and short chains creation happened, and the newly created short chains intervened during cooling and prevented a homogeneous crystallisation; the short chains pack and freeze prematurely and result in dispersed but localised crystalline domains, so during the DSC heating mode, these same dispersedly packed chains are prone to early glass transition and quick melting, resulting in decreased $\boldsymbol{T_g}$; *Heino et al.* [120] reported that reactions between the GMA-functionalised SEBS and PET lead to improved mixing between PET and PP phases and improved interfacial adhesion and shifted the $\boldsymbol{T_g}$ of the PET towards that of PP, and so, the shifting in $\boldsymbol{T_g}$ in this case, resulted from the influence of the inclusion of PP despite the absence of compatibilisers.

Extruded Samples	$\boldsymbol{T_g}$ **(°C)**		
	Mean ($\boldsymbol{\mu}$)	**ST. Error** ($\boldsymbol{S_E = \sigma/n^{0.5}}$)	**CI (95%)** ($\boldsymbol{\mu \pm 1.96 S_E}$)
Non contaminated rPET-bg	**102.63**	2.59	$\mu \pm 5.07$
95% rPET-bg / 5% PP	**90.23**	5.94	$\mu \pm 11.65$
90% rPET-bg / 10% PP	**82.40**	6.45	$\mu \pm 12.65$
85% rPET-bg / 15% PP	**99.98**	2.80	$\mu \pm 5.48$

Table 6.6 Glass Transition Temperature of Extruded Samples of rPET-bg Contaminated with PP

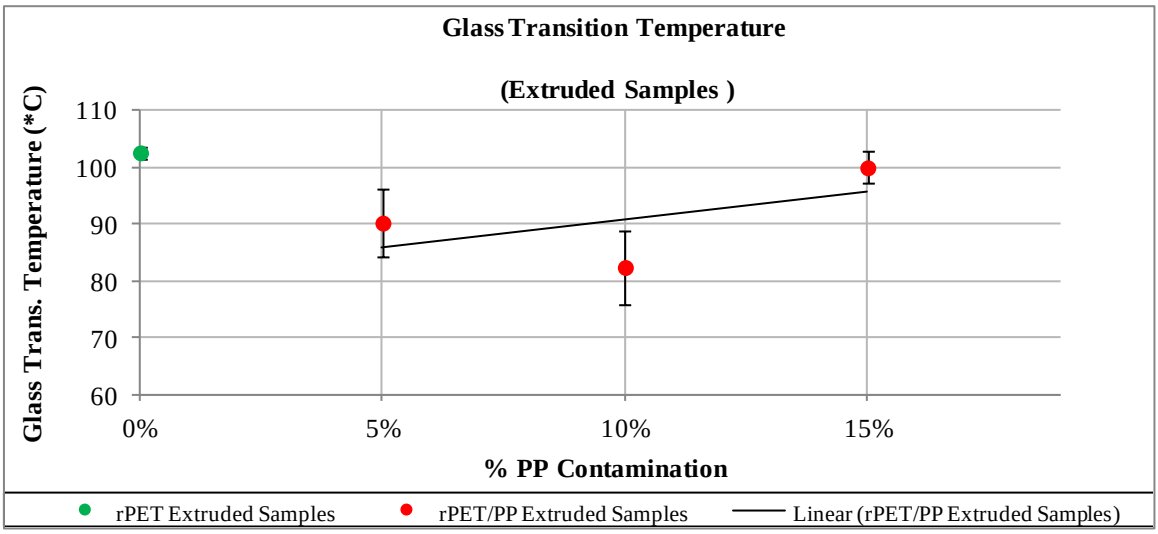

Figure 6.5 Glass Transition Temperatures of Extruded Samples of rPET-bg Contaminated with PP

Compared to non contaminated rPET-bg, as shown in *Table 6.7* and *Figure 6.6* below, the inclusion of PP decreased orderly the T_m, in all cases. It is likely that early melting of the PP chains speeded up the overall melting process, resulting in temperature decrease. Dispersed crystalline domains, usually requires less time and temperature to complete melting. The T_m in the contaminated rPET-bg increased gradually with increasing % PP contamination; showing the relationship between crystallinity and melting. As previously described with HDPE as contaminant, the absence of chemical secondary bonding, resulted in the exhibition of *double melting phases*, shown as sharply separated double melting peaks and reduced T_g; this confirmed also that PP and rPET-bg are *immiscible* and *incompatible*.

Extruded Samples	T_m (°C)		
	Mean (μ)	**ST. Error ($S_E = \sigma/n^{0.5}$)**	**CI (95%) ($\mu \pm 1.96 S_E$)**
Non contaminated rPET-bg	**254.62**	0.65	$\mu \pm 1.27$
95% rPET-bg / 5% PP	**252.45**	0.82	$\mu \pm 1.60$
90% rPET-bg / 10% PP	**253.18**	0.59	$\mu \pm 1.16$
85% rPET-bg / 15% PP	**253.64**	0.84	$\mu \pm 1.64$

Table 6.7 Melting Temperature of Extruded Samples of Extruded Samples of rPET-bg Contaminated with PP

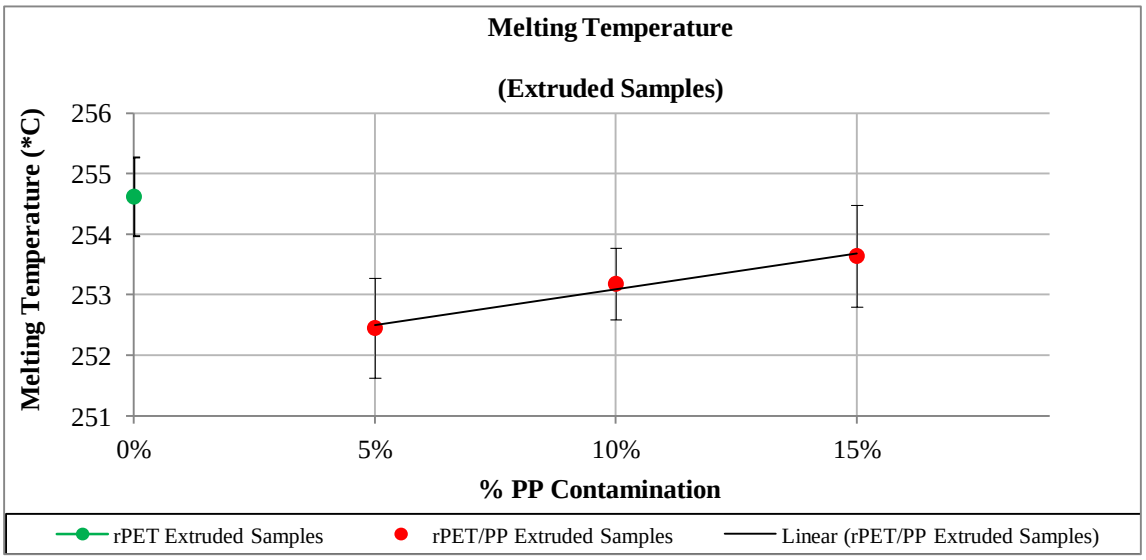

Figure 6.6 Melting Temperature of Extruded Samples of rPET-bg Contaminated with PP

Compared to non contaminated rPET-bg, as shown in *Table 6.8* and *Figure 6.7* below, the inclusion of PP contributed to the overall decrease of ΔH_m, where the rate of melting was improved by the early melting of PP. The decreased ΔH_m, once more indicated the presence of crystalline domains sporadically distributed within the rPET.bg matrix, and the endothermic heat required is proportional to the density of crystalline domains; these crystalline domains resulted from the formation of very short chains, and consequently, they are tiny and dispersed and required less heat absorption for melting. Furthermore, their densities decreased with increasing % PP contamination, which resulted in decreased ΔH_m with increasing % PP contamination.

Extruded Samples	ΔH_m (J.g^{-1})		
	Mean (μ)	**ST. Error ($S_E = \sigma/n^{0.5}$)**	**CI (95%) ($\mu \pm 1.96 S_E$)**
Non contaminated rPET-bg	**33.75**	4.65	$\mu \pm 9.12$
95% rPET-bg / 5% PP	**26.78**	2.53	$\mu \pm 4.96$
90% rPET-bg / 10% PP	**27.79**	0.62	$\mu \pm 1.22$
85% rPET-bg / 15% PP	**22.71**	1.02	$\mu \pm 2.00$

Table 6.8 Heat of Fusion of Extruded Samples of rPET-bg Contaminated with PP

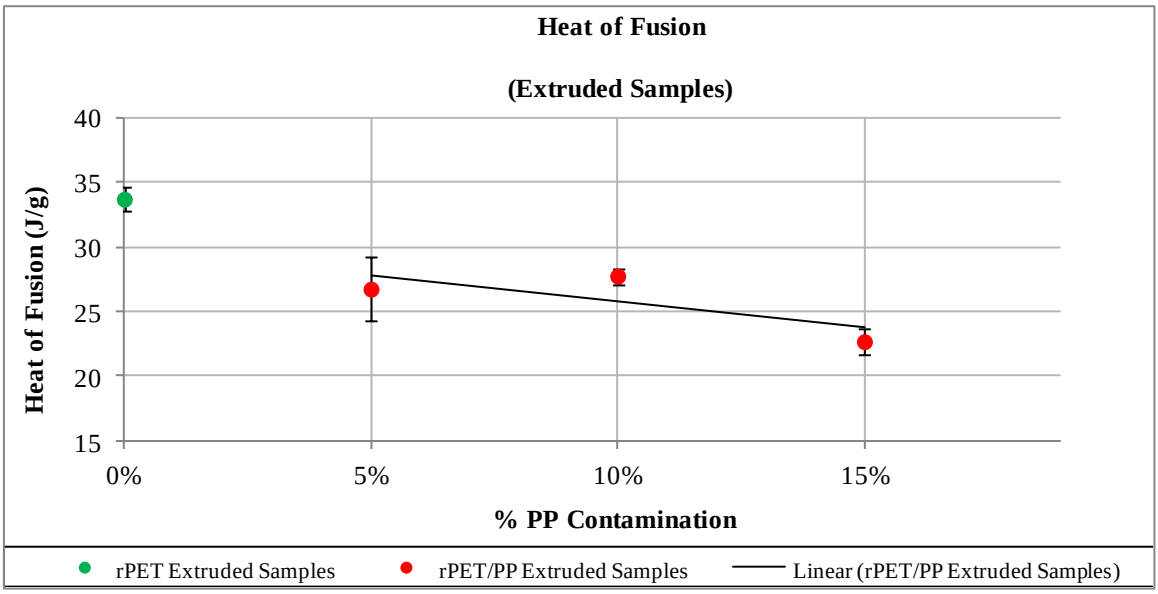

Figure 6.7 Heat of Fusion of Extruded Samples of rPET-bg Contaminated with PP

Compared to non contaminated rPET-bg, as shown in *Table 6.9* and *Figure 6.8* below, once again, the major absence of cold crystallisation peaks, indicated that following extrusion and degradation and consequently chains scissions, very small chains of PP were created and at cooling stage, they were able to stack and sporadically distributed in localised domains. Also, their fast glass transition and melting during the DSC heating, contributed to the overall ease of phase transitions and the absence of cold crystallisation peaks in major cases indicated that the melting overridden the relaxation process of chains. And the reduced $\boldsymbol{X_c}$ confirmed the pattern of the crystalline domains as being numerous but sporadically dispersed as a result of PP inclusion.

Extruded Samples	X_c **(%)**		
	Mean (μ)	**ST. Error** ($S_E = \sigma/n^{0.5}$)	**CI (95%)** ($\mu \pm 1.96 S_E$)
Non contaminated rPET-bg	**24.11**	3.32	$\mu \pm 6.51$
95% rPET-bg / 5% PP	**19.13**	1.81	$\mu \pm 3.54$
90% rPET-bg / 10% PP	**19.85**	0.44	$\mu \pm 0.87$
85% rPET-bg / 15% PP	**16.22**	0.73	$\mu \pm 1.43$

Table 6.9 % Crystallinity of Extruded Samples of rPET-bg Contaminated with PP

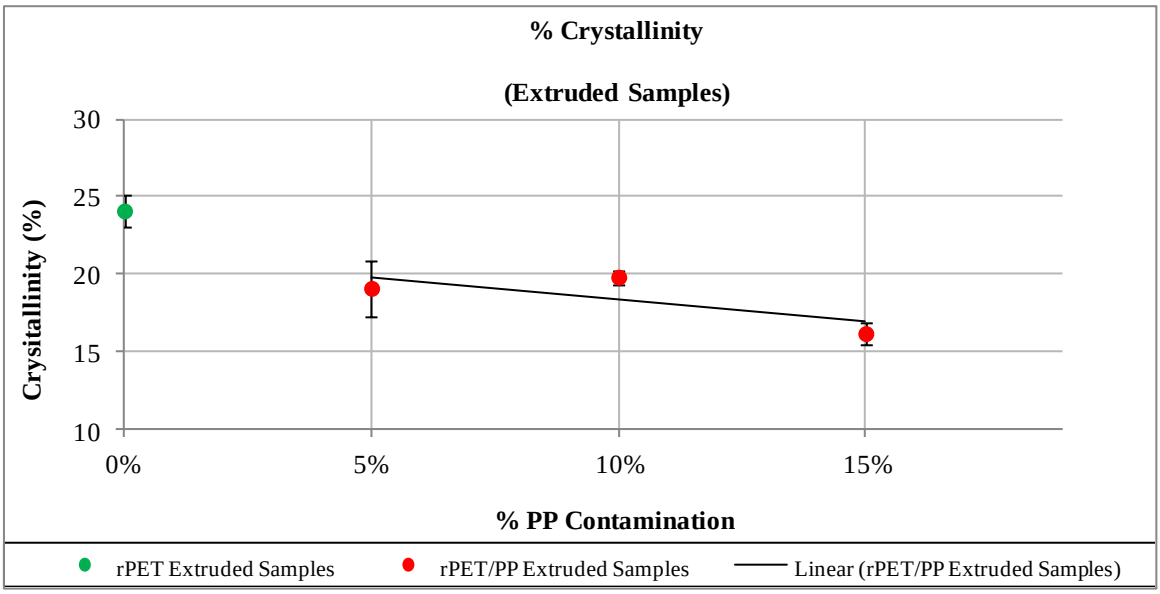

Figure 6.8 % Crystallinity of Extruded Samples of rPET-bg Contaminated with PP

6.1.2 FTIR results of *Extruded Samples*

In *experiments 6, 7* and *8*, the FTIR analysis yielded the data below.

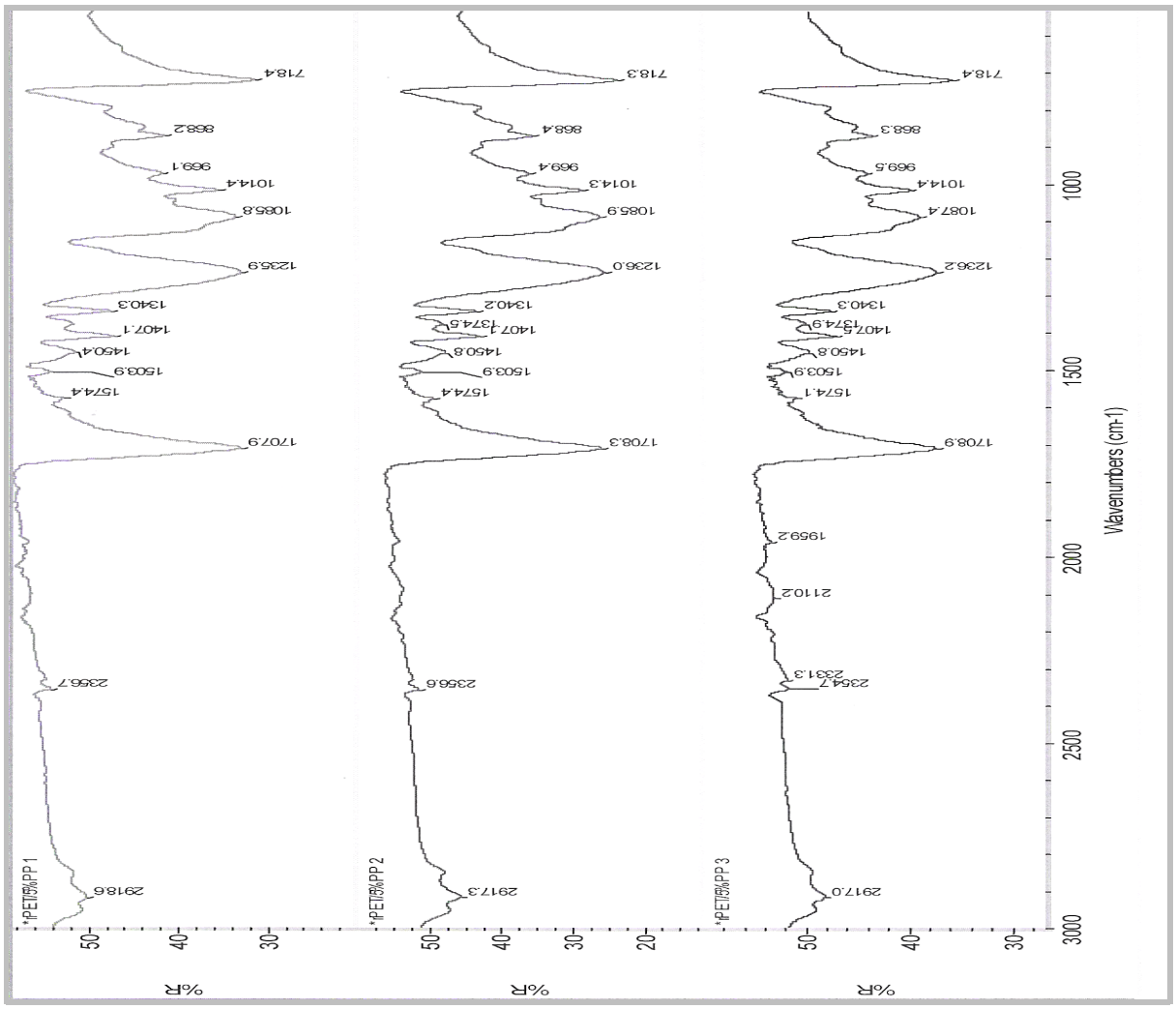

Figure 6.9 Spectra of Extruded Samples of rPET-bg contaminated with 5% PP

Wavenumber (cm^{-1})			Bond	Wavenumber (cm^{-1})	Compound Type
Scan 1	**Scan 2**	**Scan 3**			
2918	2917	2917	C-H	2850-2960	Alkane
1707	1708	1708	C=O	1670-1760	Ester
1503 to 1574	1503 to 1574	1503 to 1574	C=C	1500-1600	Ester Ar. Ring
718 to 868	718 to 868	718 to 868	C-H	Below 900	Ester Ar. Ring
1085 to 1235	1085 to 1236	1087 to 1236	C-O	1000-1260	Ester

Table 6.10 FTIR Data of Extruded Samples of rPET-bg Contaminated with 5% PP

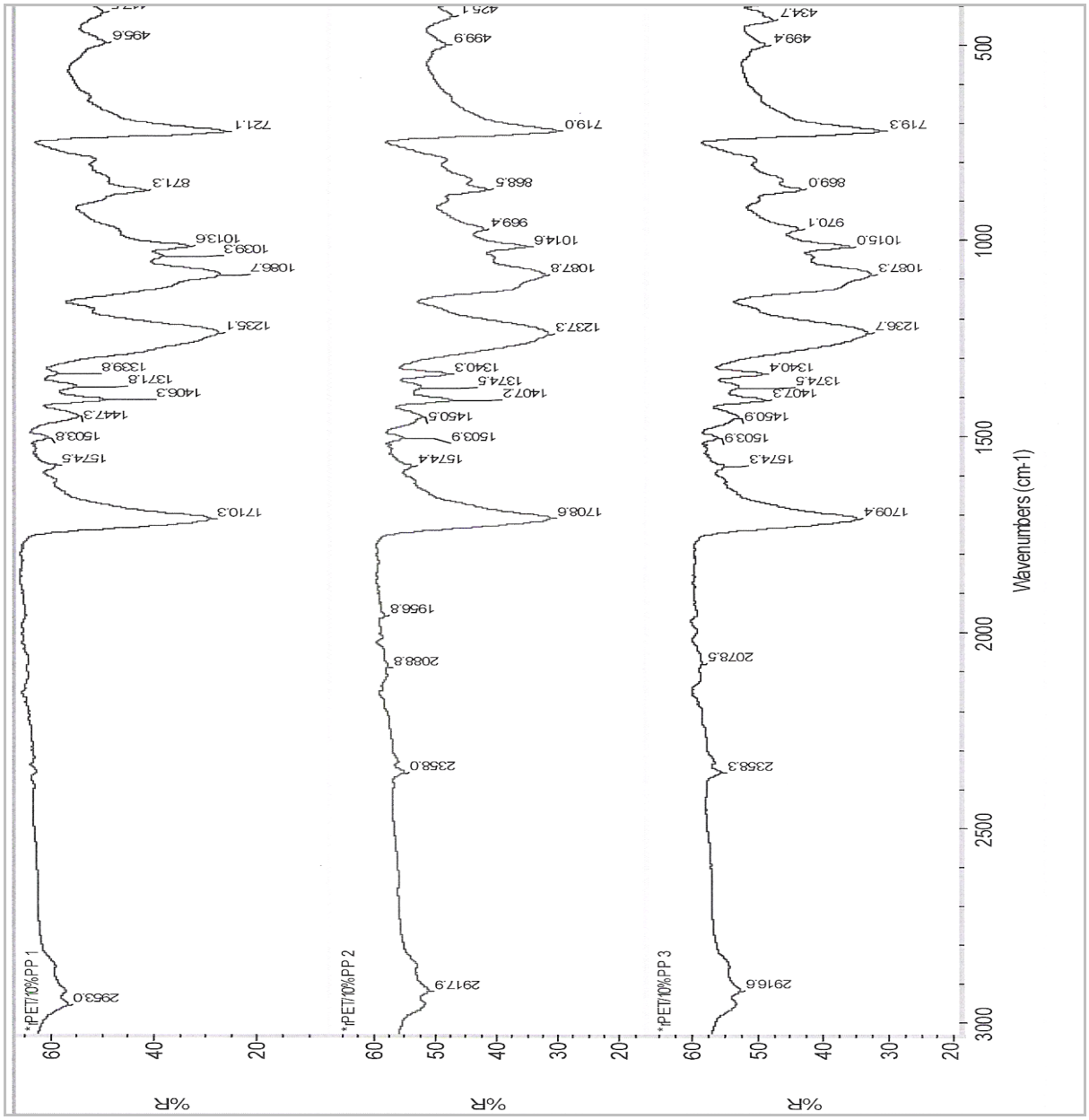

Figure 6.10 Spectra of Extruded Samples of rPET-bg contaminated with 10% PP

Wavenumber (cm^{-1})			Bond	Wavenumber (cm^{-1})	Compound Type
Scan 1	**Scan 2**	**Scan 3**			
2953	2917	2916	C-H	2850-2960	Alkane
1710	1708	1709	C=O	1670-1760	Ester
1503 to 1574	1503 to 1574	1503 to 1574	C=C	1500-1600	Ester Ar. Ring
417 to 871	425 to 868	434 to 869	C-H	Below 900	Ester Ar. Ring
1086 to 1235	1087 to 1237	1087 to 1236	C-O	1000-1260	Ester

Table 6.11 FTIR Data of Extruded Samples of rPET-bg Contaminated with 10% PP

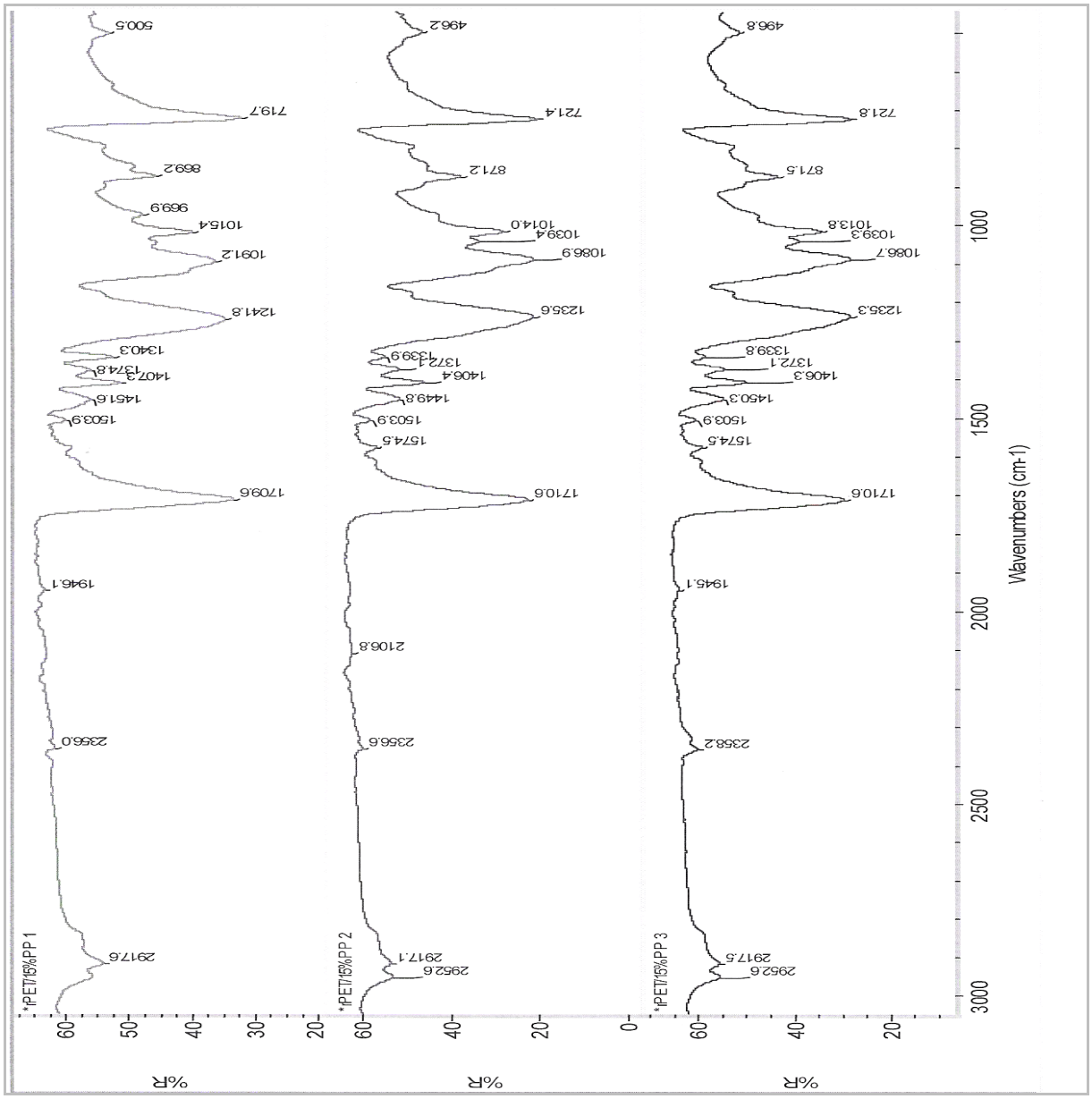

Figure 6.11 Spectra of Extruded Samples of rPET-bg contaminated with 15% PP

Wavenumber (cm^{-1})			Bond	Wavenumber (cm^{-1})	Compound Type
Scan 1	**Scan 2**	**Scan 3**			
2917	2917 to 2952	2917 to 2952	C-H	2850-2960	Alkane
1709	1710	1710	C=O	1670-1760	Ester
1503	1503 to 1574	1503 to 1574	C=C	1500-1600	Ester Ar. Ring
500 to 869	496 to 871	496 to 871	C-H	Below 900	Ester Ar. Ring
1091 to 1241	1086 to 1235	1086 to 1235	C-O	1000-1260	Ester

Table 6.12 FTIR Data of Extruded Samples of rPET-bg Contaminated with 15% PP

The results, shown in *Table 6.13* below, showed slight increase in absorptions and fusion of the *PP* and *the rPET-bg* matrix *allkane* broad *C-H* absorptions and also indicated overall changes in bonds dipoles; this indicated reduced bonds strain levels which allowed flexibility and excitation and vibrations of bonds and increased the absorbed intensity. Also, these vibration levels, as seen previously with *HDPE inclusion*, showed reduced and unbalanced molecular strains as a result of the overall sporadic crystals' dispersion and the weak interactions generated by the inclusion of *PP*. Once again, the *extruded samples*' molecular bonds in the batches of *rPET-bg contaminated with PP* compared to their counterpart of *non contaminated rPET-bg* showed slight increase of vibrations as a result of reduced molecular strains and density due to the *PP inclusion* and further processing and confirmed the slight decrease of % crystallinity shown by the DSC analysis.

Material	**Extruded Samples of rPET-bg** (1) **Compared to rPET-bg / PP** (5%, 10% and 15%)

Samples (1)	**5% HDPE)**	**10% HDPE**	**15% HDPE**	**Reference**		
Wavenumber (cm^{-1})				**Bonds**	**Wavenumber (cm^{-1})**	**Compound Type**
2915 to 2919	2917 to 2918	2916 to 2953	2917 to 2952	C-H	2850-2960	Alkane
1705 to 1708	1707 to 1708	1708 to 1710	1709 to 1710	C=O	1670-1760	Ester
1503 to 1574	1503 to 1574	1503 to 1574	1503 to 1574	C=C	1500-1600	Ester Ar. Ring
410 to 867	718 to 868	417 to 871	496 to 871	C-H	Below 900	Ester Ar. Ring
1084 to 1236	1085 to 1236	1086 to 1237	1086 to 1241	C-O	1000-1260	Ester

Table 6.13 FTIR Data of Extruded Samples of rPET-bg contaminated with PP

6.1.3 MFR results of *Extruded Samples*

In *experiments 6, 7* and *8*, the MFR analysis yielded the data below.

Extrudates	Weight Averages (g)	Time (s)	MFR (g/10min)
Run 1	**1.43**	15	57.27
Run 2	**0.87**	10	52.34
Run 3	**0.45**	05	53.68
Mean (μ)			**54.43**
STDEV (σ)			2.55
ST. Error ($S_E = \sigma/n^{0.5}$)			1.47
CI (95%), ($\mu \pm 1.96 S_E$)			$\mu \pm 2.88$

Table 6.14 MFR of Extruded Samples of rPET-bg Contaminated with 5% PP

Run 1	**1.78**	15	71.15
Run 2	**1.21**	10	72.70
Run 3	**0.60**	05	72.20
Mean (μ)			**72.02**
STDEV (σ)			0.79
ST. Error ($S_E = \sigma/n^{0.5}$)			0.46
CI (95%), ($\mu \pm 1.96 S_E$)			$\mu \pm 0.90$

Table 6.15 MFR of Extruded Samples of rPET-bg Contaminated with 10% PP

Run 1	**1.92**	15	76.91
Run 2	**1.39**	10	83.58
Run 3	**0.71**	05	85.20
Mean (μ)			**81.90**
STDEV (σ)			4.40
ST. Error ($S_E = \sigma/n^{0.5}$)			2.54
CI (95%), ($\mu \pm 1.96 S_E$)			$\mu \pm 4.97$

Table 6.16 MFR of Extruded Samples of rPET-bg Contaminated with 15% PP

Compared to non contaminated rPET-bg, as shown in *Table 6.17* and *Figure 6.12* below, The low *MFR* of PP, *1g /10min* as shown in *Table 3.2*, *Section 3.1.3*, contributed to the decrease of MFR in most cases of contaminated rPET-bg. Quantitatively, the MFR increased proportionally with increasing the % PP contamination in the contaminated samples; this showed that despite its low MFR, this grade of PP is characterised by excellent flow behaviour, good dimensional stability and ease of shear under thermal conditions, characteristics of a multi-processes material as shown in *Data Sheet , Appendix 2*. In addition, the degradation process and the incompatibility of PP and rPET-bg increased further the number of very short chains, which promoted the shear of lamellae and consequently increased the MFR proportionally with increasing % PP contamination. *Pracella et al.* [114], *Friedrich et al.* [115] and *Inoya et al.* [118, 119] reported that for improved properties of the PET/PP, the use of compatibilisers is a necessity.

Extruded Samples	**MFR (g/10mins)**		
	Mean (μ)	**ST. Error ($S_E = \sigma/n^{0.5}$)**	**CI (95%) ($\mu \pm 1.96 S_E$)**
Non contaminated rPET-bg	**74.30**	0.52	$\mu \pm 1.02$
95% rPET-bg / 5% PP	**54.43**	1.47	$\mu \pm 2.88$
90% rPET-bg / 10% PP	**72.02**	0.46	$\mu \pm 0.90$
85% rPET-bg / 15% PP	**81.90**	2.54	$\mu \pm 4.97$

Table 6.17 MFR of Extruded Samples of rPET-bg Contaminated with PP

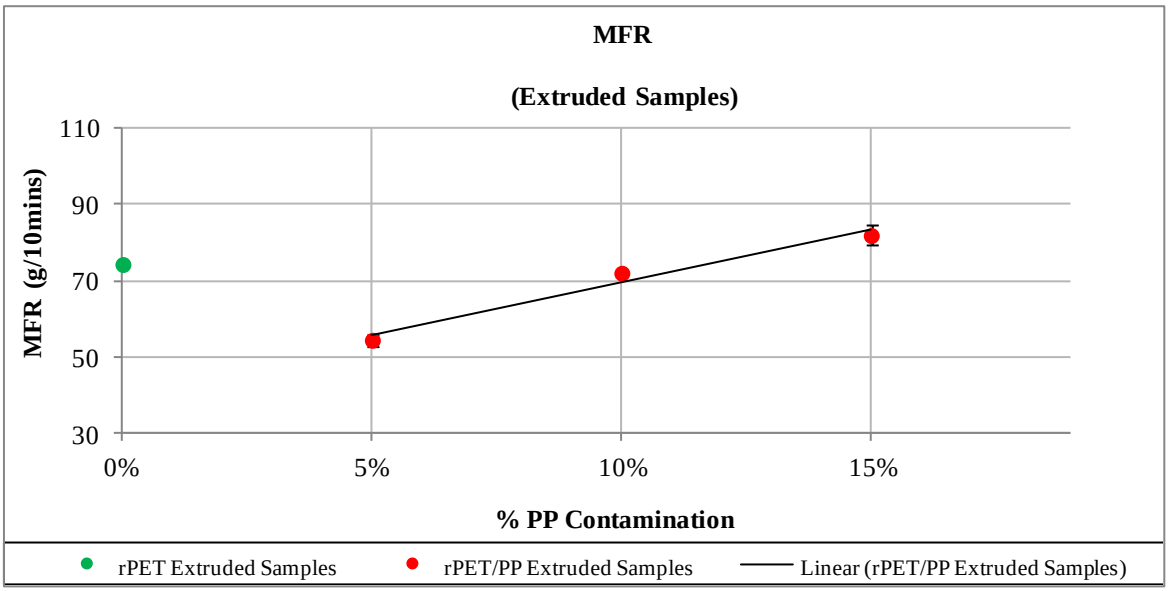

Figure 6.12 MFR of Extruded Samples of rPET-bg Contaminated with PP

By analysis of *Figure 6.13* below, the curves of rPET- bg contaminated with PP showed a slight inverse proportionality between MFR and % torque; the % torque, which defines the viscosity behaviour during extrusion, showed balanced and good processing stability slightly affected by the increased % PP contamination.

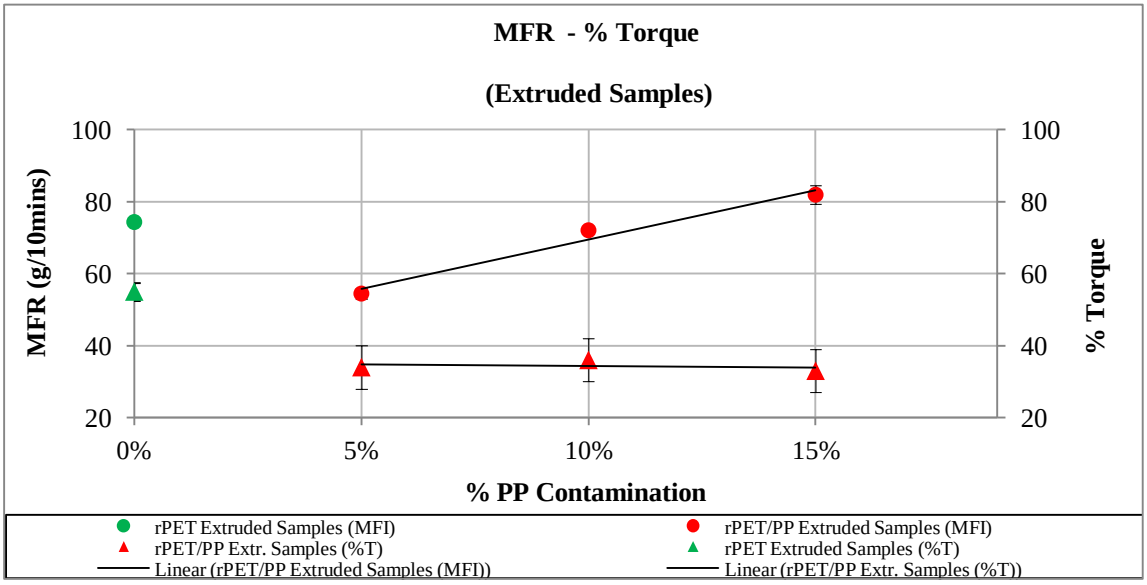

Figure 6.13 MFR Compared to % Torque of Extruded Samples of rPET-bg Contaminated with PP

Again, by analysis of *Figure 6.14* below, the curves of rPET- bg contaminated with PP showed balanced screw speed despite the increasing % PP contamination; this indicated the excellent flow behaviour and dimensional stability of the PP despite the effects of chains-scissions in easing the screw speed. It is assumed that polyolefins would undergo thermal degradation, within a processing temperature range of *200 - 230^{o}C*, in rPET/ PP blends where rPET is the minor phase, as reported by *Dealy* and *Wissbrun* [176] and consequently decreases dramatically the screw speed; this may be the case but when the PET phase is the major, as in this work, even up to *270^{o}C* the screw speed appeared to stabilise, which indicated not only chains' scissions is taking place during extrusion.

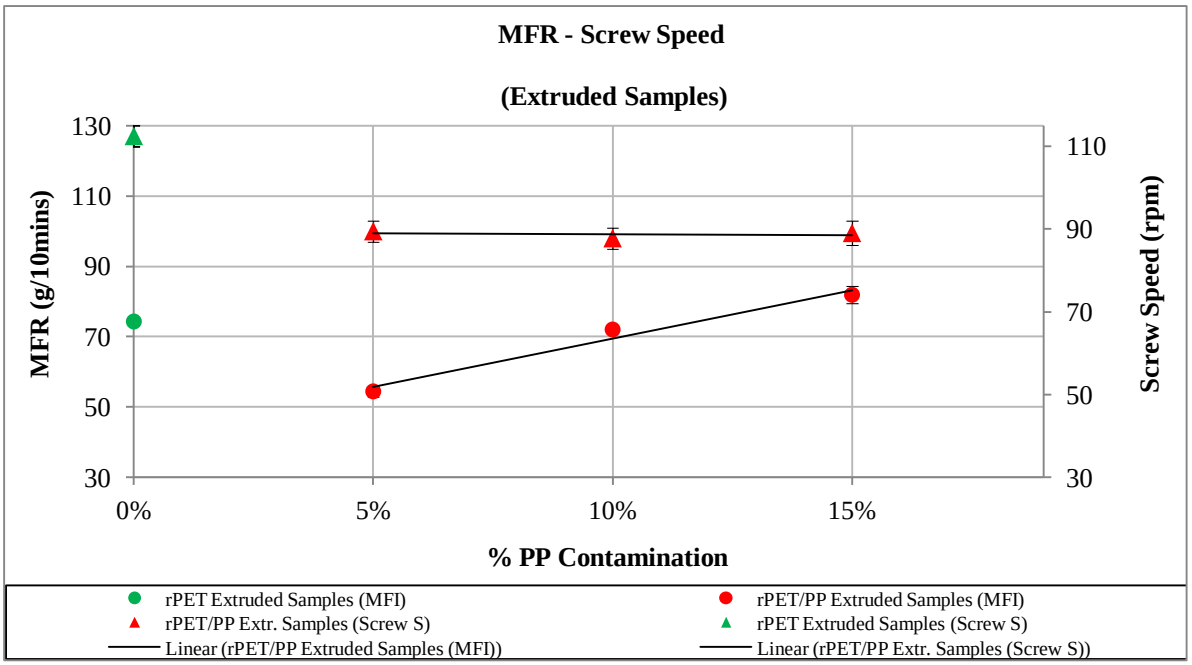

Figure 6.14 MFR Compared to Screw Speed of Extruded Samples of rPET-bg Contaminated with PP

In *experiments 6, 7* and *8*, the *extruded pellets* of rPET-bg, contaminated respectively with *5%, 10%* and *15%* PP, were injection moulded into *dumbbells* and *impact bars*. Again, *injection moulded samples* were analysed by DSC, FTIR, MFR and the *dumbbells* and *impact bars* were tested for their tensile and impact properties and investigated and the results are shown and discussed below.

Furthermore, the inclusion of PP contamination decreased the injection and packing pressures, as shown in *Table 6.18* below; this showed the ease of flow of PP and its dimension stability. The increased packing pressure with increasing % PP contamination indicated decreased shear of lamellae due to early cooling of PP chains in the mould cavity. Compared to non contaminated rPET-bg, the stability of the injection pressure in the contaminated materials indicated homogeneous melt and balanced flow promoted by the contaminant, PP.

Injection Moulded Samples	Injection Pressure (Bars)	Packing Pressure (Bars)	Mould Temp. (^{o}C)	Injection Time (s)	Packing Pressure (%)
Non contaminated rPET-bg	**180**	**75**	60	1.35	45%
95% rPET-bg / 5% PP	**165**	**70**	60	1.35	45%
90% rPET-bg / 10% PP	**165**	**72**	60	1.35	45%
85% rPET-bg / 15% PP	**165**	**73**	60	1.35	45%

Table 6.18 Variation of Injection Moulding Condition of rPET-bg Contaminated with PP

6.1.4 DSC results of *Injection Moulded Samples*

In *experiments 6, 7* and *8*, the DSC analysis yielded the data below.

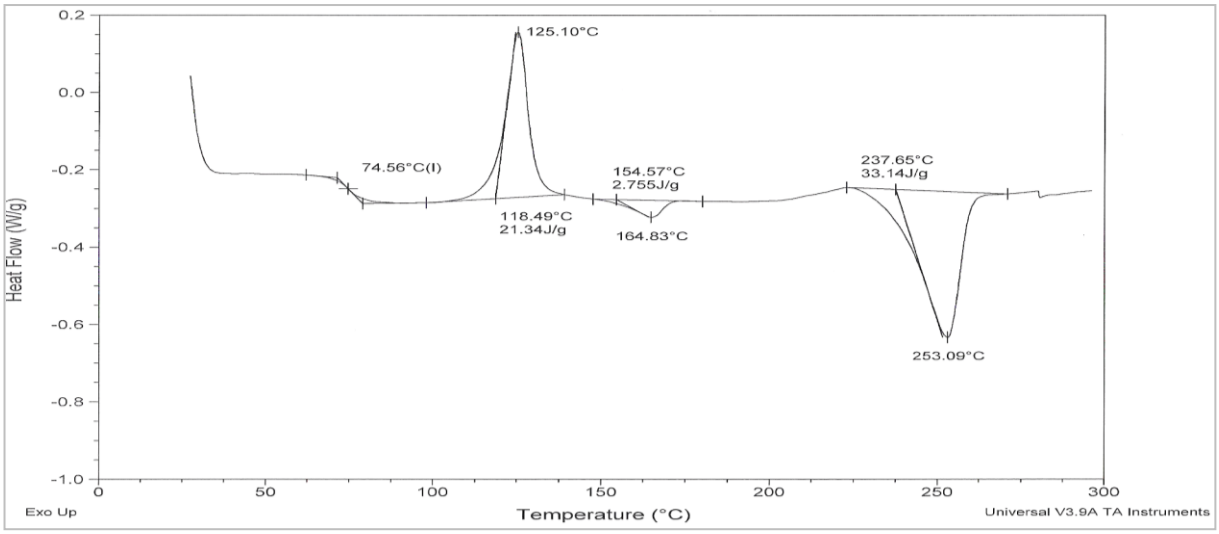

Figure 6.15 Thermogram of Inj. Moulded Sample 1 of rPET-bg contaminated with 5% PP

	T_g (^{o}C)	T_m (^{o}C)	ΔH_m (J/g)	T_c (^{o}C)	ΔH_c (J/g)	ΔH_m^0 (J/g)	X_c (%)	T_d (^{o}C)
Run 1	74.56	253.09	33.14	125.10	21.34	140	23.67	Nil
Run 2	74.13	251.96	36.14	124.80	23.97	140	25.81	Nil
Run 3	77.67	252.93	30.46	123.00	19.46	140	21.76	Nil
Mean (μ)	**75.45**	**252.66**	**33.25**	**124.30**	**21.59**		**23.75**	
STDEV (σ)	1.93	0.61	2.84	1.14	2.26		2.03	
ST. Error ($S_E = \sigma/n^{0.5}$)	1.11	0.35	1.64	0.66	1.31		1.17	
CI (95%), ($\mu \pm 1.96 S_E$)	$\mu \pm 2.19$	$\mu \pm 0.69$	$\mu \pm 3.21$	$\mu \pm 1.28$	$\mu \pm 2.56$		$\mu \pm 2.30$	

Table 6.19 DSC Data of Inj. Moulded Samples of rPET-bg Contaminated with 5% PP

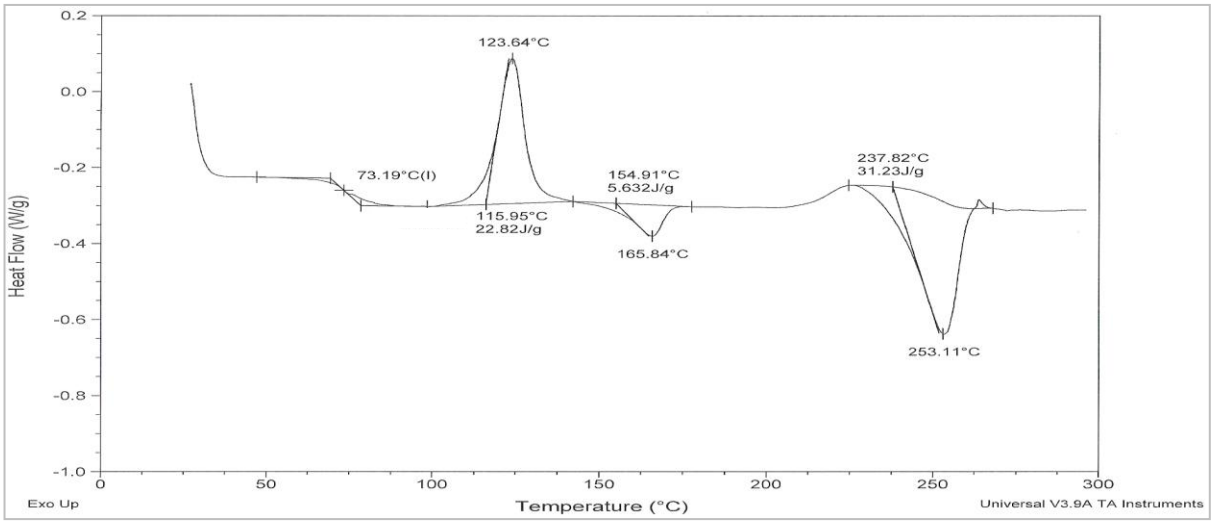

Figure 6.16 Thermogram of Inj. Moulded Sample 1 of rPET-bg contaminated with 10% PP

	T_g (^{o}C)	T_m (^{o}C)	ΔH_m (J/g)	T_c (^{o}C)	ΔH_c (J/g)	ΔH_m^0 (J/g)	X_c (%)	T_d (^{o}C)
Run 1	73.19	253.11	31.23	123.64	22.82	140	22.31	Nil
Run 2	73.42	253.06	34.26	Nil	Nil	140	24.47	Nil
Run 3	74.33	255.03	12.32	Nil	Nil	140	8.80	Nil
Mean (μ)	**73.65**	**253.73**	**25.94**				**18.53**	
STDEV (σ)	0.60	1.12	11.89				8.49	
ST. Error ($S_E = \sigma/n^{0.5}$)	0.35	0.65	6.86				4.90	
CI (95%), ($\mu \pm 1.96S_E$)	$\mu \pm 0.68$	$\mu \pm 1.27$	$\mu \pm 13.45$				$\mu \pm 9.61$	

Table 6.20 DSC Data of Inj. Moulded Samples of rPET-bg Contaminated with 10% PP

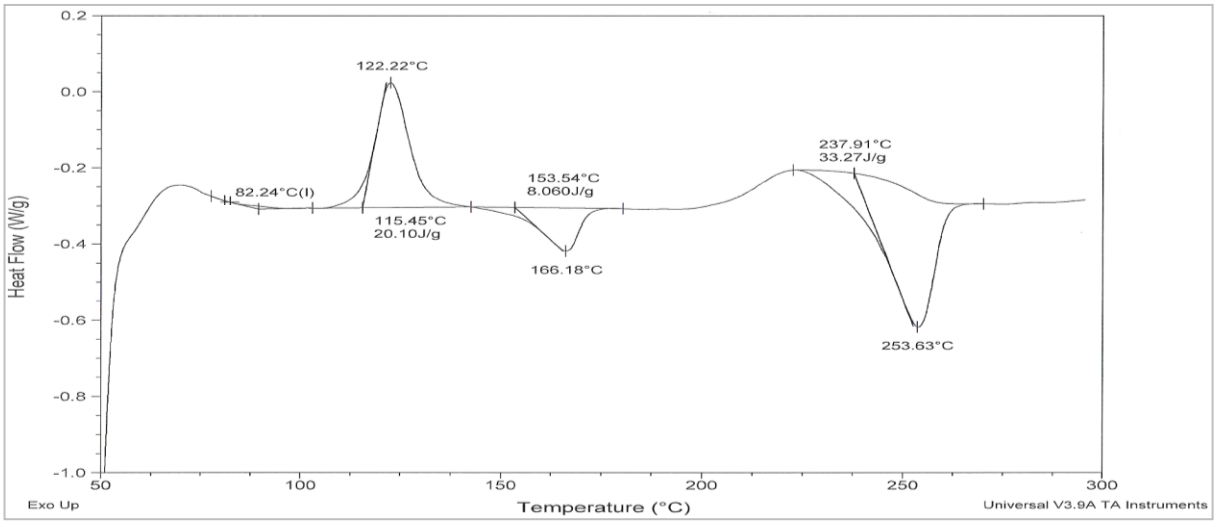

Figure 6.17 Thermogram of Inj. Moulded Sample 1 of rPET-bg contaminated with 15% PP

	T_g (^{o}C)	T_m (^{o}C)	ΔH_m (J/g)	T_c (^{o}C)	ΔH_c (J/g)	ΔH_m^0 (J/g)	X_c (%)	T_d (^{o}C)
Run 1	82.24	253.63	33.27	122.22	20.10	140	23.76	Nil
Run 2	80.28	253.00	31.11	123.96	20.33	140	22.22	Nil
Run 3	76.84	252.89	30.70	121.95	15.98	140	21.93	Nil
Mean (μ)	**79.79**	**253.17**	**31.69**	**122.71**	**18.80**		**22.64**	
STDEV (σ)	2.73	0.40	1.38	1.09	2.45		0.99	
ST. Error ($S_E = \sigma/n^{0.5}$)	1.58	0.23	0.80	0.63	1.41		0.57	
CI (95%), ($\mu \pm 1.96S_E$)	$\mu \pm 3.09$	$\mu \pm 0.45$	1.56	$\mu \pm 1.23$	$\mu \pm 2.77$		$\mu \pm 1.12$	

Table 6.21 DSC Data of Inj. Moulded Samples of rPET-bg Contaminated with 15% PP

Note: DSC Thermograms are available in ***Appendix 6*** **(***7, 8, 9***)**.

Compared to non contaminated rPET-bg, as shown in *Table 6.22* and *Figure 6.18* below, the T_g of the rPET-bg contaminated with PP decreased randomly with increasing % PP contamination, indicating larger domains of dispersed very small chains; this random arrangement of chains was promoted by the increased packing pressure in the cavity of the mould. These very short chains required larger scales of time and temperatures to re-arrange during the DSC heating process, resulting in random T_g with increasing % PP contamination.

Inj. Moulded Samples	T_g (°C)		
	Mean (μ)	**ST. Error ($S_E = \sigma/n^{0.5}$)**	**CI (95%) ($\mu \pm 1.96 S_E$)**
Non contaminated rPET-bg	**79.60**	3.29	$\mu \pm 6.45$
95% rPET-bg / 5% PP	**75.45**	1.11	$\mu \pm 2.19$
90% rPET-bg / 10% PP	**73.65**	0.35	$\mu \pm 0.68$
85% rPET-bg / 15% PP	**79.79**	1.58	$\mu \pm 3.09$

Table 6.22 Glass Transition Temperature of Inj. Moulded Samples of rPET-bg Contaminated with PP

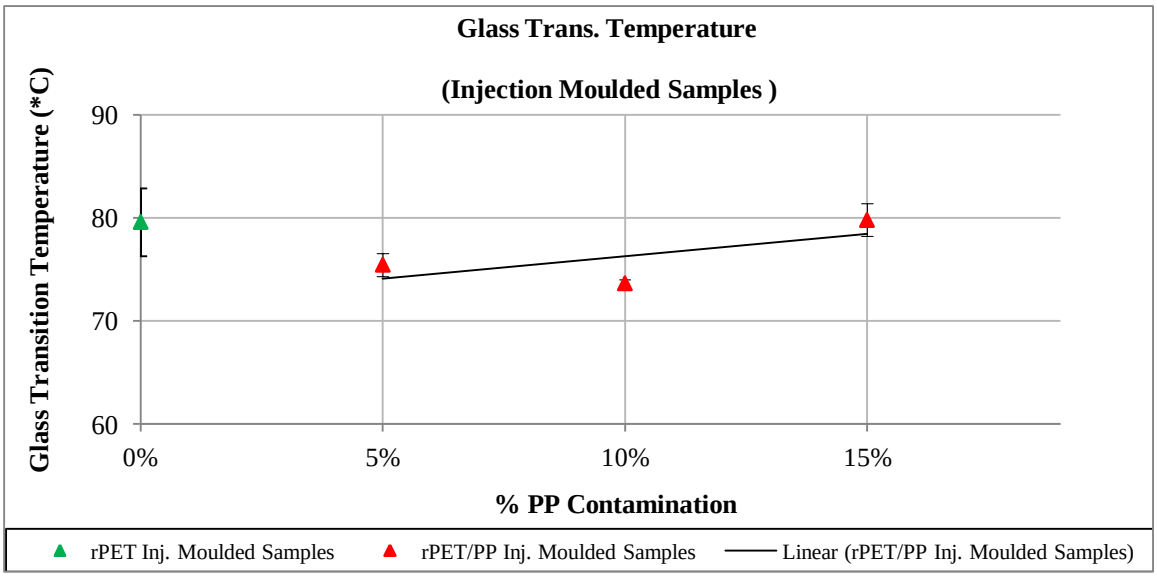

Figure 6.18 Glass Transition Temperature of Inj. Moulded Samples of rPET-bg Contaminated with PP

Compared to non contaminated rPET-bg, as shown in *Table 6.23* and *Figure 6.19* below, once more the effect of packing pressure can be seen by the quantities of randomly dispersed domains of very small chains; which decreased with increasing both % PP contamination and packing pressure in the cavity. During the DSC heating mode, proportional temperature was required for chains of the retained amorphous domains from previous cooling, to relax and crystallise and release proportional amounts of energy for achieving cold crystallisation.

Inj. Moulded Samples	**T_c (°C)**		
	Mean (μ)	**ST. Error ($S_E = \sigma/n^{0.5}$)**	**CI (95%) ($\mu \pm 1.96 S_E$)**
Non contaminated rPET-bg	**120.23**	1.07	$\mu \pm 2.09$
95% rPET-bg / 5% PP	**124.30**	0.66	$\mu \pm 1.28$
90% rPET-bg / 10% PP	**123.64**	0.00	$\mu \pm 0.00$
85% rPET-bg / 15% PP	**122.71**	0.63	$\mu \pm 1.23$

Table 6.23 Cold Crystallisation Temperature of Inj. Moulded Samples of rPET-bg Contaminated with PP

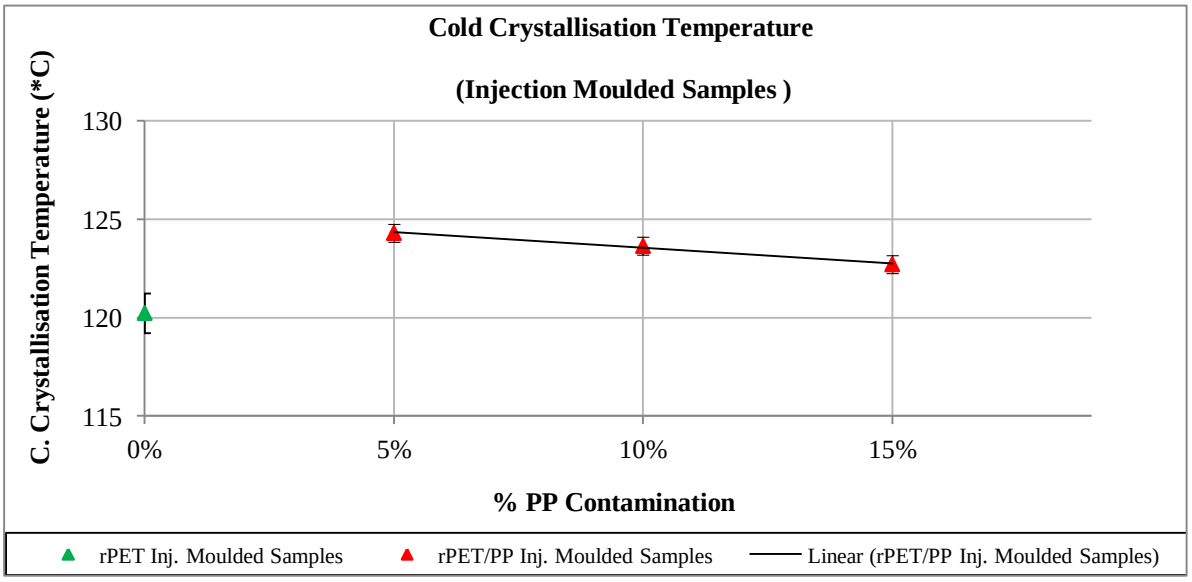

Figure 6.19 Cold Crystallisation Temperature of Inj. Moulded Samples of rPET-bg Contaminated with PP

Compared to non contaminated rPET-bg, as shown in *Table 6.24* and *Figure 6.20* below, as with HDPE, the decrease of enthalpy of cold crystallisation ΔH_c indicated presence of small crystalline domains and very small and sporadically dispersed large number of very small chains, so during the DSC heating mode, their re-straightening and repacking released decreased amounts of heat and the early melting of PP promoted the overall melting and prevented the completion of cold crystallisation.

Inj. Moulded Samples	ΔH_c (J.g^{-1})		
	Mean (μ)	**ST. Error ($S_E = \sigma/n^{0.5}$)**	**CI (95%) ($\mu \pm 1.96 S_E$)**
Non contaminated rPET-bg	**23.46**	2.72	$\mu \pm 5.33$
95% rPET-bg / 5% PP	**21.59**	1.31	$\mu \pm 2.56$
90% rPET-bg / 10% PP	**22.82**	0.00	$\mu \pm 0.00$
85% rPET-bg / 15% PP	**18.80**	1.41	$\mu \pm 2.77$

Table 6.24 Heat of Cold Crystallisation of Inj. Moulded Samples of rPET-bg Contaminated with PP

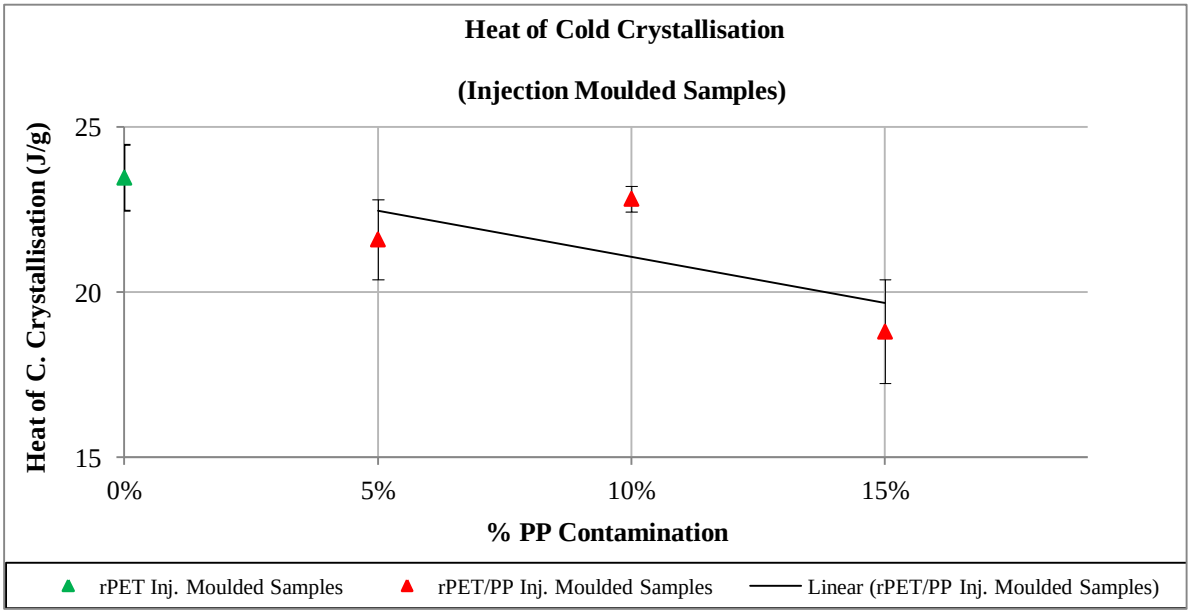

Figure 6.20 Heat of Cold Crystallisation of Inj. Moulded Samples of rPET-bg Contaminated with PP

Compared to non contaminated rPET-bg, as shown in *Table 6.25* and *Figure 6.21* below, following injection moulding, the T_m slightly decreased in all cases showing that the early melting of crystalline domains including PP and the very small chains activated further and speeded up the melting process, and resulted in reduced T_m. The exhibition of two melting phases showed that miscibility of PP and rPET-bg did not improve despite further processing, hence, the degree of *incompatibility* and *immiscibility* is still high.

Inj. Moulded Samples	T_m (°C)		
	Mean (μ)	**ST. Error ($S_E = \sigma/n^{0.5}$)**	**CI (95%) ($\mu \pm 1.96 S_E$)**
Non contaminated rPET-bg	**253.86**	0.80	$\mu \pm 1.57$
95% rPET-bg / 5% PP	**252.66**	0.35	$\mu \pm 0.69$
90% rPET-bg / 10% PP	**253.73**	0.65	$\mu \pm 1.27$
85% rPET-bg / 15% PP	**253.17**	0.23	$\mu \pm 0.45$

Table 6.25 Melting Temperature of Inj. Moulded Samples of rPET-bg Contaminated with PP

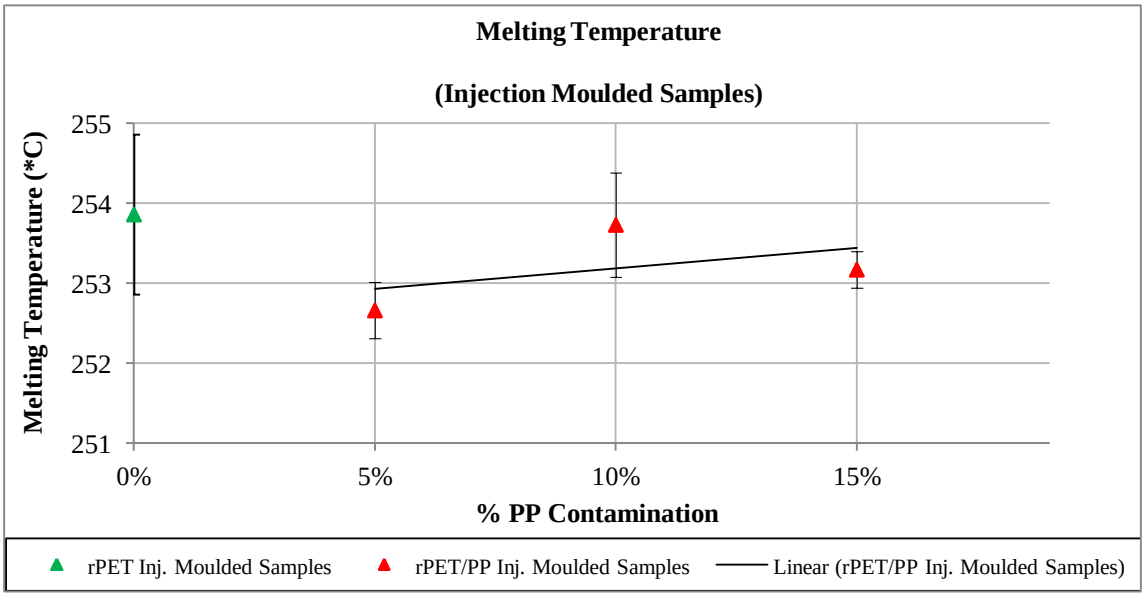

Figure 6.21 Melting Temperature of Inj. Moulded Samples of rPET-bg Contaminated with PP

Compared to non contaminated rPET-bg, as shown in *Table 6.26* and *Figure 6.22* below, the ΔH_m decreased in all cases, showing the effect of early melting of PP on the overall endothermic reaction. Furthermore, the unbalanced fluctuation of ΔH_m in the contaminated rPET-bg, indicated unbalanced distribution of crystalline domains, and suggested presence of localised entangled chains, which triggered formation of localised amorphous domains, like at 10% PP contamination, which required decreased heat absorption for melting.

Inj. Moulded Samples	ΔH_m (J.g^{-1})		
	Mean (μ)	**ST. Error** ($S_E = \sigma/n^{0.5}$)	**CI (95%)** ($\mu \pm 1.96 S_E$)
Non contaminated rPET-bg	**46.22**	3.21	$\mu \pm 6.29$
95% rPET-bg / 5% PP	**33.25**	1.64	$\mu \pm 3.21$
90% rPET-bg / 10% PP	**25.94**	6.86	$\mu \pm 13.45$
85% rPET-bg / 15% PP	**31.69**	0.80	$\mu \pm 1.56$

Table 6.26 Heat of Fusion of Inj. Moulded Samples of rPET-bg Contaminated with PP

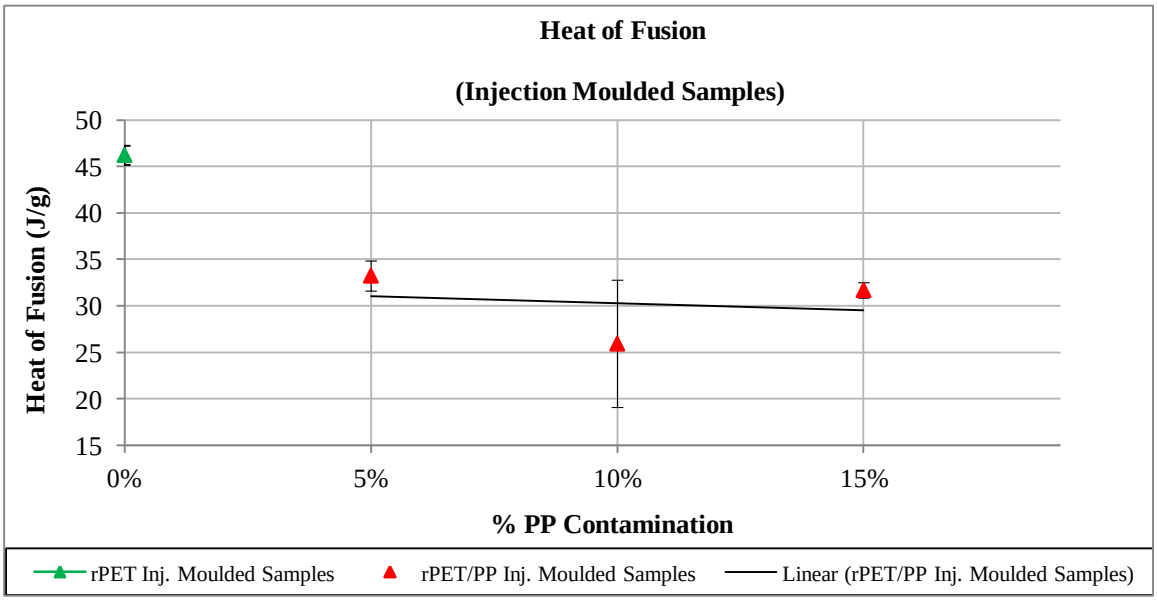

Figure 6.22 Heat of Fusion of Inj. Moulded Samples of rPET-bg Contaminated with PP

Compared to non contaminated rPET-bg, as shown in *Table 6.27* and *Figure 6.23* below, the % crystallinity, $\boldsymbol{X_c}$, of the rPET-bg contaminated with PP decreased in all cases, indicating that the PP inclusion interfered in the orderly packing of the matrix chains by intersecting and delaying the overall process of crystallisation. Furthermore, localised entangled chains at 10%, possibly resulting from unbalanced packing due to the presence of other contaminants, as described previously, decreased further the % crystallinity, $\boldsymbol{X_c}$ at 10% PP contamination.

Inj. Moulded Samples	$\boldsymbol{X_c}$ **(%)**		
	Mean ($\boldsymbol{\mu}$)	**ST. Error** ($\boldsymbol{S_E = \sigma/n^{0.5}}$)	**CI (95%)** ($\boldsymbol{\mu \pm 1.96 S_E}$)
Non contaminated rPET-bg	**33.01**	2.29	$\mu \pm 4.49$
95% rPET-bg / 5% PP	**23.75**	1.17	$\mu \pm 2.30$
90% rPET-bg / 10% PP	**18.53**	4.90	$\mu \pm 9.61$
85% rPET-bg / 15% PP	**22.64**	0.57	$\mu \pm 1.12$

Table 6.27 % Crystallinity of Inj. Moulded Samples of rPET-bg Contaminated with PP

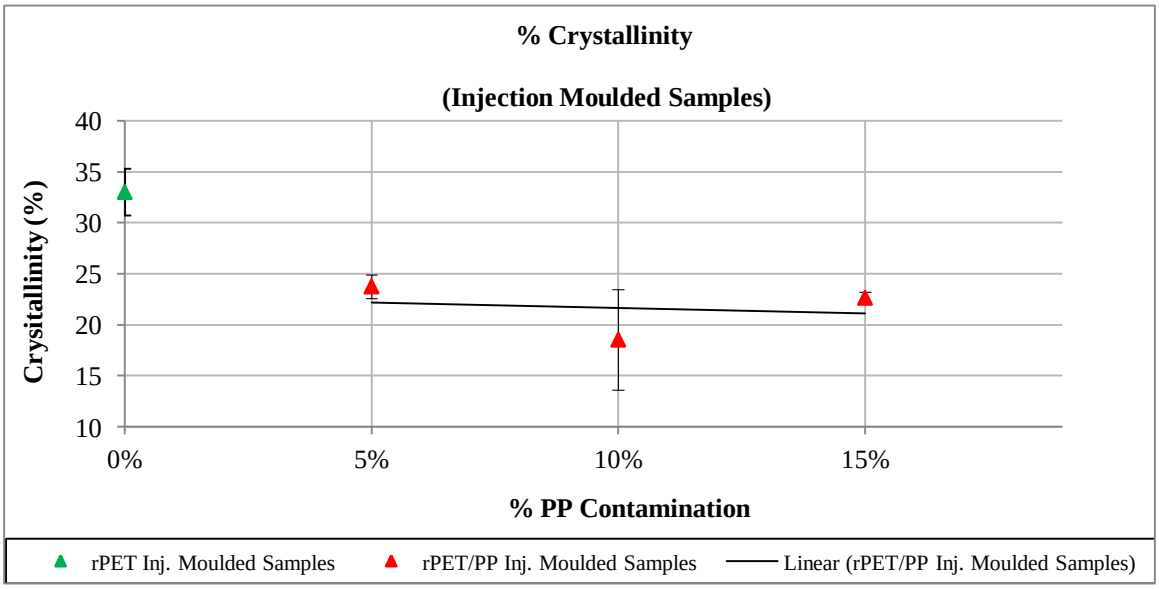

Figure 6.23 % Crystallinity of Inj. Moulded Samples of rPET-bg Contaminated with PP

6.1.5 FTIR results of *Injection Moulded Samples*

In *experiments 6, 7* and *8*, the FTIR analysis yielded the data below.

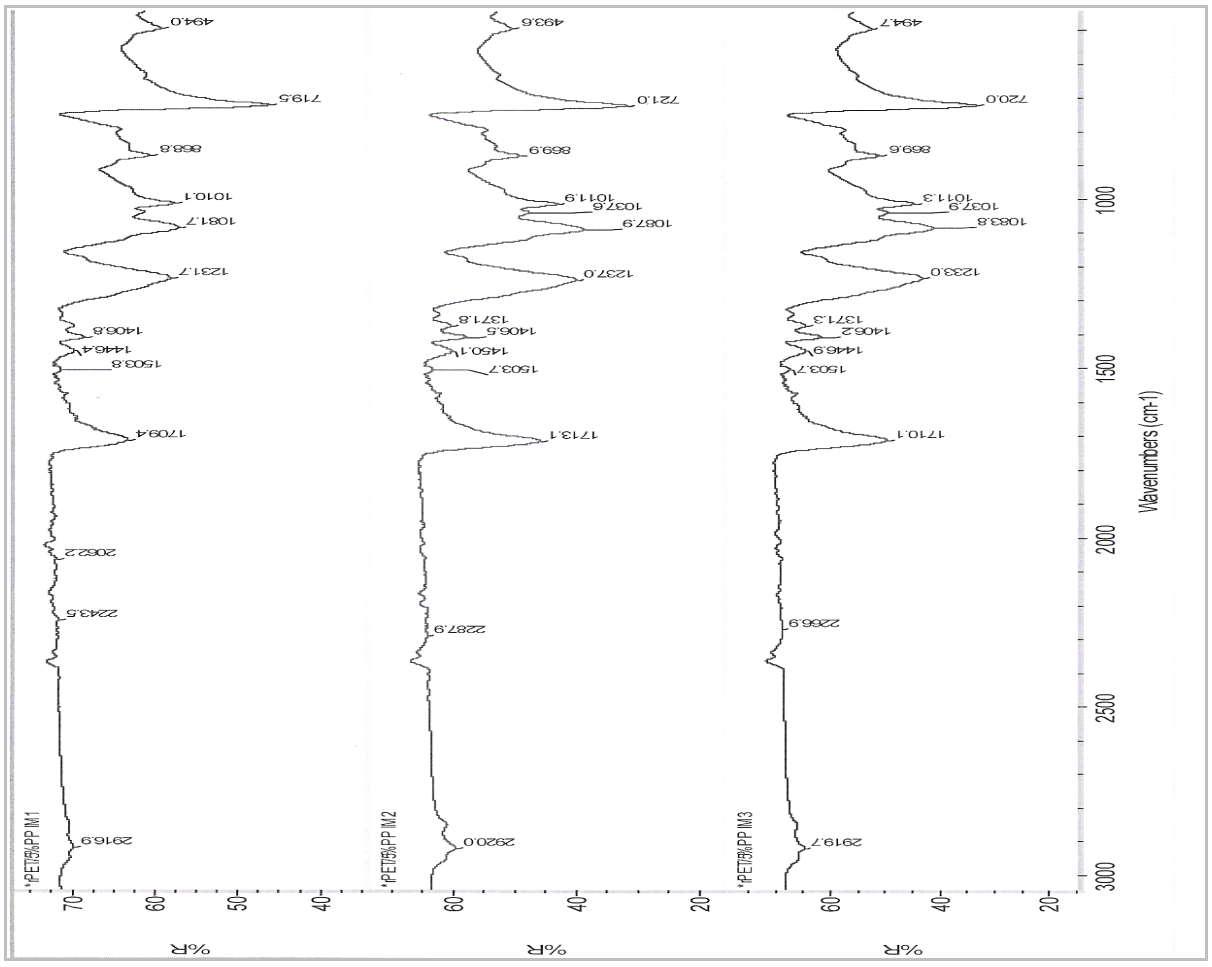

Figure 6.24 Spectra of Inj. Moulded Samples of rPET-bg contaminated with 5% PP

Wavenumber (cm^{-1})			Bond	Wavenumber (cm^{-1})	Compound Type
Scan 1	**Scan 2**	**Scan 3**			
2916	2920	2919	C-H	2850-2960	Alkane
1709	1713	1710	C=O	1670-1760 stretch	Ester
1503	1503	1503	C=C	1500-1600	Ester Ar. Ring
494 to 868	493 to 869	494 to 869	and C-H	Below 900	Ester Ar. Ring
1081 to 1231	1087 to 1237	1083 to 1233	C-O	1000-1260	Ester

Table 6.28 FTIR Data of Inj. Mould. Samples of rPET-bg Contaminated with 5% PP

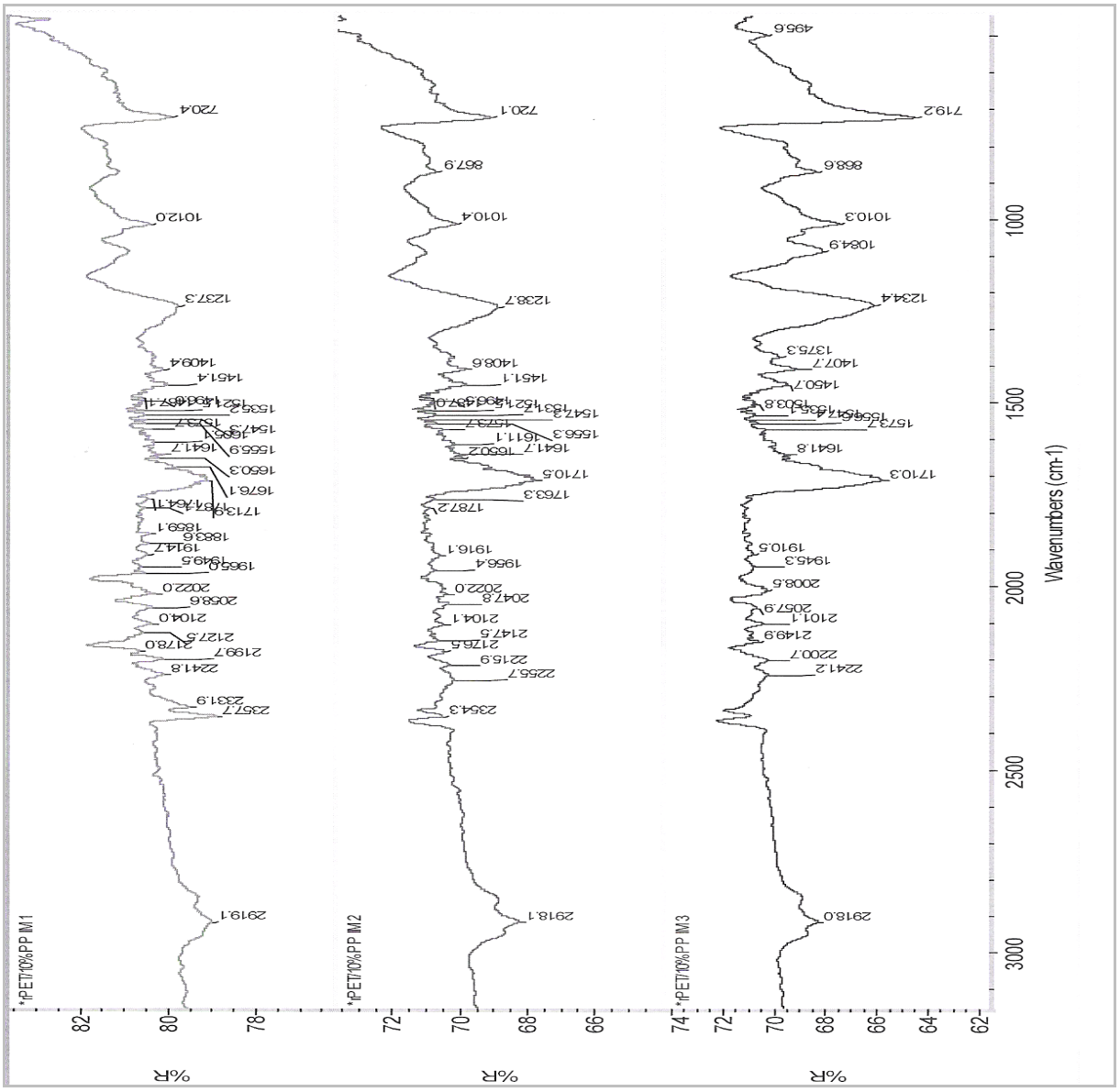

Figure 6.25 Spectra of Inj. Moulded Samples of rPET-bg contaminated with 10% PP

Wavenumber (cm^{-1})			Bond	Wavenumber (cm^{-1})	Compound Type
Scan 1	**Scan 2**	**Scan 3**			
2919	2918	2918	C-H	2850-2960	Alkane
1713	1710	1710	C=O	1670-1760 stretch	Ester
1504 to 1573	1504 to 1573	1503 to 1573	C=C	1500-1600	Ester Ar. Ring
720	720 to 867	495 to 868	and C-H	Below 900	Ester Ar. Ring
1237	1238	1084 to 1234	C-O	1000-1260	Ester

Table 6.29 FTIR Data of Inj. Mould. Samp. of rPET-bg Contaminated with 10% PP

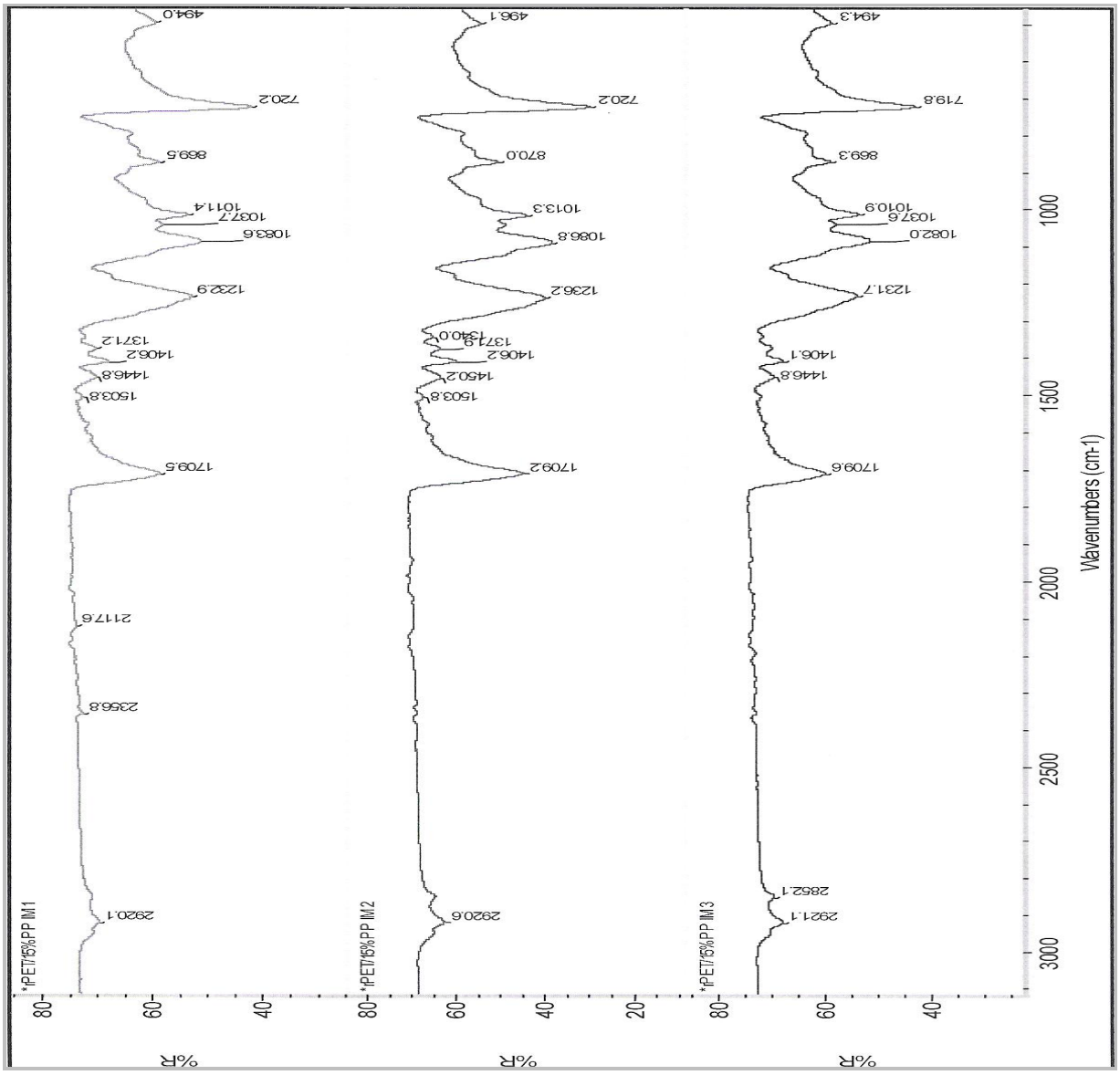

Figure 6.26 Spectra of Inj. Moulded Samples of rPET-bg contaminated with 15% PP

Wavenumber (cm^{-1})			Bond	Wavenumber (cm^{-1})	Compound Type
Scan 1	**Scan 2**	**Scan 3**			
2920	2920	2852 to 2921	C-H	2850-2960	Alkane
1709	1709	1709	C=O	1670-1760 stretch	Ester
1503	1503		C=C	1500-1600	Ester Ar. Ring
494 to 869	496 to 869	494 to 869	and C-H	Below 900	Ester Ar. Ring
1083 to 1232	1086 to 1236	1082 to 1231	C-O	1000-1260	Ester

Table 6.30 FTIR Data of Inj. Mould. Samp. of rPET-bg Contaminated with 15% PP

The results, shown in *Table 6.31* below, showed instability in the overall absorptions, especially the absorption of the *alkane CH*, as a result of interaction between the molecular *alkane CH bonds* of the PP and the rPET-bg matrix. The *ester carbonyl C-O* showed apparent change in dipole showed by increased vibration and intensity of absorption. Once again, these variation in intensity absorptions and dipole changes allowed to conclude that molecular bonds ability of excitation and vibration were promoted by the reduced chains' strain, which resulted in reduced bonds' stiffness, as a result of reduced density, dispersed instable crystals and instable reduced % crystallinity as shown by the DSC analysis.

Material	**Injection Moulded Samples of rPET-bg** (1) **Compared to rPET-bg / PP** (5%, 10% and 15%)

Samples (1)	**5% PP**	**10% PP**	**15% PP**	**Reference**		
Wavenumber (cm^{-1})				**Bonds**	**Wavenumber (cm^{-1})**	**Compound Type**
2919 to 2953	2916 to 2920	2918 to 2919	2852 to 2921	C-H	2850-2960	Alkane
1697 to 1731	1709 to 1713	1710 to 1713	1709	C=O	1670-1760 stretch	Ester
1503 to 1574	1503	1503 to 1573	1503	C=C	1500-1600	Ester Ar. Ring
493 to 869	493 to 869	495 to 868	494 to 869	C-H	Below 900	Ester Ar. Ring
1081 to 1233	1081 to 1237	1084 to 1238	1082 to 1236	C-O	1000-1260	Ester

Table 6.31 FTIR Data of Injection Moulded Samples of rPET-bg contaminated with PP

6.1.6 MFR results of *Injection Moulded Samples*

In *experiments 6, 7* and *8*, the MFR yielded the data below.

Extrudates	Weight (g)	Time (s)	MFR (g/10min)
Run 1	**1.75**	15	70.08
Run 2	**1.21**	10	72.78
Run 3	**0.75**	05	90.36
Mean (μ)			**77.74**
STDEV (σ)			11.01
ST. Error ($S_E = \sigma/n^{0.5}$)			6.36
CI (95%), ($\mu \pm 1.96 S_E$)			$\mu \pm 12.46$

Table 6.32 MFR Values of Inj. Moulded Samples of rPET-bg contaminated with 5% PP

Run 1	**2.01**	15	80.44
Run 2	**1.41**	10	84.66
Run 3	**0.83**	05	99.84
Mean (μ)			**88.31**
STDEV (σ)			10.20
ST. Error ($S_E = \sigma/n^{0.5}$)			5.89
CI (95%), ($\mu \pm 1.96 S_E$)			$\mu \pm 11.55$

Table 6.33 MFR Values of Inj. Mould. Samples of rPET-bg contaminated with 10% PP

Run 1	**2.21**	15	88.52
Run 2	**1.67**	10	100.32
Run 3	**1.02**	05	122.76
Mean (μ)			**103.87**
STDEV (σ)			17.39
ST. Error ($S_E = \sigma/n^{0.5}$)			10.04
CI (95%), ($\mu \pm 1.96 S_E$)			$\mu \pm 19.68$

Table 6.34 MFR Values of Inj. Mould. Samples of rPET-bg contaminated with 15% PP

The comparative *melt flow* results, shown in *Table 6.35* and *Figure 6.27* below, showed pronounced effect of PP inclusion, especially at high %. At lower % PP contamination, the PP chains were able to fill quickly the void of interstices and creating sort of entanglement which resulted in reduced MFR. By increasing the % PP contamination, the MFR increased greatly because of the overwhelming ease of flow of PP which increased dramatically the shear of lamellae leading to decreased overall viscosity and consequently increased the MFR. Also, the increase in MFR is attributed to the effects of degradation and chains scissions which increased proportionally with increasing % PP contamination.

Inj. Moulded Samples	**MFR (g/10mins)**		
	Mean (μ)	**ST. Error ($S_E = \sigma/n^{0.5}$)**	**CI (95%) ($\mu \pm 1.96S_E$)**
Non contaminated rPET-bg	**96.23**	8.06	$\mu \pm 15.80$
95% rPET-bg / 5% PP	**77.74**	6.36	$\mu \pm 12.46$
90% rPET-bg / 10% PP	**88.31**	5.89	$\mu \pm 11.55$
85% rPET-bg / 15% PP	**103.87**	10.04	$\mu \pm 19.68$

Table 6.35 MFR of Injection Moulded Samples of rPET-bg contaminated with PP

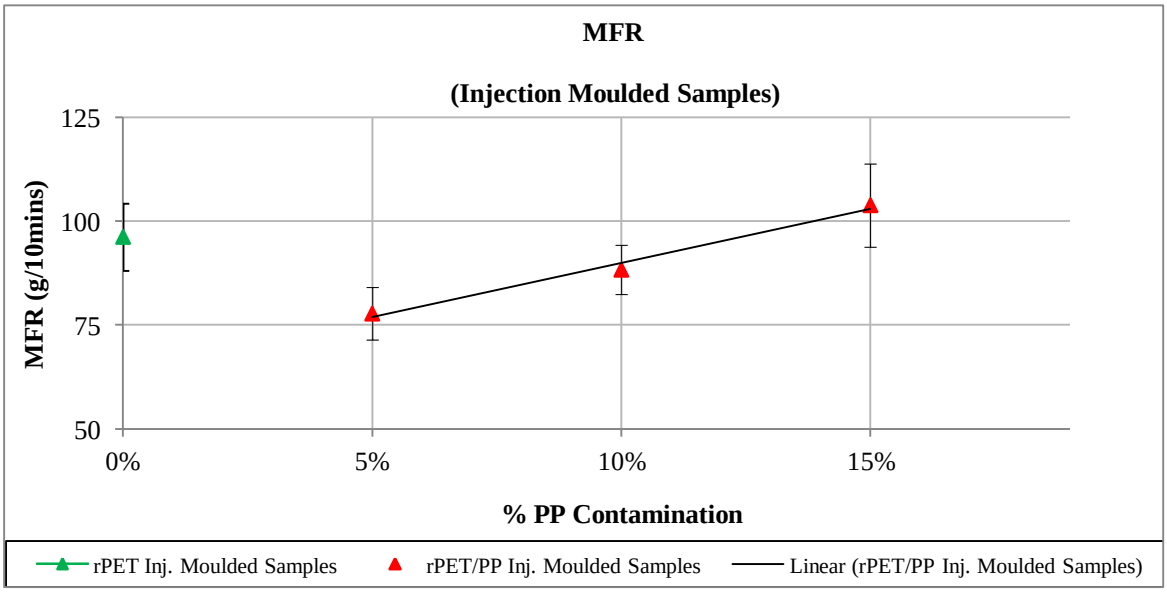

Figure 6.27 MFR of Injection Moulded Samples of rPET-bg contaminated with PP

6.1.7 Tensile Testing results of *Injection Moulded Dumbbells*

In *experiments 6, 7* and *8*, the tensile testing yielded the data below.

The collected data were converted into *stress-strain* curve as shown in *Figure 6.28* and from which the tensile properties were extracted and listed in *Table 6.36* below.

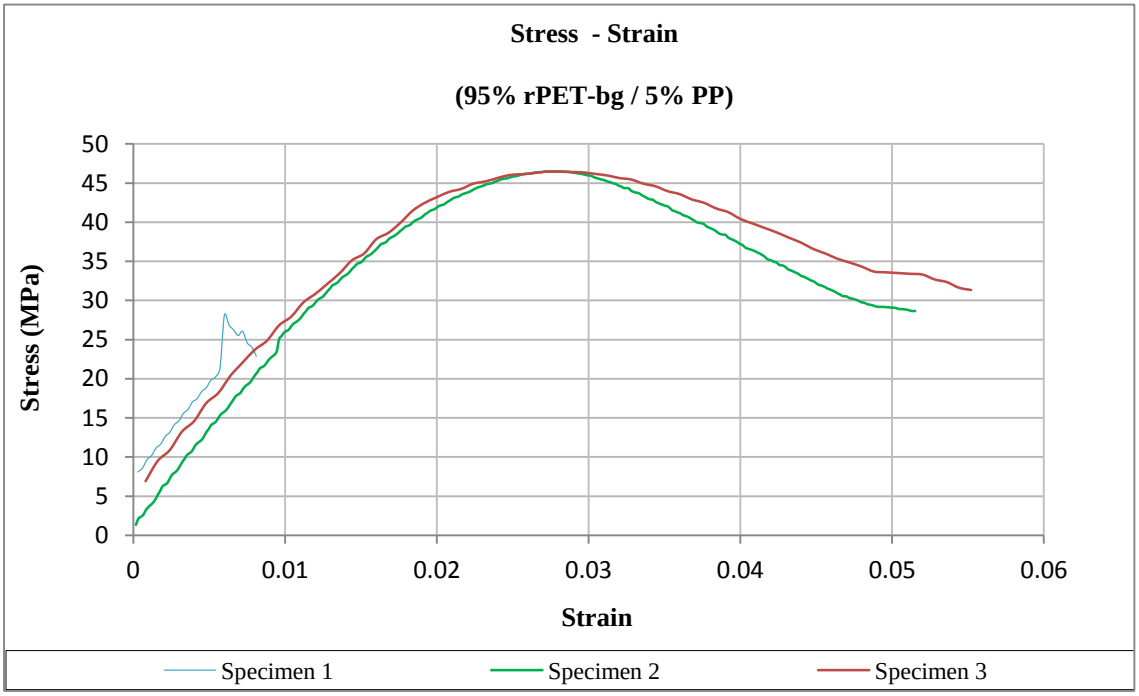

Figure 6.28 Stress-Strain Curves of Dumbbells of rPET-bg contaminated with 5% PP (1 to 3)

Material	95% rPET-bg contaminated with 5% PP			
Specimen	Modulus, E (GPa)	Yield Stress, σ_y (MPa)	Stress @ Break, σ_f (MPa)	Strain @ Yield, e_y
1	2.22	28.14*	22.88	0.006*
2	2.33	46.51	28.67	0.028
3	2.00	46.48	31.35	0.028
Mean (μ)	**2.18**	**46.50**	**27.63**	**0.028**
STDEV (σ)	0.17	0.02	4.33	0.00
ST. Error ($S_E = \sigma/n^{0.5}$)	0.10	0.01	2.50	0.00
CI (95%), ($\mu \pm 1.96 S_E$)	$\mu \pm 0.19$	$\mu \pm 0.03$	$\mu \pm 4.90$	$\mu \pm 0.00$

Table 6.36 Tensile Data of Dumbbells of rPET-bg contaminated with 5% PP

*: This' an "outlier" displayed but not included in the calculation.

From the stress-strain curves, the *stress at yield*, *stress at failure* (break), *strain at yield* and the secant *modulus*, elastic modulus, were extracted as previously described in *Figure 3.23, Section 3.2.4.2* and *Section 5.1.7*.

.

Note: The calculations were done by Excel, so results were rounded to the nearest decimal and may differ from the displayed data.

The results are shown in *Table 6.37* below. The same applied for results at 10% and 15% PP contamination.

Material	**95% rPET-bg / 5% PP**

	Stress , (MPa)			**Strain, e_x**			**$E = (\sigma_y / e_x)$**	
Specimen	**σ_{y1}**	**σ_{y2}**	**σ_y**	**e_{x1}**	**e_{x2}**	**e_x**	**MPa**	**GPa**
1	12.607	17.037	4.43	0.002	0.004	0.002	2215.00	2.22
2	6.478	20.450	13.97	0.002	0.008	0.005	2328.67	2.33
3	13.252	26.840	13.59	0.003	0.010	0.007	1998.24	2.00

Mean (μ)	**2.18**
STDEV (σ)	0.17
ST. Error ($S_E = \sigma/n^{0.5}$)	0.10
CI (95%), ($\mu \pm 1.96 S_E$)	$\mu \pm 0.19$

Table 6.37 Tensile Modulus of Dumbbells of rPET-bg contaminated with 5% PP

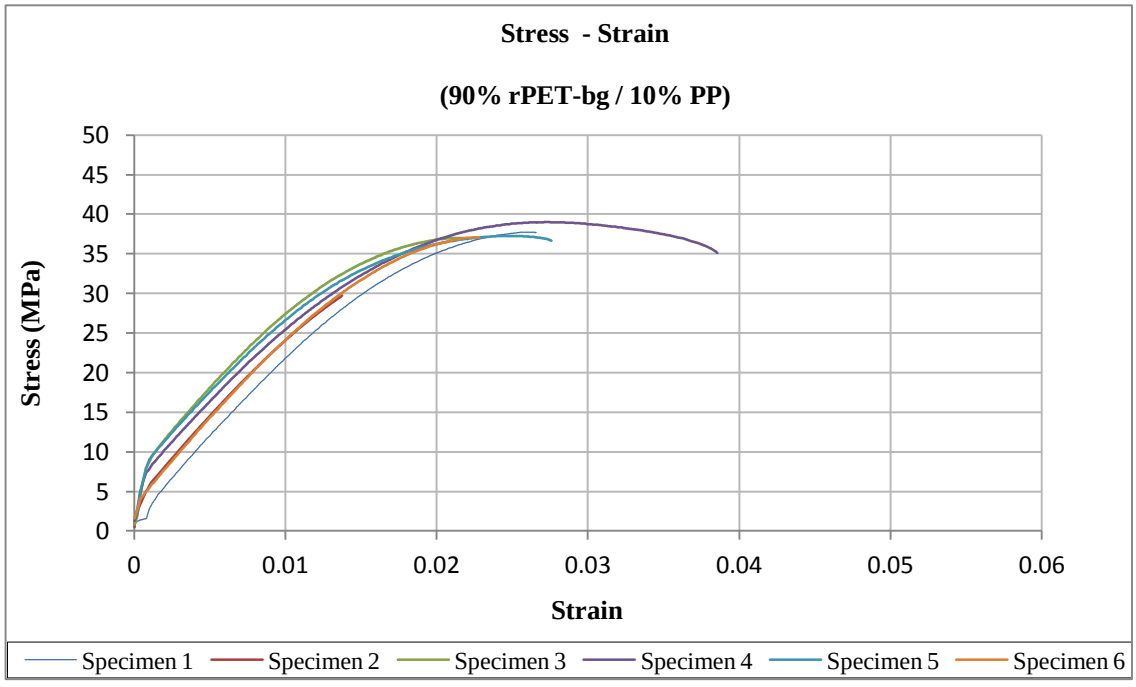

Figure 6.29 Stress-Strain Curves of Dumbbells of rPET-bg contaminated with 10% PP (1 to 6)

Material	90% rPET-bg contaminated with 10% PP			
Dumbbells	Modulus, E (GPa)	Yield Stress, σ_y (MPa)	Stress @ Break, σ_f (MPa)	Strain @ Yield, e_y
1	2.08	37.72	37.67	0.025
2	2.07	29.76	29.76	0.014
3	2.07	36.97	36.83	0.022
4	1.98	39.05	35.14	0.027
5	1.99	37.22	36.64	0.026
6	2.12	37.10	37.05	0.023
Mean (μ)	**2.05**	**36.30**	**35.52**	**0.023**
STDEV (σ)	0.05	3.29	2.94	0.00
ST. Error ($S_E = \sigma/n^{0.5}$)	0.02	1.34	1.20	0.00
CI (95%), ($\mu \pm 1.96 S_E$)	$\mu \pm 0.04$	$\mu \pm 2.64$	$\mu \pm 2.35$	$\mu \pm 0.00$

Table 6.38 Tensile Data of Dumbbells of rPET-bg contaminated with 10% PP

Material	90% rPET-bg contaminated with 10% PP							
	Stress , (MPa)			Strain, e_x			$E = (\sigma_y / e_x)$	
Specimen	σ_{y1}	σ_{y2}	σ_y	e_{x1}	e_{x2}	e_x	MPa	GPa
1	7.697	16.020	8.323	0.003	0.007	0.004	2080.75	2.08
2	10.279	18.561	8.282	0.003	0.007	0.004	2070.50	2.07
3	13.786	22.078	8.292	0.003	0.007	0.004	2073.00	2.07
4	12.292	20.198	7.906	0.003	0.007	0.004	1976.50	1.98
5	13.449	21.403	7.954	0.003	0.007	0.004	1988.50	1.99
6	9.934	18.429	8.495	0.003	0.007	0.004	2123.75	2.12
Mean (μ)								**2.05**
STDEV (σ)								0.05
ST. Error ($S_E = \sigma/n^{0.5}$)								0.02
CI (95%), ($\mu \pm 1.96 S_E$)								$\mu \pm 0.04$

Table 6.39 Tensile Modulus of Dumbbells of rPET-bg contaminated with 10% PP

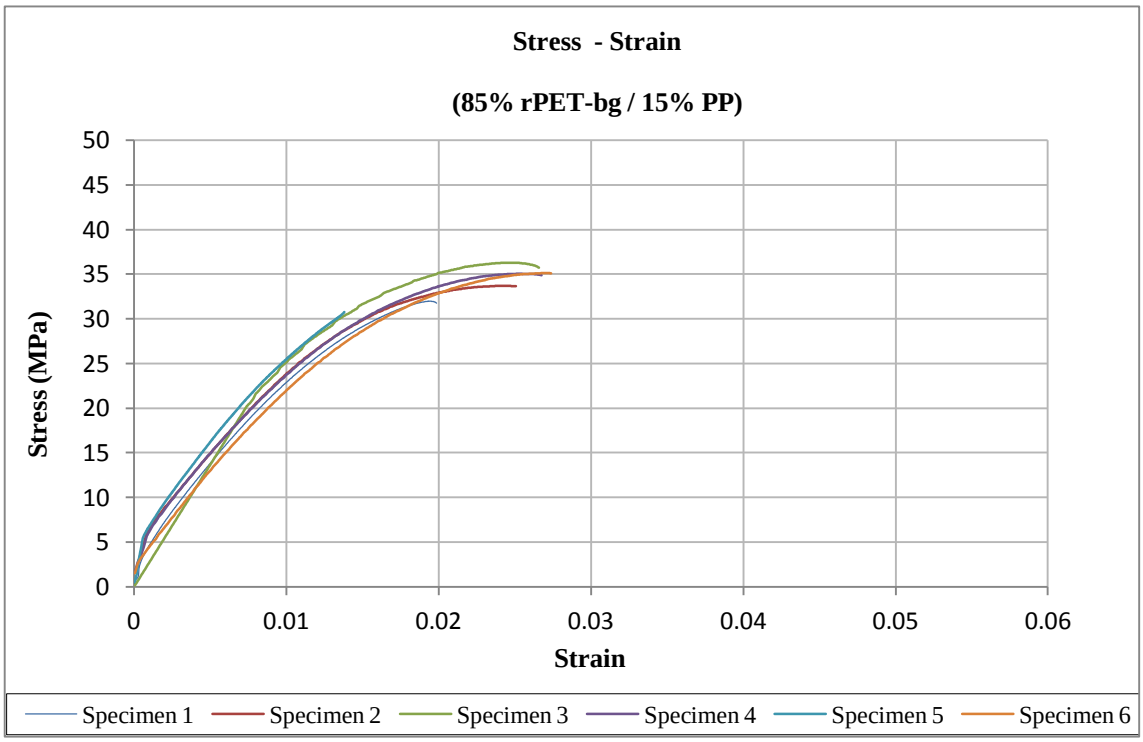

Figure 6.30 Stress-Strain Curves of Dumbbells of rPET-bg contaminated with 15% PP (1 to 6)

Material	**85% rPET-bg contaminated with 15% PP**			
Dumbbells	**Modulus, E (GPa)**	**Yield Stress, σ_y (MPa)**	**Stress @ Break, σ_f (MPa)**	**Strain @ Yield, e_y**
1	2.05	31.98	31.75	0.019
2	1.98	33.71	33.67	0.025
3	2.73	36.31	35.77	0.025
4	1.95	35.08	34.90	0.025
5	2.19	30.78	30.78	0.014
6	1.99	35.10	35.07	0.027
Mean (μ)	**2.15**	**33.83**	**33.66**	**0.023**
STDEV (σ)	0.30	2.10	2.00	0.00
ST. Error ($S_E = \sigma/n^{0.5}$)	0.12	0.86	0.81	0.00
CI (95%), ($\mu \pm 1.96 S_E$)	$\mu \pm 0.24$	$\mu \pm 1.68$	$\mu \pm 1.60$	$\mu \pm 0.00$

Table 6.40 Tensile Data of Dumbbells of rPET-bg contaminated with 15% PP

Material	85% rPET-bg contaminated with 15% PP

	Stress , (MPa)			Strain, e_x			E = (σ_y/e_x)	
Specimen	σ_{y1}	σ_{y2}	σ_y	e_{x1}	e_{x2}	e_x	MPa	GPa
1	11.767	15.861	4.094	0.004	0.006	0.002	2047.00	2.05
2	12.976	16.927	3.951	0.004	0.006	0.002	1975.50	1.98
3	10.937	16.406	5.469	0.004	0.006	0.002	2734.50	2.73
4	12.978	16.872	3.894	0.004	0.006	0.002	1947.00	1.95
5	13.972	18.352	4.38	0.004	0.006	0.002	2190.00	2.19
6	11.055	15.039	3.984	0.004	0.006	0.002	1992.00	1.99

Mean (μ)	**2.15**
STDEV (σ)	0.30
ST. Error ($S_E = \sigma/n^{0.5}$)	0.12
CI (95%), ($\mu \pm 1.96 S_E$)	$\mu \pm 0.24$

Table 6.41 Tensile Modulus of Dumbbells of rPET-bg contaminated with 15% PP

Note: Other Graphs are available in ***Appendix 6*** **(***13, 14, 15***)**.

The tensile results of *dumbbells*, shown in *Figures 6.28, 6.29* and *6.30* and *Tables 6.36, 6.38* and *6.40* above, showed clearly the influence of the inclusion of PP contamination on the overall tensile characteristics of non contaminated rPET-bg. All the *dumbbells* yielded, especially at 5% PP, and the degree of yielding indicated that the degree of ductility decreased with increasing % PP contamination from 5% to 15%. It is clear that the crystalline phase is increasing the ductility; the % crystallinity decreased with increasing % PP contamination, so the ductility decreased too. In comparison, the ductility factor increased the overall elongation of the contaminated rPET-bg and was higher with PP contamination, as shown in *Figure 6.31* below.

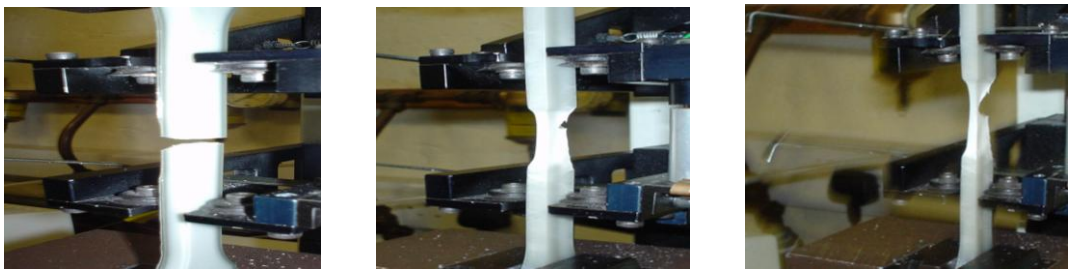

Figure 6.31 Sharp Failure of non contaminated rPET-bg Dumbbell (Left) Compared to Necked Dumbbell of rPET-bg contaminated with 15% HDPE (Middle) and rPET-bg contaminated with 15% PP (Right)

The following discussions show the variations in terms of individual characteristics, such as modulus, stress at yield and at break and the strain at yield of the materials.

Compared to non contaminated rPET-bg, as shown in *Table 6.42* and *Figure 6.31* below, the *stiffness* decreased as a result of decreased *modulus*; two factors contributed to this decrease, the incompatibility of PP and rPET-bg and the decreased crystallinity of the matrix due to the inclusion of PP as contaminant, same case scenario as with HDPE as contaminant, showing that crystallinity is a determinant factor in promoting or demoting tensile characteristics. In their study on recycled PET and PP blends, *Friedrich et al.* [115] reported that mechanical properties, such as flexural modulus and strength of the samples were 50% better than those of the clean PP in the presence of compatibilisers. Furthermore, the dispersion of PP phase in rPET-bg and the finesse of the particle sizes in the blend is an important factor in reducing the stress concentration and enhancing the mechanical efficiency of the blends. *Leong et al.* [177] reported that the inclusion of compatibilisers reduced the PP particle size and improved the overall homogeneity of the rPET/PP blends. The *stiffness,* in the rPET-bg contaminated with PP, decreased proportionally with *crystallinity*. As *crystallinity* is proportional to *ductility* and *toughness,* so, the toughness of the contaminated rPET-bg matrix decreased with increasing % PP contamination, similar findings were reported by *Inoya et al*. [118, 119] with compatibilised rPET/PP blends. The above results indicated formation of graft

co-polymers resulting from the reaction of the generated oligomers during the thermo-mechanical degradation and this is in line with the findings of *Samperi et al.* [66], *Romao et al.* [67] and *Cooney et al* [68].

Materials	Elastic Modulus, E, (GPa)		
	Mean (μ)	**ST. Error ($S_E = \sigma/n^{0.5}$)**	**CI (95%) ($\mu \pm 1.96 S_E$)**
Non contaminated rPET-bg	**3.10**	0.07	$\mu \pm 0.15$
95% rPET-bg / 5% PP	**2.18**	0.10	$\mu \pm 0.19$
90% rPET-bg / 10% PP	**2.05**	0.02	$\mu \pm 0.04$
85% rPET-bg / 15% PP	**2.15**	0.12	$\mu \pm 0.24$

Table 6.42 Modulus of rPET-bg contaminated with PP

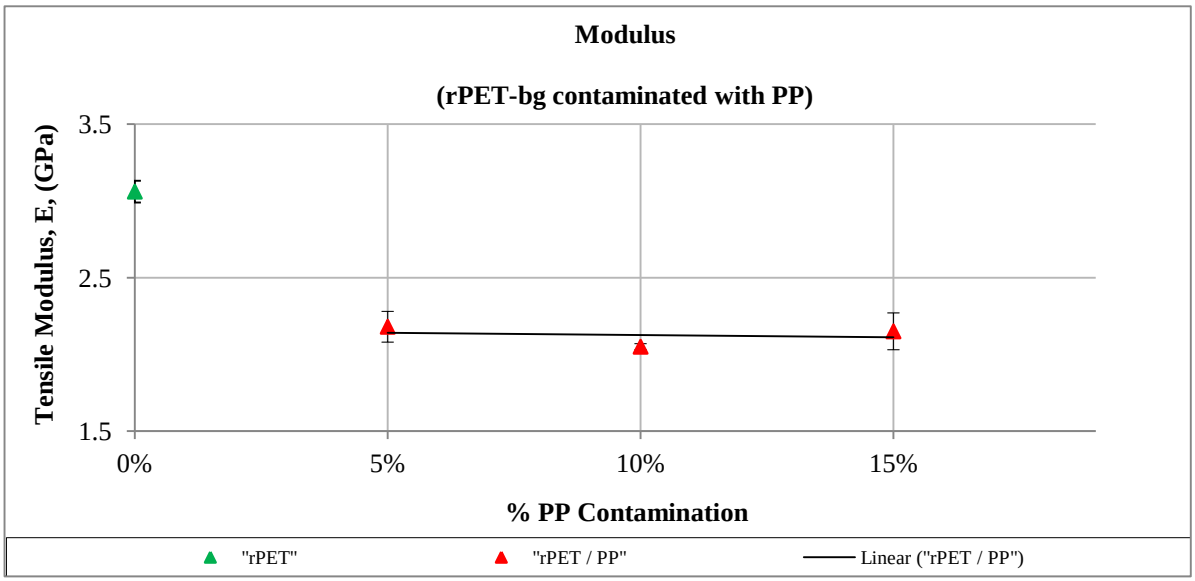

Figure 6.32 Modulus of rPET-bg contaminated with PP

Compared to non contaminated rPET-bg, as shown in *Table 6.43* and *Figure 6.32* below, the *stress at yield*, σ_y , increased by the inclusion of PP; this increase is attributed to the strength of PP and the readiness of its crystalline domains in enhancing resistance to fracture. In the other hand, the *stress at yield* decreased orderly with increasing % PP contamination showing the flow characteristics of PP and the readiness of lamellae in shearing under tensile force, resulting in decreased resistance to failure, hence decreased stress at yield with increasing % PP contamination.

Materials	**Stress at Yield, σ_y (MPa)**		
	Mean (μ)	**ST. Error ($S_E = \sigma/n^{0.5}$)**	**CI (95%) ($\mu \pm 1.96 S_E$)**
Non contaminated rPET-bg	**18.90**	2.91	$\mu \pm 5.69$
95% rPET-bg / 5% PP	**46.50**	0.01	$\mu \pm 0.03$
90% rPET-bg / 10% PP	**36.30**	1.34	$\mu \pm 2.64$
85% rPET-bg / 15% PP	**33.83**	0.86	$\mu \pm 1.68$

Table 6.43 Stress at Yield of rPET-bg contaminated with PP

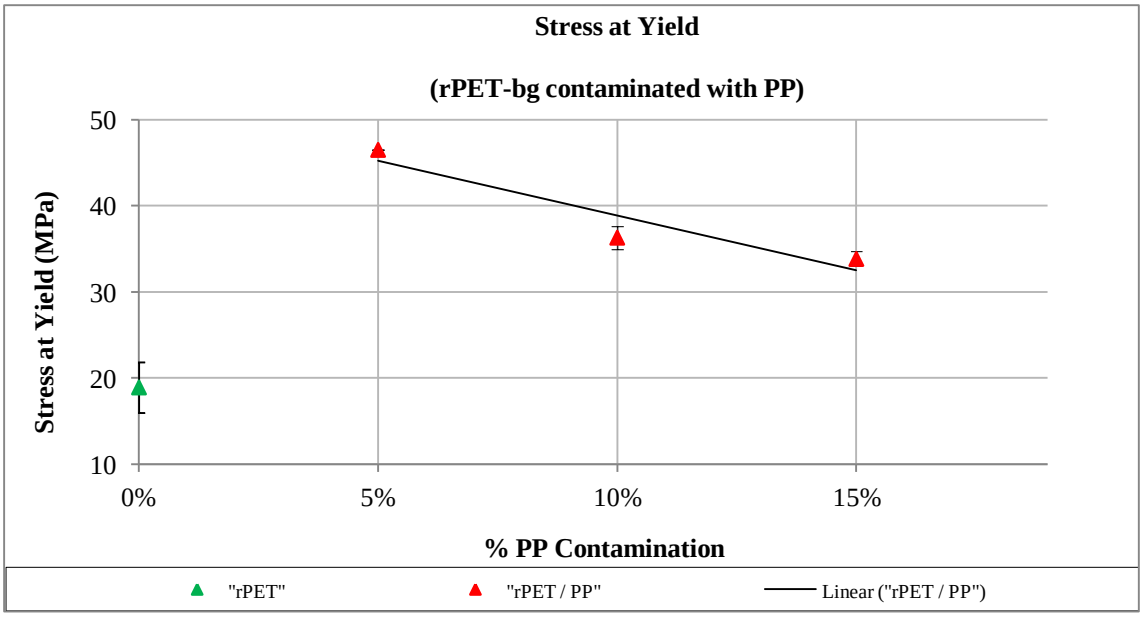

Figure 6.33 Stress at Yield of rPET-bg contaminated with PP

Compared to non contaminated rPET-bg, as shown in *Table 6.44* and *Figure 6.33* below, the increase of the *stress at break*, σ_f ,in the contaminated matrices, showed the capability of PP molecular structure in promoting elongation and improving elasticity. In the other hand, the random increase of stress at break with increasing % PP contamination indicated unbalanced distribution of PP chains in the matrix or potential presence of failure promoting contaminants, such as soil particulates.

Materials	**Stress at Break, σ_f, (MPa)**		
	Mean (μ)	**ST. Error ($S_E = \sigma/n^{0.5}$)**	**CI (95%) ($\mu \pm 1.96 S_E$)**
Non contaminated rPET-bg	**18.90**	2.91	$\mu \pm 5.69$
95% rPET-bg / 5% PP	**27.63**	2.50	$\mu \pm 4.90$
90% rPET-bg / 10% PP	**35.52**	1.20	$\mu \pm 2.35$
85% rPET-bg / 15% PP	**33.66**	0.81	$\mu \pm 1.60$

Table 6.44 Stress at Break of rPET-bg contaminated with PP

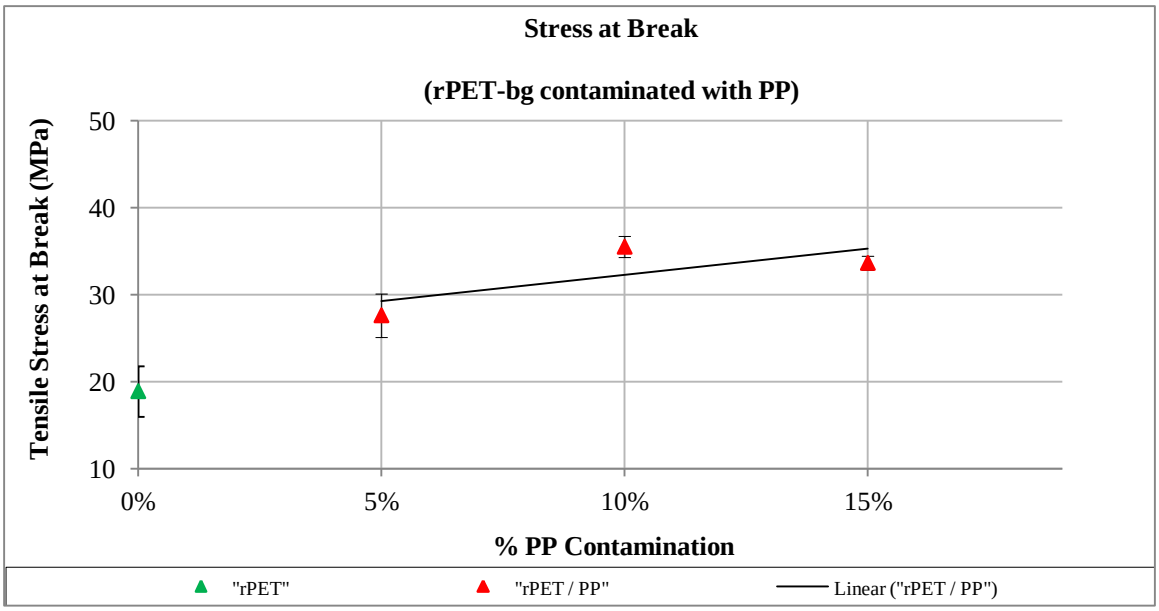

Figure 6.34 Stress at Break of rPET-bg contaminated with PP

Compared to non contaminated rPET-bg, as shown in *Table 6.45* and *Figure 6.34* below, the inclusion of PP increased the strain encountered for yielding to happen; which indicated acquired strength by the matrix. The strain decreased with increasing % PP contamination, which showed the influence of crystallinity in dictating the amount of strain at yielding. Once again, proportionality *stress at yield - strain at yield* is shown as both properties decreased proportionally with crystallinity.

Materials	**Strain at Yield**		
	Mean (μ)	**ST. Error ($S_E = \sigma/n^{0.5}$)**	**CI (95%) ($\mu \pm 1.96 S_E$)**
Non contaminated rPET-bg	**0.007**	0.00	$\mu \pm 0.00$
95% rPET-bg / 5% PP	**0.028**	0.00	$\mu \pm 0.00$
90% rPET-bg / 10% PP	**0.023**	0.00	$\mu \pm 0.00$
85% rPET-bg / 15% PP	**0.023**	0.00	$\mu \pm 0.00$

Table 6.45 Strain at Yield of rPET-bg contaminated with PP

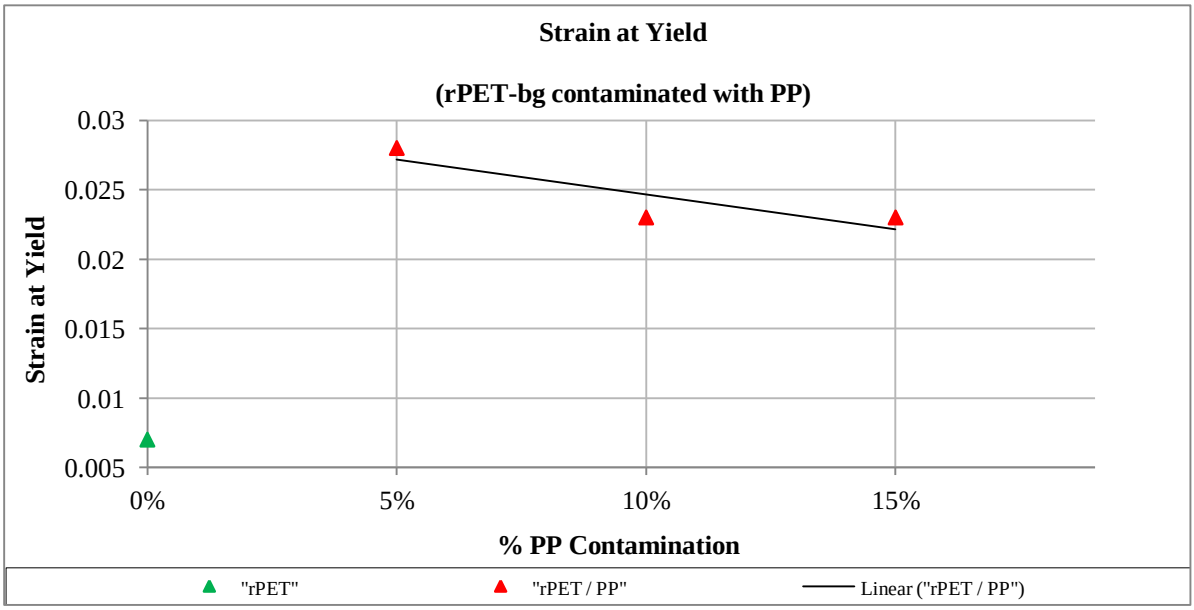

Figure 6.35 Strain at Yield of rPET-bg contaminated with PP

6.1.8 Impact Testing results of *Injection Moulded Impact Bars*

In *experiments 6, 7* and *8*, the impact testing yielded the data below.

Number	Width (B) (mm)	Thickness (t) (mm)	Energy Absorbed (J)	Impact Strength ($kJ.m^{-2)}$
1	10.08	4.07	1.29	**31.44**
2	10.04	4.09	1.45	**35.31**
3	10.10	4.06	1.47	**35.85**
4	10.11	4.09	1.36	**32.89**
5	10.09	4.10	1.33	**32.15**
6	10.10	4.08	1.27	**30.82**
7	10.09	4.09	1.31	**31.74**
8	10.11	4.10	1.29	**31.12**
9	10.12	4.07	1.39	**33.75**
10	10.10	4.11	1.43	**34.45**
Mean	**10.09**	**4.09**	**1.36**	**32.95**
STDEV	0.02	0.02	0.07	1.80
ST. Error ($S_E = \sigma/n^{0.5}$)	0.01	0.01	0.02	0.57
CI (95%), ($\mu \pm 1.96 S_E$)	$\mu \pm 0.01$	$\mu \pm 0.01$	$\mu \pm 0.04$	$\mu \pm 1.11$

Table 6.46 Charpy Impact Strength of rPET-bg contaminated with 5% PP

1	10.04	4.09	1.14	**27.76**
2	10.09	4.12	1.12	**26.94**
3	10.01	4.07	1.17	**28.72**
4	9.98	4.11	1.22	**29.74**
5	10.04	4.09	1.24	**30.20**
6	10.07	4.02	1.20	**29.64**
7	10.00	4.03	1.22	**30.27**
8	10.01	4.10	1.17	**28.51**
9	10.05	4.09	1.19	**28.95**
10	9.99	4.07	1.21	**29.76**
Mean	**10.03**	**4.08**	**1.19**	**29.05**
STDEV	0.04	0.03	0.04	1.09
ST. Error ($S_E = \sigma/n^{0.5}$)	0.01	0.01	0.01	0.34
CI (95%), ($\mu \pm 1.96 S_E$)	$\mu \pm 0.02$	$\mu \pm 0.02$	$\mu \pm 0.02$	$\mu \pm 0.67$

Table 6.47 Charpy Impact strength of rPET-bg contaminated with 10% PP

Number	Width (B) (mm)	Thickness (t) (mm)	Energy Absorbed (J)	Impact Strength ($kJ.m^{-2}$)
1	10.03	4.07	0.93	**22.78**
2	10.06	4.02	0.58	**14.34**
3	10.01	4.05	0.73	**18.01**
4	10.06	4.10	0.75	**18.18**
5	10.03	4.02	0.59	**14.63**
6	10.05	4.08	0.72	**17.56**
7	10.04	4.02	0.91	**22.55**
8	10.05	4.05	0.82	**20.15**
9	10.01	4.07	0.71	**17.43**
10	10.03	4.10	0.73	**17.75**
Mean	**10.04**	**4.06**	**0.75**	**18.34**
STDEV	0.02	0.03	0.12	2.83
ST. Error ($S_E = \sigma/n^{0.5}$)	0.01	0.01	0.04	0.90
CI (95%), ($\mu \pm 1.96 S_E$)	$\mu \pm 0.01$	$\mu \pm 0.02$	$\mu \pm 0.07$	$\mu \pm 1.76$

Table 6.48 Charpy Impact Strength of rPET-bg contaminated with 15% PP

Compared to non contaminated rPET-bg, as shown in *Table 6.49* and *Figure 6.35* below, The increased *impact strength* indicated predominance of crystalline domains over amorphous ones. The previously shown increase in toughness and strength of the rPET-bg contaminated with PP is shown again by the increased impact strength. Furthermore, the impact strength decreased with increasing % PP contamination as for the stress at yield; this showed proportionality between impact strength and stress at yield, where in both cases, the crystalline domains and their distribution within the matrix dictated the amount of energy required to accomplish a failure mechanism. In their study on PET/PP blend, *Abdul Razak et al.* [178] reported that maximum improvement of impact strength was obtained in the presence of the compatibiliser SEBS-g-MAH at 8%, the improvement was attributed to the elastomeric nature of the SEBS-g-MAH, whereas in this work, the improvement in impact strength is solely attributed to the inclusion of PP and its influence on the rPET-bg matrix. Also, the probability that newly generated oligomers could react and reinforced the interfacial strength is also acceptable.

Materials	Impact Strengths (J/m^2)		
	Mean (μ)	**ST. Error ($S_E = \sigma/n^{0.5}$)**	**CI (95%) ($\mu \pm 1.96 S_E$)**
Non contaminated rPET-bg	**2.40**	0.12	$\mu \pm 0.23$
95% rPET-bg / 5% PP	**32.95**	0.57	$\mu \pm 1.11$
90% rPET-bg / 10% PP	**29.05**	0.34	$\mu \pm 0.67$
85% rPET-bg / 15% PP	**18.34**	0.90	$\mu \pm 1.76$

Table 6.49 Charpy Impact Strength of rPET-bg contaminated with PP

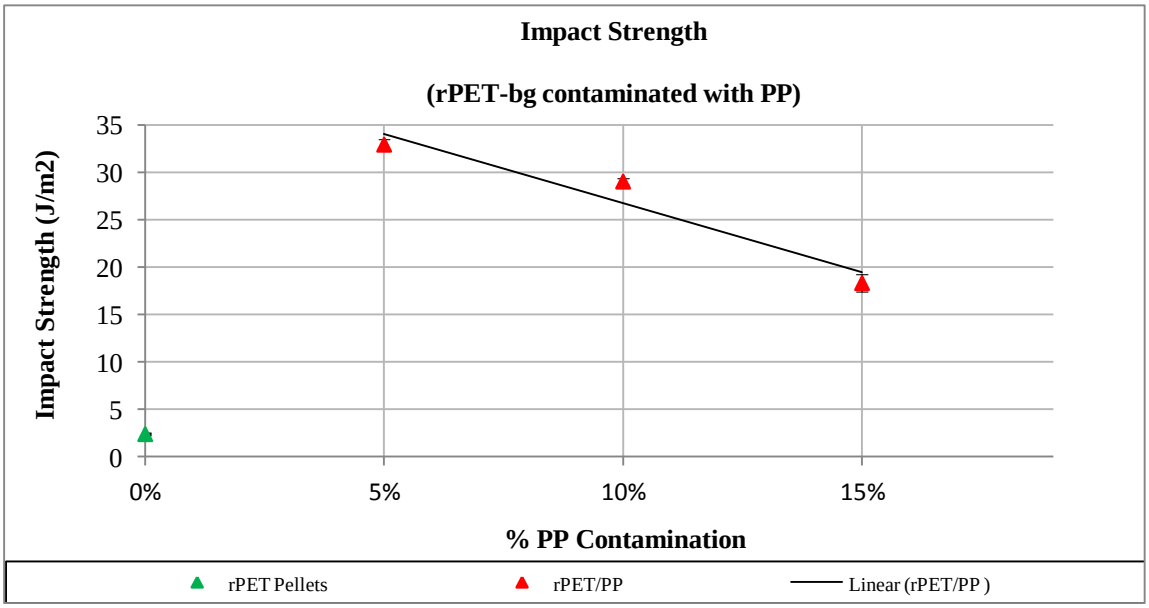

Figure 6.36 Impact Strengths of rPET-bg contaminated with PP

6.1.9 Overall Data Comparisons

In terms of processing, from the comparative *Table 6.50* below, the decrease in screw speed due to the inclusion of PP contamination, is the result of very low *melt flow* property of PP, which is *1g /10min* in (*Table 3.2, Section 3.2.2*) compared to the non contaminated rPET-bg flakes' of *61.35g/10min* previously determined and shown in (*Table 4.3, Section 4.1.3*); this pronounced difference allowed an increase in viscosity proportionally equivalent to the % torque. The overall % torque decreased; this is attributed to the % PP contaminations applied and their proportional effect in influencing this property; which is proportional to the volume of very short chains created as a result of thermo-mechanical degradation. Additionally, the degradation encountered during extrusion, allowed to some degree the decrease of the melt injection and packing pressures during injection moulding; indicating overall balance of processing temperatures and melt flow.

	***Screw Speed* (*rpm*)**	***% T***	***Injection Pressure* (*Bar*)**	***Packing Pressure* (*Bar*)**
Extruded Samples **rPET-bg / PP** *compared to* **rPET-bg**	↓	↓		
Inj. Moulded Samples **rPET-bg / PP** *compared to* **rPET-bg**			↓	↓

Table 6.50 Variation of Processing Conditions of rPET-bg contaminated with PP

In terms of thermal and flow properties, the inclusion of PP, as shown in *Table 6.51* below, the decreased $\boldsymbol{T_g}$ indicated well dispersion of PP chains within the rPET-bg matrix, coupled with chains entanglement which narrowed glass transition. The effects of thermo-mechanical degradation can be seen through the presence of very short chains which froze prematurely and result in dispersed but localised crystalline domains. In contrast, after injection moulding, larger amorphous domains of the dispersed very small chains were promoted by the increased packing pressure in the cavity of the mould; the re-arrangement of the very small chains required larger scales of time and temperature, which resulted in narrowed and decreased $\boldsymbol{T_g}$. Once more the effect of packing pressure can be seen by the quantity of randomly distributed very small chains, which required proportional temperature for chains to complete cold crystallisation, and therefore increased the $\boldsymbol{T_c}$. These very small and sporadically dispersed chains were able to cold crystallise at minimum rate, resulting in decreased enthalpy of cold crystallisation, $\boldsymbol{\Delta H_c}$, because of the competition with the early melting of PP, which promoted the overall melting and prevented further propagation of cold crystallisation. The inclusion of PP speeded up the overall melting process, resulting in decreased $\boldsymbol{T_m}$. Unlike large crystalline domains, dispersed small crystalline domains usually require less time and temperature to complete melting, and this showed the relationship between crystallinity and melting. As with HDPE as contaminant, the absence of chemical secondary bonding, resulted in the exhibition of *double melting phases*, shown as sharply separated double melting peaks, which confirmed that PP and rPET-bg are *immiscible* and *incompatible*. Furthermore, the rate of melting was improved by the early melting of PP, which decreased the $\boldsymbol{\Delta H_m}$, which indicated the presence of very small sporadic distributed crystalline domains within the rPET.bg matrix, and as the enthalpy of melting is proportional to the density of crystalline domains, therefore $\boldsymbol{\Delta H_m}$ decreased with decreasing crystallinty. The inclusion of PP contamination, decreased crystallinity, $\boldsymbol{X_c}$, which confirmed the pattern of the crystalline domains as being numerous but sporadically dispersed, and that PP chains interfered in the orderly packing of the matrix chains by intersecting, entangling and delaying the overall process of crystallisation. The low MFR of PP of *1g /10min*, contributed to the overall decrease of MFR of contaminated rPET-bg. Despite its low MFR, this grade of PP is characterised by excellent flow behaviour, good dimensional stability and ease of shear under thermal conditions. Furthermore, the degradation process and the incompatibility of PP and rPET-bg decreased the overall viscosity and promoted the shear of lamellae and consequently increased the MFR proportionally with increasing % PP contamination.

	T_g (^oC)	T_c (^oC)	ΔH_c ($J.g^{-1}$)	T_m (^oC)	ΔH_m ($J.g^{-1}$)	X_c (%)	MFI (g/10min)
Extruded Samples **rPET-bg / PP** *compared to* **rPET-bg**	↓	NA	NA	↓	↓	↓	↑
Inj. Moulded Samples **rPET-bg / PP** *compared to* **rPET-bg**	↓	↑	↓	↓	↓	↓	↑

Table 6.51 Variation of Thermal and Flow Properties of rPET-bg contaminated with PP

In terms of tensile and impact properties, as shown in *Table 6.52* below, The inclusion of PP contamination influenced the overall tensile characteristics of non contaminated rPET-bg. The *stiffness* decreased as a result of decreased *modulus* and decreased crystallinity of the matrix; showing that crystallinity is a determinant factor in promoting or demoting tensile characteristics. The *stress at yield*, σ_y , increased, which is attributed to the readiness of the crystalline domains of PP in enhancing resistance to fracture. In the other hand, the *stress at yield* decreased orderly with increasing % PP contamination showing the flow characteristics of PP and the ease of PP lamellae in shearing under tensile force, which increased resistance to failure. The increased *stress at break*, σ_f , in the contaminated matrices, showed the capability of PP molecular structure in promoting elongation and improving elasticity of the more stiff structure of rPET-bg. The inclusion of PP increased the strain encountered for yielding to happen; which indicated acquired strength by the matrix. The strain decreased with increasing % PP contamination, which showed the influence of crystallinity in dictating the amount of strain at yielding. Once again, proportionality *stress at yield - strain at yield* is shown as both properties decreased proportionally with crystallinity. Furthermore, the increased *impact strength* indicated predominance of crystalline domains over amorphous ones., and showed proportionality with toughness and strength of the rPET-bg contaminated with PP. Additionally, proportionality is shown between impact strength, stress at yield and strain at yield. Once again, the crystalline domains and their distribution within the matrix dictated the amount of energy required to accomplish a failure mechanism.

	E (*GPa*)	σ_y (*MPa*)	σ_f (*MPa*)	e *at Yield*	*I.S* ($J.m^{-2}$)
Inj. Moulded Samples rPET-bg / PP *compared to* **rPET-bg**	↓	↑	↑	↑	↑

Table 6.52 Variation of Tensile and Impact Properties of Inj. Moulded Samples of rPET-bg contaminated with PP

The injection moulded samples of contaminated rPET-bg with PP, as shown in *Table 6.53* below, influenced the overall thermal and flow properties; this is shown in additional thermo-mechanical degradation, chains scissions and formation of very small chains. The decreased T_g allowed to understand the influence of processing conditions in enhancing molecular structure domains and showed optimised flow and cooling conditions. The increased T_m indicated high volume of sporadic very small crystalline domains which required increased temperature for melting. The melting process, the increased volume of small crystalline domains required extra energy to complete the process and consequently increased the ΔH_m. The increase in % crystallinity, X_c, confirmed the formation of additional crystalline domains resulting from further arrangement, straightening and packing of newly created very small chains. The increased ***MFR*** indicated the influence of the high shear and reduced viscosity, which were further promoted by degradation, chains scissions and ease of lamellae shearing of the main matrix.

	T_g (^oC)	T_m (^oC)	ΔH_m ($J.g^{-1}$)	X_c (%)	*MFI* (*g/10min*)
Inj. Moulded Samples *compared to* **Extruded Samples** *of* **rPET-bg contaminated with PP**	↓	↑	↑	↑	↑

Table 6.53 Comparison of Inj. Moulded Samples to Extruded Samples of rPET-bg contaminated with PP

Where: ↑ means increase, ↓ means decrease.

6.2 Conclusion

In light of the above investigation, it was shown that the inclusion of small amounts of *PP*, as a polymeric contaminant at *5%, 10%* and *15 %*, influenced the overall properties of the *rPET-bg* matrix. The thermal, spectroscopic, flow and mechanical analyses confirmed the presence of very small polymer chains, resulting from thermo-mechanical degradation encountered during processing operations. These very short chains allowed the formation of sporadic crystalline domains which influenced the overall properties. As seen with rPET-bg contaminated with HDPE, the exhibition of two well separated melting peaks indicated *incompatibility* and *immiscibility* of the polar PET and the non polar PP. Also, the premature melting of PP primary crystals speeded up and balanced the overall rate of melting. Once more, the decreased *crystallinity* showed that PP inclusion promoted the creation of sporadic and dispersed small crystalline domains. Additionally, the PP allowed high increase in shear and high decrease in viscosity, shown by an apparent increase in MFR. Furthermore, the inclusion of PP influenced the tensile and impact characteristics, resulting in decreased *stiffness*, increased *toughness* and increased *impact strength* of the contaminated matrix, and all of these variations showed a change in fracture mechanism, as seen with rPET-bg contaminated with HDPE, coupled with high energy absorption at failure.

Stage 1

Closing work and statement

The outcome of the experiments performed in ***stage 1*** allowed the selection of a contaminated batch which was further studied in ***stage 2***. The selection was done as follow.

Selection of a suitable contaminated batch for Further Research Work

The following criteria helped selecting the candidate contaminated batch.

1. The batch with the nearest T_g compared to PET-bg range.
2. The batch with the nearest % crystallinity to PET-bg range.
3. The batch with lowest T_m compared to PET-bg range.
4. The batch with the lowest ΔH_m compared to PET-bg range.
5. The batch with the lowest *MFR* compared to PET-bg range.
6. The batch with the nearest *E* compared to PET-bg range.
7. The batch with the nearest σ_y compared to PET-bg range.
8. The batch with the nearest σ_f compared to PET-bg range.
9. The batch with the nearest e_y compared to PET-bg range.
10. The batch with the highest $I.S$ compared to PET-bg range.

	T_g (^oC)	X_c (%)	T_m (^oC)	ΔH_m ($J.g^{-1}$)	*MFI* (*g/10min*)
PET-bg range	**69-115**	**30-40**	**255-265**	**30-140**	**20-35**
Non contaminated rPET-bg	**79.60**	**33.01**	**253.90**	**46.22**	**96.23**
95% rPET-bg / 5% HDPE	**76.23**	**24.90**	**253.72**	**34.80**	**49.51**
90% rPET-bg / 10% HDPE	**75.80**	**18.60**	**252.44**	**26.00**	**57.00**
85% rPET-bg / 15% HDPE	**73.31**	**18.50**	**252.53**	**25.90**	**68.71**
95% rPET-bg / 5% PP	**75.50**	**23.80**	**252.70**	**33.30**	**77.74**
90% rPET-bg / 10% PP	**73.70**	**18.53**	**253.73**	**25.94**	**88.31**
85% rPET-bg / 15% PP	**79.80**	**22.64**	**253.20**	**31.70**	**103.90**

Table 6.54 Comparison of Samples in terms of Thermal and Flow Properties

	E (GPa)	σ_y (MPa)	σ_f (MPa)	e_y	$I.S$ ($J.m^{-2}$)
PET-bg range	**2.8-3.1**	**55-75**	**50**	**0.005 0.015**	**3.6**
Non contaminated rPET-bg	**3.10**	**18.90**	**18.90**	**0.007**	**2.40**
95% rPET-bg / 5% HDPE	**2.29**	**17.27**	**17.27**	**0.008**	**3.74**
90% rPET-bg / 10% HDPE	**1.91**	**34.44**	**34.44**	**0.021**	**15.40**
85% rPET-bg / 15% HDPE	**1.93**	**40.23**	**40.23**	**0.024**	**29.31**
95% rPET-bg / 5% PP	**2.18**	**46.50**	**27.63**	**0.028**	**33.00**
90% rPET-bg / 10% PP	**2.10**	**36.30**	**35.52**	**0.023**	**29.10**
85% rPET-bg / 15% PP	**2.20**	**33.83**	**33.70**	**0.023**	**18.34**

Table 6.55 Comparison of Samples in terms of Mechanical Properties

Note: "green colour" for rPET-bg contaminated with HDPE and "red colour" for rPET-bg contaminated with PP.

The *rPET-bg* contaminated with *5% PP* showed good match and selected for further investigation.

Closing statement

As a result of this investigation, it was shown that the inclusion of small amounts of polyolefin contaminants, *HDPE* or *PP*, at *5%*, *10%* and *15 %*, influenced the overall properties of the *rPET-bg*. By comparing the results obtained in the performed experiments, a selection process, as shown above in *Tables 6.54* and *6.55*, led to the selection of *rPET-bg* contaminated with *5% PP* for *further research work*. *rPET-bg* is more likely to be contaminated by *PP* more than by *HDPE* during the *mechanical recycling*, especially during the *sorting* and *separation process* of *bottle grades PET* (see *Section 2.1.6*), where cross contamination with other plastic materials, mainly bottles of *HDPE* and mostly *PP* caps and *closures*, which are sometimes difficult to separate from the *recycled PET bottles*, take place and influence the properties of the final *bottle grade recycled PET*. Furthermore, a *5% PP weight* in the form of *bottle caps* and *closures* can easily pass through the sorting process during recycling. Additionally, the *selected batch* showed good reasons to believe that its resulting *crystallinity* was affected by the inclusion of *PP*. Furthermore, the resulting *crystallinity* influenced the *selected batch*'s thermal, flow and mechanical characteristics, as shown in *Tables 6.54* and *6.55*, compared to other *batches.* As the *cooling rate* is an important processing parameter which influence the thermal characteristics in the field of bottle manufacturing and the *repetitive extrusions* is a method of choice in compounding *recycled polymers*, therefore, it was decided to subject *extruded samples* of *non contaminated rPET-bg* and the *selected batch*, i.e. *rPET-bg contaminated with 5% PP*, to DSC analysis at *various cooling rates* and also DSC analysis of *repetitively extruded samples* of both materials in order to investigate and determine the influence of *PP contamination* on the *thermal characteristics* of the *rPET-bg matrix*, with emphasis on *crystallinity* and *crystallisation process*. These investigations were carried out in ***stage 2***.

Stage 2

Chapter 7

Effect of *cooling rates* on the *thermal characteristics* of *non contaminated rPET-bg* and *rPET-bg contaminated with 5% PP*

7.1 Results and Discussions

This section discusses the various experimental results obtained in *experiment 9*; where extruded samples of non contaminated rPET-bg and the *selected batch* of *stage 1*, i.e. rPET-bg contaminated with *5%* PP, were thermally analysed by DSC at various *heating* and *cooling rates*, as described in *Experiment 9, Section 3.2.1.2* and *Experiment 9, Section 3.4*, and their thermal *characteristics* investigated, especially *crystallinity* which was analysed by *Avrami* and *Ozawa equations* for *non-isothermal crystallisation process*, as described in *Section 1.2.3.2*.

As in ***stage 1***, the results of ***Stage 2*** were assessed statistically, validated and compared to other literature and research works. The results are displayed first and then discussed as below.

7.1.1 DSC Results of *non contaminated rPET-bg at various heating / cooling rates*

In *experiments 9*, the DSC analysis yielded the data below.

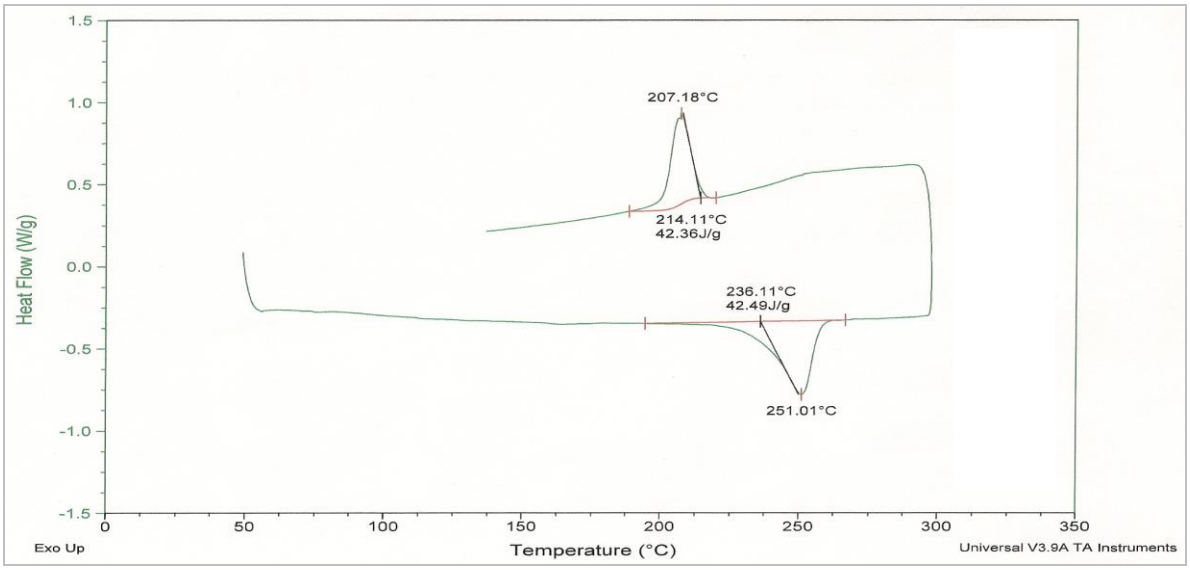

Figure 7.1 Thermogram of Extruded Sample 1 of non contaminated rPET-bg at 10°C/min

	T_m (°C)	ΔH_m (J.g^{-1})	T_c (°C)	ΔH_c (J.g^{-1})	ΔH_m^0 (J.g^{-1}	X_c (%)
Material	**Extruded Samples of rPET-bg at 10°C/min**					
Mean (μ)	**251.14**	**43.86**	**207.05**	**41.77**	**140**	**29.83**
STDEV (σ)	0.18	1.93	0.18	0.84		0.60
ST. Error ($S_E = \sigma/n^{0.5}$)	0.13	1.36	0.13	0.59		0.43
CI (95%), ($\mu \pm 1.96 S_E$)	$\mu \pm 0.25$	$\mu \pm 2.68$	$\mu \pm 0.25$	$\mu \pm 1.17$		$\mu \pm 0.83$

Table 7.1 Non contaminated rPET-bg Samples at 10°C/min heating / cooling Rate

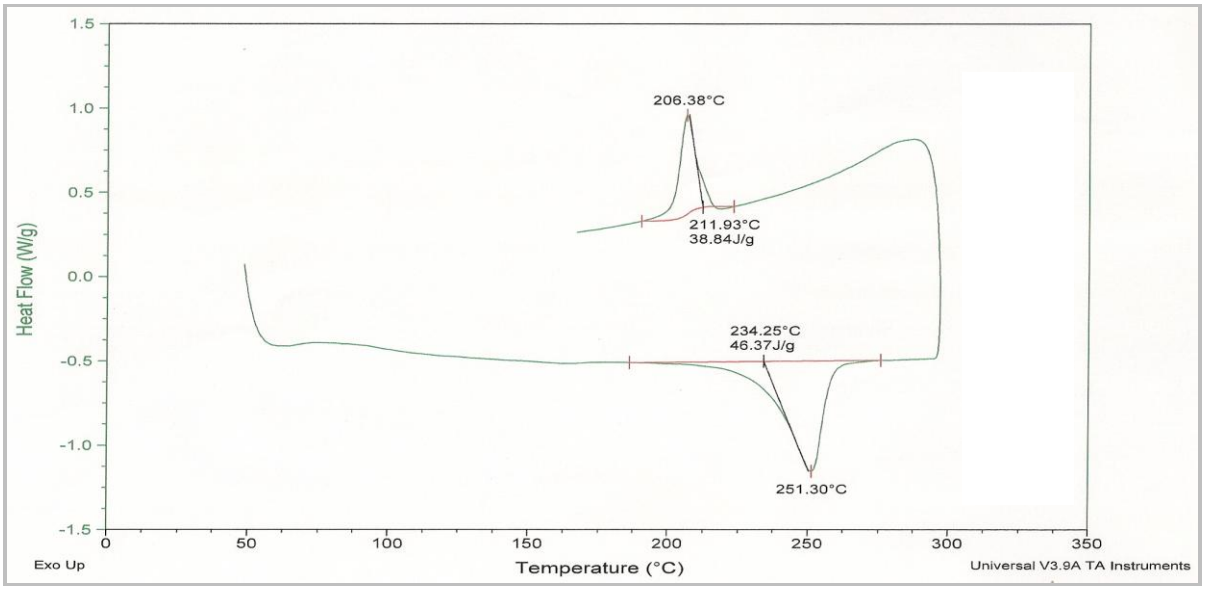

Figure 7.2 Thermogram of Extruded Sample 1 of non contaminated rPET-bg at 15°C/min

	T_m (°C)	ΔH_m (J.g^{-1})	T_c (°C)	ΔH_c (J.g^{-1})	ΔH_m^0 (J.g^{-1}	X_c (%)
Material	**Extruded Samples of rPET-bg at 15°C/min**					
Mean (μ)	**251.30**	**46.20**	**206.38**	**39.43**	**140**	**28.16**
STDEV (σ)	0.00	0.25	0.00	0.83		0.59
ST. Error ($S_E = \sigma/n^{0.5}$)	0.00	0.18	0.00	0.59		0.42
CI (95%), ($\mu \pm 1.96 S_E$)	$\mu \pm 0.00$	$\mu \pm 0.34$	$\mu \pm 0.00$	$\mu \pm 1.15$		$\mu \pm 0.82$

Table 7.2 Samples of non contaminated rPET-bg at 15°C/min heating / cooling Rate

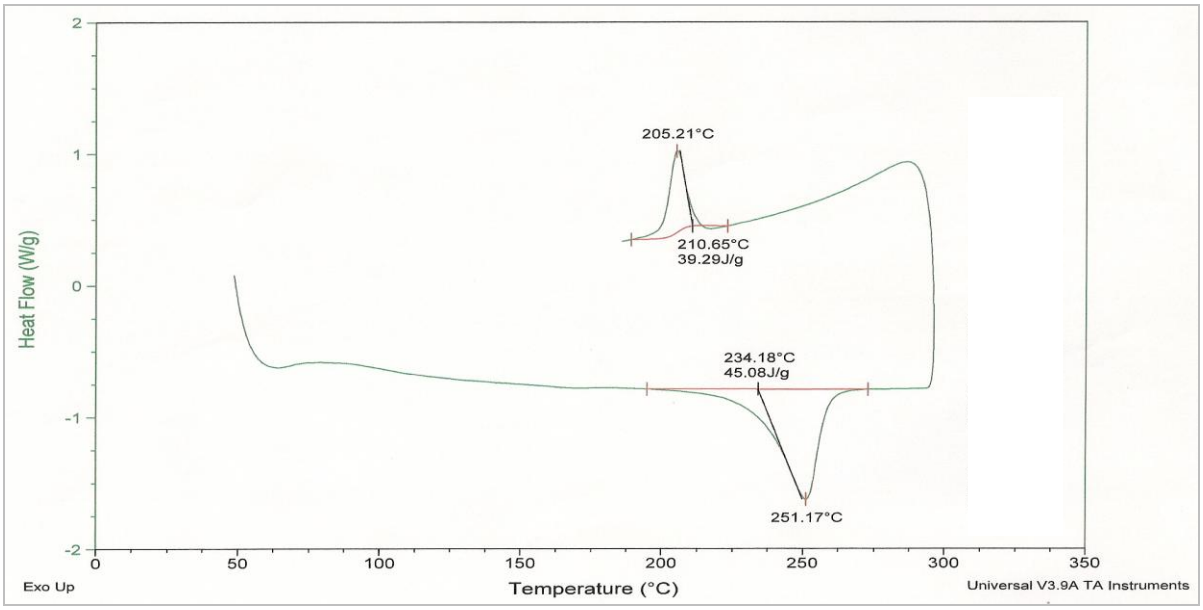

Figure 7.3 Thermogram of Extruded Sample 1 of non contaminated rPET-bg at 20°C/min

	T_m (°C)	ΔH_m (J.g^{-1})	T_c (°C)	ΔH_c (J.g^{-1})	ΔH_m^0 (J.g^{-1}	X_c (%)
Material	**Extruded Samples of rPET-bg at 20°C/min**					
Mean (μ)	**251.17**	**45.40**	**205.27**	**40.89**	**140**	**29.21**
STDEV (σ)	0.00	0.45	0.08	2.26		1.62
ST. Error ($S_E = \sigma/n^{0.5}$)	0.00	0.32	0.05	1.60		1.14
CI (95%), ($\mu \pm 1.96S_E$)	$\mu \pm 0.00$	$\mu \pm 0.62$	$\mu \pm 0.11$	$\mu \pm 3.14$		$\mu \pm 2.24$

Table 7.3 Samples of non contaminated rPET-bg at 20°C/min heating / cooling Rate

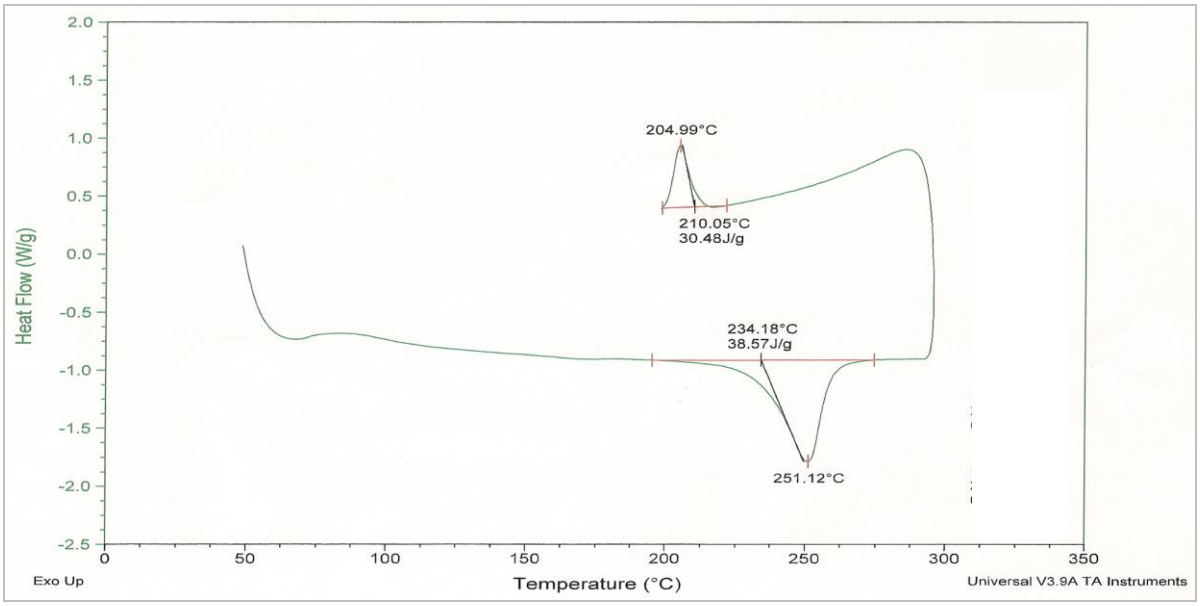

Figure 7.4 Thermogram of Extruded Sample 1 of non contaminated rPET-bg at 25°C/min

	T_m (°C)	ΔH_m (J.g^{-1})	T_c (°C)	ΔH_c (J.g^{-1})	ΔH_m^0 (J.g^{-1}	X_c (%)
Material	**Extruded Samples of rPET-bg at 25°C/min**					
Mean (μ)	**251.12**	**38.43**	**204.99**	**30.88**	**140**	**22.06**
STDEV (σ)	0.00	0.20	0.00	0.57		0.40
ST. Error ($S_E = \sigma/n^{0.5}$)	0.00	0.14	0.00	0.40		0.29
CI (95%), ($\mu \pm 1.96 S_E$)	$\mu \pm 0.00$	$\mu \pm 0.27$	$\mu \pm 0.00$	$\mu \pm 0.78$		$\mu \pm 0.56$

Table 7.4 Samples of non contaminated rPET-bg at 25°C/min heating / cooling Rate

7.1.2 DSC Results of *rPET-bg contaminated with 5% PP at various cooling rates*

In *experiments 9*, the DSC analysis yielded the data below.

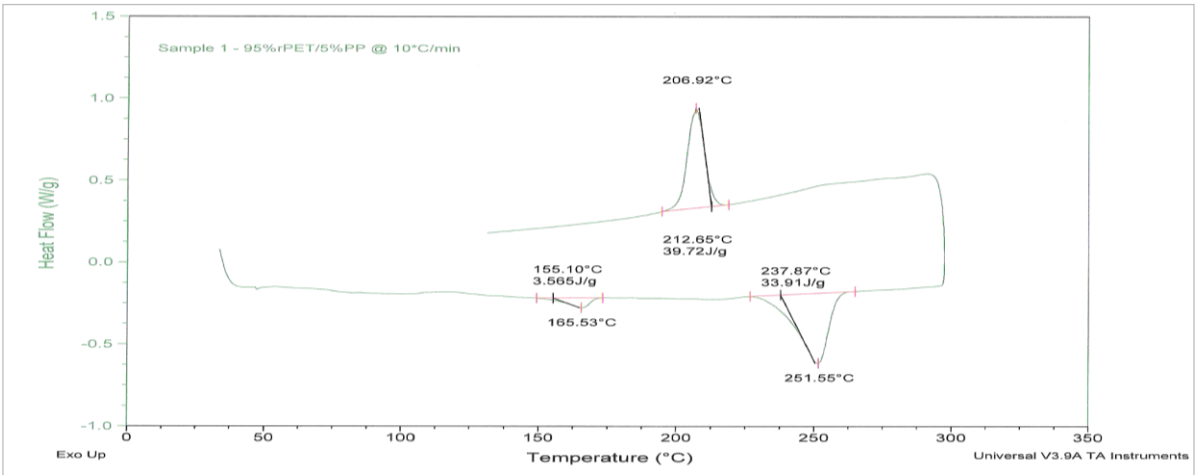

Figure 7.5 Thermogram of Extruded Sample 1 of rPET-bg contaminated with 5% PP at 10°C/min

	T_m (°C)	ΔH_m (J.g^{-1})	T_c (°C)	ΔH_c (J.g^{-1})	ΔH_m^0 (J.g^{-1})	X_c (%)
Material	**Extruded Samples of 95% rPET-bg / 5% PP at 10°C/min**					
Mean (μ)	**251.83**	**33.42**	**205.64**	**37.56**	**140**	**26.83**
STDEV (σ)	0.26	0.63	1.13	2.41		1.72
ST. Error ($S_E = \sigma/n^{0.5}$)	0.15	0.36	0.65	1.39		0.99
CI (95%), ($\mu \pm 1.96 S_E$)	$\mu \pm 0.30$	$\mu \pm 0.71$	$\mu \pm 1.28$	$\mu \pm 2.73$		$\mu \pm 1.95$

Table 7.5 Samples of rPET-bg contam. with 5% PP at 10°C/min heating / cooling Rate

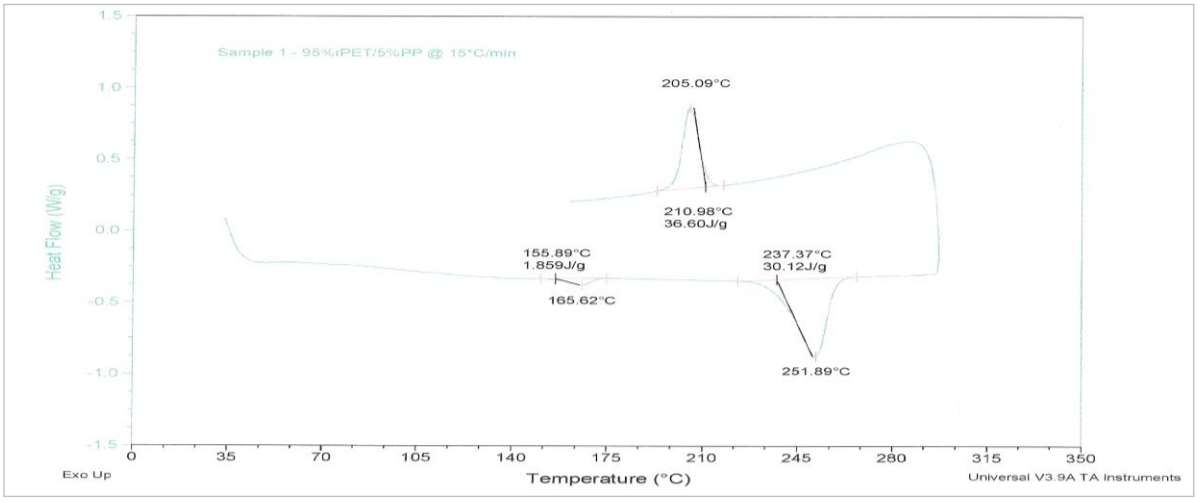

Figure 7.6 Thermogram of Extruded Sample 1 of rPET-bg contaminated with 5% PP at 15°C/min

	T_m (°C)	ΔH_m (J.g^{-1})	T_c (°C)	ΔH_c (J.g^{-1})	ΔH_m^0 (J.g^{-1}	X_c (%)
Material	**Extruded Samples of 95% rPET-bg / 5% PP at 15°C/min**					
Mean (μ)	**251.86**	**29.85**	**205.14**	**36.85**	**140**	**26.32**
STDEV (σ)	0.10	0.31	0.57	1.29		0.92
ST. Error ($S_E = \sigma/n^{0.5}$)	0.06	0.18	0.33	0.74		0.53
CI (95%), ($\mu \pm 1.96 S_E$)	$\mu \pm 0.12$	$\mu \pm 0.35$	$\mu \pm 0.65$	$\mu \pm 1.46$		$\mu \pm 1.04$

Table 7.6 Samples of rPET-bg contam. with 5% PP at 15°C/min heating / cooling Rate

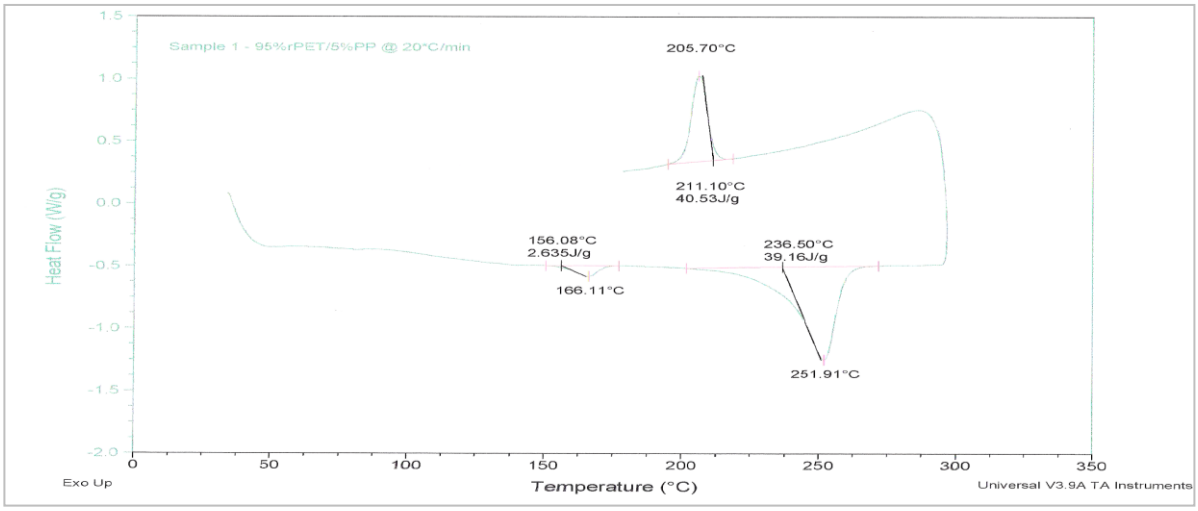

Figure 7.7 Thermogram of Extruded Sample 1 of rPET-bg contaminated with 5% PP at 20°C/min – *Stage 2*

	T_m (°C)	ΔH_m (J.g^{-1})	T_c (°C)	ΔH_c (J.g^{-1})	ΔH_m^0 (J.g^{-1}	X_c (%)
Material	**Extruded Samples of 95% rPET-bg / 5% PP at 20°C/min**					
Mean (μ)	**252.30**	**36.16**	**205.20**	**39.34**	**140**	**28.10**
STDEV (σ)	0.34	5.43	0.77	3.07		2.19
ST. Error ($S_E = \sigma/n^{0.5}$)	0.19	3.13	0.44	1.77		1.26
CI (95%), ($\mu \pm 1.96 S_E$)	$\mu \pm 0.38$	$\mu \pm 6.14$	$\mu \pm 0.87$	$\mu \pm 3.47$		$\mu \pm 2.48$

Table 7.7 Samples of rPET-bg contam. with 5% PP at 20°C/min heating / cooling Rate

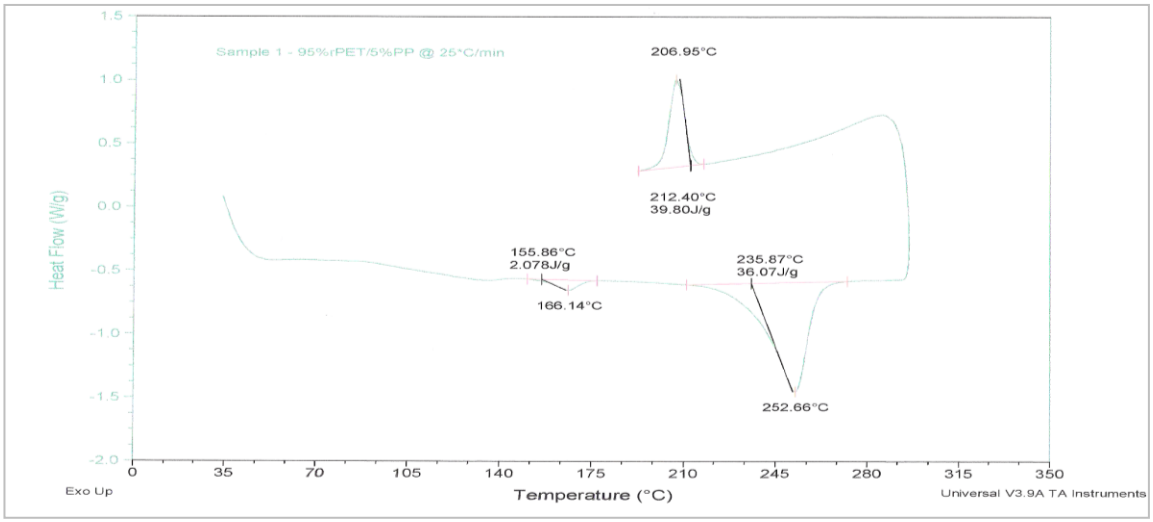

Figure 7.8 Thermogram of Extruded Sample 1 of rPET-bg contaminated with 5% PP at 25°C/min

	T_m (°C)	ΔH_m (J.g^{-1})	T_c (°C)	ΔH_c (J.g^{-1})	ΔH_m^0 (J.g^{-1}	X_c (%)
Material	**Extruded Samples of 95% rPET-bg / 5% PP at 25°C/min**					
Mean (μ)	**253.31**	**33.30**	**205.75**	**36.79**	**140**	**26.28**
STDEV (σ)	1.34	2.65	1.22	3.14		2.24
ST. Error ($S_E = \sigma/n^{0.5}$)	0.78	1.53	0.70	1.81		1.29
CI (95%), ($\mu \pm 1.96 S_E$)	$\mu \pm 1.52$	$\mu \pm 3.00$	$\mu \pm 1.38$	$\mu \pm 3.55$		$\mu \pm 2.53$

Table 7.8 Samples of rPET-bg contam. with 5% PP at 25°C/min heating / cooling Rate

Note: Additional DSC Thermograms are available in ***Appendix 7*** **(***1 to 8***)**.

7.1.3 Melting Temperature, T_m

DSC analysis in the *heating mode*, as shown in *Table 7.9* and *Figure 7.9* below, showed stability with narrow fluctuation of the T_m of *non contaminated rPET-bg* between *251.12* and *251.30°C*; this narrow melting point indicated orderly structures of the crystalline domains. Whereas, the T_m of *rPET-bg contaminated with 5% PP* fluctuated with an increase from *251.83* to *253.31°C*; this is attributed to random distribution of amorphous and crystalline domains which resulted in irregular and broader melting points due to the various degrees of interfacial interaction, i.e. the mobility of the molecular chains increased proportionally with heating rates, promoted by the early melting of PP which allowed further chains' mobility, orientation and re-arrangement before melting. As the crystalline domains becomes more ordered, the degree of entropy decreases and the T_m increases; the increased T_m of the rPET-bg contaminated with PP indicated that crystalline domains are larger than amorphous ones. Furthermore, this showed the effect of heterogeneous nucleation of PP and rPET-bg on each other, similar findings were reported by *Hao et al.* [127] and *Tao* and *Mai* [128] in their studies. The different thermal history is evidenced by the presence of individual endotherms, as reported by *Murayama* and *Bell* [179], and showed individual crystallisation of the materials, as reported by *Oyman* and *Tincer* [180].

	Extruded Samples Non contaminated rPET-bg			Extruded Samples 95% rPET-bg / 5% PP		
	T_m (°C)					
Heating Rates (°C/min.)	**Mean (μ)**	**ST. Error ($S_E = \sigma/n^{0.5}$)**	**CI (95%) ($\mu \pm 1.96S_E$)**	**Mean (μ)**	**ST. Error ($S_E = \sigma/n^{0.5}$)**	**CI (95%) ($\mu \pm 1.96S_E$)**
10	**251.14**	0.13	$\mu \pm 0.25$	**251.83**	0.15	$\mu \pm 0.30$
15	**251.30**	0.00	$\mu \pm 0.00$	**251.86**	0.06	$\mu \pm 0.12$
20	**251.17**	0.00	$\mu \pm 0.00$	**252.30**	0.19	$\mu \pm 0.38$
25	**251.12**	0.00	$\mu \pm 0.00$	**253.31**	0.78	$\mu \pm 1.52$

Table 7.9 Melting Temperature at Various Heating Rates

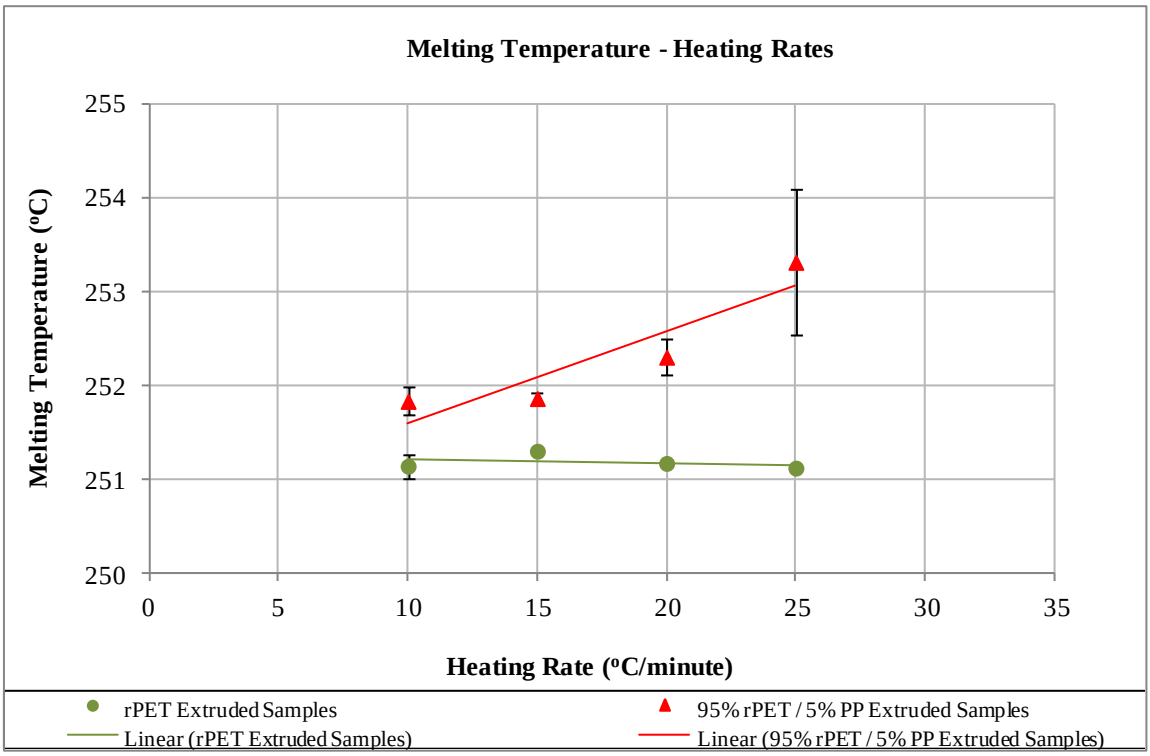

Figure 7.9 Melting Temperature at Various Heating Rates

7.1.4 Heat of Fusion, ΔH_m

The *heat of fusion* or *enthalpy of melting*, ΔH_m, of the *rPET-bg contaminated with 5% PP*, as shown in *Table 7.10* and *Figure 7.10* below, increased by fluctuating randomly between *29.85* and *36.16* $J.g^{-1}$ and were lower than their counterparts of *non contaminated rPET-bg* which decreased by fluctuating randomly between *38.43* and *46.20* $J.g^{-1}$; this random fluctuation was the result of heterogeneous distribution of crystalline domains due to entanglement and heterogeneous nucleation, as described previously, and also could be caused by other contaminants or impurities, such as soil particulates, which are the main issues in post consumer plastic recycling. *Fann et al.* [126] and *Pracella et al.* [181] respectively, related the roles of heterogeneous nucleation, phase dispersion and interfacial adhesion on the variation of enthalpy and crystallinity. It is apparent that the inclusion of *5% PP* increased the free energy, resulting in improved melting process and consequently decreased the ΔH_m.

	Extruded Samples Non contaminated rPET-bg			Extruded Samples 95% rPET-bg / 5% PP		
	ΔH_m $(J.g^{-1})$					
Heating Rates (°C/min.)	**Mean (μ)**	**ST. Error ($S_E = \sigma/n^{0.5}$)**	**CI (95%) ($\mu \pm 1.96 S_E$)**	**Mean (μ)**	**ST. Error ($S_E = \sigma/n^{0.5}$)**	**CI (95%) ($\mu \pm 1.96 S_E$)**
10	**43.86**	1.36	$\mu \pm 2.68$	**33.42**	0.36	$\mu \pm 0.71$
15	**46.20**	0.18	$\mu \pm 0.34$	**29.85**	0.18	$\mu \pm 0.35$
20	**45.40**	0.32	$\mu \pm 0.62$	**36.16**	3.13	$\mu \pm 6.14$
25	**38.43**	0.14	$\mu \pm 0.27$	**33.30**	1.53	$\mu \pm 3.00$

Table 7.10 Heat of Fusion at Various Heating Rates

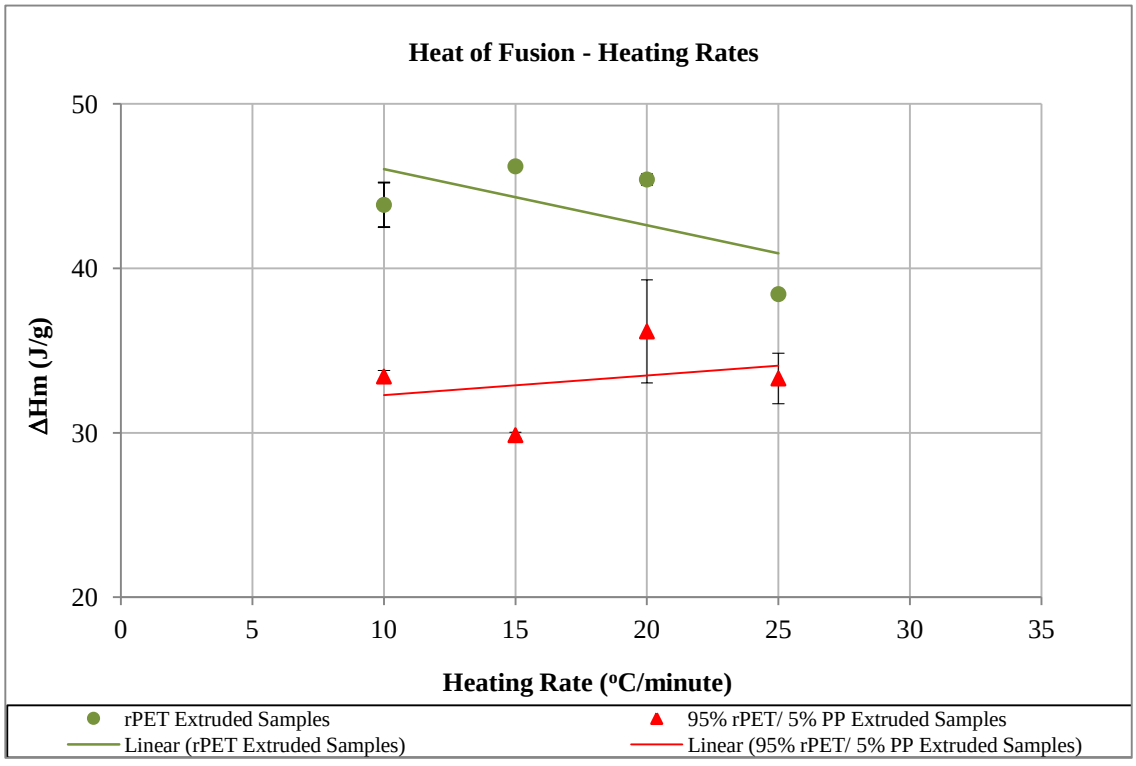

Figure 7.10 Heat of Fusion at Various Heating Rates

7.1.5 Crystallisation Temperature, T_c

DSC analysis in the *cooling mode*, as shown in *Table 7.11* and *Figure 7.11* below, showed that the T_c of *non contaminated rPET-bg* decreased from *207.05* to *204.99°C*, and stabilised by fluctuating between *205.14* and *205.75°C* for the *rPET-bg contaminated with 5%*; the *exotherms* associated with crystallisation shifted to lower temperatures with *increase* of *cooling rates*. The T_c for the *earlier* indicated logical inverse proportionality confirming that the crystallisation propagation depended on cooling temperature, i.e. the faster the cooling the lower the crystallisation and the higher amorphous is the resulting material, as reported by *Awaja* and *Pavel* [153], whereas the fluctuation in the *latter* showed that T_c slightly increased because of the influence of *contaminant* but tended to stabilise as shown by the narrow gap in reduction, i.e. the T_c of *rPET-bg contaminated with 5%* were lower than those of *non contaminated rPET-bg*; this observable difference showed obvious difference in the crystallisation behaviour and that rPET phase has nucleation ability for crystallisation in the presence of PP, similar outcomes were reported by *Zhu et al.* [182], [183] and by *Jayanarayanan et al.* [184]. *Non contaminated rPET-bg* displayed an ease of *crystallisation* at *lower cooling rate* and crystallised at higher temperatures from the melt compared with *rPET-bg contaminated with 5%*, which displayed lower temperatures from the melt; this meant, in real time processing the *latter* needs a lower temperature to crystallise and therefore is not easy to crystallise at a high temperature, therefore, during processing, it is easier for the *earlier* to have very low crystallinity than the *latter* at higher cooling rates. This difference in crystallisation behaviour may be attributed to the effect of contaminant, i.e. the *5% PP* which hindered the propagation of temperature to higher level and acting as a defect, i.e. as a short chain branching or interfering in the formation of larger crystals, therefore formation of small crystals which required lower crystallisation temperature; this contradicts what was reported by *Torres et al.*[23] that the presence of contaminants and residual moisture contribute or facilitate the crystallisation of the *recycled PET*, this may be the case for impurities but not with *PP* as *contaminant*.

	Extruded Samples Non contaminated rPET-bg			Extruded Samples 95% rPET-bg / 5% PP		
	T_c (^oC)					
Cooling Rates (^oC/min.)	**Mean (μ)**	**ST. Error ($S_E = \sigma/n^{0.5}$)**	**CI (95%) ($\mu \pm 1.96 S_E$)**	**Mean (μ)**	**ST. Error ($S_E = \sigma/n^{0.5}$)**	**CI (95%) ($\mu \pm 1.96 S_E$)**
10	**207.05**	0.13	$\mu \pm 0.25$	**205.64**	0.65	$\mu \pm 1.28$
15	**206.38**	0.00	$\mu \pm 0.00$	**205.14**	0.33	$\mu \pm 0.65$
20	**205.27**	0.05	$\mu \pm 0.11$	**205.20**	0.44	$\mu \pm 0.87$
25	**204.99**	0.00	$\mu \pm 0.00$	**205.75**	0.70	$\mu \pm 1.38$

Table 7.11 Crystallisation Temperature at Various Cooling Rates

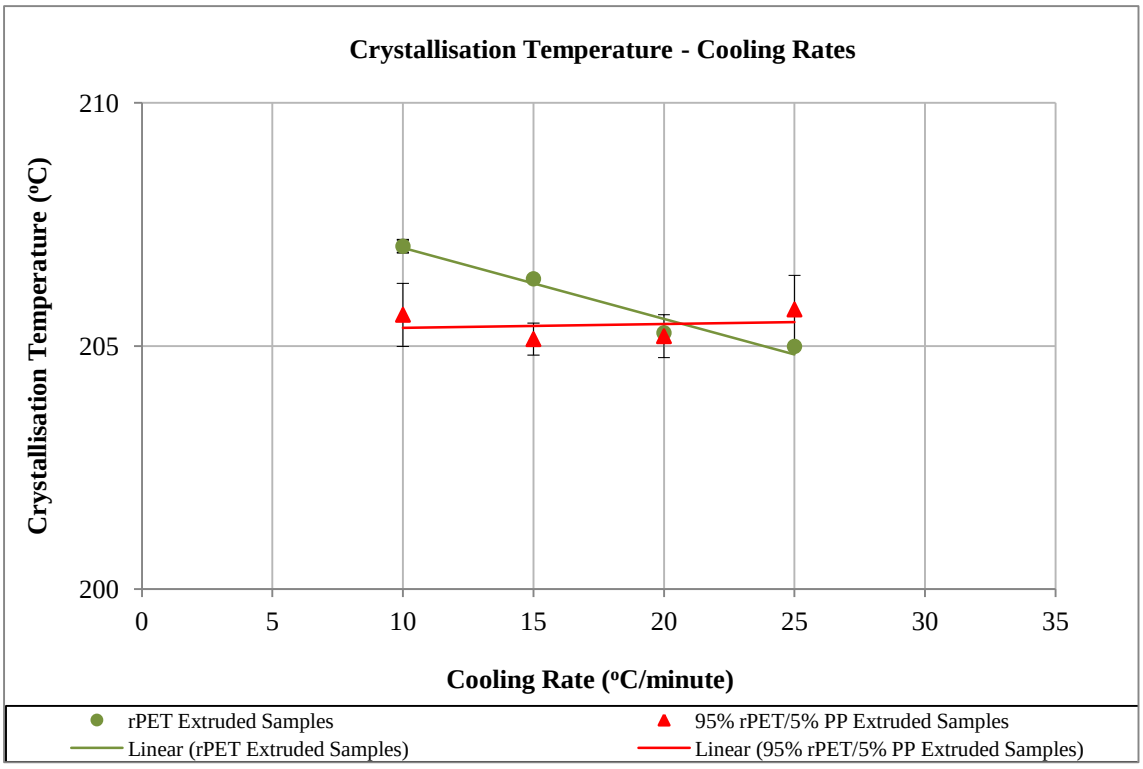

Figure 7.11 Crystallisation Temperature at Various Cooling Rates

7.1.6 Heat of Crystallisation, ΔH_c

The *heat of crystallisation* or enthalpy of crystallisation, ΔH_c , of *non contaminated rPET-bg* tended to *decrease* from *41.77* to *30.88 J.g*$^{-1}$, as shown in *Table 7.12* and *Figure 7.12* below, which indicated that crystals were forming faster at lower cooling temperature and decreased with increasing cooling rate; indicating a balanced nucleation and growth with respect to crystals densities. In the other hand, the ΔH_c of *rPET-bg contaminated with 5% PP* fluctuated randomly and tended to stabilise between *39.34* and *36.79 J.g*$^{-1}$, the above ΔH_c ranges of fluctuations showed that the *PP inclusion* influenced the *crystallisation process* by interfering in the stability of the microscopic structure of the main matrix and by bridging the polymer chains and filling the vacant interstices and interfering with nucleation and crystallite growth process, resulting in decreased T_c as seen previously. It can be seen that the crystalline domains formation in *non contaminated rPET-bg* was reducing with increasing cooling rates than in *rPET-bg contaminated with 5% PP*. *By assumption, from the extrapolation of the linear trend line of rPET-bg, in Figure 7.4 below, one can predict that the minimum cooling rate for reaching 0% crystallinity should be high, probably no less than 65*^{o}*C*. The above, confirmed that the inclusion of *PP* contributed to the stabilisation of the crystallisation process in the *rPET-bg* main matrix and consequently tended to stabilise the decreasing T_c and ΔH_c.

	Extruded Samples Non contaminated rPET-bg			Extruded Samples 95% rPET-bg / 5% PP		
	ΔH_c ($J.g^{-1}$)					
Cooling Rates (^{o}C/min.)	**Mean (μ)**	**ST. Error ($S_E = \sigma/n^{0.5}$)**	**CI (95%) ($\mu \pm 1.96 S_E$)**	**Mean (μ)**	**ST. Error ($S_E = \sigma/n^{0.5}$)**	**CI (95%) ($\mu \pm 1.96 S_E$)**
10	**41.77**	0.59	$\mu \pm 1.17$	**37.56**	1.39	$\mu \pm 2.73$
15	**39.43**	0.59	$\mu \pm 1.15$	**36.85**	0.74	$\mu \pm 1.46$
20	**40.89**	1.60	$\mu \pm 3.14$	**39.34**	1.77	$\mu \pm 3.47$
25	**30.88**	0.40	$\mu \pm 0.78$	**36.79**	1.81	$\mu \pm 3.55$

Table 7.12 Heat of Crystallisation at Various Cooling Rates

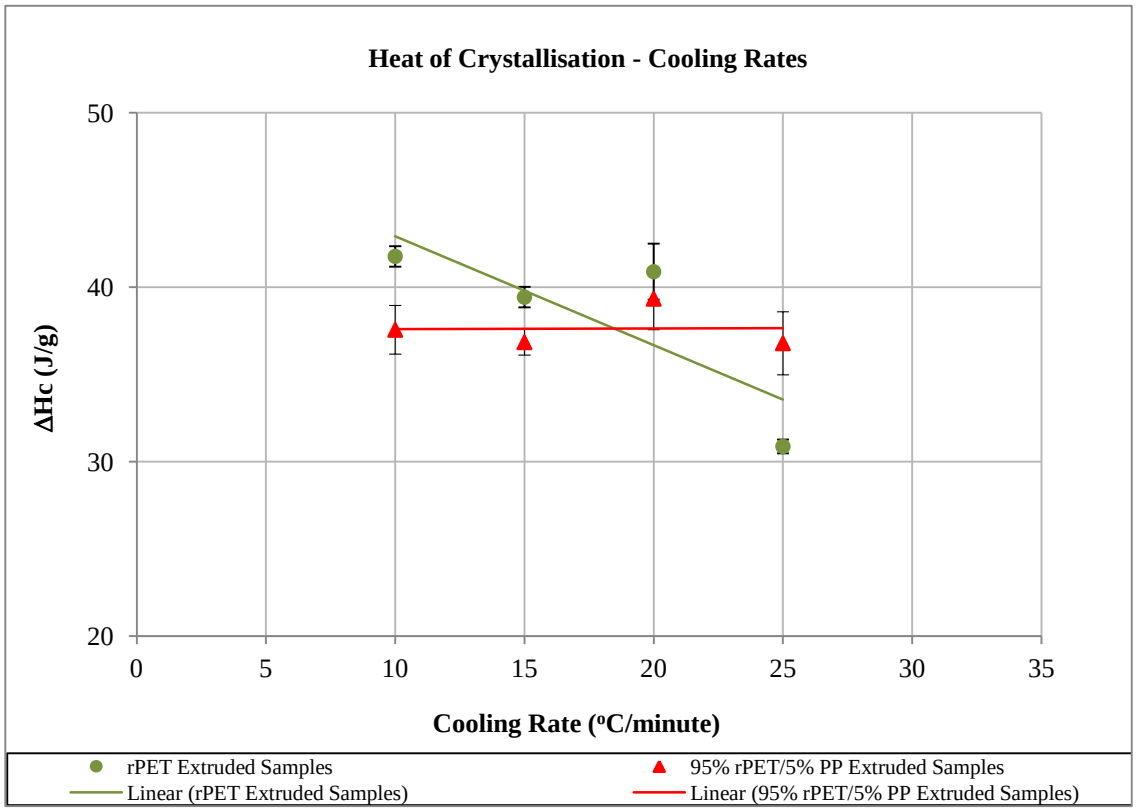

Figure 7.12 Heat of Crystallisation at Various Cooling Rates

7.1.7 % Crystallinity, X_c

The *% crystallinity*, X_c, of *non contaminated rPET-bg decreased* from *29.21* to *22.06 %*, as shown in *Table 7.13* and *Figure 7.13* below, indicating *slow* crystallisation at proportional nucleation and growth rate with increasing cooling rates. The stability tendency of crystallinity in the *rPET-bg contaminated with 5% PP*, indicated *fast* formation of *crystallites* of various densities, meaning that the crystallisation process was hindered by the time required at each cooling rate; the increase in cooling rates, reduced the time required for the chains' disentanglement and straightening, and disturbed the heterogeneous nucleation, which in turn slowed or retarded the formation of crystallites within the matrix. In real time bottle processing, during the cooling stage, the nucleation and growth processes of *PET* spherulites are the main controlling factors governing the degree of crystallinity in the final product. In our case, the small amount of contaminant, *5% PP*, contributed in delaying and stabilising the % crystallinity with increasing cooling rates; this indicated that the presence of such *contaminant* influenced to some extend the

propagation of crystallinity with increasing cooling rates. In the sense of non-isothermal crystallisation, the pre-melting of PP influenced the crystallisation and melting behaviour of the rPET-bg matrix, improved crystallinity and other characteristics in the rPET/PP blend, similar findings were reported by *Tao* and *Mai* [128] and *Martinelli et al.* [185]. The process of crystallisation is initiated by the formation of primary stable nuclei, as described in *Section 1.2.3*, then, crystallisation propagates to form primary spherulites and continues through the primary and secondary phases until spherulites filled all the *area* under the *exotherm*; this *area* under the *exotherm* is proportional to ΔH_c, which is used in determining the amount of *crystallinity* and their proportionality is shown in the similarity of the curves in *Figure 7.12* above and *Figure 7.13* below. In most cases, crystallinity starts on the surfaces of impurities or on deliberately added nucleating agents, and as no nucleating agents were added in this case, therefore, the *5% PP* contributed in stabilising the chains' mobility and the heterogeneous nucleation of the rPET-bg matrix, and consequently stabilising the formation of crystalline domains with increasing cooling rates.

	Extruded Samples Non contaminated rPET-bg			**Extruded Samples 95% rPET-bg / 5% PP**		
	X_c (%)					
Cooling Rates (°C/min.)	**Mean (μ)**	**ST. Error ($S_E = \sigma/n^{0.5}$)**	**CI (95%) ($\mu \pm 1.96 S_E$)**	**Mean (μ)**	**ST. Error ($S_E = \sigma/n^{0.5}$)**	**CI (95%) ($\mu \pm 1.96 S_E$)**
10	**29.83**	0.43	$\mu \pm 0.83$	**26.83**	0.99	$\mu \pm 1.95$
15	**28.16**	0.42	$\mu \pm 0.82$	**26.32**	0.53	$\mu \pm 1.04$
20	**29.21**	1.14	$\mu \pm 2.24$	**28.10**	1.26	$\mu \pm 2.48$
25	**22.06**	0.29	$\mu \pm 0.56$	**26.28**	1.29	$\mu \pm 2.53$

Table 7.13 % Crystallinity at Various Cooling Rates

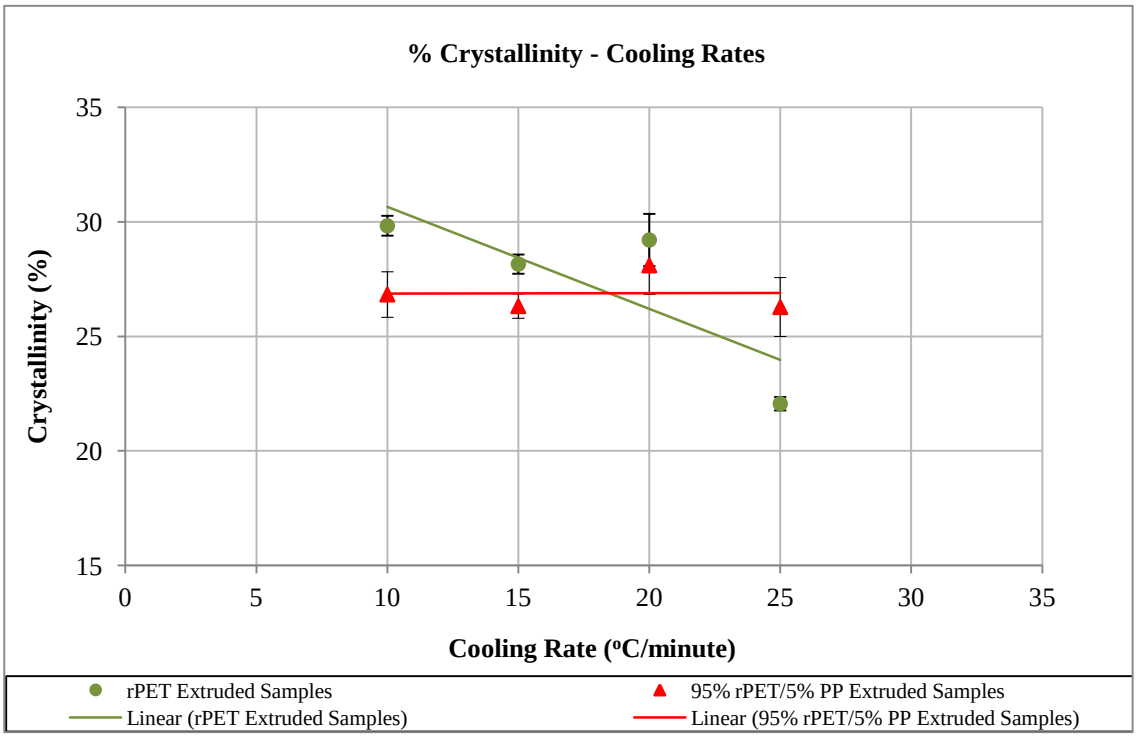

Figure 7.13 % Crystallinity at Various Cooling Rates

7.1.8 Heat of Crystallisation - Crystallinity Relationship

Once more, data comparison in *Table 7.14* and the linearity in *Figure 7.14* below showed clearly the proportionality between heat of crystallisation and the formed crystalline domains described as % crystallinity.

	Extruded Samples Non contaminated rPET-bg		Extruded Samples 95% rPET-bg / 5% PP	
	ΔH_c ($J.g^{-1}$)	X_c (%)	ΔH_c ($J.g^{-1}$)	X_c (%)
Cooling Rates (°C/min.)	**Mean (μ)**	**Mean (μ)**	**Mean (μ)**	**Mean (μ)**
10	**41.77** ± 1.17	29.83 ± 0.83	**37.56** ± 2.73	26.83± 1.95
15	**39.43** ± 1.15	28.16 ± 0.82	**36.85** ± 1.46	26.32± 1.04
20	**40.89** ± 3.14	29.21 ± 2.24	**39.34** ± 3.47	28.10± 2.48
25	**30.88** ± 0.78	22.06 ± 0.56	**36.79** ± 3.55	26.28± 2.53

Table 7.14 Heat of Crystallisation and Crystallinity at Various Cooling Rates

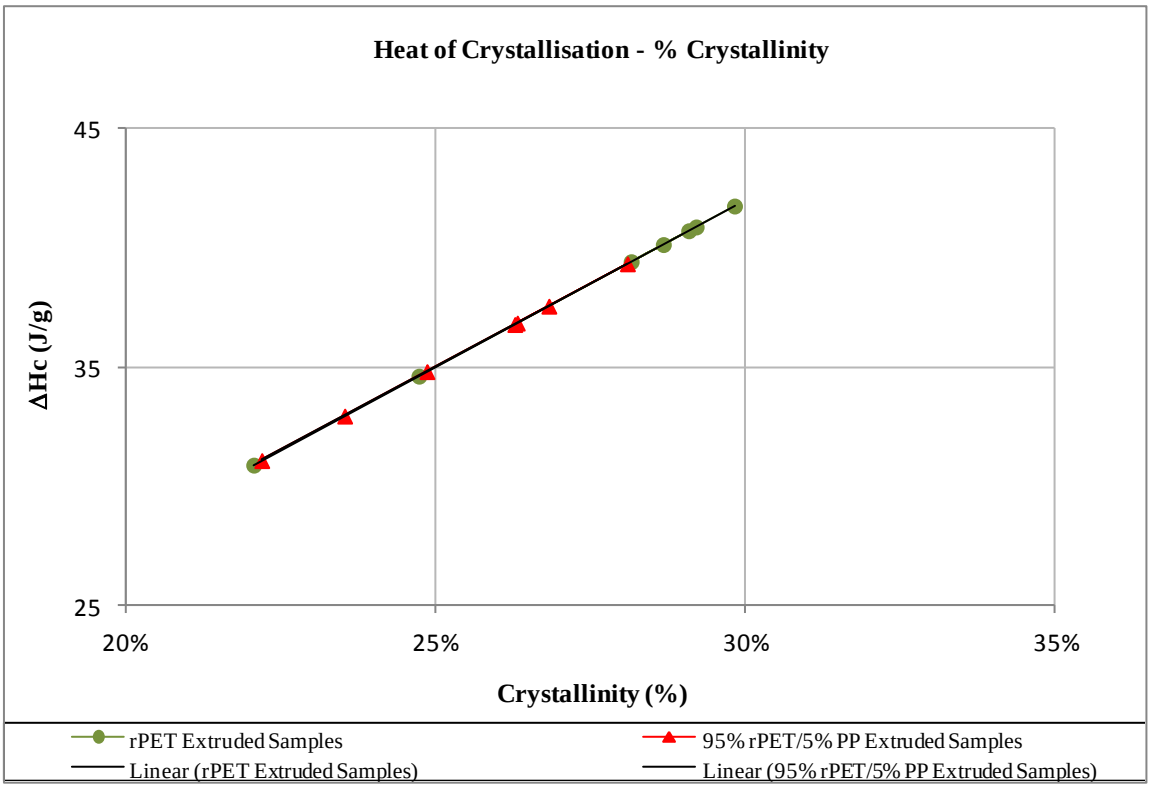

Figure 7.14 Heat of Crystallisation Vs Crystallinity at Various Cooling Rates

7.1.9 Overall Data Comparison

The comparison of the thermal characteristics obtained, as shown in *Table 7.15* below, showed clearly the influence of PP inclusion on the rPET-bg matrix. The increased $\boldsymbol{T_m}$ in the *rPET-bg contaminated with 5% PP* showed the random distribution of amorphous and crystalline domains in affecting the mobility of molecular chains and their dependency on the variation of cooling rates, which meant that the early melting of PP allowed further chains' mobility and reinforced the entangling state, resulting in slow melting and consequently an increased temperature. This heterogeneous distribution of crystallites coupled with early melting of PP chains generated further entropy and increased the free energy, resulting in unbalanced melting process and consequently decreased the $\boldsymbol{\Delta H_m}$. The crystallisation process showed decreased $\boldsymbol{T_c}$ of *rPET-bg contaminated with 5%*, which tended to stabilise; this indicated influence of PP and change of crystallisation behaviour in the main matrix. *Non contaminated rPET-bg* displayed an ease of *crystallisation* at *lower cooling rate* and crystallised at higher

temperatures from the melt compared with *rPET-bg contaminated with 5%*, which displayed lower temperatures from the melt; this showed the influence of PP, which crystallises at lower temperature from the melt of the matrix, and consequently increasing the chains' mobility and stabilising and reducing the % crystallinity. It can be seen that the crystallisation of PP at lower temperature had an effect on the crystalline domains formation in *rPET-bg* matrix, and this shown by the reduction and stability of T_c and ΔH_c with increasing cooling rates. Furthermore, the stability tendency of crystallinity in the *rPET-bg contaminated with 5% PP,* indicated *fast* formation of heterogeneous *crystallites* of various densities, meaning that the crystallisation process was hindered by the time required at each cooling rate; the cooling time overridden the overall crystallisation process with increasing cooling rates. And the inclusion of PP retarded further the crystallisation process within the matrix, resulting in slight decrease of $\% X$.

	T_m (^oC)	ΔH_m ($J.g^{-1}$)	T_c (^oC)	ΔH_c ($J.g^{-1}$)	X_c (%)
Extruded Samples *rPET-bg contaminated with 5% PP* **compared to** *non contaminated rPET-bg*	↑	↓	↓ / St.	↓ / St.	↓ / St.

Table 7.15 Variation of Thermal Characteristics with cooling rates of rPET-bg contaminated with 5% PP

Where: ↑ means increase, ↓ means decrease and ↓ / St. decrease with stability.

It appears that the overall thermal characteristics were affected by the inclusion of *5% PP*, especially the *% crystallinity*. There is indication of change in molecular chains' mobility and crystallisation behaviour following the inclusion of *5% PP*, and to clarify the influence of PP on the crystallisation process of the rPET-bg matrix with increasing *cooling rates*, it is important to analyse this crystallisation process by existing theoretical models. The *Avrami* and *Ozawa equations* are well known for offering good explanations and describing the *crystallisation process* through the mechanism of *nucleation* and *growth* of crystallites for *non-isothermal processes*. These equations were used to describe the process of crystallisation and investigating the influence of *PP inclusion* in the *rPET-bg matrix*, as a result of variation of *cooling rates*

7.1.10 Validation by *Avrami Equation* for non-isothermal crystallisation

The *Avrami equation* is well known for *isothermal* crystallisation and can still offer good explanation in describing *non isothermal* crystallisation through the *mechanism* of *nucleation* and *growth* of crystallites. This equation, as described in *Section 1.2.3.2*, was used to describe the *non-isothermal* crystallisation at various *cooling rates* for *non contaminated rPET-bg* and *rPET-bg contaminated with 5% PP*.

The following table lists the data extracted at various cooling rates.

	Extruded Samples Non contaminated rPET-bg		Extruded Samples 95% rPET-bg / 5% PP	
Cooling Rate, ($^oC/min$)	***Time* (*min*)**	X_t	***Time* (*min*)**	X_t
10	0.99	0.013	0.97	0.010
	1.31	0.022	1.29	0.017
	1.44	0.027	1.46	0.023
	1.63	0.034	1.70	0.034
	1.88	0.041	1.96	0.044
15	0.93	0.013	0.97	0.028
	1.24	0.020	1.27	0.044
	1.37	0.024	1.42	0.056
	1.57	0.030	1.68	0.091
	1.83	0.044	2.03	0.144
20	0.97	0.012	0.88	0.026
	1.28	0.020	1.16	0.043
	1.40	0.023	1.28	0.054
	1.60	0.030	1.57	0.084
	1.93	0.047	1.88	0.135
25	1.00	0.015	0.80	0.025
	1.30	0.023	1.03	0.042
	1.42	0.027	1.08	0.052
	1.61	0.036	1.30	0.078
	1.86	0.051	1.80	0.130

Table 7.16 Relative Crystallinity and Time at Various Cooling Rates

Note: Additional Data are available in ***Appendix 7* (9)**.

Figures 7.15 and *7.16* below, showed sigmoid curves describing the relationship between cooling time and crystallisation. In the *non contaminated rPET-bg*, the increase of cooling rate allowed less time for the crystallisation process and resulted in gradual slow crystallisation. Whereas, in the *rPET-bg contaminated with 5% PP*, crystallisation increased faster with increasing cooling rates, but the crystallisation speed seemed very slow at low cooling rate because of the large allowable cooling time.

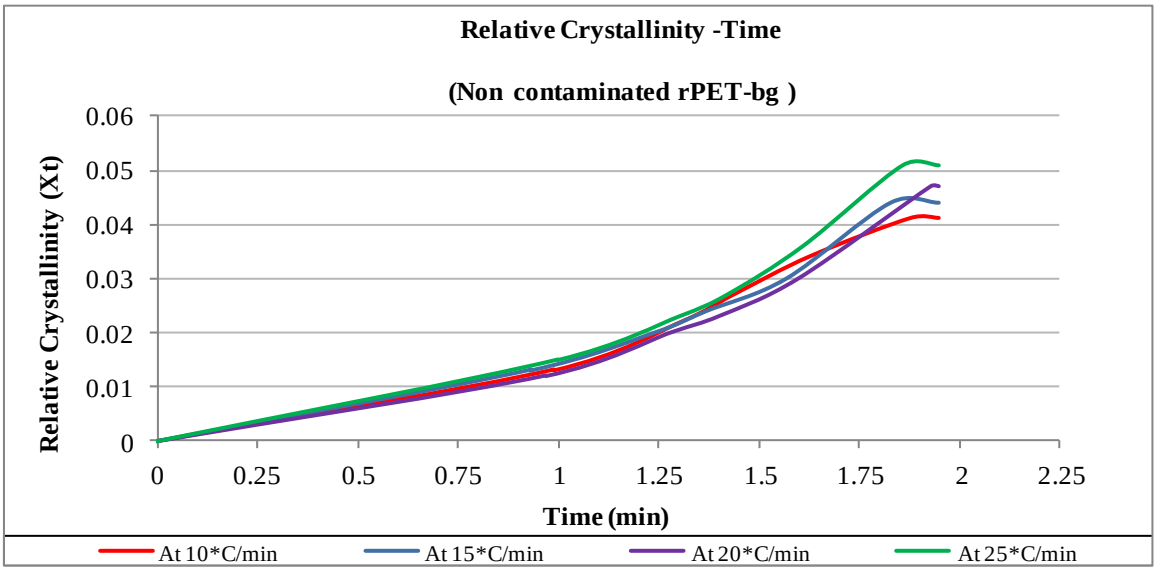

Figure 7.15 Relative Crystallinity Vs Time for Non-Isothermal Crystallisation at Various Cooling Rates of non contaminated rPET-bg

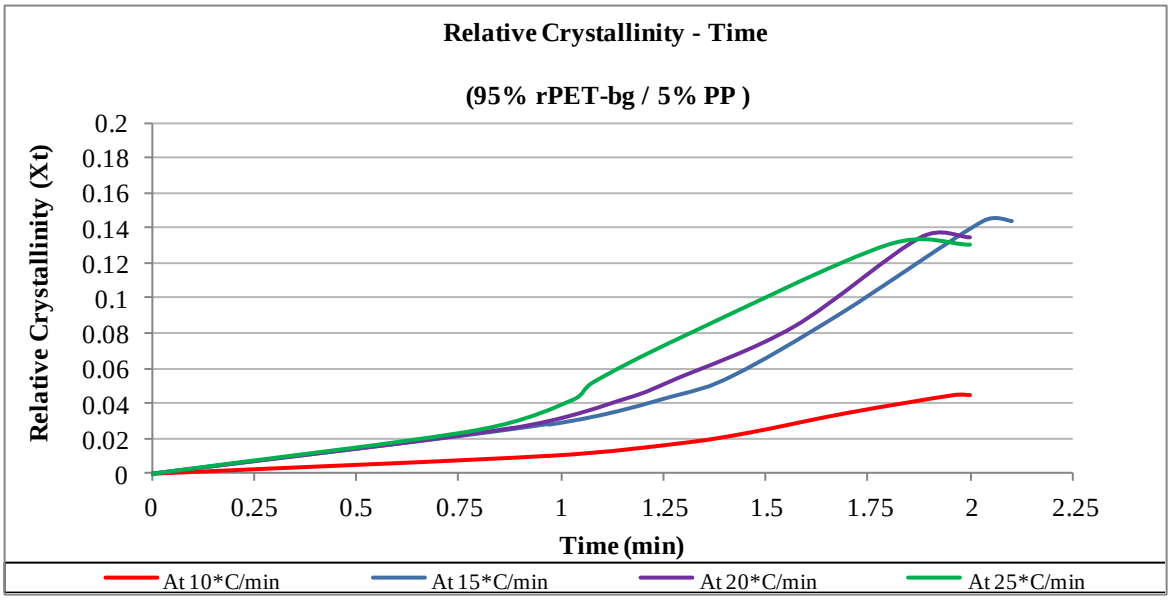

Figure 7.16 Relative Cryst. Vs Time for Non-Isothermal Crystallisation at Various Cooling Rates of rPET-bg contaminated with 5% PP

The following table lists the transformed data at various cooling rates.

	Extruded Samples Non contaminated rPET-bg		Extruded Samples 95% rPET-bg / 5% PP	
Cooling Rate, ($^oC/min$)	***log t***	***log(-ln(1-X_t)***	***log t***	***log(-ln(1-X_t)***
10	0.00	-1.879	-0.01	-2.000
	0.12	-1.650	0.11	-1.763
	0.16	-1.568	0.16	-1.627
	0.21	-1.465	0.23	-1.461
	0.27	-1.381	0.29	-1.345
15	-0.03	-1.896	-0.01	-1.553
	0.09	-1.700	0.10	-1.351
	0.14	-1.605	0.15	-1.236
	0.20	-1.521	0.23	-1.022
	0.26	-1.347	0.31	-0.808
20	-0.01	-1.925	-0.06	-1.578
	0.11	-1.721	0.06	-1.360
	0.15	-1.640	0.11	-1.257
	0.20	-1.512	0.19	-1.056
	0.29	-1.315	0.27	-0.837
25	0.00	-1.821	-0.10	-1.602
	0.11	-1.636	0.02	-1.371
	0.15	-1.561	0.04	-1.273
	0.21	-1.441	0.11	-1.089
	0.27	-1.285	0.25	-0.855

Table 7.17 Data at Various Cooling Rates

The curves in *Figures 7.17* and *7.18* showed the *straight portion* of the *Avrami primary phase* of crystallisation.

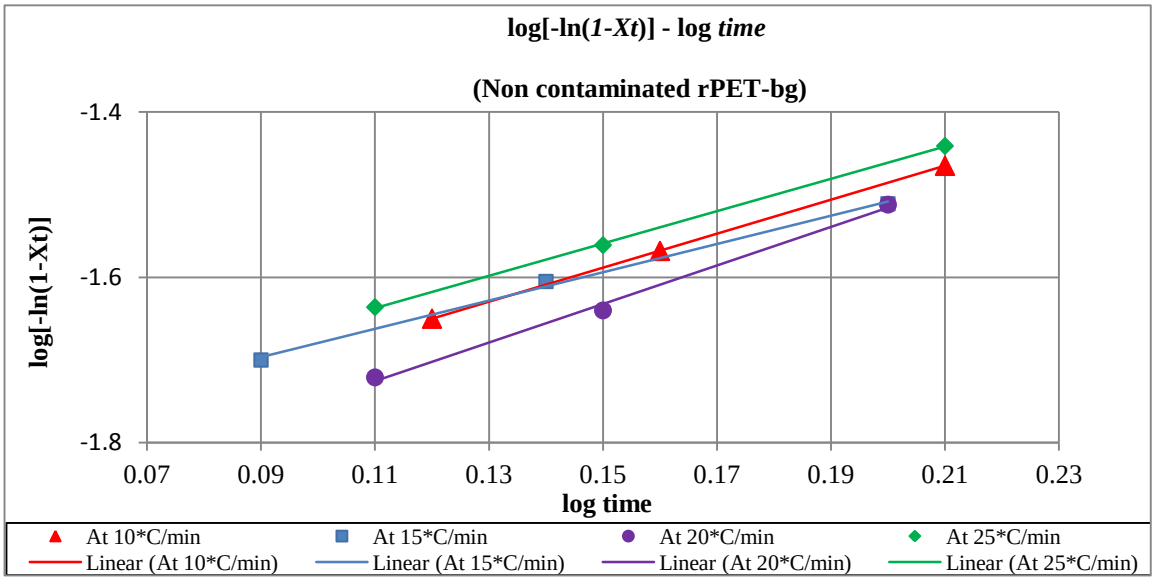

Figure 7.17 *Avrami* Plots of log [-ln(1-X_t)] Vs log t for Non-Isothermal Crystallisation at Various Cooling Rates of non contaminated rPET-bg

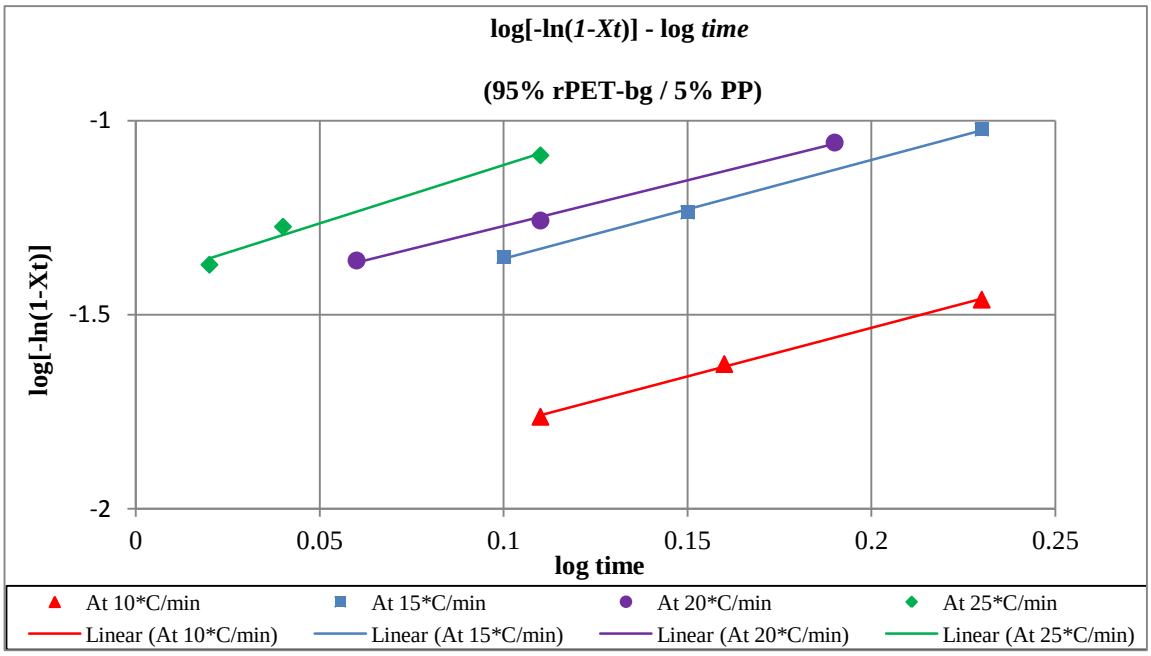

Figure 7.18 *Avrami* Plots of log [-ln(1-X_t)] Vs log t for Non-Isothermal Crystallisation at Various Cooling Rates of rPET-bg contaminated with 5% PP

The *Avrami exponent* ***n*** and the calculated $\boldsymbol{Z_C}$ from the *corrected* ***log*** $\boldsymbol{Z_C}$ which is calculated from the ***intercept log*** $\boldsymbol{Z_t}$; because of the influence of *cooling rates*, this *correction* is required for *non-isothermal crystallisation process*, as reported in the literature [45].

$$\log Z_C = \frac{\log Z_t}{a} \tag{1.11}$$

Where: ***a*** is the cooling rate.

As shown in *Table 7.18* below, the ***n*** values increased randomly and tended to stabilise with increasing cooling rates in the *non contaminated rPET-bg*, which indicated random nucleation and variation of spherulites from sporadic nuclei to disc and rod like, indicating random, slow and complex crystallisation process. The crystallisation time is inversely proportional to the rate of crystallisation, as reported by *Kim et al.* [19], i.e. a higher *cooling rate* resulted in lower *crystallisation time* accompanied by a higher *rate* of *growth* of crystallites, $\boldsymbol{Z_C}$. So, the low $\boldsymbol{Z_C}$ values of the *non contaminated rPET-bg*, accounted for *slow crystallisation.*

Whereas, in the *rPET-bg contaminated with 5% PP*, as shown in *Table 7.19* below, the ***n*** values increased randomly and the spherulites growth varied from sporadic nuclei to spherulitic, indicating that nucleation and growth in the *latter* were faster than in the *earlier*, as shown in *Figures 7.19* and 7.20 below, from which one can see that both nucleation and growth increased with increasing cooling rates. By increasing cooling rates, and because of the fast crystallisation, the area under the exotherm filled quickly with crystallites, which confirmed the lower temperature of crystallisation in the *rPET-bg contaminated with 5% PP* compared to the *non contaminated rPET-bg* and confirmed that the *non contaminated rPET-bg* was crystallising slower than the *rPET-bg contaminated with 5% PP* with increasing cooling rates. The random distribution of the ***n*** values in both materials showed that the mechanism of nucleation seemed more complex because of the irregular growth rate of crystallites. Also, the inclusion of 5% PP influenced the crystallisation mechanism of the rPET-bg matrix by increasing both nucleation and growth rates compared to non contaminated rPET-bg.

Extruded Samples **Non contaminated rPET-bg**				
Cooling Rates ($^oC/min$)	***n***	***Nucleation Characteristics***	***Type***	***Z_C*** **(min.$^oC^{-1}$)**
10	2.055	(n = 2) - Rod-Shaped Growth from Sporadic Nuclei (n =2)- Disc- Shaped Growth from Instantaneous Nuclei (n = 3) - Disc-Shaped Growth from Sporadic Nuclei	1 D 2 D 3 D	0.646
15	1.713	(n < 2) - Sporadic Nucleation		0.753
20	2.332	(n = 2) - Rod-Shaped Growth from Sporadic Nuclei (n = 2)- Disc- Shaped Growth from Instantaneous Nuclei (n = 3) - Disc-Shaped Growth from Sporadic Nuclei	1 D 2 D 3 D	0.796
25	1.954	(n < 2) - Sporadic Nucleation		0.843

Table 7.18 *Avrami's* ***n*** and Z_C for non-isothermal Crystallisation of non contaminated rPET-bg

Extruded Samples **95% rPET-bg / 5% PP**				
Cooling Rates ($^oC/min$)	***n***	***Nucleation Characteristics***	***Type***	***Z_C*** **(min.$^oC^{-1}$)**
10	2.507	(n = 2) - Rod-Shaped Growth from Sporadic Nuclei	1 D	0.626
15	2.544	(n =2)- Disc- Shaped Growth from Instantaneous Nuclei	2 D	0.781
20	2.355	(n = 3) - Disc-Shaped Growth from Sporadic Nuclei	3 D	0.841
25	3.002	(n = 3) - Disc-Shaped Growth from Sporadic Nuclei (n = 3) - Spherilitic Growth from Instantaneous	2 D 3 D	0.878

Table 7.19 *Avrami's* ***n*** and Z_C for non-isothermal Crystallisation of rPET-bg contaminated with 5% PP

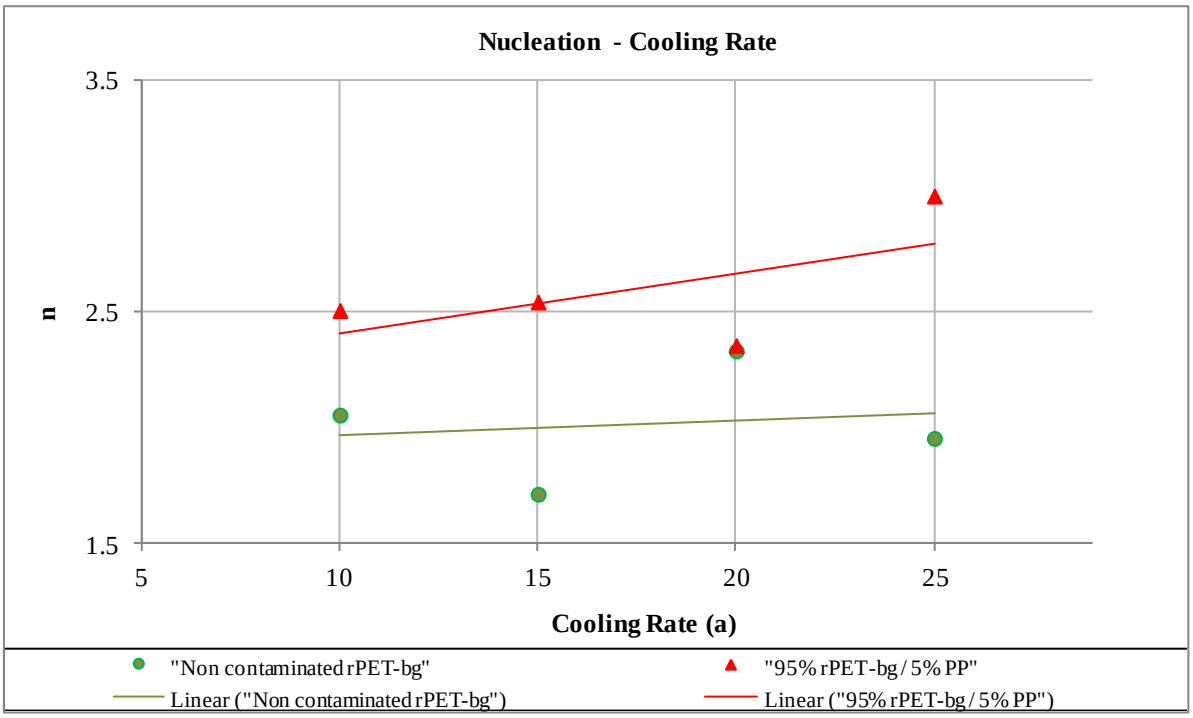

Figure 7.19 *Avrami's Exponent, n,* at Various Cooling Rates for Non-Isothermal Crystallisation

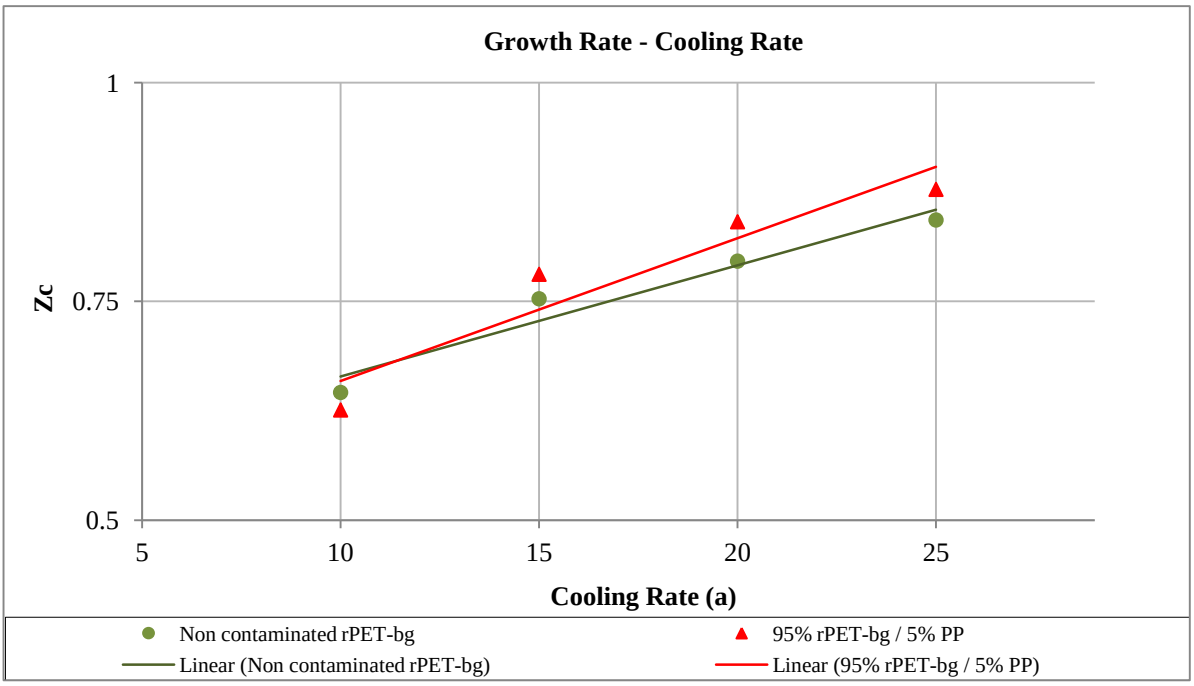

Figure 7.20 *Avrami's Growth Rate,* Z_C, at Various Cooling Rates for Non-Isothermal Crystallisation

7.1.11 Validation by *Ozawa Equation* for non-isothermal crystallisation

The *Ozawa equation*, which was extended from the *Avrami equation*, is used in describing the *non-isothermal crystallisation*, as previously described in *Section 1.2.3.2*. The *Ozawa exponent*, ***m***, and the K_T parameter described the *mechanism* of *crystallisation* under *non-isothermal crystallisation* condition during the variation of *cooling rates* for *non contaminated rPET-bg* and *rPET-bg contaminated with 5% PP*.

The following table lists the data extracted at various cooling rates.

		Extruded Samples Non contaminated rPET-bg	Extruded Samples 95% rPET-bg / 5% PP
Cooling Rate, ($^oC/min$)	**Temp. (^oC)**	X_T	X_T
10	212	0.013	0.010
	210	0.022	0.017
	209	0.027	0.023
	208	0.034	0.034
	206	0.041	0.044
15	212	0.013	0.028
	210	0.020	0.044
	209	0.024	0.056
	208	0.030	0.091
	206	0.044	0.144
20	212	0.012	0.026
	210	0.012	0.043
	209	0.023	0.054
	208	0.029	0.084
	206	0.047	0.135
25	212	0.015	0.025
	210	0.023	0.042
	209	0.027	0.052
	208	0.036	0.078
	206	0.051	0.130

Table 7.20 Relative Crystallinity and Temperatures at Various Cooling Rates

In *Figures 7.21* and *7.22* below, the curves obeyed the Ozawa pattern and described the relationship between cooling temperature and crystallisation. In the *non contaminated rPET-bg*, the increase of cooling rate allowed an unbalanced decrease of crystallisation with temperature. Whereas, in the *rPET-bg contaminated with 5% PP*, crystallisation increased faster with increasing cooling rates and decreasing temperature, but very slow crystallisation can be seen at low cooling rate.

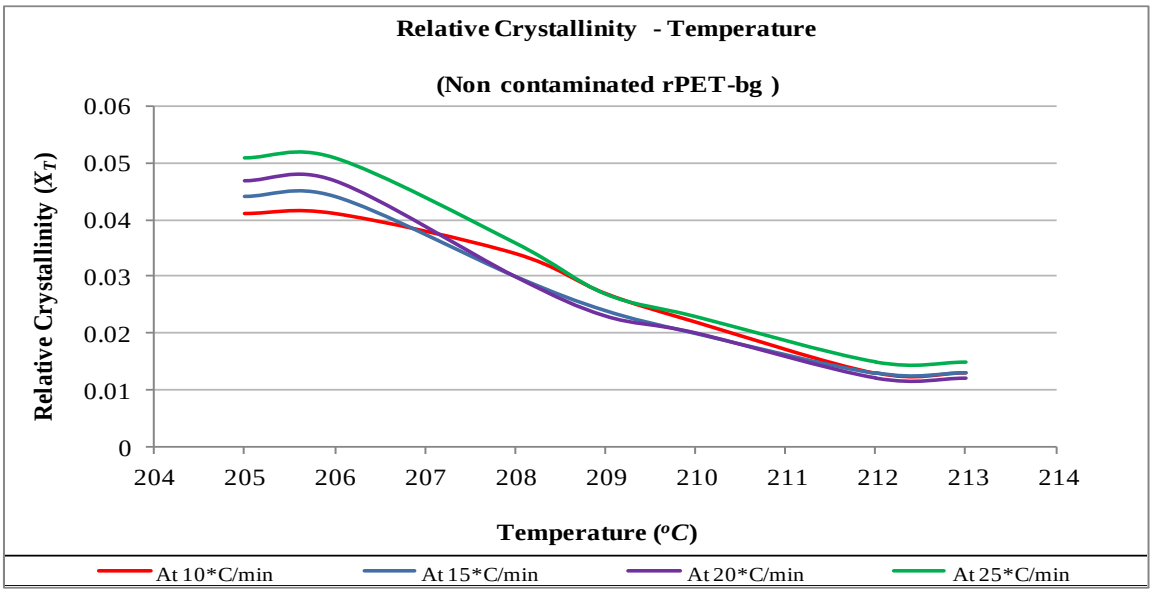

Figure 7.21 Relative Crystallinity Vs Temperature for Non-Isothermal Crystallisation at Various Cooling Rates of non contaminated rPET-bg

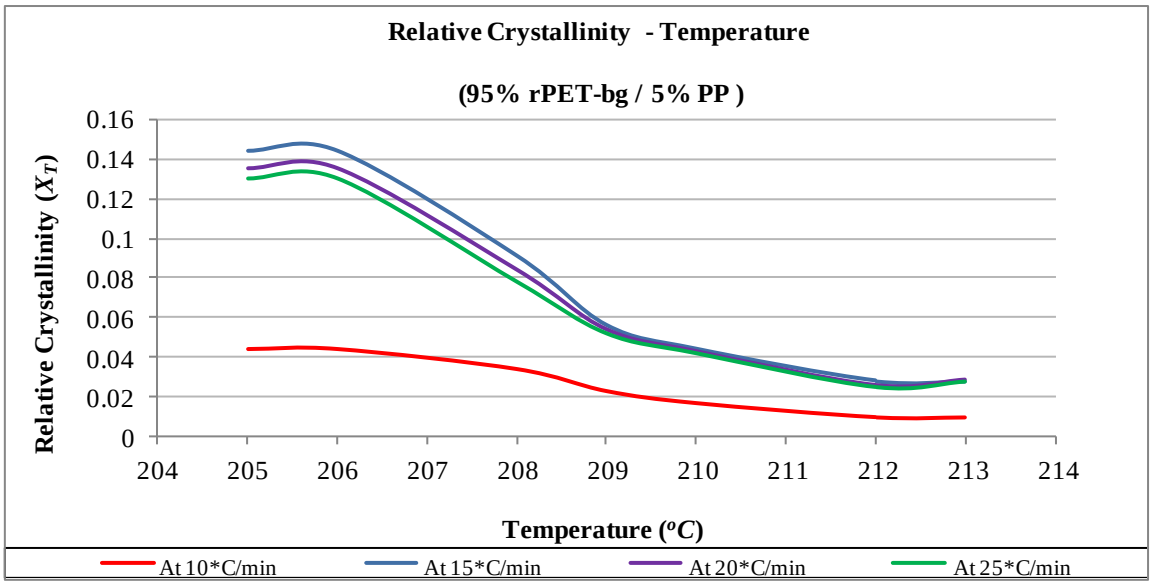

Figure 7.22 Relative Crystallinity Vs Temperature for Non-Isothermal Crystallisation at Various Cooling Rates of rPET-bg contaminated with 5% PP

The following table lists the transformed data at various cooling rates.

			Extruded Samples Non cont. rPET-bg	Extruded Samples 95% rPET-bg / 5% PP
Cooling Rate, (*a*) (*$^oC/min$*)	**Temp. (*^oC*)**	***log a***	***log(-ln(1-X_T)***	***log(-ln(1-X_T)***
10	**212**	1.000	-1.879	-2.000
15		1.176	-1.896	-1.553
20		1.301	-1.925	-1.578
25		1.398	-1.821	-1.602
10	**210**	1.000	-1.650	-1.763
15		1.176	-1.700	-1.351
20		1.301	-1.721	-1.360
25		1.398	-1.636	-1.371
10	**209**	1.000	-1.568	-1.627
15		1.176	-1.605	-1.236
20		1.301	-1.640	-1.257
25		1.398	-1.561	-1.273
10	**208**	1.000	-1.465	-1.461
15		1.176	-1.521	-1.022
20		1.301	-1.526	-1.056
25		1.398	-1.441	-1.089
10	**206**	1.000	-1.381	-1.345
15		1.176	-1.347	-0.808
20		1.301	-1.315	-0.837
25		1.398	-1.285	-0.855

Table 7.21 Other Data at Various Cooling Rates and Various Temperatures

The curves in *Figures 7.23* and *7.24* showed *Ozawa's negative straight line* of the relationship crystallisation – cooling rates. The curve at *206°C* did not obey the rule of *Ozawa equation* of negative exponent; this may be attributed to the fact that the slow secondary crystallisation was not considered and this could result in this non conformance or it could be that the measurements taken were at the end (Plateau) of the crystallisation.

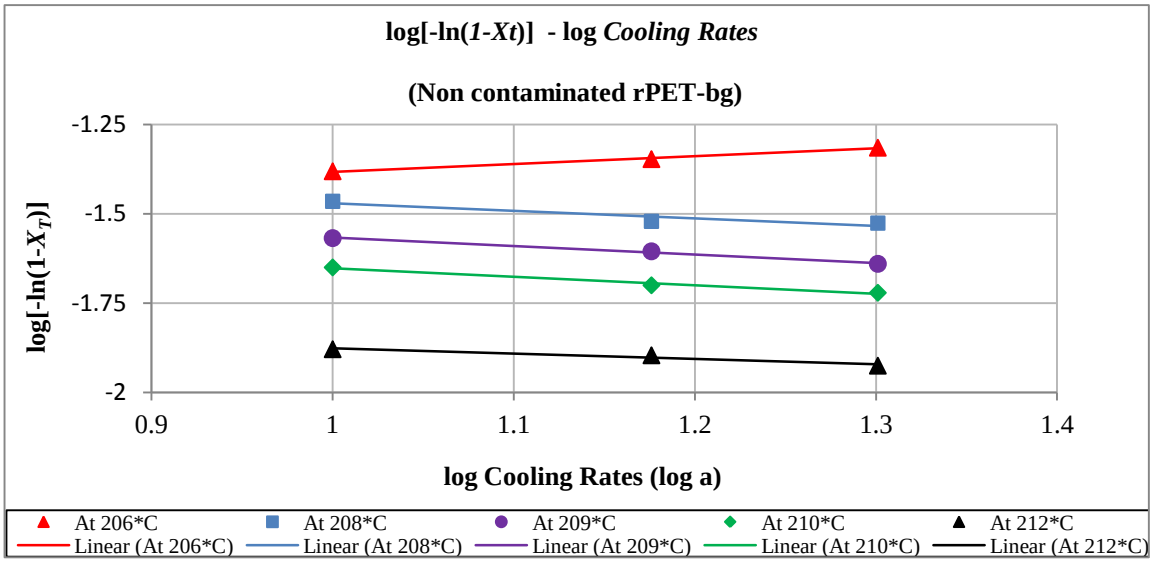

Figure 7.23 *Ozawa* Plots of log[-ln(1-X_T)] Vs log Cooling Rates of non contaminated rPET-bg

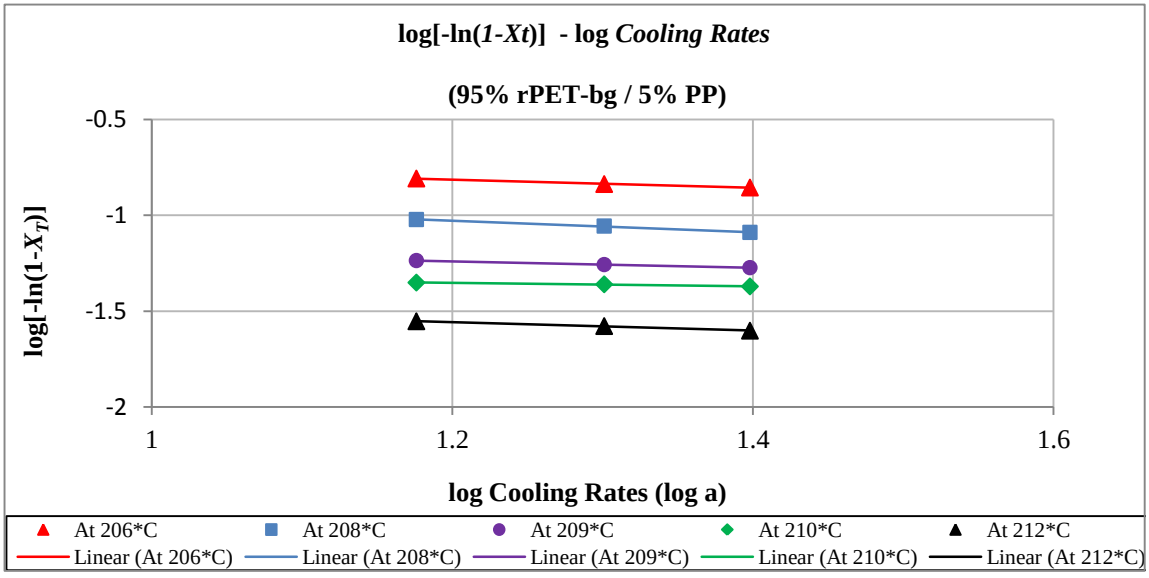

Figure 7.24 *Ozawa* Plots of log[-ln(1-X_T)] - log Cooling Rates of rPET-bg contaminated With 5% PP

The Ozawa exponent ***m*** and rate of growth $\boldsymbol{K_T}$ as a function of cooling temperatures were extracted from the *linear curves' equations* in *Figures 7.23* and *7.24* above.
As shown in *Tables 7.22* and *7.23*, the *Ozawa exponent*, ***m***, in both materials had very low values and fluctuated randomly with decreasing cooling temperatures from the melt; this is attributed to the unbalanced nucleation and imperfect crystals in the materials. The *non contaminated rPET-bg* randomly displayed lower values than the *rPET-bg contaminated with 5% PP*, showing that at a given temperature but under different cooling rates, the high crystallisation could be just at the latest or earliest stage of cooling, as showed by the increased rate of growth with decreasing temperatures. Nucleation in both materials decreased with decreasing temperature, as shown in *Figure 7.25* below, which suggested sporadic nuclei could occur at high temperatures from the melt, and the *inclusion* of *PP* promoted further this sort of nucleation and shown by the pronounced growth rate of spherullites in *Figure 7.18* below. Low $\boldsymbol{K_T}$ values, i.e. growth rate values, indicate the degree of transparency in amorphous *PET* as reported by *Jabarin* [20], and both materials displayed low values of $\boldsymbol{K_T}$ and also showed slow crystallisation process. Furthermore, the growth rate in *non contaminated rPET-bg*, as shown in *Figures 7.26* below, was much lower than in *rPET-bg contaminated with 5% PP*, which accounted for *slower crystallisation* compared to *faster crystallisation* of the *latter*, i.e. the *non contaminated rPET-bg* tended to crystallise less than *rPET-bg contaminated with 5% PP* with decreasing temperature.

Extruded Samples **Non contaminated rPET-bg**		
Temp. **(^oC)**	**- *m***	**K_T**
206	+0.218	0.025
208	-0.210	0.055
209	-0.237	0.047
210	-0.239	0.039
212	-0.149	0.019

Table 7.22 *Ozawa's* **-*m*** and K_T for non-isothermal Crystallisation of non contaminated rPET-bg

Extruded Samples **95% rPET-bg / 5% PP**		
Temp. **(^oC)**	**- *m***	**K_T**
206	-0.213	0.276
208	-0.300	0.215
209	-0.167	0.091
210	-0.089	0.057
212	-0.220	0.051

Table 7.23 *Ozawa's* **-*m*** and K_T for non-isothermal Crystallisation of rPET-bg contaminated with 5% PP

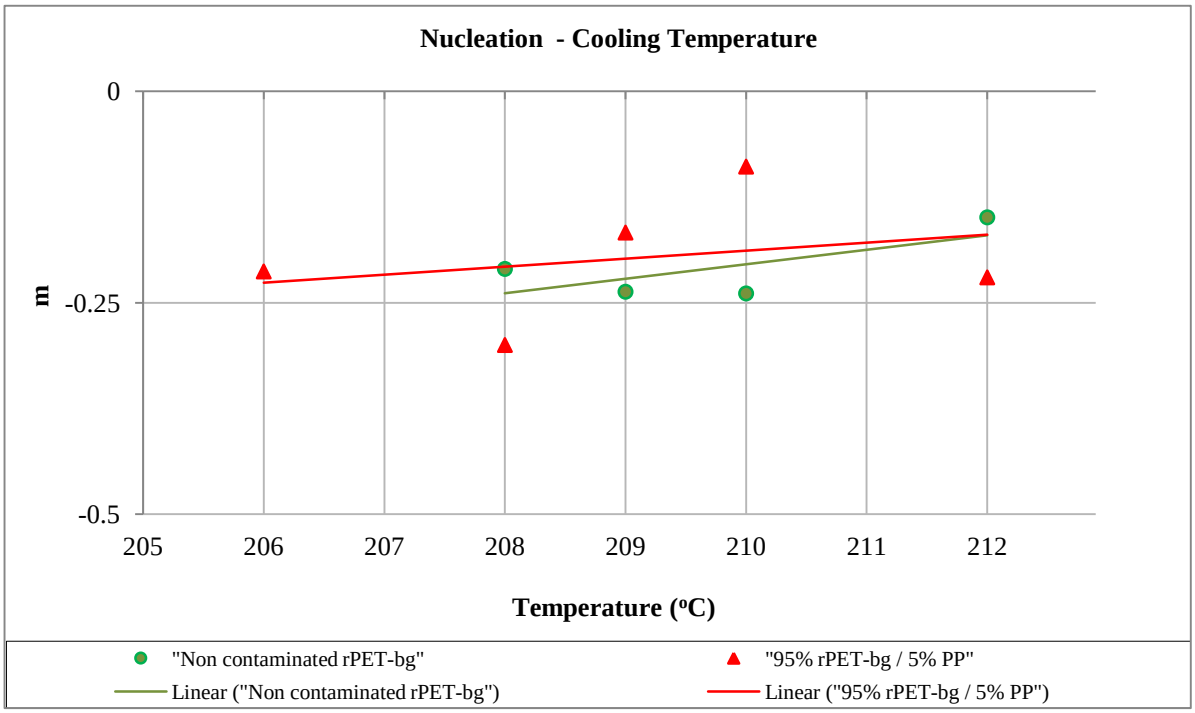

Figure 7.25 *Ozawa's Exponent, m,* at Various Cooling Temperatures for Non-Isothermal Crystallisation

Note: The ***positive m*** value at $206^{o}C$ for rPET-bg did not obey the rule and was removed.

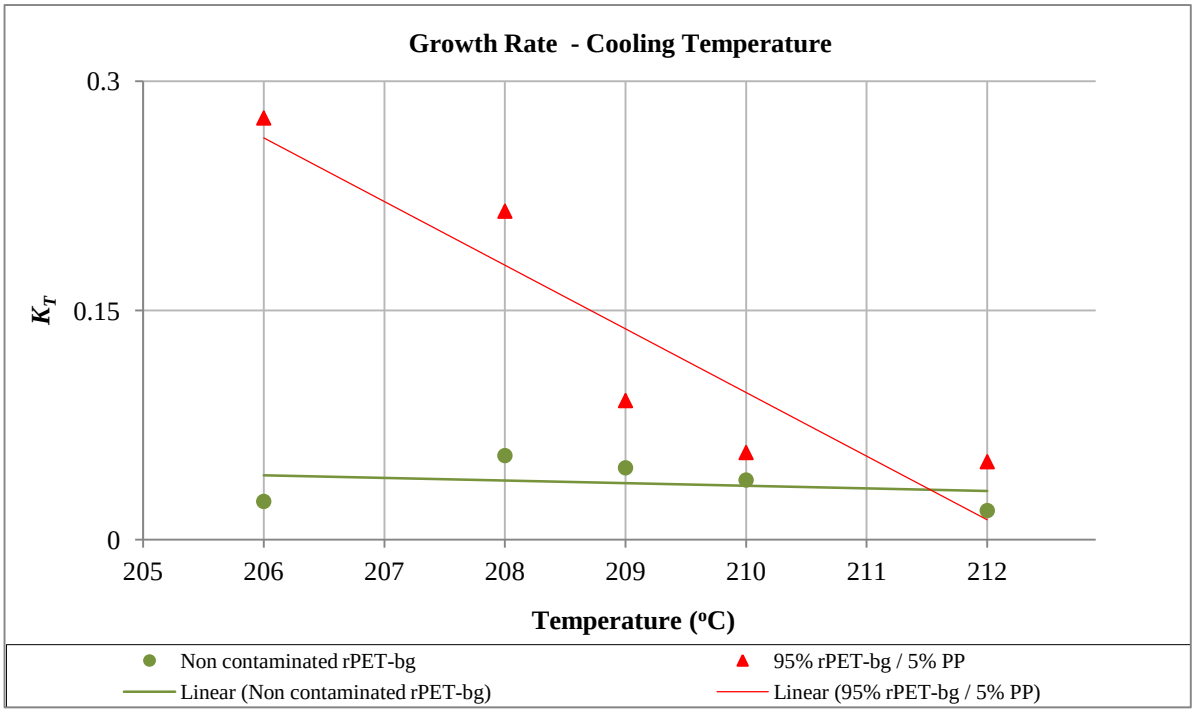

Figure 7.26 *Ozawa's Growth Rate,* K_T, at Various Cooling Temperatures for Non-Isothermal Crystallisation

7.2 Conclusion

In light of the above investigation, it was shown that the inclusion of 5% *PP* influenced the thermal characteristics of the *rPET-bg matrix*, especially *crystallinity* which decreased with tendency of stabilising with increasing cooling rates. This is confirmed by the *DSC* work performed on *extruded samples* of *rPET-bg contaminated with 5% PP* at various *cooling rates*. Also the *Avrami* and *Ozawa models* confirmed the outcome of the results obtained and showed that the crystallisation process depended on many influencing factors, such as impurities, nucleation and growth rates. The crystallisation process of the *rPET-bg* with and without *PP contamination* indicated that *nucleation* and *molecular mobility* increased with increasing *temperature* and *cooling rates*, whereas the *growth rate* decreased with increasing *temperature* and increased with increasing *cooling rates*. Throughout the crystallisation process, the *small amount* of *PP*, played dominant role in *increasing* the *chain mobility* in the *non contaminated rPET-bg matrix* and consequently stabilising and slightly increasing the degree of crystallinity.

Stage 2

Chapter 8

Effect of *repetitive extrusions* on the *thermal characteristics* of *non contaminated rPET-bg* and *rPET-bg contaminated with 5% PP*

8.1 Results and Discussion

This section discusses the various experimental results obtained in *experiment 10*; where *samples* of non contaminated rPET-bg and the *selected batch* of *stage 1*, i.e. rPET-bg contaminated with *5%* PP, were *repetitively extruded* for *5 cycles* and thermally analysed by DSC at a constant *heating / cooling rate* of $10^{o}C/min$ and isothermally kept for *2 minutes* at $300^{o}C$ to complete melting, as described in *Experiment 10, Section 3.2.1.2* and *Experiment 10, Section 3.4*, and their thermal *characteristics* investigated, especially *crystallinity* which was analysed by *Avrami equation* for *non-isothermal crystallisation* process, as described in *Section 1.2.3.2*.

The results were assessed statistically, validated and compared with other literatures and research works. The results are displayed first and then discussed as below.

8.1.1 DSC Results of *non contaminated rPET-bg* for *5 re-extrusion cycles*

In *experiments 10*, the DSC analysis yielded the data below.

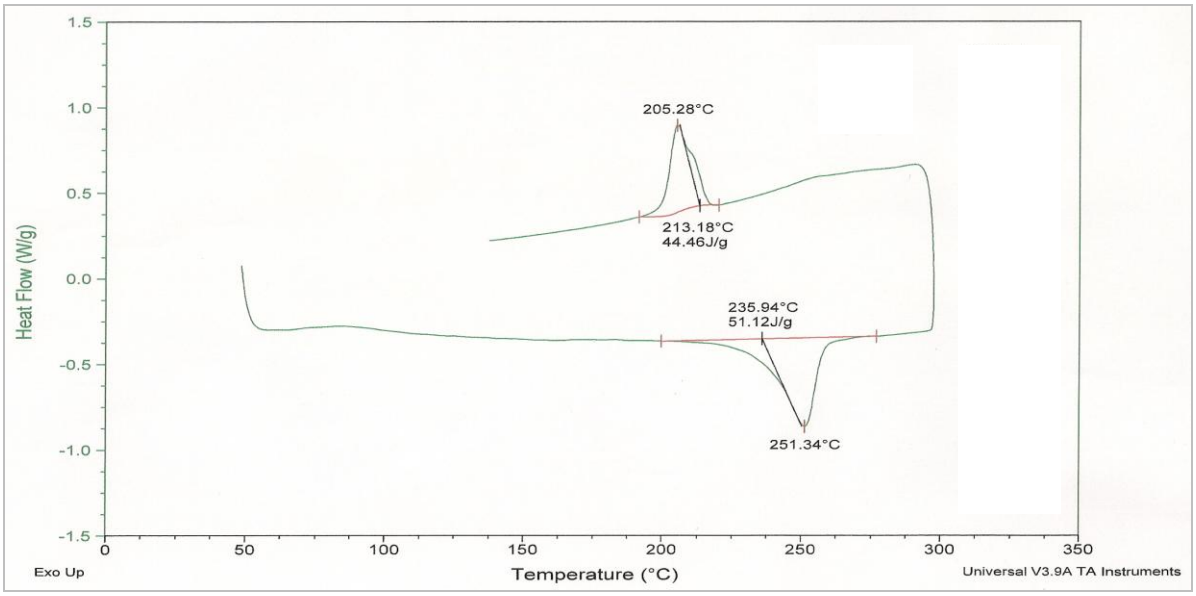

Figure 8.1 Thermogram of Extruded Samples of non contaminated rPET-bg
- 1st re-extrusion cycle -

	T_m (^{o}C)	ΔH_m (J.g^{-1})	T_c (^{o}C)	ΔH_c (J.g^{-1})	ΔH_m^0 (J.g^{-1}	X_c (%)
Material	**Re-extruded Samples of non contaminated rPET-bg at 10^{o}C/min (Cycle 1)**					
Mean (μ)	**251.34**	**49.64**	**205.28**	**43.43**	**140**	**31.02**
STDEV (σ)	0.00	2.09	0.00	1.46		1.04
ST. Error ($S_E = \sigma/n^{0.5}$)	0.00	1.48	0.00	1.03		0.74
CI (95%), ($\mu \pm 1.96 S_E$)	$\mu \pm 0.00$	$\mu \pm 2.90$	$\mu \pm 0.00$	$\mu \pm 2.02$		$\mu \pm 1.44$

Table 8.1 Samples of non contaminated rPET-bg - Re-extrusion Cycle 1

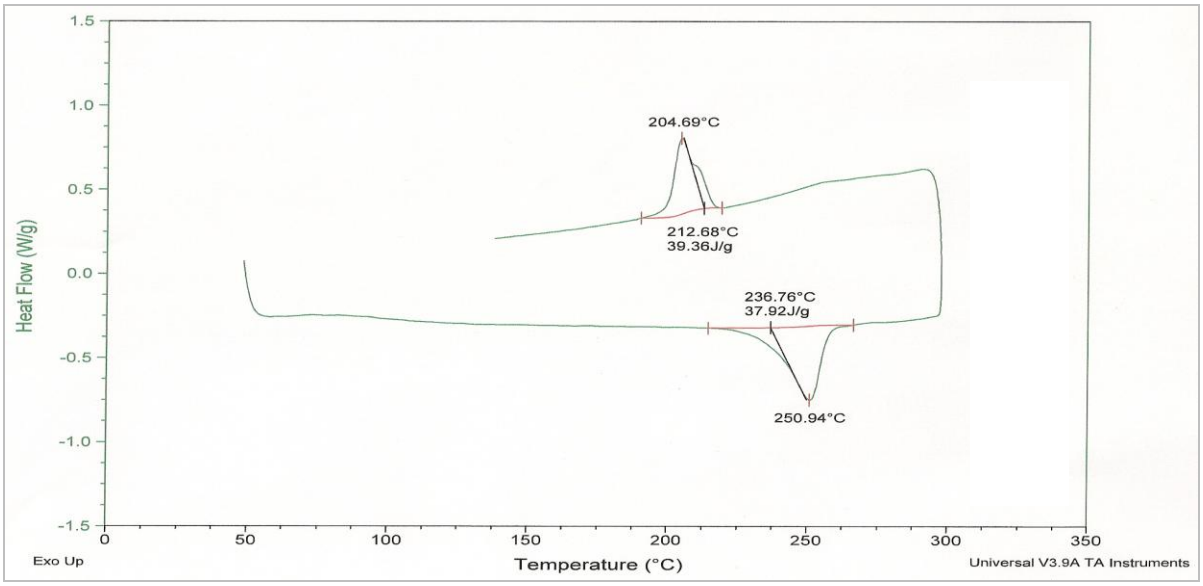

Figure 8.2 Thermogram of Extruded Sample 1 of non contaminated rPET-bg
- 2nd re-extrusion cycle -

	T_m (^oC)	ΔH_m ($J.g^{-1}$)	T_c (^oC)	ΔH_c ($J.g^{-1}$)	ΔH_m^0 ($J.g^{-1}$	X_c (%)
Material	**Re-extruded Samples of non contaminated rPET-bg at 10°C/min (Cycle 2)**					
Mean (μ)	**250.94**	**37.94**	**204.69**	**38.00**	**140**	**27.14**
STDEV (σ)	0.00	0.03	0.00	1.93		1.38
ST. Error ($S_E = \sigma/n^{0.5}$)	0.00	0.02	0.00	1.36		0.98
CI (95%), ($\mu \pm 1.96 S_E$)	$\mu \pm 0.00$	$\mu \pm 0.04$	$\mu \pm 0.00$	$\mu \pm 2.68$		$\mu \pm 1.91$

Table 8.2 Samples of non contaminated rPET-bg - Re-extrusion Cycle 2

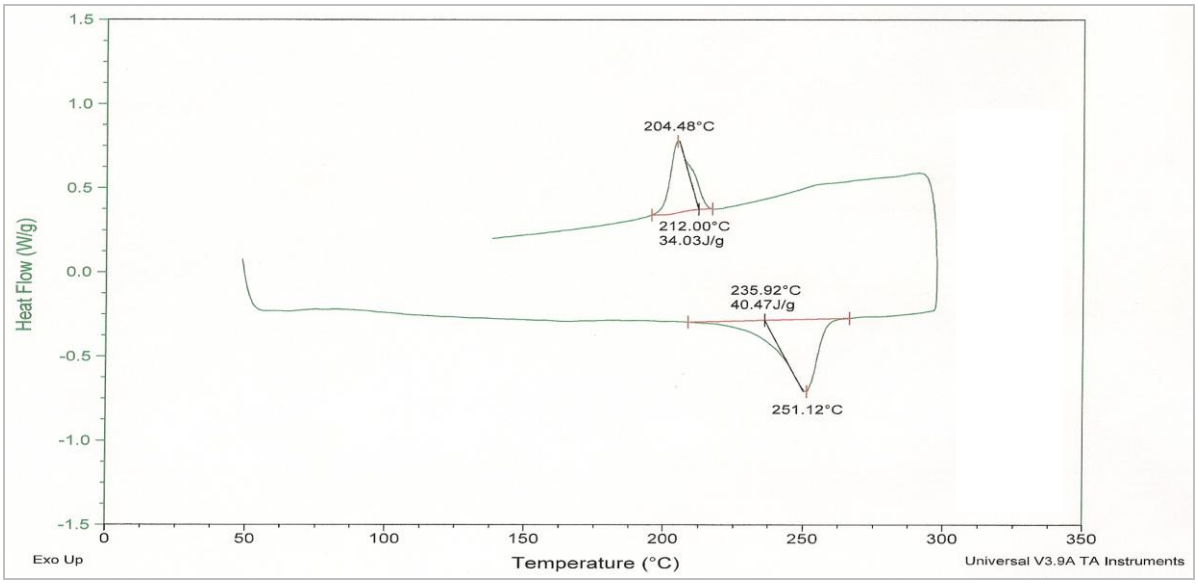

Figure 8.3 Thermogram of Extruded Sample 1 of non contaminated rPET-bg
- 3rd re-extrusion cycle -

	T_m (°C)	ΔH_m (J.g^{-1})	T_c (°C)	ΔH_c (J.g^{-1})	ΔH_m^0 (J.g^{-1}	X_c (%)
Material	**Re-extruded Samples of non contaminated rPET-bg at 10°C/min (Cycle 3)**					
Mean (μ)	**251.12**	**42.01**	**204.48**	**35.20**	**140**	**25.14**
STDEV (σ)	0.00	2.18	0.00	1.65		1.18
ST. Error ($S_E = \sigma/n^{0.5}$)	0.00	1.54	0.00	1.17		0.83
CI (95%), ($\mu \pm 1.96 S_E$)	$\mu \pm 0.00$	$\mu \pm 3.02$	$\mu \pm 0.00$	$\mu \pm 2.28$		$\mu \pm 1.63$

Table 8.3 Samples of non contaminated rPET-bg - Re-extrusion Cycle 3

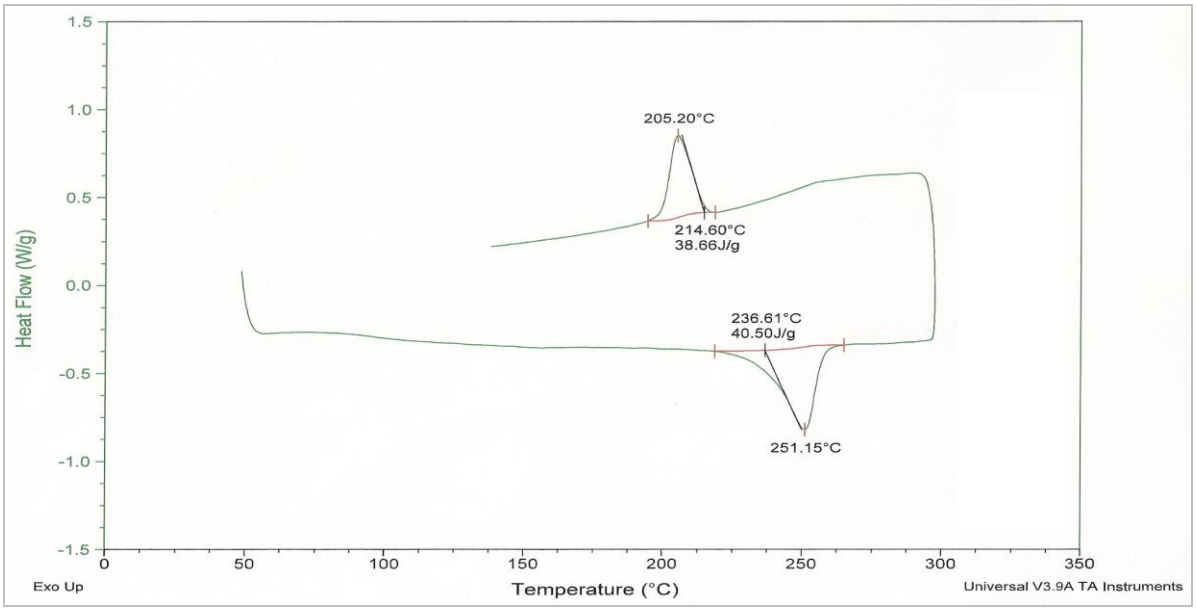

Figure 8.4 Thermogram of Extruded Sample 1 of non contaminated rPET-bg - 4th re-extrusion cycle -

	T_m (^oC)	ΔH_m ($J.g^{-1}$)	T_c (^oC)	ΔH_c ($J.g^{-1}$)	ΔH_m^0 ($J.g^{-1}$	X_c (%)
Material	**Re-extruded Samples of non contaminated rPET-bg at 10°C/min (Cycle 4)**					
Mean (μ)	**251.15**	**41.82**	**205.20**	**39.49**	**140**	**28.20**
STDEV (σ)	0.00	1.86	0.00	1.17		0.83
ST. Error ($S_E = \sigma/n^{0.5}$)	0.00	1.32	0.00	0.82		0.59
CI (95%), ($\mu \pm 1.96 S_E$)	$\mu \pm 0.00$	$\mu \pm 2.58$	$\mu \pm 0.00$	$\mu \pm 1.62$		$\mu \pm 1.15$

Table 8.4 Samples of non contaminated rPET-bg - Re-extrusion Cycle 4

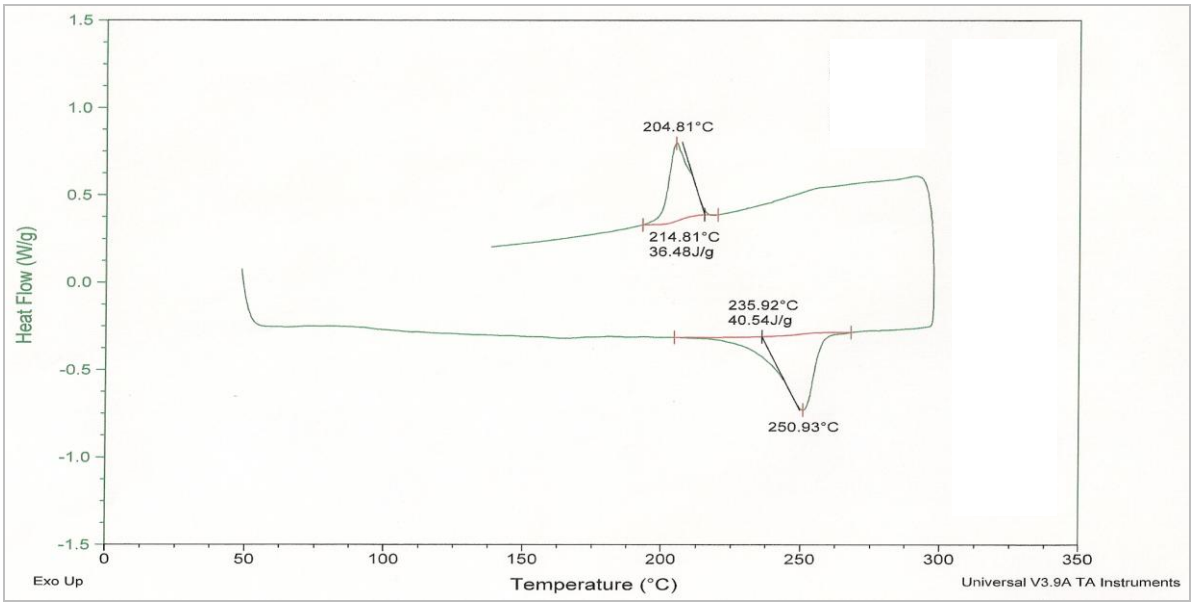

Figure 8.5 Thermogram of Extruded Sample 1 of non contaminated rPET-bg
- 5th re-extrusion cycle -

	T_m (^oC)	ΔH_m ($J.g^{-1}$)	T_c (^oC)	ΔH_c ($J.g^{-1}$)	ΔH_m^0 ($J.g^{-1}$	X_c (%)
Material	**Re-extruded Samples of non contaminated rPET-bg at 10°C/min (Cycle 5)**					
Mean (μ)	**250.93**	**39.35**	**204.88**	**35.72**	**140**	**25.51**
STDEV (σ)	0.00	1.69	0.09	1.08		0.77
ST. Error ($S_E = \sigma/n^{0.5}$)	0.00	1.20	0.06	0.77		0.55
CI (95%), ($\mu \pm 1.96 S_E$)	$\mu \pm 0.00$	$\mu \pm 2.34$	$\mu \pm 0.13$	$\mu \pm 1.50$		$\mu \pm 1.07$

Table 8.5 Samples of non contaminated rPET-bg - Re-extrusion Cycle 5

8.1.2 DSC Results of *rPET-bg contaminated with 5% PP* for *5 re-extrusion cycles*

In *experiments 10*, the DSC analysis yielded the data below.

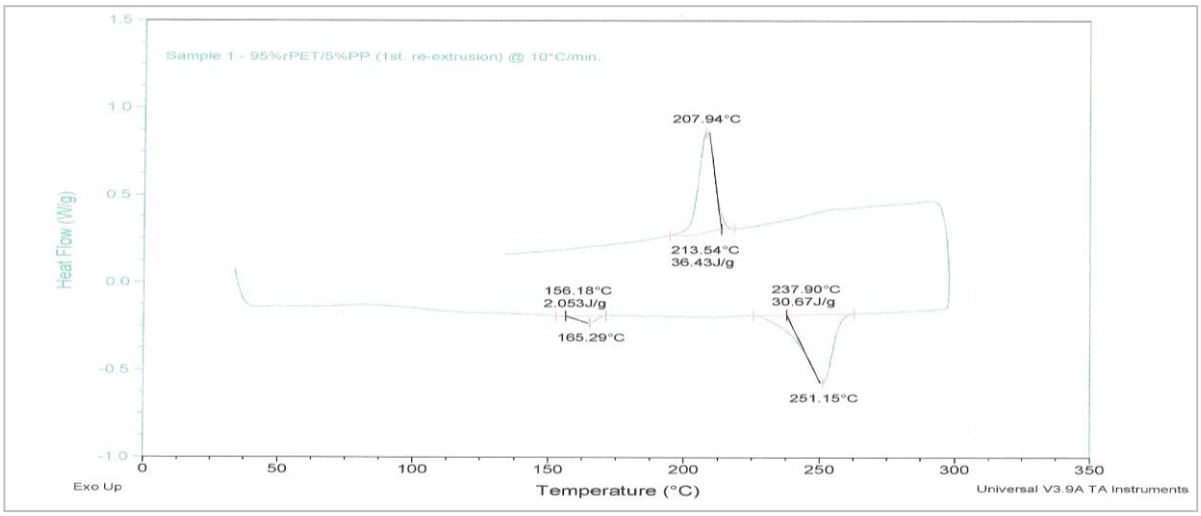

Figure 8.6 Thermogram of Extruded Sample 1 of rPET-bg contaminated with 5% PP - 1st re-extrusion cycle -

	T_m (^{o}C)	ΔH_m (J.g^{-1})	T_c (^{o}C)	ΔH_c (J.g^{-1})	ΔH_m^0 (J.g^{-1})	X_c (%)
Material	**Re-extruded Samples of 95% rPET-bg / 5% PP at 10^{o}C/min (Cycle 1)**					
Mean (μ)	**250.94**	**31.13**	**207.16**	**34.67**	**140**	**24.76**
STDEV (σ)	0.49	0.42	1.12	1.73		1.23
ST. Error ($S_E = \sigma/n^{0.5}$)	0.28	0.24	0.65	1.00		0.71
CI (95%), ($\mu \pm 1.96 S_E$)	$\mu \pm 0.55$	$\mu \pm 0.47$	$\mu \pm 1.27$	$\mu \pm 1.95$		$\mu \pm .40$

Table 8.6 Samples of rPET-bg contaminated with 5% PP - Re-extrusion Cycle 1

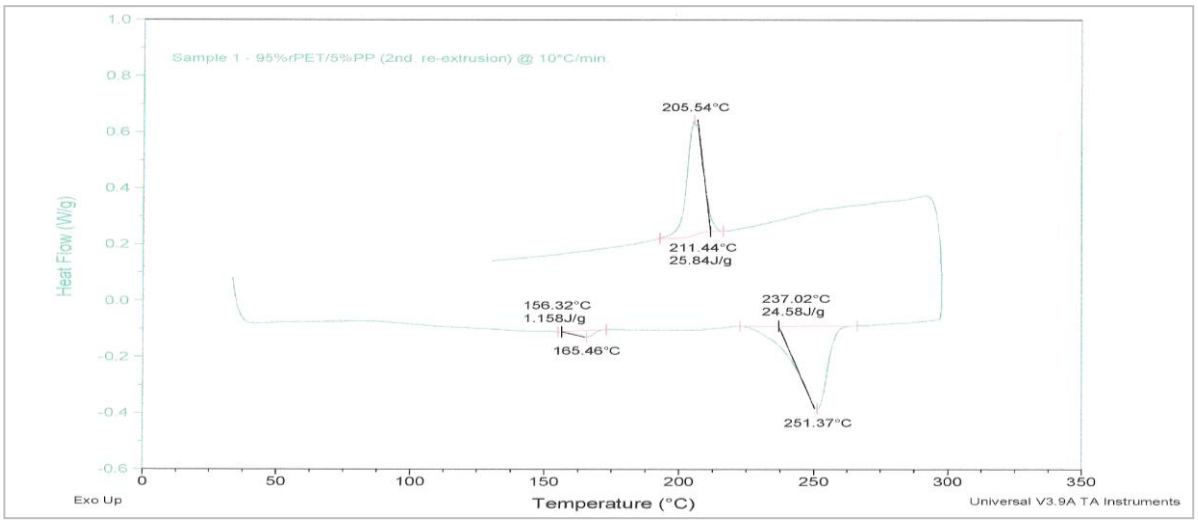

Figure 8.7 Thermogram of Extruded Sample 1 of rPET-bg contaminated with 5% PP - 2nd re-extrusion cycle -

	T_m (^{o}C)	ΔH_m (J.g^{-1})	T_c (^{o}C)	ΔH_c (J.g^{-1})	ΔH_m^0 (J.g^{-1}	X_c (%)
Material	**Re-extruded Samples of 95% rPET-bg / 5% PP at 10^{o}C/min (Cycle 2)**					
Mean (μ)	**251.02**	**22.08**	**205.62**	**23.89**	**140**	**17.07**
STDEV (σ)	0.36	2.83	0.20	3.31		2.37
ST. Error ($S_E = \sigma/n^{0.5}$)	0.21	1.63	0.11	1.91		1.37
CI (95%), ($\mu \pm 1.96 S_E$)	$\mu \pm 0.41$	$\mu \pm 3.20$	$\mu \pm 0.22$	$\mu \pm 3.75$		$\mu \pm 0.68$

Table 8.7 Samples of rPET-bg contaminated with 5% PP - Re-extrusion Cycle 2

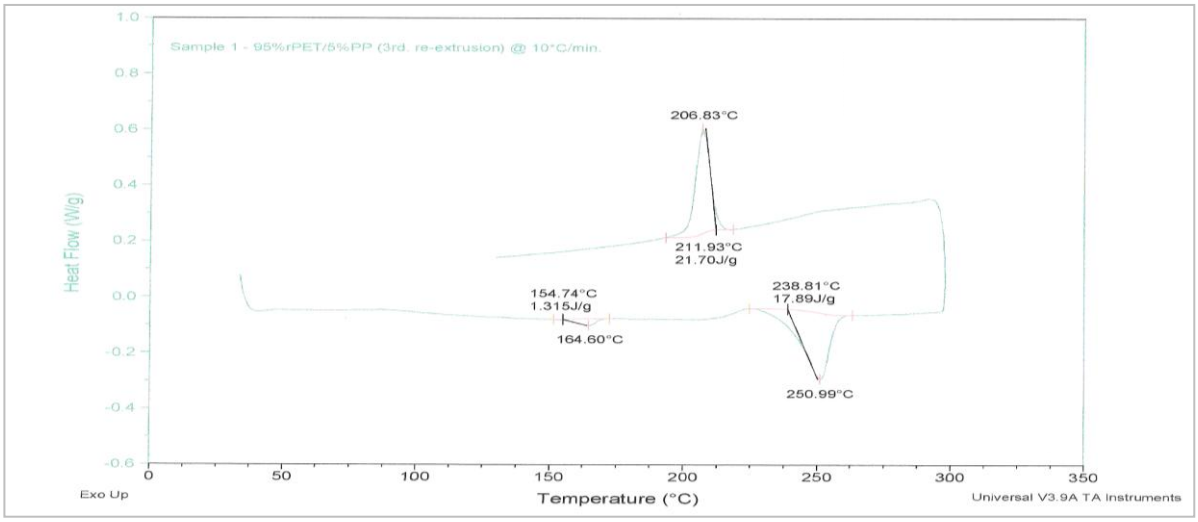

Figure 8.8 Thermogram of Extruded Sample 1 of rPET-bg contaminated with 5% PP - 3rd re-extrusion cycle -

	T_m (^oC)	ΔH_m ($J.g^{-1}$)	T_c (^oC)	ΔH_c ($J.g^{-1}$)	ΔH_m^0 ($J.g^{-1}$	X_c (%)
Material	**Re-extruded Samples of 95% rPET-bg / 5% PP at 10°C/min (Cycle 3)**					
Mean (μ)	**250.88**	**17.88**	**206.07**	**20.38**	**140**	**14.56**
STDEV (σ)	0.70	0.39	0.69	1.14		0.82
ST. Error ($S_E = \sigma/n^{0.5}$)	0.40	0.22	0.40	0.66		0.47
CI (95%), ($\mu \pm 1.96 S_E$)	$\mu \pm 0.79$	$\mu \pm 0.44$	$\mu \pm 0.78$	$\mu \pm 1.29$		$\mu \pm 0.92$

Table 8.8 Samples of rPET-bg contaminated with 5% PP - Re-extrusion Cycle 3

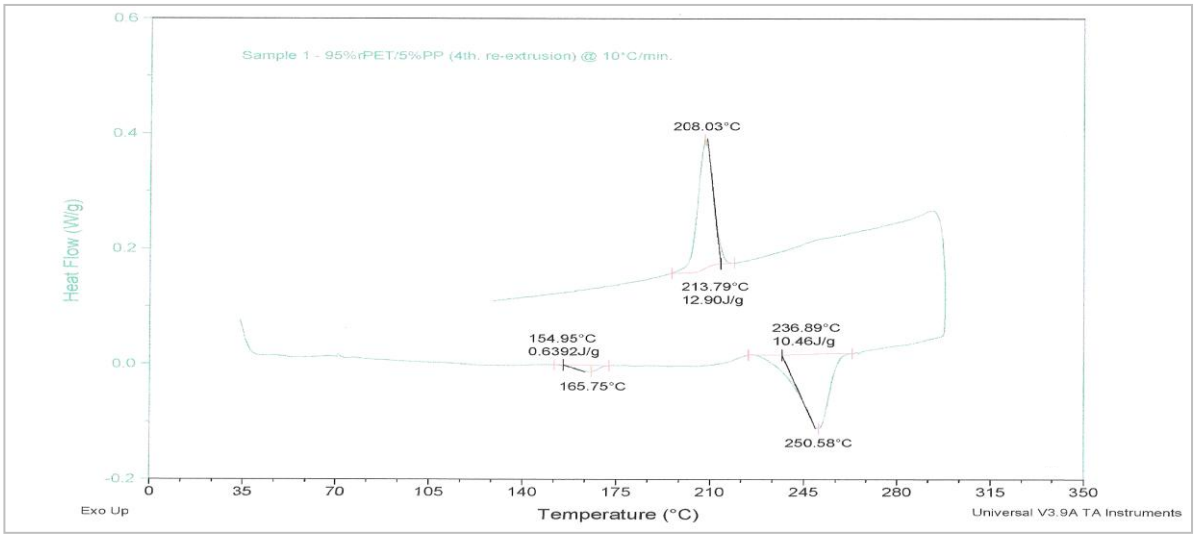

Figure 8.9 Thermogram of Extruded Sample 1 of rPET-bg contaminated with 5% PP - 4th re-extrusion cycle -

	T_m (^{o}C)	ΔH_m (J.g^{-1})	T_c (^{o}C)	ΔH_c (J.g^{-1})	ΔH_m^0 (J.g^{-1})	X_c (%)
Material	**Re-extruded Samples of 95% rPET-bg / 5% PP at 10^{o}C/min (Cycle 4)**					
Mean (μ)	**251.08**	**11.36**	**206.50**	**12.83**	**140**	**9.17**
STDEV (σ)	0.68	1.57	1.39	1.23		0.88
ST. Error ($S_E = \sigma/n^{0.5}$)	0.40	0.91	0.80	0.71		0.51
CI (95%), ($\mu \pm 1.96 S_E$)	$\mu \pm 0.77$	$\mu \pm 1.78$	$\mu \pm 1.58$	$\mu \pm 1.39$		$\mu \pm 1.00$

Table 8.9 Samples of rPET-bg contaminated with 5% PP - Re-extrusion Cycle 4

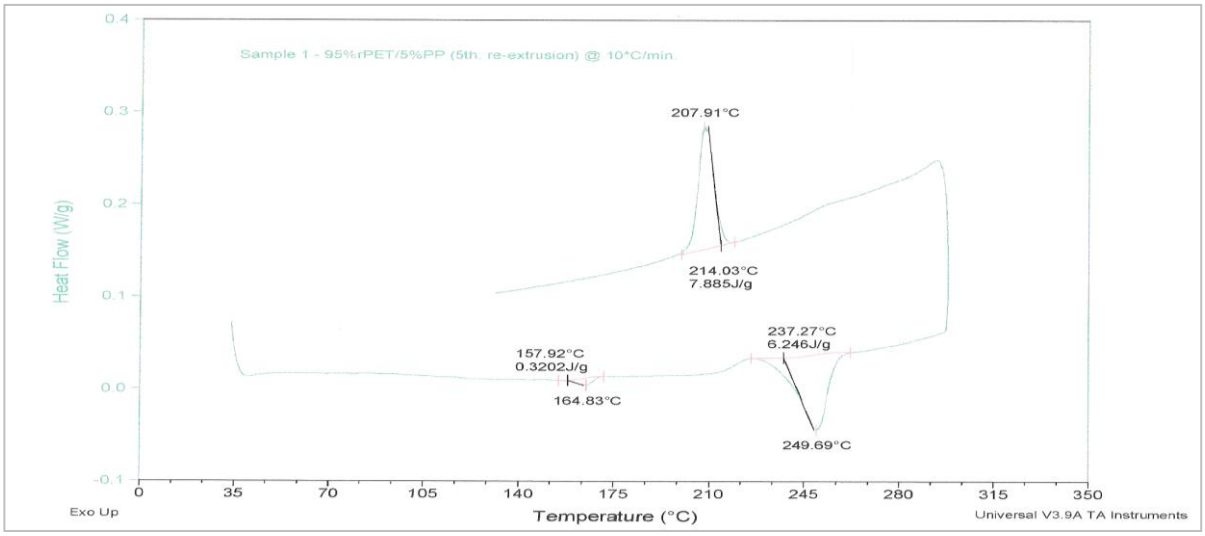

Figure 8.10 Thermogram of Extruded Sample 1 of rPET-bg contaminated with 5% PP - 5th re-extrusion cycle -

	T_m (^oC)	ΔH_m ($J.g^{-1}$)	T_c (^oC)	ΔH_c ($J.g^{-1}$)	ΔH_m^0 ($J.g^{-1}$	X_c (%)
Material	**Re-extruded Samples of 95% rPET-bg / 5% PP at 10°C/min (Cycle 5)**					
Mean (μ)	**250.30**	**6.74**	**206.27**	**7.66**	**140**	**5.47**
STDEV (σ)	0.56	1.25	1.43	1.14		0.81
ST. Error ($S_E = \sigma/n^{0.5}$)	0.33	0.72	0.83	0.66		0.47
CI (95%), ($\mu \pm 1.96 S_E$)	$\mu \pm 0.64$	$\mu \pm 1.41$	$\mu \pm 1.62$	$\mu \pm 1.29$		$\mu \pm 0.92$

Table 8.10 Samples of rPET-bg contaminated with 5% PP - Re-extrusion Cycle 5

Note: Additional DSC Thermograms are available in ***Appendix 8*** **(***1 to 10***).**

8.1.3 Melting Temperature, T_m

DSC analysis in the *heating mode*, as shown in *Table 8.11* and *Figure 8.11* below, showed fluctuating decrease in $\boldsymbol{T_m}$ of both *non contaminated rPET-bg* and *rPET-bg contaminated with 5% PP* with increasing re-extrusion cycles. The decrease in $\boldsymbol{T_m}$ is clearly higher in the *latter* than in the *earlier*; this indicated random distribution and clear reduction of crystalline domains in the *latter* and that the degree of disentanglement is higher and the amorphous domains are larger, which contributed to the overall melting speed. This showed the effect of re-extrusions in allowing favourable conditions for the PP chains to further disperse within the main matrix molecular chains and contribute to an increase of entangling which increased secondary bonding. Also, premature melting of PP and repetition of chains-scission due to thermo-mechanical degradation during the various re-extrusion cycles, and the remaining small percentage of DEG in the PET decreases the melt temperature and the thermo-oxidative stability and other physical and chemical properties, as reported respectively by *Binsack* [8]. Also, the retained DEG content can lower the physical and chemical properties, as reported by *Yu et al.* [186], *Patkar* and *Jabarin* [187] and *Seganov et al.* [99]. Other generated oligomers contribute in enhancing formation of new chains with the ability of further entangling or even allowing cross-linking of the main matrix chains, which could enhance both the amorphous domains and the degree of entropy and speed up the melting process, resulting in reduced $\boldsymbol{T_m}$. As the crystalline domains become more ordered, the degree of entropy decreases and the $\boldsymbol{T_m}$ increases; the decreased $\boldsymbol{T_m}$ of the rPET-bg contaminated with PP indicated that amorphous domains are larger than crystalline ones and showed the effect of heterogeneous nucleation of PP and rPET-bg on each other.

	Extruded Samples Non contaminated rPET-bg			Extruded Samples 95% rPET-bg / 5% PP		
	T_m (°C)					
Re-extrusion Cycles at 10 (°C/min.)	**Mean (μ)**	**ST. Error ($S_E = \sigma/n^{0.5}$)**	**CI (95%) ($\mu \pm 1.96 S_E$)**	**Mean (μ)**	**ST. Error ($S_E = \sigma/n^{0.5}$)**	**CI (95%) ($\mu \pm 1.96 S_E$)**
1st. Re-Extrusion	**251.34**	0.00	$\mu \pm 0.00$	**250.94**	0.28	$\mu \pm 0.55$
2nd. Re-Extrusion	**250.94**	0.00	$\mu \pm 0.00$	**251.02**	0.21	$\mu \pm 0.41$
3rd. Re-Extrusion	**251.12**	0.00	$\mu \pm 0.00$	**250.88**	0.40	$\mu \pm 0.79$
4th. Re-Extrusion	**251.15**	0.00	$\mu \pm 0.00$	**251.08**	0.40	$\mu \pm 0.77$
5th. Re-Extrusion	**250.93**	0.00	$\mu \pm 0.00$	**250.30**	0.33	$\mu \pm 0.64$

Table 8.11 Melting Temperature at Various Re-extrusion Cycles

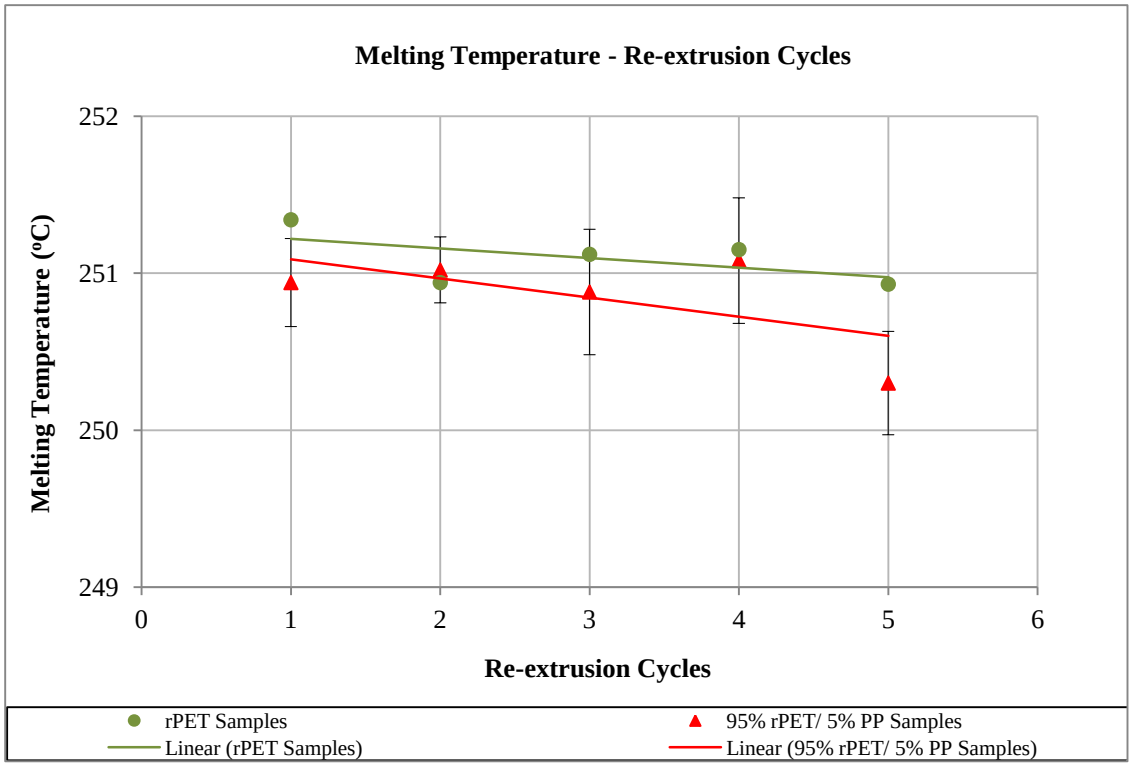

Figure 8.11 Melting Temperature at Various Re-extrusion Cycles

8.1.4 Heat of Fusion, ΔH_m

The *enthalpy* of *melting*, ΔH_m, of the *rPET-bg contaminated with 5% PP*, as shown in *Table 8.12* and *Figure 8.12* below, decreased dramatically; this clearly showed the reduced crystalline domains and the role of PP in enhancing the right conditions through its premature melting. Furthermore, this dramatic decrease of ΔH_m indicated high degree of entropy promoted by weak secondary bonding adhesion of molecular chains due to incompatibility. Also, newly generated oligomers, as a result of thermo-mechanical degradation during re-extrusions, could increase the viscosity ratio and decrease the interfacial tension between PET and PP, as reported by *Yi et al.* [188], and created some sort of weak cross-linking between molecular chains, and consequently promoted increase of amorphous domains which increased entropy and decreased the ΔH_m.

	Extruded Samples Non contaminated rPET-bg			Extruded Samples 95% rPET-bg / 5% PP		
	ΔH_m ($J.g^{-1}$)					
Re-extrusion Cycles at 10 (°C/min.)	**Mean (μ)**	**ST. Error ($S_E = \sigma/n^{0.5}$)**	**CI (95%) ($\mu \pm 1.96 S_E$)**	**Mean (μ)**	**ST. Error ($S_E = \sigma/n^{0.5}$)**	**CI (95%) ($\mu \pm 1.96 S_E$)**
1st. Re-Extrusion	**49.64**	1.48	$\mu \pm 2.90$	**31.13**	0.24	$\mu \pm 0.47$
2nd. Re-Extrusion	**37.94**	0.02	$\mu \pm 0.04$	**22.08**	1.63	$\mu \pm 3.20$
3rd. Re-Extrusion	**42.01**	1.54	$\mu \pm 3.02$	**17.88**	0.22	$\mu \pm 0.44$
4th. Re-Extrusion	**41.82**	1.32	$\mu \pm 2.58$	**11.36**	0.91	$\mu \pm 1.78$
5th. Re-Extrusion	**39.35**	1.20	$\mu \pm 2.34$	**6.74**	0.72	$\mu \pm 1.41$

Table 8.12 Heat of Fusion at Various Re-extrusion Cycles

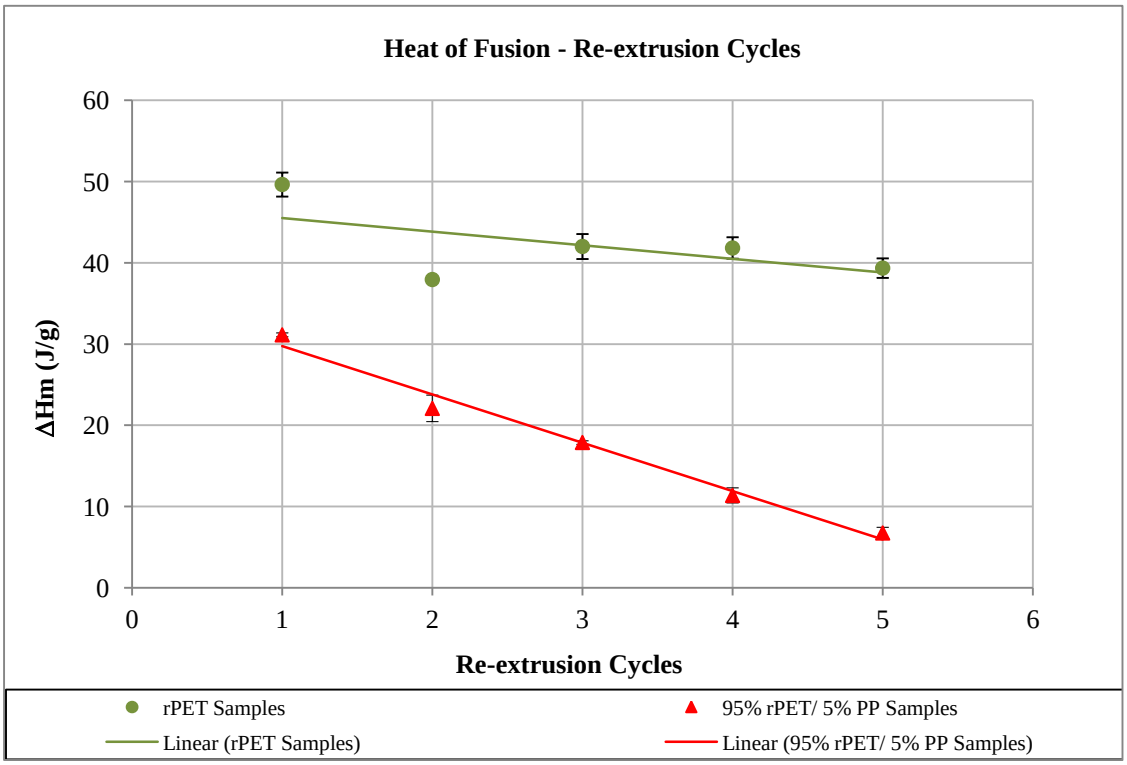

Figure 8.12 Heat of Fusion at Various Re-extrusion Cycles

8.1.5 Crystallisation Temperature, T_c

The crystallisation temperatures of *non contaminated rPET-bg* and *rPET-bg contaminated with 5% PP*, as shown in *Table 8.13* and *Figure 8.13* below, fluctuated respectively between *204.48* and *205.28°C* and between *205.62* and *207.16°C;* the inclusion of *5% PP* increased the T_c by approximately *2°C*, meaning slow crystallisation of high volume of short chains, also indicating melt thermo-mechanical degradation, as reported by *Badia et al.* [189], and also, probable reactions between relevant macro-radicals in generation of grafted copolymers, as reported by *Pospisil et al.* [24]. Both materials showed a trend of continuous reduction in T_c with an increase in re-extrusion cycles; this indicated chain branching formation and its domination over chains'-scission throughout the re-extrusion cycles.

	Extruded Samples Non contaminated rPET-bg			Extruded Samples 95% rPET-bg / 5% PP		
	T_c (^oC)					
Re-extrusion Cycles at 10°C/min.	**Mean (μ)**	**ST. Error ($S_E = \sigma/n^{0.5}$)**	**CI (95%) ($\mu \pm 1.96 S_E$)**	**Mean (μ)**	**ST. Error ($S_E = \sigma/n^{0.5}$)**	**CI (95%) ($\mu \pm 1.96 S_E$)**
1st. Re-Extrusion	**205.28**	0.00	$\mu \pm 0.00$	**207.16**	0.65	$\mu \pm 1.27$
2nd. Re-Extrusion	**204.69**	0.00	$\mu \pm 0.00$	**205.62**	0.11	$\mu \pm 0.22$
3rd. Re-Extrusion	**204.48**	0.00	$\mu \pm 0.00$	**206.07**	0.40	$\mu \pm 0.78$
4th. Re-Extrusion	**205.20**	0.00	$\mu \pm 0.00$	**206.50**	0.80	$\mu \pm 1.58$
5th. Re-Extrusion	**204.88**	0.06	$\mu \pm 0.13$	**206.27**	0.83	$\mu \pm 1.62$

Table 8.13 Crystallisation Temperature at Various Re-extrusion Cycles

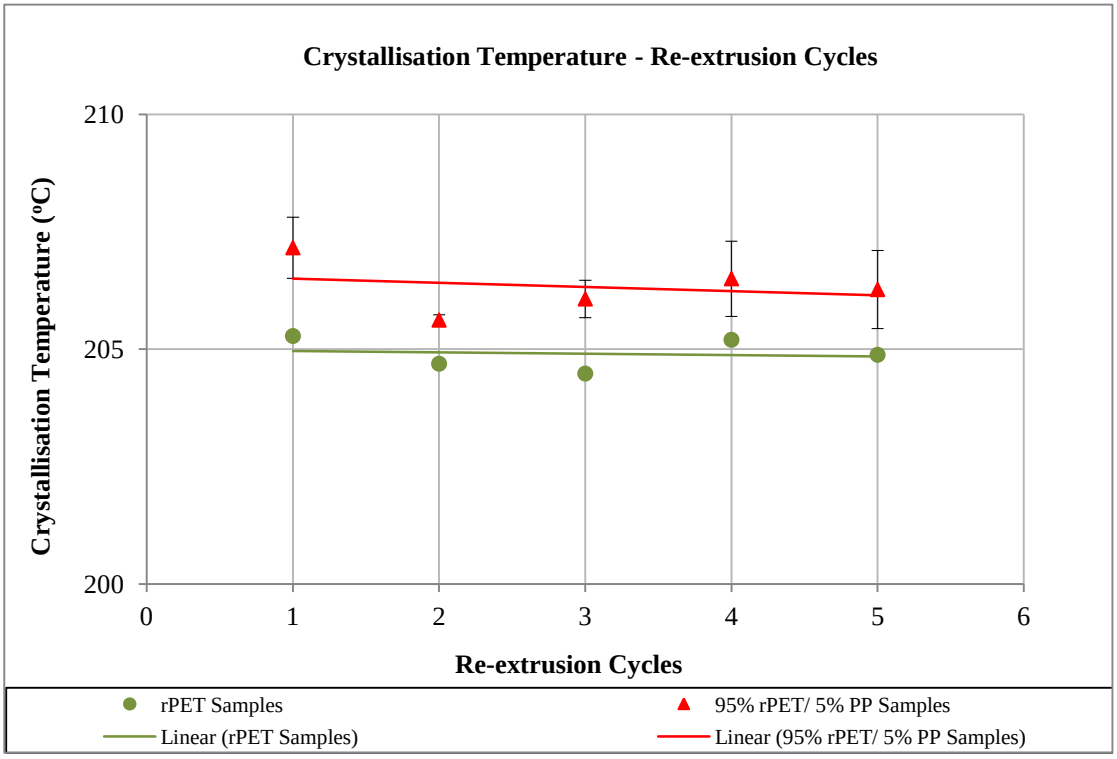

Figure 8.13 Crystallisation Temperature at Various Re-extrusion Cycles

8.1.6 Heat of Crystallisation, ΔH_c

The enthalpy of crystallization, ΔH_c , of *non contaminated rPET-bg* fluctuated with a tendency of decreasing from *43.43* to *35.20 J.g*$^{-1}$, whereas in the *rPET-bg contaminated with 5% PP*, it decreased orderly from *34.67* to *7.66 J.g*$^{-1}$, as shown in *Table 8.14* and *Figure 8.14* below; this showed clearly the slow crystallisation process in the *latter* compared with the *earlier* and meant that the inclusion of *5% PP* induced chains'-scission which contributed to generation of high volume of chains' which in return contributed to branching and enhanced both the weak secondary bonding and the amorphous domains, and consequently resulted in a reduction of crystallinity with increasing re-extrusion cycles.

	Extruded Samples Non contaminated rPET-bg			Extruded Samples 95% rPET-bg / 5% PP		
	ΔH_c ($J.g^{-1}$)					
Re-extrusion Cycles at 10 (°C/min.)	**Mean (μ)**	**ST. Error ($S_E = \sigma/n^{0.5}$)**	**CI (95%) ($\mu \pm 1.96 S_E$)**	**Mean (μ)**	**ST. Error ($S_E = \sigma/n^{0.5}$)**	**CI (95%) ($\mu \pm 1.96 S_E$)**
1st. Re-Extrusion	**43.43**	1.03	$\mu \pm 2.02$	**34.67**	1.00	$\mu \pm 1.95$
2nd. Re-Extrusion	**38.00**	1.36	$\mu \pm 2.68$	**23.89**	1.91	$\mu \pm 3.75$
3rd. Re-Extrusion	**35.20**	1.17	$\mu \pm 2.28$	**20.38**	0.66	$\mu \pm 1.29$
4th. Re-Extrusion	**39.49**	0.82	$\mu \pm 1.62$	**12.83**	0.71	$\mu \pm 1.39$
5th. Re-Extrusion	**35.72**	0.77	$\mu \pm 1.50$	**7.66**	0.66	$\mu \pm 1.29$

Table 8.14 Heat of Crystallisations at Various Re-extrusion Cycles

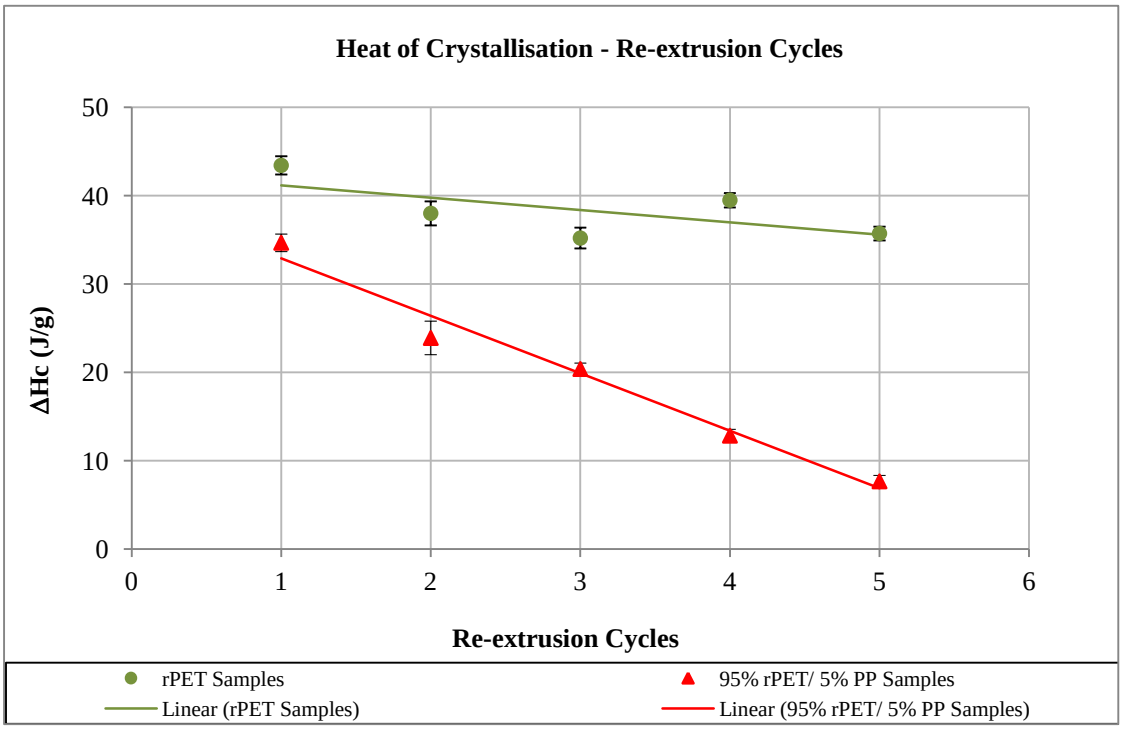

Figure 8.14 Heat of Crystallisations at Various Re-extrusion Cycles

8.1.7 % Crystallinity, X_c

The % crystallinity of *non contaminated rPET-bg* fluctuated randomly between *31.02* and *25.14 %* and decreased orderly from *24.76* to *5.47%* in the *rPET-bg contaminated with 5 % PP*, as shown in *Table 8.15* and *Figure 8.15* below; one can see the proportional relationship of enthalpy of crystallisation and % crystallinity. Reducing crystallinity in PET bottle manufacturing is of paramount importance in enhancing bottle clarity or transparency. Nucleation and growth processes of PET spherulites are the main factors governing the degree of crystallinity and the process of crystallisation is initiated by the formation of primary nuclei, then formation of folded layers of ordered chains, as reported by *Lauritzen* and *Hoffman* [190] and propagates to form primary spherulites or crystallites until all the area under the exotherm is saturated. The results shown, clearly indicated that formation of spherulites and their propagation were slowing with increasing re-extrusion cycles. The *5% PP* contributed to lowering the degree of crystallinity in the *rPET-bg* matrix with increasing re-extrusion cycles; this indicated competition between

chains'-scission and cross-linking and chains branching and also newly created chains, following reaction of newly created oligomers, generated sort of interfacial molecular forces leading to weak secondary bonding between chains despite the incompatibility of the *contaminant, PP* and the *host matrix, rPET-bg*. This explains the reduction of crystallinity in the rPET-bg contaminated with 5% PP. It is apparent that such differential crystallisation behaviour is attributed to the various phenomena taking place during re-extrusion cycles; combination of thermo-mechanical degradation, incompatibility, impurities, irregular compositions and retained DEG in the matrix can all result in unexpected decrease of crystallisation rate as in the works of *Jabarin* [191], [192] respectively by isothermal and dynamic crystallisations, and in the work of *Yu et al.* [186].

	Extruded Samples Non contaminated rPET-bg			**Extruded Samples 95% rPET-bg / 5% PP**		
	X_c (%)					
Re-extrusion Cycles at 10 (°C/min.)	**Mean (μ)**	**ST. Error ($S_E = \sigma/n^{0.5}$)**	**CI (95%) ($\mu \pm 1.96 S_E$)**	**Mean (μ)**	**ST. Error ($S_E = \sigma/n^{0.5}$)**	**CI (95%) ($\mu \pm 1.96 S_E$)**
1st. Re-Extrusion	**31.02**	0.74	$\mu \pm 1.44$	**24.76**	0.71	$\mu \pm 1.40$
2nd. Re-Extrusion	**27.14**	0.98	$\mu \pm 1.91$	**17.07**	1.37	$\mu \pm 2.68$
3rd. Re-Extrusion	**25.14**	0.83	$\mu \pm 1.63$	**14.56**	0.47	$\mu \pm 0.92$
4th. Re-Extrusion	**28.20**	0.59	$\mu \pm 1.15$	**9.17**	0.51	$\mu \pm 1.00$
5th. Re-Extrusion	**25.51**	0.55	$\mu \pm 1.07$	**5.47**	0.47	$\mu \pm 0.92$

Table 8.15 % Crystallinity at Various Re-extrusion Cycles

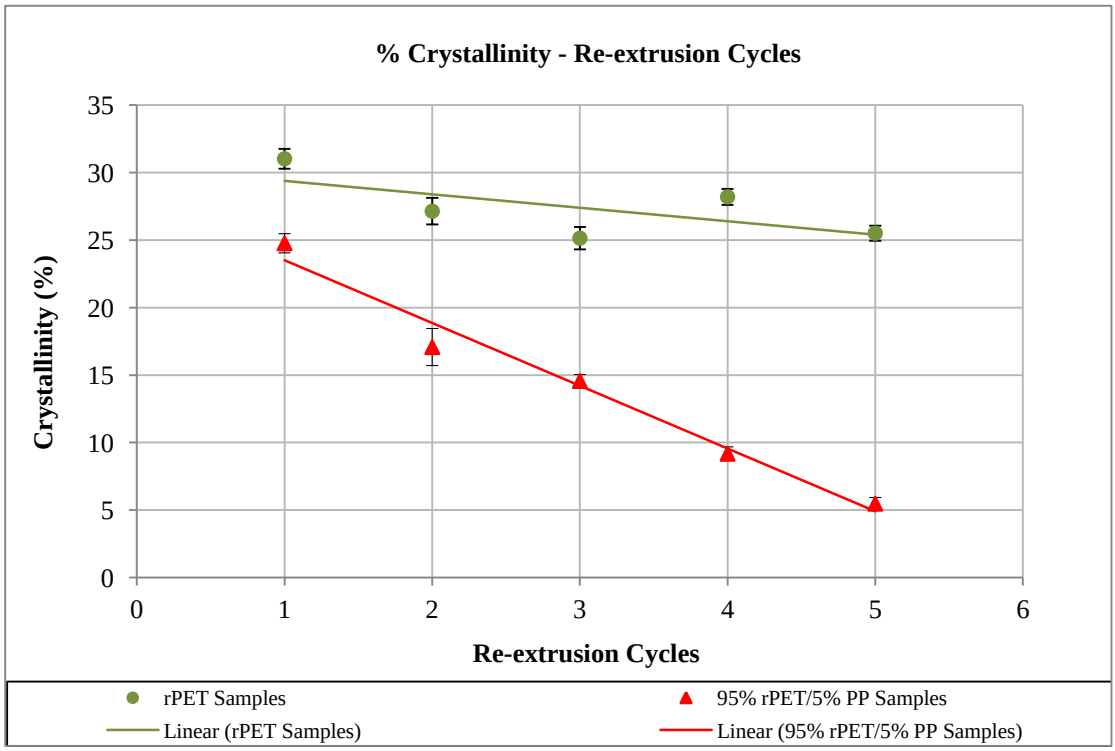

Figure 8.15 % Crystallinity at Various Re-extrusion Cycles

8.1.8 Heat of Crystallisation - Crystallinity Relationship

By comparison of data in *Table 8.16* and the linearity in *Figure 8.16* below, one can see clearly the proportionality between heat of crystallisation and the % crystallinity, which indicated crystalline domains were reducing with increasing re-extrusion cycles.

	Extruded Samples Non contaminated rPET-bg		**Extruded Samples 95% rPET-bg / 5% PP**	
	ΔH_c (J.g^{-1})	**X_c (%)**	**ΔH_c (J.g^{-1})**	**X_c (%)**
Re-extrusion Cycles	**Mean (μ)**	**Mean (μ)**	**Mean (μ)**	**Mean (μ)**
1st. Re-Extrusion	**43.43** ± 2.02	31.02 ± 1.44	**34.67** ± 1.95	24.76 ± 1.40
2nd. Re-Extrusion	**38.00** ± 2.68	27.14 ± 1.91	**23.89** ± 3.75	17.07 ± 2.68
3rd. Re-Extrusion	**35.20** ± 2.28	25.14 ± 1.63	**20.38** ± 1.29	14.56 ± 0.92
4th. Re-Extrusion	**39.49** ± 1.62	28.20 ± 1.15	**12.83** ± 1.39	9.17 ± 1.00
5th. Re-Extrusion	**35.72** ± 1.50	25.51 ± 1.07	**7.66** ± 1.29	5.47 ± 0.92

Table 8.16 Heat of Crystallisation and Crystallinity at Various Re-extrusion Cycles

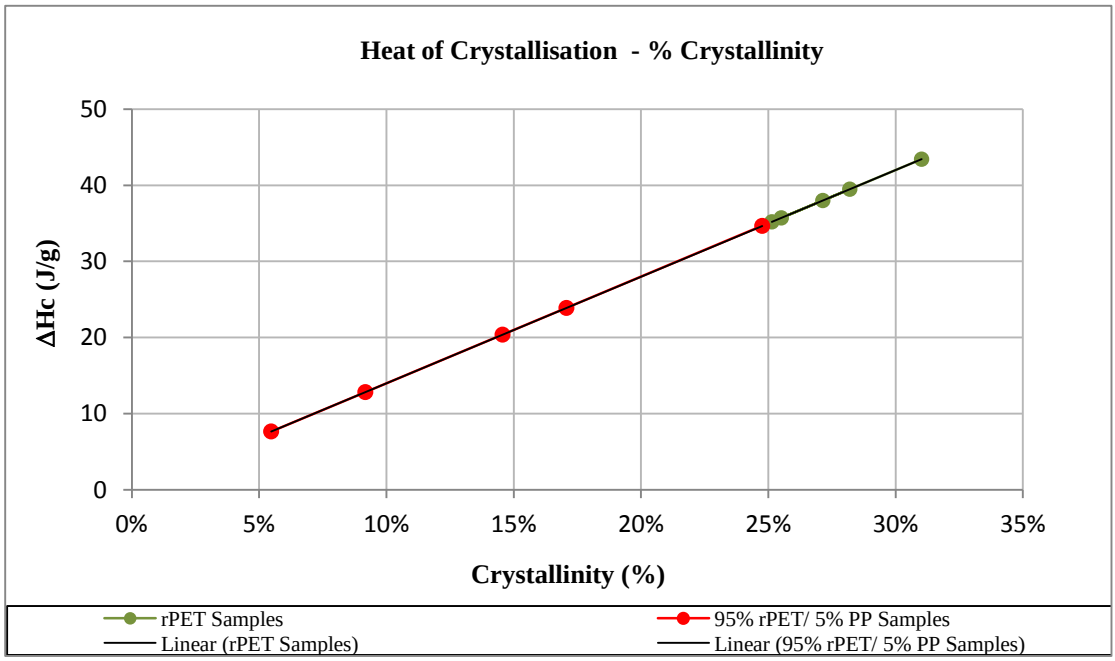

Figure 8.16 Heat of Crystallisation Vs Crystallinity at Various Re-extrusion Cycles

8.1.9 Screw Speeds and % Torques

During multiple extrusions, both *non contaminated* and *rPET-bg contaminated with 5% PP*, showed reduction in *screw speed* with increased *re-extrusion cycles*; this indicated the influence of chains' scissions on the materials' flow characteristics and highly ordered chain orientation led to ease of processability in both cases, as reported by *Cogswell et al.* [168] and *Harrison et al.* [193]. In comparison, the gap in screw speed decrease was larger with the *latter* than with the *earlier*, as shown in *Table 8.17* and *Figure 8.17* below, which indicated that *chains'- scission* and *chains' orientation*, achieved in the convergent flow at the inlet of the die, were happening simultaneously, the *latter* was promoted by the flow property of *PP* which helped reducing the melt viscosity. It is worth noting, that the chains' orientation achieved promoted the interfacial adhesion at *cooling stage* which in return enhanced the weak secondary bonding between incompatible polymer chains, hence, promoting branching and cross-linking and reducing crystallinity.

Re-extrusion Cycles	Extruded Samples Non contaminated rPET-bg		Extruded Samples 95% rPET-bg / 5% PP	
	Screw Speed	%Torque	Screw Speed	%Torque
	Mean ($\mu \pm x$) (rpm)	Mean ($\mu \pm x$) (%)	Mean ($\mu \pm x$) (rpm)	Mean ($\mu \pm x$) (%)
1st. Re-Extrusion	**112.0** ± 2.0	**55** ± 5	**99.0** ± 3.0	**35** ± 6
2nd. Re-Extrusion	**112.0** ± 2.0	**56** ± 6	**98.5** ± 2.5	**36** ± 6
3rd. Re-Extrusion	**111.5** ± 2.5	**56** ± 5	**97.5** ± 2.5	**37** ± 6
4th. Re-Extrusion	**111.0** ± 2.0	**56** ± 5	**96.0** ± 2.0	**38** ± 7
5th. Re-Extrusion	**110.5** ± 2.5	**57** ± 5	**95.0** ± 2.0	**38** ± 8

Table 8.17 Screw Speeds and % Torque at Various Re-extrusion Cycles

Note: The (± x) values represent the observed fluctuations.

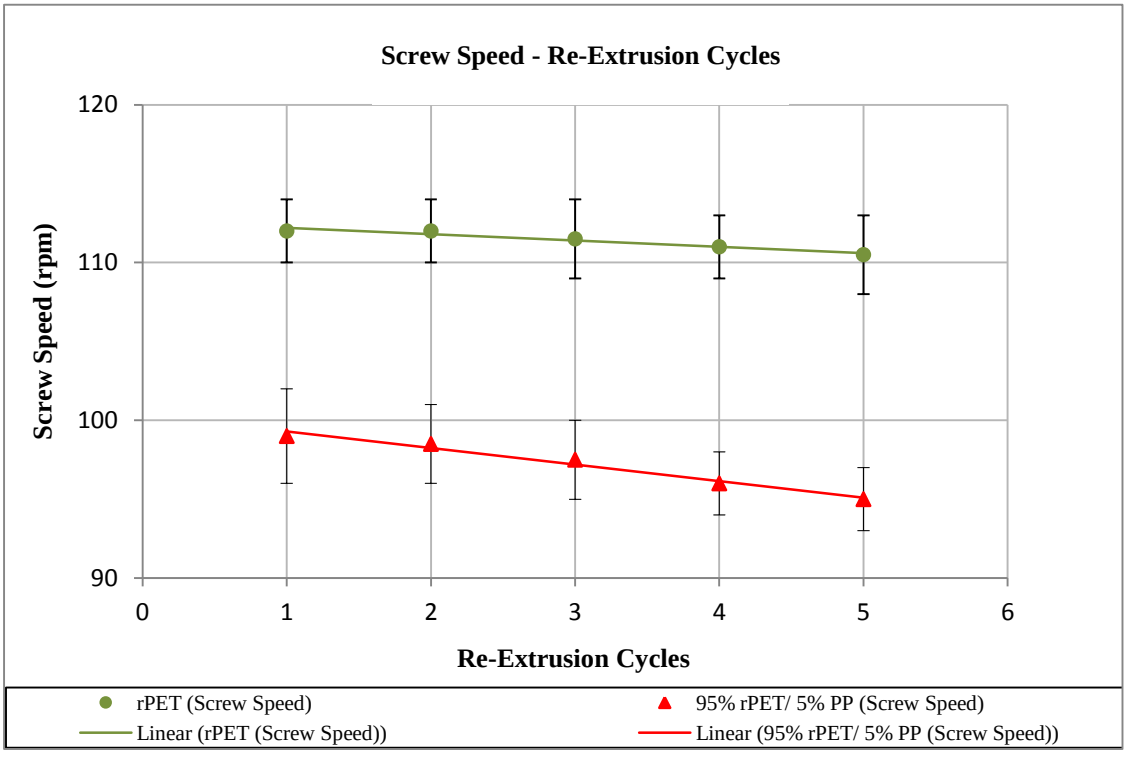

Figure 8.17 Screw Speeds at Various Re-extrusion Cycles

Furthermore, the screw *% torque*, as shown in *Table 8.17* and *Figure 8.18*, complied with the processing rule of the inverse proportionality of screw speed and % torque and it is clear to see that the gap in % torque increase is larger with the *rPET-bg contaminated with 5% PP* than with the *non contaminated rPET-bg*, indicating that the *PP contaminant* generated certain degree of cross-linking and branching resulting in an increase of viscosity despite the continuous chains' scission resulting from the thermo-mechanical degradation during re-extrusion cycles; this was in line with what was reported respectively *Paci* and *La Mantia* [22], and *Pospisil et al.* [24] and *Assadi et al.* [27] that during processing not only chain scission but also chain extension, grafted copolymers and cross-linking can occur, and contradicted *Camacho* and *Karlsson* [25] and *Badía et al.* [26] that only chain scission predominated and no chain branching or cross-linking were observed during re-extrusions.

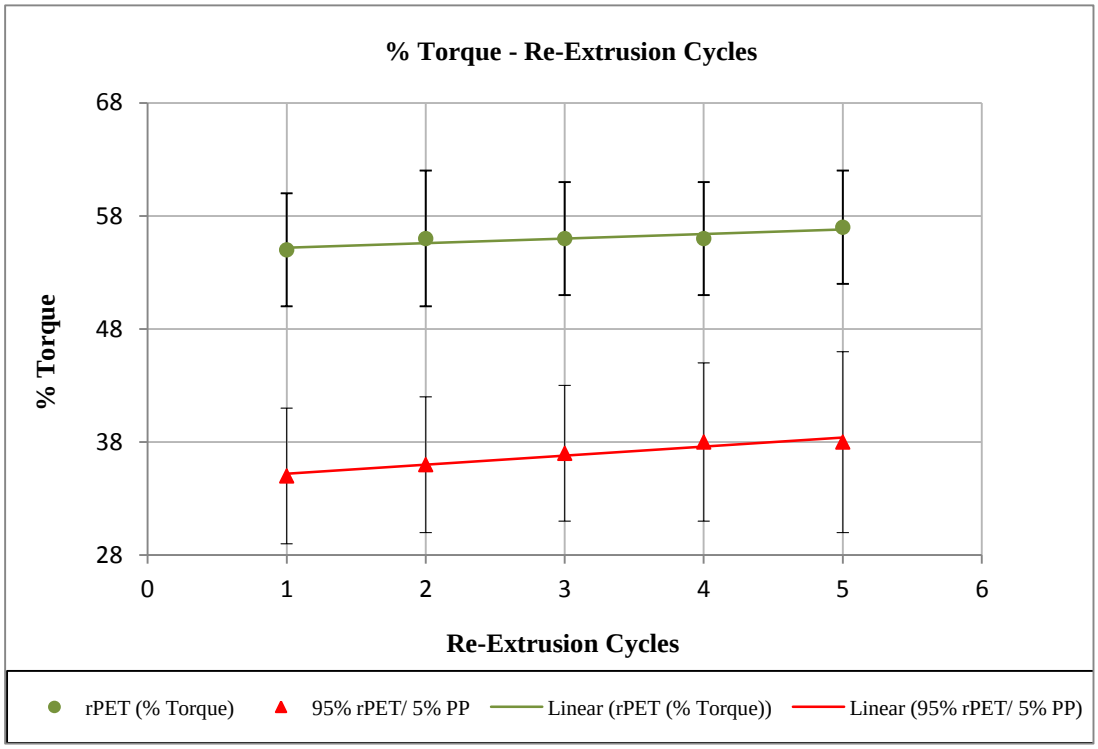

Figure 8.18 % Torques at Various Re-extrusion Cycles

8.1.10 Overall Data Comparison

The comparison of the thermal characteristics and processing conditions obtained, as shown in *Table 8.18* below, identified the extend of PP influence on the rPET-bg matrix. The decrease in $\boldsymbol{T_m}$ in the *rPET-bg contaminated with 5% PP* clearly indicated random and heterogeneous distribution and clear reduction of crystalline domains; this showed presence of less crystalline domains, which required less time and temperature for melting. The effect of *re-extrusions* is apparent, the PP chains through the re-extrusions and compounding were further dispersed within the main matrix molecular chains, and the newly generated chains, as a result of polymer chains interaction, and under favourable conditions contributed to an increase of entangling which contributed and increased secondary bonding and even allowed cross-linking of the main matrix chains, which increased the degree of entropy and the melting process, resulting in reduced $\boldsymbol{T_m}$. The increased entropy allowed quick melting due the low resistance of weak secondary bonding generated as a result of *re-extrusion*. This state of entropy promoted the speed of melting process which required less energy and resulted in decreased $\boldsymbol{\Delta H_m}$. In the other hand, the created high volume of short chains, as a result of re-extrusion and melt thermo-mechanical degradation, allowed formation of macro-radicals and generated grafted copolymers, which is a possibility as reported by *Pospisil et al.* [24]. This high volume of chains coupled with the PP low temperature of crystallisation, allowed extended temperature to complete the slow crystallisation process, which resulted in increased the $\boldsymbol{T_c}$ in the *rPET-bg contaminated with 5% PP*. This slow crystallisation process is clearly shown by the decreased $\boldsymbol{\Delta H_c}$. Furthermore, decreased $\boldsymbol{\% X}$, clearly indicated the slow formation of spherulites and their propagation with increasing *re-extrusion cycles*.

In the other hand, the decreased *screw speed* with increasing *re-extrusion cycles*, indicated the high volume of newly created chains, as a result of chains'-scissions, which influenced the overall melt flow and interacted with the efficiency of the *screw speed*, as a result of interaction of various molecular chains and formation of *grafted copolymers* and *cross-linking*, which *increased* the melt *viscosity*, shown by the *increased* screw *% torque*, despite the continuous chains' scission resulting from the thermo-mechanical degradation during *re-extrusion cycles*; this competition between *chains'-scission* and *cross-linking* and *branching* is in line with the finding reported respectively by *Paci* and *La Mantia* [22], and *Pospisil et al.* [24] and *Assadi et al.* [27] that during processing not only

chains'-scission but also chain extension, grafted copolymers and cross-linking can occur, and contradicted *Camacho* and *Karlsson* [25] and *Badía et al.* [26] that only chain scission predominated and no chain branching or cross-linking were observed during *re-extrusions.* It is worth noting, that the chains' orientation achieved, in the convergent flow of the extruder's die, promoted the chains' interfacial adhesion at *cooling stage*, which in return enhanced the weak secondary bonding between incompatible polymer chains, hence, promoted branching and cross-linking and reduced most of thermal characteristics, especially the % crystallinity. The *5% PP* contributed in lowering the degree of crystallinity in the *rPET-bg* matrix with increasing *re-extrusion cycles*; this indicated competition between chains'-scission and cross-linking and chains' branching and also the newly created chains, following reaction of newly created oligomers, generated sort of interfacial molecular forces leading to weak secondary bonding between chains despite the incompatibility of the *contaminant, PP* and the *host matrix, rPET-bg.*

	T_m (^oC)	ΔH_m ($J.g^{-1}$)	T_c (^oC)	ΔH_c ($J.g^{-1}$)	X_c (%)	Screw Speed (rpm)	% T
Extruded Samples *rPET-bg contaminated with 5% PP* **compared to** *non contaminated rPET-bg*	↓	↓	↑	↓	↓	↓	↑

Table 8.18 Variation of Thermal Characteristics and Processing Conditions with re-extrusion cycles of rPET-bg contaminated with 5% PP

Following the *re-extrusions*, there is indication of competition between *chains'-scission* and *cross-linking* and *chains branching* in the *rPET-bg contaminated with 5% PP*, and to see which one is predominating the other and contributing to the variation of thermal characteristics, especially the reduction of *crystallinity*, it is of paramount importance to understand the influence of the *PP contaminant* on the crystallisation process of the *rPET-bg* matrix at *constant cooling rate* post *re-extrusions*. So, the *crystallisation process* was analysed by the *Avrami equation* for *non-isothermal process*, which was used to describe the mechanism of crystallisation and investigating the *competition* and *predominance*, between cross-linking and branching or chains' scission.

8.1.11 Validation by *Avrami equation* for non-isothermal crystallisation

The *Avrami equation*, as described in *Section 1.2.3.2*, was used to describe the process of *non-isothermal* crystallisation for *non contaminated rPET-bg* and *rPET-bg contaminated with 5% PP* and to validate if cross-linking and branching were dominating chains'-scission during *repetitive extrusions*. The obtained data are as follow.

	Extruded Samples Non contaminated rPET-bg		**Extruded Samples 95% rPET-bg / 5% PP**	
Re-extrusion Cycles	***Time (min)***	X_t	***Time (min)***	X_t
1	0.95	0.014	0.99	0.012
	1.33	0.022	1.34	0.023
	1.46	0.025	1.47	0.029
	1.65	0.030	1.59	0.034
	1.91	0.038	1.91	0.044
2	1.02	0.015	0.98	0.035
	1.27	0.021	1.28	0.057
	1.46	0.025	1.40	0.071
	1.65	0.029	1.53	0.089
	1.91	0.037	1.81	0.132
3	1.02	0.014	0.98	0.039
	1.33	0.022	1.24	0.061
	1.46	0.025	1.40	0.081
	1.65	0.030	1.57	0.107
	2.17	0.048	1.85	0.147
4	0.95	0.013	0.97	0.048
	1.33	0.022	1.26	0.078
	1.46	0.026	1.39	0.095
	1.52	0.027	1.55	0.120
	1.85	0.038	1.81	0.154
5	1.01	0.014	1.01	0.067
	1.33	0.022	1.30	0.099
	1.45	0.026	1.42	0.117
	1.65	0.031	1.60	0.147
	1.97	0.041	1.85	0.185

Table 8.19 Relative Crystallinity and Time at Various Re-extrusion Cycles

The crystallisation process analysis, as shown in *Figures 8.19* and *8.20* below, gave sigmoid curves, as described by *Avrami equation*, and clearly showed the influence of *repetitive extrusions* on the *crystallisation process* and the influence of PP contaminant on the main matrix. The curves of *non contaminated rPET-bg* showed random, narrow and fast crystallisation with increased repetitive extrusion cycles, indicating dependency of crystallisation on re-extrusion cycles and the ability of the material in withstanding thermo-mechanical degradation and that the crystallisation process as a result of re-extrusions showed uniform and balanced nucleation and growth rate. Whereas, in the *rPET-bg contaminated with 5% PP*, the rate of crystallisation gradually decreased uniformly with increasing re-extrusion cycles, indicating ability of the polymer chains in maintaining disordered and entangled forms and requiring higher activation energy for disentangling and straightening which was the result of branching and cross-linking generated during the re-extrusions.

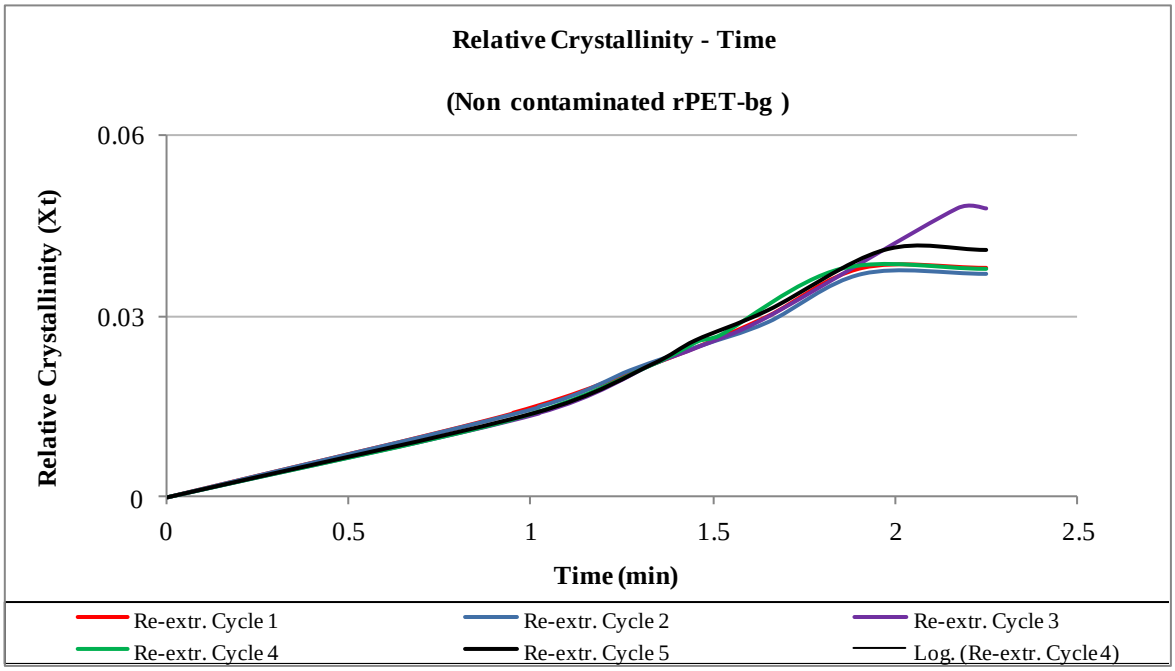

Figure 8.19 Relative Crystallinity Vs Time for Non-isothermal Crystallisation at Various Re-extrusion Cycles of non contaminated rPET-bg

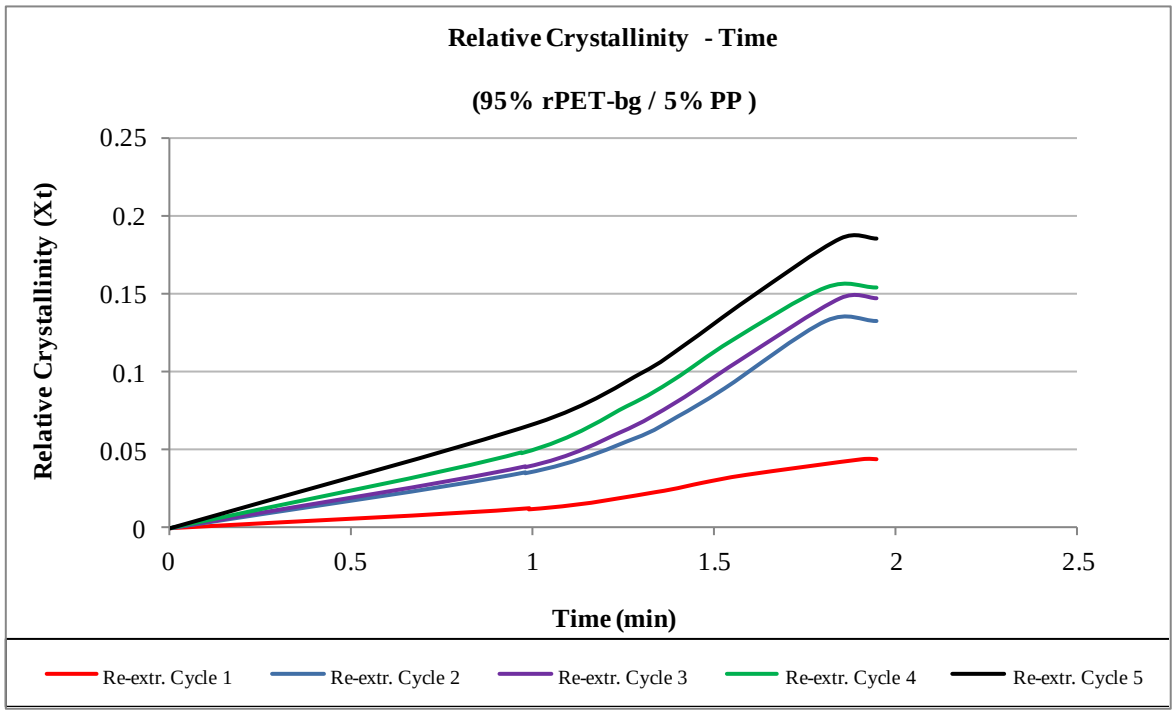

Figure 8.20 Relative Crystallinity Vs Time for Non-isothermal Crystallisation at Various Re-extrusion Cycles of rPET-bg contaminated with 5% PP

The following table lists the transformed data at various re-extrusion cycles.

	Extruded Samples Non contaminated rPET-bg		Extruded Samples 95% rPET-bg / 5% PP	
Re-extrusion Cycles	***log t***	***log(-ln(1-X_t)***	***log t***	***log(-ln(1-X_t)***
1	-0.02	-1.857	0.00	-1.935
	0.12	-1.645	0.13	-1.639
	0.16	-1.595	0.17	-1.534
	0.22	-1.520	0.20	-1.460
	0.28	-1.411	0.28	-1.348
2	0.01	-1.812	-0.01	-1.452
	0.10	-1.673	0.11	-1.232
	0.16	-1.600	0.15	-1.132
	0.22	-1.533	0.18	-1.033
	0.28	-1.419	0.26	-0.849
3	0.01	-1.844	-0.01	-1.400
	0.12	-1.646	0.09	-1.203
	0.16	-1.588	0.15	-1.073
	0.22	-1.515	0.20	-0.945
	0.34	-1.309	0.27	-0.798
4	-0.02	-1.897	-0.01	-1.307
	0.12	-1.653	0.10	-1.091
	0.16	-1.585	0.14	-1.003
	0.18	-1.555	0.19	-0.892
	0.27	-1.414	0.26	-0.778
5	0.00	-1.849	0.01	-1.159
	0.12	-1.646	0.11	-0.984
	0.16	-1.586	0.15	-0.906
	0.22	-1.506	0.20	-0.800
	0.29	-1.376	0.27	-0.690

Table 8.20 Data at Various Re-extrusion Cycles and Various Temperatures

Note: Additional Data are available in ***Appendix 8*** **(***11***)**.

The curves in *Figures 8.21* and *8.22* showed the *straight portion* of the *Avrami primary phase* of crystallisation.

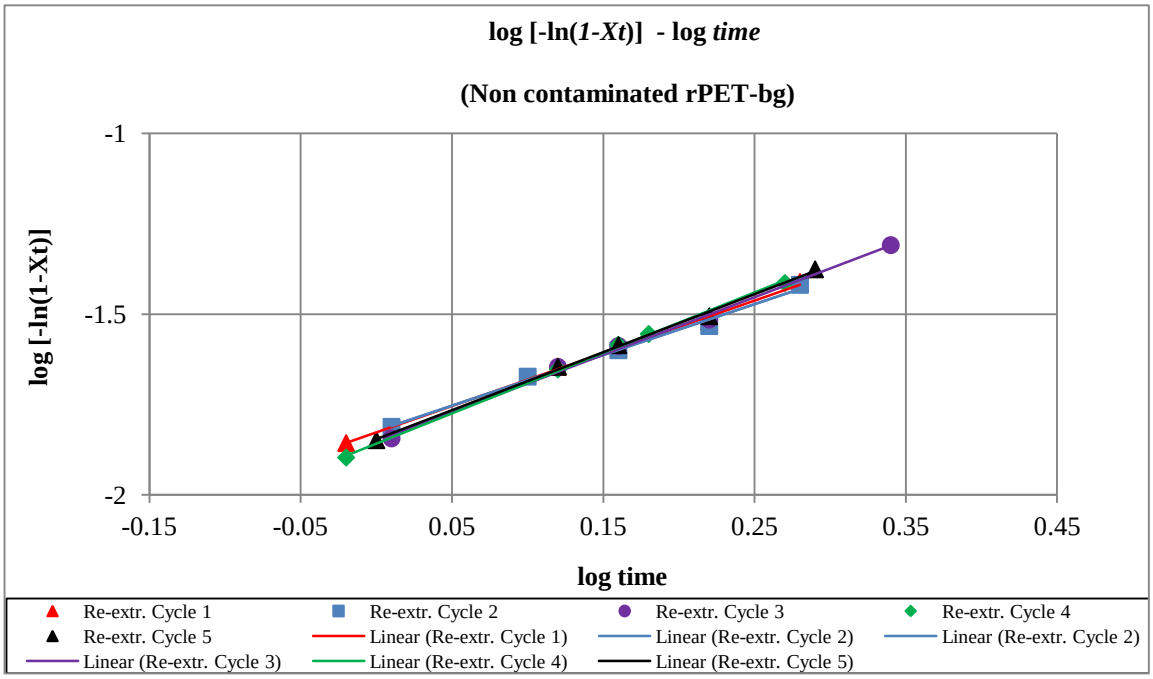

Figure 8.21 *Avrami* Plots of log [-ln(1-X_t)] Vs log*t* for Non-isothermal Crystallisation at Various Re-extrusion Cycles of non contaminated rPET-bg

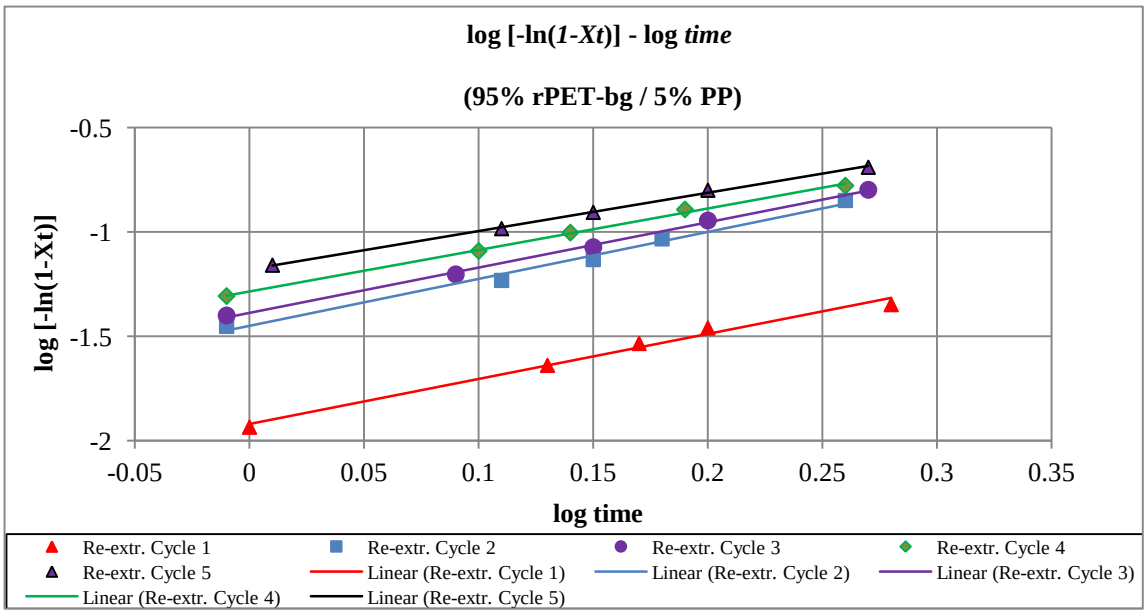

Figure 8.22 *Avrami* Plots of log [-ln(1-X_t)] Vs log*t* for Non-isothermal Crystallisation at Various Re-extrusion Cycles of rPET-bg contaminated with 5% PP

The *Avrami exponent* ***n*** and the calculated *rate* of *growth* $\boldsymbol{Z_t}$ as a function of *re-extrusion cycles* were extracted from the curves in *Figures 8.21* and *8.22* above and recorded in *Tables 8.21* and *8.22* below. Unlike for $\boldsymbol{Z_t}$ in the previous *Chapter 7*, which was corrected into $\boldsymbol{Z_C}$ because of the variation of *cooling rates*, the $\boldsymbol{Z_t}$ in this *Chapter 8*, was not corrected because the cooling rate was *constant*, $10^oC/min$, for all the *re-extruded samples* of the *5 cycles*.

As shown in *Table 8.21* below, the ***n*** values increased randomly with increased re-extrusion cycles in the *non contaminated rPET-bg*, which indicated random sporadic nucleation due to the large allowable crystallisation time. Whereas, in the *rPET-bg contaminated with 5% PP*, as shown in *Table 8.22* below, the ***n*** values increased at the start of the crystallisation process due to the presence of small amount of short chains which crystallised faster and resulted in a primary increase, but then decreased orderly and the spherulites growth varied from rod to disc and to sporadic shapes indicating that nucleation was slower than in the *non contaminated rPET-bg* with increasing re-extrusion cycles, as shown in *Figure 8.23*; this indicated that by increasing re-extrusion cycles, further cross-linking and branching were generated which made it difficult for *rPET-bg contaminated with 5% PP* to crystallise at lower cooling temperatures even with large allowable time. This confirmed the previously discussed lower crystallinity in the *rPET-bg contaminated with 5% PP* due to the inclusion of the PP contaminant. Also, this indicated that the *non contaminated rPET-bg* was crystallising faster. Both sporadic nucleation and fast crystallisation indicated the tendency of the *non contaminated* and *contaminated rPET-bg* in remaining less crystalline as shown by the very low $\boldsymbol{Z_t}$ values, which indicated unique characteristics of transparency and clarity. Despite the large allowable crystallisation time as function of low cooling rate, both materials showed tendency in crystallising at very slow rate which confirmed that re-extrusions contributed in strengthening the disordered nature of entangled chains making crystallisation more complex. $\boldsymbol{Z_t}$ values of *non contaminated rPET-bg* are lower than those of the *rPET-bg contaminated with 5% PP*; this could be attributed to the degree of diffusion which is a controlling factor at low temperature, whereas the rate of nucleation dominates at high temperature according to *Keith* and *Padden* [39], this diffusion rendered the growth rate extremely slow, i.e. at the low cooling rate of $10^oC/min$, crystallisation time was largely

available and accompanied by a lower Z_t. Therefore, the higher Z_t values of the *rPET-bg contaminated with 5% PP* accounted for slow crystallisation compared with fast crystallisation of the non contaminated *rPET-bg*, as shown in *Figure 8.24* below.

Extruded Samples **Non contaminated rPET-bg**				
Re-extrusion Cycles	***n***	***Nucleation Characteristics***	***Type***	Z_t
1	1.457	(n < 2) - Sporadic Nuclei		0.015
2	1.405			0.015
3	1.593			0.014
4	1.673			0.014
5	1.605			0.014

Table 8.21 *Avrami's* n and Z_t for non-isothermal Crystallisation of non contaminated rPET-bg

Extruded Samples **95% rPET-bg / 5% PP**				
Re-extrusion Cycles	***n***	***Nucleation Characteristics***	***Type***	Z_t
1	2.154	(n = 2) - Rod-Shaped Growth from Sporadic Nuclei	1 D	0.012
2	2.250	(n =2)- Disc- Shaped Growth from Instantaneous Nuclei	2 D	0.035
3	2.171	(n = 3) - Disc-Shaped Growth from Sporadic Nuclei	3 D	0.041
4	1.990	(n < 2) - Sporadic Nuclei		0.052
5	1.832			0.066

Table 8.22 *Avrami's* n and Z_t for non-isothermal Crystallisation of rPET-bg contaminated with 5% PP

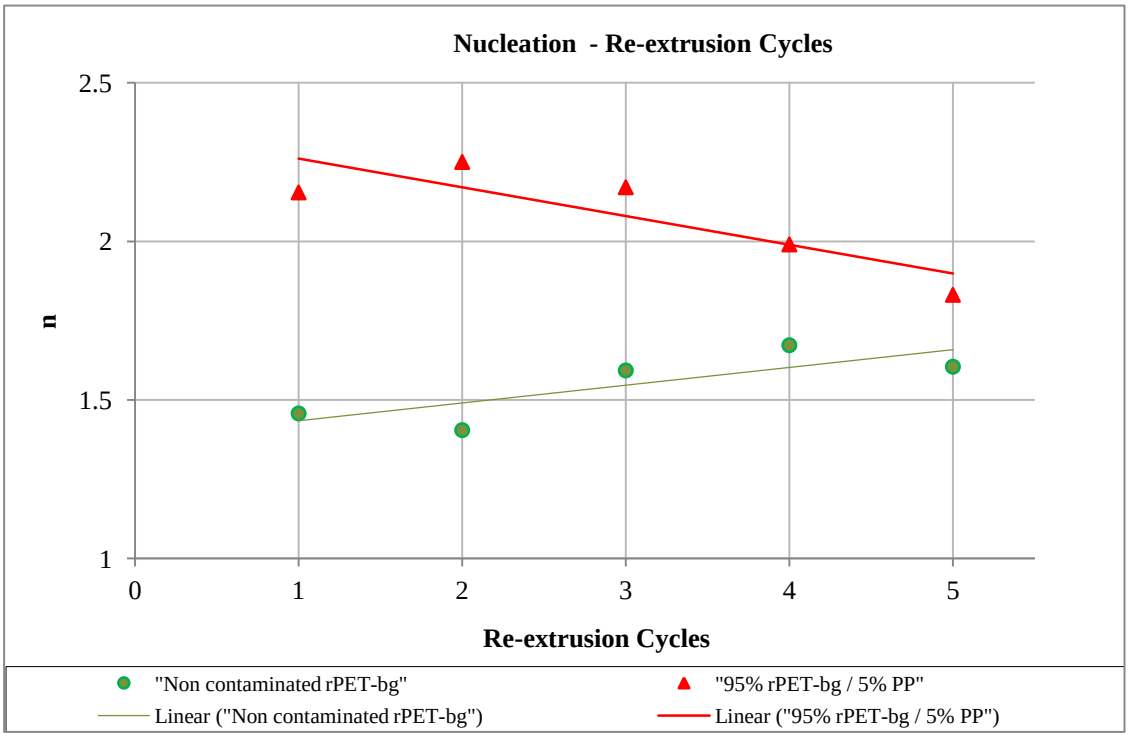

Figure 8.23 *Avrami's Exponent, n,* at Various Re-extrusion Cycles for Non-isothermal Crystallisation

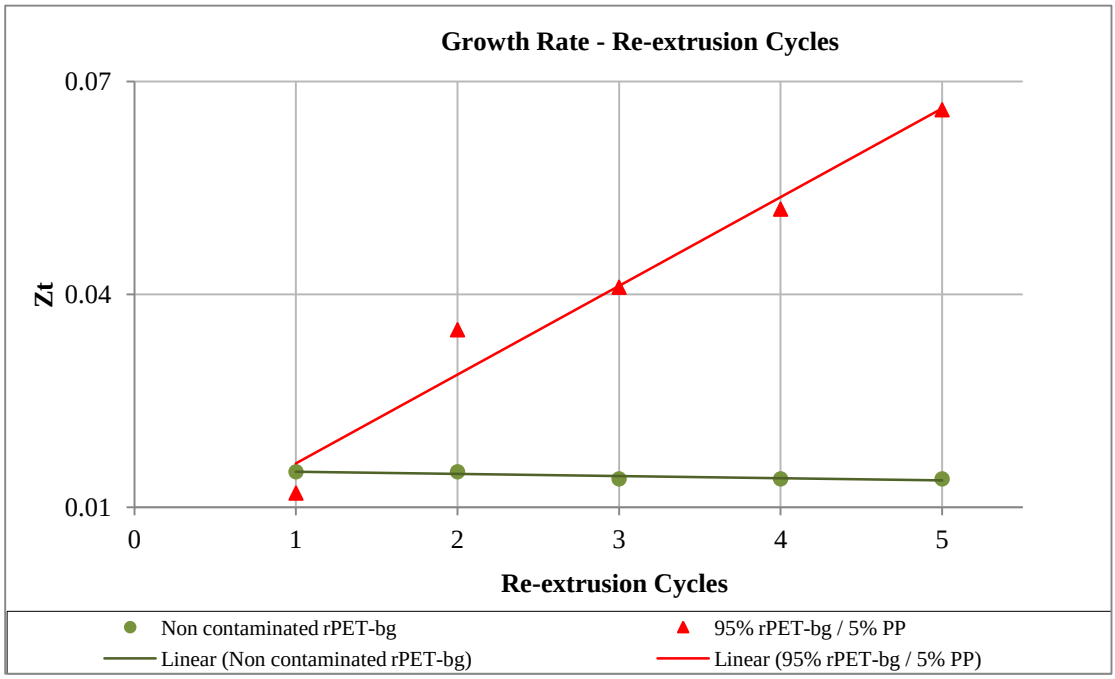

Figure 8.24 *Avrami's Growth Rate,* Z_t, at Various Re-extrusion Cycles for Non-isothermal Crystallisation

8.2 Conclusion

In light of the above investigation, it was shown that the inclusion of 5% *PP* influenced the thermal characteristics of the *rPET-bg matrix*, especially *crystallinity* which decreased with increasing *re-extrusions cycles* and that *cross-linking* and chains' branching predominated over *chains'-scission*. Also the *Avrami model* confirmed the outcome of the results obtained and showed that the crystallisation process depended on the re-extrusion cycles and their influence on nucleation and growth rates. By increasing *re-extrusion cycles*, the crystallisation process of the *rPET-bg contaminated with 5% PP* showed that *nucleation* and *molecular mobility* were competing together but decreased. Throughout the crystallisation process, the *small amount* of *contaminant, PP, lowered* the *chain mobility* of the *rPET-bg* matrix due to the *cross-linking*, chains' entanglement and *chains' branching* generated during *repetitive extrusions*, which contributed in *decreasing* the *nucleation* and consequently *decreasing crystallinity*

Thesis closing statement

As a result of this body of work it has been possible to show that the inclusion of *Small amounts* of *polyolefin contamination, HDPE* or *PP*, in the *rPET-bg* matrix had an impact on its overall characteristics. *rPET-bg* is more likely to be contaminated by *PP* more than by *HDPE* during the *mechanical recycling*, especially during the *sorting* and *separation process* of *bottle grade PET*, where cross contamination with bottles of *HDPE* and mostly *PP* caps and *closures* can happen easily and influence the properties of the final *bottle grade recycled PET*. Furthermore, a *5% PP weight* in the form of *bottle caps* and *closures* can easily pass through the sorting process during recycling. The DSC work performed on *non contaminated rPET-bg* and *rPET-bg contaminated with 5% PP* extruded samples at various *heating / cooling rates* and also at various *re-extrusions cycles* (*multiple extrusions*) and low *constant heating / cooling rates* and the validation by *Avrami* and *Ozawa models*, confirmed the outcome of this research work.

It was shown that the inclusion of small amounts of 5% *PP* influenced the thermal characteristics of the *rPET-bg matrix*, especially *crystallinity* which was *disrupted* and stabilised with increasing *cooling rates* and also *reduced* with *increasing re-extrusion cycles* as a result of generated cross-linking and molecular chains' branching.

Furthermore, the *Avrami* and *Ozawa models* confirmed that the crystallisation process of the *rPET-bg contaminated with 5% PP* depended on many influencing factors, such as impurities and the processing history but fully depended on the nucleation and spherulite growth mechanism. By increasing *cooling rates*, the crystallisation process of the *rPET-bg contaminated with 5% PP* showed that *nucleation* and *molecular mobility* increased with increasing *temperature*. In contrast, by increasing *re-extrusion cycles*, the crystallisation process of the *rPET-bg contaminated with 5% PP* showed that *nucleation* and *molecular mobility* were competing together but decreased. Throughout the crystallisation process, the *small amount* of *contaminant*, *PP*, played dominant role in *lowering* the *chain mobility* of the *rPET-bg* matrix due to the *cross-linking* coupled with chains' branching generated during *repetitive extrusions*, which contributed to *decreasing* the *nucleation* and *decreasing crystallinity*. Reducing *crystallinity* in *PET bottle* manufacturing is of paramount importance in enhancing bottles' clarity or transparency with respect to related characteristics which are required in bottle manufacturing, such as the degree of *toughness* and resistance to failure under stress of the produced bottles,

especially during storage. A *crystallinity-toughness* requirement should be taken in consideration when designing bottles and products with minimum *crystallinity*. From industrial perspective, recyclers of post-consumer polymeric materials, such as *PET* or other polymeric materials, are continuously spending enormous manpower and expensive cost in tackling the problem of contamination and its impact on the final produce, especially in the bottle manufacturing field where the primary priority is the continuous processes' optimization to reduce and minimise crystallinity. The growth of recycling post-consumer polymeric materials means that *polyolefin contaminants*, especially *PP*, must be taken in consideration for potential re-usability to enhance the recycling capabilities, reaching environmental protection targets and reducing overall costs. Recycling is the future of manufacturing in the field of polymers and recycling involves *repetitive extrusions* for cost effectiveness and the confirmation of cross-linking and chains' branching generated as a result of *repetitive extrusions* is of paramount importance in tackling *crystallinity* related complications. ***This research work*** showed originality in investigating the role of *small amounts* of *polyolefin* contamination on the overall characteristics, with emphasis on the influence of *5% PP* on the *thermal characteristics* of bottle grade recycled polyethylene terephthalate, *rPET-bg*. Despite the research works done in the field of *PET recycling*, this research work dealt with a particular grade, *bottle grade*, which is used vastly and had an important impact on the environment when recycled, so specific research works dealing with its fundamental characteristics is of paramount importance and it is exactly what this research work had delivered. Furthermore, the confirmation of *crystallinity reduction* by *Avrami* and *Ozawa models* in the *rPET-bg contaminated with 5% PP* is a step forward in changing thoughts and an *original* insight on the *influence* of *polyolefin contamination* at industrial scale. As previously mentioned, recycling is the future of manufacturing in the field of polymers and the use of *repetitive extrusions* as a compounding mean and its cost effectiveness coupled with the outcome of this research work on the cross-linking and chains' branching generation, is of paramount importance in tackling crystallinity related complications, and this outcome added to the acquired knowledge in the field and made of this research work original.

Chapter 9

Summary of Conclusions and Future Research Work

9.1 Summary of Conclusions

The outcome of this research work showed that:

1. The thermal, spectroscopic, flow, mechanical and processing investigation of the material supplied by *Closed Loop Recycling limited* in the form of *flakes* showed that the *flakes* originated from an *amorphous* material which underwent cooling stages at elevated cooling rates by a *processing technique* using engineering materials of excellent flow properties coupled with excellent stretch-ability, such as *PET* and intended to produce clear and *transparent* products, such as *bottles.* Also, the determined tensile and impact properties showed characteristics, such as *brittleness* and *impact strength*, similar and inherited from *PET*. Furthermore, some characteristics showed *history* of *processing* and *degradation* in properties and presence of *contaminants*, such as soil particulates, which confirmed that the *flakes* originated from a *recycled* source of mixed batches of different colours and encountered direct contact with soil either before or at *recycling* stage. The obtained information allowed the identification of the *flakes* supplied as *recycled bottle grade PET*, or *rPET-bg*.

2. The inclusion of small amounts of polyolefin contaminants, *HDPE* or *PP* influenced the overall characteristics of the *rPET-bg matrix* and the various analyses confirmed the generation of very small polymer chains, resulting from thermo-mechanical degradation encountered during processing, which contributed to the formation of sporadic crystalline domains and influenced the overall characteristics. The exhibition of individual melting peaks indicated *incompatibility* and *immiscibility* of the polar *PET* and the non polar *HDPE* and *PP*, which in poor to nil chemical bonding. The premature melting of *HDPE* and *PP* primary crystals improved the overall balanced rates

and the decreased *crystallinity* confirmed the presence of reduced sporadic and dispersed small crystalline domains. Additionally, the *HDPE* and *PP* influenced the processing conditions and consequently affected the overall characteristics. Furthermore, the tensile and impact properties showed decrease of *stiffness* as a result of decreased *crystallinity* and confirmed once more the *incompatibility* of the contaminants *HDPE* or *PP* and the *rPET-bg*. In contrast, the *HDPE* or *PP* inclusion showed a fracture mechanism change from craze crack growth, for *rPET-bg*, to ductile shear yielding for the contaminated materials, resulting in decreased *stiffness*, increased *toughness* and increased *impact strength*.

3. The inclusion of *5% PP* influenced the thermal characteristics of the *rPET-bg matrix*, especially *crystallinity* which decreased with tendency of stabilising with increasing *cooling rates*, and the *Avrami* and *Ozawa models* confirmed this finding and showed that the crystallisation process depended on many influencing factors, such as *impurities*, *nucleation* and *growth rates*. And that *nucleation* and *molecular mobility* increased with increasing *cooling temperature* and *cooling rates*, whereas the *growth rate* decreased with increasing *cooling temperature* and increased with increasing *cooling rates*. Throughout the crystallisation process, the *5% PP*, played dominant role in *increasing* the *chain mobility* in the *non contaminated rPET-bg matrix* and consequently stabilising the % crystallinity.

4. The inclusion of 5% *PP* influenced the thermal characteristics of the *rPET-bg matrix*, especially *crystallinity* which decreased with increasing *re-extrusions cycles* and that *cross-linking* and *chains' branching* predominated over *chains'-scission*. Also the *Avrami model* confirmed this finding and showed that the crystallisation process depended on the *re-extrusion cycles* and their influence on *nucleation* and *growth rates*. By increasing *re-extrusion cycles*, the crystallisation process of the *rPET-bg contaminated with 5% PP* showed that *nucleation* and *molecular mobility* were competing together but decreased. Throughout the crystallisation process, the inclusion of *PP lowered* the *chain mobility* of the *rPET-bg* matrix due to the *cross-linking* and *chains' branching* generated during *repetitive extrusions*, which contributed in *decreasing* the *nucleation* and consequently *decreasing crystallinity*.

9.2 Future Research Work

Recycled post-consumer polymeric materials, such as *PET*, *polyolefin* or others, are in continuous demand because of the dramatic decrease of raw polymeric materials. Research works on the potential of these recycled polymeric materials will enhance the understanding of their potential with or without polymeric contamination and the improvement and development of recycling processes capable of overcoming the problem of polymeric contamination or others. For these purposes and despite the researches done in this field, many areas are still to be investigated and explored in the purpose of changing thoughts about the presence of small amounts of polymeric contaminants in specialist polymeric matrices.

The following are some of the suggested future research works:

1. Investigating the *effect* of *post-consumer polyolefin contaminants* on *rPET-bg* in the presence of *chain extender* at *various extrusion screw speeds*; this investigation will give an insight on the *combination* of *chain extender* and *polyolefin contaminants* in the *rPET matrix*.

2. Investigating the *crystallisation-crosslinking competition* in *contaminated rPET-bg* with both *small amounts* of *HDPE* and *PP* as *contaminants* in the presence of *chain extender*; this investigation will clarify the *effect* of combined *multi-contamination-crosslinking* on the *transparency* of *rPET*.

3. Investigating the *effect* of *chain extender* on the *permeability* of bottles made from *contaminated rPET-bg* with polyolefin; this investigation will enhance the understanding of *fluid permeation mechanism* in *contaminated rPET bottles*.

References and Bibliography

[1] *Frank Welle,* Twenty years of PET bottle to bottle recycling- An overview, *Resources, Conservation and Recycling, Volume 55, Issue 11, Pages 865-875, Sept. 2011*

[2] Plastics: The Facts 2014-15 Report, *http://www.plasticseurope.org/Document/plastics-the-facts-20142015.aspx?Page=DOCUMENT&FolID=2*
Accessed on: 23.01.2015

[3] *http://ec.europa.eu/environment/waste/framework/*
Accessed on: 15.03.2015

[4] *http://www.legislation.gov.uk/ukpga/2008/27/contents*
Accessed on: 17.03.2015

[5] *http://ec.europa.eu/clima/policies/package/index_en.htm*
Accessed on: 10.01.2010

[6] *Santosh K. Gupta* and *Anil Kumar,* Reaction Engineering of Step Growth Polymerization, Plenum Press, New York and London, 1987.

[7] *T. Rieckmann and S. Völker,* Poly(ethylene Terephthalate, in Modern Polyesters: Chemistry and Technology of Polyesters and Copolyesters, in *John Scheirs and Timothy E. Long* (Ed.), John Wiley and Sons Publishers, Pages 31-116, England, 2003.

[8] *R. Binsack*, "Thermoplastic Polyesters", *in* Engineering Thermoplastics: Polycarbonates, Polyacetals, Polyesters and Cellulose Esters, *Ludwig Bottenbruch* (Ed.), Hanser Publishers, Munich. Vienna. New York, 1996, Pages 06-111

[9] *B. Culbert and A. Christel*, "Continuous SSP of Polyesters", in Modern Polyesters: Chemistry and Technology of Polyesters and Copolyesters, *John Scheirs and Timothy E.* Long (Ed.), John Wiley and Sons Publishers. England, 2003, Pages 143-194

[10] *G. Reese*, "Polyester Fibers", in Modern Polyesters: Chemistry and Technology of Polyesters and Copolyesters, *John Scheirs and Timothy E.* *Long* (Ed.), John Wiley and Sons Publishers. England, 2003, Pages 401-434

[11] *H. Zhang, Z-G. Wen,* The consumption and recycling collection system of PET bottles, *Waste Management, Volume 34, Issue 6, Pages 987-998, June 2014*

[12] *L. Shen, E. Worrell, MK. Patel,* Open-loop recycling: A LCA case study of PET bottle-to-fibre recycling,
Resources, Conservation and Recycling, Volume 55, Issue 1, Pages 34-52, Nov. 2010

[13] *Y. Liu, M. Wang, Z. Pan,* Catalytic depolymerization of polyethylene terephthalate in hot compressed water,
The Journal of Supercritical Fluids, Volume 62, Pages 226-231, Feb. 2012

[14] *H. Kurokawa, M-A. Ohshima, K. Sugiyama, H. Miura,* Methanolysis of polyethylene terephthalate (PET) in the presence of aluminium tiisopropoxide catalyst to form dimethyl terephthalate and ethylene glycol,
Polymer Degradation and Stability, Volume 79, Issue 3, Pages 529-533, March 2003

[15] *M. Ghaemy, K. Mossaddegh,* Depolymerisation of poly(ethylene terephthalate) fibre wastes using ethylene glycol,
Polymer Degradation and Stability, Volume 90, Issue 3, Pages 570-576, Dec. 2005

[16] *M. del M. C. Lopez, A. I. A. Pernas, M. J. A. López, A. L. Latorre, J.M. L. Vilariño, M. V. G. Rodríguez ,* Assessing changes on poly(ethylene terephthalate) properties after recycling: Mechanical recycling in laboratory versus postconsumer recycled material,
Materials Chemistry and Physics, Volume 147, Issue 3, Pages 884-894, Oct. 2014
[17] *R. Navarro, S. Ferrándiz, J. López, V.J. Seguí,* The influence of polyethylene in the mechanical recycling of polyethylene terephtalate,
J. of Materials Processing Tech., Volume 195, Issue 1-3, Pages 110-116, January 2008

[18] *K. Friedrich, M. Evstatiev,S. Fakirov, O. Evstatiev, M. Ishir, M. Harrass,* Microfibrillar reinforced composites from PET/PP blends: processing, morphology and mechanical properties,
Composites Science and Technology, Volume 65, Issue 1, Pages 107-116, January 2005

[19] *S.H. Kim, S.H. Ahn, T. Hirai,* Crystallisation Kinetics and Nucleation Activity of silica nanoparticle filled poly(ethylene 2,6 naphtalene), *Polymer, Volume 44, Issue 19, Pages 5625-5634, September 2003*

[20] *S.A Jabarin,* Crystallization kinetics of polyethylene terephthalate. II. Dynamic crystallization of PET,
Journal of Applied Polymer Science, Volume 34, Issue 1, Pages 97-102, July 1987

[21] *M. R. Tant and W.T. Culberson,* Effect of molecular weight on spherulite growth rate of poly(ethylene terephthalate) via real-time small angle light scattering
Polymer Engineering and Science, Volume 33, Issue 17, Pages 1152-1156, Sept.1993

[22] *M. Paci, F.P. La Mantia,* Competition between degradation and chain extension during processing of reclaimed poly(ethylene terephthalate),
Polymer Degradation and Stability, Volume 61, Issue 3, Pages 417-420, 1998

[23] *N. Torres, J.J. Robin, B. Boutevin,* Study of thermal and mechanical properties of virgin and recycled poly(ethylene terephthalate) before and after injection molding,
European Polymer Journal, Volume 36, Issue 10, Pages 2075-2080, 1 October 2000

[24] *Jan Pospíšil, Zdeněk Horák, Zdeněk Kruliš, Stanislav Nešpůrek, Shin-ichi Kuroda,* Degradation and aging of polymer blends I. Thermomechanical and thermal degradation,
Polymer Degradation and Stability, Volume 65, Issue 3, Pages 405-414, September 1999

[25] *W. Camacho, S. Karlsson,* Assessment of thermal and thermo-oxidative stability of multi-extruded recycled PP, HDPE and a blend thereof,
Polymer Degradation and Stability, Volume 78, Issue 2, 2002, Pages 385-391

[26] *J. D. Badía, F. Vilaplana, S. Karlsson, A. Ribes-Greus,* Thermal analysis as a quality tool for assessing the influence of thermo-mechanical degradation on recycled polyethylene terephthalate,
Polymer Testing, Volume 28, Issue 2, Pages 169-175, April 2009

[27] *R. Assadi, X. Colin, J. Verdu,* Irreversible structural changes during PET recycling by extrusion, *Polymer, Volume 45, Issue 13, Pages 4403-4412, June 2004*

[28] *LK. Nait-Ali, X. Colin, A. Bergeret,* Kinetic analysis and modelling of PET macromolecular Changes during its mechanical recycling by extrusion,
Polymer Degradation and Stability, Volume 96, Issue 2, Pages 236-246, February 2011

[29] *J. W. Nicholson***,** The Chemistry of Polymers, Royal Society of Chemistry, Turpin Distribution Services Ltd.

[30] *D. C. Bassett,* Principles of polymer morphology, D. C. Bassett, Cambridge Solid State Series, Cambridge University Press, Cambridge, England, 1981

[31] *S. A. Jabarin, D. C. Balduff,* Gel Permeation Chromatography of Polyethylene Terephalate,
Journal of Liquid Chromatography, Volume 5, Issue 10, Pages 1825-1845, 1982

[32] *J.C. Moore,* Gel permeation chromatography. I. A new method for molecular weight distribution of high polymers,
J. of Polym. Sc. Part A: General Papers, Volume 2, Issue 2, Pages 835-843, Feb. 1964

[33] *R. J. Young and P. A. Lovell,* Introduction to polymers (second edition), Chapman and Hall, London, 1991.

[34] *A. Galeski, E. Piorkowska,* Localized volume deficiencies as an effect of spherulite growth. I. The two dimensional cases.
Journal of Polymer Science: Polymer Physics Edition, Volume 21, Issue 8, Pages 1299-1312, August 1983

[35] *K. A. Granath, B. E. Kyist,* Molecular weight distribution analysis by gel chromatography on sephadex,
Journal of Chromatography A, Volume 28, Pages 69-81, 1967

[36] *M R Milana, M Denaro, L Arrivabene, A Maggio, L Gramiccioni,*
Gel permeation chromatography (GPC) of repeatedly extruded polyethylene terephthalate (PET),
Food Additives and Contaminants, Volume 15, Issue 3, 1998

[37] *R. E. Robertson,* Polymer Order and Polymer Density,
Journal of Physical Chemistry, Volume 69, Issue 5, Pages 1575-1578, 1965

[38] *J. D. Badia, E. Strömberg, S. Karlsson, A. Ribes-Greus,* The role of crystalline, mobile amorphous and rigid amorphous fractions in the performance of recycled poly (ethylene terephthalate) (PET),
Polymer Degradation and Stability, Volume 97, Issue 1, Pages 98-107, January 2012

[39] *H. D. Keith, F. J, Padden Jr,* Spherulitic Crystallization from the Melt. I. Fractionation and Impurity Segregation and Their Influence on Crystalline Morphology,
Journal of Applied Physics, Volume 35, 1270 (1964)

[40] *VBF. Mahot,* Crystallization of polymers,
J. of Thermal Analysis and Calorimetry, Volume 102, Issue 2, Pages 403-412, Nov. 2010

[41] *W. Banks, A. Sharples, JN. Hay,* The effect of simultaneously occurring processes on the course of polymer crystallization,
Journal of Polymer Science, Part A, Volume 2, Issue 9, Pages 4059-4067, 1964

[42] *C. C. Price,* Some relative monomer reactivity factors,
Journal of Polymer Science, Part A, Volume 3, Issue 5,
Pages 772-775, October 1948

[43] *I H. Hillier,* Modified avrami equation for the bulk crystallization kinetics of spherulitic polymers,
Journal of Polymer Science, Part A, Volume 3, Issue 9, Pages 3067-3078, 1965

[44] *O. Verhoyen, F. Dupret, R. Legras,* Isothermal and non-isothermal crystallization kinetics of polyethylene terephthalate: Mathematical modeling and experimental measurement,
Polymer Eng. and Science, Volume 38, Issue 9, Pages 1594-1610, Sept. 1998

[45] *X. F Lu, J. N Hay,* Isothermal crystallization kinetics and melting behaviour of poly(ethylene terephthalate), *Polymer, Volume 42, Pages 9423-31, November 2001*

[46] *A. Bishara, H.I. Shaban,* Nonisothermal crystallization kinetics of poly(ethylene terephthalate) and poly(methyl methacrylate) blends.
Journal of Applied Polymer Science, Volume 101, Issue 6, Pages 3565-3571, Sept. 2006

[47] *A. A-Mulla, H. I. Shaban,* Degradation kinetics of poly(ethylene terephthalate) and poly(methyl methacrylate) blends.
Polymer Bulletin, Volume 58, Issue 5-6, Pages 893-902, December 2006

[48] *M. Avrami,* Kinetics of Phase Change. I. General Theory,
Journal of Chemical Physics, Volume 7, Issue 12, Pages 1103, 1939

[49] *M. Avrami,* Kinetics of Phase Change. II. Transformation-Time Relations for Random Distribution of Nuclei.
Journal of Chemical Physics, Volume 8, Issue 2, Pages 212, 1940

[50] *M. Avrami,* Kinetics of Phase Change. III. Granulation, Phase Change, and Microstructure,
Journal of Chemical Physics, Volume 9, Issue 2, Pages 177, 1941

[51] *T. Ozawa,* Kinetics of Non-Isothermal Crystallisation, *Polymer, Volume 12, Issue 3, Pages 150-158, March 1971.*

[52] *A Sharples,* Introduction to Polymer Crystallisation, Chapter 4, Edward Arnold (Publisher), London 1966.

[53] *E. N. Doyle,* The Development and Use of Polyester Products,
Mc Graw-Hill Book Company. London, New York, S/Francisco, Toronto, Sydney. 1969.

[54] *C-C. Lin, S. Baliga,* A study on the polycondensation of bis-hydroxyethyl terephthalate,
Journal of Applied Polymer Science, Volume 31, Issue 8, Pages 2483-2489, 1986

[55] *S. Collins, S. K. Peace, R. W. Richards,* Transesterification in Poly(ethylene terephthalate), Molecular Weight and End Group Effects,
Macromolecules, Volume 33, Issue 8, Pages 2981-2988, 2000

[56] *K. Ravindranath, R. A. Mashelkar,* Polyethylene terephthalate—I. Chemistry, thermodynamics and transport properties,
Chemical Engineering Science, Volume 41, Issue 9, Pages 2197-2214, 1986

[57] *W. R. Sorenson, T. W. Cambell,* Preparative methods of polymer chemistry, 2nd Ed.
J. of Polym Sc. Part A-1: Polymer Chemistry, Volume 8, Issue 1, Page 283, Jan. 1970

[58] *J. H. Youk, R. P. Kambour, WJ. MacKnight,* Polymerization of Ethylene Terephthalate Cyclic Oligomers with Antimony Trioxide,
Macromolecules, Volume 33, Issue 10, Pages 3594-3599, 2000

[59] *H. Zimmermann, N. T. Kim,* Investigations on thermal and hydrolytic degradation of poly(ethylene terephthalate),
Polymer Eng. And Science, Volume 20, Issue 10, Pages 680-683, July 1980

[60] *D. G. Baird, D. I. Collias,* Polymer Processing: Principles and Design, 2nd Edition,
Macromolecules, Volume 33, Issue 10, Pages 3594-3599, 2000

[61] *P. J. Flory,* Principles of Polymer Chemistry, Chapter 3, Cornell Univ. Press, 1953.

[62] *V.V. Korshak, S. V. Vinogradova,* Polyesters, Chapter 6, Pergamon Press, 1964.

[63] *H. W. Coover Jr.,* F. B. Joyner, *N. H. Shearer Jr.,* Solid Phase Process for Linear Superpolyesters, U.S. Patent 3,075, 952, 1963.

[64] *F. Villain, J. Goudane, M. Vert,* Thermal degradation of polyethylene terephthalate: study of polymer stabilization,
Polymer Degradation and Stability, Volume 49, Issue 3, Pages 393-397, 1995

[65] *J. A. Brydson,* Plastics Materials, (Fifth Edition), *Pages 72-104, 1989*

[66] *F. Samperi, C. Puglisi, R. Alicata, G. Montaudo*, Thermal degradation of poly(ethylene terephthalate) at the processing temperature,
Polymer Degradation and Stability, Volume 83, Issue 1, Pages 3-10, Jan. 2004

[67] *W. Romao, MF. Franco, YE. Corilo, MN. Eberlin, MAS. Spinace, M-A. De Paoli*, Poly (ethylene terephthalate) thermo-mechanical and thermo-oxidative degradation mechanisms,
Polymer Degradation and Stability, Volume 94, Issue 10, Pages 1849-1859, Oct. 2009

[68] *J. D. Cooney, M. Day, D. M. Wiles*, Thermal degradation of poly(ethylene terephthalate): A kinetic analysis of thermogravimetric data,
Journal of Applied Polymer Science, Volume 28, Issue 9, Page 2887-2902, 1983

[69] *G. Wypych*, Data on Specific Polymers,
Handbook of Material Weathering (Fifth Edition), *Pages 351-546, 2013*

[70] *J. C. Arnold*, Environmental Effects on Crack Growth in Polymers,
Comprehensive Structural Integrity, Volume 6, Pages 281-319, 2003

[71] *V. B. Gupta and Z. Bashir*, "PET Fibers, Films and Bottles", in Handbook of thermoplastic Polyesters: Homopolymers, Copolymers, Blends and Composites, *Stoyko Fakirov* (Ed.), Volume 1, Wiley-VCH. Weinheim, 2002

[72] Closed Loop Recycling Ltd, *http://www.closedlooprecycling.co.uk/*
Accessed on: 30.09.2009

[73] *J. Scheirs*, Polymer recycling: science, technology and application,
John Wiley and Sons, Chichester, 1998.

[74] *D. Paszun, T. Spychaj*, Chemical Recycling of Poly(ethylene terephthalate),
Ind. and Engineering Chemistry Research, Volume 36, Issue 4, Pages 1373-1383, 1997

[75] *J. Milgrom*, PET, in Plastics recycling (Ed. Ehring R J), Hanser Verlag, Pages 45-72, 1992.

[76] *M. N. Marathe, D. A. Dabholkar, M. K. Jain*, Process for the recovery of dimethyl terephthalate from polyethylene terephthalate,
GB Patent 2641916, 1980.

[77] *R. Scheirs*, Recycling of PET, in Polymer recycling: science, technology and application, John Wiley and Sons, Chichester, Pages 119-182, 1998.

[78] *D. D. Cornell*, Depolymerization of PET for food packaging,
Proceeding Conference, Recycling RETEC, Society of Plastics Engineers, 1993.

[79] *A. Fujita, M. Sato, M. Murakami*, Depolymerization of polyester scraps,
Japanese Patent 06 248 646; CA 105:7063, 1985

[80] *H. S. Ostrowski*, Continuous atmospheric depolymerization of polyester,
US Patent 3884850, 1975.

[81] *S. Baliga, W. T. Wong,* Depolymerization of PET recycled from post-consumer soft-drink bottles,
J. of Polymer Science: Part A, Polym Chem, Vol.27, Issue 6, Pages 2071-2082, May 1989

[82] *J. Y. Chen, C. F. Ou, Y. C. Hu, C. C. Lin,* Depolymerization of poly(ethylene terephthalate) resin under pressure,
J. of Applied Polymer Science, Volume 42, Issue 6, Pages 1501-1507, March 1991

[83] *J. R. Campanelli, M. R. Kamal, D. G. Cooper,* Kinetics of glycolysis of poly(ethylene terephthalate) melts,
J. of Applied Polymer Science, Volume 54, Issue 11, Pages 1731-1740, December 1994

[84] *G. Guclu, A. Kasgoz, S. Ozbudak, S. Ozgumus, M. Orbay,* Glycolysis of poly(ethylene terephthalate) wastes in xylene,
J. of Applied Polymer Science, Volume 69, Issue 12, Pages 2311-2319, September 1998

[85] *T. Yoshioka, T. Sato, A. Okuwaki,* Hydrolysis of waste PET by sulfuric acid at 150^{o}C for a chemical recycling,
J. of Applied Polymer Science, Volume 52, Issue 9, Pages 1353-1355, September 1994

[86] *H. Kamatani, S. Konagaya, S. Nakamura,* Effect of phosphoric acid on the polycondensation of bis(2-hydroxyethyl) terephthalate catalyzed by Sb (III) compounds,
Polymer Journal, Volume 12, Pages 125-130, 1980

[87] *K. S. Seo, J. D. Cloyd,* Kinetics of hydrolysis and thermal degradation of polyester melts,
J. of Applied Polymer Science, Volume 42, Issue 3, Pages 845-850, February 1991

[88] *C. Y. Kao, B. Z. Wan, W. H. Cheng,* Kinetics of hydrolytic depolymerisation of melt poly(ethylene terephthalate),
Ind. and Engineering Chemistry Research, Volume 37, Issue 4, Pages 1228-1234, 1998

[89] *J R. Campanelli, D G Cooper, M R Kamal,* Catalyzed hydrolysis of poly(ethylene terephthalate) melts,
J. of Applied Polymer Science, Volume 53, Issue 8, Pages 985-991, August 1994

[90] *T Yoshioka, M Ota, A. Okuwaki,* Conversion of a Used Poly(ethylene terephthalate) Bottle into Oxalic Acid and Terephthalic Acid by Oxygen Oxidation in Alkaline Solutions at Elevated Temperatures,
Ind. and Eng. Chemistry Research, Volume 42, Issue 4, Pages 675-679, Jan. 2003

[91] *C Y Kao, W H Cheng, B Z Wan,* Investigation of alkaline hydrolysis of poly(ethylene terephthalate) by differential scanning calorimetry and thermogravimetric analysis,
J. of Applied Polymer Science, Volume 70, Issue 10, Pages 1939-1945, December 1998

[92] *B Z Wan, C Y Kao, W H Cheng,* Kinetics of depolymerization of polyethylene terephthalate in potassium hydroxide solution,
Ind. and Eng. Chemistry Research, Volume 40, Issue 2, Pages 509-514, 2001

[93] *J R Campanelli, M R Kamal, D G Cooper,* A Kinetic study of the degradation of poly(ethylene terephthalate) at high temperatures,
J. of Applied Polymer Science, Volume 48, Issue 3, Pages 443-451, April 1993

[94] *A Noritake, M Hori, M Shigematsu and M Tanahashi,* Recycling of PET using High- Pressure Steam Treatment, *Polymer, Volume 40, Issue 6, Pages 498-502, 2008*

[95] *M. Lopez, A. Pernas, M. Lopez, A. Latorre,JM. Vilarino, M. Rodriguez,* Assessing changes on poly(ethylene terephthalate) properties after recycling: Mechanical recycling in laboratory versus postconsumer recycled material,
Materials Chemistry and Physics, Volume 147, Issue 3, Pages 884-894, Oct. 2014

[96] *K. Hamad, M. Kaseem, F. Deri,* Recycling of waste from polymer materials: An overview of the recent works,
Polymer Degradation and Stability, Volume 98, Issue 12, Pages 2801-2812, Dec. 2013

[97] *B Gumther, H G Zachmann,* Influence of molar mass and catalysts on the kinetics of crystallization and on the orientation of poly(ethylene terephthalate),
Polymer, Volume 24, Issue 8, Pages 1008-1014, August 1983

[98] *L.H Sperling,* Introduction to Physical Polymer Science, 2nd Edition, John Wiley and Sons, Singapore, *Pages 232-235, 1993*

[99] *I. Seganov, J. M. Schultz, S. Fakirov,* Effect of diethylene glycol content and annealing temperature on the structure and properties of poly(ethylene terephthalate),
Journal of Applied Polymer Science, Volume 32, Issue 2, Pages 3371–3392, August 1986

[100] *F. Awaja, D. Pavel,* Statistical models for optimisation of properties of bottles produced using blends of reactive extruded recycled PET and virgin PET,
European Polymer Journal, Volume 41, Issue 9, Pages 2097-2106, September 2005

[101] *F. Awaja, D. Pavel,* Inj. stretch blow moulding process of reactive extruded Recycled and virgin PET blends,
European Polymer Journal, Volume 41, Issue 11, Pages 2614-2634, November 2005

[102] *A. Oromiehie, A. Mamizadeh,* Recycling PET beverage bottles and improving properties,
Polymer International, Volume 53, Issue 6, pages 728–732, June 2004

[103] *L. Incarnato, P. Scarfato, L. Di Maio, D. Acierno,* Structure and rheology of recycled PET modified by reactive extrusion,
Polymer, Volume 41, Issue 18, Pages 6825-6831, August 2000

[104] *F. Daver, R. Gupta, E. Kosior,* Rheological characterisation of recycled poly(ethylene terephthalate) modified by reactive extrusion,
J. of Materials Processing Tech., Volume 204, Issues 1–3, Pages 397-402, August 2008

[105] *L A Utracki,* PP/PET blends, in Commercial Polymer Blends,
Chapman and Hall, London, Pages 276-278.

[106] *N Kunimune, K Yamada, Y W Leong, S Thumsorn, H Hamada,* Influence of the Reactive Processing of Recycled Poly(ethylene terephthalate) / Poly(ethylene-co-glycidyl methacrylate) Blends,
Journal of Applied Polymer Science, Volume 120, Issue 1, Pages 50-55, April 2011

[107] *C P Papadopoulou, N K Kalfoglou,* Comparison of Compatibilizer Effectiveness for PET/PP Blends: Their Mechanical, Thermal and Morphology Characterization,
Polymer, Volume 41, Issue 7, Pages 2543-2555, March 2000

[108] *L. Yao and C. Beatty,* The in situ Compatibilization of HDPE/PET Blends,
Copyright © 1999 Plastics Design Library Published by Elsevier Inc.

[109] *T L Carté, A Moet,* Morphological origin of super thoughness in poly(ethylene terephthalate) / polyethylene blends,
J. of Applied Polymer Science, Volume 48, Issue 4, Pages 611-624, April 1993

[110] *S Kim, C E Park, J H An, D Lee, J Kim,* The Effect of Functional Group Content on Poly(ethylene terephthalate)/High Density Polyethylene Blends Compatibilized with Poly(ethylene-*co*-acrylic acid),
Polymer Journal, Volume 29, Pages 274-278, 1997, Doi:10.1295/polymj.29.274

[111] *T D Traugott, J W Barlow, D R Paul,* Mechanical compatibilization of high density polyethylene-poly(ethylene terephthalate) blends,
J. of Applied Polymer Science, Volume 28, Issue 9, Pages 2947-2959, September 1983

[112] *N. K. Kalfoglou, D. S. Skafidas, J. K. Kallitsis, J-C. Lambert, L V-Der Stappen,* Comparison of compatibilizer effectiveness for PET/HDPE blends,
Polymer, Volume 36, Issue 23, Pages 4453-4462, 1995

[113] *D-H. Kim, K-Y Park, K-D Suh,* Improved compatibility of high density polyethylene / poly(ethylene terephthalate) blend by the use of blocked isocyanate group,
J. of Applied Polymer Science, Volume 78, Issue 5, Pages 1017-1024, October 2000

[114] *M. Pracella, D. Chionna, R. Ishak, A. Galeski,* Recycling of PET and Polyolefin Based Packaging Materials by Reactive Blending,
Polymer-Plastics Tech. and Eng., Volume 43, Issue 6, Pages 1711-1722, 2004

[115] *K. Friedrich, M. Evstatiev, S. Fakirov, O. Evstatiev, M. Ishii, M. Harrass,* Microfibrillar reinforced composites from PET/PP blends: processing, morphology and mechanical properties,
Composite Science and Technology, Volume 65, Issue 1, Pages 107-116, January 2005

[116] *S Thumsorn, K Yamada, Y W Leong, H Hamada,* Development of Cockleshell-Derived CaCO3 for Flame Retardancy of Recycled PET / Recycled PP Blend,
Materials Sciences and Applications, Volume 2, Issue 2, Pages 59-69, February 2011

[117] *K Yamada, S Thumsorn,* Effectiveness of Talc Filler on Thermal Resistance of Recycled PET Blends,
Advances in Materials Physics and Chemistry, Vol. 3, Issue 8, Pages 327-331, Dec. 2013

[118] *H Inoya, Y W Leong, W Klinklai, S Thumsorn, Y Makata, H Hamada,* Compatibilization of Recycled Poly(Ethylene Terephthalate) and Polypropylene Blends: Effect of Polypropylene Molecular Weight on Homogeneity and Compatibility,
Journal of Applied Polymer Science, Volume 124, Issue 5, Pages 3947-3955, June 2012

[119] *H Inoya, Y W Leong, W Klinklai, Y Takai, H Hamada,* Compatibilization of Recycled Poly(Ethylene Terephthalate) and Polypropylene Blends: Effect of Compatibilization on Blend Toughness, Dispersion of Minor Phase and Thermal Stability,
Journal of Applied Polymer Science, Volume 124, Issue 6, Pages 5260-5269, June 2012

[120] *M Heino, J Kirjava, P Hietaoja, J A Seppala,* Compatibilization of polyethylene terephthate / polypropylene blends with styrene-ethylene/butylene-styrene (SEBS) block copolymers,
J. of Applied Polymer Science, Volume 65, Issue 2, Pages 241-249, July 1997

[121] *Y. Zhu, C. Liang, Y. Bo, S. Xu,* Compatibilization of polypropylene/recycled polyethylene terephthalate blends with maleic anhydride grafted polypropylene in the presence of diallyl phthalate,
Journal of Polymer Research, Volume 22, Issue 35, 2015
DOI: 10.1007/s10965-014-0591-4

[122] *A L F de Moura Giraldi, R. Cardoso de Jesus, L. H. Innocentini Mei,*The influence of extrusion variables on the interfacial adhesion and mechanical properties of recycled PET composites,
J. of Materials Processing Technology, Volumes 162-163, Pages 90- 95, 15 May 2005

[123] *.L.F. de M. Giraldi, M. Bizarria, A.A. Silva, J.I. Velasco, M.A. d'Ávila, L.H.I. Mei,* Effects of extrusion conditions on the properties of recycled poly(ethylene terephthalate)/nanoclay nanocomposites prepared by a twin-screw extruder,
Journal of Applied Polymer Science, Volume 108, Issue 4, pages 2252–2259, May 2008

[124] *A Pawlak, M Pluta, J Morawiec, A. Galeski, M Pracella,* Characterization of scrap poly(ethylene terephthalate),
European Polymer Journal, Volume 36, Issue 9, Pages 1875-1884, September 2000

[125] *G. Giannotta, R. Po, N. Cardi, E. Tampellini, E. Occhiello, F. Garbassi, L. Nicolais,* Processing effects on poly(ethylene terephthalate) from bottle scraps,
Polymer Eng. and Science, Volume 34, Issue 15, Pages: 1219–1223, August 1994

[126] *D-M. Fann, S. K. Huang, J. Y. Lee,* Kinetics and thermal crystallinity of recycled PET. II. Topographic study on thermal crystallinity of the injection-molded recycled PET,
J. of Applied Polymer Science, Volume 61, Issue 2, Pages 261-271, July 1996

[127] *W. Hao, X. Wang, W. Yang, K. Zheng,* Non-isothermal crystallization kinetics of recycled PET-Si_3N_4 nanocomposites,
Polymer Testing, Volume 31, Issue 1, Pages 110-116, February 2012

[128] *Y. Tao, K. Mai,* Non-isothermal crystallization and melting behavior of compatibilized polypropylene / recycled poly(ethylene terephthalate) blends,
European Polymer Journal, Volume 43, Issue 8, Pages 3538–3549, August 2007

[129] HDPE Material Data Sheet, *http://prospector.ides.com/DataView.aspx?E=51685*
Accessed on: 30.07.2010

[130] PP Material Data Sheet,
https://prospector.ides.com/DataView.aspx?I=34&TAB=DV_DS&E=124101
Accessed on: 30.07.2010

[131] *GW. Ehrenstein*, Gabriela Riedel, Pia Trawiel, Thermal Analysis of Plastics, Carl Hanser Verlag, Munich 2004

[132] *G Widmann, M Jandali*, Collected Applications of Thermal Analysis, Thermoplaste, Mettler-Toledo Gmbh, Page 19, 1997

[133] *GW Ehrenstein*, Polymeric Materials, Carl Hanser Publishers, Munich 2001

[134] *VBF Mathot*, Calorimetry and Thermal Analysis of Polymers,
Carl Hanser Publisher, Munich 1994

[135] ISO 11357-1: 2009, Differential Scanning Calorimetry, Part 1 – General Principles

[136] DIN 51005: 1999, Thermal Analysis (TA) – Terms/Note: Intended as Replacement for DIN 51005: 1993

[137] *SM Sarge*, Thermal Calibration of Differential Calorimeters,
PTB-Information 103, June 1993

[138] CRC Handbook of Chemistry and Physics, 53rd Edition, USA: CRC Press,
Page B-241, 1972

[139] *GWH Hohne*, Temperature Calibration of Differential Calorimeters,
PTB-Information 100, January 1990

[140] *B Wunderlich*, Thermal Analysis, Academic Press, San Diego, 1990

[141] ISO 11357-3: 2011, Differential Scanning Calorimetry (DSC)
Part 3 – Determination of Temperature and Enthalpy of Melting and Crystallization

[142] *Y. Kong, J.N. Hay*, Measurement of the crystallinity of polymers by DSC,
Polymer, Volume 43, Issue 14, Pages 3873-3878, June 2002

[143] ASTM E168-06 - Standard Practices for General Techniques of Infra-Red Quantitative Analysis

[144] *R.M. Silverstein, G.C. Bassler, T.C. Morrill*, Spectrometric Identification of Organic Compound, 5th Edition, John Wiley and Sons, New York 1991

[145] *T. Hirschfeld, B. Chase*, Fourier transform-raman spectroscopy: Development and justification,
Applied Spectroscopy, Volume 40, Issue 2, Pages 133-137, 1986

[146] *C.Q. Yang, R.R. Bresee, W.G. Fateley,* Studies of chemically modified poly(ethylene terephthalate) fibers by FT-IR photoacoustic spectroscopy and X-ray photoelectron spectroscopy,
Applied Spectroscopy, Volume 44, Issue 6, Pages 1035-1039, 1990

[147] ISO 1133-1:2011 - Plastics - Determination of the melt mass-flow rate (MFR) and melt volume-flow rate (MVR) of thermoplastics.

[148] ASTM D1238-13 - Standard Test Method for Melt Flow Rates of Thermoplastics by Extrusion Plastometer.

[149] ISO 527-1:2012 - Determination of tensile properties: General principles.

[150] ISO 527-2:2012 (en) - Determination of tensile properties: Test Conditions for Moulding and Extrusion Plastics.

[151] ISO 179-1:2000 - Determination of Charpy impact properties.

[152] ISO 1872-2:2007 - Plastics – Polyethylene moulding and extrusion materials

[153] *F. Awaja, D. Pavel*, Recycling of PET,
European Polymer Journal,Volume 41, Pages1453-1477, 2005

[154] ISO 294-1-2:1996 - Plastics – Inj. moulding of test specimens of thermoplastics mat.

[155] *British Plastics and Rubber, Edition October 2008, Page 5*

[156] *Olabisi O*, Handbook of thermoplastics,New York,USA, Marcel Dekker Inc., 1997.

[157] *H.F Mark*, Encyclopedia of polymer science and engineering,
New York, USA, John Wiley and Sons, 1985.

[158] *F. Medellin-Rodriguez*, Phillips PJ, Lin JS, Campos RJ,
The triple melting behaviour of poly(ethylene terephthalate), molecular weight effects,
Journal of Polymer Science, Part B, PolymPhys, Volume 35, Pages 1757–1762, 1997

[159] *V. B. F. Mathot*, Calorimetry and thermal analysis of polymers,
New York: Hanser Publishers; 1994.

[160] *W. G. Kampert WG, Sauer BB*, Temperature modulated DSC studies of melting and recrystallization in poly(ethylene-2,6-naphthalene dicarboxylate) (PEN) and blends with poly(ethylene terephthalate) (PET),
Polymer, Volume 42, Issue 21, Pages 8703-8714, October 2001

[161] *Z. G. Wang, B. S. Hsiao, B. B. Sauer, W. G. Kampert*, The nature of secondary crystallization in poly(ethylene tere-phthalate), *Polymer, 40, Pages 4615-27, 1999*

[162] *J. A. Brydson*, Plastics materials. Oxford, UK: Butter-worth-Heinemann; 1995.

[163] *R. Bhargava, S-Q Wang,J.L. Koenig*, FTIR Microspectroscopy of Polymeric Systems,
Advances in Polymer Science, Volume 163, Issue 1, Pages 137-191, 2003

[164] *A-M.M. Baker, C.M.F. Barry*, Effects of Composition, Processing and Structure on Properties of Engineering Plastics,
Materials Selection and Design, Volume 20, Pages 434-456, ASM Hand-book, ASM International, 1997

[165] *A. Pawlak, M. Pluta, J. Morawiec, A. Galeski, M. Pracella*, Characterization of scrap poly(ethylene terephthalate),
European Polymer Journal, Volume 36, Issue 9, Pages 1875-1884, 1 September 2000

[166] *R. J. Crawford*, Plastics engineering, Oxford, UK: Butter-worth-Heinemann; 1998

[167] *M. K. Akkapeddi, B. Van Buskirk, C. D. Mason*, Performance blends based on recycled Polymers,
Polymer Engineering and Science, Volume 35, Issue 1, Pages 72-78, 1995

[168] *F.N. Cogswell*, Converging flow of polymer melts in extrusion dies,
Polymer Engineering and Science, Volume 12, Issue 1, Pages 64-73, Jan. 1972

[169] *A.V. Shenoy, D.R. Saini*, Melt flow index: More than just a quality control rheological parameter. Part I,
Advances in Polymer Technology, Volume 6, Issue 1, Pages 1-58, 1986

[170] *B. Boutevin, J. M. Lusinchi, Y. Pietrasanta, J. J. Robin*, Improving poly(ethylene terephthalate)/high-density polyethylene blends by using graft copolymers,
Polymer Engineering and Science, Volume 36, Issue 6, Pages 879-884, March 1996

[171] *C. Guerrero, T. Lozano, V. Gonzales, E. Arroyo*, Properties and morphology of poly(ethylene terephthalate) and high-density polyethylene blends,
Journal of Applied Polymer Science, Volume 82, Issue 6, Pages 1382-1390, Nov. 2001

[172] *S. Mbarek, M. Jaziri, Y. Chalamet, C. Carrot*, Effect of the viscosity ratio on the morphology and properties of PET/HDPE blends with and without compatibilization,
Journal of Applied Polymer Science, Volume 117, Issue 3, Pages 1683-1694, Aug. 2010

[173] *R.S. Chen, M. H. A. Ghani, M. N. Salleh, S. Ahmed, S. Gan*, Influence of Blend Composition and Compatibilizer on Mechanical and Morphological Properties of Recycled HDPE/PET Blends, *Scientific Research Publication, MSA, Volume 5, Issue 13, Pages 943-952, Nov. 2014*
DOI: 10.4236/msa.2014.513096

[174] *M. Pracella, L. Rolla, D. Chionna, A. Galeski*, Compatibilization and properties of poly(ethylene terephthalate)/polyethylene blends based on recycled materials,
Macromol. Chem. and Physics, Volume 203, Issues 10-11, Pages 1473–1485, July 2002

[175] *Y. Lei, Q. Wu, Q. Zhang*, Morphology and properties of microfibrillar composites based on recycled poly(ethylene terephthalate) and high density polyethylene. Composites A,
Applied Science and Manufacturing, Volume 40, Issues 6-7, Pages 904–912, July 2009
doi:10.1016/j.compositesa.2009.04.017

[176] *J.M. Dealy, K.F. Wissbrun*, Melt Rheology and Its Role in Plastics Processing, Chapman and Hall, London,1996.

[177] *Y. W. Leong, H. Inoya, S. Thumsorn, H. Hamada*, Effect of Dispersed Phase Particle Dispersion on the Thermal Stability of Recycled Poly(ethylene terephthalate)/Polypropylene Blend,
The 10th International Conference on Flow Processes in Composite Materials (FPCM10) Monte Verità, Ascona, CH – July 11-15, 2010

[178] *N.C. Abdul Razak, I.M. Inuwa, A. Hassan, S.A. Samsudin*, Effects of compatibilizers on mechanical properties of PET/PP blend,
Composite Interfaces, Volume 20, Issue 7, Pages 507-515, 2013
DOI: 10.1080/15685543.2013.811176

[179] *T. Murayama, J. P. Bell*, Relation between the network structure and dynamic mechanical properties of a typical amine-cured epoxy polymer,
J. of Polym. Sc., Part A-2: Polym. Physics, Volume 8, Issue 3, Pages 437-445, 1970

[180] *Z. O. Oyman, T. Tincer*, Melt blending of poly(ethylene terephthalate) with polypropylene in the presence of silane coupling agent,
Journal of Applied Polymer Science, Volume 89, Issue 4, Pages 1039-1048, July 2003

[181] *M. Pracella, D. Chionna, A. Pawlak, A. Galeski*, Reactive mixing of PET and PET/PP blends with glycidyl methacrylate–modified styrene-*b*-(ethylene-*co*-olefin) block copolymers,
J. of Applied Polymer Science, Volume 98, Issue 5, Pages 2201–2211, December 2005

[182] *Y. Zhu, C. Liang, Y. Bo, S. Xu*, Non-isothermal crystallization behavior of compatibilized polypropylene/recycled polyethylene terephthalate blends,
J. of Therm. Analy. and Calorim., Volume 119, Issue 3, Pages 2005-2013, March 2015

[183] *Y. Zhu, C. Liang, Y. Bo, S. Xu*, Compatibilization of polypropylene/recycled polyethylene terephthalate blends with maleic anhydride grafted polypropylene in the presence of diallyl phthalate,
Journal of Polymer Research, Volume 22, Issue 35, 2015

[184] *K. Jayanarayanan, S. S. Bhagawan, S. Thomas, K. Joseph*, Morphology development and non isothermal crystallization behaviour of drawn blends and microfibrillar composites from PP and PET,
Polymer Bulletin, Volume 60, Issue 4, Pages 525-532, April 2008

[185] *A. Martinelli, C. De Souza, C. B. Caldeira*, An investigation on recycled PET/PP and recycled PET/PP-EP compatibilized blends: Rheological, morphological, and mechanical properties,
Journal of Applied Polymer Science, Volume 132, Issue 17, May 2015

[186] *T. Yu, H. Bu, J. Chen, J. Mei, J. Hu,* The effect of units derived from diethylene glycol on crystallization kinetics of poly(ethylene terephthalate),
Macrom. Chem. and Physics (Die Makromolekulare Chemie), Volume 187, Issue 11, Pages 2697–2709, November 1986

[187] *M. Patkar, S. A. Jabarin,* Effect of diethylene glycol (DEG) on the crystallization behavior of poly(ethylene terephthalate) (PET),
J. of Applied Polymer Science, Volume 47, Issue 10, Pages 1749–1763, March 1993

[188] *X. Yi, L. Xu, Y-L. Wang, G-J. Zhong, X. Ji, Z-M. Li,* Morphology and properties of isotactic polypropylene/poly(ethylene terephthalate) in situ microfibrillar reinforced blends: Influence of viscosity ratio,
European Polymer Journal, Volume 46, Issue 4, Pages 719-730, April 2010

[189] *J. D. Badia, E. Strömberg, S. Karlsson, A. Ribes-Greus,* Thermal analysis as a quality tool for assessing the influence of thermo-mechanical degradation on recycled poly(ethylene terephthalate),
Polymer Testing, Volume 28, Issue 2, Pages 169-175, April 2009

[190] *John I. Lauritzen Jr.* and *John D. Hoffman,* Extension of theory of growth of chain-folded polymer crystals to large undercoolings,
Journal of Applied Physics, Volume 44, Pages 4340-53, 1973

[191] *S. A. Jabarin,* Crystallization kinetics of polyethylene terephthalate. I. Isothermal crystallization from the melt,
Journal of Applied Polymer Science, Volume 34, Issue 1, Pages 85-96, July 1987

[192] *S. A. Jabarin,* Crystallization kinetics of polyethylene terephthalate. II. Dynamic crystallization of PET,
Journal of Applied Polymer Science, Volume 34, Issue 1, Pages 97-102, July 1987

[193] *P. J. Harrison, J. M. Newton, R. C. Rowe,* Convergent flow analysis in the extrusion of wet powder masses,
J. of Pharmacy and Pharmacology, Volume 36, Issue 12, pages 796-798, December 1984

[194] *http://statweb.stanford.edu/~naras/jsm/NormalDensity/NormalDensity.html*
Accessed on: 30.08.2011
Appendix 9

[195] *D. B. Rorabacher,* Statistical treatment for rejection of deviant values: critical values of Dixon's "Q" parameter and related subrange ratios at the 95% confidence level,
Analytical Chemistry, Volume 63, Issue 2, Pages 139-146, 1991
DOI: 10.1021/ac00002a010

[196] University internal academic paper, *Dixon's Q Test Methodology*
Appendix 9

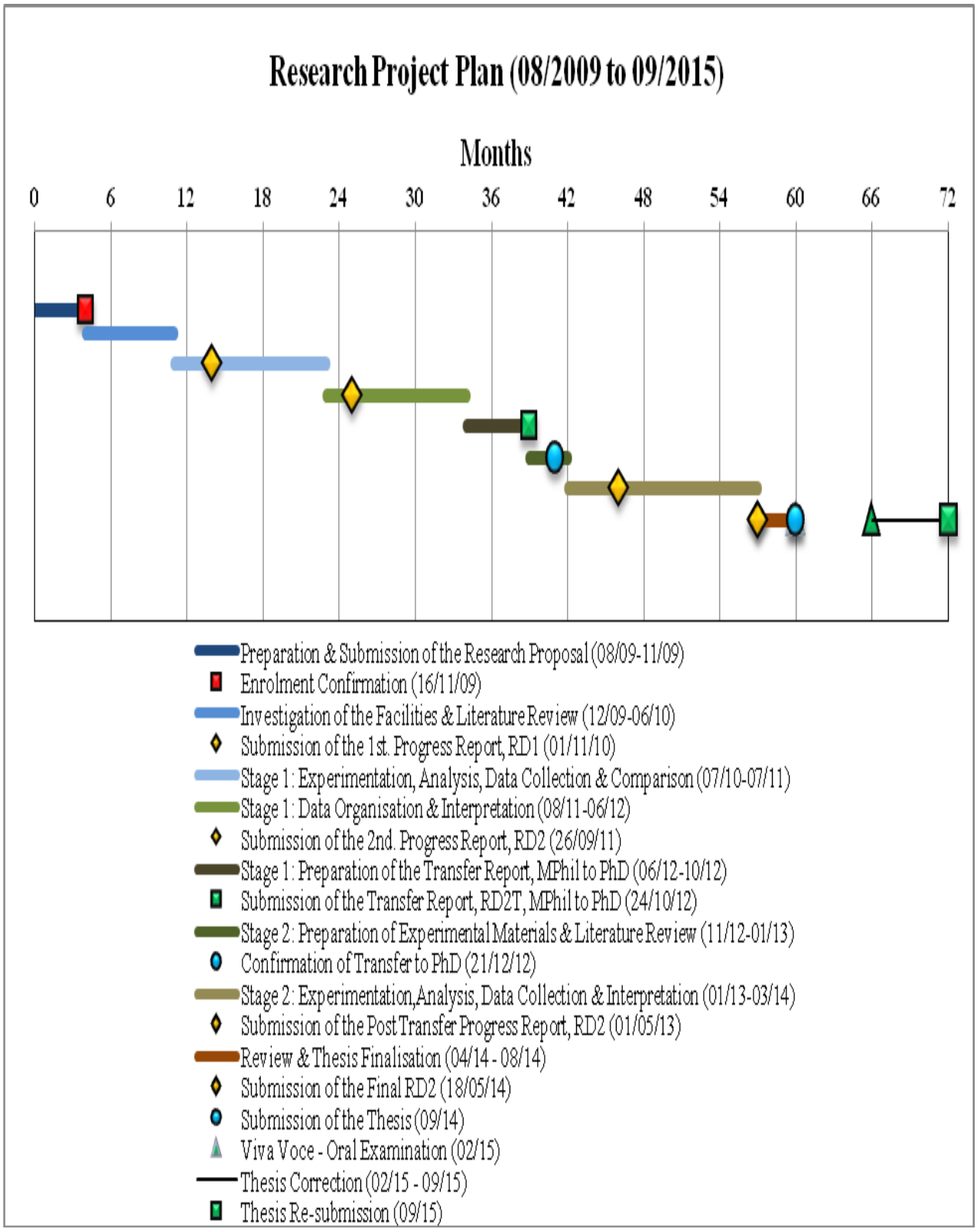
Research Project Plan (08/2009 to 09/2015)
Months
0
6
12
18
24
30
36
42
48
54
60
66
72
Preparation & Submission of the Research Proposal (08/09-11/09)
Enrolment Confirmation (16/11/09)
Investigation of the Facilities & Literature Review (12/09-06/10)
Submission of the 1st. Progress Report, RD1 (01/11/10)
Stage 1: Experimentation, Analysis, Data Collection & Comparison (07/10-07/11)
Stage 1: Data Organisation & Interpretation (08/11-06/12)
Submission of the 2nd. Progress Report, RD2 (26/09/11)
Stage 1: Preparation of the Transfer Report, MPhil to PhD (06/12-10/12)
Submission of the Transfer Report, RD2T, MPhil to PhD (24/10/12)
Stage 2: Preparation of Experimental Materials & Literature Review (11/12-01/13)
Confirmation of Transfer to PhD (21/12/12)
Stage 2: Experimentation,Analysis, Data Collection & Interpretation (01/13-03/14)
Submission of the Post Transfer Progress Report, RD2 (01/05/13)
Review & Thesis Finalisation (04/14 - 08/14)
Submission of the Final RD2 (18/05/14)
Submission of the Thesis (09/14)
Viva Voce - Oral Examination (02/15)
Thesis Correction (02/15 - 09/15)
Thesis Re-submission (09/15)

Appendices

APPENDIX 1 – Published and Submitted Journal Articles

1. B. Itim, M. Philip, *Effect of multiple extrusions and influence of PP contamination on the thermal characteristics of bottle grade recycled PET*,
   Polymer Degradation and Stability, Volume 117, Pages 84-89, 2015

   Received 4th January 2015,
   Received in revised form 15th March 2015,
   Accepted 5th April 2015 2012,
   Available online 11th April 2015

2. B. Itim, M. Philip, *Effect of cooling rates and influence of PP contamination on the crystallization of bottle grade recycled PET,*

   Article submitted to Polymer Degradation and Stability on 10th September 2015

Polymer Degradation and Stability 117 (2015) 84–89

Contents lists available at ScienceDirect

Polymer Degradation and Stability

journal homepage: www.elsevier.com/locate/polydegstab

Review article

Effect of multiple extrusions and influence of PP contamination on the thermal characteristics of bottle grade recycled PET

Bachir Itim, Mathew Philip*

Sir John Cass Faculty of Art, Architecture and Design, London Metropolitan University, London E1 1LA, UK

ARTICLE INFO

Article history:
Received 4 January 2015
Received in revised form
15 March 2015
Accepted 5 April 2015
Available online 11 April 2015

Keywords:
Bottle grade recycled PET
PP contamination
Chain scission
Cross-linking
Crystallinity

ABSTRACT

The thermal characteristics of bottle grade recycled PET pellets contaminated with 5% PP prepared by multiple extrusions were studied by differential scanning calorimetry (***DSC***) at constant heating rate of 10 °C/min for various extrusion cycles. The peak temperature of crystallization T_c, the enthalpy of crystallization ΔH_c and the degree of crystallinity X_c were found to be dependent on the number of extrusion cycles. From the dependence on extrusion cycles, the analysis of the crystallization mechanism by Avrami model has been determined, the Avrami exponent n and the rate constant Z_t were calculated and the influence of the 5% PP on the bottle grade recycled PET matrix during multiple extrusions and its effect on crystallinity was thoroughly discussed.

1. Introduction

Bottle grade recycled PET referred to in future as rPET-bg can replace and be used as an alternative to virgin PET and reducing environmental issues related to landfilling and incineration. rPET-bg is considered to lose its inherited properties through recycling and reprocessing cycles. During recycling, rPET-bg gets cross contaminated with other polymeric materials, especially PP. This cross contamination is a major issue in rPET-bg recycling industry because of its influence on the characteristics of the final produce. Furthermore, during reprocessing of the contaminated rPET-bg, the transparency of the final produce is altered as a result of contamination. The present study, focussed on the influence of PP contamination on the thermal characteristics of rPET-bg, especially crystallinity which dictates transparency in PET, and its importance in bottle manufacturing. Crystallization kinetics of engineering grades have been extensively studied [1,2]. However, studies on recycled materials such as rPET-bg have been rare. The influence of polymeric contaminants, such as PP, on the crystallization of rPET is particularly important as PP bottle tops are easily mixed with rPET-bg when recycling. Their presence in small amounts in rPET-bg can significantly affect crystallinity during multiple extrusions. Some researchers have studied the degradation of rPET during processing and concluded that chain scission can occur and that formation of grafted copolymers and crystallization can be facilitated [4,5] and others concluded that during repetitive extrusion, chain scission predominated and no chain branching or cross-linking were observed which decreased capabilities and crystallinity [7,8], whereas others concluded that cross-linking and chain branching occur during extrusion [9,10]. This research study investigates the influence of thermo-mechanical degradation during repetitive extrusion cycles on the crystallinity of non-contaminated and contaminated rPET matrix with 5% PP. Furthermore, the Avrami model may properly describe the behaviour of crystallization of the non-contaminated and contaminated rPET under isothermal crystallization process.

2. Materials and method

The rPET-bg flakes, mixture of multicolored flakes were supplied by Closed Loop Recycling Ltd [11].

The PP addition selected was the grade 7011L1 manufactured by ExxonMobil Chemical with properties given in Table 1. Samples of non contaminated rPET-bg and others with 5% PP were prepared by multiple extrusions for 5 cycles using a Leistritz twin screw extrusion machine. The samples were dried for 5 h at a temperature of 120 °C and all processed under same temperature range of 250–270 °C and a screw speed of 120 rpm.

* Corresponding author. Tel.: +44 2073202843.
E-mail address: M.Philip@londonmet.ac.uk (M. Philip).

http://dx.doi.org/10.1016/j.polymdegradstab.2015.04.004
0141-3910/

Bachir

From: "Polymer Degradation and Stability" <ees.pdst.0.33d8ee.dc8697a0@eesmail.elsevier.com>
Date: 10 September 2015 04:55
To: <bachiritim@yahoo.co.uk>
Subject: Editor handles PDST-D-15-00666

Polymer Degradation and Stability
Ref: PDST-D-15-00666
Title: Effect of cooling rates and influence of polypropylene contamination on the crystallization of bottle grade recycled poly(ethylene terephthalate)
Authors: Bachir ITIM, PhD student; Mathew PHILIP, Dr
Article Type: Review Article

Dear Bachir,

Your submission entitled "Effect of cooling rates and influence of polypropylene contamination on the crystallization of bottle grade recycled poly(ethylene terephthalate)" will be handled by Administrative Support Agent [24-Feb-11] Administrative Support Agent.

You may check on the progress of your paper by logging on to the Elsevier Editorial System as an author. The URL is http://ees.elsevier.com/pdst/.

Your username is: bachiritim@yahoo.co.uk

If you need to retrieve password details, please go to:
http://ees.elsevier.com/pdst/automail_query.asp

Thank you for submitting your work to this journal. Please do not hesitate to contact me if you have any queries.

Kind regards,

Polymer Degradation and Stability

****

For further assistance, please visit our customer support site at http://help.elsevier.com/app/answers/list/p/7923. Here you can search for solutions on a range of topics, find answers to frequently asked questions and learn more about EES via interactive tutorials. You will also find our 24/7 support contact details should you need any further assistance from one of our customer support representatives.

ExxonMobil™ HDPE HMA 025
High Density Polyethylene Resin
ExxonMobil Chemical Web

ExxonMobil Chemical IDES Prospector

Product Description			
HMA 025 is a HDPE grade, characterized by excellent dimensional stability, impact strength and very high stiffness.			
General			
Material Status	• Commercial: Active		
Literature [1]	• Typical Values Datasheet		
Availability	• Africa & Middle East	• Asia Pacific	• Europe
Additive	• Heat Stabilizer		
Physical	**Nominal Value**	**Unit**	**Test Method**
Melt Mass-Flow Rate (MFR) (190°C/2.16 kg)	8.0	g/10 min	ASTM D1238
Environmental Stress-Cracking Resistance (10% Igepal)	3.00	hr	ASTM D1693
Mechanical	**Nominal Value**	**Unit**	**Test Method**
Tensile Stress (Yield)	26.0	MPa	ISO 527-2/1A/50
Tensile Strain			ISO 527-2/1A/50
Yield	9.0	%	
Break	> 100	%	
Flexural Modulus	1100	MPa	ISO 178
Impact	**Nominal Value**	**Unit**	**Test Method**
Notched Izod Impact Strength	7.0	kJ/m²	ISO 180/1A
Thermal	**Nominal Value**	**Unit**	**Test Method**
Heat Deflection Temperature (0.45 MPa, Unannealed)	69.0	°C	ISO 75-2/B
Melting Temperature	134	°C	ASTM D3418

Additional Information

The molded properties were measured on 4 mm (157.5 mil) thick injection molded specimen based on ISO 294-1.
1. 0.45 MPa, 70 psi
2. ESCR was measured on 2 mm (78.7 mil) thick compression molded plate (F50, 10 % Igepal, 50°C, 122°F)

Legal Statement

Contact your ExxonMobil Chemical Customer Service Representative for potential food contact application compliance (e.g. FDA, EU, HPFB).

This product is not intended for use in medical applications and should not be used in any such applications.

Notes

[1] These links provide you with access to supplier literature. We work hard to keep them up to date; however you may find the most current literature from the supplier.

Revision History
Added to Prospector: April 2001
Last Updated: 12/02/2011

Figure 1 Material Data Sheet for *HDPE HMA025*

ExxonMobil™ PP7011L1
Polypropylene Impact Copolymer
ExxonMobil Chemical Web

ExxonMobil Chemical IDES Prospector

Product Description			
An impact copolymer resin for extrusion applications with high melt viscosity and excellent low-temperature impact strength. It is suitable for cables, pipes, profiles, sheets and thermoforming.			
General			
Material Status	• Commercial: Active		
Literature [1]	• Typical Values Datasheet		
Availability	• Africa & Middle East	• Europe	
Features	• High Impact Resistance	• Low Flow	
Uses	• Compounding • Corrugated Pipe	• Electrical/Electronic Applications • Industrial Applications	
Appearance	• Natural Color		
Forms	• Pellets		
Processing Method	• Extrusion • Extrusion Blow Molding	• Injection Molding • Profile Extrusion	• Sheet Extrusion • Thermoforming

Physical	**Nominal Value**	**Unit**	**Test Method**
Melt Mass-Flow Rate (MFR)			ISO 1133
230°C/2.16 kg	1.0	g/10 min	
230°C/5.0 kg	4.0	g/10 min	
Hardness	**Nominal Value**	**Unit**	**Test Method**
Shore Hardness (Shore D)	65		ISO 868
Mechanical	**Nominal Value**	**Unit**	**Test Method**
Tensile Modulus - Secant	1100	MPa	ISO 527-2/1
Tensile Stress (Yield)	26.0	MPa	ISO 527-2/50
Tensile Strain (Yield)	10	%	ISO 527-2/50
Flexural Modulus - Secant	1150	MPa	ISO 178
Impact	**Nominal Value**	**Unit**	**Test Method**
Charpy Notched Impact Strength			ISO 179/1eA
-20°C	4.5	kJ/m²	
0°C	6.0	kJ/m²	
23°C	33	kJ/m²	
Notched Izod Impact Strength (23°C)	35	kJ/m²	ISO 180/1A
Thermal	**Nominal Value**	**Unit**	**Test Method**
Heat Deflection Temperature			
0.45 MPa, Unannealed	83.0	°C	ISO 75-2/B
1.8 MPa, Unannealed	50.0	°C	ISO 75-2/A
Vicat Softening Temperature	149	°C	ISO 306/A50
Melting Temperature (DSC)	161	°C	ISO 3146
Peak Crystallization Temperature (DSC)	112	°C	ISO 3146

Legal Statement

Contact your ExxonMobil Chemical Customer Service Representative for potential food contact application compliance (e.g. FDA, EU, HPFB).

This product is not intended for use in medical applications and should not be used in any such applications.

Notes

[1] These links provide you with access to supplier literature. We work hard to keep them up to date; however you may find the most current literature from the supplier.

Revision History
Added to Prospector: February 2009
Last Updated: 12/02/2011

Figure 2 Material Data Sheet for *PP7011L1*

APPENDIX 3 – Injection Mouding Setting Sheet, F60

45: (% Packing Pressure)

KLOCKNER FERROMATIK

F60

A	B	C	D	E	F	G	H

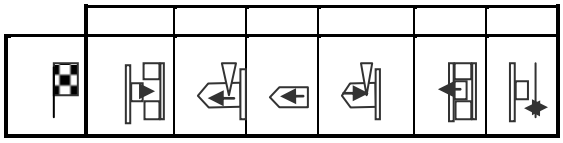

		090	5

C

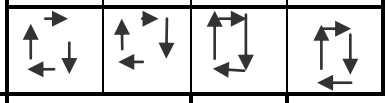

t	1	2	3	4	5	6	7	8	9
sec	00	4.0	0.0	0.0	0.0	0.0	0.0	0.0	0.0
f (x)									

START

STOP

1	2	3	4	5	6	7	8	9	10	11	12	13	14	15
X	0	0	X	2	0	2	2	3	0	0	X	X	0	0

t	1	2	3	4	5	6	7	8	9	10	11
sec	1.5	13.0	02.0	03.0	24.0	0	0.3	0.5	00.0	000	001

p	1	2	3	4	5	6	7	8	9	10	11
%	95	45	35	35	X	X	X	1	X	50	60

v/p	1	2	3	4	5	6	7	8	9	10	11
%	95	015	055	055	42	10	95	45	40	56	04

s		1	2	3	4	5	6	7
mm		004.5	007.4	037.0	X	X	080.0	229

s		1	2	3	4	5	6	7	8	9
mm	247	224	026	009	00	X	025	030	000	000

TEMPS	TEMPS	TEMPS	TEMPS
290	270	260	260

Table 1 Injection Machine Setting Sheet, *F60*

APPENDIX 4 – *Experiments 1* and *2* - **Non Contaminated rPET-bg**

(Stage 1)

1. DSC Thermograms of *Flakes*

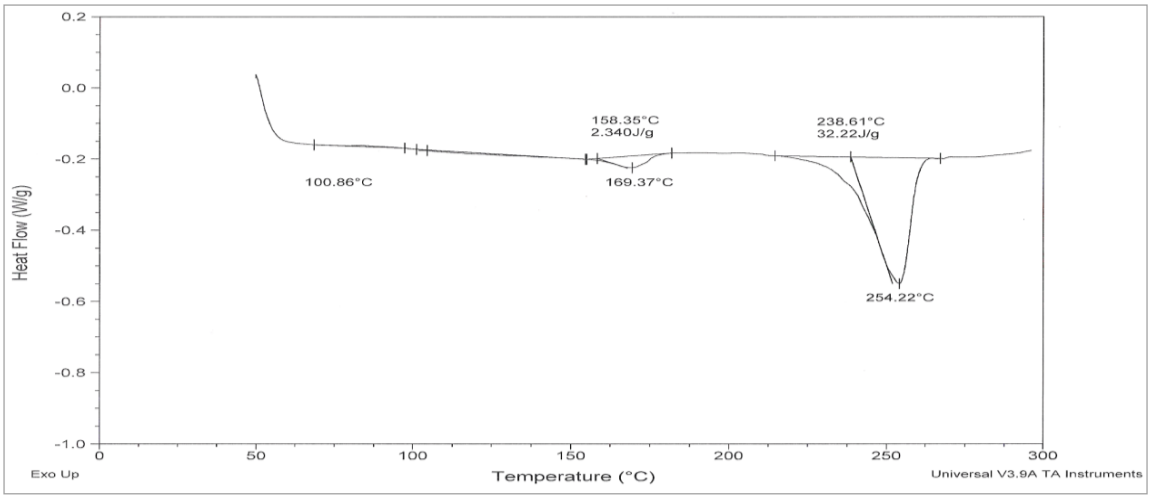

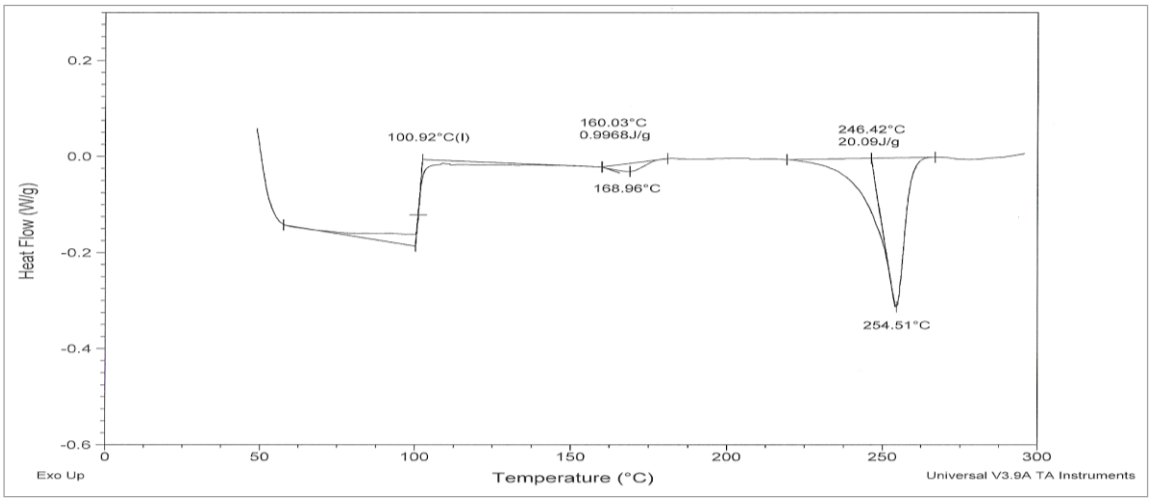

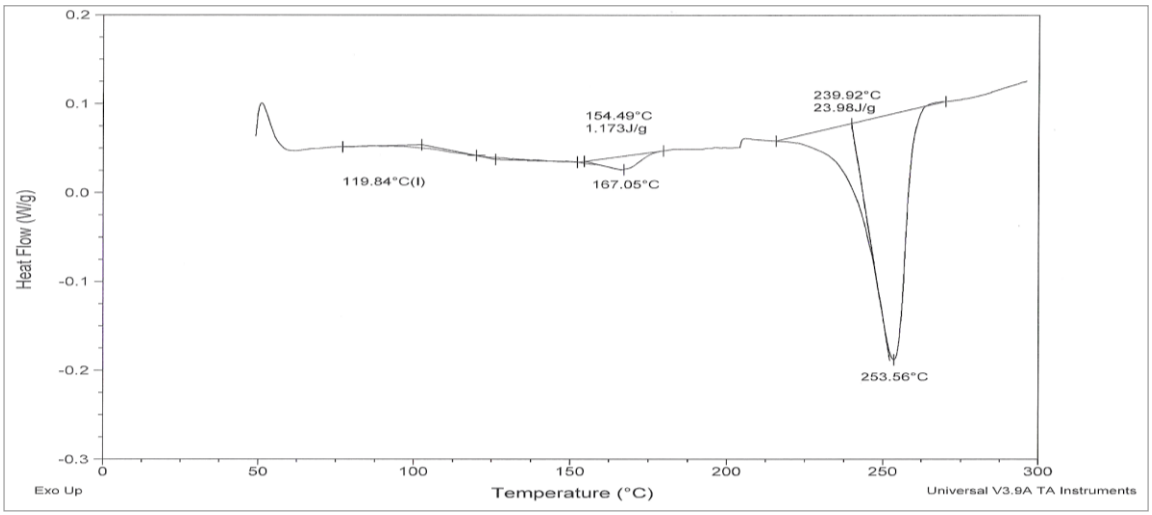

Figure 3 DSC Thermograms of non contaminated rPET-bg Flakes

2. FTIR Spectra of *Flakes*

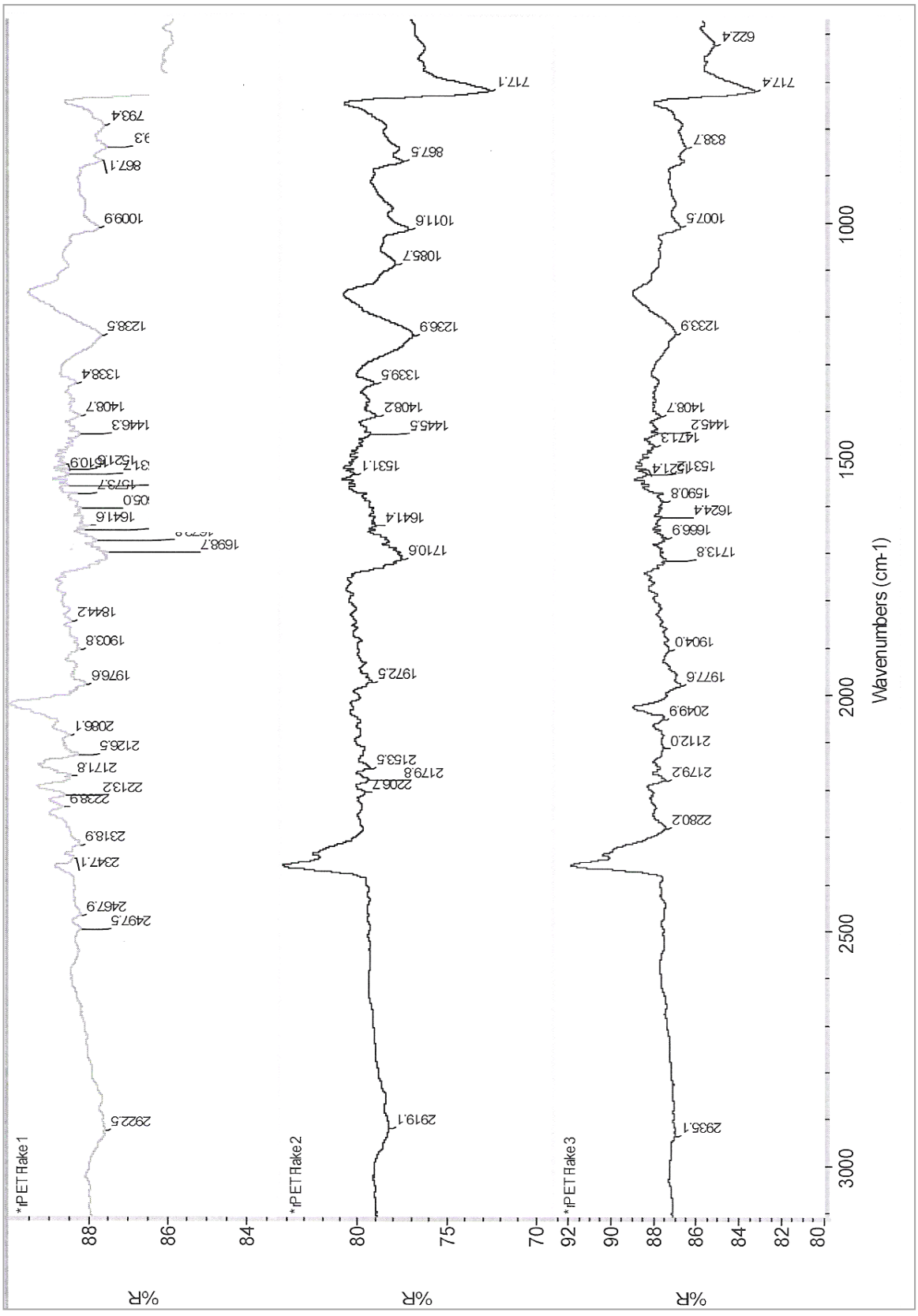

Figure 4 FTIR Spectra of non contaminated rPET-bg Flakes

3. DSC Thermograms of *Extruded Samples*

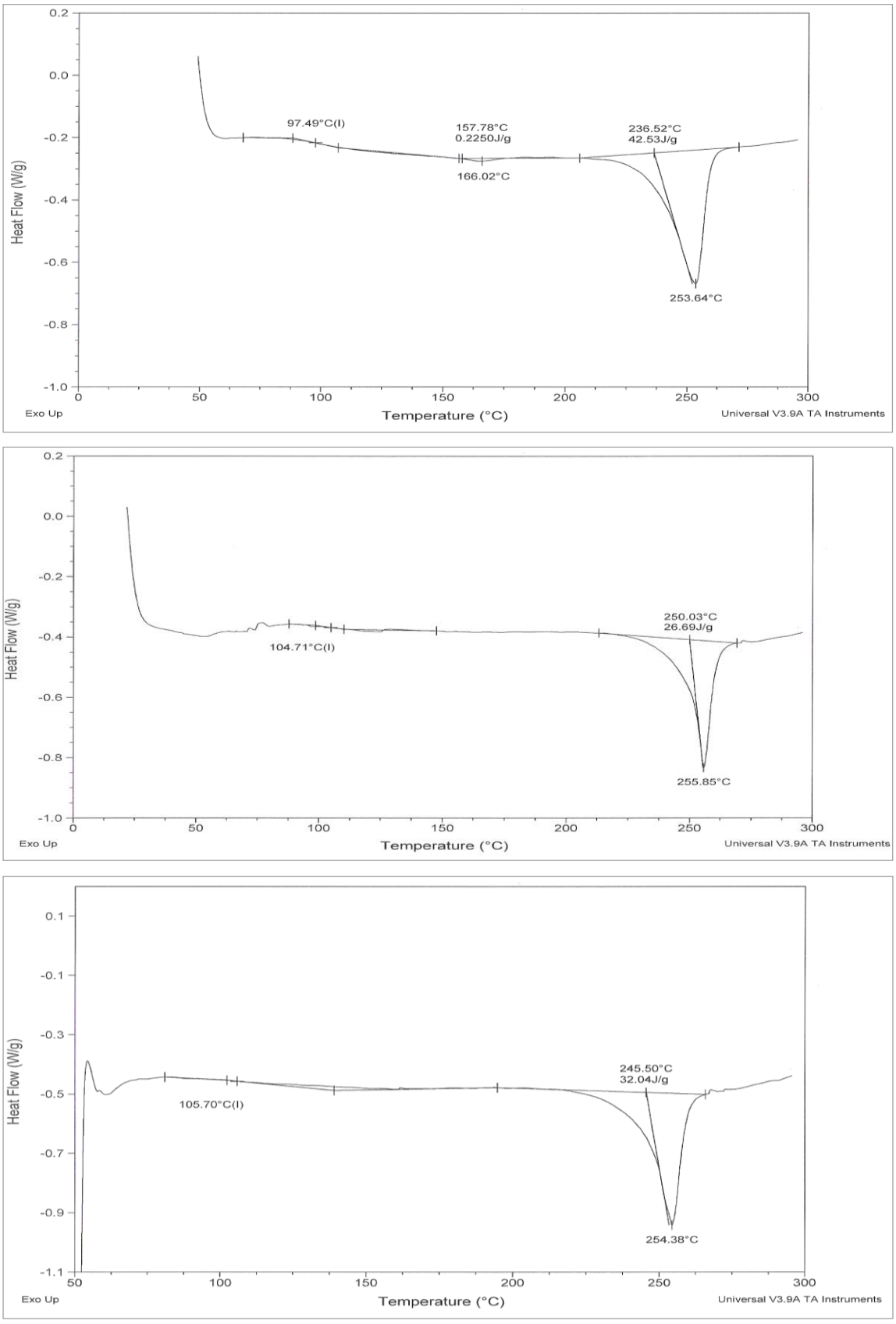

Figure 5 DSC Thermograms of non contaminated rPET-bg Extruded Samples

4. FTIR Spectra of *Extruded Samples*

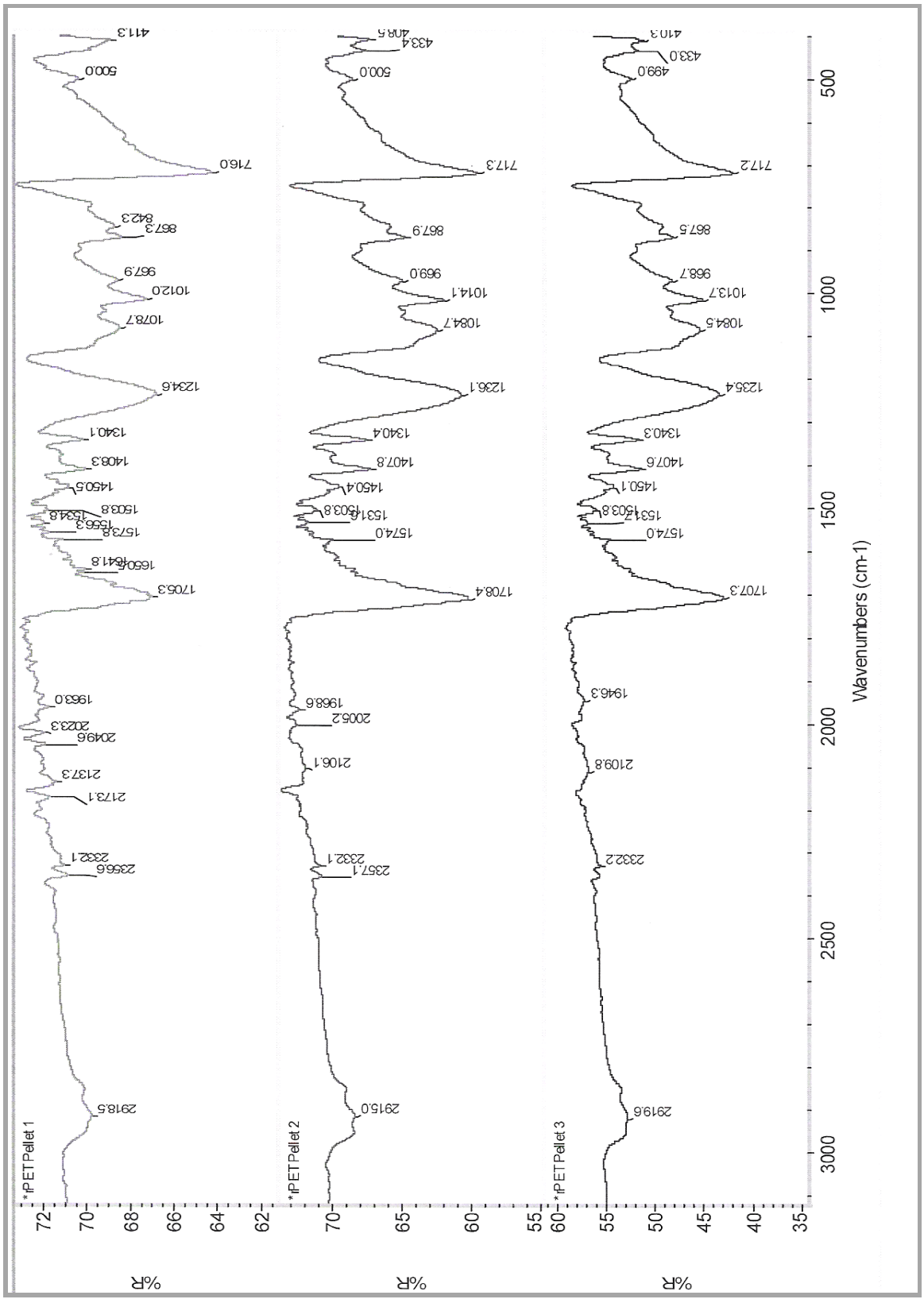

Figure 6 FTIR Spectra of non contaminated rPET-bg Extruded Samples

5. DSC Thermograms of *Injection Moulded Samples*

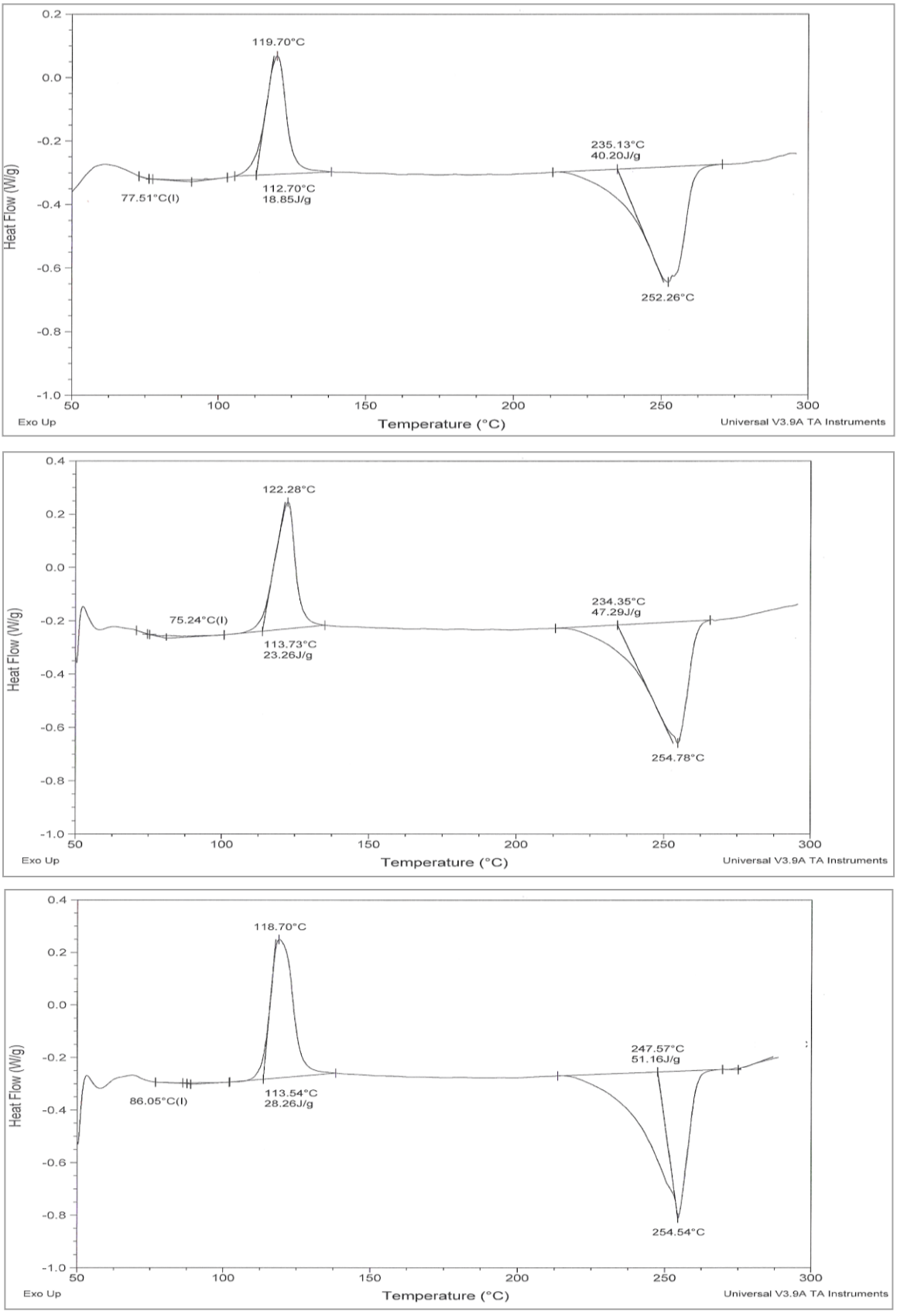

Figure 7 DSC Thermograms of non contaminated rPET-bg Inj. Moulded Samples

6. FTIR Spectra of *Injection Moulded Samples*

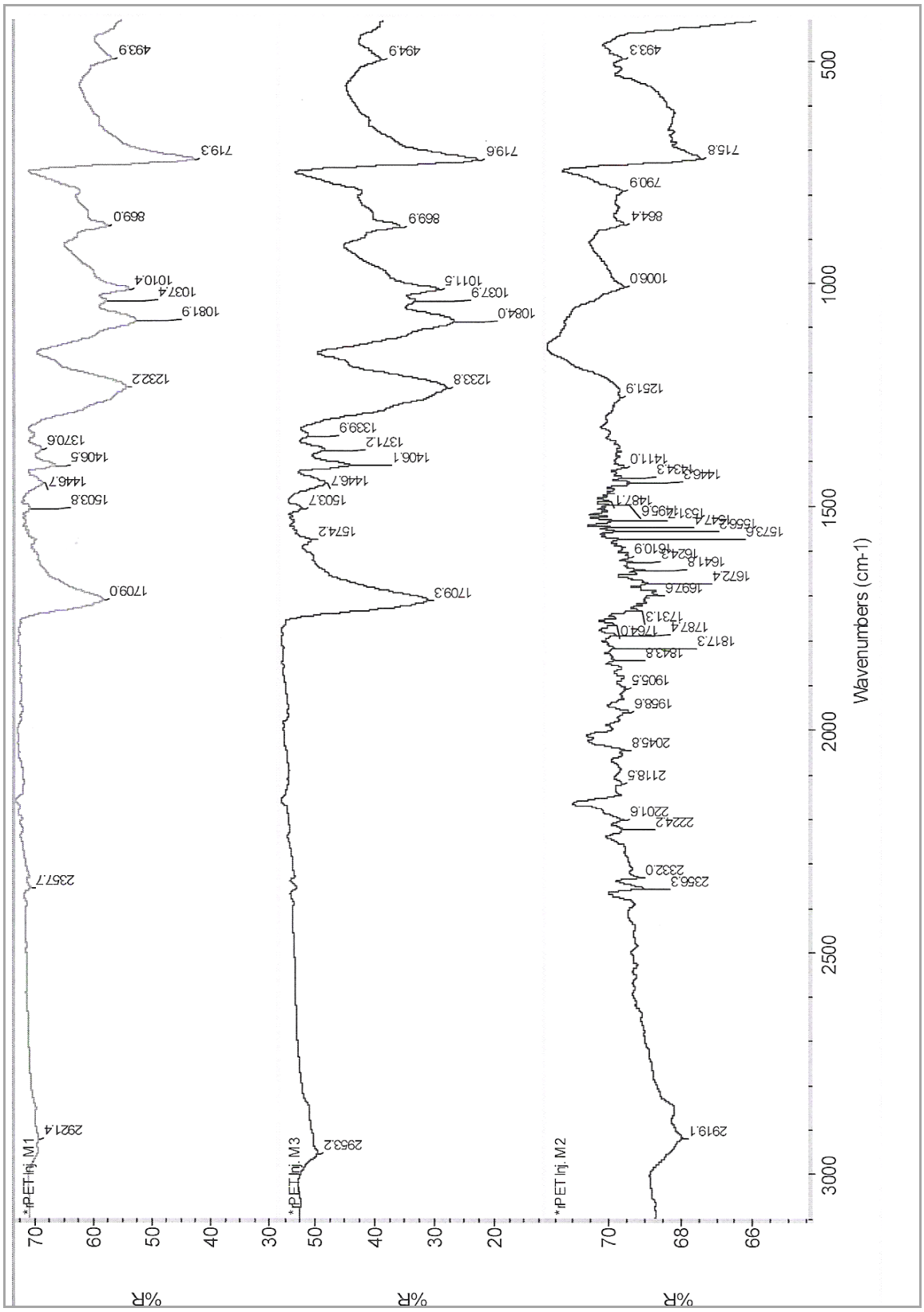

Figure 8 FTIR Spectra of non contaminated rPET-bg Inj. Moulded Samples

APPENDIX 5 **–** *Experiments 3, 4* and *5* **- rPET-bg Contaminated with HDPE**

(Stage 1)

1. DSC Thermograms of *Extruded Samples* (95% rPET-bg / 5% HDPE)

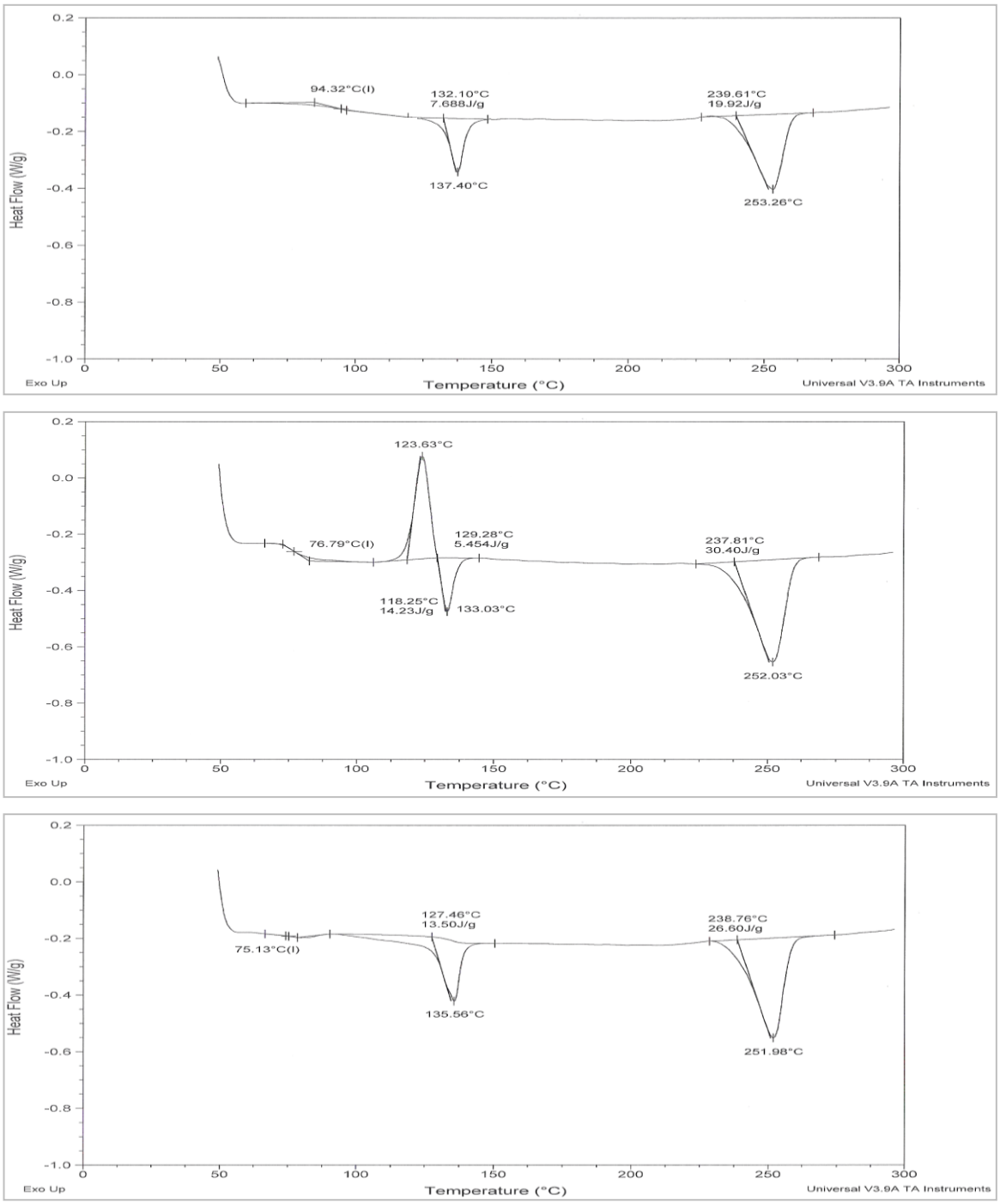

Figure 9 Thermograms of Extruded Samples of rPET-bg contaminated with 5% HDPE

2. DSC Thermograms of *Extruded Samples* (90% rPET-bg / 10% HDPE)

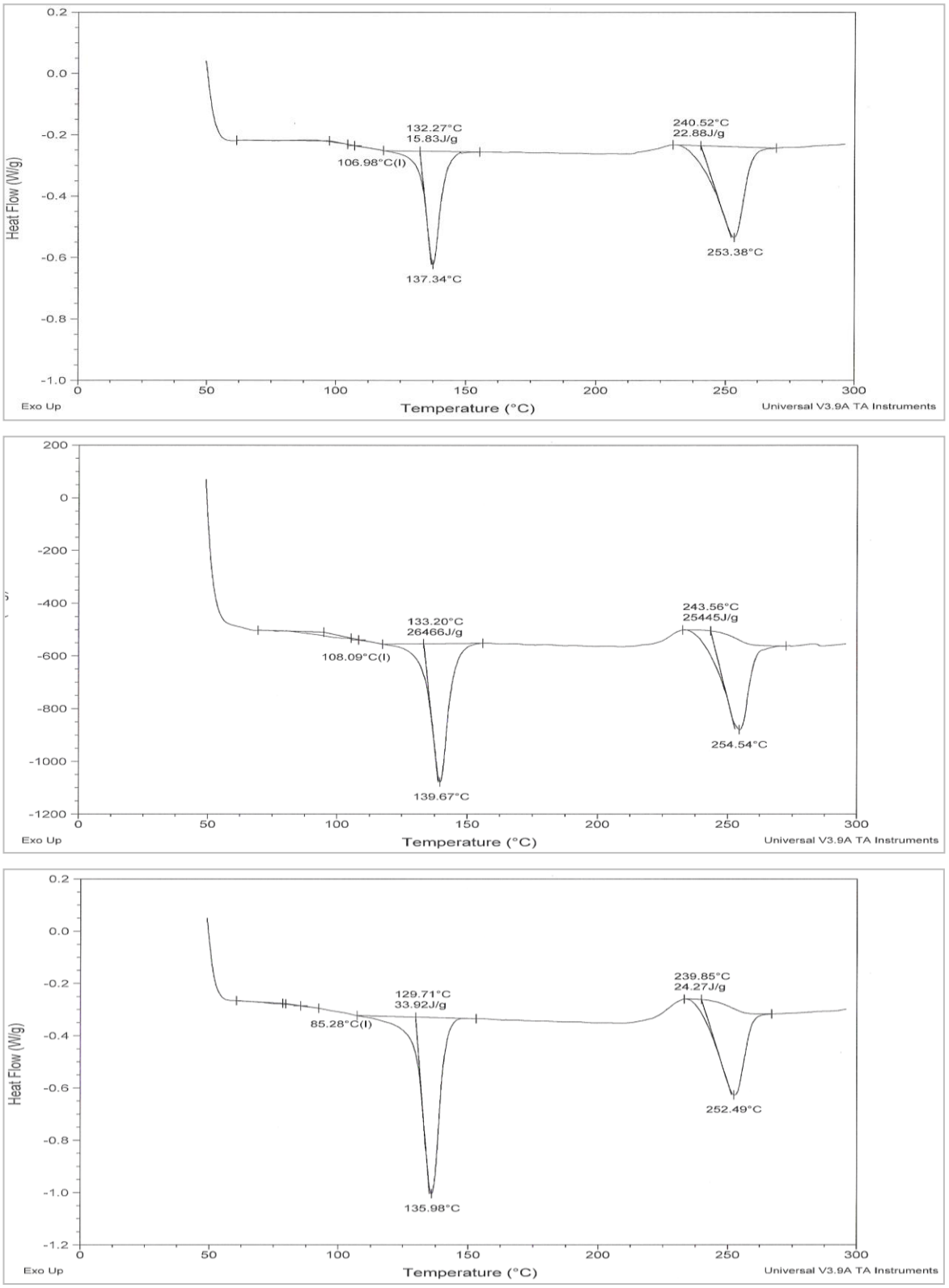

Figure 10 Thermograms of Extruded Samples of rPET-bg contaminated with 10% HDPE

3. DSC Thermograms of *Extruded Samples* (85% rPET-bg / 15% HDPE)

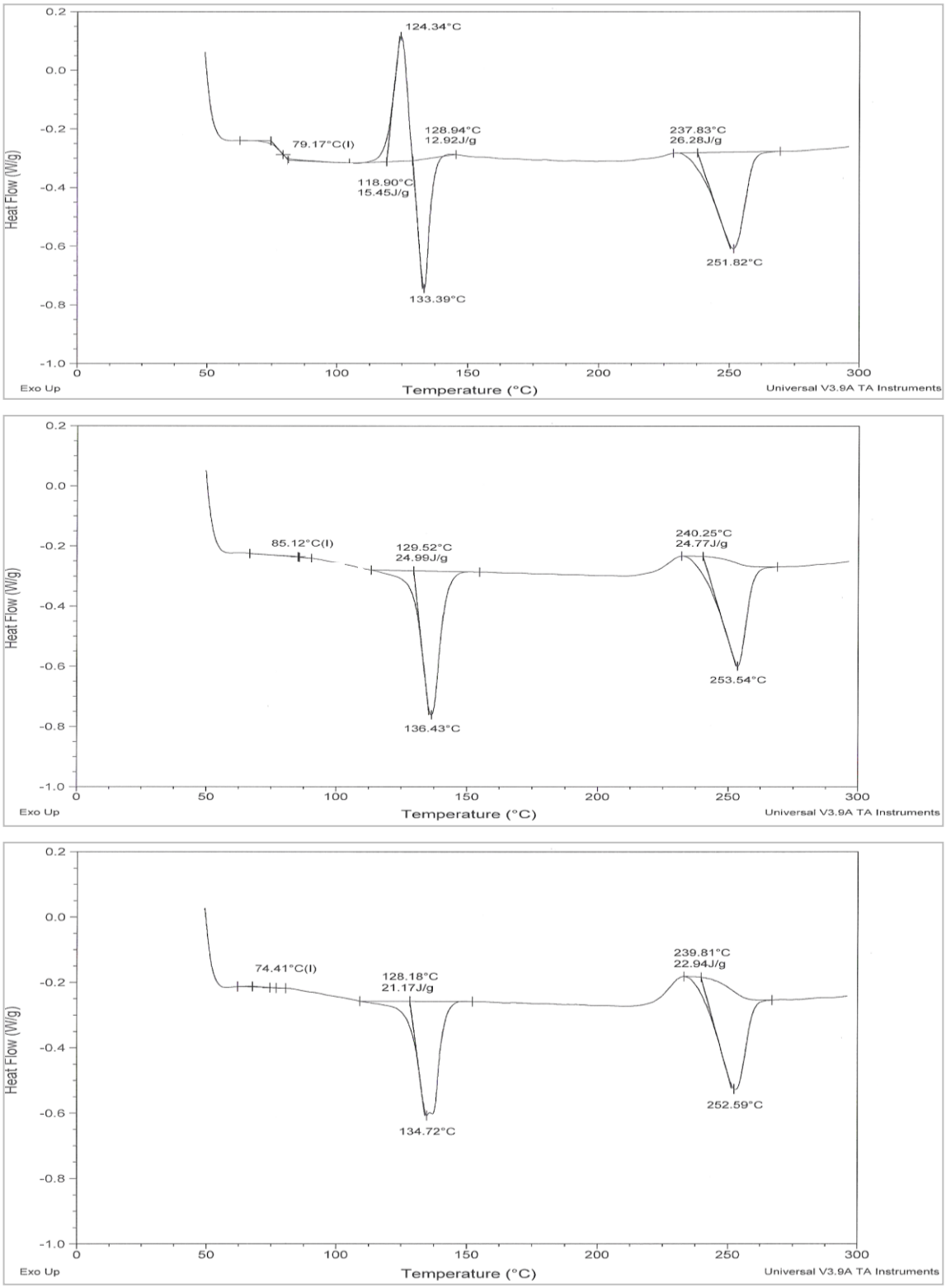

Figure 11 Thermograms of Extruded Samples of rPET-bg contaminated with 15% HDPE

4. FTIR Spectra of *Extruded Samples* (95% rPET-bg / 5% HDPE)

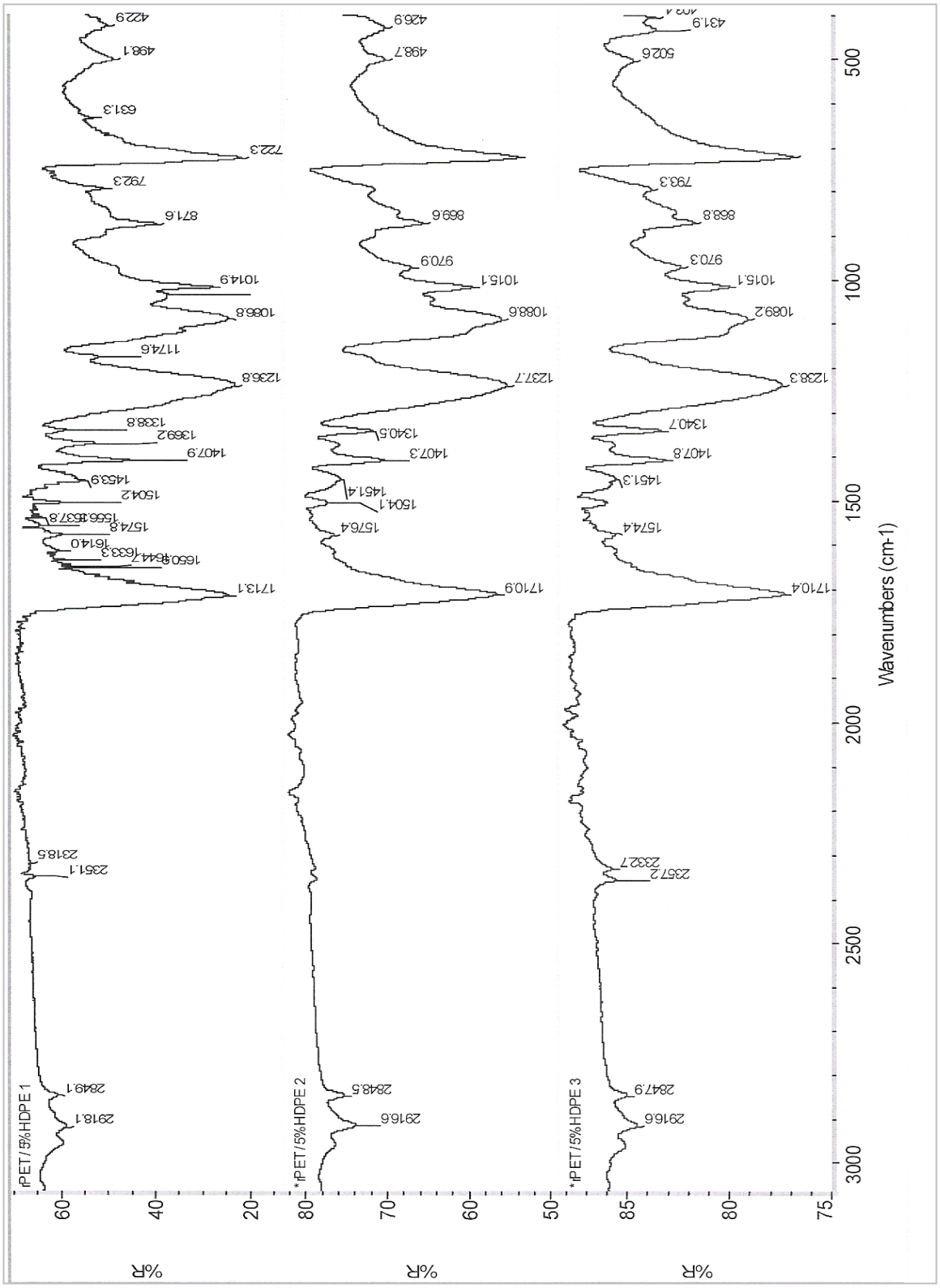

Figure 12 FTIR Spectra of Extruded Samples of rPET-bg contaminated with 5% HDPE

5. FTIR Spectra of *Extruded Samples* (90% rPET-bg / 10% HDPE)

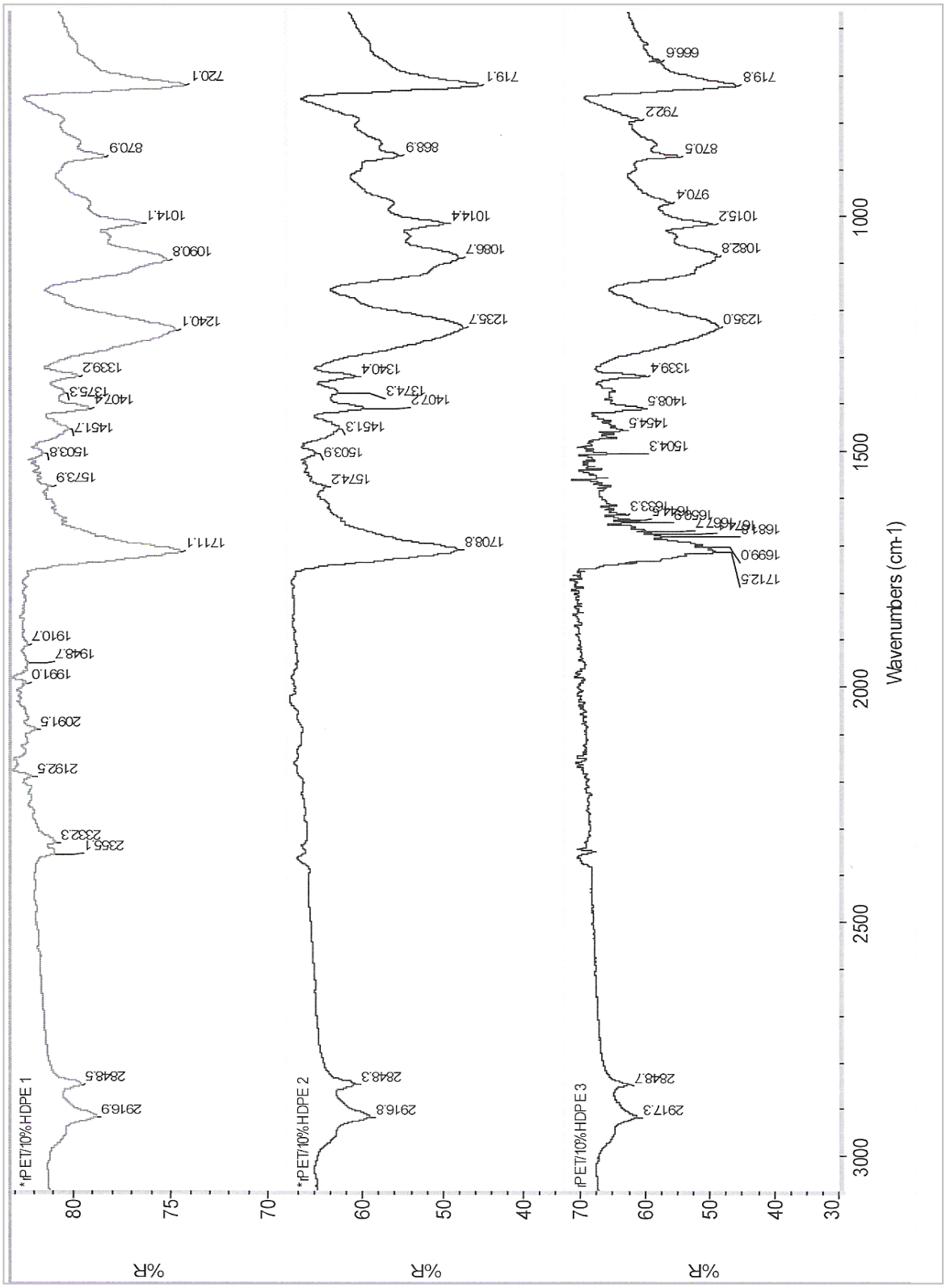

Figure 13 Spectra of of Extruded Samples of rPET-bg contaminated with 10% HDPE

6. FTIR Spectra of *Extruded Samples* (85% rPET-bg / 15% HDPE)

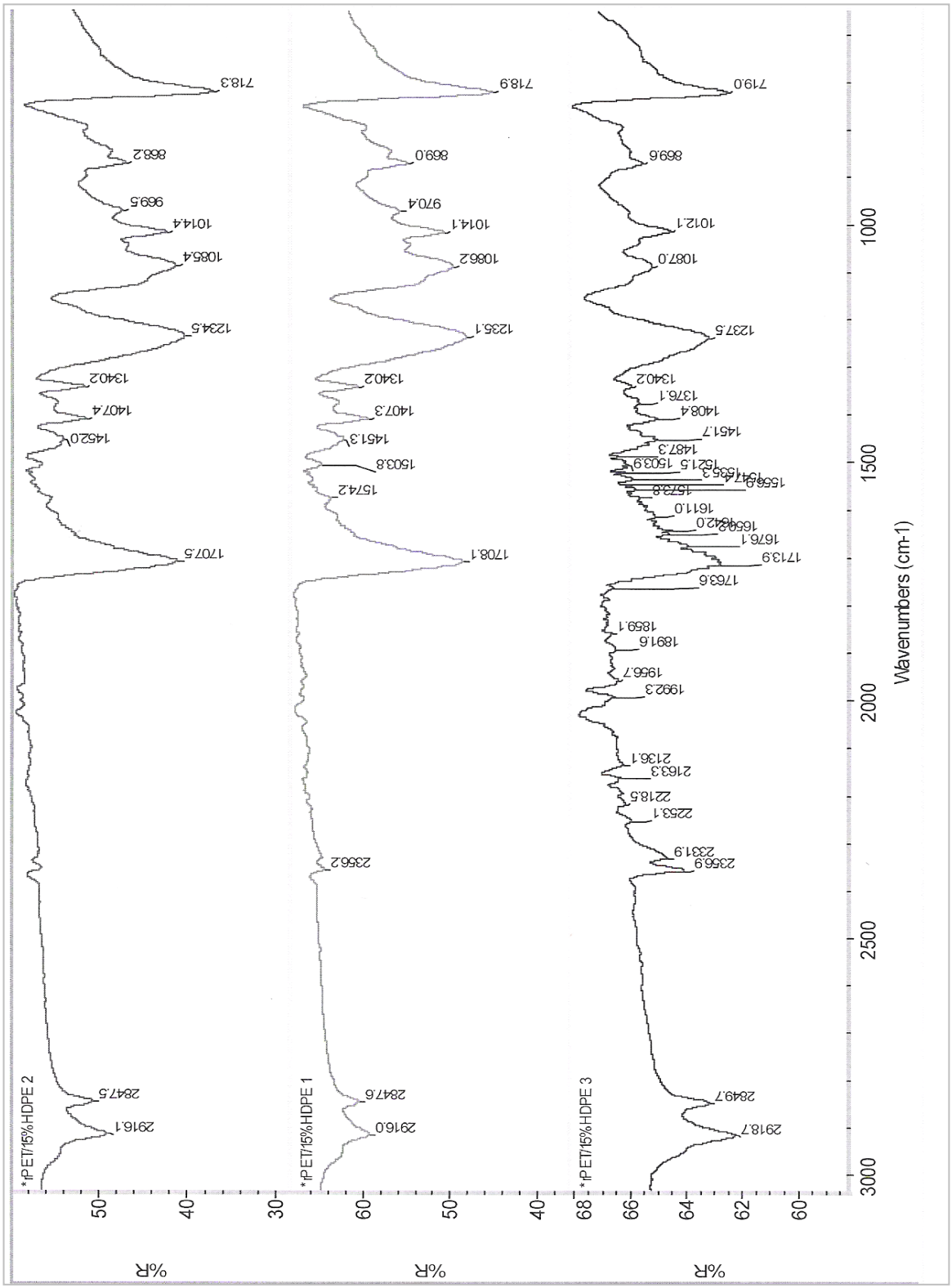

Figure 14 Spectra of of Extruded Samples of rPET-bg contaminated with 15% HDPE

7. DSC Thermograms of *Injection Moulded Samples* (95% rPET-bg / 5% HDPE)

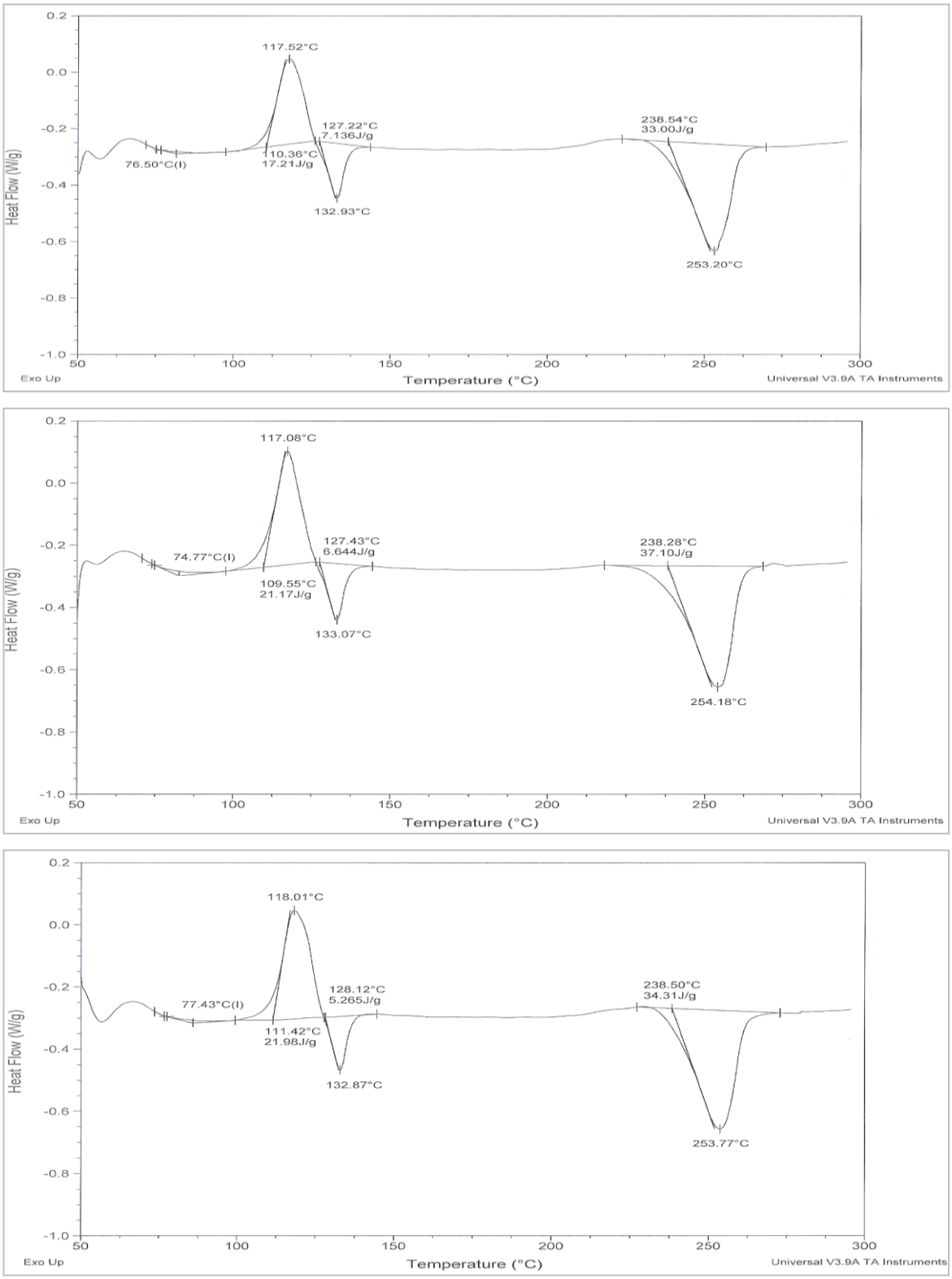

Figure 15 Thermograms of Inj. Moulded Samples of rPET-bg contaminated with 5% HDPE

8. DSC Thermograms of *Injection Moulded Samples* (90% rPET-bg / 10% HDPE)

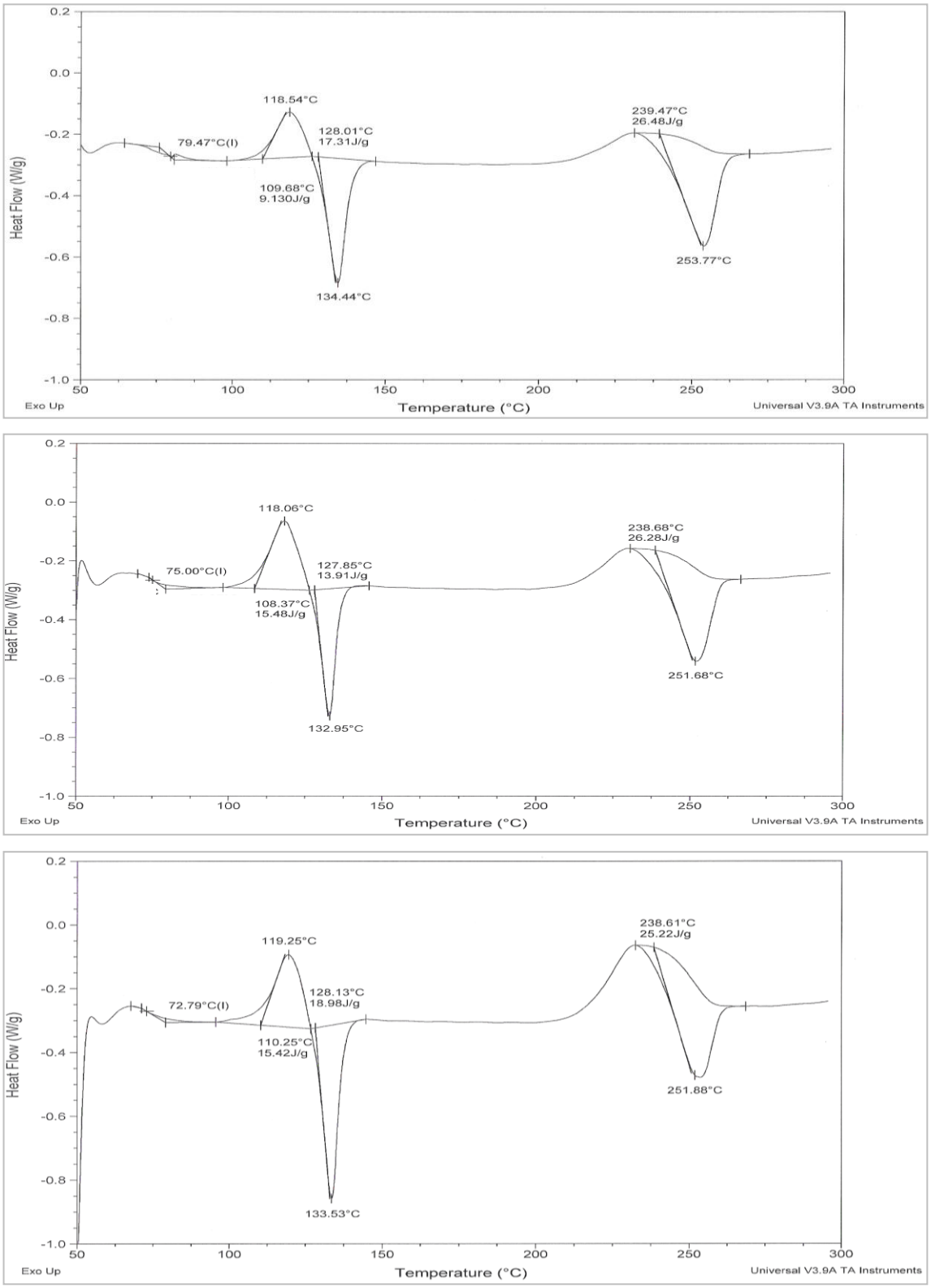

Figure 16 Thermograms of Inj. Moulded Samples of rPET-bg contaminated with 10% HDPE

9. DSC Thermograms of *Injection Moulded Samples* (85% rPET-bg / 15% HDPE)

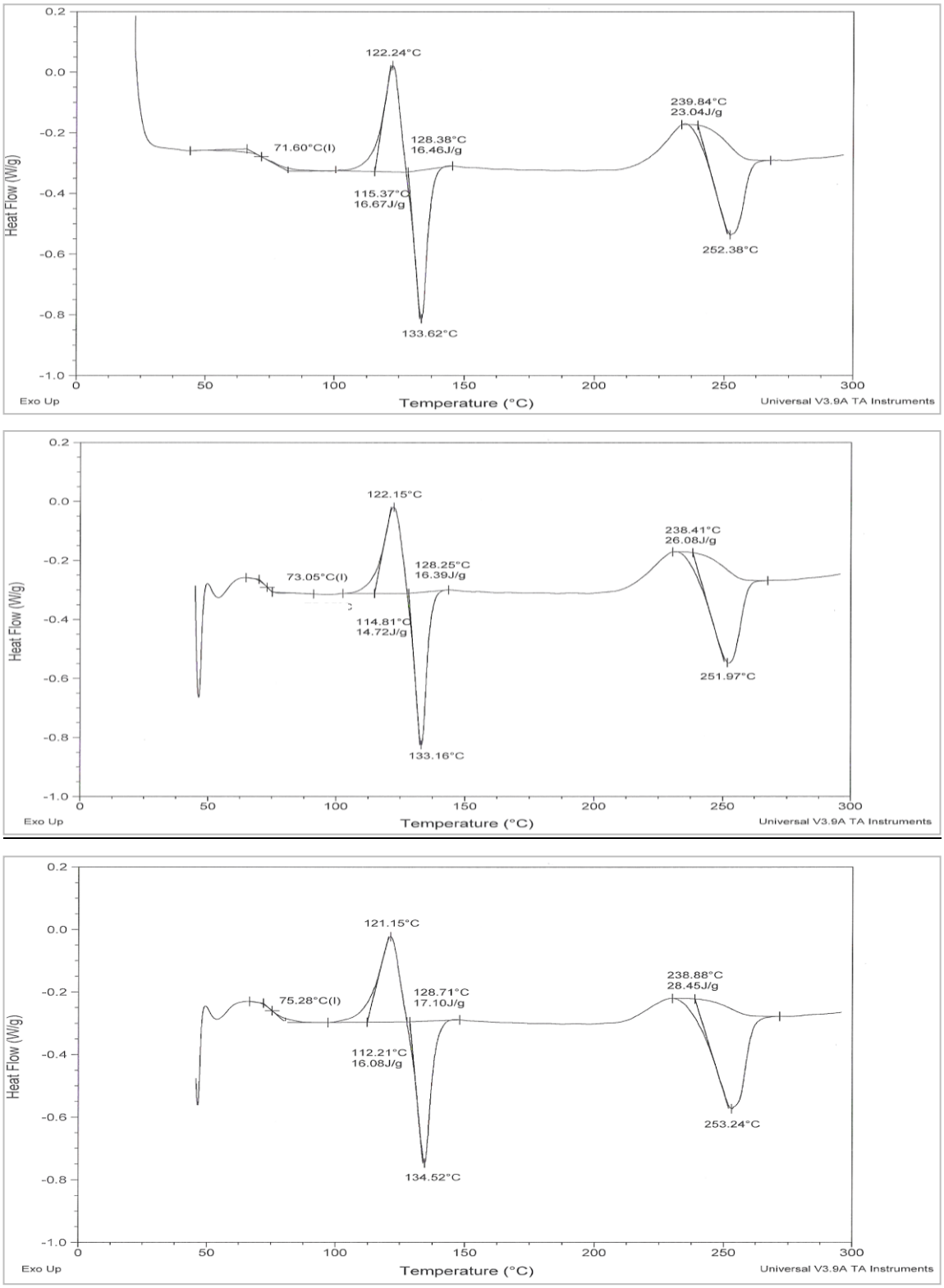

Figure 17 Thermograms of Inj. Moulded Samples of rPET-bg contaminated with 15% HDPE

10. FTIR Spectra of *Inj. Moulded Samples* (95% rPET-bg / 5% HDPE)

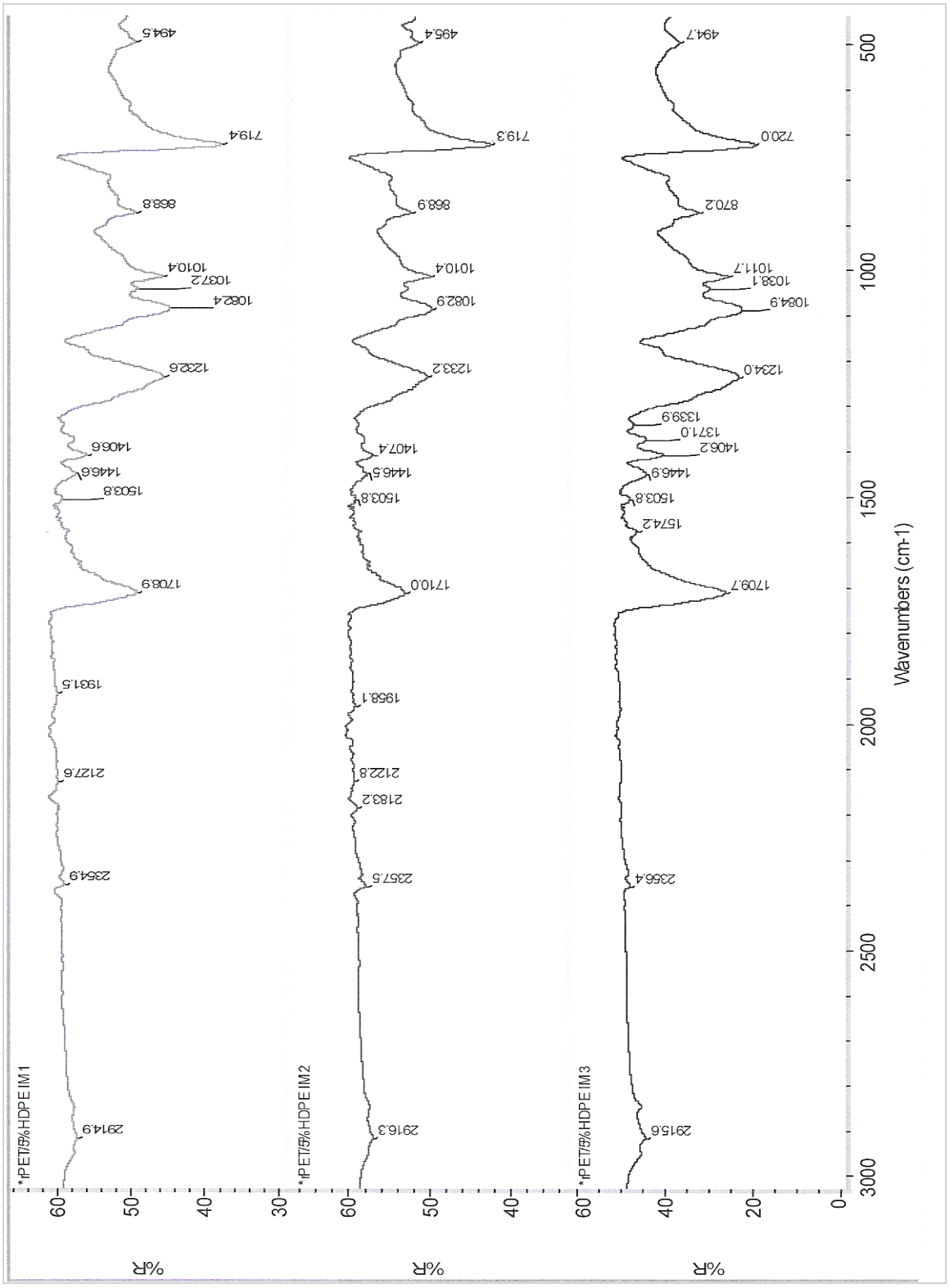

Figure 18 FTIR Spectra of Inj. Moulded Samples of rPET-bg contaminated with 5% HDPE

11. FTIR Spectra of *Inj. Moulded Samples* (90% rPET-bg / 10% HDPE)

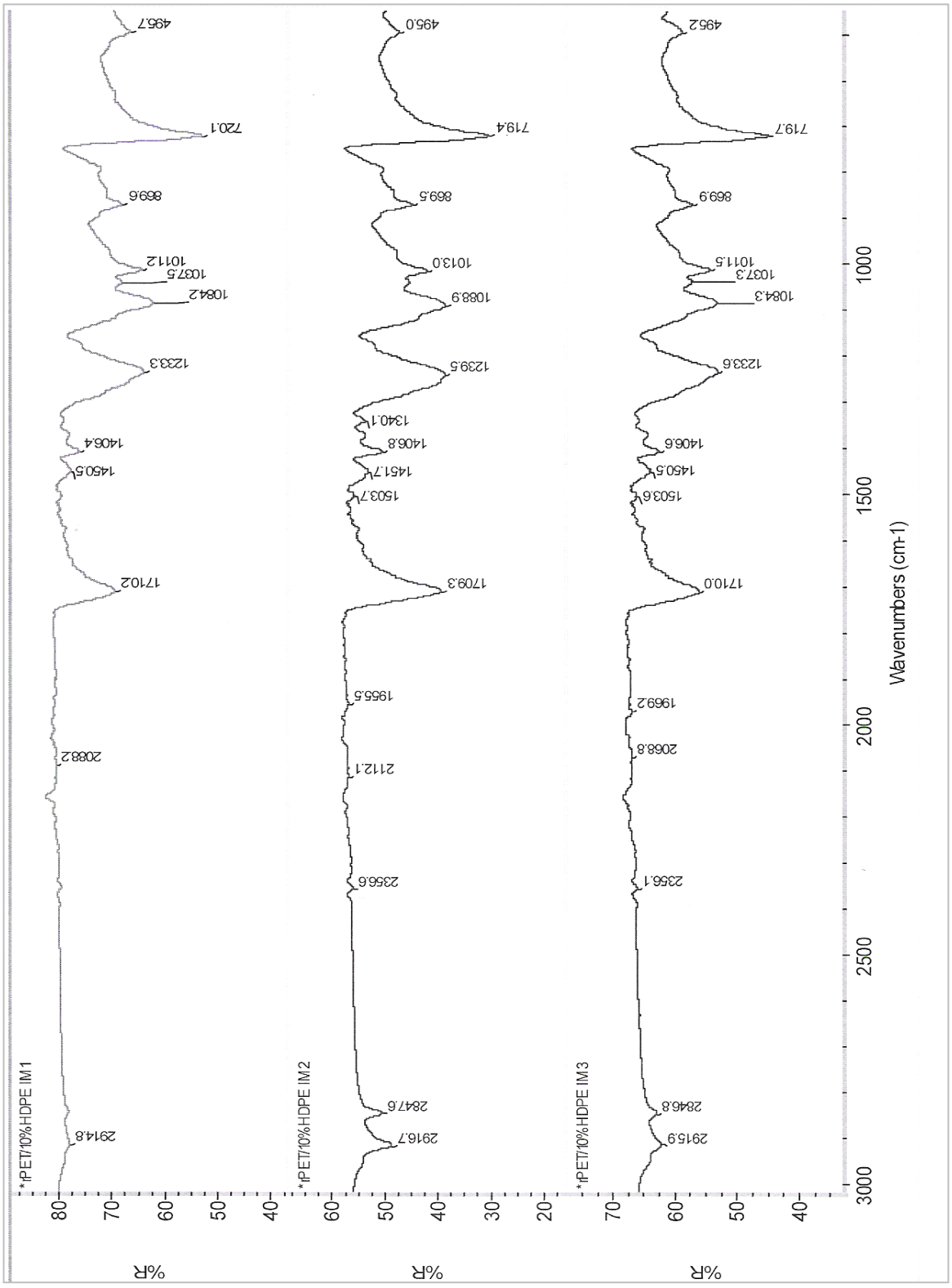

Figure 19 FTIR Spectra of Inj. Moulded Samples of rPET-bg contaminated with 10% HDPE

12. FTIR Spectra of *Inj. Moulded Samples* (85% rPET-bg / 15% HDPE)

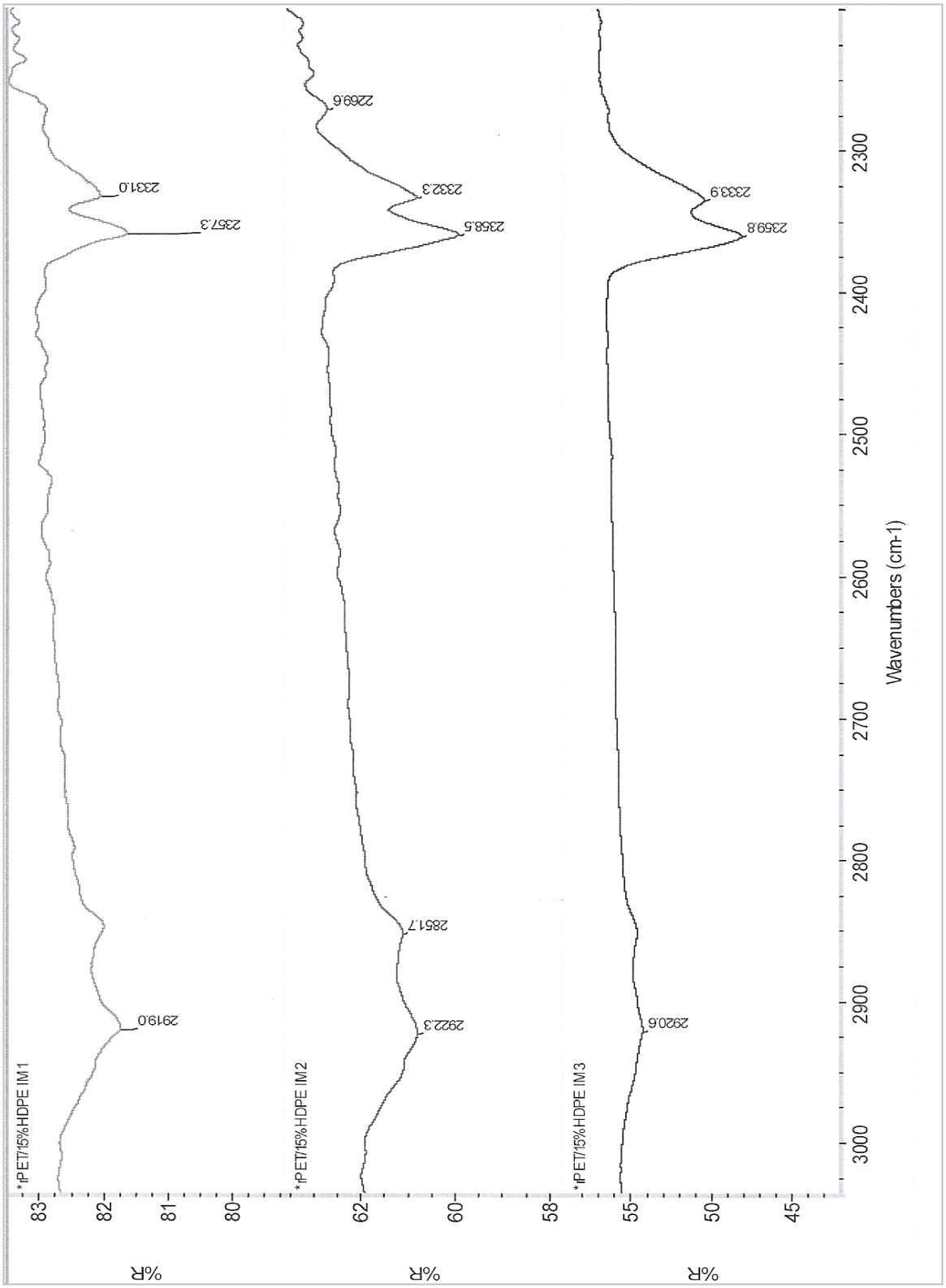

Figure 20 Spectra of Inj. Moulded Samples of rPET-bg contaminated with 15% HDPE

13. Tensile Graph of *Dumbbells* (95% rPET-bg / 5% HDPE)

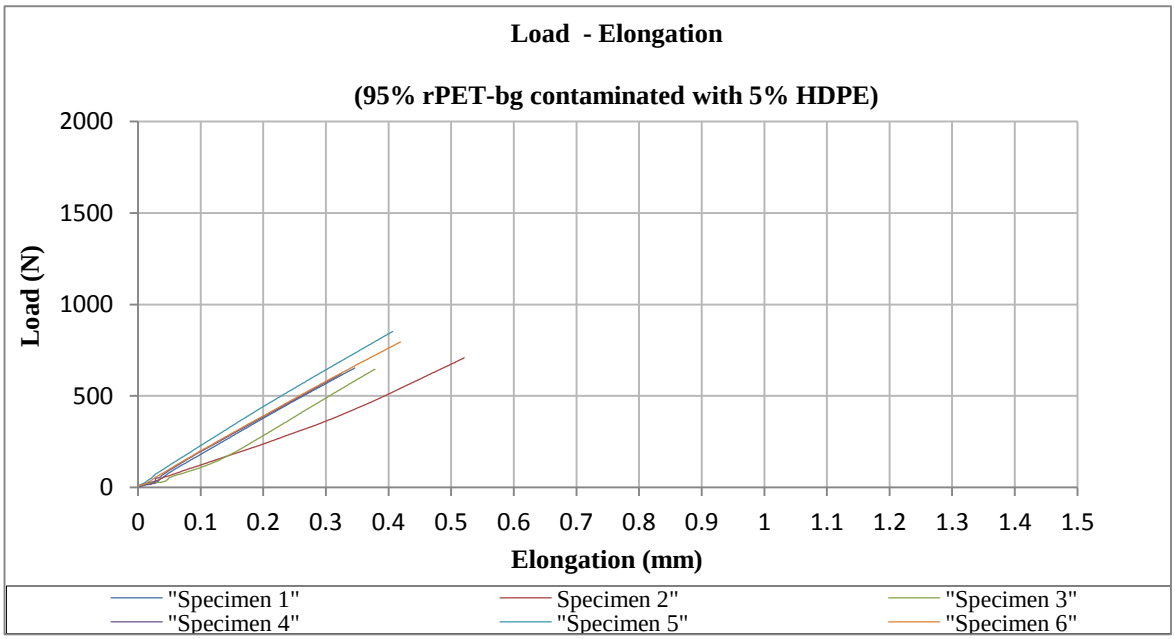

Figure 21 Curves of Dumbbells of rPET-bg contaminated with 5% HDPE

14. Tensile Graph of *Dumbbells* (90% rPET-bg / 10% HDPE)

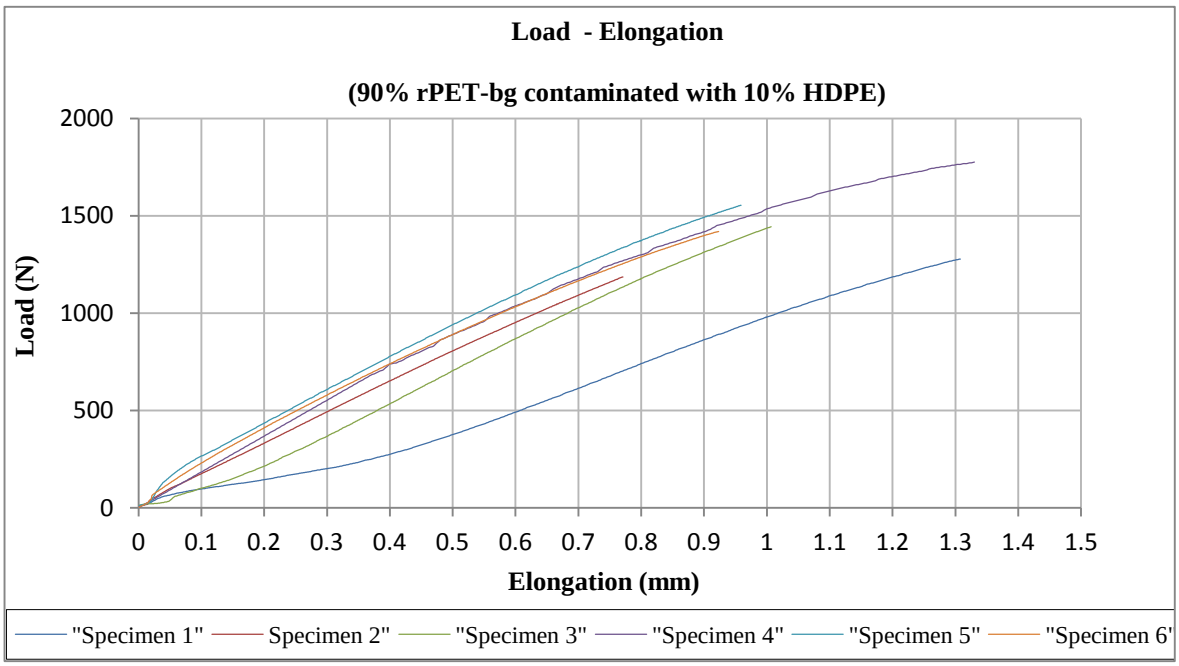

Figure 22 Curves of Dumbbells of rPET-bg contaminated with 10% HDPE

15. Tensile Graph of *Dumbbells* (85% rPET-bg / 15% HDPE)

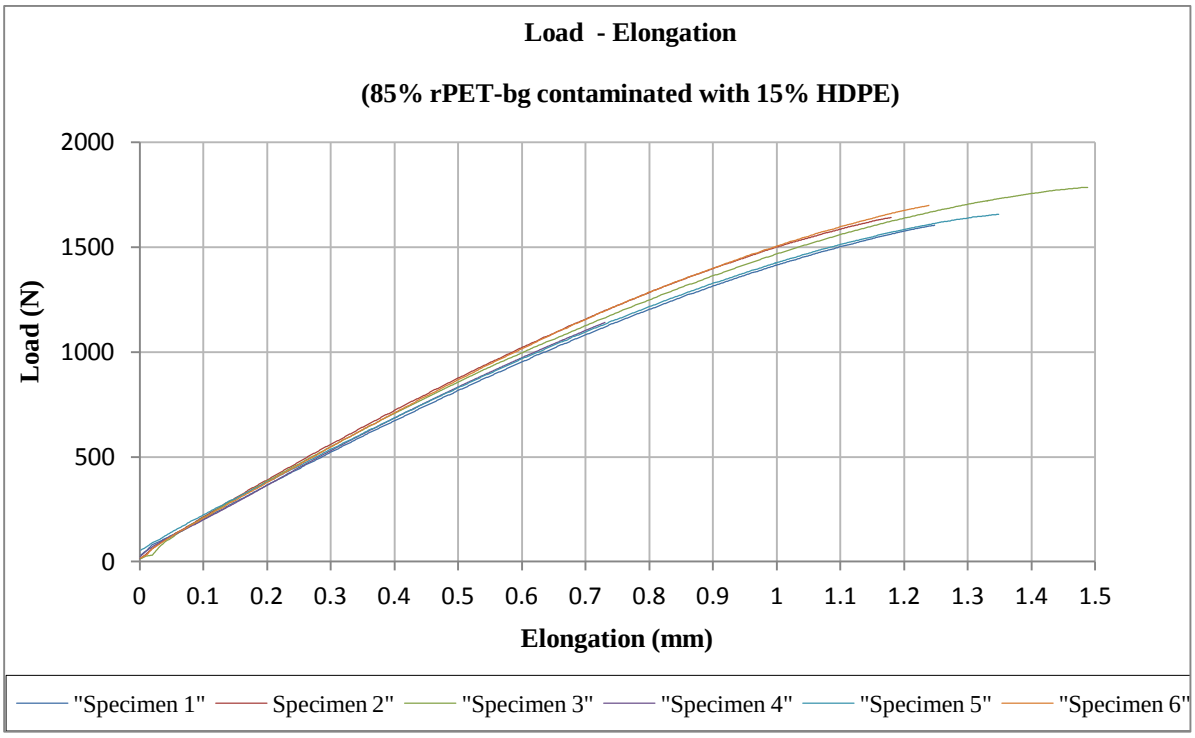

Figure 23 Curves of Dumbbells of rPET-bg contaminated with 15% HDPE

APPENDIX 6 – *Experiments 6, 7* and *8* - **rPET-bg Contaminated with PP**

(Stage 1)

1. DSC Thermograms of *Extruded Samples* (95% rPET-bg / 5% PP)

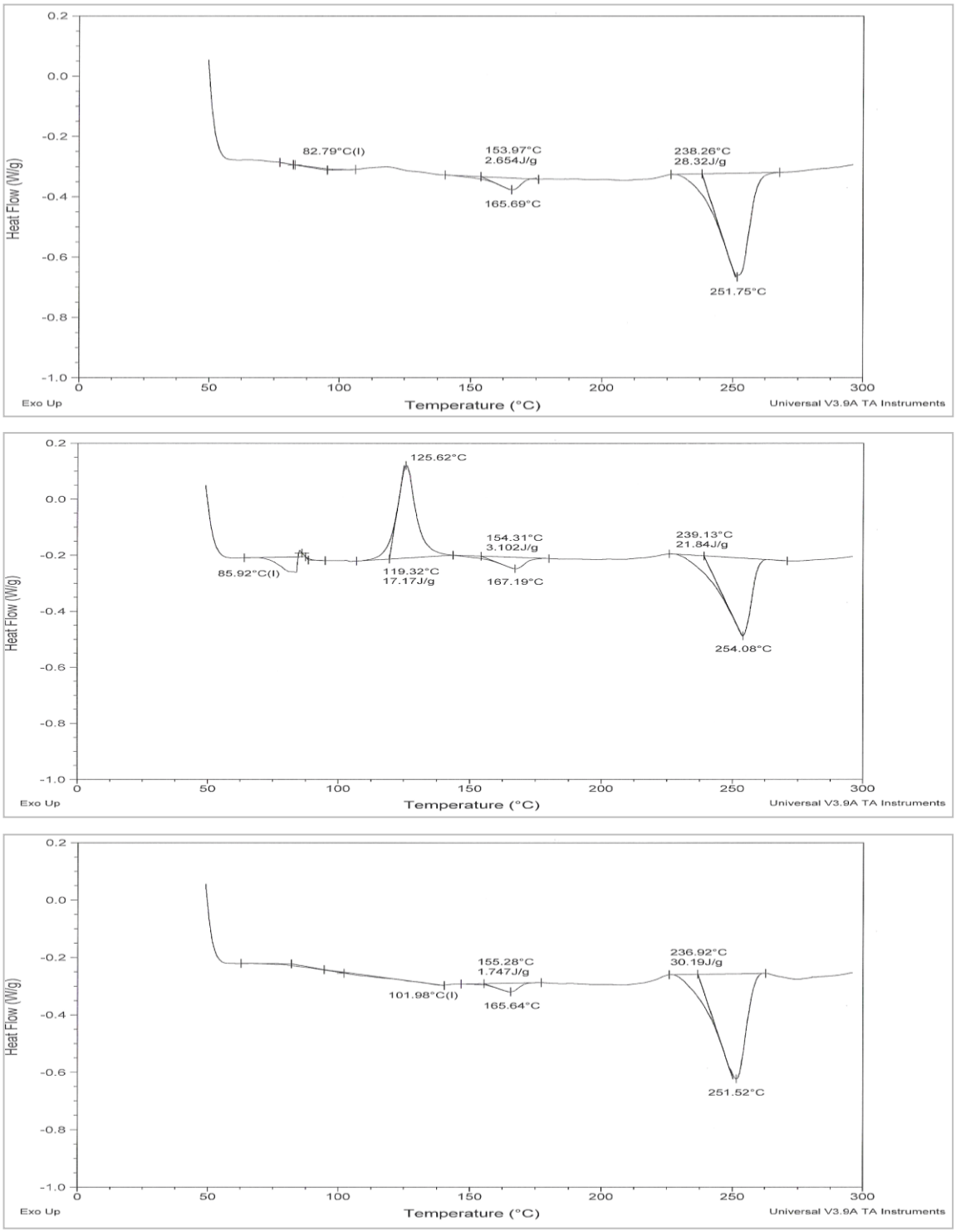

Figure 24 Thermograms of Extruded Samples of rPET-bg contaminated with 5% PP

2. DSC Thermograms of *Extruded Samples* (90% rPET-bg / 10% PP)

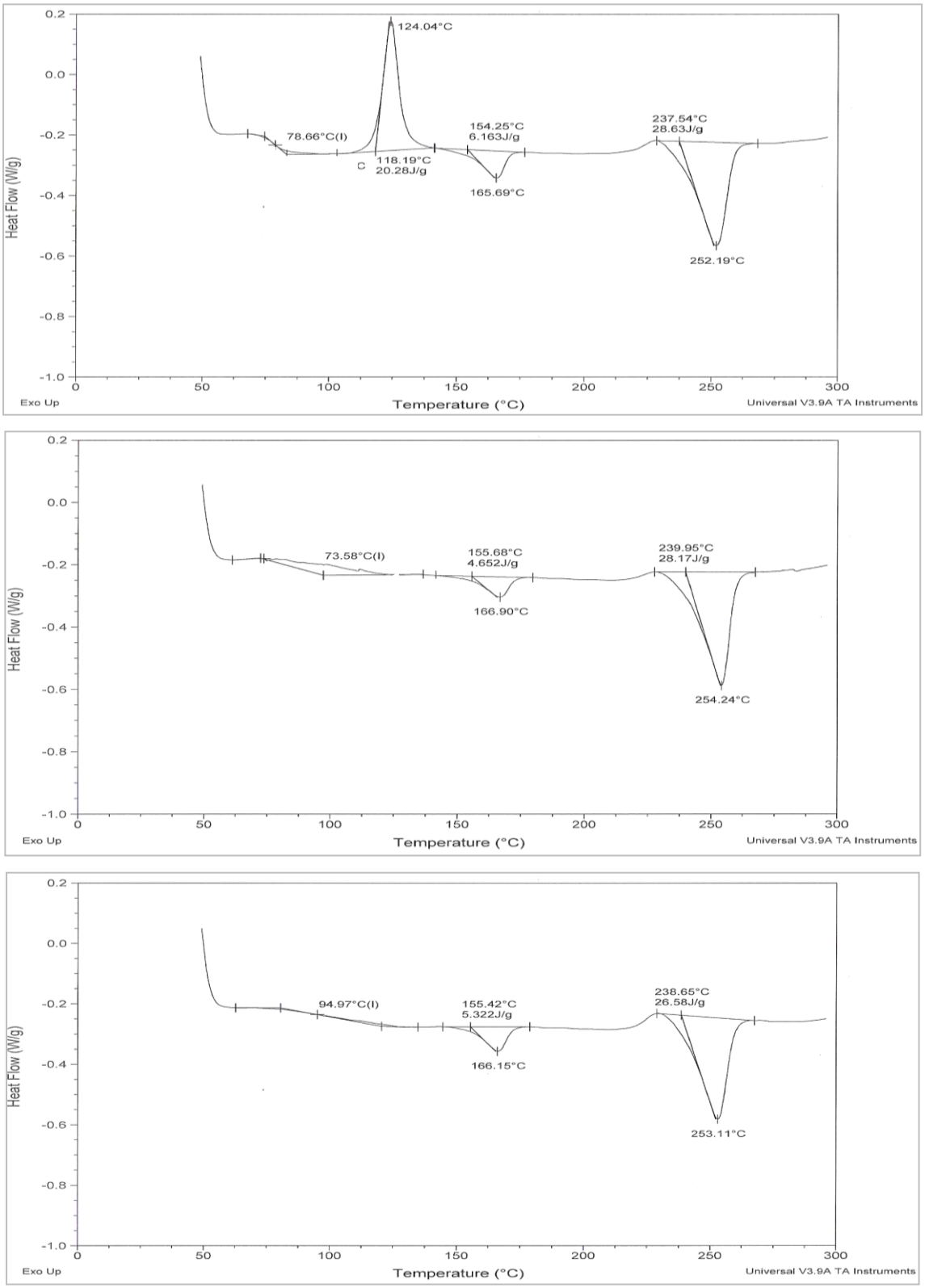

Figure 25 Thermograms of Extruded Samples of rPET-bg contaminated with 10% PP

3. DSC Thermograms of *Extruded Samples* (85% rPET-bg / 15% PP)

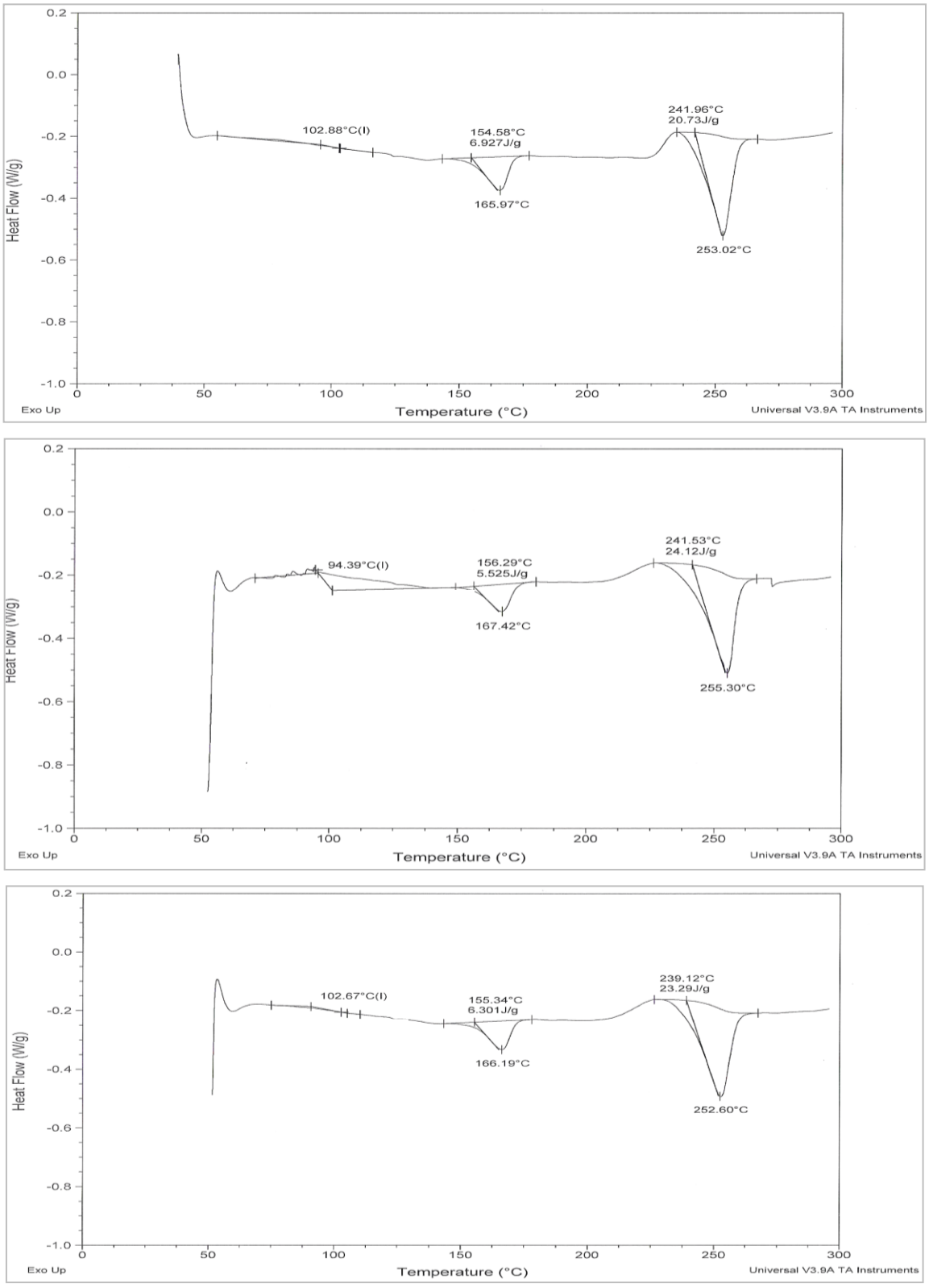

Figure 26 Thermograms of Extruded Samples of rPET-bg contaminated with 15% PP

4. FTIR Spectra of *Extruded Samples* (95% rPET-bg / 5% PP)

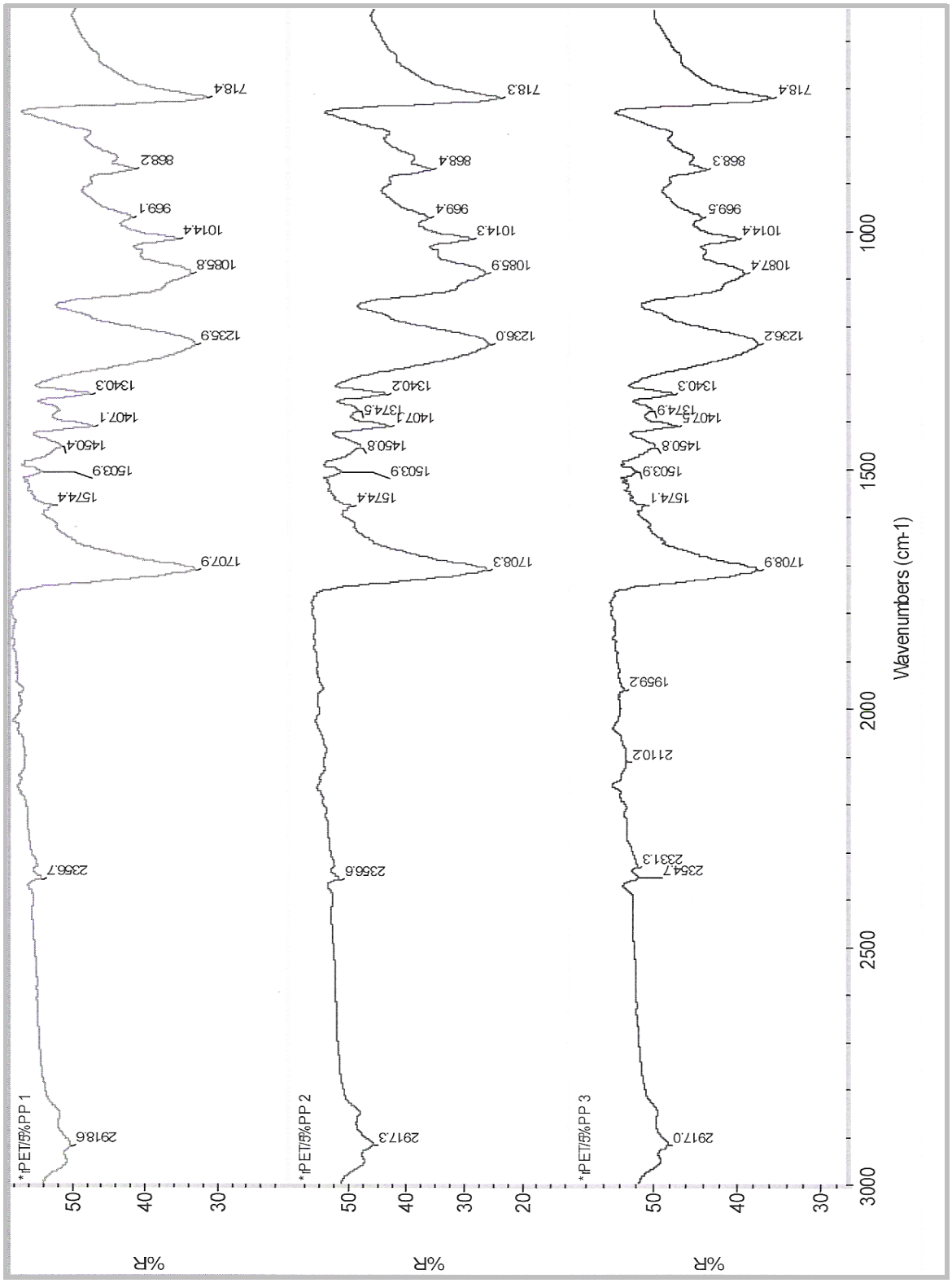

Figure 27 Spectra of Extruded Samples of rPET-bg contaminated with 5% PP

5. FTIR Spectra of *Extruded Samples* (90% rPET-bg / 10% PP)

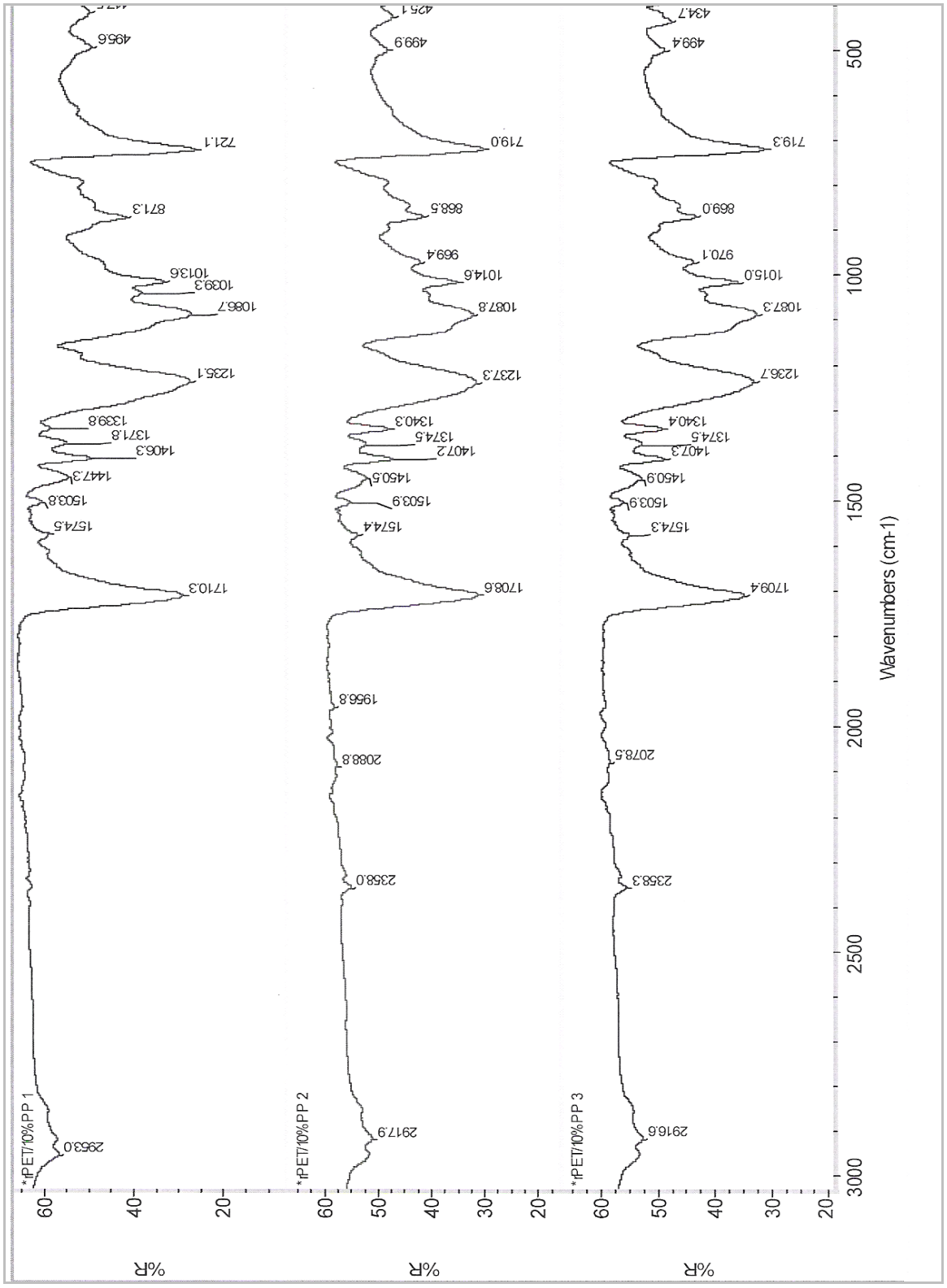

Figure 28 Spectra of Extruded Samples of rPET-bg contaminated with 10% PP

6. FTIR Spectra of *Extruded Samples* (85% rPET-bg / 15% PP)

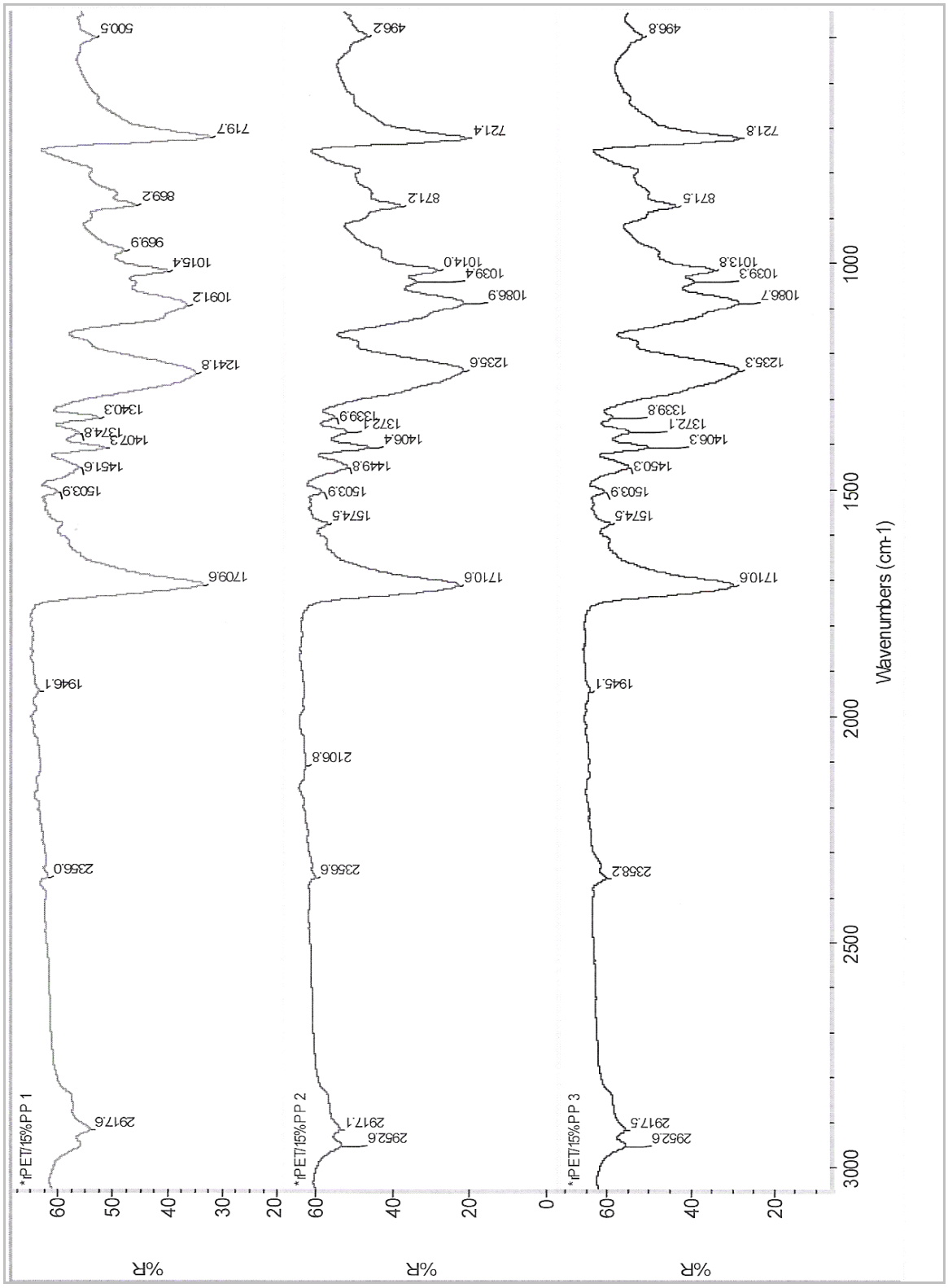

Figure 29 Spectra of Extruded Samples of rPET-bg contaminated with 15% PP

7. DSC Thermograms of *Inj. Moulded Samples* (95% rPET-bg / 5% PP)

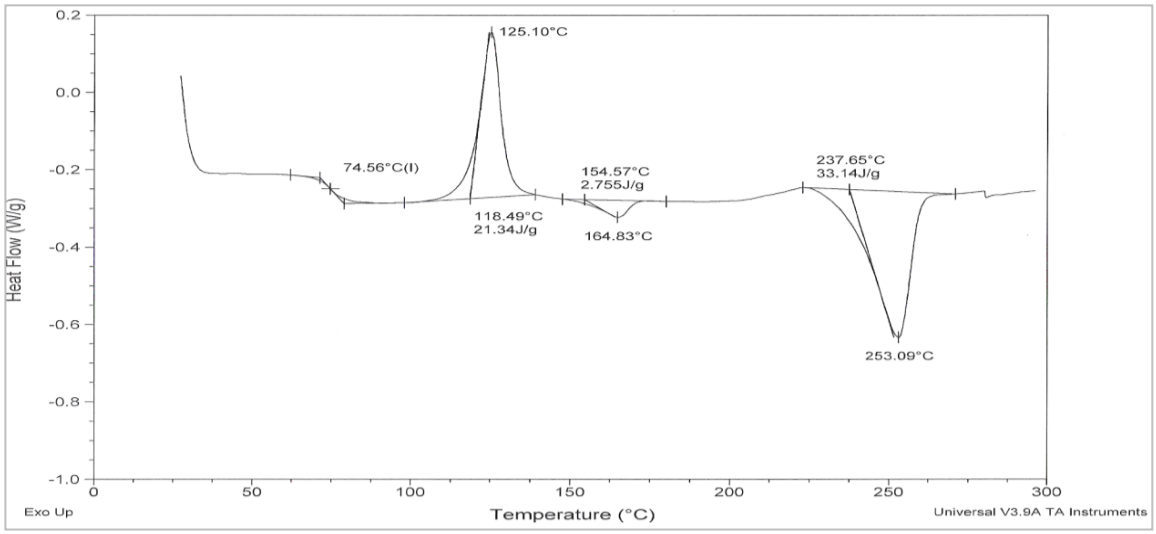

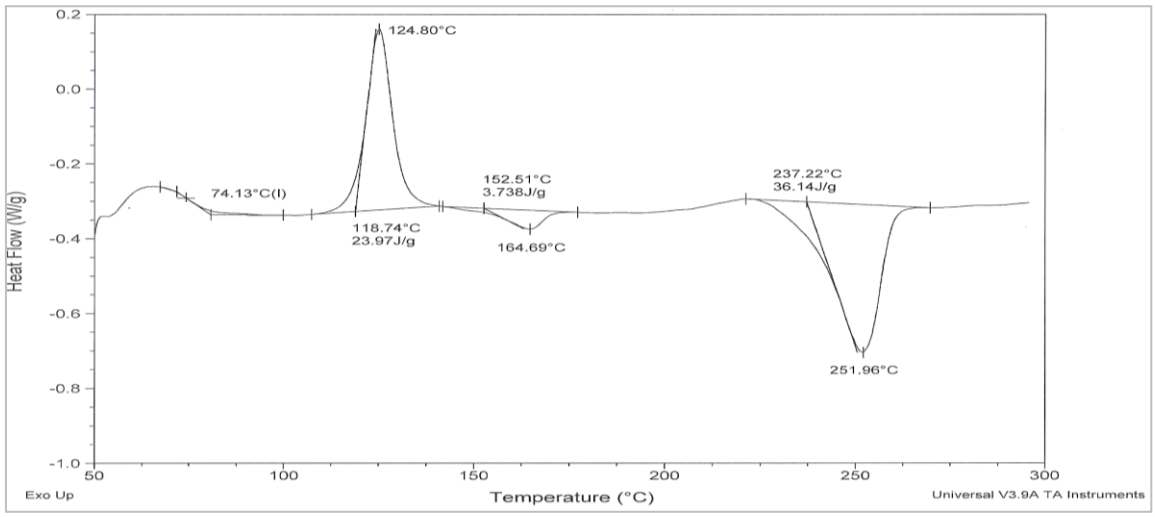

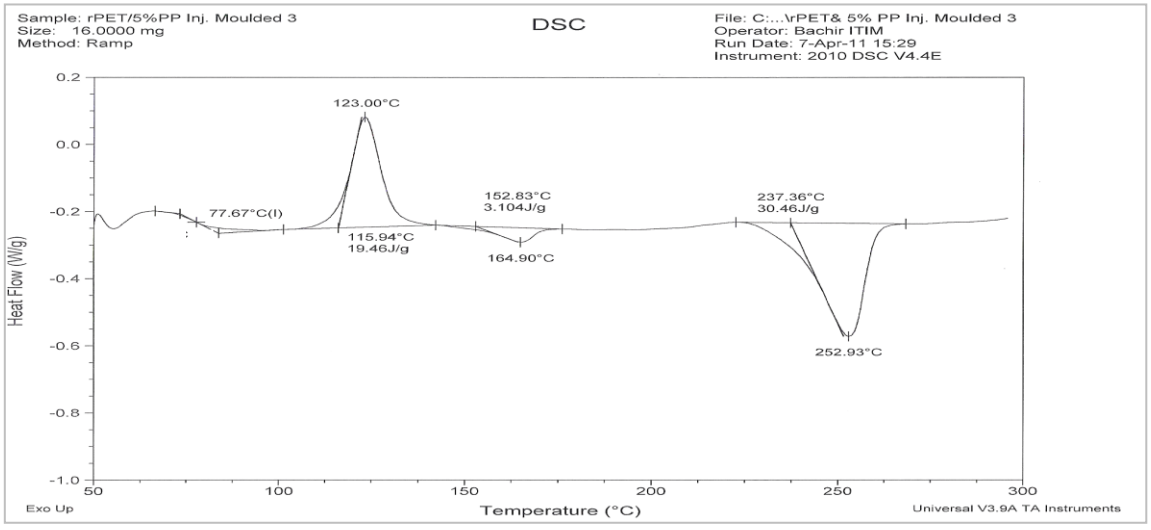

Figure 30 Thermograms of Inj. Moulded Samples of rPET-bg contaminated with 5% PP

8. DSC Thermograms of *Inj. Moulded Samples* (90% rPET-bg / 10% PP)

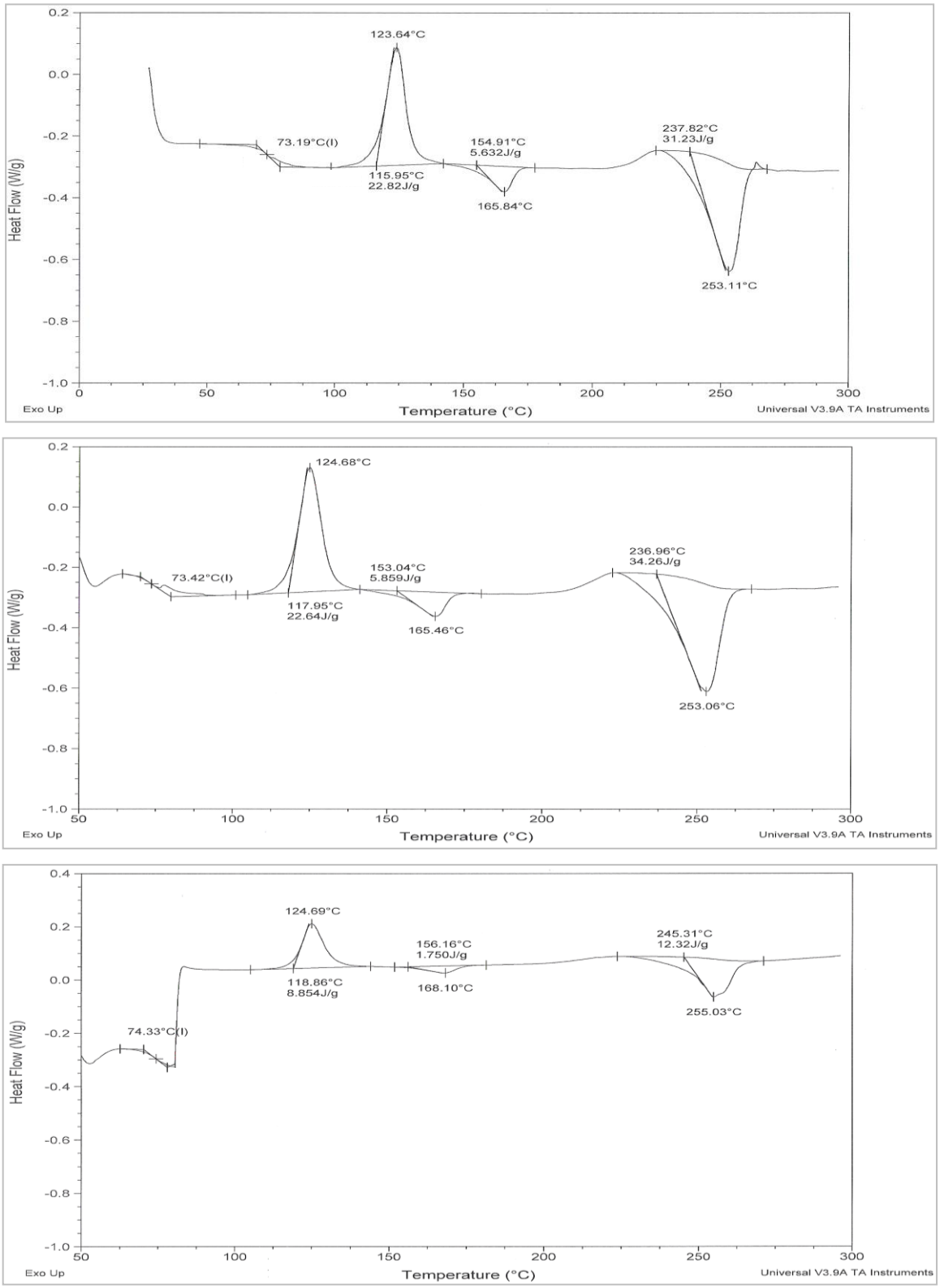

Figure 31 Thermograms of Inj. Moulded Samples of rPET-bg contaminated with 10% PP

9. DSC Thermograms of *Inj. Moulded Samples* (85% rPET-bg / 15% PP)

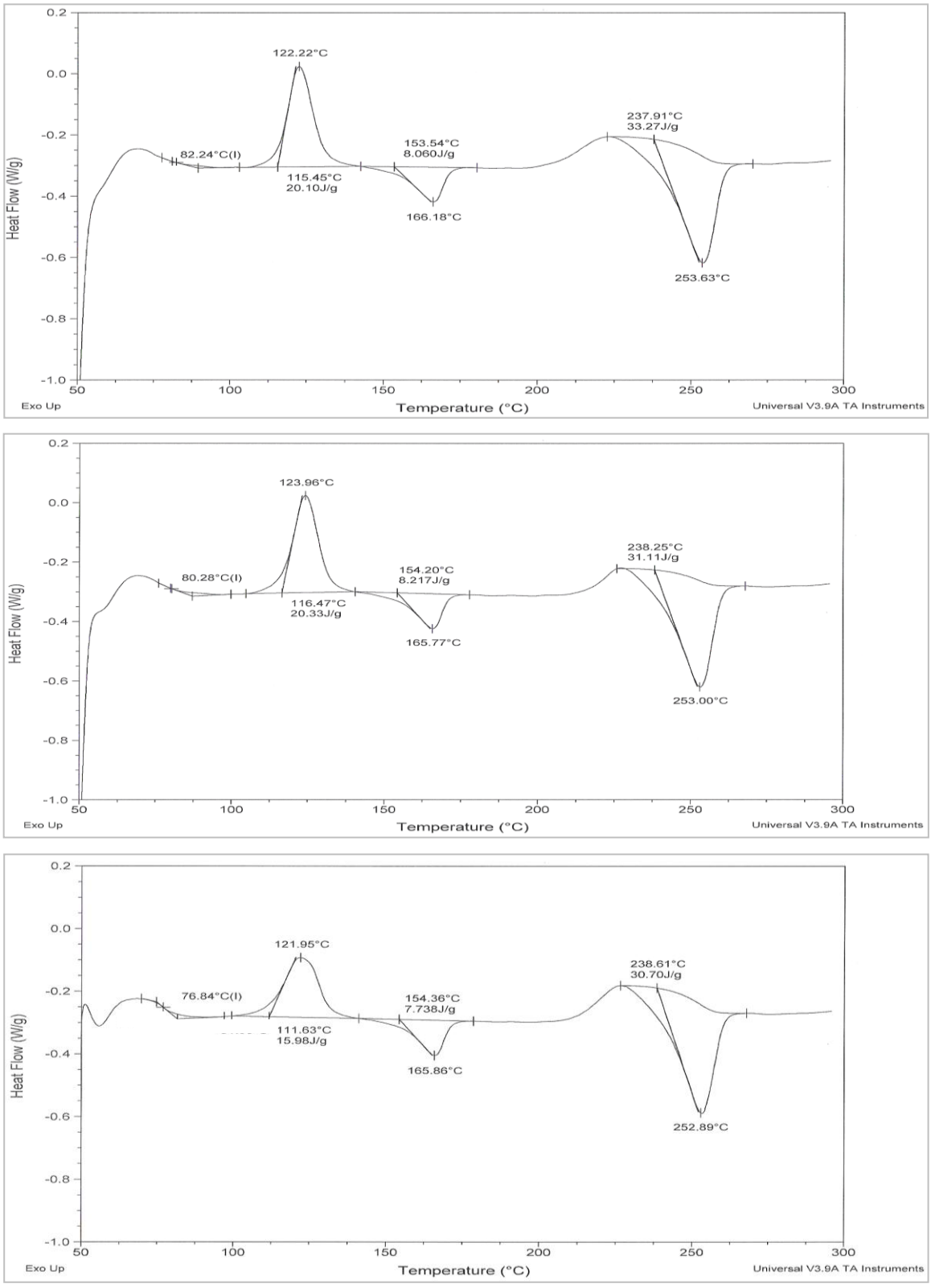

Figure 32 Thermograms of Inj. Moulded Samples of rPET-bg contaminated with 15% PP

10. FTIR Spectra of *Inj. Moulded Samples* (95% rPET-bg / 5% PP)

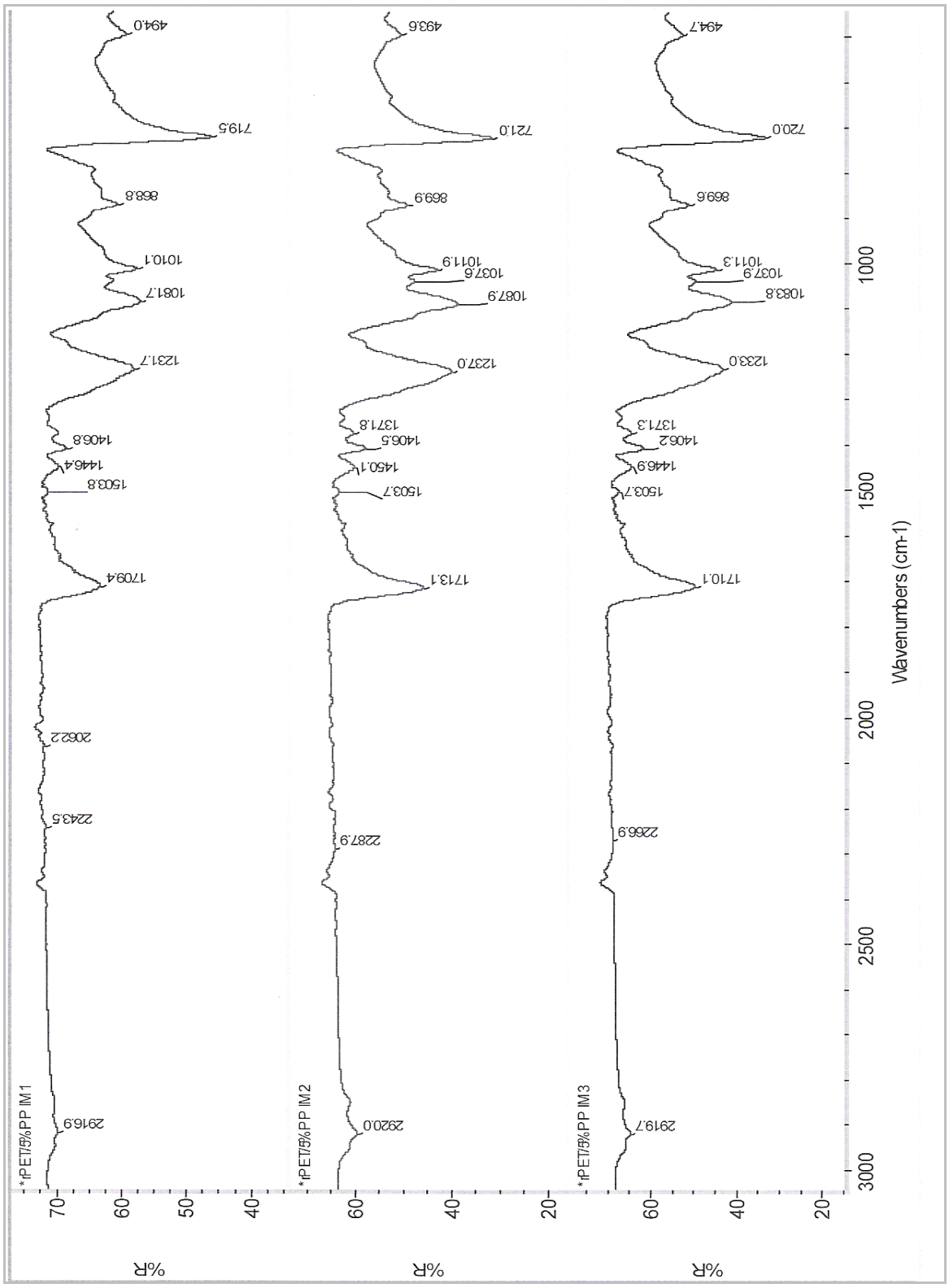

Figure 33 Spectra of Inj. Moulded Samples of rPET-bg contaminated with 5% PP

11. FTIR Spectra of *Inj. Moulded Samples* (90% rPET-bg / 10% PP)

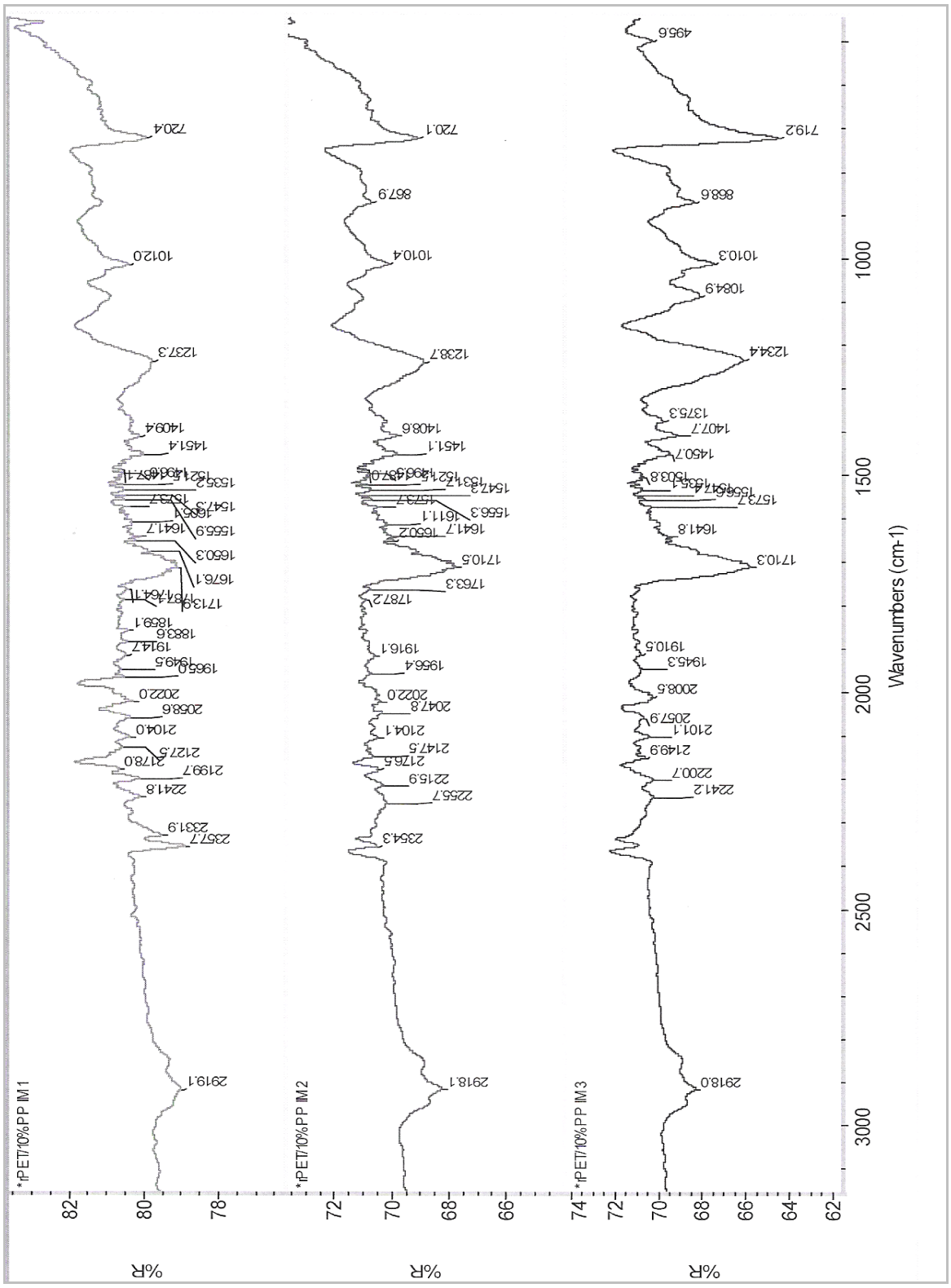

Figure 34 Spectra of Inj. Moulded Samples of rPET-bg contaminated with 10% PP

12. FTIR Spectra of *Inj. Moulded Samples* (85% rPET-bg / 15% PP)

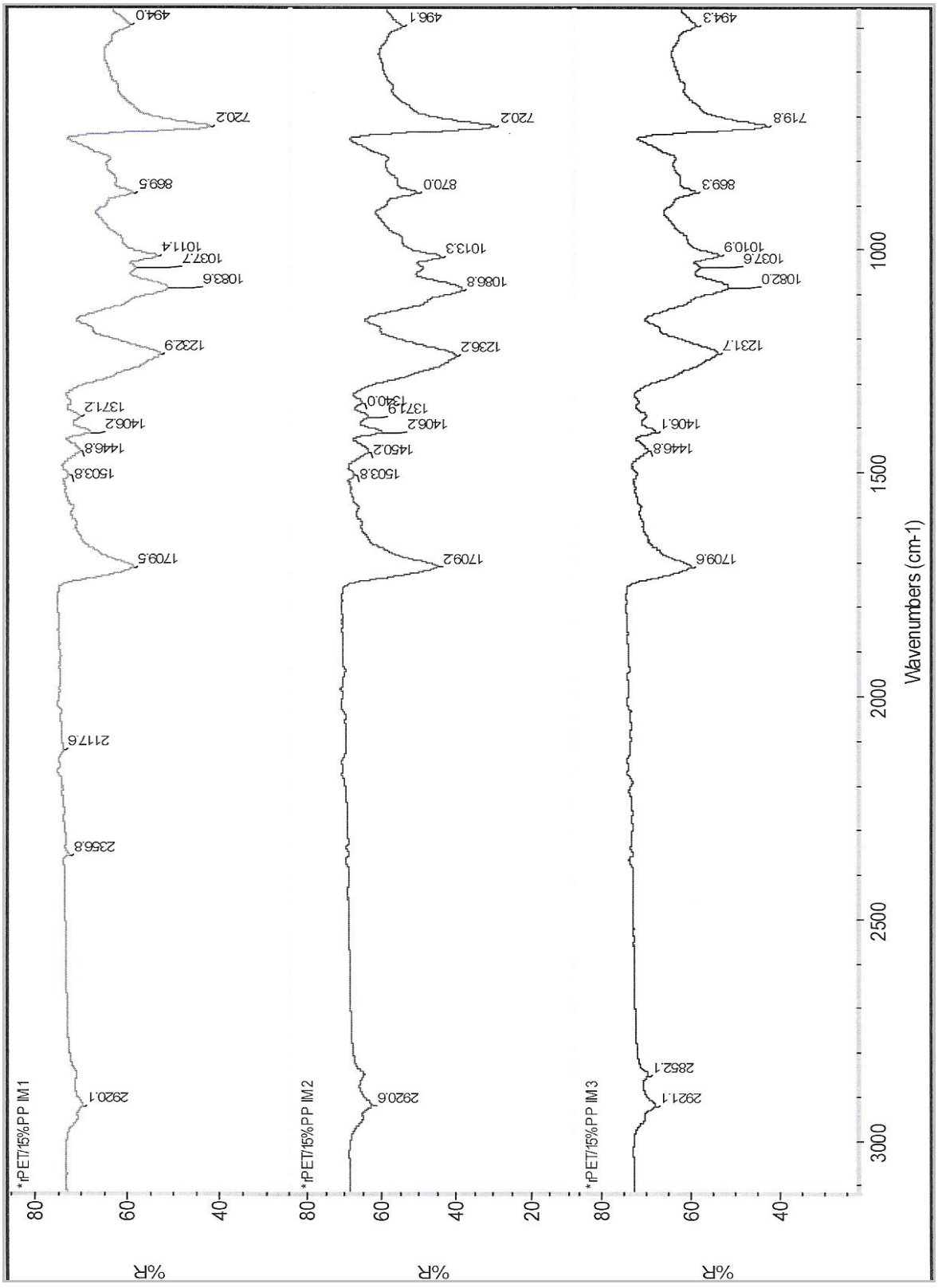

Figure 35 Spectra of Inj. Moulded Samples of rPET-bg contaminated with 15% PP

13. Tensile Graph of *Dumbbells* (95% rPET-bg / 5% PP)

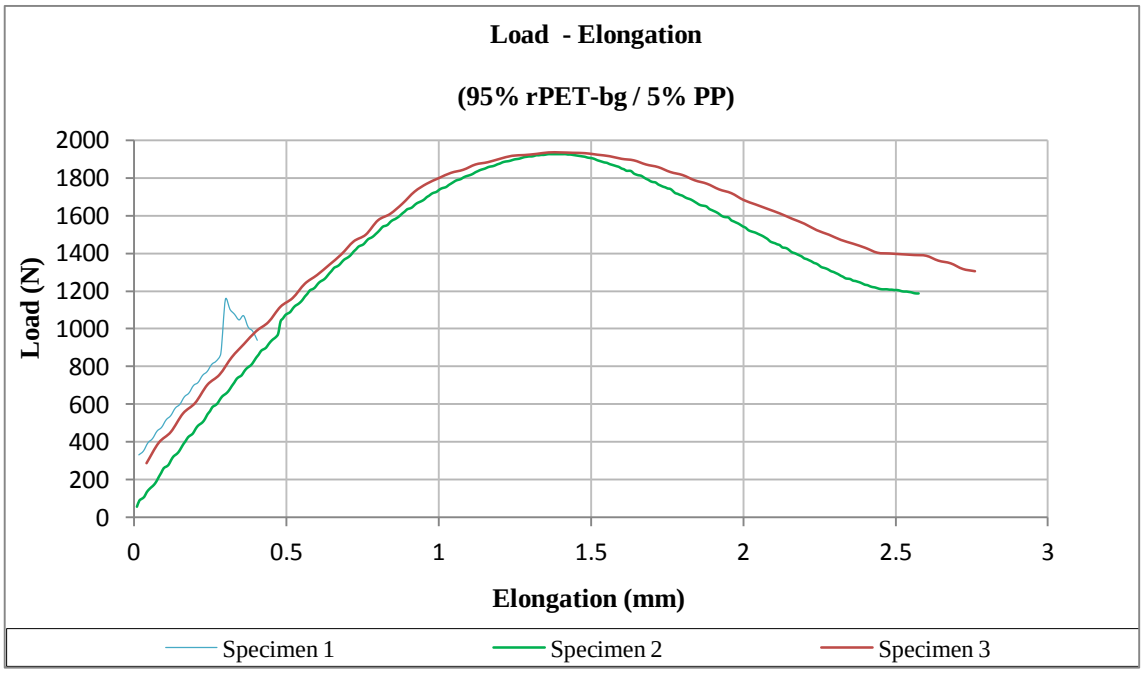

Figure 36 Tensile Curves of of rPET-bg contaminated with 5% PP

14. Tensile Graph of *Dumbbells* (90% rPET-bg / 10% PP)

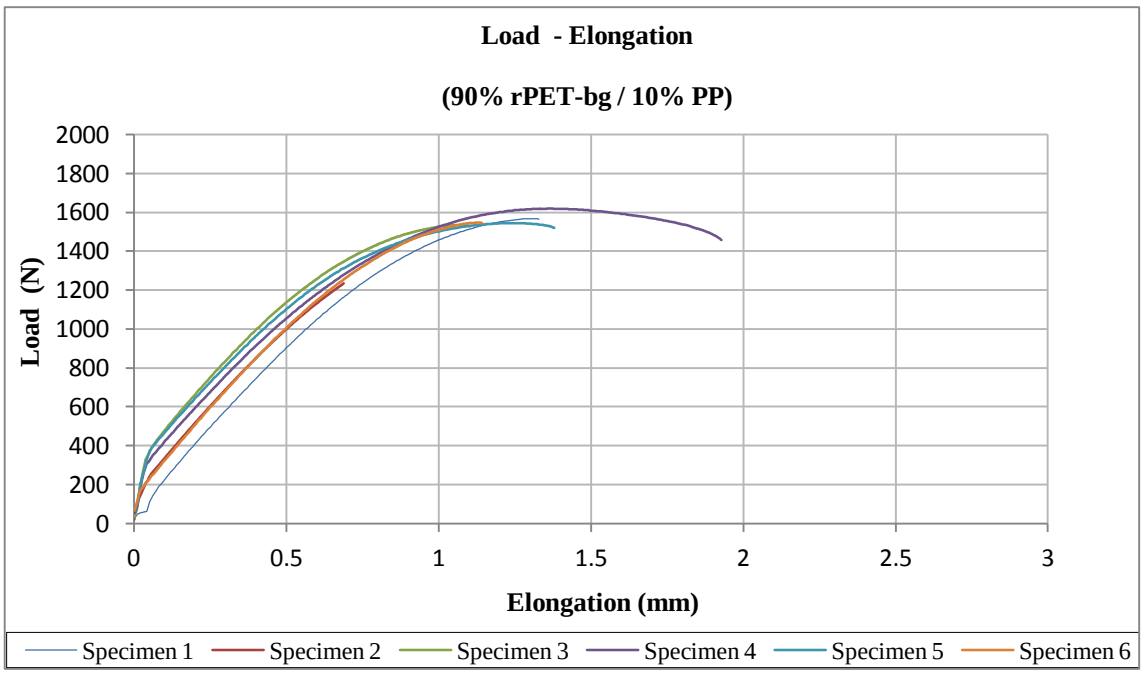

Figure 37 Tensile Curves of of rPET-bg contaminated with 10% PP

15. Tensile Graph of *Dumbbells* (85% rPET-bg / 15% PP)

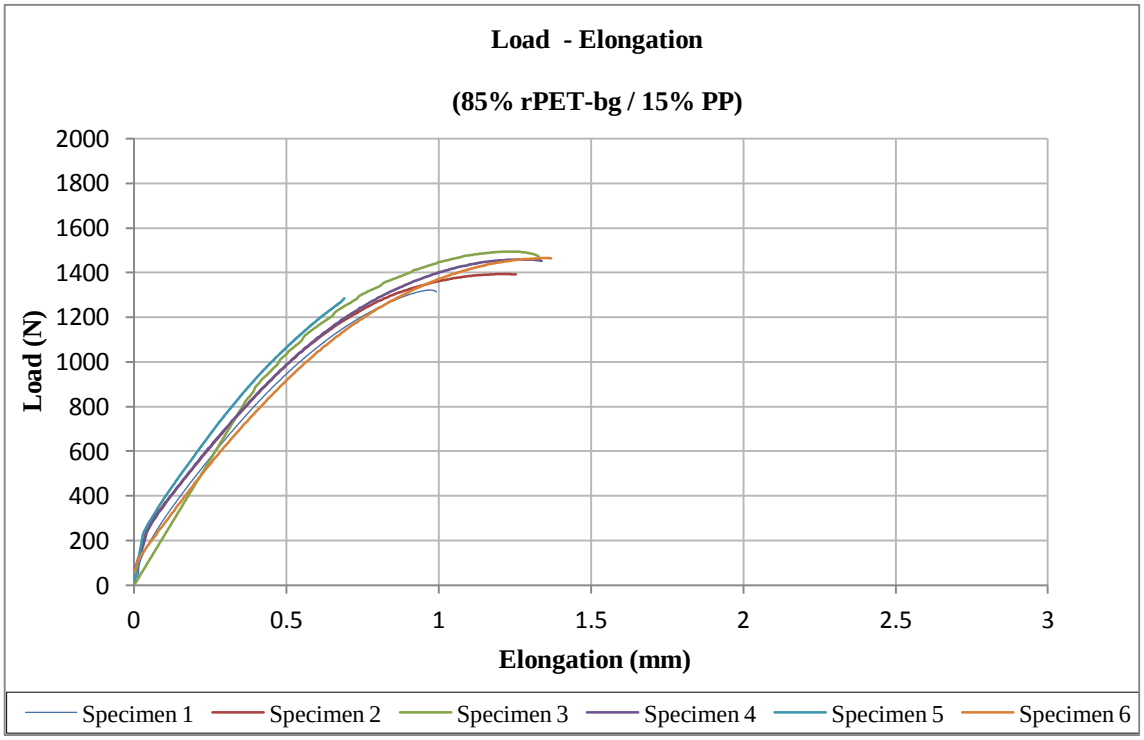

Figure 38 Tensile Curves of of rPET-bg contaminated with 15% PP

Effect of *cooling rates* **on the** *thermal characteristics* **of** *non contaminated rPET-bg* **and** *rPET-bg contaminated with 5% PP*

(Stage 2)

1. DSC Thermograms of *non contaminated rPET-bg at a heating / cooling rate of* ***10°C/min***

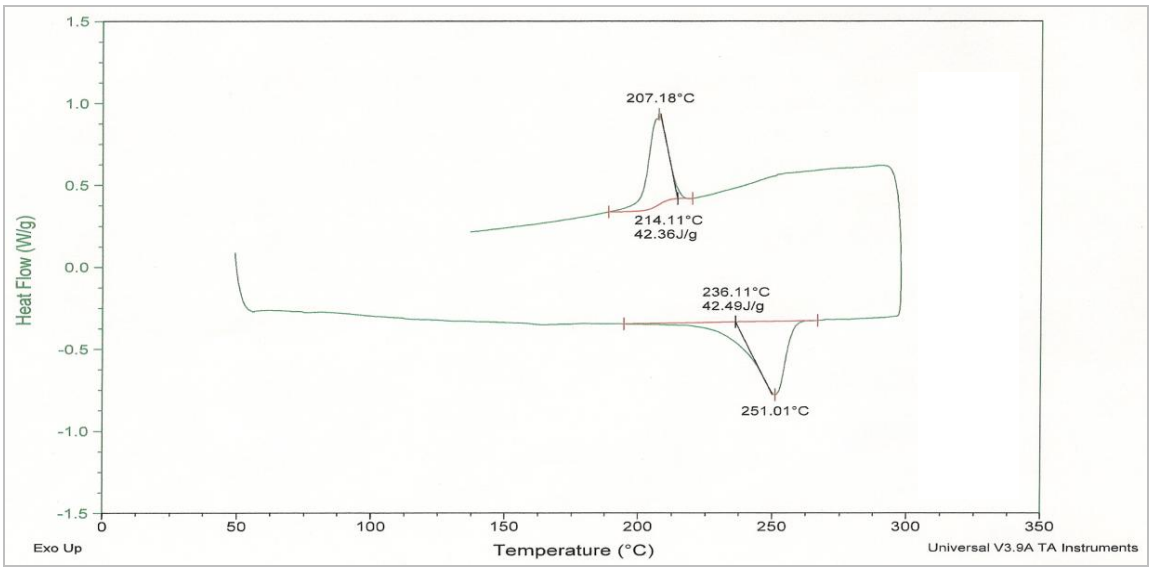

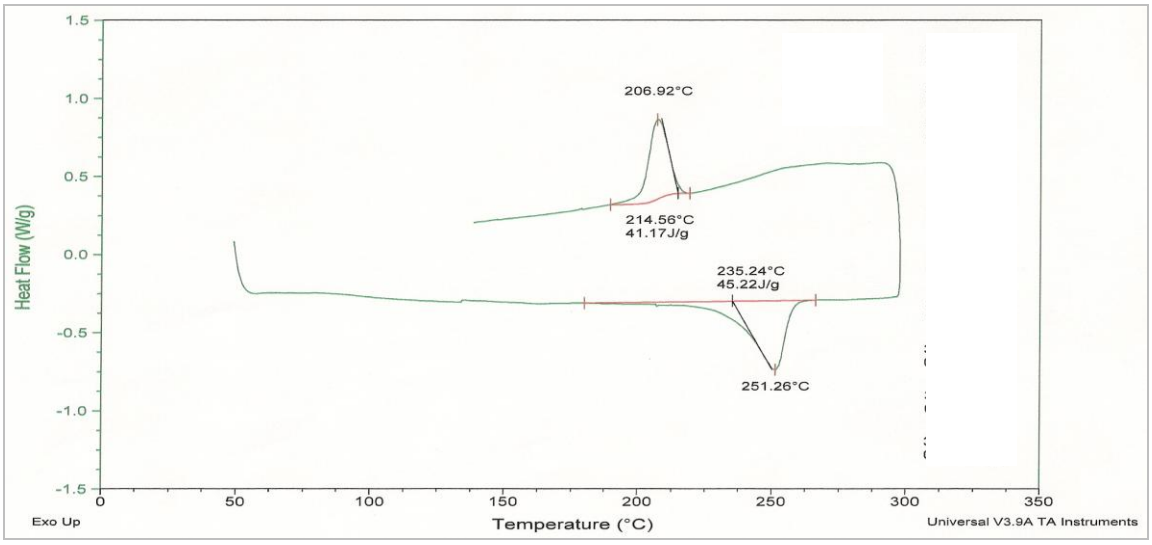

Figure 39 Thermograms of Extruded Samples of non contaminated rPET-bg at 10°C/min

2. DSC Thermograms of *rPET-bg contaminated with 5% PP at a heating / cooling rate of* ***10°C/min***

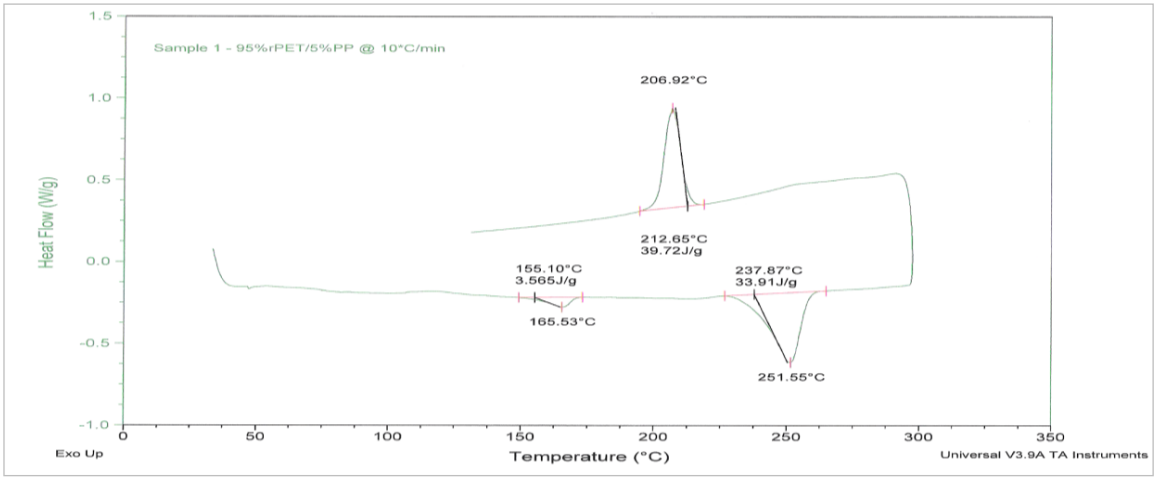

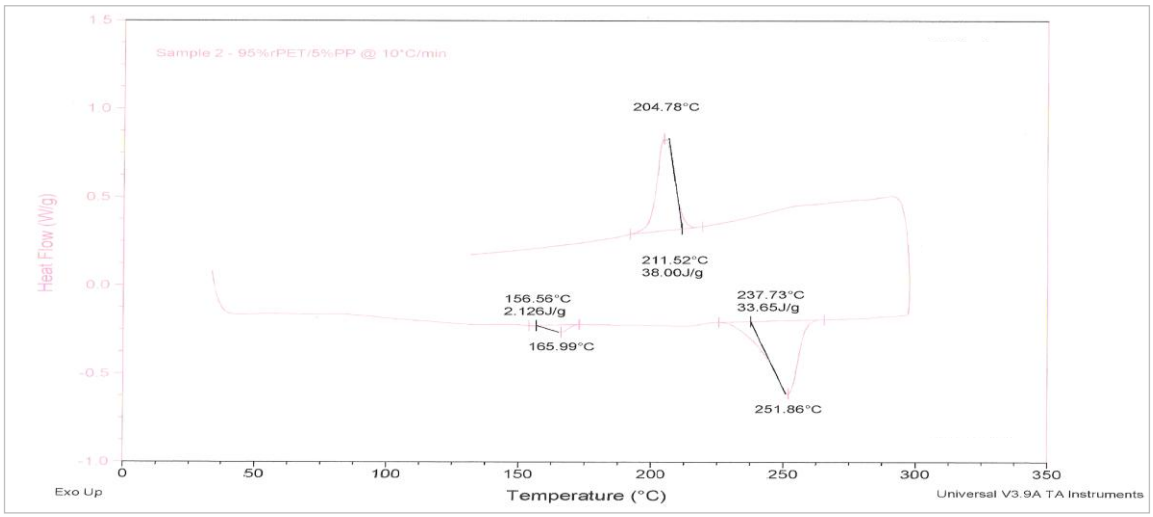

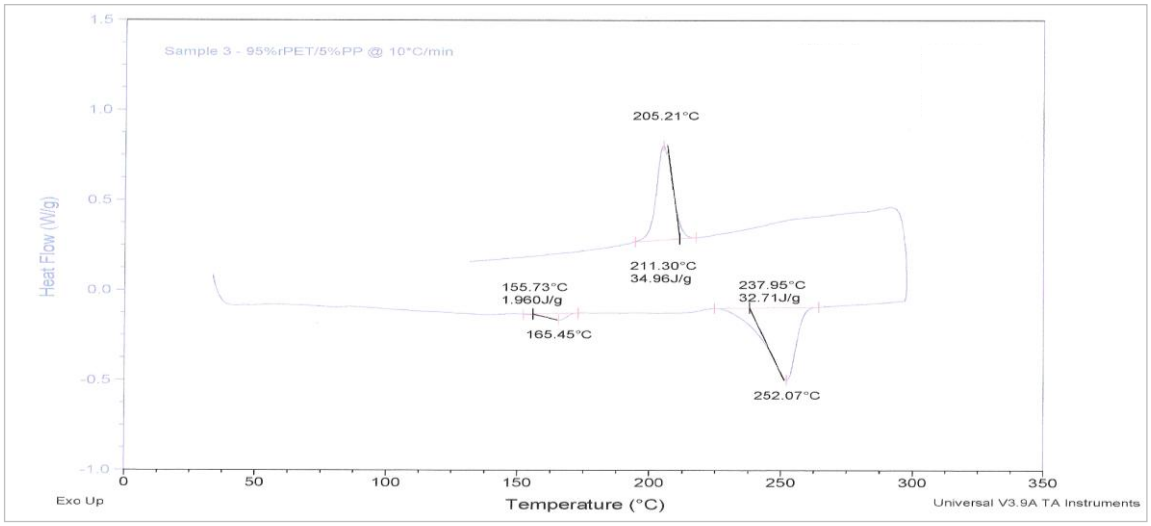

Figure 40 Thermograms of Extruded Samples of rPET-bg contaminated with 5% PP at 10°C/min

2. **DSC Thermograms of** *non contaminated rPET-bg at a heating / cooling rate of* ***15°C/min***

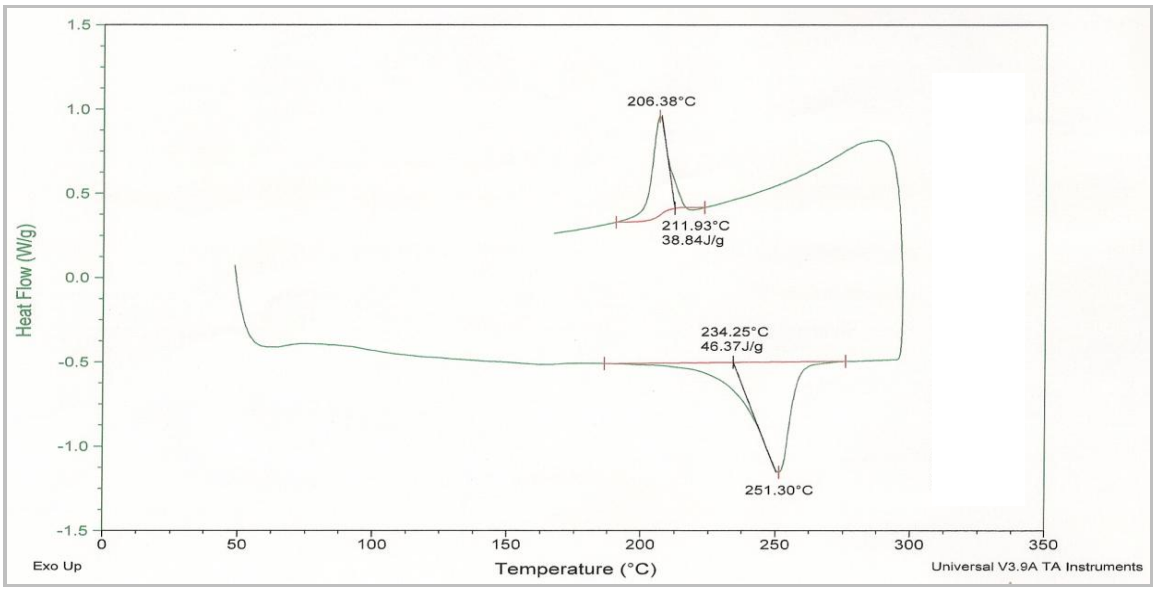

Figure 41 Thermograms of Extruded Samples of non contaminated rPET-bg at 15°C/min

4. DSC Thermograms of *rPET-bg contaminated with 5% PP at a heating / cooling rate of* ***15°C/min***

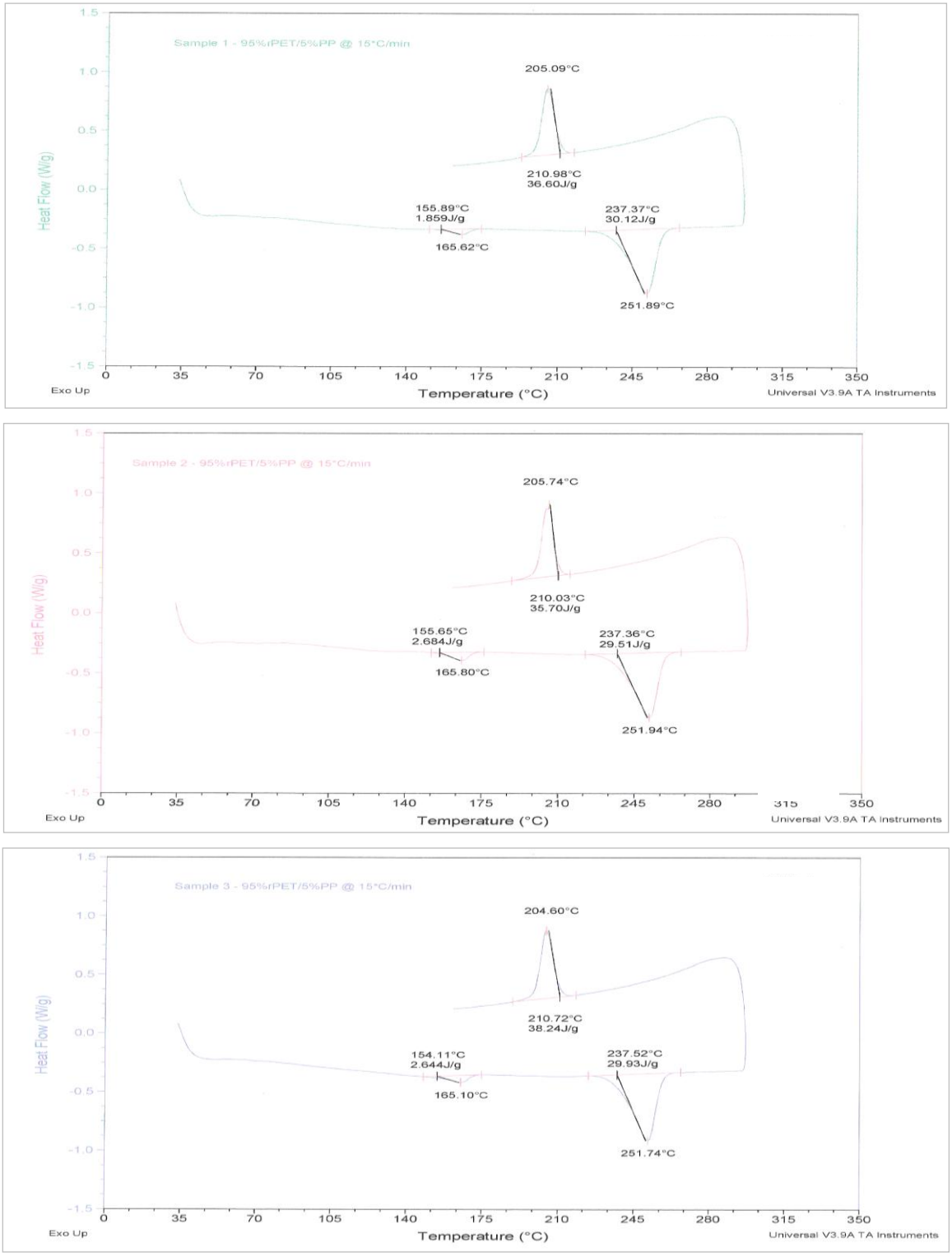

Figure 42 Thermograms of Extruded Samples of rPET-bg contaminated with 5% PP at 15°C/min

5. DSC Thermograms of *non contaminated rPET-bg at a heating / cooling rate of* ***20°C/min***

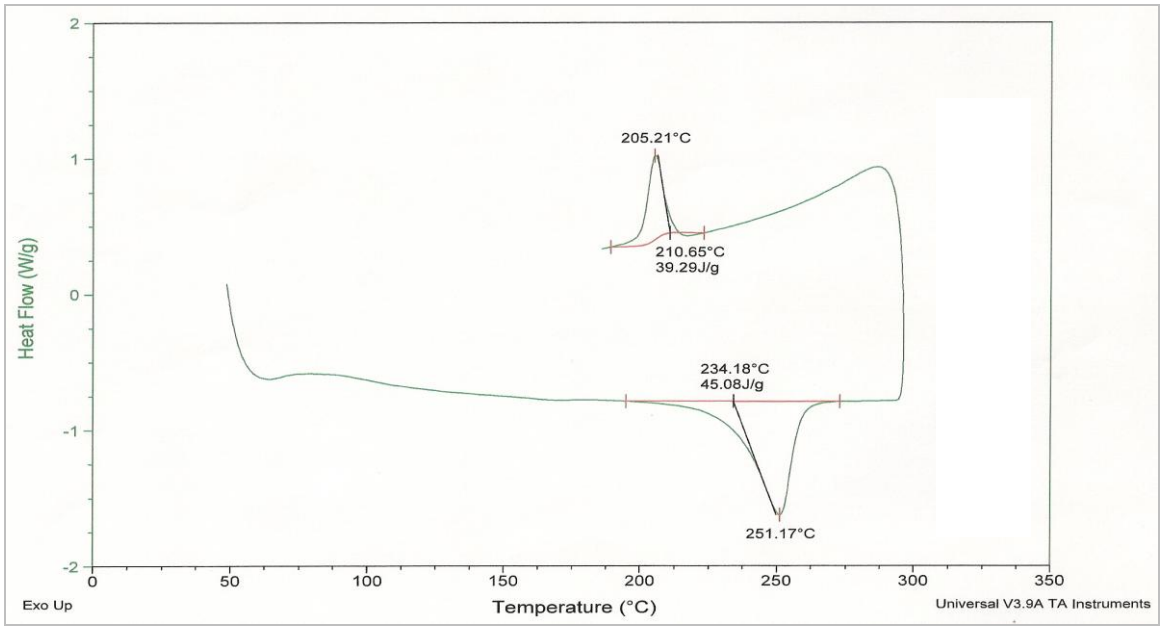

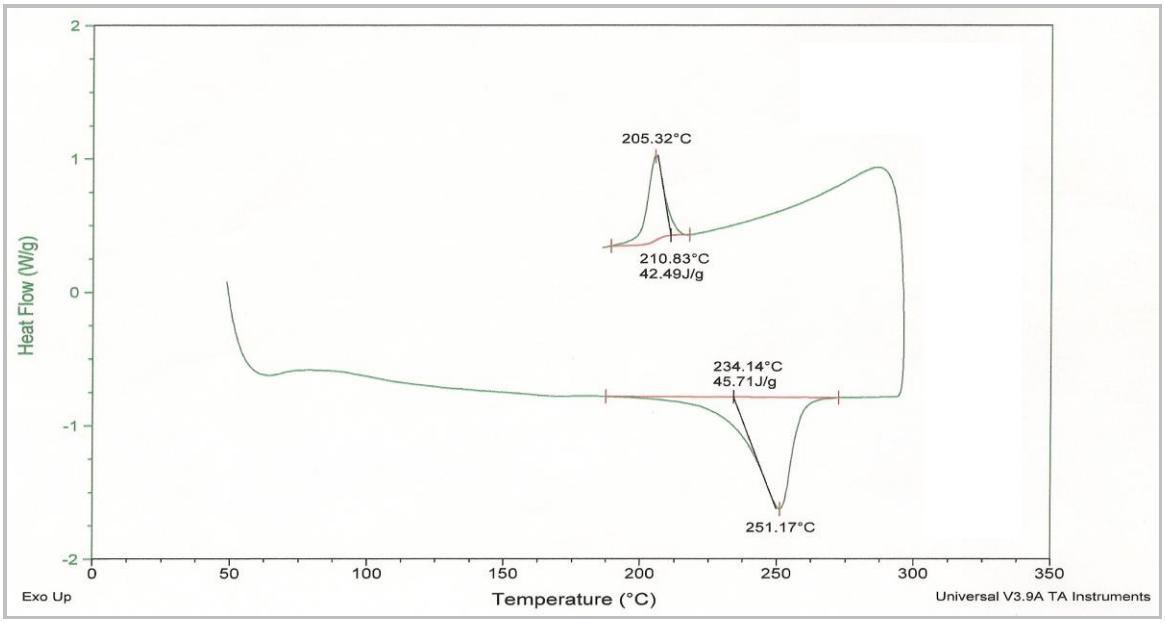

Figure 43 Thermograms of Extruded Samples of non contaminated rPET-bg at 20°C/min

6. DSC Thermograms of *rPET-bg contaminated with 5% PP at a heating / cooling rate of* ***20°C/min***

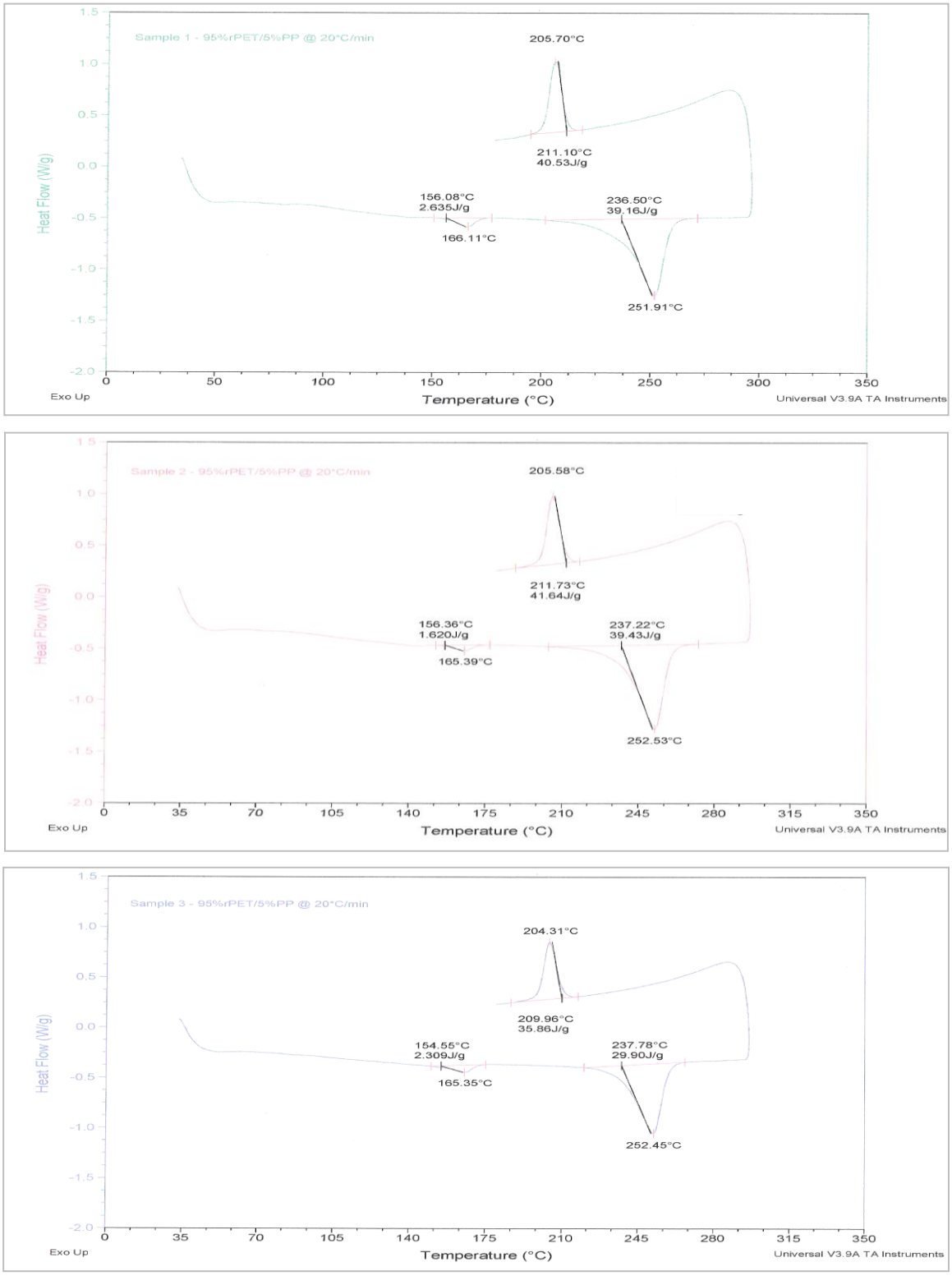

Figure 44 Thermograms of Extruded Samples of rPET-bg contaminated with 5% PP at 20°C/min – *Stage 2*

7. DSC Thermograms of *non contaminated rPET-bg at a heating / cooling rate of* ***25°C/min***

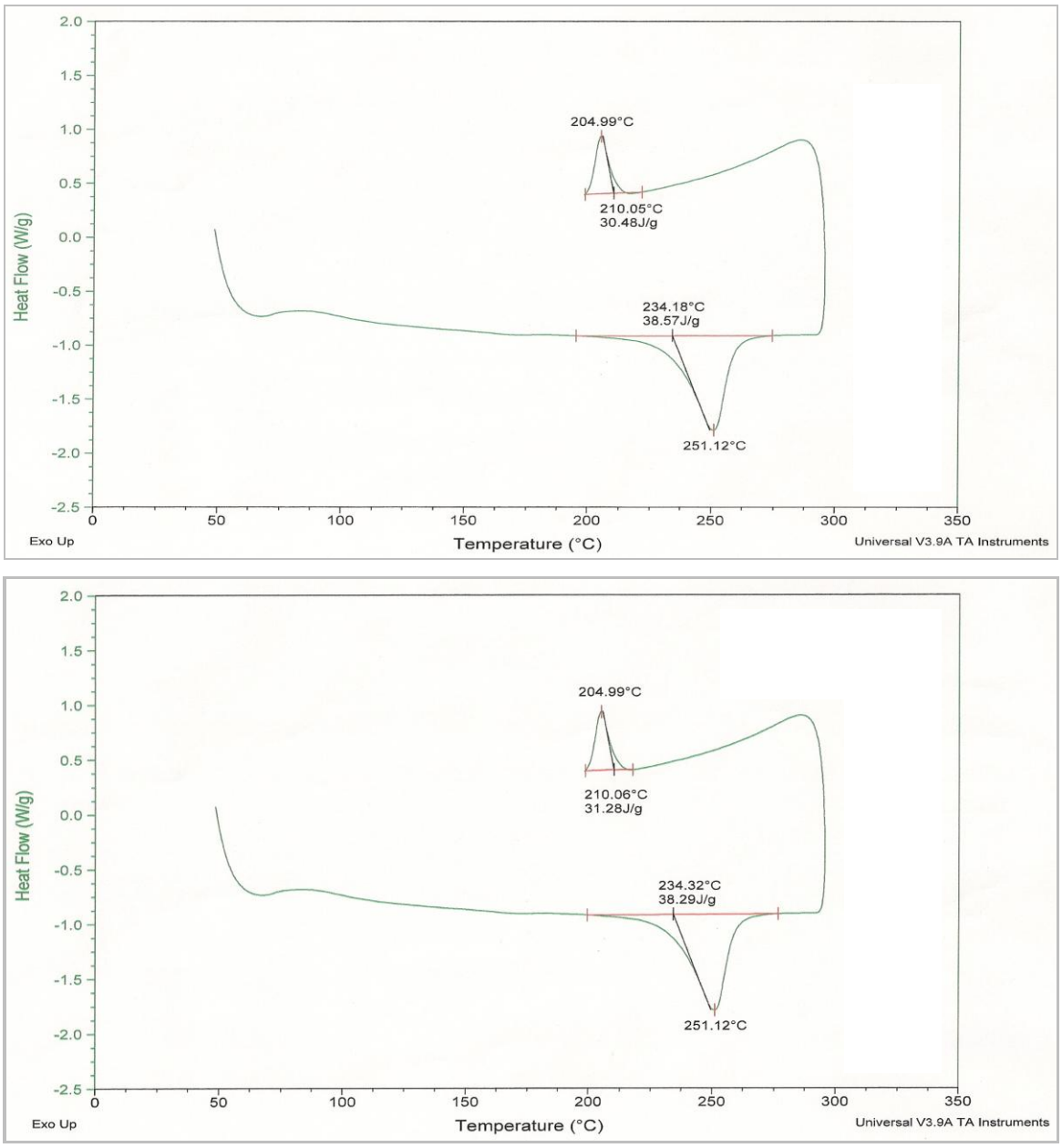

Figure 45 Thermograms of Extruded Samples of non contaminated rPET-bg at 25°C/min

8. DSC Thermograms of *rPET-bg contaminated with 5% PP at a heating / cooling rate of* ***25°C/min***

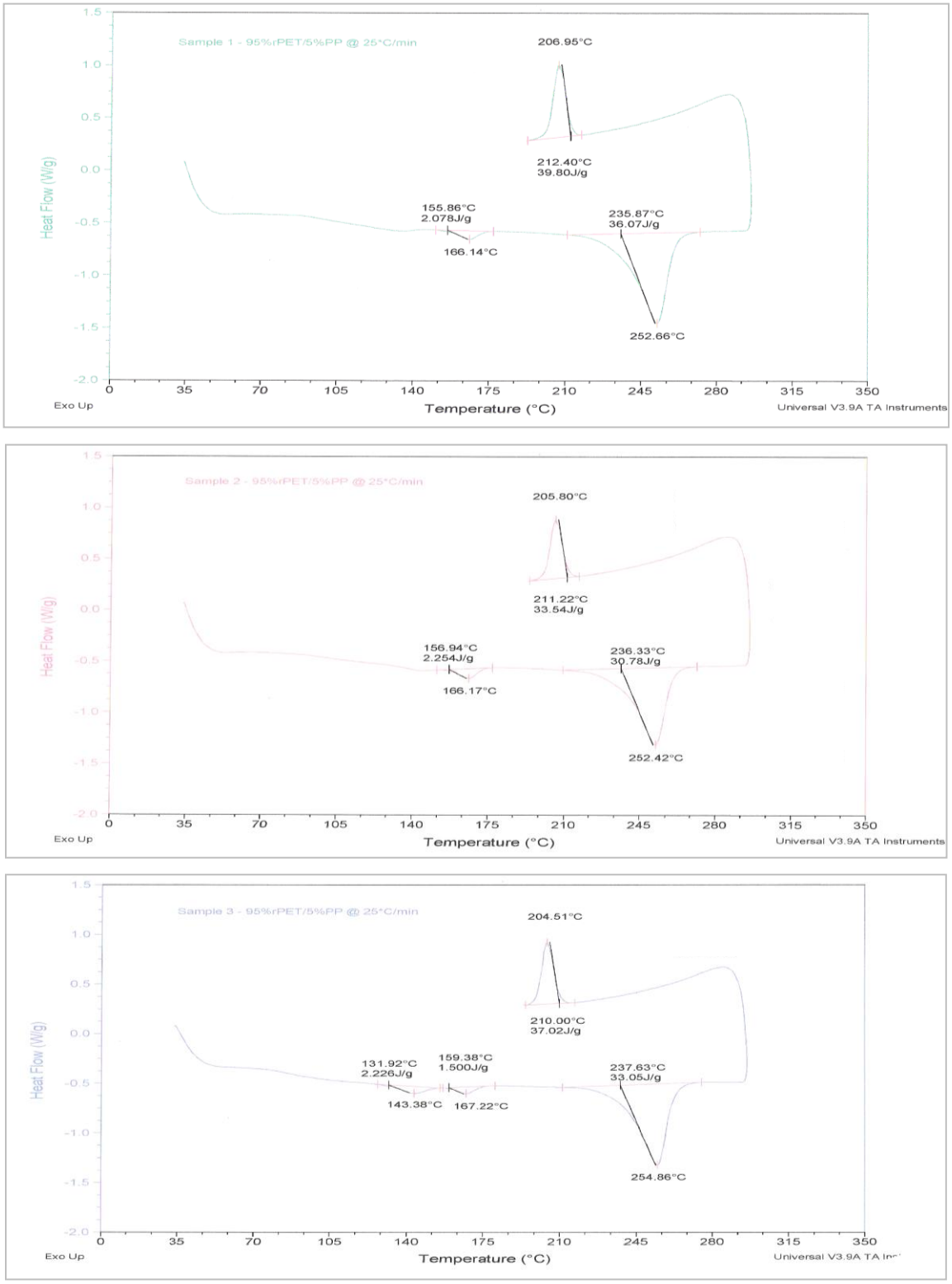

Figure 46 Thermograms of Extruded Samples of rPET-bg contaminated with 5% PP at 25°C/min

9. Evaluation by Avrami and Ozawa Equations

9.1 Overall Data at various cooling rates

		Extruded Samples Non contaminated rPET-bg				Extruded Samples 95% rPET-bg / 5% PP			
Cooling Rate, ($^oC/min$)	***Temp.* (^oC)**	***Time* (*min*)**	***log t***	**X_t**	***log(-ln(1-X_t))***	***Time* (*min*)**	***log t***	**X_t**	***log(-ln(1-X_t))***
10	212	0.99	0.00	0.013	-1.879	0.97	-0.01	0.010	-2.000
	210	1.31	0.12	0.022	-1.650	1.29	0.11	0.017	-1.763
	209	1.44	0.16	0.027	-1.568	1.46	0.16	0.023	-1.627
	208	1.63	0.21	0.034	-1.465	1.70	0.23	0.034	-1.461
	206	1.88	0.27	0.041	-1.381	1.96	0.29	0.044	-1.345
15	212	0.93	-0.03	0.013	-1.896	0.97	-0.01	0.028	-1.553
	210	1.24	0.09	0.020	-1.700	1.27	0.10	0.044	-1.351
	209	1.37	0.14	0.024	-1.605	1.42	0.15	0.056	-1.236
	208	1.57	0.20	0.030	-1.521	1.68	0.23	0.091	-1.022
	206	1.83	0.26	0.044	-1.347	2.03	0.31	0.144	-0.808
20	212	0.97	-0.01	0.012	-1.925	0.88	-0.06	0.026	-1.578
	210	1.28	0.11	0.020	-1.721	1.16	0.06	0.043	-1.360
	209	1.40	0.15	0.023	-1.640	1.28	0.11	0.054	-1.257
	208	1.60	0.20	0.030	-1.512	1.57	0.19	0.084	-1.056
	206	1.93	0.29	0.047	-1.315	1.88	0.27	0.135	-0.837
25	212	1.00	0.00	0.015	-1.821	0.80	-0.10	0.025	-1.602
	210	1.30	0.11	0.023	-1.636	1.03	0.02	0.042	-1.371
	209	1.42	0.15	0.027	-1.561	1.08	0.04	0.052	-1.273
	208	1.61	0.21	0.036	-1.441	1.30	0.11	0.078	-1.089
	206	1.86	0.27	0.051	-1.285	1.80	0.25	0.130	-0.855

Table 2 Data at Various Cooling Rates and Various Temperatures

9.2 Data of non contaminated rPET-bg at various cooling rates and fixed temeratures

Cooling Rates (a) (^oC/min)	Temp. (^oC)	*Time (min)*	ΔH_t	ΔH_c	log t	log R	X_t	log$(-ln(1-X_t)$
10	**212**	0.99	0.55	41.77	0.00	1.000	0.0131	-1.879
15		0.93	0.50	39.43	-0.03	1.176	0.0126	-1.896
20		0.97	0.48	40.89	-0.01	1.301	0.0118	-1.925
25		1.00	0.46	30.88	0.00	1.398	0.0150	-1.821
10	**210**	1.31	0.92	41.77	0.12	1.000	0.0221	-1.650
15		1.24	0.78	39.43	0.09	1.176	0.0197	-1.700
20		1.28	0.77	40.89	0.11	1.301	0.0188	-1.721
25		1.30	0.71	30.88	0.11	1.398	0.0229	-1.636
10	**209**	1.44	1.11	41.77	0.16	1.000	0.0267	-1.568
15		1.37	0.97	39.43	0.14	1.176	0.0245	-1.605
20		1.40	0.93	40.89	0.15	1.301	0.0226	-1.640
25		1.42	0.84	30.88	0.15	1.398	0.0271	-1.561
10	**208**	1.63	1.41	41.77	0.21	1.000	0.0337	-1.465
15		1.57	1.17	39.43	0.20	1.176	0.030	-1.521
20		1.55	1.20	40.89	0.19	1.301	0.029	-1.526
25		1.61	1.10	30.88	0.21	1.398	0.0356	-1.441
10	**206**	1.88	1.70	41.77	0.27	1.000	0.0408	-1.381
15		1.83	1.73	39.43	0.26	1.176	0.0440	-1.347
20		1.93	1.93	40.89	0.29	1.301	0.0473	-1.315
25		1.86	1.56	30.88	0.27	1.398	0.0506	-1.285

Table 3 Data of non contaminated rPET-bg at Various Cooling Rates and Various Temperatures

9.3 Data of rPET-bg contaminated with 5% PP at various cooling rates and fixed temperatures

Cooling Rates (a) (^oC/min)	Temp. (^oC)	*Time (min)*	ΔH_t	ΔH_c	log t	log R	X_t	log$(-ln(1-X_t)$
10	**212**	0.97	0.37	37.56	-0.01	1.000	0.010	-2.000
15		0.97	1.02	36.85	-0.01	1.176	0.028	-1.553
20		0.88	1.03	39.34	-0.06	1.301	0.026	-1.578
25		0.80	0.91	36.79	-0.10	1.398	0.025	-1.602
10	**210**	1.29	0.64	37.56	0.11	1.000	0.017	-1.763
15		1.27	1.61	36.85	0.10	1.176	0.044	-1.351
20		1.16	1.68	39.34	0.06	1.301	0.043	-1.360
25		1.03	1.53	36.79	0.02	1.398	0.042	-1.371
10	**209**	1.46	0.88	37.56	0.16	1.000	0.023	-1.627
15		1.42	2.08	36.85	0.15	1.176	0.056	-1.236
20		1.28	2.12	39.34	0.11	1.301	0.054	-1.257
25		1.08	1.91	36.79	0.04	1.398	0.052	-1.273
10	**208**	1.70	1.28	37.56	0.23	1.000	0.034	-1.461
15		1.68	3.35	36.85	0.23	1.176	0.091	-1.022
20		1.57	3.31	39.34	0.19	1.301	0.084	-1.056
25		1.30	2.88	36.79	0.11	1.398	0.078	-1.089
10	**206**	1.96	1.66	37.56	0.29	1.000	0.044	-1.345
15		2.03	5.31	36.85	0.31	1.176	0.144	-0.808
20		1.88	5.33	39.34	0.27	1.301	0.135	-0.837
25		1.80	4.80	36.79	0.25	1.398	0.130	-0.855

Table 4 Data of rPET-bg contaminated with 5% PP at Various Cooling Rates and Various Temperatures

Effect of *repetitive extrusions* **on the** *thermal characteristics* **of** *non contaminated rPET-bg* **and** *rPET-bg contaminated with 5% PP*

(Stage 2)

1. **DSC Thermograms of** *non contaminated rPET-bg – 1st extrusion cycle*

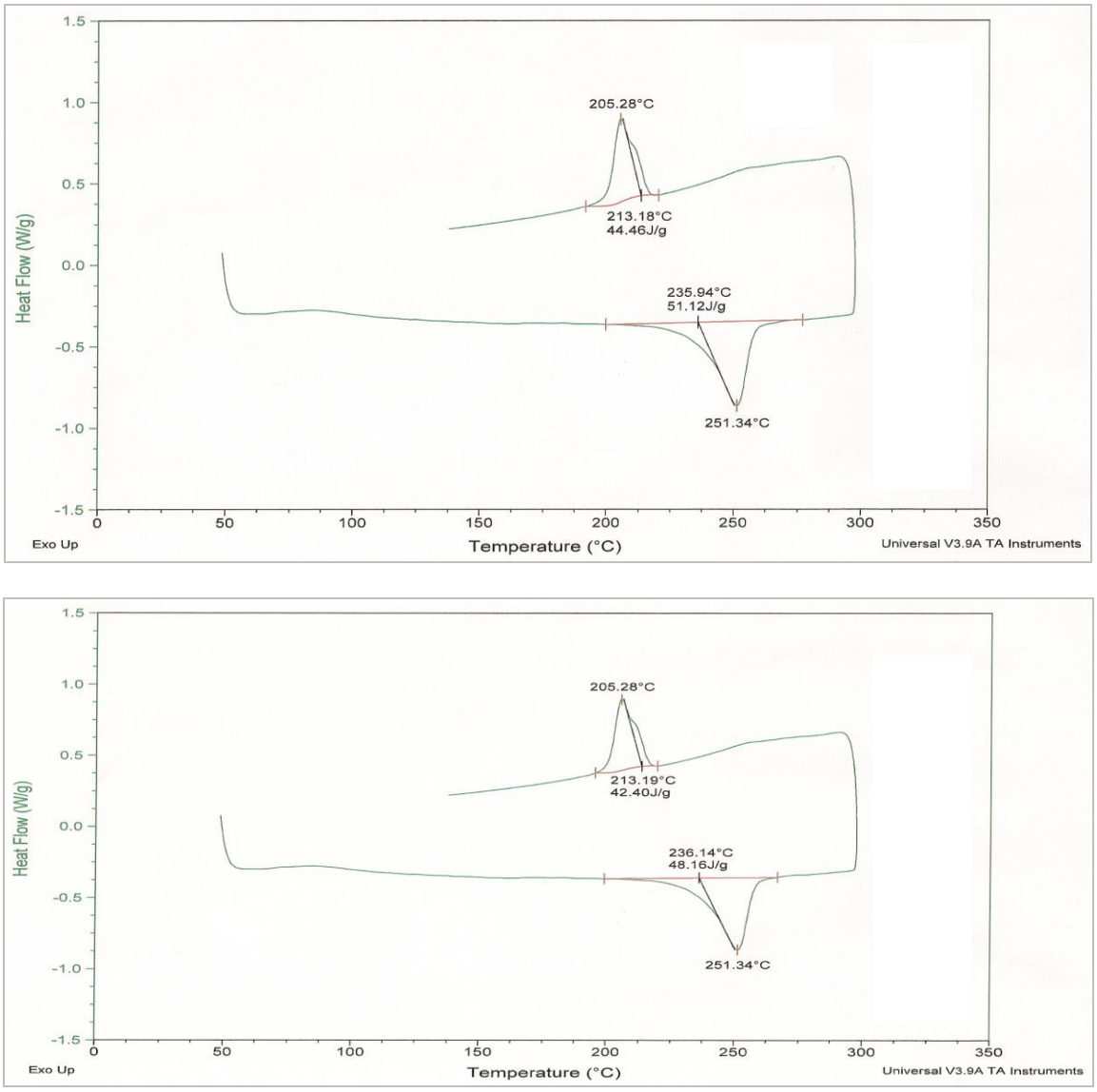

Figure 47 Thermograms of Extruded Samples of non contaminated rPET-bg – 1st extrusion cycle

2. DSC Thermograms of *rPET-bg contaminated with 5% PP – 1st extrusion cycle*

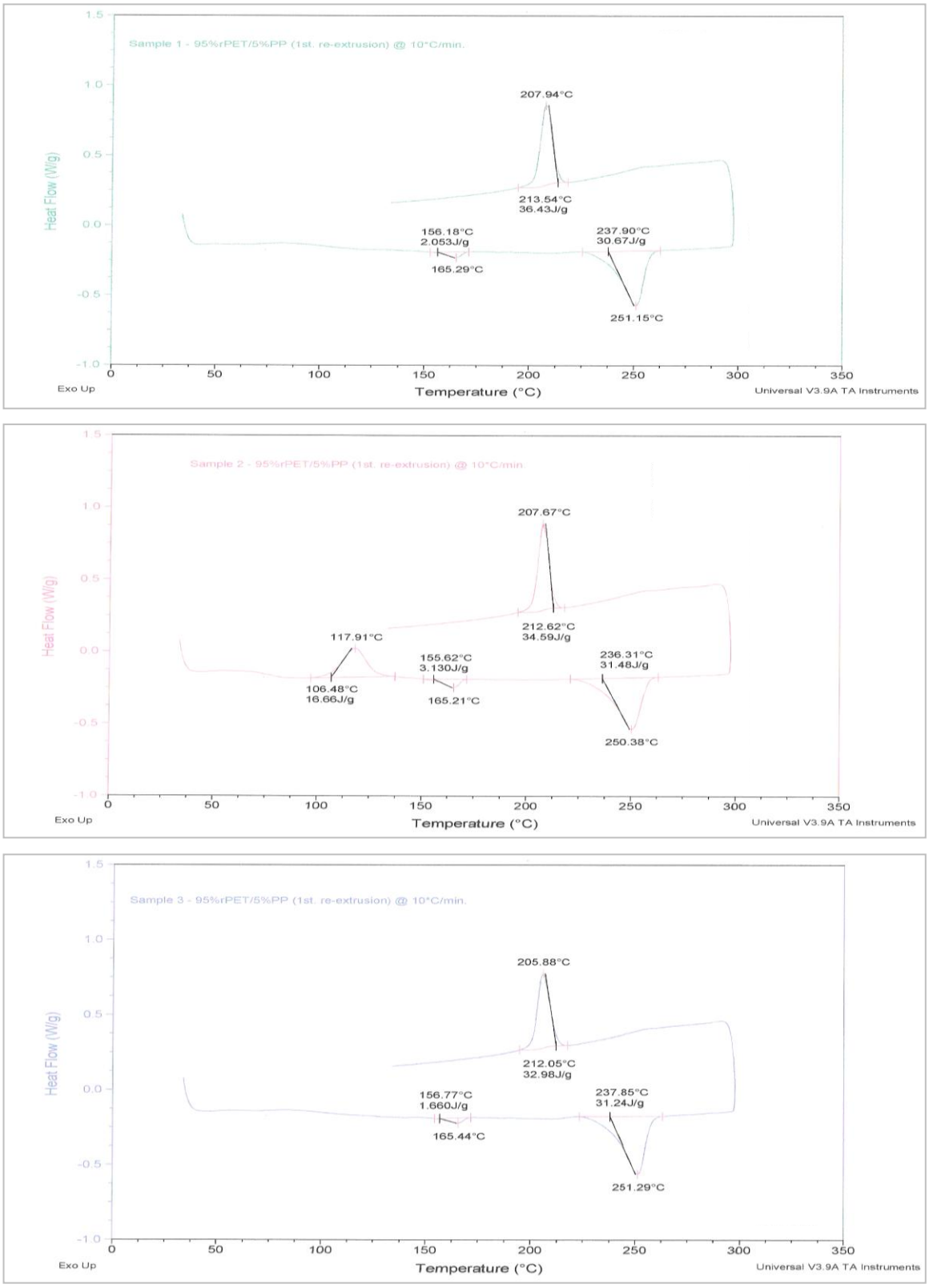

Figure 48 Thermograms of Extruded Samples of rPET-bg contaminated with 5% PP – 1st extrusion cycle

3. **DSC Thermograms of** *non contaminated rPET-bg – 2nd extrusion cycle*

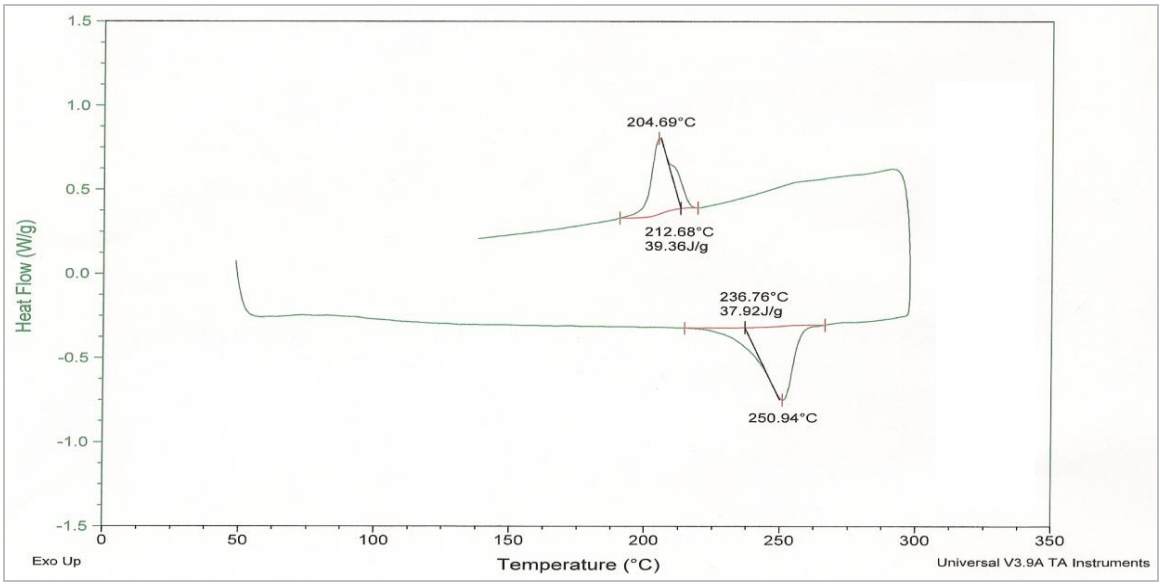

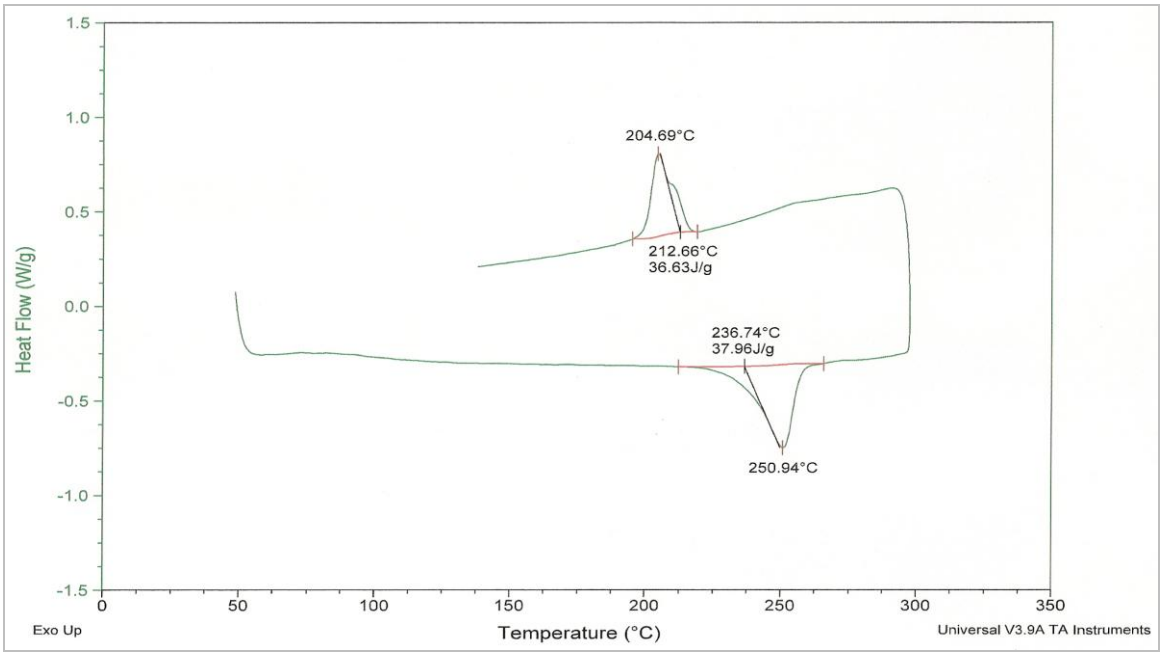

Figure 49 Thermograms of Extruded Samples of non contaminated rPET-bg – 2nd extrusion cycle

4. DSC Thermograms of *rPET-bg contaminated with 5% PP – 2nd extrusion cycle*

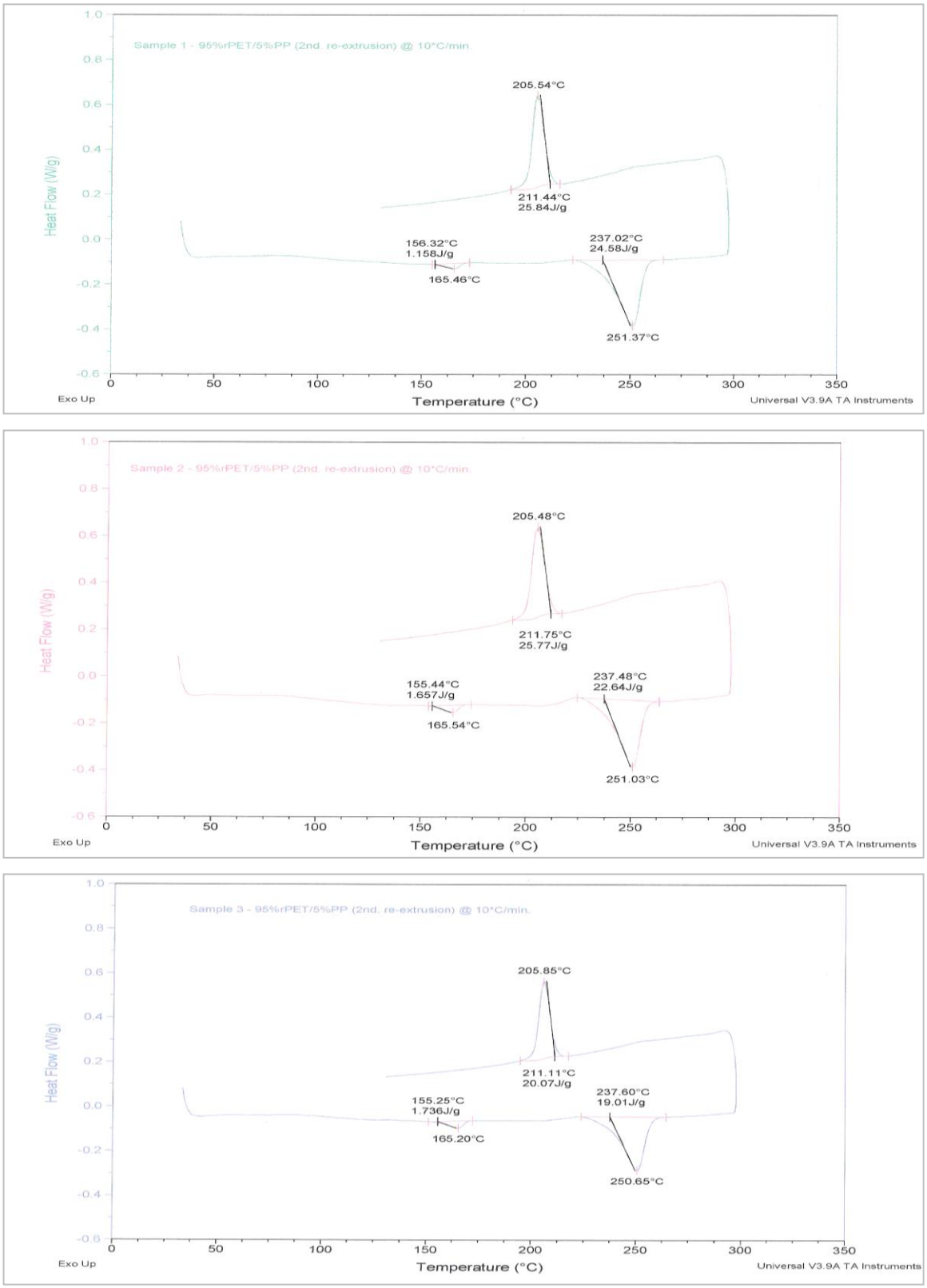

Figure 50 Thermograms of Extruded Samples of rPET-bg contaminated with 5% PP – 2nd extrusion cycle

5. DSC Thermograms of *non contaminated rPET-bg – 3rd extrusion cycle*

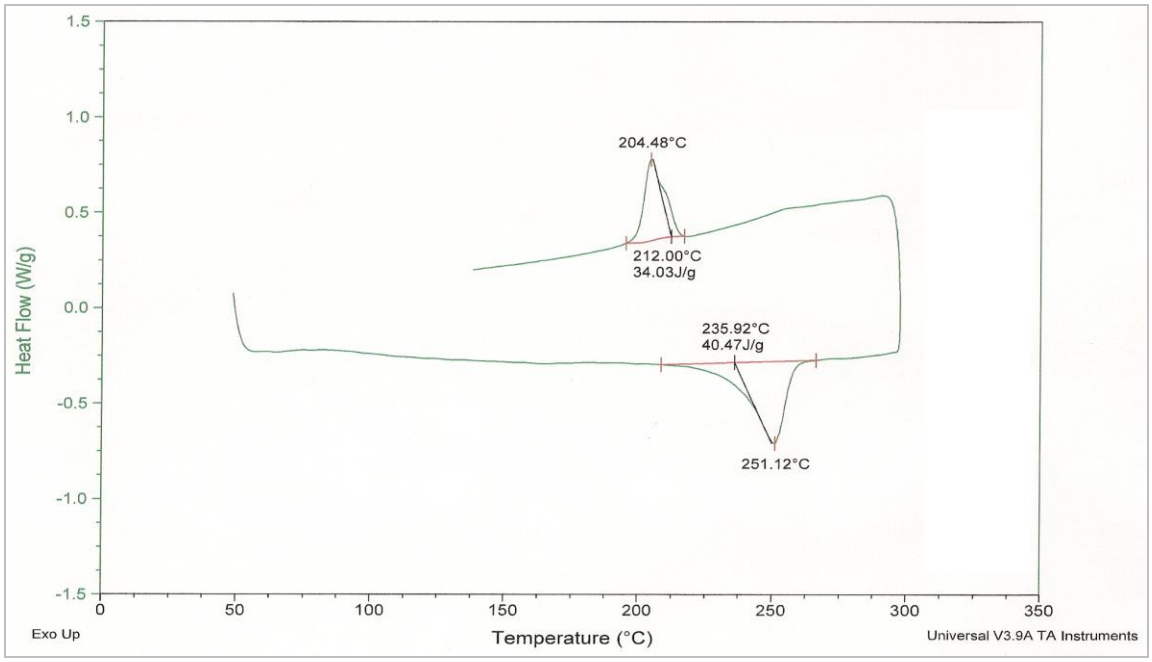

Figure 51 Thermograms of Extruded Samples of non contaminated rPET-bg – 3rd extrusion cycle

6. DSC Thermograms of *rPET-bg contaminated with 5% PP – 3rd extrusion cycle*

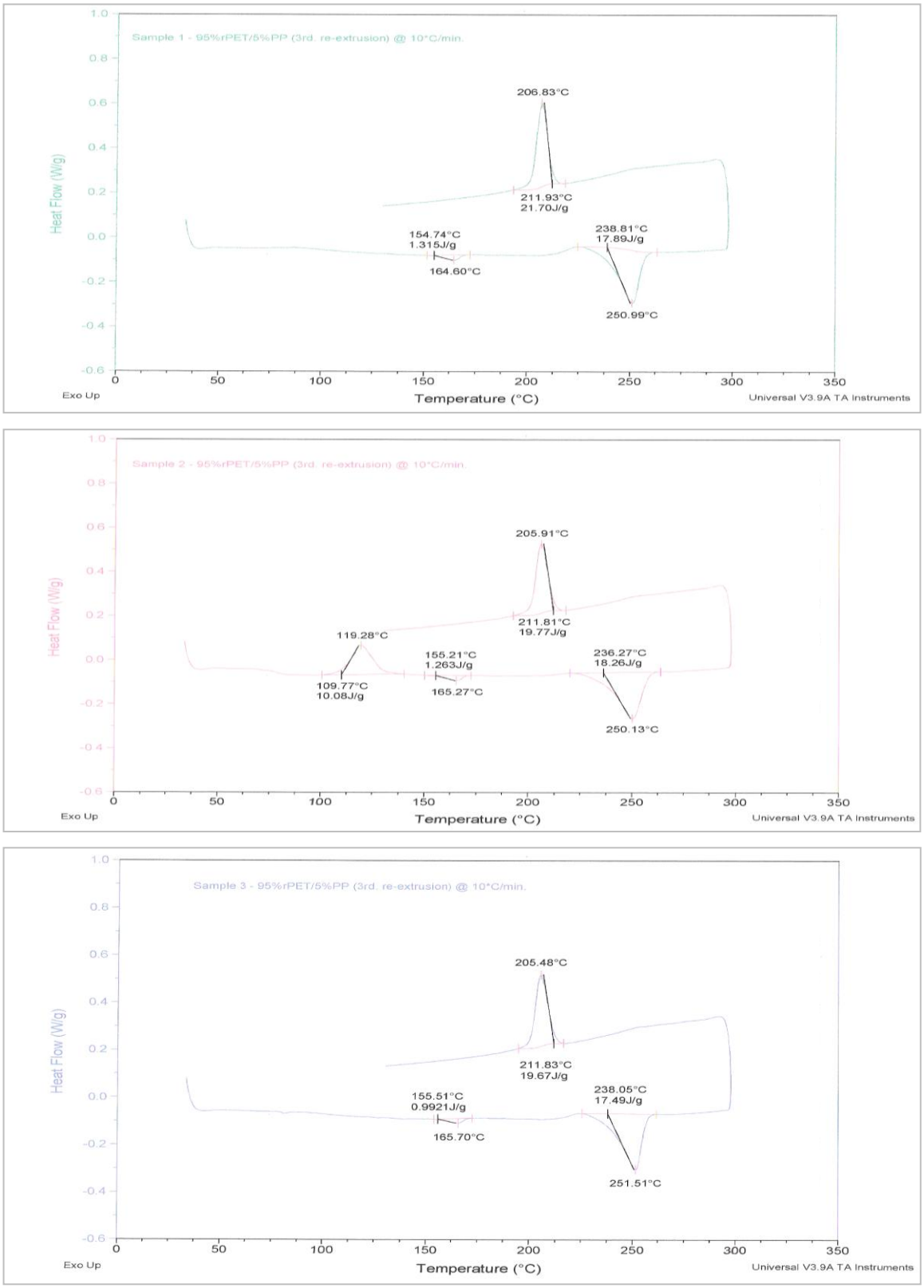

Figure 52 Thermograms of Extruded Samples of rPET-bg contaminated with 5% PP – 3rd extrusion cycle

7. DSC Thermograms of *non contaminated rPET-bg – 4th extrusion cycle*

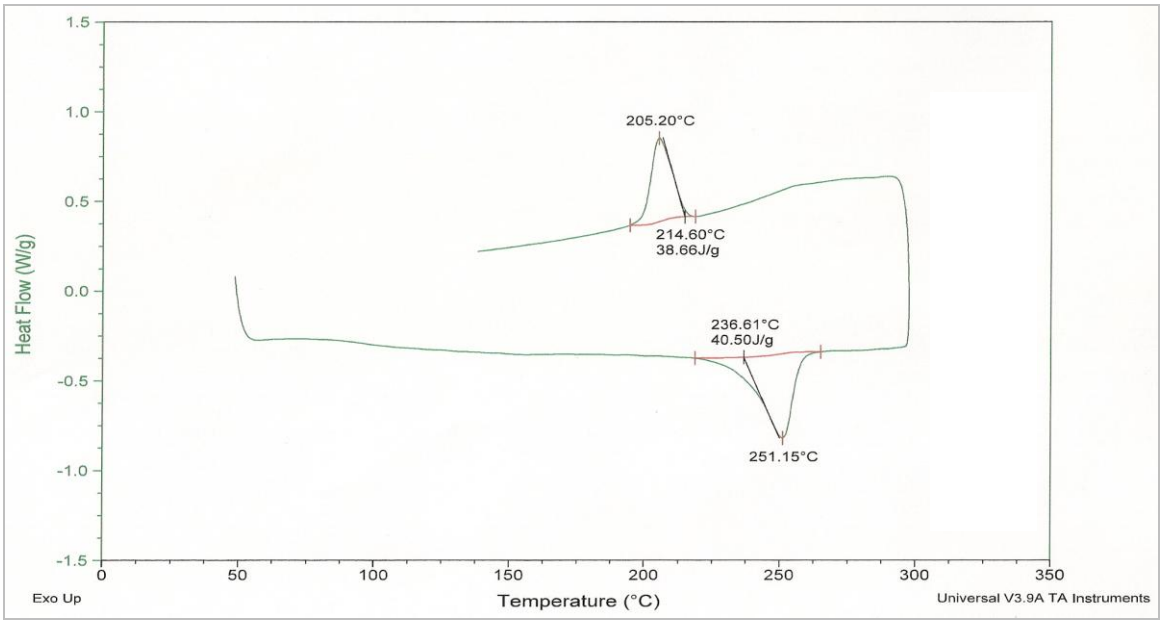

Figure 53 Thermograms of Extruded Samples of non contaminated rPET-bg – 4th extrusion cycle

8. DSC Thermograms of *rPET-bg contaminated with 5% PP – 4th extrusion cycle*

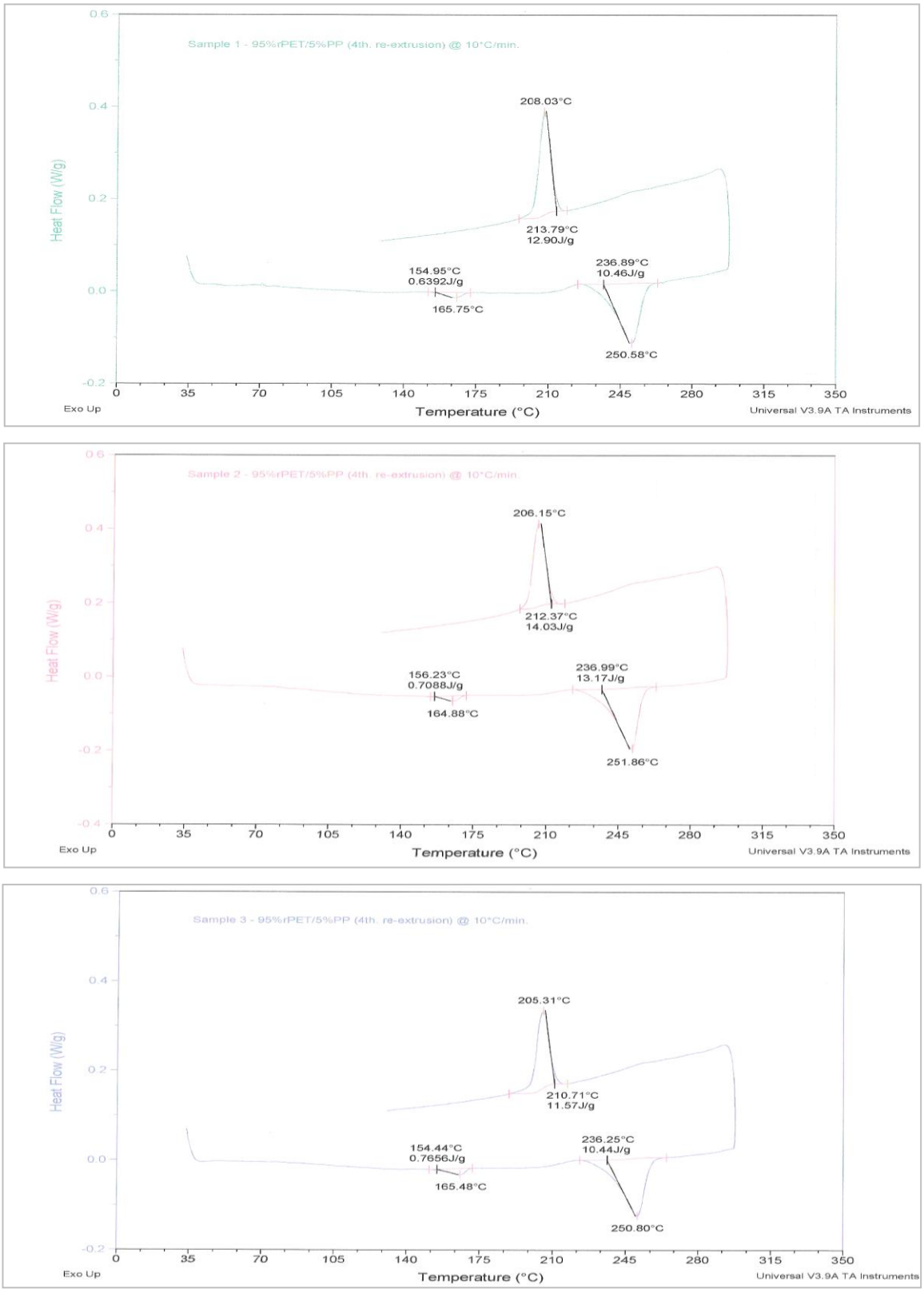

Figure 54 Thermograms of Extruded Samples of rPET-bg contaminated with 5% PP – 4th extrusion cycle

9. DSC Thermograms of *non contaminated rPET-bg – 5th extrusion cycle*

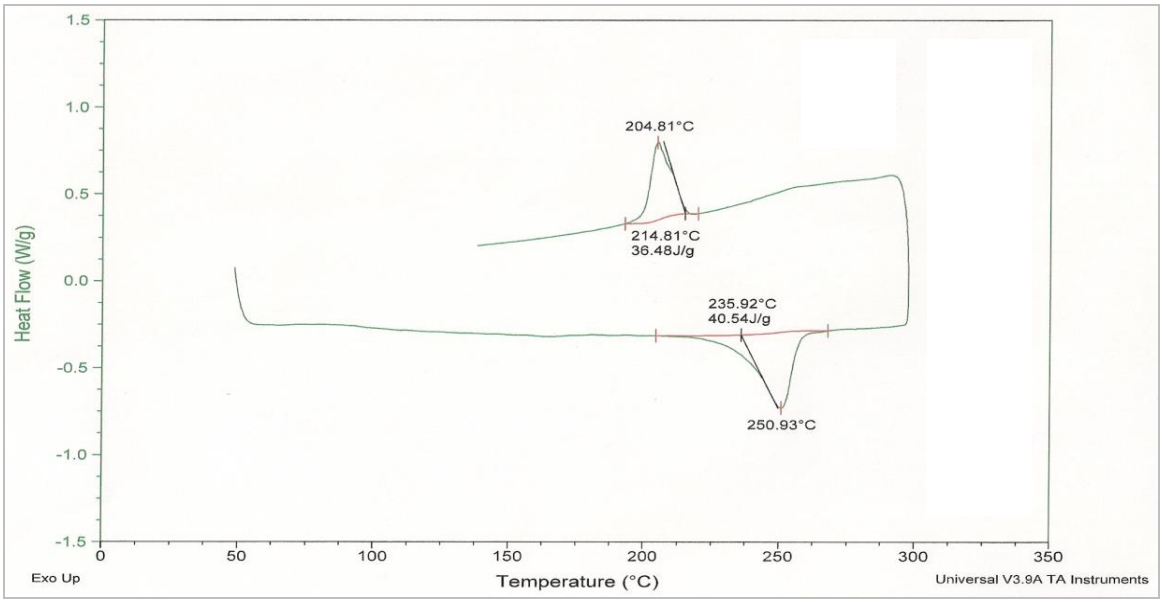

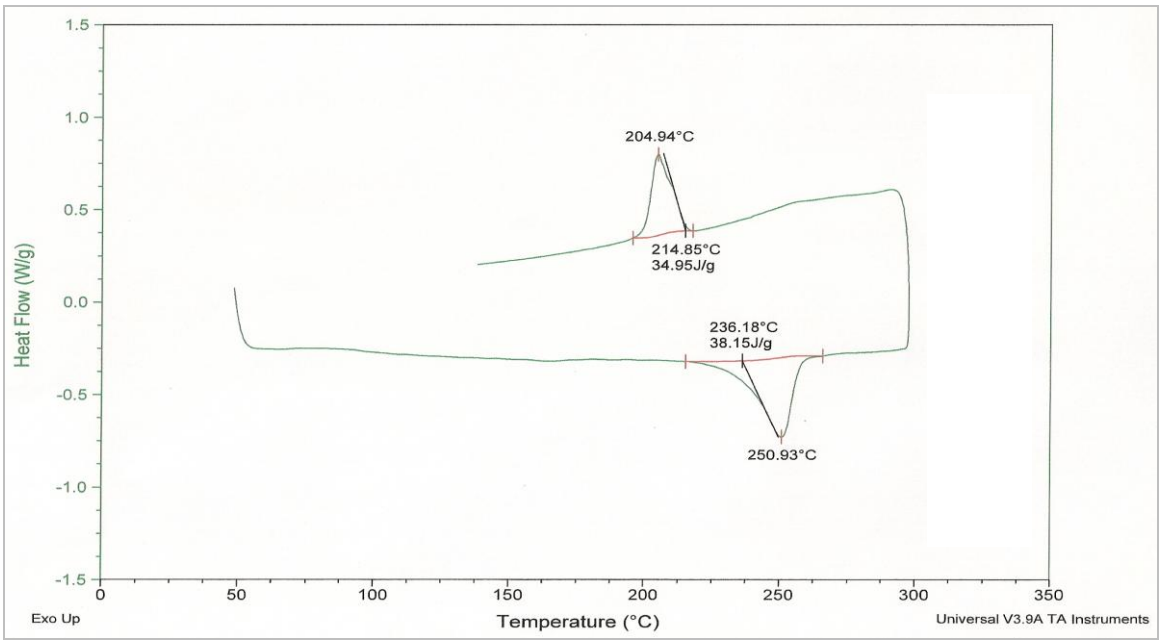

Figure 55 Thermograms of Extruded Samples of non contaminated rPET-bg – 5th extrusion cycle

10. DSC Thermograms of *rPET-bg contaminated with 5% PP – 5th extrusion cycle*

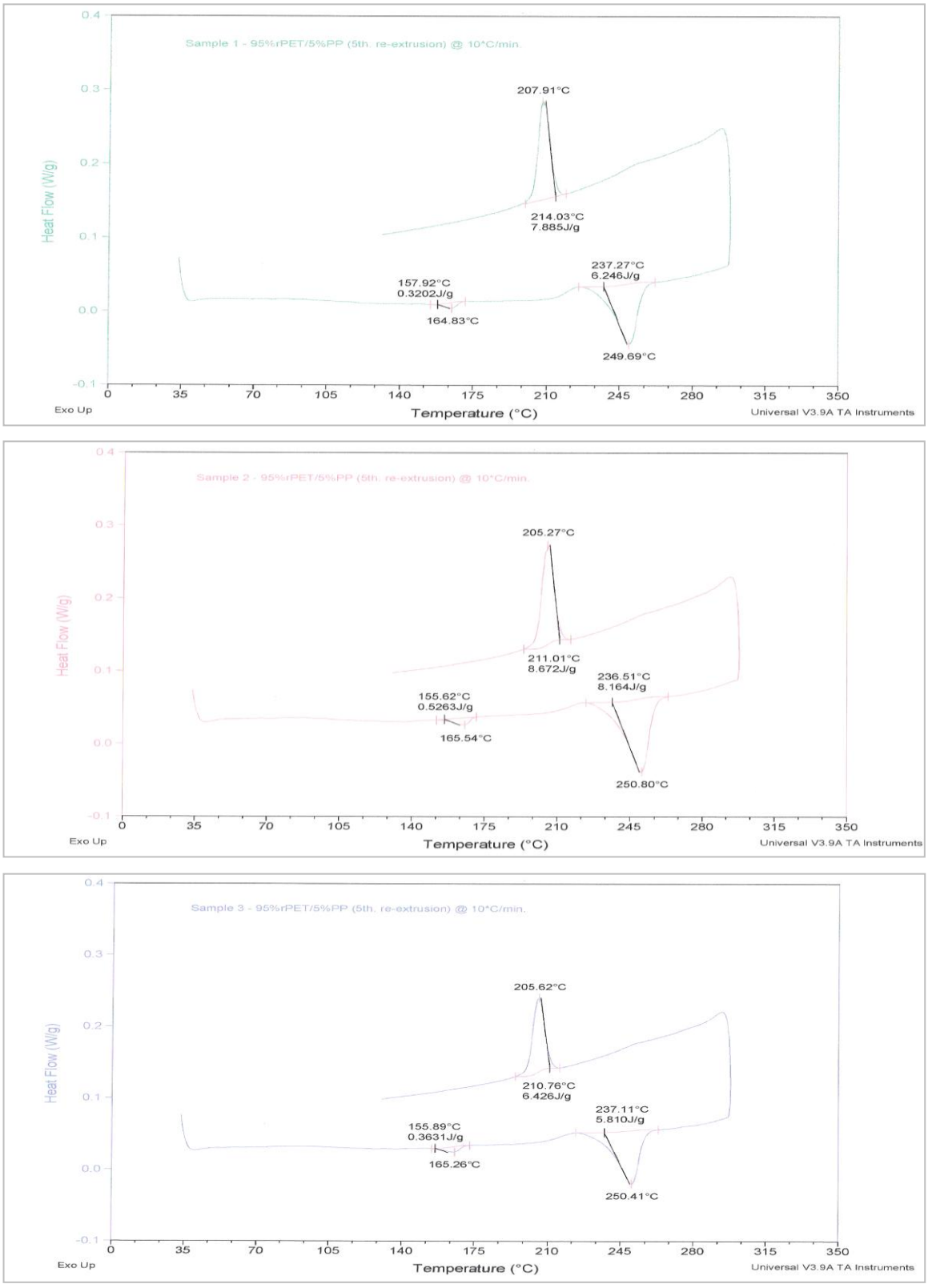

Figure 56 Thermograms of Extruded Samples of rPET-bg contaminated with 5% PP – 5th extrusion cycle

11. Evaluation by Avrami Equation, overall data for 5 re-extrusions cycles

		Extruded Samples Non contaminated rPET-bg				Extruded Samples 95% rPET-bg / 5% PP			
Re-extrusion Cycles	**Temp. (^oC)**	***Time (min)***	***log t***	X_t	$log(-ln(1-X_t)$	***Time (min)***	***log t***	X_t	$log(-ln(1-X_t)$
1	212	0.95	-0.02	0.014	-1.857	0.99	0.00	0.012	-1.935
	210	1.33	0.12	0.022	-1.645	1.34	0.13	0.023	-1.639
	209	1.46	0.16	0.025	-1.595	1.47	0.17	0.029	-1.534
	208	1.65	0.22	0.030	-1.520	1.59	0.20	0.034	-1.460
	206	1.91	0.28	0.038	-1.411	1.91	0.28	0.044	-1.348
2	212	1.02	0.01	0.015	-1.812	0.98	-0.01	0.035	-1.452
	210	1.27	0.10	0.021	-1.673	1.28	0.11	0.057	-1.232
	209	1.46	0.16	0.025	-1.600	1.40	0.15	0.071	-1.132
	208	1.65	0.22	0.029	-1.533	1.53	0.18	0.089	-1.033
	206	1.91	0.28	0.037	-1.419	1.81	0.26	0.132	-0.849
3	212	1.02	0.01	0.014	-1.844	0.98	-0.01	0.039	-1.400
	210	1.33	0.12	0.022	-1.646	1.24	0.09	0.061	-1.203
	209	1.46	0.16	0.025	-1.588	1.40	0.15	0.081	-1.073
	208	1.65	0.22	0.030	-1.515	1.57	0.20	0.107	-0.945
	206	2.17	0.34	0.048	-1.309	1.85	0.27	0.147	-0.798
4	212	0.95	-0.02	0.013	-1.897	0.97	-0.01	0.048	-1.307
	210	1.33	0.12	0.022	-1.653	1.26	0.10	0.078	-1.091
	209	1.46	0.16	0.026	-1.585	1.39	0.14	0.095	-1.003
	208	1.52	0.18	0.027	-1.555	1.55	0.19	0.120	-0.892
	206	1.85	0.27	0.038	-1.414	1.81	0.26	0.154	-0.778
5	212	1.01	0.00	0.014	-1.849	1.01	0.01	0.067	-1.159
	210	1.33	0.12	0.022	-1.646	1.30	0.11	0.099	-0.984
	209	1.45	0.16	0.026	-1.586	1.42	0.15	0.117	-0.906
	208	1.65	0.22	0.031	-1.506	1.60	0.20	0.147	-0.800
	206	1.97	0.29	0.041	-1.376	1.85	0.27	0.185	-0.690

Table 5 Overall Data at Various Re-extrusion Cycles and Various Temperatures

APPENDIX 9 – Statistical Analysis

Statistical analysis of the collected *observations* is very important in experimental work. *Observations* or *values* are considered *normally distributed* if they lie within *3 standard deviations.* This is called the ***3 σ Rule*** or the ***68-95-99 rule*** or the ***Empirical rule*** [194].

68% of the observations fall within **1 standard deviation** of the **mean**,

95% of the observations fall within **2 standard deviations** of the **mean**,

99.7% of the observations fall within **3 standard deviations** of the **mean**,

In science, the *95% coverage* is frequently used for statistical distribution evaluation, i.e. when the data are normally distributed, *95%* of the *shaped bell area*, is within ***1.96 σ*** of the *mean*. ***1.96*** represents approximately ***97.5*** percentile point of the ***normal distribution***

Any *observation* which falls outside this *normal distribution* should be rejected and considered as an *outlier*. Among the statistical tests used to determine if *observations* are *accepted* or *rejected*, the *Dixon's Q Test*.

1 Dixon's Q Test

Dixon's Q test [195], [196] is applied to individual results or to the means of sets of data to identify cases where observations' values need to be *rejected* or *accepted*. *Dixon's Q Test* is an effective simplified statistical method for small numbers of observations.
Only values which are within the acceptable interval, i.e. within the $Q_{95\%}$ and $Q_{99\%}$ confidence levels are considered and accepted. Any value outside this interval is considered as an ***outlier*** and *rejected*. ***Outliers*** are not included in the evaluation of the sample's ***mean***.

A summary of some critical values for *Dixon's Q test* are tabulated below:

Critical Values for Dixon's Q Test		
n	**Critical Values**	
	$Q_{95\%}$	**$Q_{99\%}$**
3	0.970	0.994
4	0.829	0.926
5	0.710	0.821
6	0.628	0.740
7	0.569	0.680
8	0.608	0.717
9	0.564	0.672
10	0.530	0.635

Table 6 Summarised Critical Values for *Dixon's Q Test*

Where: **$Q_{95\%}$** and **$Q_{99\%}$** are the confidence levels or *Confidence Intervals* and any *observation* outside these limits must be *rejected*.

Before the application of *Dixon Q Test*, the random *observations' values* or *results* have to be arranged in ascending order, i.e. from the lowest observation's value to the highest one. That is, X_1 the smallest through to X_n the largest as shown below:

Observation number (*n*)	**Observation Values (X_i)**	**Observation Order (*Ascending*)**
1	X_1	**Lowest**
2	X_2	↓
3	X_3	↓
4	X_4	↓
5	X_5	↓
and so on	and so on to X_n	**Largest**

Table 7 Arrangement of Observations

The ***larger*** value of the following quotients is recorded and compared to the critical values of the equivalent (*n*) observations in *Dixon's Q Test* Table:

$$Q_1 = \frac{X_2 - X_1}{X_n - X_1} \qquad (1)$$

And

$$Q_2 = \frac{X_n - X_{(n-1)}}{X_n - X_1} \qquad (2)$$

Example of application of Dixon's test

Consider the following *5 observations' values* for analysis by *Dixon's Q test*.

Observation number (*n*)	**Random Observation Values**
1	**2.24**
2	**2.51**
3	**2.00**
4	**2.72**
5	**2.23**

Table 8 Test of 5 Observations

From an examination of the results given in *Table 6.1*, the ***2.00*** result is somewhat abnormal. Let us carry out the *Dixon's test* to see if we *keep* or *reject* the ***2.00*** value.

First arrange the values of the *5 observations* in ascending order as shown below:

Observation number (*n*)	**Observation Values (X_i)**	**Observation Order (*Ascending*)**
1	X_1	**2.00**
2	X_2	**2.23**
3	X_3	**2.24**
4	X_4	**2.51**
5	X_5	**2.72**

Table 9 Ascending Order of the Observations' Values

From the above *Table 6.1*, we see that the number of observation (*n*) is *5*.

That is $n = 5$

That means, (*n*) satisfies $3 \leq n \leq 7$

Therefore, application of the equations (1) and (2):

$$Q_1 = \frac{X_2 - X_1}{X_n - X_1} \quad \text{and} \quad Q_2 = \frac{X_n - X_{(n-1)}}{X_n - X_1}$$

From *Table 6.2* above, we deduce that;

$$X_1=2.00, \quad X_2=2.23, \quad X_3=2.24, \quad X_4=2.51 \quad and \quad X_5=2.72$$

In terms of expressions of the quotients, we conclude that;

$$X_1=2.00, \quad X_2=2.23, \quad X_n= X_5=2.72 \quad and \quad X_{(n-1)}= X_4 =2.51$$

By introducing the above values in the given quotients it leads to:

$$Q_1 = \frac{X_2 - X_1}{X_n - X_1} = \frac{2.23 - 2.00}{2.72 - 2.00} = \frac{0.23}{0.72} = 0.319$$

And

$$Q_2 = \frac{X_n - X_{(n-1)}}{X_n - X_1} = \frac{2.72 - 2.51}{2.72 - 2.00} = \frac{0.21}{0.72} = 0.291$$

The ***larger*** value of the above quotients is ***0.319***, compared with the critical values for ***n=5*** (see *Table 2.4*, ***Section 2.3.1***) which are as follow:

- At *95% confidence level* is ***0.710***
- At *99% confidence level* is ***0.821***

Our ***larger*** value of ***0.319*** did not even exceed the ***critical value*** at *95% confidence level*. Since ***0.319*** is far below the critical value of ***0.710***, therefore there is ***NO*** justification for rejecting the low result value ***2.00***, hence it is ***accepted*** with the other values and not rejected.

2 Estimation of the Mean's Confidence Interval

After statistically evaluating the results and the rejection of any ***outliers*** and in respect to the above, the estimation of *95% confidence interval* for the *mean* is calculated as follow:

Sample Mean ± 1.96 Standard Error

Or $$\mu \pm 1.96 S_E \qquad (3)$$

Where: $\boldsymbol{\mu}$ is the sample mean, ± is the upper and lower limits, ***1.96*** is the ***97.5*** percentile point of the normal distribution for ***95%*** coverage and $\boldsymbol{S_E}$ is the standard error of the sample mean.

Note: To not confuse with the *sample standard deviation* (***σ***), the *standard error* (***S_E***) of a *sample mean* is the estimated standard deviation of the *error*, i.e. it is the standard deviation of the sampling distribution.

Whereas, the *standard error of the mean* (variation of the mean) is determined as follow:

$$S_E = \frac{\sigma}{\sqrt{n}} \qquad (4)$$

Where: ***σ*** is the sample standard deviation, ***n*** the number of observations.

APPENDIX 10 – Research Skills Development

Workshops and conferences Attended 2009 / 2014

Workshops	Date & Time	Facilitator	Venue
Research Philosophy	20.11.2009 10.00 – 16.00	GS	North Campus T1-20
Critical Review of the Literature	27.11.2009 10.00 – 16.00	GS	North Campus T1-20
The Context, Politics and Ethics of Research	04.12.2009 10.00 – 16.00	GS	North Campus T1-20
Project Management	25.03.2010 10.00 – 16.00	Kay Dudman	North Campus LCG-13B
Academic Writing	02.06.2010 10.00 – 13.00	Tom Burns	North Campus BEL-09
Presentation Skills	03.06.2010 10.00 – 16.00	Dave Griffiths	North Campus BEL1-09
Career Planning	30.06.2010 10.00 – 16.00	Neelam Thapar Jennifer reay	North Campus GCG-08
Census Data Workshop	24.11.2010 09.00 – 17.00	David Hall	North Campus TMG-08
Research Ethics & the MPhil/PhD process	01.12.2010 10.00 – 14.00	Georgie Parry	N/ Campus GCG-09
Real-world research	15.12.2010 10.00 – 12.00	Jim Price	N/ Campus T9-05
Introduction to NVivo	25.01.2011 13.30 – 16.30	Cathy Sullivan	N/ Campus TMG-08
Researchers' Tools: Zetoc, Copac and the Archives Hub	27.01.2011 13.00 – 15.00	Lisa Jenkins	N/ Campus TMG-08
Preparing for Fieldwor	02.02.2011 10.00 – 12.00	Paul MC Dermott	N/ Campus T9-05
Postgraduate Research Welcome and Induction – Part 1	01.03.2011 14.00 – 16.00	George Alison & Sabri	Moorgate MG2-19
Postgraduate Research Welcome and Induction – Part 2	08.03.2011 14.00 – 16.00	Deborah Albon	Moorgate MG2-19
Getting Published	09.03.2011 10.00 – 12.00	Graham Hobbs Philip Mudd	N/ Campus GCG-09

Writing Abstracts for Conferences	28.09.2011 02.30 – 17.00	Catherine Lee	N/ Campus GC1-15
Communicating Your Ideas Clearly	07.11.2011 10.00 – 13.00	Caron King	N/ Campus TSG-04
Identifying What You Want From Your Research	07.11.2011 14.00 – 17.00	Caron King	N/ Campus TSG-04
12th BPF Annual International Conference **PVC: New Challenges - New Opportunities**	10.11.2011 10.25 – 15.15	The British Plastics Federation 6 Bath Place, Rivington Street, London EC2A 3JE	
Managing Stress For PhD Students	07.12.2011 10.00 – 12.00	Hugh Clark	N/ Campus T9-05
Practical Project Management For Researchers	23.01.2012 10.00 – 17.00	Chris Hopkins	N/ Campus T9-05
Becoming An Even More Effective Researcher	22.03.2012 10.00 – 17.00	Dr Caron King	N/ Campus T9-05
Preventing Plagiarism	02.05.2012 10.00 – 13.00	Sandra Sinfield	N/ Campus T9-05
Advanced Practical Project Management For Researchers	25.06.2012 10.00 – 17.00	Dr Caron King	N/ Campus LCG 07
Media Skills	21.11.2012 09.30 – 17.00	Lily & Tim	N/ Campus LCG-07
Research Leadership	24.04.2013 14.00 – 16.30	Peter Mc Caffery	N/ Campus TM2-35
Intellectual Property	01.05.2013 10.00 – 11.00	Richard Celm	N/ Campus T9-05
What to Expect During the Viva Process	15.05.2013 10.00 – 12.00	?	N/ Campus GCG-08
REPLAST: **6th Annual Plastics Recycling Conference**	06.11.2013 10.00 – 17.00	*By BPF at RSC:* 1 Carlton House Terrace, London SW1Y 5DB	
Thermoplastic Composites	27.02.2014 10.00 – 15.00	The British Plastics Federation, 6 Bath Place, Rivington Street, London EC2A 3JE	
REACH Masterclass	15.05.2014 10.00 – 16.00	The British Plastics Federation, 6 Bath Place, Rivington Street, London EC2A 3JE	

Table 10 Workshops and conferences Attended 2009 / 2014